Natural Resources Canada | Ressources naturelles Canada

GEOLOGICAL SURVEY OF CANADA
OPEN FILE 7856

Targeted Geoscience Initiative 4: Canadian Nickel-Copper-Platinum Group Elements-Chromium Ore Systems — Fertility, Pathfinders, New and Revised Models

D.E. Ames and M.G. Houlé
(Editors)

2015

Canada

GEOLOGICAL SURVEY OF CANADA
OPEN FILE 7856

Targeted Geoscience Initiative 4: Canadian Nickel-Copper-Platinum Group Elements-Chromium Ore Systems — Fertility, Pathfinders, New and Revised Models

D.E. Ames[1] **and M.G. Houlé**[2]

[1]Geological Survey of Canada, Ottawa, Ontario
[2]Geological Survey of Canada, Québec, Quebec

2015

© Her Majesty the Queen in Right of Canada, as represented by the Minister of Natural Resources Canada, 2015

doi:10.4095/296674

This publication is available for free download through GEOSCAN (http://geoscan.nrcan.gc.ca/)

Recommended citation

Ames, D.E. and Houlé, M.G. (ed.), 2015. Targeted Geoscience Initiative 4: Canadian Nickel-Copper-Platinum Group Elements-Chromium Ore Systems — Fertility, Pathfinders, New and Revised Models; Geological Survey of Canada, Open File 7856, 305 p. doi:10.4095/296674

Publications in this series have not been edited; they are released as submitted by the author.

Contribution to the Geological Survey of Canada's Targeted Geoscience Initiative 4 (TGI-4) Program (2010-2015)

TABLE OF CONTENTS

FERTILITY AND PATHFINDERS: ADVANCES IN THE DETECTION OF Ni-Cu-PGE

GEOLOGICAL SURVEY OF CANADA
OPEN FILE 7856

Targeted Geoscience Initiative 4: Canadian Nickel-Copper-Platinum Group Elements-Chromium Ore Systems — Fertility, Pathfinders, New and Revised Models

A synthesis of the TGI- 4 Canadian nickel-copper-platinum group elements-chromium ore systems project — revised and new genetic models and exploration tools for Ni-Cu-PGE, Cr-(PGE), Fe-Ti-V-(P), and PGE-Cu deposits

Doreen E. Ames[1] and Michel G. Houlé[2]

[1]Geological Survey of Canada, Ottawa, Ontario
[2]Geological Survey of Canada, Québec, Quebec

2015

© Her Majesty the Queen in Right of Canada, as represented by the Minister of Natural Resources Canada, 2015

This publication is available for free download through GEOSCAN (http://geoscan.nrcan.gc.ca/)

Recommended citation

Ames, D.E. and Houlé, M.G., 2015. A synthesis of the TGI-4 Canadian nickel-copper-platinum group elements-chromium ore systems project — revised and new genetic models and exploration tools for Ni-Cu-PGE, Cr-(PGE), Fe-Ti-V-(P), and PGE-Cu deposits, *In:* Targeted Geoscience Initiative 4: Canadian Nickel-Copper-Platinum Group Elements-Chromium Ore Systems — Fertility, Pathfinders, New and Revised Models, (ed.) D.E. Ames and M.G. Houlé; Geological Survey of Canada, Open File 7856, p. 1–15.

Publications in this series have not been edited; they are released as submitted by the author.

Contribution to the Geological Survey of Canada's Targeted Geoscience Initiative 4 (TGI-4) Program (2010–2015)

TABLE OF CONTENTS

A synthesis of the TGI- 4 Canadian nickel-copper-platinum group elements-chromium ore systems project — revised and new genetic models and exploration tools for Ni-Cu-PGE, Cr-(PGE), Fe-Ti-V-(P), and PGE-Cu deposits

Doreen E. Ames[1]* and Michel G. Houlé[2]

[1]Geological Survey of Canada, 601 Booth Street, Ottawa, Ontario K1A 0E8
[2]Geological Survey of Canada, 490 rue de la Couronne, Québec, Quebec G1K 9A9
*Corresponding author's e-mail: Doreen.Ames@NRCan.gc.ca

ABSTRACT

The Canadian Ni-Cu-PGE-Cr ore systems project, under the fourth phase of the Targeted Geoscience Initiative (TGI-4), spanned a breadth of ore deposit types, tectonic environments (crustal boundaries, supra-subduction zones, astrobleme, intracratonic rift), and processes of formation (magmatic to hydrothermal). This report summarizes key project activities for six mineral districts completed by a collaborative group of more than fifty contributors from the GSC, four provincial geological surveys, academia, and industry to develop and refine genetic models and exploration techniques to determine fertility and pathfinders.

Sixty-six new age determinations provide important geochronological constraints to build and refine models for many Cr-(PGE), Ni-Cu-PGE, Cu-PGE, and Fe-Ti-V-(P) prospective and fertile regions. These include Ni-Cu-PGE in convergent-margin settings, Cr in the Bird River and McFaulds Lake ("Ring of Fire") greenstone belts, Cr in La Grande Rivière-Eastmain domains, Cu-PGE in Midcontinent Rift, and Ni-Cu-PGE in the enormous Sudbury mining district.

New exploration techniques to detect fertility using advanced mineral chemical microanalytical techniques and discriminant diagrams were developed for oxide phases (chromite, magnetite) in barren and fertile intrusions through examination of Canada's districts (Sudbury Igneous Complex, Ontario; Voisey's Bay, Labrador and Newfoundland) and Archean komatiite (Alexo, Abitibi). The first in situ determination of actual ore-metal concentrations from an early trapped melt hosting a major mining district was completed. Various new indicator minerals and assemblages, such as apatite, biotite, and epidote-amphibole-titanite assemblages, were identified with distinctive chemistry to aid in vectoring towards buried Ni-Cu-PGE and Cu-PGE mineralization.

INTRODUCTION

This Geological Survey of Canada (GSC) Open File publication highlights collaborative research completed over five years (2010–2015) under the fourth phase of the Targeted Geoscience Initiative (TGI-4). The goal of this federal geoscience program was the development of new geoscientific knowledge and techniques to promote more effective exploration for buried ore deposits. Several key objectives were established to meet the main goals of the TGI-4 program: (a) characterize and model mineral systems, (b) develop targeting criteria – specifically fertility indicators (which indicate the presence of a mineral system) and vectors (which allow navigation within a system), (c) develop methods/protocols to apply these criteria, and (d) train and mentor students. The concept of "ore system" research was used to formulate TGI-4 projects and differs from ore deposits (e.g. mineral systems and mineral deposits; Hronsky and Groves, 2008; McCuaig et al., 2010). Economic mineral concentrations (ore deposits) are the culmination of a complex process chain, operating at a vast range of scales, and accurate predictive models for the distribution of ore deposits in space and time need to be based on a deep understanding of the entire "ore system", not just the deposits or orebodies themselves.

The TGI-4 nickel-copper-platinum element group-chromium (Ni-Cu-PGE-Cr) ore systems project focussed on orthomagmatic mineral systems and the exploration challenge of detecting new Ni-Cu-PGE-Cr mineral deposits by tackling knowledge gaps assessed for the ore system type and choosing the best sites to solve them across the country (Fig. 1). This project was designed to improve our knowledge of the magmatic ore systems and hydrothermal-magmatic processes to improve exploration criteria and better target the highly

Ames, D.E. and Houlé, M.G., 2015. A synthesis of the TGI-4 Canadian nickel-copper-platinum group elements-chromium ore systems project — revised and new genetic models and exploration tools for Ni-Cu-PGE, Cr-(PGE), Fe-Ti-V-(P), and PGE-Cu deposits, *In:* Targeted Geoscience Initiative 4: Canadian Nickel-Copper-Platinum Group Elements-Chromium Ore Systems — Fertility, Pathfinders, New and Revised Models, (ed.) D.E. Ames and M.G. Houlé; Geological Survey of Canada, Open File 7856, p. 1–15.

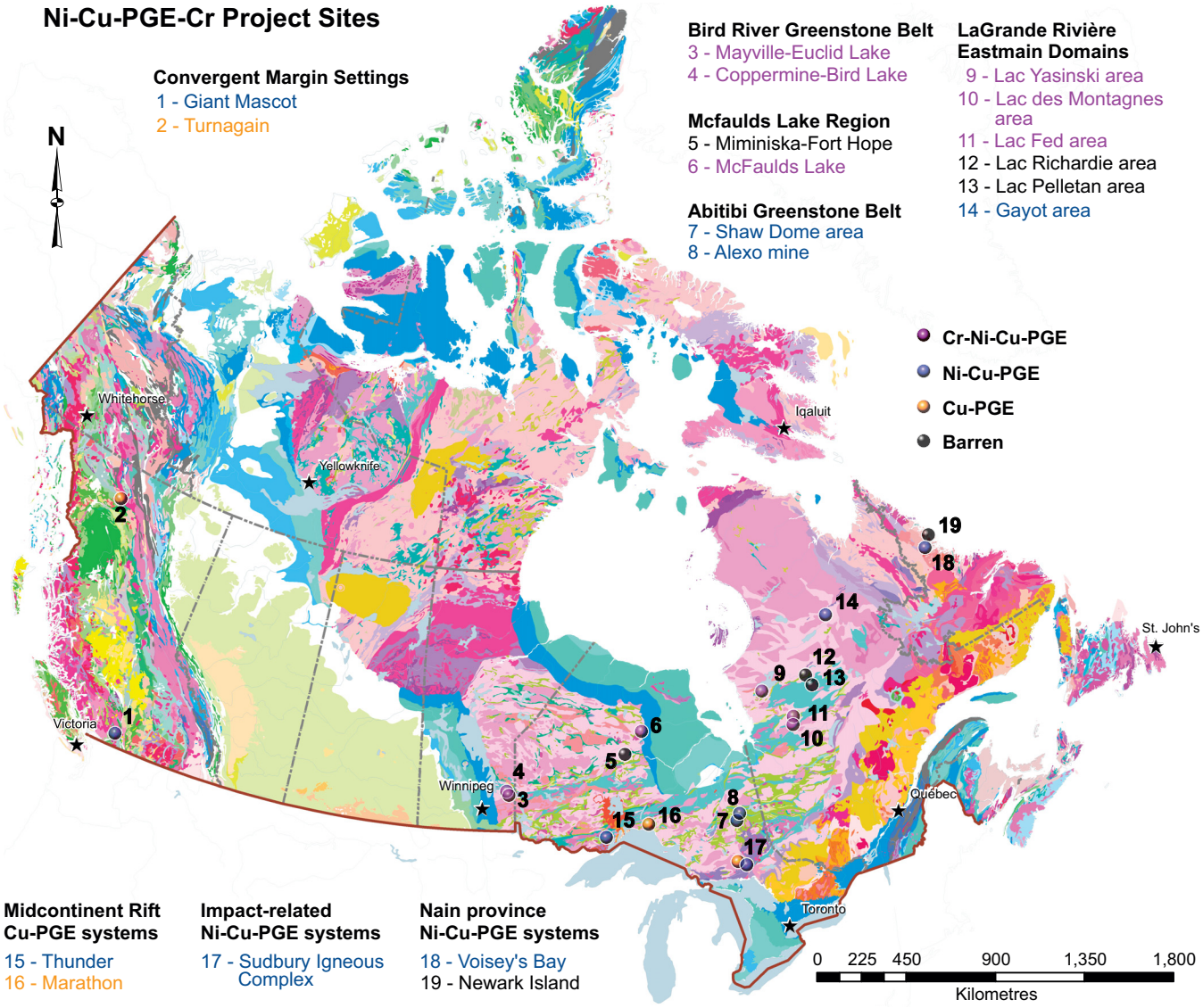

Figure 1. Location map for the TGI-4 Ni-Cu-PGE-Cr ore systems project study sites in Canada (modified from Wheeler et al., 1996). **1-2:** *Convergent margin Ni-Cu-PGE* (Nixon et al., 2015). **3-4:** *Bird River greenstone belt Ni-Cu-PGE* (Bécu et al., 2015). **5-6:** *McFaulds Lake region Cr-Ni-Cu-PGE-V* (Carson et al., 2015; Kuzmich et al., 2015; Metsaranta et al., 2015; Sappin et al., 2015; Spath et al., 2015). **7-8:** *Abitibi komatiite* (Hiebert et al., 2015; Pagé et al., 2015). **9-14:** *Eeyou Istchee Baie James region Cr-Ni-PGE* (Houlé et al., 2015). **15-16:** *Midcontinent Rift Cu-PGE* (Brzozowski et al., 2015; Shahabi Far et al., 2015; Trevisan et al., 2015). **17:** *Sudbury mining district Ni-Cu-PGE* (Adibpour et al., 2015; Ames and Tuba, 2015; Bleeker et. al., 2015; Dare et al., 2015; Hanley et al., 2015; Kontak et al., 2015). **18:** *Voiseys Bay and Newark Island* (Dare et al., 2015).

profitable Ni-Cu-PGE-Cr deposit types in hidden environments within established or emerging camps. It also provided an opportunity to acquire knowledge on less understood and mostly underexplored Ni-Cu-PGE-Cr deposit types. Collaborative and complementary work was crucial to the successful delivery of the project (and this volume) and involved more than fifty participants from the GSC, the geological surveys of British Columbia (BCGS), Manitoba (MGS), Ontario (OGS), and Quebec (MERN), nine universities, and industry.

The Canadian Ni-Cu-PGE-Cr project embraces a vast breadth of mineral deposit styles in the Cr- Ni-Cu-PGE-Fe-Ti-V-(P) realm (e.g. Ni-Cu-PGE, Cu-PGE, PGE only, Cr-Ni-Cu-PGE and/or Fe-Ti-V-(P)) that occur in different time periods (i.e. Archean, Proterozoic, and Mesozoic) through a diversity of ore-forming processes (orthomagmatic, magmatic-hydrothermal, hydrothermal) and formed in diverse tectonic and contrasting geological environments (e.g. rift-related, convergent-margin/supra-subduction zone, impact crater, terrane boundaries, and intracratonic sutures).

The project has generated sixty-five new high-precision Isotope Dilution – Thermal Ionization Mass Spectrometry (ID-TIMs) ages including nine from convergent-margin Ni deposits, six from the chrome-bearing Bird River greenstone belt, twenty-four from the McFaulds Lake area with Cr-(PGE), Ni-Cu-PGE, and

Fe-Ti-V-(P) mineralization, three from the Eeyou Istchee Baie James Cr-bearing region, one in the Midcontinent rift, and twenty-two from the Ni-Cu-PGE Sudbury mining district. An additional ten ages were determined by Laser Ablation Inductively Coupled Mass Spectrometry (LA-ICP-MS) at University of British Columbia (UBC) and Laurentian University, and five $^{40}Ar/^{39}Ar$ analyses were carried out at UBC and GSC-Ottawa.

This volume contains twenty-one papers highlighting the main results from two major themes: (1) new and revised genetic models for Ni-Cu-PGE, Cr-(PGE), Fe-Ti-V-(P), and Cu-PGE mineral systems, and (2) advances in the detection of Ni-Cu-PGE-Cr systems through innovative techniques developed for fertility and pathfinder indicators.

NEW AND REVISED GENETIC MODELS FOR Cr-Ni-Cu-PGE DEPOSITS: REGIONAL-, DISTRICT-, AND BELT-SCALE METALLOGENY

Geological advances were made in six Canadian Ni-Cu-PGE-Cr mineral districts and/or tectonic environments: (1) supra-subduction zone/convergent-margins (BC), (2) the Bird River greenstone belt (MB), (3) the McFaulds Lake area (also known as Ring of Fire: ON), (4) La Grande Rivière and Eastmain domains in the Eeyou Istchee Baie James region (QC), (5) the Midcontinent Rift (ON), and (6) the Sudbury astrobleme (ON) (Fig. 1).

Ni-Cu-PGE Ore Systems in Convergent Margin Tectonic Settings

Although magmatic Ni-Cu-PGE deposits hosted by mafic-ultramafic intrusions in convergent-margin settings have become increasingly important in recent years (e.g. Aquablanca, Spain), they remain poorly understood and little explored. Relevant mineral deposit models have just begun to emerge (e.g. Ural-Alaskan NC-7: Naldrett, 2010). The paper by Nixon and co-workers (2015) includes a global compilation of convergent-margin deposit traits and presents a new classification scheme built on the petrology of large-tonnage (> 200 Mt), low-grade Ni deposits in Alaskan-type intrusions (i.e. Turnagain), which are characteristically composed of clinopyroxene-bearing rocks, and Giant Mascot-type intrusions (Manor, 2014; Manor et al., 2014a,b, 2015a,b), which are characteristically orthopyroxene-bearing rocks. The Ni-Cu-PGE deposit in the Giant Mascot intrusion, which was studied under this TGI-4 program, has similarities to the Xiarihamu deposit that was recently discovered in China, which at 100 Mt at 0.8% Ni and 0.1% Cu is among the 20 largest magmatic Ni-Cu deposits in the world (Nixon et al., 2015).

A joint BCGS-GSC geological map of the Giant Mascot Ni mine (1958–1974) area was published in 2014, which also documented the previously unknown PGE content of the ores (Manor et al., 2014). This publication has now been augmented with new geochronology, a longitudinal section of orebodies, mine plans, and exploration history (Manor et al., 2015a).

Superior Province Cr-PGE-Ni-Cu Ore Systems

Recent discoveries of major chromite deposits (e.g. Black Thor, Big Daddy), Ni-Cu-(PGE) deposits (e.g. Eagle's Nest: Mungall et al., 2010), and significant Fe-Ti-V occurrences (e.g. Thunderbird) in the McFaulds Lake greenstone belt (MLGB) in northern Ontario (see Metsaranta et al., 2015) highlight the mineral potential not only of this region but also of possible correlative areas across the Superior Province, such as the La Grande Rivière and Eastmain domains within the Eeyou Istchee Baie James region in northern Quebec, and the Bird River greenstone belt (BRGB) in Manitoba (Houlé et al., 2015a,b). This TGI-4 project included collaborative regional bedrock mapping in the MLGB and the BRGB as well as extensive geochronology (n=35), and regional and detailed mineral deposit studies across the Superior Province (Laarman et al., 2012; Farhangi et al., 2013; Fecteau, 2013; Mehrmanesh et al., 2013; Carson et al., 2015; Kuzmich et al., 2015; Spath et al., 2015; and other student work reported in Houlé et al., 2015a).

A potential correlation of domains enriched in mafic to ultramafic intrusions hosting Cr-PGE-Ni-Cu across the Superior Province is proposed through an updated (Stott et al., 2010) understanding of the spatial and temporal distribution of Archean chromite deposits and occurrences across Ontario, Quebec, and Manitoba (Fig. 1, sites 3–6, 9–14). These observations combined with TGI-4 results from regional mapping, and geochronological and petrogenetic profiling of fertile and barren mafic-ultramafic intrusions led to the proposal of a new Cr-PGE metallogenic province through the Superior Province (Houlé et al., 2013; 2015b). This metallogenic province coincides with the proposed correlation between the Oxford-Stull/Uchi/ La Grande Rivière/Eastmain domains by Stott et al. (2010) across the Superior Province and identifies a possible link with the Bird River greenstone belt south of the North Caribou terrane. Cratonic-scale boundaries may be crucial to the genesis of these Cr-(PGE) orthomagmatic deposits and spatially associated Ni-Cu-(PGE) and Fe-Ti-(V) mineralization.

Bird River Greenstone Belt

The Bird River greenstone belt (BRGB) in southeastern Manitoba contains numerous Neoarchean mafic-

ultramafic intrusions that host significant Ni-Cu-(PGE) deposits and Cr-(PGE) deposits and occurrences, and has been the focus of regional bedrock mapping by the Manitoba Geological Survey (Gilbert et al., 2008; Yang et al., 2012, 2013). At least nine main intrusions occur over a strike length of 75 km and width of 20 km, with the older Maskwa Lake Batholith in the centre. The intrusion stratigraphy forms two distinct groups: (1) the very well layered Bird River Sill, which contains a lower ultramafic zone overlain by an upper mafic zone, and (2) the poorly stratified Mayville intrusion in which a lower heterolithic intrusive breccia zone with sporadic mafic to ultramafic zones along the basal contact is overlain by a mafic zone. Despite these differences, Bécu et al. (2015) shows that the mafic components (e.g. Coppermine Bay, Euclid Lake, and Mayville intrusions, Bird River Sill) have similar textural, compositional, and geochemical characteristics and thus are potentially petrogenetically linked. New geochronology of the mafic-ultramafic intrusions within the Bird River greenstone belt supports the petrogenetic connection between the intrusions and provides evidence for the existence of a widespread Neoarchean mafic-ultramafic magmatic event between 2744 to 2742 Ma (Table 1 in Houlé et al., 2015b). This unequivocal correlation across the belt also provides a new metallogenic context for the distribution of significant basal (e.g. Maskwa deposit, Bird River Sill) or near basal (e.g. M2 deposit, Mayville intrusion) Ni-Cu-(PGE) mineralization, and for the Cr mineralization (e.g. Chrome deposit, Bird River intrusion) higher in the stratigraphy, near the contact between the ultramafic and mafic zones of the intrusions throughout the Bird River greenstone belt. All of these intrusions were generated from a single fertile, volumetrically significant magmatic event at ca. 2744–27423 Ma, which was the source for base metal, PGE, and chromium.

McFaulds Lake Region – McFaulds Lake and Miminiska-Fort Hope Greenstone Belts

The unusual endowment of mafic to ultramafic intrusive rocks is the most prominent feature of the McFaulds Lake region, particularly as these rocks host significant chromite deposits, a major Ni-Cu-(PGE) magmatic sulphide deposit, and numerous significant Fe-Ti-(V) occurrences. The work conducted in this TGI-4 Ni-Cu-PGE-Cr project presents the characteristics of one of Canada's most important Cr-Ni-Cu-PGE discoveries in the last decade: the McFaulds Lake greenstone belt (Ring of Fire) in the Oxford-Stull domain of the Superior Province. No chromium deposits associated with mafic-ultramafic rocks were potentially mineable under likely price scenarios in the Western hemisphere (USGS, 2015) until the discovery of chromite under cover in the McFaulds Lake greenstone belt, which has a chromite resource estimate of 285.8 Mt at 31.5 % Cr_2O_3 in 5 deposits (Table 1 in Metsaranta et al., 2015).

As part of the Ni-Cu-PGE-Cr project, the Ontario Geological Survey, as in-kind contribution, has conducted regional bedrock mapping, compilation, re-logging of more than 1,500 diamond-drilled cores, and extensive new U-Pb geochronology (Metsaranta et al., 2015). This has been integrated with regional studies of the mafic-ultramafic intrusions in the McFaulds Lake region and within the eastern part of the Uchi domain of the Superior Province (Sappin et al., 2015). New 1:100,000 and 1:20,000 scale geological maps are being generated (see section *Forthcoming Releases* below) that portray the most recent advances in our understanding of the geological framework of the Ring of Fire region and the stratigraphy of the MLGB.

Mafic and ultramafic intrusions in the Ring of Fire region occur in at least two main age intervals, at ca. 2810 Ma and ca. 2735 Ma. The Mesoarchean, Highbank Lake intrusive complex (HBIC), located south of the MLGB, is a mafic-dominated intrusion with marginal Fe-Ti-V mineralization hosted within a magnetite-rich horizon. The Neoarchean intrusions, however, have two main magmatic suites (1) an ultramafic-dominated suite that contains the chromite deposits (Black Thor-Black Label, Big Daddy, Blackbird, Black Creek, Black Horse) and a major Ni-Cu-PGE deposit (Eagle's Nest) and (2) a regionally widespread, mafic-dominated "ferrogabbro" suite that hosts many significant occurrences of Fe-Ti-V-(P). Several detailed studies of these mineralized intrusions were undertaken by graduate students (Houlé et al., 2012; Carson et al., 2015; Kuzmick et al., 2015; Spath et al., 2015). The ultramafic to mafic Black Thor intrusive complex (BTIC), is a layered sill containing a conduit-hosted chromite deposit for which a new genetic model was proposed: the partial assimilation of local oxide-silicate facies iron formation by a Cr-rich magma (Carson et al., 2015). Other aspects of the BTIC that are addressed by other graduate studies include the emplacement of a co-genetic pyroxenitic magma into the BTIC and its implications for ore genesis (Spath et al., 2015), the internal stratigraphy and the textural facies distribution of the Black Label deposit (Mehrmanesh et al., 2013), and the distribution and the petrogenesis of Ni-Cu-(PGE) mineralization in the BTIC (Farhangi et al., 2013). Investigations of the petrogenesis and Fe-Ti-(V) mineralization of a mafic-dominated "ferrogabbro" suite were undertaken in the Thunderbird and the Butler (West and East) intrusions (Kuzmick et al., 2015) and at the Big Mac intrusion (Sappin et al., 2015).

Industry's Cr, and Ni-Cu discoveries in the Ring of Fire region, which are under the extensive Phanerozoic

and glacial cover of the James Bay lowlands, led Canada's geoscience community not only to investigate individual chromite-endowed regions within each province (Quebec, Ontario, Manitoba) but also to refine a metallogenic framework using high-resolution geochronology to define a new Cr-(PGE) metallogenic province across the Canadian Shield, the so-called Bird River–Uchi–Oxford-Stull–La Grande–Eastmain domains (BUOGE "domains": Houlé et al., 2012, 2013, 2015b). These geoscience studies highlight the likelihood of discovering major deposits within the frontier areas of Canada.

La Grande Rivière-Eastmain Domains

The spatial and temporal distribution of the ultramafic and mafic intrusions is still poorly constrained across the Eeyou Istchee James Bay region despite our TGI-4 investigations in collaboration with the ministère de l'Énergie et des Ressources naturelles (MERN) at several localities predominantly within the La Grande Rivière and Eastmain domains as well as within the subjacent Opinaca basin domains (Houlé et al., 2015a). The ultramafic-mafic magmatism occurred over more than 200 Ma, between ca. 2.88 Ga (David et al., 2009), and 2.63 Ga (Houlé et al., 2015a), and generated different types of ultramafic to mafic intrusions and lavas, including komatiitic ultramafic intrusions /lavas, ultramafic-dominated intrusions, mafic-dominated intrusions, alkaline ultramafic to mafic intrusions, and ultramafic lamprophyre.

Several of these ultramafic- to mafic-intrusion types contain Cr-(PGE), Ni-Cu-(PGE), or Fe-Ti-(V) occurrences but no deposits have been discovered. The most important examples examined in the course of the Ni-Cu-PGE-Cr project include the Menarik Complex (Cr-PGE), the Lac des Montagnes intrusions (Cr-PGE), the Lac Gayot intrusions (Ni-Cu-PGE), the Nisk intrusion (Ni-Cu-PGE), and the baie Chapus Pyroxenite (Fe-Ti-V) (Houlé et al., 2015a). Initial mineralogical data for chromite and magnetite in many of these intrusions have similar compositions to those analyzed from chromite deposits and the vanadiferous intrusions in the MLGB, indicating that the intrusions in the Eeyou Istchee James Bay region are prospective for significant mineralization (Houlé et al., 2015a). The most prospective units are associated with ultramafic bodies that exhibit a komatiitic affinity and are enriched in olivine.

Midcontinent Rift Cu-PGE Ore Systems

Numerous Cu-PGE occurrences associated with crosscutting gabbroic to ultramafic intrusions occur in the early-rift phase of the Midcontinent Rift at 1.1 Ga (e.g. Marathon Series gabbros, Thunder, Sunday, Current Lake) along with the high-grade Ni-Cu-PGE Eagle deposit discovered in 2002 in Michigan (Ding et al., 2010; Trevisan et al., 2015). A series of mafic to ultramafic intrusions and their associated mineralization were investigated in the Ni-Cu-PGE-Cr project at the Coldwell Alkaline Complex near Marathon (Good et al., 2015b) and also at the Thunder intrusion, a small buried body on the outskirts of Thunder Bay. The mineralized ca. 1108 Ma Thunder intrusion is the only known occurrence of Midcontinent Rift magma emplaced within an Archean greenstone belt (i.e. Shebandowan greenstone belt). This was interpreted as an evolved mantle-derived magma that ascended along a reactivated Archean Wawa and Quetico subprovince boundary fault that may also control the Current Lake (Cu-PGE) and Sunday Lake (Cu-PGE) intrusions (Trevisan et al., 2015). In the Coldwell Alkaline Complex, petrogenesis, geochemistry, and ore mineral chemistry of five distinct zones of Cu-Pd mineralization within three co-genetic intrusions (Main zone and W horizon in the Two Duck Lake gabbro, upper and lower zones in the Area 41 intrusion, and main zone in the Geordie Lake intrusion) revealed three distinctive platinum group mineral assemblages for the orebodies. A proposed PGM mineral index suggests that the Area 41 occurrence is similar to the high-PGE, low-Cu W horizon orebody of the Two Duck Lake gabbro (Good et al., 2015a), making Area 41 intrusion a viable exploration target. Furthermore, geochemical evidence for the Coubran basalt and the co-genetic Two Duck Lake gabbro suggests that they were derived from partial melting of a LILE- and LREE-enriched mantle source generated at intermediate depth (Good et al., 2015c).

Results from a detailed study at the Geordie Lake intrusion show that mineralization is characterized by a sulphide assemblage of bornite and chalcopyrite and is associated with intense albite and actinolite alteration within a crosscutting heterogeneous augite-bearing troctolite unit, which is characterized by the presence of skeletal olivine and relatively low trace element abundances (Meghji et al., 2013). These results suggest that two augite-bearing troctolite intrusions located east and north of the Geordie Lake intrusion represent potential host rocks and therefore prospective exploration targets. Other graduate students investigated the role of volatile components during crystallization of the Two Duck Lake gabbro and the potential for Cl-rich fluids to mobilize metals (Shahabi Far et al., 2015) and the trace element geochemistry of late-stage alteration (Brzozowski et al., 2015). These studies are highlighted in section *Pathfinders* below.

Impact-Related Ni-Cu-PGE Ore Systems

New geochronology results (~ 22 samples) acquired during the Ni-Cu-PGE-Cr project significantly improves our understanding of the geological frame-

work of the Sudbury Igneous Complex (SIC) and its enormous Ni-Cu-PGE resource (Bleeker et al., 2015; Kontak et al., 2015). The basement country rocks have been increasingly recognized as important host rocks for high-value, precious metal-rich orebodies (Pt, Pd Ag, Au) and enhanced U-Pb geochronological techniques (e.g. improved mineral separation, micro-sampling of complex and shocked zircons, "chemical abrasion" pre-treatment, and evaporative pre-treatment) finally allow ages to be determined at sufficient accuracy and precision to resolve key geological relationships for the SIC and its footwall. These high-precision U-Pb ages are starting to resolve different events within the ~1 million year time frame of the SIC and its mineralization. An integration of these new ages within the existing geological framework of the 250–300 km Sudbury structure will help constrain a regional geological cross-section (Bleeker et al., 2013, 2014a) that will accompany a revised version of the GIS digital map (Ames et al., 2006, 2008a,b).

Several mafic dyke swarms have been identified both pre- and post-dating the SIC, including the first documentation of a ca. 2507 Ma dyke swarm in this part of the Superior craton. A number of recently identified dykes that potentially are part of the offset dyke system of the SIC were also analyzed. A precise age for the Pele offset dyke (1848.5 ±0.8 Ma) is statistically different from the age of the Main Mass Mg-rich norite unit of the SIC (1849.7 ±0.2 Ma) and may represent the youngest injection of magma into the footwall of the SIC (Bleeker et al., 2015). This young SIC magma injection (Pele offset) significantly also contains melt inclusions that are metal depleted (Hanley et al., 2015).

Determining the Archean age of the gabbroic host rock to much of the Podolsky Cu-PGE sharp-walled vein deposit (so-called "Grey gabbro") solved the controversy of its origin, i.e., whether it is (1) a fragment of the Archean footwall rocks or (2) an 1850 Ma SIC-related melt (Kontak et al., 2015). The age is similar to the Joe Lake gabbro situated ~5 km to the west in the immediate footwall to the SIC on the North Range (Bleeker et al., 2015), suggesting that Archean mafic intrusions were a much larger component of the North Range target rocks. Remarkably, this large Archean fragment in the Podolsky deposit, approximately 250 x 250 m, is situated in the "neck" of the radial Whistle Offset structure below the Sublayer, perhaps causing a local impediment to sulphide melt/flow/fluid/gas into these structures in the footwall.

Field observations and better age constraints of the Creighton Granite and overlying Copper Cliff Rhyolite on the South Range demonstrate a single felsic magmatic system at 2455–2460 Ma that developed immediately following the main pulse of mafic Matachewan magmatism at 2460 Ma (Bleeker et al., 2015).

Mineral District Databases

The Sudbury district Ni-Cu-PGE ore geochemical database and accompanying high-reolution ore sample photographs linked to each analysed sample was recently released (Ames et al., 2014a) providing the foundation for the geochemical attributes for the various ore types from forty-four Ni-Cu-PGE deposits in the contact, footwall, offset, and breccia belt environments of the Sudbury mining district (Ames et al., 2010). A companion ore mineralogy and mineral chemistry database from thirty-nine Sudbury mines follows the first release of geochemistry (Kjarsgaard and Ames, 2010; Ames et al., 2015). Four other manuscripts using the SIC and Ni-Cu-PGE orebodies as test sites for fertility (Dare et al., 2015; Hanley et al., 2015) and pathfinder indicators (Adibpour et al., 2015; Hanley et al., 2015; Kontak et al., 2015) are discussed below and the supporting TGI-4 databases have been released (Dare et al., 2013; MacInnis et al., 2014; Watts et al., 2015).

FERTILITY AND PATHFINDERS: ADVANCES IN THE DETECTION OF Ni-Cu-PGE-Cr MINERALIZATION

Standard geochemical and geophysical techniques have been used for decades in mineral exploration to detect Ni-Cu precious metal minerals (Pt, Pd, Au). In this volume, we identify new indicator minerals (chromite, apatite, magnetite, epidote, sulphides) that define new discriminants for global use in exploration, use advanced microanalytical techniques to apply melt chemistry to ore systems research to delineate "metal-depleted" and "metal-enriched" parts of large igneous intrusions, and describe a numerical method that significantly improves interpretation of geophysical responses from gravity-gradiometer surveys.

Gravity-gradiometer surveys are generating large datasets for vast areas in search of buried mineral deposits (i.e. James Bay lowlands, Strange lake area) generating considerable multivariate data for manipulation and interpretation. Use of the geophysical data is dependent on the quality of the data and an understanding of what information the data contain. A practical method to suppress the noise in the data was developed that increases the effectiveness of data presentation and the knowledge gained by selecting individual and combinations of tensor components (Pilkington et al., 2015). Exploration for orthomagmatic mineralization in buried terrains using gravity-gradiometer data should use the high-resolution gravity signal that, when combined with co-located magnetic data, may identify mafic-ultramafic units prospective for Ni-Cu-PGE, Cr-(PGE), and Fe-Ti-V deposits. This new numerical method significantly improves interpretation of geophysical response and is of global use for industry.

Fertility

Conventional geochemical techniques that have been used for decades in Ni-Cu-PGE exploration typically include calculating chalcophile depletion ratios (e.g. Ni/Ni*, Cu/Zr, Cu/Pd) ratios in whole rock and/or Ni content of olivine (low-Ni preferred)), to distinguish Ni-Cu-PGE mineral deposit-endowed regions from potentially barren regions (e.g. Duke and Naldrett, 1978; Naldrett et al., 1984; Li et al., 2000; Barnes and Lightfoot, 2005). These techniques can been used effectively when studying a number of mafic-ultramafic intrusions in a region (e.g. McFaulds Lake area: Sappin et al., 2015; Eeyou Istchee James Bay region: Houlé et al., 2015a).

To update our understanding of "fertility" requires the development of new techniques that allow determination of trace elements at the mineral scale and new isotopic systems allow this to be undertaken better now than at any time in the past. Two of Canada's largest Ni-deposits were used as test sites to develop new methods: the 1.85 Ga Sudbury Igneous Complex (Ontario) and 1.34 Ga Voisey's Bay (Newfoundland and Labrador). The primary fertility of the magma is critically important and therefore the use of newer analytical techniques, such as laser ablation ICP-MS to determine oxide trace-element chemistry in silicate host intrusions (Dare et al., 2015) and/or melt-inclusion chemistry of apatite (Watts, 2014; Hanley et al., 2015; Watts et al., 2015), were tested to discriminate barren from fertile Ni-Cu-PGE regions and/or intrusions.

The Archean Alexo and Hart komatiite-associated Ni-Cu-(PGE) occurrences in the Abitibi greenstone belt were studied to develop new geochemical techniques with chromite chemistry to distinguish between barren and mineralized komatiitic units (Pagé et al., 2015) and multiple S and Fe isotopes to identify crustal contamination processes that are critical to the formation of magmatic Ni-Cu ore deposits (Hiebert et al., 2015).

The timing of mineral crystallization in the magma is critical for recording metal depletion upon sulphide crystallization (i.e. early chromite-PGE; late Fe-oxide-Ni-Cu; early apatite-bulk metal resource) and may identify processes of intrusion formation (i.e. immiscibility, fractional crystallization of one liquid). Distinct trace element signatures of two mineral phases (chromite and magnetite) were used to distinguish mineralized and unmineralized environments and to identify which elements maybe useful as post-magmatic discriminants for chromite. Melt inclusions in early crystallized apatite indicate the ore metal concentrations at that point in the evolution of the magmatic system.

Fe-Oxide Geochemistry

The Fe-oxide geochemistry of mafic layered complexes and ostensibly barren anorthosite suites (e.g. Newark Island, Newfoundland and Labrador; Bushveld, South Africa; Sept-Iles, Quebec; Anorthosite suite of Saguenay-Lac St-Jean, Quebec) were also studied to place constraints on the discriminators of intrusions in barren versus fertile environments. The elements Ni, Cu, and Cr in Fe-oxide minerals provide critical knowledge on the sulphide saturation and segregation histories of the intrusions. Barren intrusions lie on a single Ni-Cr trend, whereas fertile intrusions record sulphide saturation with a parallel Ni-Cr trend but at lower Ni concentrations. Similarly, Cu depletion of oxides in fertile intrusions is also an indicator of fertility.

Melt Inclusions in Apatite

Major breakthroughs using innovative methods were made in an apatite melt inclusion study of the SIC (Watts, 2014) by developing parameters that would enhance exploration success in mafic-ultramafic ore systems where post-magmatic processes have severely limited the application of bulk rock geochemistry. Melt inclusions are tiny droplets of melt trapped in host crystal phases (e.g. apatite) that provide a snapshot in time of the physiochemical characteristics of the melt at that stage in magmatic evolution. The geochemistry of melt inclusions hosted in apatite that formed early in the crystallization history of the intrusion therefore, provide a means of constraining compositions of parental magmatic liquids and reveal trends of liquid evolution (Veksler, 2006).

The first in situ determination of actual ore-metal concentrations from an early trapped melt of the SIC and the partitioning behaviour of ore metals and other trace elements between immiscible Fe-rich and Si-rich liquids is presented (Watts, 2014; Hanley et al., 2015; Watts et al., 2015). In the SIC and its offset dykes, melt-inclusion data revealed immiscible melts in the SIC main mass and young Pele offset dykes that were metal depleted compared to melt inclusions in the mineralized quartz diorite of the Whistle offset dyke and thus, identified spatial differences in the fertility of the intrusion hosting one of Canada's major Ni-Cu-PGE mining districts (Watts, 2014; Hanley et al., 2015).

Pathfinders to Mineralization

New techniques and unconventional methods for Ni-Cu-PGE-Cr exploration were tested in barren and mineralized sites and discriminants were identified to define pathfinders as vectors towards ore using bedrock indicator mineral chemistry. Minerals not previously considered as pathfinders and their identified distinctive chemistry may aid explorationists in their search for buried mineralization (i.e. *apatite*: Shahabi Far et al., 2015; *biotite*: Hanley et al., 2015; Warren et.

al., 2015; *chlorite*: Brzozowski et al., 2015; *epidote-actinolite*: Ames and Tuba, 2015) and aim to distinguish important mineralizing processes (*sulphide*: Adibpour et al., 2015). In addition, analytical techniques were optimized (Doherty et al., 2014).

A series of papers examine alteration associated with Ni-Cu, Cu-PGE, and PGE deposits. Hydrothermal and/or post-magmatic processes involving fluid/volatile interaction was examined to define a signature that may be used in targeting Ni-Cu-PGE ore deposits. Controversies regarding the role of fluids in PGE mineralization at the Marathon Cu-PGE deposit (Coldwell Alkaline Complex, Midcontinent Rift) and the Cu-PGE and PGE footwall ores in the Sudbury mining district underline the need for targeted and focussed research on this controversial topic. If fluids are integral to ore formation, indicators resulting from fluid mobility constitute a footprint of the deposits (e.g. Kerr et al., 2015). At the Marathon Cu-Pd deposit, changes in plagioclase compositions in growth and resorption zones, some of which contain base metals, reflect new influxes of magma and an overall model of zone refining with various stages of magma infiltration (Shahabi Far et al., 2015).

Exciting new exploration targets exist for the mature Sudbury mining district, from which over 19 million ounces of PGEs have been produced since 1990 (Wallbridge Mining Company Ltd., www.walbridgemining.com, April 2015). The trend to mine at increasing depths (e.g. Sudbury 2.5 km below surface) has been alleviated somewhat by the recognition of near and on-surface economic concentrations of Cu-, Pt-, Pd-, Ag- and Au-rich deposits (e.g. Broken Hammer open pit, Capre at < 200 m depth, Denison 109 zone) compared with the traditionally much deeper Ni-Cu-Co-PGE contact- and offset-type deposits. The discovery, in the last decade, of mineable low-sulphide PGE orebodies (Farrow et al., 2005) caused a shift in exploration focus to the detection of these precious metal-rich resources.

Examination of alteration proximal to footwall-style sharp-walled chalcopyrite-PGE veins provides a time frame for sulphide injection relative to cooling of the igneous complex (i.e. 0.5 to <1 Ma: Ames et al., 1998; Bleeker et al., 2015) and is the result of interaction with high-temperature magmatic-derived fluids (Kontak et al., 2015). In contrast, a spectacular of "no sulphide" PGE-rich mineralization composed of quartz-epidote and 2 cm sperrylite ($PtAs_2$) crystals at the Broken Hammer open pit (Ames et al., 2013, 2014b) is unequivocally hydrothermal in origin. Current models in the literature for the genesis of the high-sulphide sharp-wall chalcopyrite-PGE veins are related to magmatic/magmatic-hydrothermal processes and/or remobilization by high-temperature volatiles (e.g. Li et al., 1992; Naldrett et al., 1999; Péntek et al., 2008; Hanley et al., 2011 and references therein). In contrast, low-sulphide PGE-rich ores have been attributed to circulating metal-rich hydrothermal fluids (e.g. Péntek et al. 2008; Nelles et al. 2010; Tuba et al., 2010, 2014; White, 2012). In the McCreedy West PM (precious metal) zone, Farrow and coworkers (2005) used mine assay data to geochemically distinguish the low-sulphide type of ore (Farrow et al., 2005) and defined the first classification of this new style of Sudbury "footwall" ore deposit. This led MacMillan and coworkers (MacMillan, 2014; Hanley et al., 2015) to systematically classify the mineralogical (sulphide ore and alteration), fluid inclusion, and bulk rock geochemical differences between footwall-style low-sulphide PGE mineralization and high-sulphide sharp-walled vein mineralization.

Due to the absence of chalcopyrite or sulphide minerals, detecting low-sulphide deposits in the field using traditional geophysical methods for magmatic deposits was a challenge that required development of unconventional exploration techniques. To address this, Ames and Tuba (2015) delve into the regional geochemical and mineralogical indicators for low-sulphide PGE-rich mineralization along the North Range footwall environment to the SIC. Trace element signatures were defined for alteration minerals epidote, amphibole, allanite, and titanite in paragenetically different hydrothermal assemblages produced during the diverse post-impact magmatic-hydrothermal history of the footwall and hanging-wall units of the Sudbury structure. Typical element associations and behaviours were established and a unique signature for alteration related to the high-tenor PGE mineralization was recognized.

A few authors emphasize how understanding the entire coeval silicate mineral assemblage (i.e. epidote-amphibole) is critical to the development of robust exploration vectors to target buried PGE-(Cu) mineralization and caution against the use of single minerals (Ames and Tuba, 2015; Brzozowski et al., 2015). Similarly, the trace element signatures of a sulphide assemblage (pyrrhotite-pentlandite-chalcopyrite-pyrite), which was traced through a series of deposit styles with depth from the contact-style Ni-Co-Cu Levack deposit to high-sulphide Cu-PGE vein and low-sulphide PGE ores in the Morrison deposit, demonstrates the importance of mineral-pair partitioning of the trace elements to create discrimination plots (Adibpour et al., 2015).

Mineral-pair partition coefficients are thoroughly documented by Ames and Tuba (2015) for epidote-amphibole, titanite-amphibole, and titanite-epidote and provide insights into the use of "green minerals" for exploration. Significantly, Adibpour and coworkers (2015), using sulphide mineral chemistry, show that more than just magmatic fractionation of a sulphide

liquid is required to explain the differences in partition coefficients of Se in chalcopyrite-pentlandite from (1) contact-style Ni-Co ores linked to (2) Cu-PGE high-sulphide vein ores in the immediate footwall rocks below.

Typical radial, quartz diorite offset dykes along the South Range of the Sudbury structure include the Ni-Cu-PGE ore-bearing Copper Cliff and Worthington offset structures. At the Totten Ni-Cu (PGE) offset deposit, situated ~ 7 km from the basal contact of the SIC with the Paleoproterozoic Southern province metasedimentary rocks, basalt, and gabbro, the background metal content in biotite content established for each lithology and the mineral chemical variations with proximity to ore systematically were tested (Hanley et al., 2015; Warren et al., 2015). In Sudbury's offset dyke environment, the Ni, Cr, and Cu content of biotite, analyzed by LA-ICP-MS, was measured systematically in the surrounding country rocks to the offset dyke along a distal to proximal transect towards a Ni-Cu-PGE ore zone. The highly elevated Ni content and Ni/Cr ratios in biotite associated with mineralization are shown to be pathfinders to explore for buried Ni-Cu mineralization using drill core and/or soils and tills.

FORTHCOMING RELEASES

Many key geological, geophysical, geochemical, and mineral chemical datasets used in the TGI-4 Ni-Cu-PGE-Cr studies have been released as open file reports and will continue to be released in scientific papers as reported in individual manuscripts in this volume in the near future. Some of the forthcoming publications include the bedrock geological maps of the McFaulds Lake greenstone belt, which are to be published jointly by the Geological Survey of Canada and Ontario Geological Survey:

1. Precambrian geology of the McFaulds Lake greenstone belt (Ring of Fire area); South sheet. 1:100 000;
2. Precambrian geology of the McFaulds Lake geenstone belt (Ring of Fire area); Central sheet. 1:100 000;
3. Precambrian geology of the McFaulds Lake greenstone belt (Ring of Fire area); North sheet. 1:100 000;
4. Precambrian geology of the McFaulds Lake area: 1:20 000;
5. Precambrian geology of the Butler Lake area: 1:20 000.

ACKNOWLEDGEMENTS

Firstly, we would like to acknowledge the involvement and participation of numerous researchers, students, and mining company geologists in the TGI-4 Ni-Cu-PGE-Cr ore systems project of the Geological Survey of Canada. The authors would like to sincerely thank Elizabeth Ambrose for editorial reviews (all manuscripts in this volume), which genuinely helped to improve the final documents, and Valérie Bécu for her input and efficiency. We would like to express our appreciation to the reviewers of the 21 manuscripts in this volume (see list below) and the dedication of the government, academic, and industry contributors and organizations that allowed completion of the TGI-4 Ni-Cu-PGE-Cr synthesis volume in the project's final year. We are also grateful to Murray Duke for his thorough and constructive review that improved this manuscript.

Reviewers

Ms. Valérie Bécu	Geological Survey of Canada, Québec, Quebec
Dr. Wouter Bleeker	Geological Survey of Canada, Ottawa, Ontario
Dr. Thomas Clark	Université du Québec en Abitibi-Témiscamingue and Ministère de l'Énergie et des Ressources naturelles, Québec, Quebec
Dr. Sarah Dare	University of Ottawa, Ottawa, Ontario
Dr. Murray Duke	retired, Geological Survey of Canada, Ottawa
Dr. Céline Dupuis	Geological Survey of Canada, Québec, Quebec
Dr. Michael Easton	Ontario Geological Survey, Sudbury, Ontario
Dr. Alan Galley	Canada Mining Innovation Council, Ottawa, Ontario
Dr. Simon Jackson	Geological Survey of Canada, Ottawa, Ontario
Dr. Ingrid Kjarsgaard	Consulting Mineralogist, Ottawa, Ontario
Mr. Riku Metsaranta	Ontario Geological Survey, Sudbury, Ontario
Mr. James Moorhead	Ministère de l'Énergie et des Ressources naturelles, Val-d'Or, Quebec
Dr. Léopold Nadeau	Geological Survey of Canada, Québec, Quebec
Mr. Jack Parker	Ontario Geological Survey, Sudbury, Ontario
Dr. Jon Scoates	retired, Geological Survey of Canada, Nanaimo, British Columbia
Dr. Greg Stott	retired, Ontario Geological Survey, Sudbury, Ontario
Dr. Mike Thomas	Geological Survey of Canada, Ottawa
Ms. Katherine Venance	Geological Survey of Canada, Ottawa, Ontario
Dr. Natasha Wodicka	Geological Survey of Canada, Ottawa, Ontario
Dr. Alex Zagorevski	Geological Survey of Canada, Ottawa, Ontario

REFERENCES

Adibpour, M., Jugo, P.J., and Ames, D.E., 2015. Trace element distribution in sulphide assemblages of the Levack-Morrison ore system, Sudbury, Ontario: Looking for chemical fingerprints of mineralization processes, *In:* Targeted Geoscience Initiative 4: Canadian Nickel-Copper-Platinum Group Elements-Chromium Ore Systems — Fertility, Pathfinders, New and Revised Models, (ed.) D.E. Ames and M.G. Houlé; Geological Survey of Canada, Open File 7856, p. 257–268.

Ames, D.E. and Tuba, G., 2015. Epidote-amphibole and accessory phase mineral chemistry as a vector to low-sulphide platinum group element mineralization, Sudbury: laser ablation ICP-MS trace element study of hydrothermal alteration, *In:* Targeted Geoscience Initiative 4: Canadian Nickel-Copper-Platinum Group Elements-Chromium Ore Systems — Fertility, Pathfinders, New and Revised Models, (ed.) D.E. Ames and M.G. Houlé; Geological Survey of Canada, Open File 7856, p. 269–286.

Ames, D.E., Watkinson, D.H., and Parrish, R.R., 1998. Dating of a hydrothermal system induced by the 1850 Ma Sudbury impact event; Geology, v. 26, p. 447–450.

Ames, D.E., Singhroy, V., Buckle, J., Davidson, A., and Molch, K., 2006. Integrated bedrock geology – Radarsat – Digital elevation data of Sudbury, Ontario. Geological Survey of Canada, Open File 4571, scale 1: 75,000.

Ames, D.E., Davidson, A., and Wodicka, N., 2008a. Geology of the giant Sudbury polymetallic mining camp, Ontario, Canada; Economic Geology, v. 103, p. 1057–1077.

Ames, D.E., Card, K., Wodicka, N., and Davidson, A., 2008b. 100K Geological map of the Sudbury mining camp and Surrounding area, Ontario, Canada; Supplement to Ames, D.E. and Wodicka, N., 2008, Geology of the Giant Sudbury Polymetallic Mining Camp, Ontario, Canada; Economic Geology, v. 3, p. 1057–1077.

Ames, D.E., Golightly, J.P. Kjargaard, I.M. and Farrow, C.E.G., 2010. Minor element composition of Sudbury ores: Implications for source contributions, genesis and exploration of Ni-Cu-PGE in diverse settings. 11th International Platinum Symposium, extended abstract, Ontario Geological Survey, Miscellaneous Release Data 269, p. 1–4.

Ames, D.E., Hanley, J.J., and Jackson, S.E., 2013. High-grade sperrylite zone reveals primitive source in the Sudbury impact structure; Mineralogical Magazine, v. 77, p. 587. doi:10.1180/minmag.2013.077.5.1

Ames, D.E., Farrow, C.E.G, Pattison E.F., and Golightly, J.P., 2014a. Geochemistry of 44 Ni-Cu-platinum group element deposits in the contact, footwall, offset and breccia belt environments, Sudbury mining district, Canada; Geological Survey of Canada, Open File 6578, 11 p. doi:10.4095/295176

Ames, D.E., Hanley, J.J., and Jackson, S.E., 2014b. Low sulfide high-grade sperrylite-epidote-quartz zone, (Sudbury, Canada): implications for hydrothermal-magmatic processes, *In:* Abstracts; International Mineralogical Association 2014, Johannesburg, South Africa.

Ames, D.E., Kjarsgaard, I.M., and Tuba, G. 2015. Mineral chemistry database of 39 Ni-Cu-Platinum group element sulphide and low sulphide deposits and occurrences, Sudbury mining district, Canada; Geological Survey of Canada, Open File 7596.

Barnes, S.-J. and Lightfoot, P.C., 2005. Formation of magmatic nickel sulfide ore deposits and processes affecting their copper and platinum-group element contents, *In:* Economic Geology 100th Anniversary Volume, (ed.) J.W. Hedenquist, J.F.H. Thompson, R.J. Goldfarb, and J.P. Richards; Society of Economic Geologists, Littleton, Colorado, p. 179–213.

Bécu, V., Houlé, M.G., McNicoll, V.J., Yang, X.M., and Gilbert, H.P., 2015. Mafic intrusive rocks from the Bird River intrusive suite, Bird River greenstone belt, southeast Manitoba, *In:* Targeted Geoscience Initiative 4: Canadian Nickel-Copper-Platinum Group Elements-Chromium Ore Systems — Fertility, Pathfinders, New and Revised Models, (ed.) D.E. Ames and M.G. Houlé; Geological Survey of Canada, Open File 7856, p. 49–60.

Bleeker, W., Kamo, S., and Ames, D.E., 2013. New field observations and U-Pb age data for footwall (target) rocks at Sudbury: Towards a detailed cross-section through the Sudbury Structure. *In:* Extended abstract; Large Meteorite Impacts and Planetary Evolution V Meeting, August 5-8, 2013, Sudbury, Ontario., Lunar Planetary Institute contribution No. 1737, p. 13.

Bleeker, W., Kamo, S., and Ames, D.E., 2014a. Towards a detailed geological cross-section of the deformed Sudbury impact basin: New observations and new geochronology; Ontario Exploration and Geoscience Symposium, November 3-4, 2014, Sudbury, Ontario.

Bleeker, W., Kamo, S., Ames, D., and Smith, D., 2014b. New U-Pb ages for some key events in the Sudbury area, including the Creighton Granite and Joe Lake metagabbro. Geological Association of Canada Annual Meeting, May 21-23, Fredericton, Abstract Volume 37, p. 32–33.

Bleeker, W., Kamo, S.L., Ames, D.E., and Davis, D., 2015. New field observations and U-Pb ages in the Sudbury area: toward a detailed cross-section through the deformed Sudbury Structure, *In:* Targeted Geoscience Initiative 4: Canadian Nickel-Copper-Platinum Group Elements-Chromium Ore Systems — Fertility, Pathfinders, New and Revised Models, (ed.) D.E. Ames and M.G. Houlé; Geological Survey of Canada, Open File 7856, p. 151–166.

Brzozowski, M.J., Samson, I.M., Gagnon, J.E., Linnen, R.L., Good, D.J., Ames, D.E., and Flemming, R.L., 2015. Variation in vein mineralogy and mineral chemistry around the Marathon Cu-Pd deposit, Ontario: Insights into the development of an exploration tool, *In:* Targeted Geoscience Initiative 4: Canadian Nickel-Copper-Platinum Group Elements-Chromium Ore Systems — Fertility, Pathfinders, New and Revised Models, (ed.) D.E. Ames and M.G. Houlé; Geological Survey of Canada, Open File 7856, p. 245–255.

Carson, H.J.E., Lesher, C.M., and Houlé, M.G., 2015. Geochemistry and petrogenesis of the Black Thor intrusive complex and associated chromite mineralization, McFaulds Lake greenstone belt, Ontario *In:* Targeted Geoscience Initiative 4: Canadian Nickel-Copper-Platinum Group Elements-Chromium Ore Systems — Fertility, Pathfinders, New and Revised Models, (ed.) D.E. Ames and M.G. Houlé; Geological Survey of Canada, Open File 7856, p. 87–102.

Dare, S.A.S., Ames, D.E., Lightfoot, P.C., Barnes, S.-J. and Beaudoin, G. 2014. Mineral chemistry and supporting databases for TGI-4 project on "Trace elements in Fe-oxides from fertile and barren igneous complexes: Investigating their use as a vectoring tool in Ni-Cu-PGE deposits; Geological Survey of Canada, Open File 7538, 45 p.

Dare, S.A.S., Ames, D.E., Lightfoot, P.C., Barnes, S.-J., and Beaudoin, G., 2015. Trace elements in Fe-oxide minerals from fertile and barren igneous complexes: Investigating their use as a vectoring tool for Ni-Cu-PGE sulphide mineralization, *In:* Targeted Geoscience Initiative 4: Canadian Nickel-Copper-Platinum Group Elements-Chromium Ore Systems — Fertility, Pathfinders, New and Revised Models, (ed.) D.E. Ames and M.G. Houlé; Geological Survey of Canada, Open File 7856, p. 175–185.

David, J., Maurice, C., and Simard, M., 2009. Datations isotopiques effectuées dans le nord-est de la Province du Supérieur;

Travaux de 1998-1999-2000; Ministère des Ressources naturelles du Québec, DV 2008-05, 92 p.

Ding, X., Li., C., Ripley, E.M., Rossell, D., and Kamo, S., 2010. The Eagle and East Eagle sulfide ore-bearing mafic-ultramafic intrusions in the Midcontinent Rift System, upper Michigan: geochronology and petrologic evolution; Geochemistry Geophysics Geosystems, v. 11, p. 1–22.

Doherty, W., Lightfoot, P.C., and Ames, D.E., 2014. A drift correction optimization technique for the reduction of the inter-measurement dispersion of isotope ratios measured using a multi-collector plasma mass spectrometer; Spectrochimica Acta, Part B, v. 98, p. 28–38.

Duke, J.M. and Naldrett, A.J., 1978. A numerical model of the fractionation of olivine and molten sulfide from komatiite magma. Earth and Planetary Science Letters, v. 39, p .255–266.

Farhangi, N., Lesher, C.M., and Houlé, M.G., 2013. Mineralogy, Geochemistry and Petrogenesis of nickel-copper-platinum group element mineralization in the Black Thor Intrusive Complex, McFaulds Lake greenstone belt, Ontario, *In:* Summary of Field Work and Other Activities 2013; Ontario Geological Survey, Open File Report 6290, p. 55-1 to 55-7.

Farrow C.E.G., Everest J.O., King D.M., and Jolette C., 2005. Sudbury Cu(-Ni)-PGE systems: Refining the classification using McCreedy West Mine and Podolsky project case studies, *In:* Exploration for Deposits of Platinum-Group Elements, (ed.) J.E. Mungall; Mineralogical Association of Canada, Short Course Series, v. 33, p. 163–1180.

Fecteau, A., 2013. Pétrographie et géochimie des roches du Complexe mafique et ultramafique du lac Fed; Thèse B.Sc., Université Laval, Québec, 61 p.

Gilbert, H.P., Davis, D.W., Duguet, M., Kremer, P.D., Mealin, C.A., and MacDonald, J., 2008. Geology of the Bird River Belt, southeastern Manitoba (parts of NTS 52L5, 6). Manitoba Science, Technology, Energy and Mines; Manitoba Geological Survey, Geoscientific Map MAP2008-1, scale 1:50 000 (plus notes and appendix).

Good, D.J., Cabri L.J., and Ames, D.E., 2015a. PGM assemblages as an index to Cu-Pd deposition in the Coldwell Alkaline Complex, Ontario; Canada. Institute of Lake Superior Geology conference, Kenora, Ontario, May 2015.

Good, D.J., Epstein, R., McLean, K., Linnen, R.L. and Samson, I.M., 2015b. Evolution of the Main Zone at the Marathon Cu-PGE sulfide deposit, Midcontinent Rift, Canada: spatial relationships in a magma conduit setting; Economic Geology, in press.

Good D.J., Hollings P., Cundari R.M., and Ames D.E., 2015c. A petrogenetic model for LREE-enriched basalt and gabbros in the Coldwell Alkaline Complex, Midcontinent Rift, Ontario, *In:* Program with Abstract; Joint Assembly Annual Meeting American Geophysical Union-Geological Assocation of Canada-Mineralogical Association of Canada-Canadian Geophysical Union, Montréal, Québec, May 2015.

Hanley, J.J., Ames, D.E., Barnes, J., Sharp, Z., and Guillong, M., 2011. Interaction of magmatic fluids and silicate melt residues with saline groundwater in the footwall of the Sudbury Igneous Complex, Ontario, Canada: New evidence from bulk rock geochemistry, fluid inclusions and stable isotopes; Chemical Geology, v. 281, p.1–25.

Hanley J.J., MacMillan, M.A., Kerr, M.J., Watts, K.M., Warren, M.R., and Ames, D.E., 2015. Recent advances in fluid- and melt-inclusion and applied mineralogical research in the Sudbury mining camp: improving ore genesis models and exploration success, *In:* Targeted Geoscience Initiative 4: Canadian Nickel-Copper-Platinum Group Elements-Chromium Ore Systems — Fertility, Pathfinders, New and Revised Models, (ed.) D.E. Ames and M.G. Houlé; Geological Survey of Canada, Open File 7856, p. 209–231.

Hiebert, R.S., Bekker, A., Houlé, M.G., Rouxel, O.J., and Wing, B.A., 2015. Identifying and tracing crustal contamination in the Hart komatiite-associated Ni-Cu-(PGE) deposit using multiple S and Fe isotopes: Abitibi greenstone belt, Ontario, *In:* Targeted Geoscience Initiative 4: Canadian Nickel-Copper-Platinum Group Elements-Chromium Ore Systems — Fertility, Pathfinders, New and Revised Models, (ed.) D.E. Ames and M.G. Houlé; Geological Survey of Canada, Open File 7856, p. 197–207.

Houlé, M.G., Lesher, C.M., and Metsaranta, R.T., 2012. Overview of the high-magnesium ultramafic to mafic systems subproject under the Targeted Geoscience Initiative 4: An Ontario perspective, *In:* Summary of Field Work and Other Activities 2012; Ontario Geological Survey, Open File Report 6280, p. 42-1 to 42-19.

Houlé, M.G., Lesher, C.M., Metsaranta, R.T., Goutier, J., Gilbert, H.P., and McNicoll, V.J., 2013. Temporal and spatial distribution of magmatic Ni-Cu-PGE, Cr, and Fe-Ti-V deposits in the Bird River–Uchi–Oxford-Stull–La Grande–Eastmain superdomain: A new metallogenic province within the Superior Province, *In:* Proceedings; 12th Biennial Society for Geology Applied to Mineral Deposits (SGA) Meeting, Uppsala, Sweden, August 12-15, 2013, p. 1009–1012.

Houlé, M.G., Goutier, J., Sappin, A.-A., and McNicoll, V.J., 2015a. Regional characterization of ultramafic to mafic intrusions in the La Grande Rivière and Eastmain domains, Superior Province, Quebec, *In:* Targeted Geoscience Initiative 4: Canadian Nickel-Copper-Platinum Group Elements-Chromium Ore Systems — Fertility, Pathfinders, New and Revised Models, (ed.) D.E. Ames and M.G. Houlé; Geological Survey of Canada, Open File 7856, p. 125–137.

Houlé, M.G., Lesher, C.M., McNicoll, V.J., Metsaranta, R.T., Sappin, A.-A., Goutier, J., Bécu, V., Gilbert, H.P., and Yang, X.M., 2015b. Temporal and spatial distribution of magmatic Cr-(PGE), Ni-Cu-(PGE), and Fe-Ti-(V) deposits in the Bird River–Uchi–Oxford-Stull–La Grande Rivière–Eastmain domains: a new metallogenic province within the Superior Craton, *In:* Targeted Geoscience Initiative 4: Canadian Nickel-Copper-Platinum Group Elements-Chromium Ore Systems — Fertility, Pathfinders, New and Revised Models, (ed.) D.E. Ames and M.G. Houlé; Geological Survey of Canada, Open File 7856, p. 35–47.

Hronsky, J.M.A. and Groves, D.I., 2008. Science of targeting: definition, strategies, targeting and performance measurement; Australian Journal of Earth Sciences, v. 55, p. 3–12.

Kerr, M., Hanley, J., Morrison, G., Everest, J., and Bray, C., 2015. Preliminary evaluation of trace hydrocarbon speciation and abundance as exploration tool for footwall-style sulfide ores associated with the Sudbury Igneous Complex, Ontario, Canada; Economic Geology, v. 110, p. 50–76.

Kjarsgaard, I.M. and Ames, D.E., 2010. Ore mineralogy of Cu- Ni-PGE deposits in the North Range footwall environment, Sudbury, Canada, *In:* Extended Abstracts; 11th International Platinum Symposium, Ontario Geological Survey, Miscellaneous Release Data 269, p. 5–9.

Kontak, D.J., MacInnis, L.M., Ames, D.E., Rayner, N.M., and Joyce, N., 2015. A geological, petrological, and geochronological study of the Grey Gabbro unit of the Podolsky Cu-(Ni)-PGE deposit, Sudbury, Ontario, with a focus on alteration related to formation of sharp-walled chalcopyrite veins, *In:* Targeted Geoscience Initiative 4: Canadian Nickel-Copper-Platinum Group Elements-Chromium Ore Systems — Fertility, Pathfinders, New and Revised Models, (ed.) D.E. Ames and M.G. Houlé; Geological Survey of Canada, Open File 7856, p. 287–301.

Kuzmich, B., Hollings, P., and Houlé, M.G., 2015. Petrogenesis of the ferrogabbroic intrusions and associated Fe-Ti-V-(P) mineralization within the McFaulds greenstone belt, Superior Province, northern Ontario, *In:* Targeted Geoscience Initiative 4: Canadian Nickel-Copper-Platinum Group Elements-Chromium Ore Systems — Fertility, Pathfinders, New and Revised Models, (ed.) D.E. Ames and M.G. Houlé; Geological Survey of Canada, Open File 7856, p. 101–109.

Laarman, J., Barnett, R., and Duke, N., 2012. Preliminary results on the chromite geochemistry at the Black Label, Black Thor and Big Daddy chromite deposits in the McFaulds Lake Greenstone Belt, Ontario, *In:* Summary of Field Work and Other Activities 2012; Ontario Geological Survey, Open File Report 6280, p. 44-1 to 46-8.

Li, C., Naldrett A.J., Coats C.J.A., and Johannessen, P., 1992. Platinum, palladium, gold and copper-rich stringers at the Strathcona Mine, Sudbury: Their enrichment by fractionation of a sulfide liquid; Economic Geology, v. 87, p. 1584–1598.

Li, C., Lightfoot, P.C., Amelin, Y., and Naldrett A.J., 2000. Contrasting petrological and geochemical relationships in the Voisey's Bay and Mushuau intrusions Labrador, Canada: implications for ore genesis; Economic Geology, v. 95, p. 771–799.

MacInnis, L.M., Kontak, D.J., Ames, D.E., and Joyce, N.L., 2014. Geochemistry and supporting databases from an alteration study at the Podolsky Cu(-Ni)-PGE deposit, Whistle offset structure, Sudbury; Geological Survey of Canada Open File 7666, 19 p. doi:10.4095/295482

MacMillan, M.A., 2014. Mineralogical, fluid inclusion, and stable isotope constraints on the origin of footwall-style "high-sulfide" and "low-sulfide" Cu-Ni-PGE mineralization at the Coleman Mine, Sudbury Igneous Complex (SIC), Sudbury, Canada; M.Sc. thesis, Saint Mary's University, Halifax, Nova Scotia, 152 p.

Manor, M.J., Scoates, J.S., Nixon, G.T., and Ames, D.E., 2014a. Platinum-group mineralogy of the Giant Mascot Ni-Cu-PGE deposit, Hope, BC, *In:* Geological Fieldwork 2013; British Columbia Ministry of Energy and Mines, British Columbia Geological Survey, Paper 2014-1, p. 141–156.

Manor, M., Wall, C., Nixon, G., Scoates, J., Pinsent, R.H., and Ames, D.E., 2014b. Preliminary geology and geochemistry of the Giant Mascot ultramafic-mafic intrusion, Hope, southwestern British Columbia; Geological Survey of Canada, Open File 7570; British Columbia Ministry of Energy and Mines, Open File 2014-03; scale 1:10 000. doi:10.4095/293429

Manor, M.J., Wall, C.J., Friedman, R.M., Gabites, J., Nixon, G.T., Scoates, J.S., and Ames, D.E., 2015a. Geology, geochronology and Ni-Cu-PGE orebodies of the Giant Mascot ultramafic intrusion, Hope, southwestern British Columbia; British Columbia Ministry of Energy and Mines, British Columbia Geological Survey, Geoscience Map 2015-01, scale: 1:10 000 (2 sheets).

Manor, M.J., Scoates, J.S., Nixon, G.T., and Ames, D.E., 2015b. The Giant Mascot Ni-Cu-PGE deposit, southwestern British Columbia: mineralized conduits and sulphide saturation mechanisms in a convergent margin tectonic setting; Economic Geology, in press.

McCuaig, C., Beresford, S., and Hronsky, J., 2010. Translating the mineral systems approach into an effective exploration targeting system; Ore Geology Reviews, v. 38, p. 128–138.

Mehrmanesh K., Carson H.J.E., Lesher C.M. and Houlé M.G., 2013. Stratigraphy, geochemistry and petrogenesis of the Black Label chromitite horizon, Black Thor intrusive complex, McFaulds Lake greenstone belt, Ontario, *In:* Summary of Field Work and Other Activities 2013; Ontario Geological Survey, Open File Report 6290, p.53-1 to 53-6.

Meghji, I., Linnen R.L., Samson I.M., Ames D.E., and Good D.J., 2013. The character and distribution of Cu-PGE mineralization at the Geordie Lake Deposit within the Coldwell Complex, Ontario, *In:* Program with Abstracts; Geological Association of Canada – Mineralogical Association of Canada Joint Annual Meeting, Winnipeg, Manitoba, May 2013, Abstract Volume 36, p. 143–144.

Metsaranta, R.T., Houlé, M.G., McNicoll, V.J., and Kamo, S.L., 2015. Revised geological framework for the McFaulds Lake greenstone belt, Ontario, *In:* Targeted Geoscience Initiative 4: Canadian Nickel-Copper-Platinum Group Elements-Chromium Ore Systems — Fertility, Pathfinders, New and Revised Models, (ed.) D.E. Ames and M.G. Houlé; Geological Survey of Canada, Open File 7856, p. 61–73.

Mungall, J.E., Harvey, J.D., Balch, S.J., Azar, B., Atkinson, J., and Hamilton, M.A., 2010. Eagles Nest: A magmatic Ni-sulphide deposit in the James Bay lowlands, Ontario, Canada, *In:* The Challenge of Finding New Mineral Resources: Global Metallogeny, Innovative Exploration, and New Discoveries, (ed.) R.J. Goldfarb, E.E. Marsh, T. Monecke; Economic Geology, Special Publication 15, p. 539–557.

Naldrett, A.J., 2010. Secular variation of magmatic sulfide deposits and their source magmas; Economic Geology, v. 105, p. 259–262.

Naldrett, A.J., Duke, J.M., Lightfoot, P.C., and Thompson J.F.H., 1984. Quantitative modelling of the segregation of magmatic suphfides: an exploration guide; Canadian Institute of Mineralogy and Metallurgy Bulletin, v. 77, p. 46–56.

Naldrett, A.J., Asif, M., Schandl, E., and Searcy, T., 1999. Platinum-group elements in the Sudbury ores: Significance with respect to the origin of different ore zones and to the exploration for footwall orebodies; Economic Geology, v. 94, p. 185–210.

Nelles, E.W., Lesher C.M., and Lafrance B., 2010. Mineralogy and textures of Cu–PPGE–Au-rich mineralization in the Morrison (Levack footwall) Deposit, Sudbury, Ontario, *In:* Abstracts Volume; Society of Economic Geologists Annual Meeting, Keystone, Colorado, October 2010.

Nixon, G.T., Manor, M.J., Jackson-Brown, S., Scoates, J.S., and Ames, D.E., 2015. Magmatic Ni-Cu-PGE sulphide deposits at convergent margins, *In:* Targeted Geoscience Initiative 4: Canadian Nickel-Copper-Platinum Group Elements-Chromium Ore Systems — Fertility, Pathfinders, New and Revised Models, (ed.) D.E. Ames and M.G. Houlé; Geological Survey of Canada, Open File 7856, p. 17–34.

Pagé, P., Barnes, S.-J., Méric, J., and Houlé, M.G., 2015. Geochemical composition of chromite from Alexo komatiite in the western Abitibi greenstone belt: Implications for mineral exploration, *In:* Targeted Geoscience Initiative 4: Canadian Nickel-Copper-Platinum Group Elements-Chromium Ore Systems — Fertility, Pathfinders, New and Revised Models, (ed.) D.E. Ames and M.G. Houlé; Geological Survey of Canada, Open File 7856, p. 187–195.

Péntek, A., Molnár F., Watkinson D.H., and Jones P.C., 2008. Footwall-type Cu-Ni-PGE mineralization in the Broken Hammer area, Wisner township, North Range, Sudbury structure; Economic Geology, v. 103, p. 1005–1028.

Pilkington, M. and Keating, P., 2015. Gravity gradiometer data analysis in mineral exploration, *In:* Targeted Geoscience Initiative 4: Canadian Nickel-Copper-Platinum Group Elements-Chromium Ore Systems — Fertility, Pathfinders, New and Revised Models, (ed.) D.E. Ames and M.G. Houlé; Geological Survey of Canada, Open File 7856, p. 167–173.

Sappin, A.-A., Houlé, M.G., Lesher, C.M., Metsaranta, R.T., and McNicoll, V.J., 2015. Regional characterization of mafic-ultramafic intrusions in the Oxford-Stull and Uchi domains,

Superior Province, Ontario, *In:* Targeted Geoscience Initiative 4: Canadian Nickel-Copper-Platinum Group Elements-Chromium Ore Systems — Fertility, Pathfinders, New and Revised Models, (ed.) D.E. Ames and M.G. Houlé; Geological Survey of Canada, Open File 7856, p. 75–85.

Shahabi Far, M., Samson, I.M., Gagnon, J.E., Linnen, R.L., Good, D.J., and Ames, D.E., 2015. Textural character and chemistry of plagioclase and apatite in the Marathon Cu-PGE deposit, Ontario: Implications for mineralizing processes, *In:* Targeted Geoscience Initiative 4: Canadian Nickel-Copper-Platinum Group Elements-Chromium Ore Systems — Fertility, Pathfinders, New and Revised Models, (ed.) D.E. Ames and M.G. Houlé; Geological Survey of Canada, Open File 7856, p. 233–243.

Spath, C.S. III, Lesher, C.M., and Houlé, M.G., 2015. Hybridized ultramafic rocks in the Black Label hybrid zone of the Black Thor intrusive complex, McFaulds Lake greenstone belt, Ontario, *In:* Targeted Geoscience Initiative 4: Canadian Nickel-Copper-Platinum Group Elements-Chromium Ore Systems — Fertility, Pathfinders, New and Revised Models, (ed.) D.E. Ames and M.G. Houlé; Geological Survey of Canada, Open File 7856, p. 103–114.

Stott, G.M., Corkery, M.T., Percival, J.A., Simard, M., and Goutier, J., 2010. A revised terrane subdivision of the Superior Province, *In:* Summary of Field Work and Other Activities 2010; Ontario Geological Survey, Open File Report 6260, p. 20-1 to 20-10.

Trevisan, B.E., Hollings, P., Ames, D.E., and Rayner, N.M., 2015. The petrology, mineralization, and regional context of the Thunder mafic to ultramafic intrusion, Midcontinent Rift, Thunder Bay, Ontario, *In:* Targeted Geoscience Initiative 4: Canadian Nickel-Copper-Platinum Group Elements-Chromium Ore Systems — Fertility, Pathfinders, New and Revised Models, (ed.) D.E. Ames and M.G. Houlé; Geological Survey of Canada, Open File 7856, p. 139–149.

Tuba, G., Molnár, F., Watkinson, D.H., Jones, P.C., and Mogessie, A., 2010. Hydrothermal vein and alteration assemblages associated with low-sulfide footwall Cu-Ni-PGE mineralization and regional hydrothermal processes, North and East Ranges, Sudbury structure, Canada, *In:* The Challenge of Finding New Mineral Resources: Global Metallogeny, Innovative Exploration, and New Discoveries Volume I: Gold, Silver, and Copper-Molybdenum, (ed.) R.J. Goldfarb, E.E. Marsh, and T. Monecke; Society of Economic Geologists, Special Publication 15, p. 573–598.

Tuba, G., Molnár, F., Ames, D.E., Péntek, A., Watkinson, D.H., and Jones, P.C., 2014. Multi-stage hydrothermal processes involved in "low-sulfide" Cu(-Ni)-PGE mineralization in the footwall of the Sudbury Igneous Complex (Canada): Amy Lake PGE zone, East Range; Mineralium Deposita, v. 49, p. 7–47. doi 10.1007/s00126-013-0468-1

United States Geological Survey, 2015. Chromium, *In:* Minerals Yearbook 2015; United States Department of the Interior, United States Geological Survey, 2015, p. 17.1 to 17.21. http://minerals.usgs.gov/minerals/pubs/commodity/chromium/index.html#myb

Veksler, I.V., 2006. Crystallized melt inclusions in gabbroic rocks, *In:* Melt Inclusions in Plutonic Rocks, (ed.) J.D. Webster; Mineralogical Association of Canada, Short Course Series, v. 36, p. 99–122.

Warren, M., Hanley, J., Ames, D.E., and Jackson, S., 2015. The Ni-Cr-Cu content of biotite as pathfinder elements for magmatic Ni-Cu-PGE sulfide exploration associated with mafic units of the Sudbury Igneous Complex, Ontario, Canada; Journal of Exploration Geochemistry, v. 153, p. 11–29.

Watts, K., 2014. A melt inclusion study of the Sudbury Igneous Complex (Ontario, Canada): Evidence for two-liquid immiscibility and constraints on trace-element distribution; M.Sc. thesis, Saint Mary's University, Halifax, Nova-Scotia, 115 p.

Watts, K., Hanley, J., Ames, D.E., Kontak, D., and Petrus, J., 2015. Chemical databases for apatite and melt inclusions from a study of the 1850 Ma Sudbury Igneous Complex, Ontario, Canada; Geological Survey of Canada, Open File 7710.

Wheeler, J.O., Hoffman, P.F., Card, K.D., Davidson, A., Sanford, B.V., Okulitch, A.V., and Roest, W.R., 1996. Geological map of Canada; Geological Survey of Canada, "A" Series Map 1860A, scale 1: 5 000 000.

White, C.J., 2012. Low-sulfide PGE-Cu-Ni mineralization from five prospects within the footwall of the Sudbury Igneous Complex, Ontario, Canada; Ph.D. thesis, University of Toronto, Toronto, Ontario, 318 p.

Yang, X.M., Gilbert, H.P., and Houlé, M.G., 2012. Geological investigations of the Cat Creek area in the Neoarchean Bird River greenstone belt, southeastern Manitoba (part of NTS 52L12): new insights into PGE-Ni-Cu-Cr mineralization, *In:* Report of Activities 2012; Manitoba Innovation, Energy and Mines, Manitoba Geological Survey, p. 32–53.

Yang, X.M., Gilbert, H.P., and Houlé, M.G., 2013. Cat Lake–Euclid Lake area in the Neoarchean Bird River greenstone belt, southeastern Manitoba (parts of NTS 52L11, 12): preliminary results of bedrock geological mapping and their implications for geodynamic evolution and metallogeny, *In:* Report of Activities 2013; Manitoba Mineral Resources, Manitoba Geological Survey, p. 70–84.

GEOLOGICAL SURVEY OF CANADA
OPEN FILE 7856

Targeted Geoscience Initiative 4: Canadian Nickel-Copper-Platinum Group Elements-Chromium Ore Systems — Fertility, Pathfinders, New and Revised Models

Magmatic Ni-Cu-PGE sulphide deposits at convergent margins

Graham T. Nixon[1], Matthew J. Manor[2], Sarah Jackson-Brown[2], James S. Scoates[2], and Doreen E. Ames[3]

[1]British Columbia Geological Survey, Victoria, British Columbia
[2]University of British Columbia, Vancouver, British Columbia
[3]Geological Survey of Canada, Ottawa, Ontario

2015

© Her Majesty the Queen in Right of Canada, as represented by the Minister of Natural Resources Canada, 2015

This publication is available for free download through GEOSCAN (http://geoscan.nrcan.gc.ca/)

Recommended citation

Nixon, G.T., Manor, M.J., Jackson-Brown, S., Scoates, J.S., and Ames, D.E., 2015. Magmatic Ni-Cu-PGE sulphide deposits at convergent margins, *In:* Targeted Geoscience Initiative 4: Canadian Nickel-Copper-Platinum Group Elements-Chromium Ore Systems — Fertility, Pathfinders, New and Revised Models, (ed.) D.E. Ames and M.G. Houlé; Geological Survey of Canada, Open File 7856, p. 17–34.

Publications in this series have not been edited; they are released as submitted by the author.

Contribution to the Geological Survey of Canada's Targeted Geoscience Initiative 4 (TGI-4) Program (2010–2015)

TABLE OF CONTENTS

Magmatic Ni-Cu-PGE sulphide deposits at convergent margins

Graham T. Nixon[1]*, Matthew J. Manor[2], Sarah Jackson-Brown[2], James S. Scoates[2], and Doreen E. Ames[3]

[1]British Columbia Ministry of Energy and Mines, British Columbia Geological Survey, PO Box 9333, Stn Prov Govt, Victoria, British Columbia V8W 9N3

[2]Pacific Centre for Isotopic and Geochemical Research, Department of Earth, Ocean and Atmospheric Sciences, University of British Columbia, 6339 Stores Road, Vancouver, British Columbia V6T 1Z4

[3]Geological Survey of Canada, 601 Booth Street, Ottawa, Ontario K1A 0E8

*Corresponding author's e-mail: graham.nixon@gov.bc.ca

ABSTRACT

Magmatic Ni-Cu-PGE sulphide deposits hosted by ultramafic-mafic intrusions in convergent-margin tectonic settings are an increasingly important resource worldwide, yet remain poorly understood and underexplored. A compilation of global mineralized intrusions in subduction-related settings underscores their economic potential and reveals mineralogical differences that may reflect parental magma composition and ore-forming processes. Our geochemical and isotopic investigations of two mineralized ultramafic intrusions in the Cordillera, the orthopyroxene-absent Turnagain Alaskan-type intrusion and the orthopyroxene-rich Giant Mascot intrusion, emphasize (1) the importance of wall-rock assimilation in promoting sulphide saturation and formation of an immiscible sulphide liquid; and (2) the ability of narrow conduit systems to channel influxes of new metal-laden magma and serve as traps for the collection of upgraded Ni-Cu-PGE sulphides. Processes fundamental to the production of economic Ni-sulphide deposits in the oxidized and hydrous primitive magmas generated at subduction zones are similar to those that have produced world-class magmatic nickel deposits in other tectonic settings.

INTRODUCTION

Investigations of orthomagmatic nickel-copper-platinum group element (Ni-Cu-PGE) mineralization in convergent-margin or supra-subduction-zone plate tectonic settings were carried out as part of the magmatic-hydrothermal nickel-copper-PGE ore system and convergent-margin Ni subprojects under the Targeted Geoscience Initiative 4 (TGI-4; Ames and Houlé, 2011; Ames et al., 2012). Our convergent-margin Ni-Cu-PGE study has a number of objectives: (1) examine the potential for economic Ni-sulphide deposits in an unconventional convergent-margin tectonic setting; (2) determine the principal factors that influence the genesis of magmatic Ni-Cu-PGE sulphide mineralization in the subduction-zone environment; and (3) evaluate exploration criteria for the discovery of economic mineralization in Canada and orogenic belts globally. To meet these objectives, we have (1) conducted a compilation of select global ultramafic-mafic intrusions that host Ni-sulphide deposits and prospects in convergent-margin settings; (2) investigated the ore-forming characteristics and mode of occurrence of Ni-Cu-PGE mineralization in two ultramafic intrusions in the Canadian Cordillera that have contrasting petrogenetic affiliations, including the Turnagain Alaskan-type intrusion, which characteristically lacks orthopyroxene, and the orthopyroxene-rich Giant Mascot intrusion; and (3) made a preliminary evaluation of factors that may influence the prospectivity of ultramafic-mafic intrusions at convergent margins for significant Ni-Cu-PGE mineralization. From our studies, which are summarized below, we contend that (1) the nature of ultramafic-mafic intrusions that host Ni-Cu-PGE mineralization at convergent margins is more diverse than generally realized; (2) the principal factors that promote magmatic sulphide mineralization in the relatively oxidizing environment of subduction zones are akin to those involved in the generation of major Ni-sulphide deposits in other tectonic environments; and (3) the potential for the discovery of economic deposits at convergent margins is currently underestimated.

CONVERGENT-MARGIN Ni-Cu-PGE DEPOSITS

Most of the world's major magmatic Ni-Cu-PGE deposits are hosted by ultramafic-mafic intrusions and volcanic rocks in various rift-related settings (summarized by Naldrett, 2010). Magmatic Ni-Cu-PGE sulphide deposits at convergent margins are becoming an increasingly important resource worldwide, yet are still

Nixon, G.T., Manor, M.J., Jackson-Brown, S., Scoates, J.S., and Ames, D.E., 2015. Magmatic Ni-Cu-PGE sulphide deposits at convergent margins, *In:* Targeted Geoscience Initiative 4: Canadian Nickel-Copper-Platinum Group Elements-Chromium Ore Systems — Fertility, Pathfinders, New and Revised Models, (ed.) D.E. Ames and M.G. Houlé; Geological Survey of Canada, Open File 7856, p. 17–34.

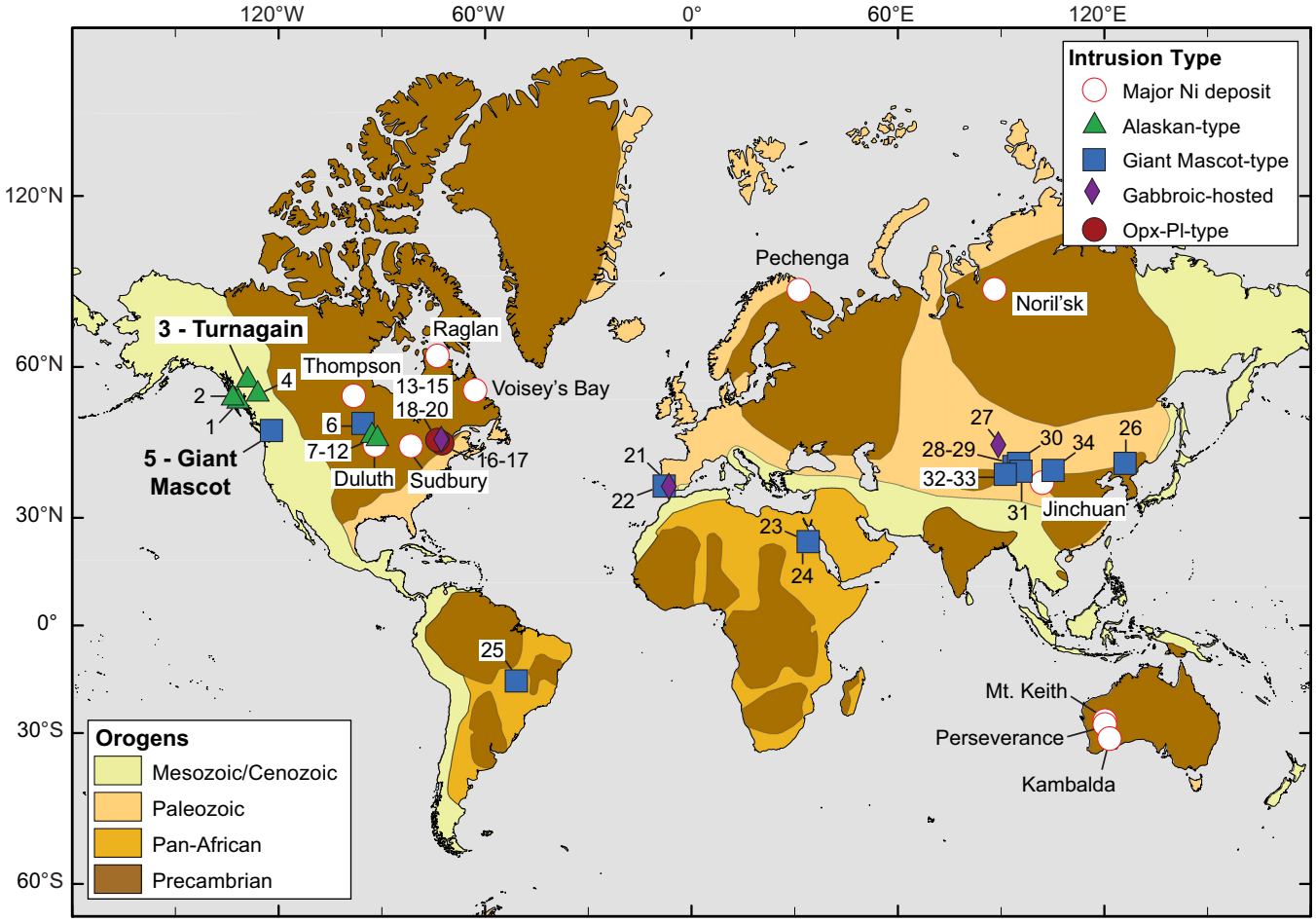

Figure 1. Global occurrences of selected orthomagmatic Ni-Cu±PGE deposits and prospects hosted by orthopyroxene-absent (Alaskan-type) and various orthopyroxene-rich ultramafic-mafic intrusions (Giant Mascot-type, gabbroic and orthopyroxene-plagioclase (Opx-Pl)-type) in convergent-margin plate tectonic settings, and world-class Ni-sulphide deposits/mining camps in other tectonic environments. Deposits listed in bold represent TGI-4 study locations. Numbered deposits/prospects correspond to those in Table 1 (generalized orogenic belts taken from Guillot et al., 2009; Mercator projection).

poorly understood and underexplored. Traditionally, subduction-zone settings have been regarded as unfavourable environments for nickel exploration due to the relative paucity of economically exploitable deposits. Consequently, mineral deposit models for magmatic Ni-sulphide mineralization at convergent margins have emerged only recently (e.g. Ural-Alaskan NC-7: Naldrett, 2010).

A compilation of selected global Ni-Cu±PGE deposits and prospects at convergent margins, which included factors such as age, host-rock characteristics, and other pertinent features, indicates that the occurrence of these deposits is more common and the number of similarities among them is greater than previously considered (Fig. 1, Table 1). All of the ultramafic-mafic intrusions that host Ni-sulphide mineralization that were compiled are in deformed and metamorphosed, arc-related accretionary terranes, and their ages range from Late Cretaceous (Giant Mascot, ca. 93 Ma) to Neoarchean (Gordon Lake and the Quetico intrusions, ca. 2.7 Ga; Table 1). All of these intrusions are reported to contain magmatic "hornblende" (typically tschermakite, pargasite, magnesiohornblende, magnesiohastingsite, and edenite), especially those with ultramafic suites. To aid in distinguishing different intrusion types, we have adopted a simple mineralogical classification (discussed below).

The intrusions are generally small (<4 km^2) and form composite or simple dykes, plugs, and sill-like bodies. They exhibit a well developed (rare) to crudely concentric, bilateral, or unilateral arrangement of rock units separated by sharp to gradational contacts, and have centimetre-scale (rare) to hectometre-scale (common) layering, or no discernible internal structure.

Intrusions considered to have been emplaced in supra-subduction regimes include Alaskan-type bodies in southeastern Alaska (Himmelberg and Loney, 1995), British Columbia (Nixon et al., 1997), and the Portneuf-Mauricie Domain intrusions in Quebec (Sappin et al., 2009, 2011). Although some intrusions bear the geochemical fingerprint of subduction-modified mantle source regions, such as the Permian intru-

Table 1. Global occurrences of selected magmatic Ni-Cu±PGE sulphide deposits and prospects in convergent-margin plate tectonic settings.

No.[1]	Type[2]	Deposit/ Prospect	Geotectonic setting[3]	Intrusion age (Ma)	Surface dimension	Internal structure	Intrusion lithologies[4]	Metamorphic grade[5]	Resource[6]	Grade (wt%) Ni	Cu
Southeast Alaska											
1	A	Duke Island (Marquis-Potato Patch-Raven)	Northern Cordillera/ Alexander terrane	Early Cretaceous (ca. 108–111)	23 km^2	composite/ layered/ crudelyzoned	dunite(±Cpx)/ wehrlite(±Hb)/ Ol clinopyroxenite(±Hb)/ Hb-Mt clinopyroxenite/ hornblendite(±Pl±Mt)	greenschist - amphibolite	prospect	<0.25	<2.8 (1g/t Pt+Pd)
2	A	Salt Chuck*		Silurian (ca. 430)	7.3 x 1.6 km	NIS	Bi-Pl-Mt clinopyroxenite(±Hb)/ Bi-Mt gabbro(±Hb)	greenschist	0.3 Mt		0.95 (2 g/t Pd)
British Columbia											
3	A	Turnagain (Horsetrail)	Northern Cordillera/ Yukon-Tanana terrane	Early Jurassic (ca. 190)	8.5 x 3 km	composite	dunite(±Cpx±Phl)/ wehrlite(±Phl)/ Ol clinopyroxenite/ Mt clinopyroxenite/ Hb clinopyroxenite(±Mt)/ hornblendite (±Pl±Bi)/ Hb diorite(±Bi)/ chromitite	lower greenschist	1841.8 Mt	0.21	(0.013 Co)
4	A	Polaris	Northern Cordillera/ Quesnellia/ Harper Ranch subterrane	Early Jurassic (ca. 186)	45 km^2	crudely zoned (asymmetric)	dunite(±Cpx±Phl)/ wehrlite(±Phl)/ clinopyroxenite (±Phl)/ Ol clinopyroxenite (±Phl)/ Hb/ hornblendite(±Pl±Bi)/ Hb clinopyroxenite(±Pl±Mt±Bi)/ gabbro-diorite(±Bi±Mt)	lower greenschist	prospect	0.25	1.2 (<1.3 g/t Pt; <1.8 g/t Pd)
5	GM	Giant Mascot*	Northern Cordillera/ Coast Plutonic Complex	Late Cretaceous (ca. 93)	3 x 1.3 km	composite/ zoned	dunite(±Opx±Hb±Cpx)/Hb harzburgite/ Hb lherzolite (rare)/ Hb orthopyroxenite(±Ol)/ Ol-Hb websterite (±Pl)/ Hb websterite(±Pl)/ hornblendite(±Pl±Cpx)/ Hb gabbro	amphibolite	4.2 Mt	0.77	0.34
Ontario											
6	GM?	Gordon Lake*	Superior/ English River subprovince	Neoarchean (ca. 2.7 Ga)	180 x 45 m	possible weak zoning	Hb harzburgite/ Hb lherzolite/ Ol-Px hornblendite/ rare Ol-Hb orthopyroxenite & Hb wehrlite	upper amphibolite - lower granulite	1.5 Mt	0.92	0.47 (0.9 g/t Pt+Pd)
7	A	Samuels Lake	Superior/ Quetico subprovince	Neoarchean (ca. 2.69 Ga)	600 x 300 m	zoned	Mt-Hb-Pl clinopyroxenite(±Bi)/ wehrlite(±Hb±Bi)/ Bi-Pl hornblendite/ Hb gabbro/ monzodiorite-diorite	upper greenschist - lower amphibolite	prospect	0.15–1.0	0.2–1.0 (<1.8 g/t Pd+Pt)
8	A	Plateau Lake			650 x 100 m	weakly zoned	Hb clinopyroxenite(±Bi±Pl)/ hornblendite(±Bi±Pl)	low-mid amphibolite	prospect	<0.73	<4.4 (<1.7 g/t Pd+Pt)
9	A	Kawene			500 x 70–130 m	crudely zoned	Hb wehrlite(±Bi)/Hb clinopyroxenite(±Ol)/ Cpx hornblendite(±Bi)/hornblendite(±Pl±Bi±Cpx)/ Hb gabbro(±Bi±Kf±Qz)	upper greenschist - lower amphibolite	prospect	<0.47	<1.1 (<5.9 g/t PGE)
10	A	Abiwin			200 x 40 m	NIS	hornblendite(±Pl±Bi)/ Hb gabbro(±Bi±Kf±Qz)	mid-amphibolite	prospect	<0.24	<2.1 (<1.4 g/t Pd+Pt)
11	A	Mudd Lake			800 x 10–100 m	NIS	hornblendite(±Pl±Cpx±Bi)/Cpx hornblendite(±Bi)/ Hb gabbro(±Bi±Kf±Qz)/diorite(±Bi±Kf±Qz)	upper greenschist - lower amphibolite	prospect	<0.1	<5.1 (<3.9 g/t Pd+Pt)
12	A	Chief Peter Lake			760 x 460 m	zoned	Hb wehrlite(±Bi)/hornblendite(±Bi±Pl)	greenscist - amphibolite	prospect	<0.24	<0.81 (<2.5 g/t Pd+Pt)
Québec[6]											
13	Opx-Pl	Lac Matte	Grenville/Portneuf-Mauricie Domain	Mesoproterozoic (ca. 1.4 Ga)	1.1 x 0.9 km	NIS	websterite-orthopyroxenite(±Ol±Pl)/norite/ gabbronorite/rare Pl harzburgite & lherzolite	amphibolite	prospect		
14	Opx-Pl	Lac Kennedy			1 x 0.5 km	layered	harzburgite/Pl websterite(±Ol)/gabbronorite/norite	amphibolite	prospect		
15	Opx-Pl	Lac Édouard*			300 m wide	layered	harzburgite/websterite-orthopyroxenite(±Ol±Pl)/ gabbronorite	amphibolite	0.082 Mt	1.5	0.5
16	G	Boivin			160 x 70 m	NIS	Pl-websterite/gabbronorite	amphibolite	prospect		
17	G	Rochette West			150 x 150 m	NIS	websterite(±Pl)/gabbronorite/norite	amphibolite	prospect		
18	Opx-Pl	Lac à la Vase (Rousseau)			3 x 0.8–1.8 km	zoned	lherzolite-wehrlite-harzburgite(±Pl)/websterite-orthopyroxenite(±Pl)/gabbronorite/norite/hornblendite	amphibolite	prospect		
19	Opx-Pl	Lac Nadeau			1.04 x 0.45+ km	zoned	lherzolite-harzburgite(±Pl)/websterite(±Ol±Pl)/Pl-orthopyroxenite/gabbronorite/norite/Qz-diorite	amphibolite	prospect		
20	Opx-Pl	Réservoir Blanc			unknown	NIS	norite/gabbronorite/anorthosite/gabbro/orthopyroxenite	amphibolite	prospect		

Table 1 continued.

No.[1]	Type[2]	Deposit/ Prospect	Geotectonic setting[3]	Intrusion age (Ma)	Surface dimension	Internal structure	Intrusion lithologies[4]	Metamorphic grade[5]	Resource[6]	Grade (wt%) Ni	Cu
Spain											
21	G	Aguablanca	Variscan/Santa Olalla Igneous Complex	Carboniferous (ca. 341)	<10 km^2	layered/ breccia pipe	Hb gabbronorite/norite/gabbro/anothosite/rare Hb dunite, rare Hb harzburgite, rare Hb websterite (±Ol±Pl)	amphibolite and greenschist	15.7 Mt	0.66	0.46 (0.47 g/t PGE)
22	GM	Tejadillas	Variscan/Cortegana Igneous Complex	Carboniferous (ca. 336)	1.4 x 0.7 km	zoned	Hb harzburgite(±Cpx±Phl)/gabbronorite(±Ol)/ norite-gabbro(±Hb±Phl)/Qz diorite	amphibolite	prospect	0.16	0.08
Egypt											
23	GM	Gabbro Akarem	Pan-African/Nubian shield	Neoproterozoic (ca. 973)	West: 3 x 0.5 km; East: 7 x 2 km	zoned	Cpx-Hb-Opx dunite/lherzolite(±Hb±Pl)/Pl websterite(±Ol±Hb)/hornblendite(±Ol±Pl)	'unmetamorphosed'	0.7 Mt	0.95 (Ni+	
24	GM	Genina Gharbia		Neoproterozoic (ca. 963)	9 x 3 km	zoned	Hb harzburgite(±Pl±Cpx)/Hb lherzolite(±Pl)/ Hb pyroxenite(±Ol±Phl)/Hb norite/Opx-Hb gabbro	'unmetamorphosed' (greenschist?)	prospect		
Brazil											
25	GM	Americano do Brasil*	Braziliano/Brazilia Belt/ Goiás Magmatic Arc	Neoproterozoic (ca. 626)	12 x 3 km	layered	S1: Pl-Hb websterite/gabbronorite; S2: dunite/ wehrlite/ lherzolite; G2: lherzolite/websterite	amphibolite-granulite	3.1 Mt	1.12	1.02
China											
26	GM	Hongqiling No.7*	CAOB/Xing'an-Mongolianterrane/ Hulan Group (early Paleozoic)	Late Triassic (ca. 216)	~130 m^2	NIS (dyke-like)	orthopyroxenite(±Phl±Pl±Hb)/harzburgite/norite	amphibolite (Early-Middle Triassic metamorphism)	0.2 Mt Ni 0.04 Mt Cu	2.31	0.63
27	G	Kalatongke* (Y1, Y2, Y3)	CAOB/Junggar Orogen/ Puerjin-Ertai terrane/ Nanmingshui Fm (Lower Carboniferous)	Permian (ca. 287)	<400 m x 150 m (5.2 x 0.5 km concealed)	composite/ layered (funnel-shaped/ tabular)	Bi-Hb-Ol norite/Bi-Hb norite/troctolite/ Qz-Bi-Hb diorite	greenschist; 20 m contact metamorphic aureole	Y1: 18 Mt Y2: 10 Mt Y3: 5 Mt	0.88 0.6 0.6	1.4 1.1 1.1
28	GM	Huangshandong* (Huangshan East)	CAOB/North Tianshan terrane/Gandu Group (mid-Carboniferous)	Permian (ca. 274)	3.5 x 1.2 km ~2.8 km^2	composite/ layered	Bi-Pl-Hb lherzolite/ Ol websterite(±Pl±Phl)/ gabbro/ Ol gabbro/ Hb gabbro/ troctolite/ gabbronorite(±Ol±Hb)/ Hb diorite(±Qz±Bi)	greenschist; weak contact metamorphic aureole <100m wide	>50 Mt 135 Mt	0.52 0.30	0.27 0.16
29	GM	Huangshanxi* (Huangshan)	CAOB/North Tianshan terrane/Gandu Group (mid-Carboniferous)	Permian (ca. 284)	3.8 x 0.8 km	composite/ layered	I. Hb lherzolite(±Pl)/gabbronorite; II. Hb-Bi gabbro(±Ol±Opx) III.Hb lherzolite(±Phl)/ Hb-Olwebsterite/ Ol orthopyroxenite(±Cpx±Hb)/ websterite	greenschist; weak contact metamorphic aureole <100m wide	80 Mt	0.54	0.3
30	GM	Hulu*	CAOB/North Tianshan terrane/Wotongwozi Fm (Lower Carboniferous)	Permian (ca. 282)	1.9 x 0.7 km	layered/ zoned (?folded sill)	Bi-Pl-Hb lherzolite-harzburgite; Hb-Pl pyroxenite/ Pl-Hb-Ol pyroxenite; Bi-Hb gabbro-diorite	amphibolite	80,200 t Ni 39600 t Cu	0.23-0.61	0.10–0.49
31	GM	Heishan	CAOB/Beishan terrane/Hulan Fm	late Devonian (ca. 366)	800 x 470 m	weakly zoned (dyke-like)	harzburgite(±Bi±Hb±Pl)/lherzolite	amphibolite?	35 Mt	0.6	0.3
32	GM	Poyi	CAOB/Beishan terrane/Pobei intrusion	Permian (ca. 271–284)	3 x 1 km	layered (pipe-like)	dunite/lherzolite(±Hb±Phl±Pl)/Ol websterite	upper greenschist?	1.3 Mt Ni 0.22 Mt Cu	0.5	
33	GM?	Poshi	CAOB/Beishan terrane/Pobei intrusion	Permian (ca. 271–284)	2 x 1.6	zoned	websterite(±Pl±Hb)/peridotite	upper greenschist?	14.7 Mt	0.3-0.6	
34	GM	Erbutu*	CAOB/Ondur Sum terrane/ Baoyintu Group (Meso-proterozoic)	Permian (ca. 294)	200 m x 170 m	layered	Ol orthopyroxenite(±Cpx±Hb±Phl)/ orthopyroxenite	amphibolite	1 Mt	0.3-2.0	

[1]Location shown in Fig. 1 [2] Intrusion type: A = Alaskan-type (orthopyroxene-free); GM = Giant Mascot-type (orthopyroxene-rich); G = gabbroic-hosted mineralization; Opx-Pl = orthopyroxene-plagioclase-hosted mineralization
[3]CAOB = Central Asian Orogenic Belt; [4] Mineral abbreviations: Ol = olivine; Opx = orthopyroxene; Cpx = clinopyroxene; Hb = hornblende (magmatic amphibole); Phl = phlogopite; Bi = biotite; Pl = plagioclase; Kf = potassium feldspar; Qz = quartz [5] Metamorphic grade of host rocks to intrusion [6] Ore tonnage or contained metal tonnage where Ni and Cu indicated separately; Mt = million metric tonnes; t = metric tonnes [7] The Portneuf-Mauricie mafic-ultramafic intrusive suites are distinguished by early crystallizing plagioclase and minor amounts of late magmatic hornblende (Sappin et al., 2009) * Active or past-producing mine

References: 1) Irvine, 1974; Saleeby, 1992; Ripley et al., 2005; 2) Holt et al., 1948; Loney and Himmelberg, 1992; 3) Clark, 1975, 1980; Scheel, 2007; Nixon et al., 2012; Mudd and Jowitt, 2014;
4) Nixon et al., 1997; Simard et al., 2003; Mowat, 2013; 5) Aho, 1954, 1956; Manor, 2014; Manor et al., 2015a; 6) Scoates, 1972; Parker, 1998; 7) Pettigrew et al., 2000; Pettigrew and Hattori, 2006;
8-12) MacTavish, 1999; 13-14, 16-20) Sappin et al., 2009, 2011, 2012; 15) Mudd and Jowitt, 2014; Sappin et al., 2009, 2011, 2012; 21) Tornos et al., 2001, 2006; Piña et al., 2006, 2008, 2010; Romeo et al., 2006;
22) Piña et al., 2012; 23) Helmy and Mogessie, 2001; Helmy and Mallahawi, 2003; Helmy et al., 2005; 24) Helmy et al., 2014; Helmy, 2004; 25) Mota-e-Silva et al., 2011; Nilson, 1981;
26) Wu et al., 2004; Lu et al., 2011; Wei et al., 2013; 27) Li et al., 2012; Gao et al., 2012; Zhang et al., 2009: Han et al., 2004; 28) Gao et al., 2013; Mao et al., 2014a; Han et al., 2004; Zhang et al., 2011; Branquet et al., 2012;
29) Zhang et al., 2011; Mao et al., 2014b; Branquet et al., 2012; 30) Han et al., 2013; 31) Xie et al., 2012, 2014; 32) Xia et al., 2013; Qin et al., 2011; 33) Mao et al., 2008; Qin et al., 2011; 34) Peng et al., 2013.

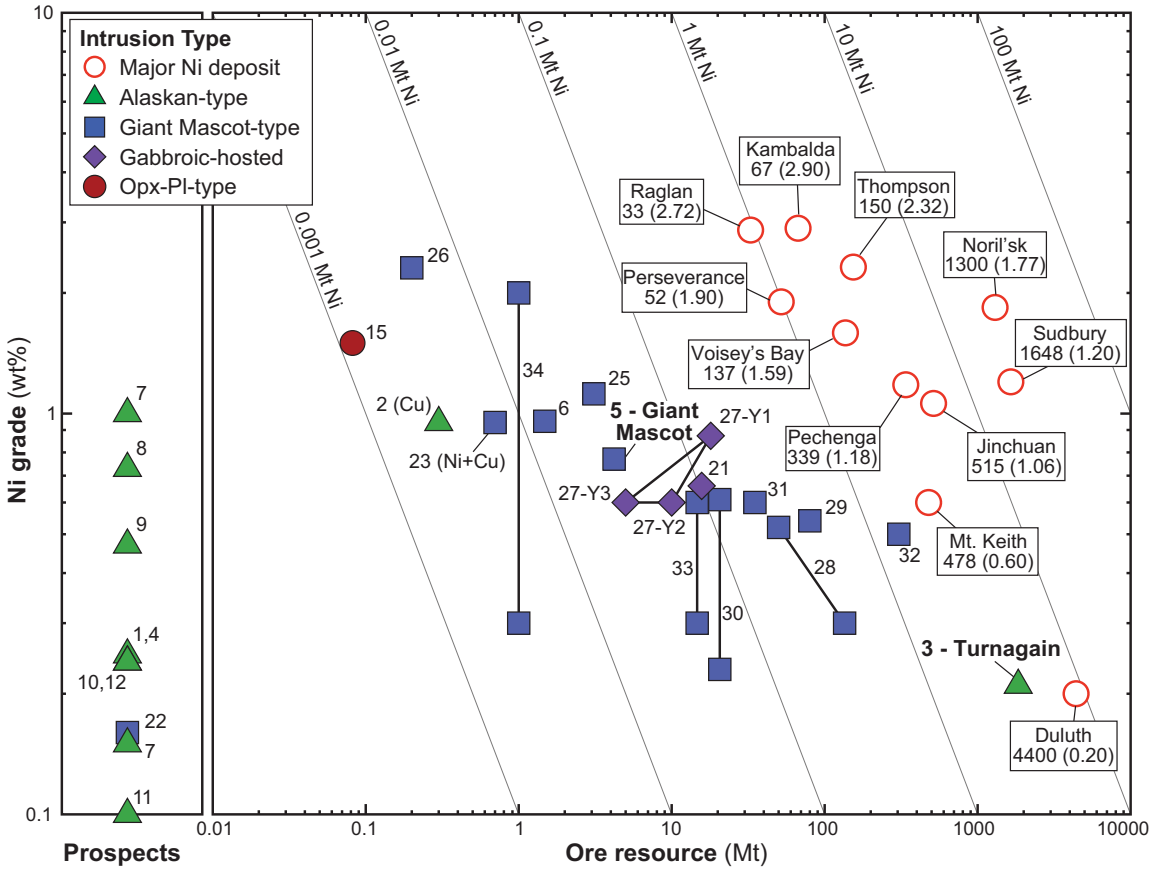

Figure 2. Ni grade in weight percent (wt%) versus ore tonnage in million metric tonnes (Mt) for the convergent-margin Ni-Cu±PGE deposits/prospects listed in Table 1 compared to world-class Ni-sulphide deposits (modified from Naldrett, 2010). Labels for major deposits denote tonnage (Mt) and wt% Ni grade (in brackets); numbered deposits and symbols correspond to those in Table 1 and Figure 1, respectively; diagonal lines represent contained Ni metal (note logarithmic scale).

sions in the Central Asian Orogenic Belt, they are regarded by some authors as "post-orogenic" (i.e. syn- or post-collisional) and are thought to be related to decompression melting of upwelling mantle asthenosphere that has been contaminated by a subduction component (Li et al., 2012; Sun et al., 2013a; Xia et al., 2013). Others consider these intrusions the result of a short-lived extensional event within the orogen generated by mantle plume activity (Zhang et al., 2010; Su et al., 2013). In the case of the Early Carboniferous (ca. 341 Ma) Aguablanca Ni-Cu-PGE deposit, which is Europe's only nickel mine, and the nearby Tejadillas prospect (ca. 336 Ma) in Spain, geochronological and geochemical data support the concept of an Andean-style convergent margin with a transpressional magmatic arc, whereas geophysical evidence has been used to invoke a mantle plume origin for the mineralized intrusions (Casquet et al., 2001; Tornos et al., 2001; Piña et al., 2006, 2010, 2012).

A plot of grade versus tonnage (Fig. 2) shows that significant Ni metal resources are contained in deposits formed in convergent-margin settings. Low-grade Ni-sulphide mineralization in the Turnagain Alaskan-type intrusion ranks among the top ten largest deposits in the world in terms of contained Ni metal, constituting a total resource of ~1842 Mt of ore with an average grade of 0.21 wt% Ni and 0.013 wt% Co (Mudd and Jowitt, 2014). Some of the largest Ni-Cu±PGE deposits being mined in China today are found in the accreted island arc terranes of the Central Asian Orogenic Belt, examples of which include the Kalatongke mine with ores grading ~0.6–0.9 wt% Ni and 1.1–1.4 wt% Cu; the 135 Mt Huangshandong deposit with a grade of 0.30 wt% Ni and 0.16 wt% Cu; and neighbouring Huangshanxi ores at 80 Mt with an average grade of 0.54 wt% Ni and 0.30 wt% Cu (Table 1). The total Ni metal resource for magmatic Ni-Cu sulphide deposits in the Huangshandong-Huangshanxi district alone approximates one million metric tonnes (Mao et al., 2008).

CLASSIFICATION: BACK TO THE FUTURE

Alaskan-type (Ural-Alaskan or concentrically zoned) intrusions in convergent-margin settings are well documented (e.g. Himmelberg and Loney, 1995; Nixon et al., 1997; Johan, 2002). The classic petrological studies of Taylor and Noble (1960), Noble and Taylor (1960),

Taylor (1967), and Irvine (1974) were influenced by a concentric zonation of rock types in the larger bodies. They defined Alaskan-type intrusions as a distinctive suite of ultramafic(±gabbroic) rocks characterized by peridotite (dunite-wehrlite) in the core, passing outward into olivine clinopyroxenite, clinopyroxenite and hornblendite ± gabbro at the margin. The principal minerals forming the ultramafic rocks are olivine (+minor chromite) and clinopyroxene with magnetite and hornblende occurring in clinopyroxenite and hornblendite; orthopyroxene is typically absent and plagioclase is extremely rare. Cumulus textures are common and provide ample evidence for differentiation by crystal fractionation and mineral concentration processes. In general, Alaskan-type intrusions are considered to occur in sulphide-poor magmatic environments and are known primarily for their dunite-hosted, chromitite-PGE mineralization that provides most of the world's important platinum placer deposits (e.g. Tulameen, British Columbia, Nixon et al., 1990; Johan, 2002; Weiser, 2002).

Modern "petrotectonic" classification schemes for Ni-sulphide deposits tend to focus on the nature of parental magmas associated with rocks that host the deposits and their plate tectonic setting (e.g. Naldrett, 2011). Since cumulus and postcumulus minerals provide information regarding the nature of parental magmas and liquid line of descent, we propose a mineralogical framework to distinguish different types of ultramafic-mafic intrusions in convergent-margin settings.

Modal analyses for ultramafic rocks from two well known Alaskan-type intrusions, Duke Island and Tulameen, and the Giant Mascot intrusion are distinct on the International Union of Geological Sciences (IUGS) classification scheme (Fig. 3). Alaskan-type intrusions lack orthopyroxene and fall exclusively along the olivine-clinopyroxene (Ol-Cpx) join in the hornblende-free plot; hornblende-bearing rocks are predominantly olivine-hornblende clinopyroxenite, hornblende clinopyroxenite, clinopyroxene hornblendite and hornblendite, and minor hornblende wehrlite (Fig. 3b). In contrast, the majority of ultramafic rocks at Giant Mascot, including those hosting Ni-sulphide ores, are hornblende harzburgite, hornblende websterite, two-pyroxene hornblendite, and hornblendite (including plagioclase-bearing pyroxenite), and minor hornblende dunite, olivine-hornblende pyroxenite, and hornblende orthopyroxenite (Fig. 3c). We have used these mineralogical traits to identify orthopyroxene-free Alaskan-type (*sensu stricto*) and orthopyroxene-rich Giant Mascot(GM)-type intrusions that host magmatic Ni-Cu±PGE sulphide mineralization (Table 1). These affiliations rely strongly on petrographic descriptions of the ultramafic rocks. Mineralized gabbroic intrusions in convergent-margin settings that appear to lack an ultramafic component (e.g. Kalatongke, Table 1) or carry unmineralized ultramafic inclusions (e.g. Aguablanca, Table 1) are designated as "gabbroic". In addition, certain ultramafic-mafic suites in the Portneuf-Mauricie Domain, a Proterozoic island arc terrane (Sappin et al., 2009, 2012), that co-crystallized plagioclase and amphibole after orthopyroxene, are provisionally distinguished as a separate orthopyroxene-plagioclase group (Opx-Pl, Table 1).

IMPLICATIONS OF THE MINERALOGICAL CLASSIFICATION

A number of mineralized ultramafic-mafic intrusions that have been documented as Alaskan-type in the literature have a clear GM-type affiliation. These include Gabbro Akarem and Genina Gharbia in Egypt (Helmy and Mogessie, 2001; Helmy and El Mahallawi, 2003; Helmy, 2004) and many intrusions in the Central Asian Orogenic Belt (Xiao et al., 2004, 2010; Table 1). Our reclassification has no impact on paleotectonic interpretations, but may have an important bearing on the interpretation of the petrogenetic history of a given intrusion, and thus critical factors that lead to the formation of an economic magmatic sulphide deposit.

The mineralogical affiliations distinguished above are taken to reflect important petrogenetic variables such as the composition of parental magma, and/or pressure and water fugacity (fH_2O) conditions of crystallization. Previous studies of magmatic Ni-Cu±PGE deposits have shown that parental magma compositions believed to be consistent with the nature and order of crystallization of cumulus phases include (1) moderately magnesian basalt (e.g. ~6–8.5 wt% MgO at Kalatongke: Li et al., 2012); (2) high-MgO basalt (e.g. ~9–13 wt% MgO at Huangshandong: Mao et al., 2014a; Huangshanxi: Mao et al., 2014b; Hongqiling No. 7: Wei et al., 2013; and Erhongwa: Sun et al., 2013b); and (3) for those intrusions particularly enriched in orthopyroxene, a "boninitic" parent has been proposed (e.g. Erbutu: Peng et al., 2013; and the recently documented Xiarihamu intrusion: Li et al., 2015). Due to the presence of hornblende±phlogopite, all authors conclude that parent magmas feeding the intrusions are hydrous, which reduces the stability of plagioclase relative to olivine and pyroxene in the melts. High modal proportions of orthopyroxene may indicate crustal contamination, which potentially has links to early sulphide saturation and ore-forming processes, as explored in the case studies summarized below.

GIANT MASCOT

Studies of the Giant Mascot Ni-Cu-PGE deposit, which is the only significant nickel deposit ever mined in

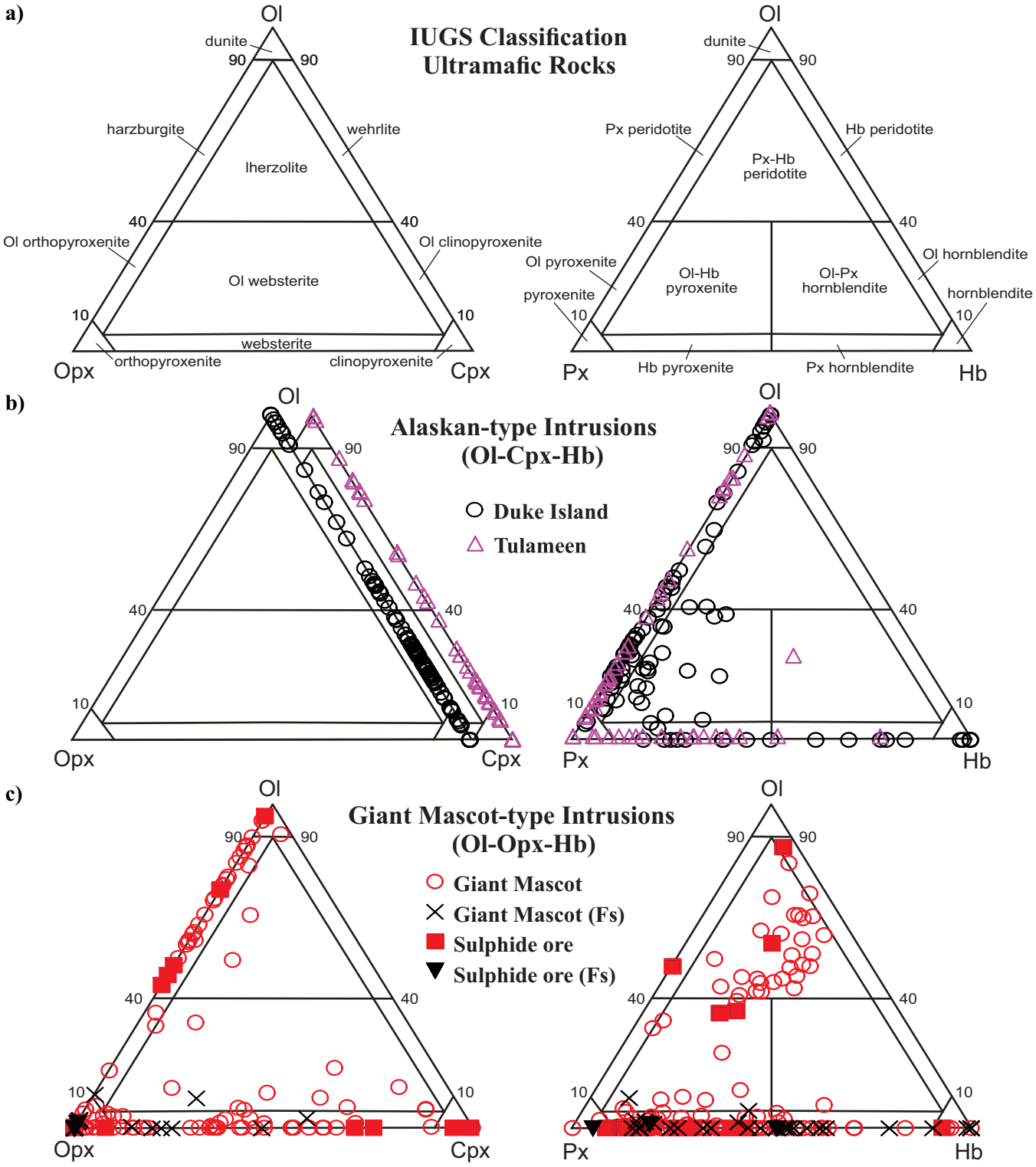

Figure 3. Modal analyses of selected ultramafic-mafic intrusive suites plotted in the IUGS classification scheme: **a)** International Union of Geological Sciences (IUGS) classification of ultramafic rocks (vol%); **b)** Duke Island (Irvine, 1959, Table 7; 1974, Table 18B) and Tulameen (Findlay, 1963, Appendices I and III) Alaskan-type intrusions with characteristic orthopyroxene-absent mineral assemblages; **c)** Giant Mascot ultramafic suite characterized by orthopyroxene-rich, feldspar-free and feldspar(Fs)-bearing (Fs <10%) ultramafic rocks and magmatic Ni-Cu sulphide ores (Muir, 1971, Appendix 1) . Mineral abbreviations: Cpx = clinopyroxene; Hb = hornblende; Ol = olivine; Opx = orthopyroxene; Px = pyroxene.

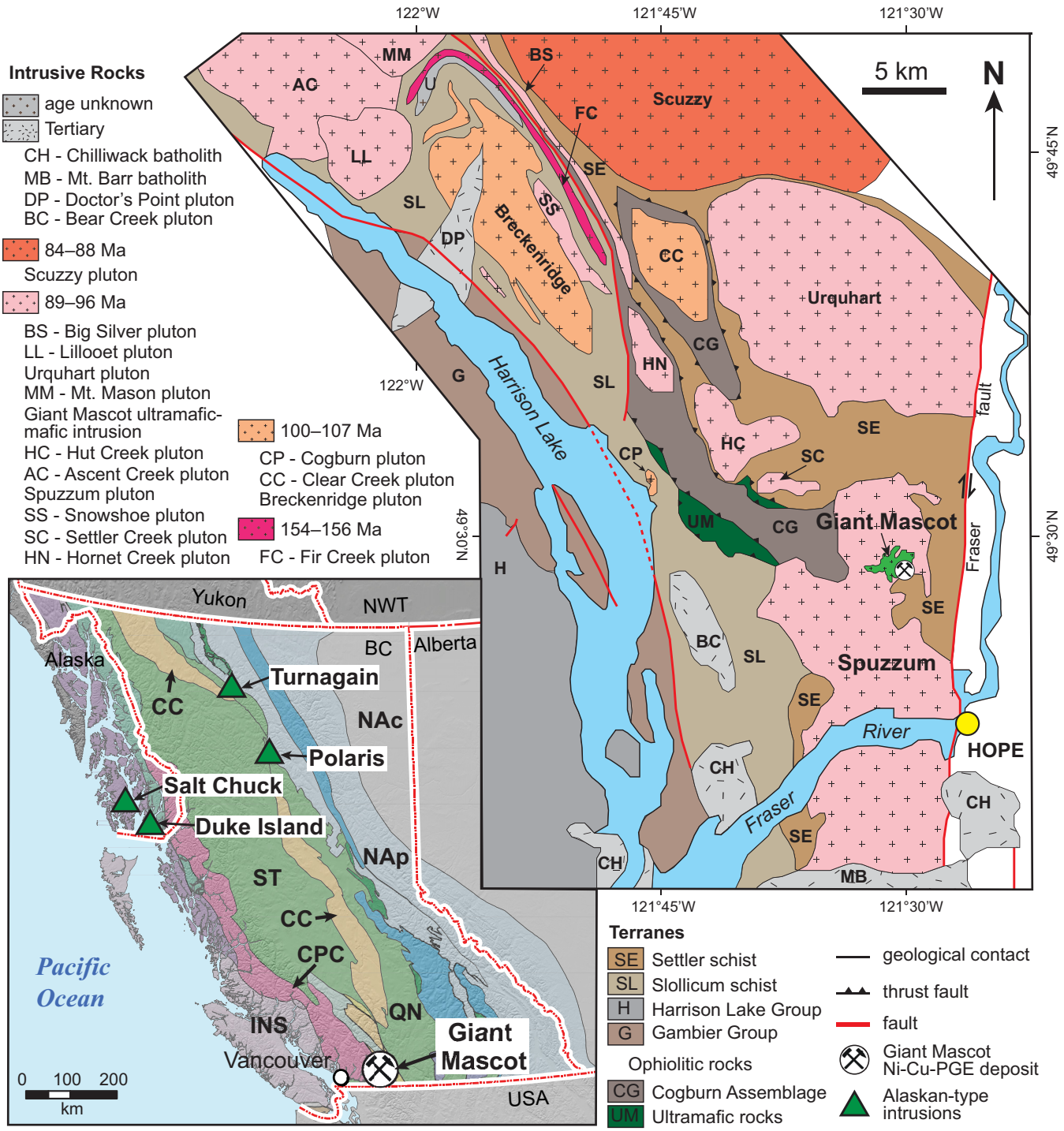

Figure 4. Location of sulphide-rich ultramafic-mafic intrusions in British Columbia and southeastern Alaska (inset) and geology of the Harrison Lake region showing the location of the Giant Mascot ultramafic intrusion and associated Ni-Cu-PGE deposit (after Manor et al., 2015a). Inset shows location of Alaskan-type intrusions referenced in the text and Table 1, and tectonic elements of the northern Cordillera: INS = Insular terranes (Alexander-Wrangellia); arc terranes of Quesnellia (QN) and Stikinia (ST); and Cache-Creek-Bridge River (CC) oceanic terranes; CPC = Coast Plutonic Complex; NAc = North America craton and cover; Nap = North America platform.

British Columbia (1958–1974; Table 1), build upon the pioneering work of Aho (1954, 1956). The deposit is hosted by the Giant Mascot ultramafic intrusion situated at the southeastern margin of the Coast Plutonic Complex (Fig. 4). The ultramafic body forms a small elliptical plug (3 x 1.3 km) intruding amphibolite-facies metasedimentary rocks of the Upper Triassic Settler schist and Late Cretaceous Spuzzum pluton (Fig. 5). A crude zonation of ultramafic lithologies has been mapped ranging from an olivine-rich core (dunite-peri-

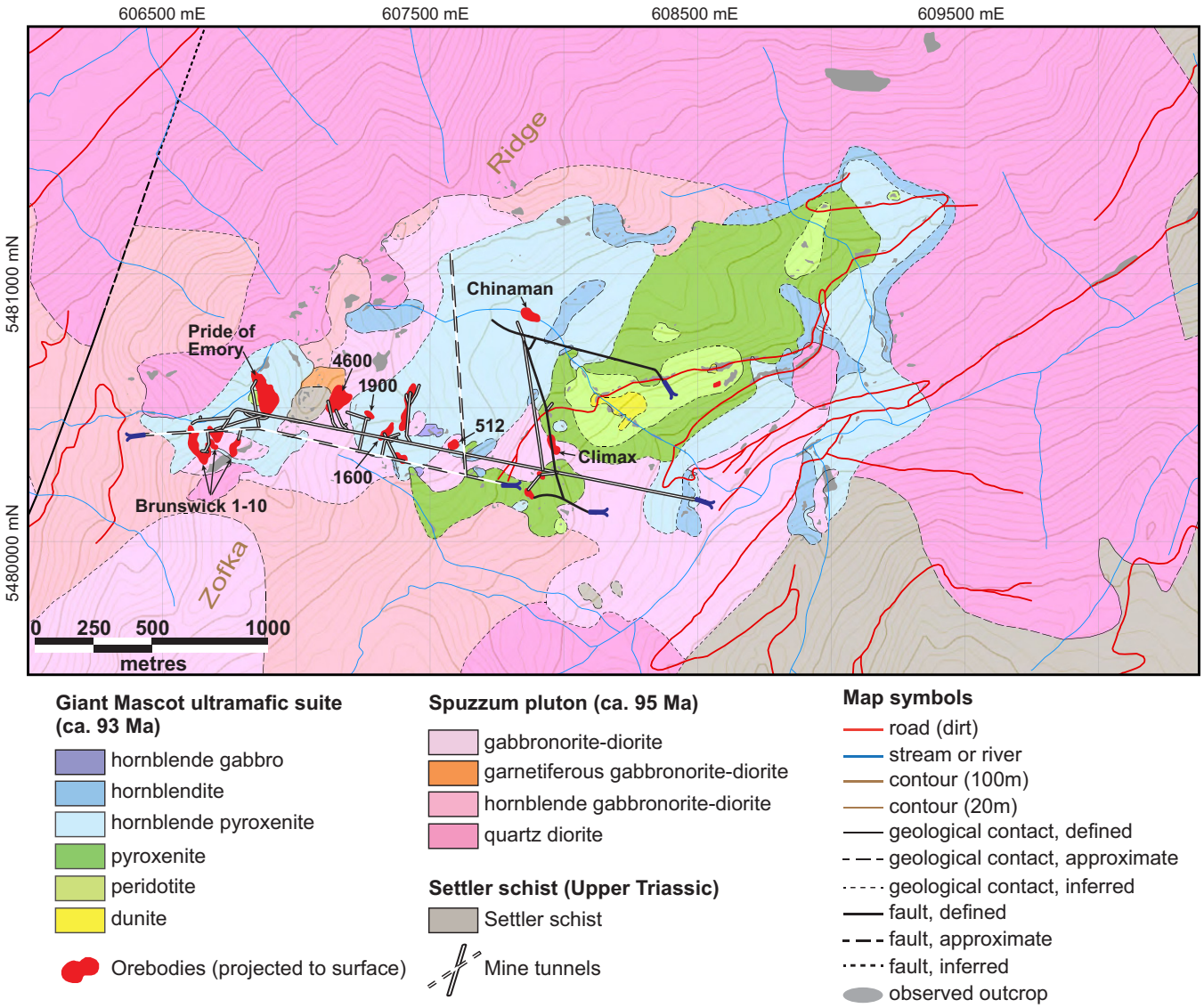

Figure 5. Geology of the Late Cretaceous (ca. 93 Ma) Giant Mascot ultramafic intrusion and surrounding rocks of the Late Cretaceous (ca. 95 Ma) Spuzzum pluton and Upper Triassic Settler schist (after Manor et al., 2015a). Orebodies and mine tunnels shown projected to surface and important orebodies are labeled (projection is NAD83 UTM Zone 10).

dotite) through pyroxenite to a thin, discontinuous rim of hornblendite and hornblende gabbro (Figs. 3, 5; Manor et al., 2014, 2015a). Chemical abrasion-isotope dilution-thermal ionization mass spectrometry (CA-ID-TIMS) U-Pb and $^{40}Ar/^{39}Ar$ geochro-nology on zircon and hornblende/biotite, respectively, has established the Giant Mascot ultramafic suite as Late Cretaceous (ca. 93 Ma) and the Spuzzum diorite as slightly older, but statistically distinct (ca. 95 Ma: Manor, 2014).

Structure of Sulphide Orebodies

The main locus of mineralization at Giant Mascot is oriented at N70°E, passing through Zofka Ridge (Brunswick to Climax orebodies, Fig. 5). The Ni-sulphide ore shoots form steeply plunging, pipe-like and lensoid structures, and atypical, steeply dipping tabular bodies that are ~5–75 m long, ~5–30 m wide and extend ~15–350 m in depth (Manor et al., 2015a). Orebodies are classified as zoned or unzoned, based primarily on textures of the ores (Aho, 1954, 1956). Zoned orebodies are concentrically zoned with disseminated to net-textured sulphides surrounding massive ore, where mineralization is confined to olivine-rich host rocks (dunite and peridotite). Unzoned orebodies are predominantly lensoid to tabular structures containing semimassive to massive mineralization. All orebodies are associated with olivine-bearing ultramafic rocks. We follow the original descriptions of Aho (1954, 1956) and interpret the Giant Mascot orebodies to represent subvertical crustal conduits through which multiple magma pulses ascended. This is evidenced by sharp lithological contacts, reversely zoned ore shoots cored by barren peridotite, and arcuate ore lenses pos-

sibly formed by collapse of partially solidified wall-rock cumulates (Manor et al., 2015a).

Ni-Cu-PGE Sulphide Mineralization

Sulphides at Giant Mascot exhibit orthomagmatic textures involving disseminated, net-textured, semimassive, and massive ores, and local Cu-rich veins. The principal base-metal sulphide minerals are pyrrhotite (both monoclinic and hexagonal varieties), pentlandite, chalcopyrite, minor pyrite, and trace amounts of troilite (exsolution flames in pyrrhotite), violarite and polydymite. Sulpharsenide minerals (e.g. gersdorffite, cobaltite, nickeline) are commonly associated with platinum group telluride or bismuthotelluride minerals (e.g. merenskyite, moncheite, palladian melonite), rare arsenide (sperrylite, hollingworthite) and precious metal minerals (hessite, altaite: Manor et al., 2014). The mineralogical and textural relationships between platinum group minerals and sulphide in Giant Mascot ores suggest that PGE were initially collected by an immiscible sulphide liquid and subsequently fractionated and crystallized from a semimetal-rich melt (Manor et al., 2014).

Platinum group elements in the ores are characterized by variable concentrations that define two geographic groupings: iridium-group PGE (IPGE: Ir, Ru) are depleted in the western part of the mineralized zone (WMZ: Pride of Emory and Brunswick cluster; Fig. 5), whereas IPGE are enriched in the central and eastern orebodies (EMZ: all orebodies east of and including 4600; Fig. 5). These differences broadly correlate with the texture and base-metal tenor of sulphide ores (i.e. concentration in 100 wt% sulphide equivalent) such that higher tenor sulphides are more common in disseminated ores of the EMZ, whereas moderate tenor sulphides are more typical of net-textured and massive ores in the WMZ (Manor et al., 2015a). The differences in IPGE concentrations and mantle-normalized enrichment patterns indicate the presence of two distinct parental magmas (Manor et al., in press). Modeling results detailed by Manor et al. (in press) indicate that disseminated ores represent sulphide melt with upgraded metal contents due to extensive interaction and scavenging of metals from silicate melt, whereas net-textured sulphides with low-PGE but high-Cu concentrations, originated from a more fractionated monosulphide solid solution.

Parental Magma and Ore-Forming Mechanisms

Olivine compositions in barren and mineralized ultramafic rocks of the Giant Mascot intrusion range from Fo_{80} to Fo_{89}, with the greatest variation in nickel contents (386–3859 ppm Ni) occuring in mineralized peridotite and pyroxenite (Manor, 2014). Petrographic evidence and modeling results indicate that anomalously high-Ni content in olivine appears to reflect subsolidus equilibration with Ni-rich sulphide liquid, which appeared early in the crystallization history (<20% crystallized) of a moderately magnesian (~9 wt% MgO) parental magma (Manor et al., in press). From the partitioning of Ni and Fe between olivine and sulphide liquid, we determined that the oxygen fugacity of the system at the time of formation of the Giant Mascot ores was relatively reduced (~1 log unit above the quartz-fayalite-magnetite buffer; ΔQFM+1), similar to sulphide deposits formed worldwide in less oxidizing tectonic environments (e.g. rift-related settings). The mechanism for reduction of these parental arc magmas is considered to be assimilation of graphite from the Settler schist. Sulphur isotopic compositions of mineralized samples occupy a narrow range of $\delta^{34}S$ values (-3.4 to -1.3‰) that overlap with those determined for pyrite in graphitic Settler schist ($\delta^{34}S$ = -5.4 to -1.2‰), and are permissive of assimilation of crustal sulphur as a principal mechanism for sulphide saturation (Manor et al., in press). Independent evidence for addition of silica to the parental magma, which also serves to promote sulphide saturation (e.g. Irvine, 1975), is found as abundant xenoliths of diorite and Settler schist, and zircon xenocrysts in Giant Mascot pyroxenite derived from the Spuzzum pluton (Manor et al., 2015a).

TURNAGAIN

The Turnagain Alaskan-type ultramafic-mafic intrusion is hosted in Late Paleozoic metasedimentary and metavolcanic rocks of the Yukon-Tanana terrane in northern British Columbia (Figs. 4, 6). Our study has focused primarily on the youngest hornblende-bearing ultramafic intrusive phase with an anomalous Cu-PGE signature, the DJ/DB zone, and augments previous investigations of the geology and significant Ni-Cu-Co sulphide resource of the Horsetrail zone (Figs. 4, 6; Clark, 1975, 1980; Nixon et al., 1989; Nixon, 1998; Scheel, 2007; Scheel et al., 2009). Below we summarize some aspects of the earlier work in order to place our current studies in context.

Recent fieldwork has confirmed that the elongate (8.5 x 3 km) Turnagain ultramafic body is a composite intrusion with at least four distinct intrusive phases, comprising dunite and wehrlite(±phlogopite), clinopyroxenite(±olivine±hornblende±phlogopite/biotite± magnetite), and minor hornblendite with a dioritic intrusion in the core (Fig. 6). U-Pb Thermal Ionization Mass Spectrometry (TIMS) and $^{40}Ar/^{39}Ar$ geochronology on zircon/titanite and hornblende/phlogopite, respectively, have yielded an Early Jurassic age (ca. 190 Ma) for the intrusion as a whole (Scheel, 2007).

The DJ/DB prospect is hosted by a poorly exposed, younger ultramafic intrusion centred 2.5 km northwest

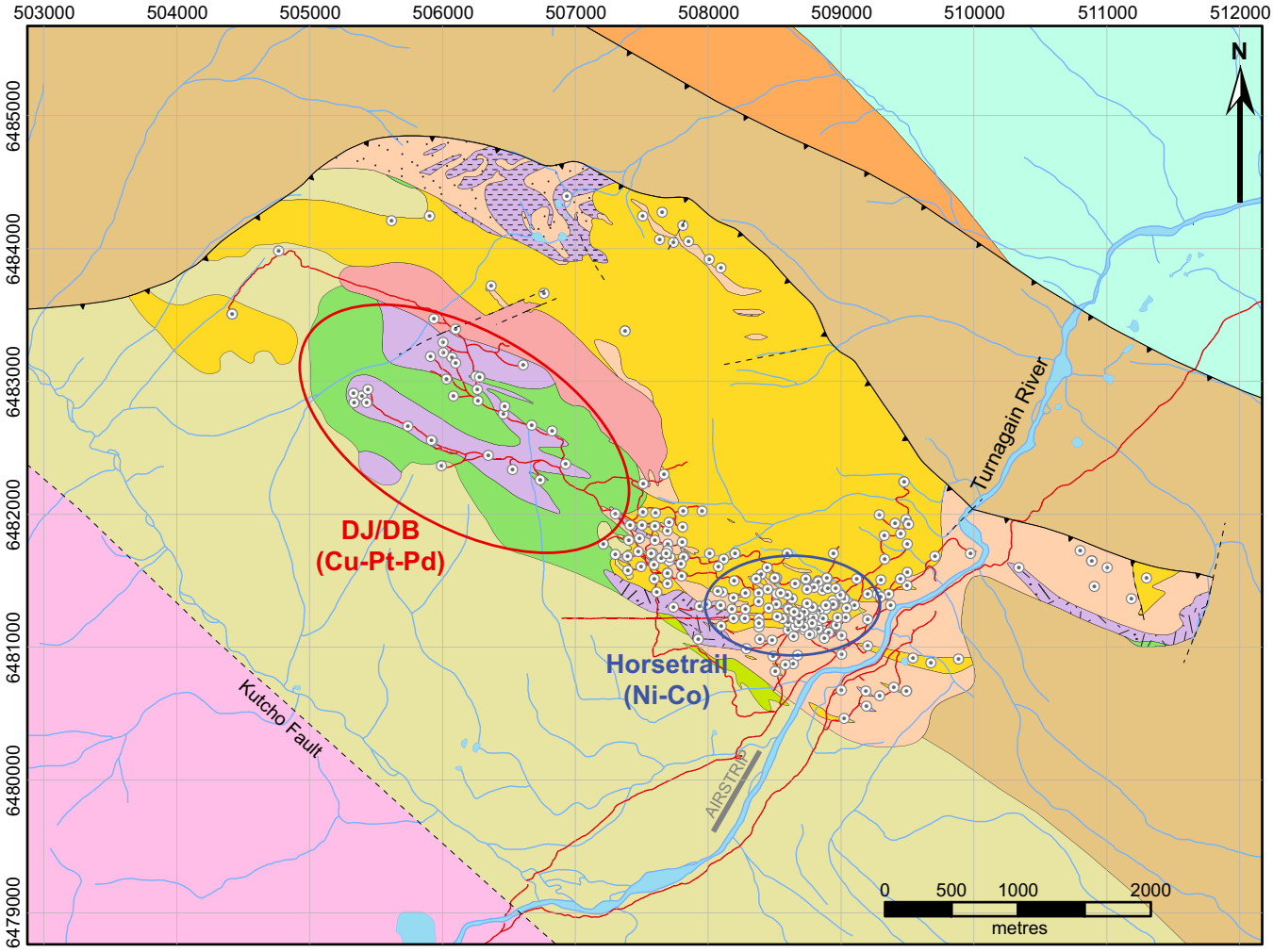

Figure 6. Geology of the Early Jurassic (ca. 190 Ma) Turnagain ultramafic intrusion and host rocks showing the Cu-PGE-enriched DJ/DB zone and the Ni-Co-enriched Horsetrail zone, which is the main Ni-sulphide ore resource (modified from Nixon et al., 2012; projection is NAD83 UTM Zone 9).

of the Horsetrail zone (Fig. 6). The main lithologies are hornblende(±biotite) clinopyroxenite, magnetite-rich (<20 vol%) clinopyroxenite, olivine clinopyroxenite, and hornblendite with minor wehrlite, locally cut by veins of hornblende- or biotite-rich pegmatite, and dioritic dykes of the younger Phase 4 pluton (Fig. 6). The rocks are fine to very coarse grained, interlayered with sharp to gradational (>10 m) contacts, and thicknesses of the different rock types in drill core range from 15 to 155 m (Jackson-Brown et al., 2014).

Ni-Cu-PGE Sulphide Mineralization

The large tonnage, low-grade Ni-sulphide resource defined by Hard Creek Nickel Corporation (Table 1) is hosted by olivine-clinopyroxene cumulates (dunite-wehrlite with minor olivine clinopyroxenite) in the

Horsetrail zone (Fig. 6). Sulphide concentrations (~2–20 vol%) are commonly disseminated with localized net-textures and thin (<20 cm), laterally discontinuous semimassive zones. The principal sulphide minerals are pyrrhotite (~90 vol%), pentlandite with minor chalcopyrite and pyrite, accompanied by trace amounts of violarite, bornite, millerite, molybdenite, valleriite, and mackinawite (Clark, 1975). PGE concentrations in mineralized samples reach ~4 g/t Pt+Pd but are typically much less (<100 ppb) and sulphide-rich samples overall have an average Pt/Pd ratio of ~0.9 and a median ratio of approximately 1 (Hard Creek Nickel Corporation, unpub. data; Scheel, 2007).

The abundance of sulphides in the DJ/DB zone varies greatly (0–55 vol%) and textures range from disseminated and net-textured to locally semimassive. PGE abundances in mineralized samples reach up to 4.9 g/t Pd+Pt with average Pd/Pt ~1 (Jackson-Brown et al., 2014, 2015, in prep). Mineralogical studies of mineralized samples from drill core have been conducted by Jackson-Brown et al. (2014). The principal base-metal sulphides are pyrrhotite and chalcopyrite with minor pyrite and pentlandite, and accessory millerite, sphalerite, bornite, siegenite, marcasite, galena, and molybdenite. Sulpharsenide, sulphantimonide, and arsenide minerals (<1 vol%; <100 μm) include cobaltite, gersdorffite-ullmannite, tucekite, hauchecornite, and nickeline. A variety of platinum group minerals (<40 μm) have been identified (all are platinum and/or palladium species), including sperrylite, sudburyite, palladian melonite, ungavaite, hongshiite, genkinite, and testibiopalladite.

Parental Magma and Ore-Forming Mechanisms

Investigations of the composition of parental magmas and ore-forming processes at Turnagain are currently underway (Jackson-Brown, in prep.). However, some observations from previous work are pertinent here.

The petrology of rocks from the Turnagain Alaskan-type intrusion indicates that it was formed by the successive emplacement and crystallization of primitive, Mg-rich hydrous magma in a subduction setting (Clark, 1975, 1980; Scheel, 2007). Evidence for the primitive nature of the parental magma is found in the most magnesian olivine ($Fo_{92.5}$) in dunite that has not re-equilibrated with chromite. The hydrous nature of the parental magma is supported by (1) primary interstitial phlogopite in olivine-clinopyroxene cumulates; (2) late interstitial to cumulus hornblende in the younger part of the composite intrusion; and (3) late appearance of plagioclase as an interstitial or cumulus phase relative to clinopyroxene and hornblende.

The unusual occurrence of abundant magmatic sulphide in the Turnagain Alaskan-type intrusion is related to the graphitic and sulphidic nature of its wall rocks. Sulphide minerals from the Turnagain intrusion have $\delta^{34}S$ values from +1‰ (i.e. mantle-like) to -9.7‰, shifted towards the composition of pyrite (-17.9‰) from the enclosing graphitic phyllite (Scheel, 2007). These results indicate that crustal sulphur was added to the Turnagain parental magma and presumably aided in achieving sulphide saturation. Inclusions of partially digested, carbonaceous phyllite are abundant in drill core from the Horsetrail zone, and graphite is commonly observed in ultramafic rocks in the mineralized zones. The presence of graphite indicates that, at least locally, the Turnagain parental magma may have had fO_2 near the carbon-carbon monoxide buffer (ΔFMQ = -1) at upper crustal pressures and hydrous conditions. Therefore, the phyllite inclusions acted as both a sulphur source and a reducing agent, allowing the Turnagain intrusion to reach early sulphide saturation in an otherwise oxidizing subduction zone environment.

IMPLICATIONS FOR EXPLORATION

The economic potential of magmatic Ni-Cu-PGE mineralization hosted by a diverse suite of ultramafic-mafic intrusions in convergent-margin tectonic settings is presently underestimated. The prime example of this deposit type in the Canadian Cordillera is the large tonnage, low-grade Ni sulphide endowment of the Turnagain Alaskan-type intrusion, which is currently subeconomic. Other prospects are hosted by Giant Mascot-type intrusions in the southern Coast Plutonic Complex and include the Sable (BC MINFILE 092HNW077), KATT (092GNE044), Jason (092HNW076), and AL (092HNW040), as well as others in the vicinity of the former Giant Mascot mine (and see Pinsent, 2002). Exploration potential in other subduction-related settings is underscored by the recently discovered Xiarihamu Ni-sulphide deposit in the East Kunlun orogenic belt at the northern margin of the Tibetan Plateau, western China. Despite its current subeconomic status, this magmatic Ni-Cu sulphide deposit contains 100 Mt of ore at an average grade of 0.8 wt% Ni and 0.1 wt% Cu, which makes it one of the 20 largest magmatic Ni deposits in the world (Li et al., 2015). Like most of the other deposits in convergent-margin settings in China, ultramafic host rocks have Giant Mascot-type affinity (Table 1).

Factors that appear fundamental to the genesis of potentially economic magmatic Ni-Cu±PGE deposits in subduction-related settings are similar to those that determine world-class Ni deposits in other tectonic environments. These include (1) primitive MgO- and Ni-rich parental magmas; (2) favourable wall rocks that can contribute crustal sulphur and/or reductants to relatively oxidized and hydrous arc magmas, thereby

promoting early sulphide saturation and formation of an immiscible sulphide melt; and (3) restrictive conduit systems capable of channelling new influxes of metal-laden parent magma and serving as suitable traps for the collection of upgraded Ni-Cu-PGE-enriched sulphides.

ACKNOWLEDGEMENTS

Funding for this collaborative project is provided by Natural Resources Canada through the Geological Survey of Canada's Targeted Geoscience Initiative 4 (TGI-4) Nickel-Copper-PGE-Chrome Ore System Project, and the British Columbia Geological Survey. Additional funding was provided by Society of Economic Geologists, Canadian Foundation Graduate Student Research Grants awarded to Matthew Manor and Sarah Jackson-Brown in 2013, and an NSERC Discovery Grant to James Scoates. We thank Mark Jarvis and Tony Hitchins of Hard Creek Nickel Corporation for logistical support, and access to drill core and proprietary data. The manuscript benefited from a thorough review by Dr. Alex Zagorevski and editorial comments by Dr. Lawrence Aspler.

REFERENCES

Aho, A.E., 1954. Geology and ore deposits of the property of Pacific Nickel Mines near Hope, British Columbia; Ph.D. thesis, University of California, California, 148 p.

Aho, A.E., 1956. Geology and genesis of ultrabasic nickel-copper-pyrrhotite deposits at the Pacific Nickel Property, southwestern British Columbia; Economic Geology, v. 51, p. 441–481.

Ames, D.E. and Houlé, M.G., 2011. Overview of the Targeted Geoscience Initiative 4 Nickel-Copper-Platinum Group Elements-Chromium Project (2010–2015) — Mafic to Ultramafic Ore Systems: Footprint, Fertility and Vectors, *In:* Summary of Field Work and Other Activities 2011; Ontario Geological Survey, Open File Report 6270, p. 37-1 to 37-7.

Ames D.E., Dare S.A., Hanley, J.J. Hollings, P., Jackson, S., Jugo, P.J., Kontak, D., Linnen R., and Samson, I.M., 2012. Update on Research Activities in the Targeted Geoscience Initiative 4 Magmatic-Hydrothermal Nickel-Copper-Platinum Group Elements Ore System subproject: System Fertility and Ore Vectors, *In:* Summary of Field Work and Other Activities 2012; Ontario Geological Survey, Open File Report 6280, p. 41-1 to 41-11.

Branquet, Y., Gumiaux, C., Sizaret, S., Barbanson, L., Wang, B., Cluzel, D., Li, G., and Delaunay, A., 2012. Synkinematic mafic/ultramafic sheeted intrusions: emplacement mechanism and strain restoration of the Permian Huangshan Ni–Cu ore belt (Eastern Tianshan, NW China); Journal of Asian Earth Sciences, v. 56, p. 240–257. doi:10.1016/j.jseaes.2012.05.021.

Casquet, C., Galindo, C., Tornos, F., Velasco, F., and Canales, A., 2001. The Aguablanca Cu-Ni ore deposit (Extremadura, Spain), a case of synorogenic orthomagmatic mineralization: age and isotope composition of magmas (Sr, Nd) and ore (S); Ore Geology Reviews, v. 18, p. 237–250.

Clark, T., 1975. Geology of an ultramafic complex on the Turnagain River, northwestern British Columbia; Ph.D. thesis, Queen's University, Kingston, Ontario, 453 p.

Clark, T., 1980. Petrology of the Turnagain ultramafic complex, northwestern British Columbia; Canadian Journal of Earth Sciences, v. 17, p. 744–757. doi:10.1139/e80-071

Findlay, D.C., 1963. Petrology of the Tulameen ultramafic complex, Yale District, British Columbia; Ph.D. thesis, Queen's University, Kingston, Ontario, 415 p.

Gao, J.-F., Zhou, M.-F., Lightfoot, P.C., Wang, C.Y., and Qi, L., 2012. Origin of PGE-poor and Cu-rich magmatic sulfides from the Kalatongke deposit, Xinjiang, Northwest China; Economic Geology, v. 107, p. 481–506.

Gao, J.-F., Zhou, M.-F., Lightfoot, P.C., Wang, C.Y., Qi, L., and Sun, M., 2013. Sulfide saturation and magma emplacement in the formation of the Permian Huangshandong Ni-Cu sulfide deposit, Xinjiang, northwestern China; Economic Geology, v. 108, p. 1833–1848. doi:10.2113/econgeo.108.8.1833

Guillot, S., Hattori, K., Agard, P., Schwartz, S., and Vidal, O., 2009. Exhumation processes in oceanic and continental subduction contexts: a review, *In:* Subduction Zone Geodynamics, (ed.) S. Lallemand and F. Funiciello, F.; Springer, Berlin Heidelberg, p. 175–205.

Han, B., Ji, J., Song, B., Chen, L., and Li, Z., 2004. SHRIMP zircon U-Pb ages of Kalatongke No. 1 and Huangshandong Cu-Ni-bearing mafic-ultramafic complexes, North Xinjiang, and geological implications; Chinese Science Bulletin, v. 49, p. 2424–2429. doi:10.1007/BF03183432

Han, C., Xiao, W., Zhao, G., Su, B.-X., Sakyi, P.A., Ao, S., Wan, B., Zhang, J., and Zhang, Z., 2013. SIMS U-Pb zircon dating and Re-Os isotopic analysis of the Hulu Cu-Ni deposit, eastern Tianshan, Central Asian Orogenic Belt, and its geological significance; Journal of Geosciences, v. 58, p. 251–270. doi:10.3190/jgeosci.146

Helmy, H.M., 2004. Cu–Ni–PGE mineralization in the Genina Gharbia mafic–ultramafic intrusion, Eastern Desert, Egypt; The Canadian Mineralogist, v. 42, p. 351–370. doi:10.2113/gscanmin.42.2.351

Helmy, H.M. and Mogessie, A., 2001. Gabbro Akarem, Eastern Desert, Egypt: Cu–Ni–PGE mineralization in a concentrically zoned mafic–ultramafic complex; Mineralium Deposita, v. 36, p. 58–71.

Helmy, H.M. and El Mahallawi, M.M., 2003. Gabbro Akarem mafic-ultramafic complex, Eastern Desert, Egypt: a Late Precambrian analogue of Alaskan-type complexes; Mineralogy and Petrology, v. 77, p. 85–108. doi:10.1007/s00710-001-0185-9

Helmy, H.M., Ahmed, A.H., Kagami, A., and Arai, S., 2005. Sm/Nd and platinum-group element geochemistry of a late-Precambrian Alaskan-type complex from the Eastern Desert of Egypt, *In:* Proceedings; 10th International Platinum Symposium, Oulu, Finland, 2005, p. 101–104.

Helmy, H.M., Abd El-Rahman, Y.M., Yoshikawa, M., Shibata, T., Arai, S., Tamura, A., and Kagami, H., 2014. Petrology and Sm–Nd dating of the Genina Gharbia Alaskan-type complex (Egypt): Insights into deep levels of Neoproterozoic island arcs; Lithos, v. 198–199, p. 263–280. doi:10.1016/j.lithos.2014.03.028

Himmelberg, G.R. and Loney, R.A., 1995. Characteristics and petrogenesis of Alaskan-type ultramafic-mafic intrusions, southeastern Alaska; United States Geological Survey, Professional Paper 1564, 47 p.

Holt, S.P., Shepard, J.G., Thorne, R.L., Tolonen, A.W., and Fosse, E.L., 1948. Investigation of the Salt Chuck copper mine, Kasaan Peninsula, Prince of Wales Island, southeastern Alaska; United States Bureau of Mines, Report of Investigations 4358, 16 p.

Irvine, T.N., 1959. The ultramafic complex and related rocks of Duke Island, southeastern Alaska; Ph.D. thesis, California Institute of Technology, Pasadena, California, 320 p.

Irvine, T.N., 1974. Petrology of the Duke Island ultramafic complex, southeastern Alaska; Geological Society of America Memoirs, v. 138, 240 p.

Irvine, T.N., 1975. Crystallization sequences in the Muscox intrusion and other layered intrusions – II. Origin of chromitite layers and similar deposits of other magmatic ores; Geochimica et Cosmochimica Acta, v. 39, p. 991–1020.

Jackson-Brown, S., in prep. Origin of the Cu-PGE-rich sulphide mineralization in the DJ/DB zone of the Turnagain Alaskan-type intrusion, British Columbia; M.Sc. thesis, University of British Columbia, Vancouver, British Columbia.

Jackson-Brown, S., Scoates, J.S., Nixon, G.T., and Ames, D.E., 2014. Mineralogy of sulphide, arsenide, and platinum group minerals from the DJ/DB Zone of the Turnagain Alaskan-type ultramafic intrusion, north-central British Columbia, *In:* Geological Fieldwork 2013; British Columbia Ministry of Energy and Mines, British Columbia Geological Survey, Paper 2014-1, p. 157–168.

Jackson-Brown, S., Scoates, J.S., Nixon, G.T., and Ames, D.E., 2015, Preliminary observations of the geology, mineralogy and geochemistry of the DJ/DB zone of the Turnagain intrusion, north-central British Columbia; Geological Survey of Canada, Open File 7871.

Johan, Z., 2002. Alaskan-type complexes and their platinum-group-element mineralization, *In:* The Geology, Geochemistry, Mineralogy and Mineral Beneficiation of Platinum-Group Elements, (ed.) L.J. Cabri; Canadian Institute of Mining, Metallurgy and Petroleum, Special Volume 54, p. 669–719.

Li, C., Zhang, M., Fu, P., Qian, Z., Hu, P., and Ripley, E.M., 2012. The Kalatongke magmatic Ni–Cu deposits in the Central Asian Orogenic Belt, NW China: product of slab window magmatism?; Mineralium Deposita, v. 47, p. 51–67. doi:10.1007/s00126-011-0354-7

Li, C., Zhang, Z., Li, W., Wang, Y., Sun, T., and Ripley, E.M., 2015. Geochronology, petrology and Hf–S isotope geochemistry of the newly-discovered Xiarihamu magmatic Ni–Cu sulfide deposit in the Qinghai–Tibet plateau, western China; Lithos, v. 216-217, p. 224–240. doi:10.1016/j.lithos.2015.01.003

Loney, R.A. and Himmelberg, G.R., 1992. Petrogenesis of the Pd-rich intrusion at Salt Chuck, Prince of Wales Island; an early Paleozoic Alaskan-type ultramafic body; The Canadian Mineralogist, v. 30, p. 1005–1022.

Lü, L., Mao, J., Li, H., Pirajno, F., Zhang, Z., and Zhou, Z., 2011. Pyrrhotite Re–Os and SHRIMP zircon U–Pb dating of the Hongqiling Ni–Cu sulfide deposits in northeast China; Ore Geology Reviews, v. 43, p. 106–119. doi:10.1016/j.oregeorev.2011.02.003.

MacTavish, A.D., 1999. The mafic-ultramafic intrusions of the Atikokan-Quetico area, northwestern Ontario; Ontario Geological Survey, Open File Report 5997, 127 p.

Manor, M.J., 2014. Convergent margin Ni-Cu-PGE deposits: geology, geochronology, and geochemistry of the Giant Mascot magmatic sulphide deposit, Hope, British Columbia; M.Sc. thesis, University of British Columbia, Vancouver, British Columbia, 371 p.

Manor, M.J., Scoates, J.S., Nixon, G.T., and Ames, D.E., 2014. Platinum-group mineralogy of the Giant Mascot Ni-Cu-PGE deposit, Hope, BC, *In:* Geological Fieldwork 2013; British Columbia Ministry of Energy and Mines, British Columbia Geological Survey, Paper 2014-1, p. 141–156.

Manor, M.J., Wall, C.J., Nixon, G.T., Scoates, J.S., Pinsent, R.H., and Ames, D.E., 2014. Preliminary geology and geochemistry of the Giant Mascot ultramafic-mafic intrusion, Hope, southwestern British Columbia; Geological Survey of Canada Open File 7570, scale: 1:10 000 (also British Columbia Ministry of Energy and Mines, British Columbia Geological Survey, Open File 2014-03).

Manor, M.J., Wall, C.J., Friedman, R.M., Gabites, J., Nixon, G.T., Scoates, J.S., and Ames, D.E., 2015. Geology, geochronology and Ni-Cu-PGE orebodies of the Giant Mascot ultramafic intrusion, Hope, southwestern British Columbia; British Columbia Ministry of Energy and Mines, British Columbia Geological Survey, Geoscience Map 2015-01, scale: 1:10 000 (2 sheets).

Manor, M.J., Scoates, J.S., Nixon, G.T., and Ames, D.E., in press. The Giant Mascot Ni-Cu-PGE deposit, southwestern British Columbia: mineralized conduits and sulphide saturation mechanisms in a convergent margin tectonic setting: Economic Geology.

Mao, J.W., Pirajno, F., Zhang, Z.H., Chai, F.M., Wu, H., Chen, S.P., Cheng, L.S., Yang, J.M., and Zhang, C.Q., 2008. A review of the Cu–Ni sulphide deposits in the Chinese Tianshan and Altay orogens (Xinjiang Autonomous Region, NW China): Principal characteristics and ore-forming processes; Journal of Asian Earth Sciences, Geodynamics and Metallogeny of the Altaid Orogen, v. 32, p. 184–203. doi:10.1016/j.jseaes.2007.10.006

Mao, Y.-J., Qin, K.-Z., Li, C., and Tang, D.-M., 2014a. A modified genetic model for the Huangshandong magmatic sulfide deposit in the Central Asian Orogenic Belt, Xinjiang, western China; Mineralium Deposita, v. 50, p. 65–82. doi:10.1007/s00126-014-0524-5.

Mao, Y.-J., Qin, K.-Z., Li, C., Xue, S.-C., and Ripley, E.M., 2014b. Petrogenesis and ore genesis of the Permian Huangshanxi sulfide ore-bearing mafic-ultramafic intrusion in the Central Asian Orogenic Belt, western China; Lithos, v. 200–201, p. 111–125. doi:10.1016/j.lithos.2014.04.008

Mota-e-Silva, J., Ferreira Filho, C.F., Bühn, B., and Dantas, E.L., 2011. Geology, petrology and geochemistry of the "Americano do Brasil" layered intrusion, central Brazil, and its Ni–Cu sulfide deposits; Mineralium Deposita, v. 46, p. 57–90. doi:10.1007/s00126-010-0312-9.

Mowat, U.G., 2013. Sampling of the Star 5, 6, 7, 10 and 12 claims; British Columbia Assessment Report 34297, 111 p.

Mudd, G.M. and Jowitt, S.M., 2014. A detailed assessment of global nickel resource trends and endowments; Economic Geology, v. 109, p. 1813–1841.

Muir, J.E., 1971. A study of the petrology and ore genesis of the Giant Nickel 4600 orebody, Hope, B.C.; M.Sc. thesis, University of Toronto, Toronto, Ontario, 134 p.

Naldrett, A.J., 2010. Secular variation of magmatic sulfide deposits and their source magmas; Economic Geology, v. 105, p. 669–688.

Naldrett, A.J., 2011. Fundamentals of magmatic sulfide deposits; Reviews in Economic Geology, v. 17, p. 1–50.

Nilson, A.A., 1981. The nature of the Americano do Brasil mafic-ultramafic complex and associated sulfide mineralization, Goias, Brazil; Ph.D. thesis, University of Western Ontario, London, Ontario, 488 p.

Nixon, G.T., 1998. Ni-Cu sulfide mineralization in the Turnagain Alaskan-type complex; a unique magmatic environment, *In:* Geological Fieldwork 1997; Ministry of Employment and Investment, British Columbia Geological, Survey Paper 1998-1, p. 18.1–18.11.

Nixon, G.T., Ash, C.A., Connelly, J.N., and Case, G., 1989. Geology and noble metal geochemistry of the Turnagain ultramafic complex, northern British Columbia; British Columbia Ministry of Energy, Mines and Petroleum Resources, British Columbia Geological Survey, Open File 1989-18, scale: 1:16 000.

Nixon, G.T., Cabri, L.J., and Laflamme, J.H.G., 1990. Platinum-group-element mineralization in lode and placer deposits asso-

ciated with the Tulameen Alaskan-type complex, British-Columbia; The Canadian Mineralogist, v. 28, p. 503–535.

Nixon, G.T., Hammack, J.L., Ash, C.A., Cabri, L.J., Case, G., Connelly, J.N., Heaman, L.M., Laflamme, J.H.G., Nuttall, C., Paterson, W.P.E., and Wong, R.H., 1997. Geology and platinum-group-element mineralization of Alaskan-type ultramafic-mafic complexes in British Columbia; Ministry of Employment and Investment, British Columbia Geological Survey, Bulletin 93, 141 p.

Nixon, G.T., Hitchins, A.C., and Ross, G.P., 2012. Geology of the Turnagain ultramafic intrusion, northern British Columbia; British Columbia Ministry of Energy and Mines, British Columbia Geological Survey, Open File 2012-05, scale: 1: 10 000.

Noble, J.A. and Taylor, H.P., Jr., 1960. Correlation of the ultramafic complexes of southeastern Alaska with those of other parts of North America and the world; Report of the International Geological Congress, Part 13, p. 188–197.

Parker, J.R., 1998. Geology of nickel-copper-chromite deposits and cobalt-copper deposits at Werner-Rex-Bug lakes, English River Subprovince, northwestern Ontario; Ontario Geological Survey, Open File Report 5975, 178 p.

Peng, R., Zhai, Y., Li, C., and Ripley, E.M., 2013. The Erbutu Ni-Cu deposit in the Central Asian Orogenic Belt: a Permian magmatic sulfide deposit related to boninitic magmatism in an arc setting; Economic Geology, v. 108, p. 1879–1888. doi:10.2113/econgeo.108.8.1879.

Pettigrew, N.T. and Hattori, K.H., 2006. The Quetico intrusions of Western Superior Province: Neo-Archean examples of Alaskan/Ural-type mafic–ultramafic intrusions; Precambrian Research, v. 149, p. 21–42. doi:10.1016/j.precamres.2006.06.004

Pettigrew, N.T., Hattori, K.H., and Percival, J.A., 2000. Samuels Lake intrusion: a Late Archean Cu-Ni-PGE-bearing mafic-ultramafic complex in the western Quetico Subprovince, northwestern Ontario; Geological Survey of Canada, Current Research 2000-C20, 8 p.

Piña, R., Lunar, R., Ortega, L., Gervilla, F., Alapieti, T., and Martínez, C., 2006. Petrology and geochemistry of mafic-ultramafic fragments from the Aguablanca Ni-Cu ore breccia, southwest Spain; Economic Geology, v. 101, p. 865–881.

Piña, R., Gervilla, F., Ortega, L., and Lunar, R., 2008. Mineralogy and geochemistry of platinum-group elements in the Aguablanca Ni-Cu deposit (SW Spain); Mineralogy and Petrology, v. 92, p. 259–282.

Piña, R., Romeo, I., Ortega, L., Lunar, R., Capote, R., Gervilla, F., Tejero, R., and Quesada, C., 2010. Origin and emplacement of the Aguablanca magmatic Ni-Cu-(PGE) sulfide deposit, SW Iberia: A multidisciplinary approach; Geological Society of America Bulletin, v. 122, p. 915–925. doi:10.1130/B30046.1

Piña, R., Gervilla, F., Ortega, L., and Lunar, R., 2012. Geochemical constraints on the origin of the Ni–Cu sulfide ores in the Tejadillas prospect (Cortegana Igneous Complex, SW Spain); Resource Geology, v. 62, p. 263–280. doi:10.1111/j.1751-3928.2012.00194.x

Pinsent, R.H., 2002. Ni-Cu-PGE potential of the Giant Mascot and Cogburn ultramafic-mafic bodies, Harrison-Hope area, southwestern British Columbia (092H), *In:* Geological Fieldwork 2001; British Columbia Ministry of Energy and Mines, British Columbia Geological Survey, Paper 2002-1, p. 211–236.

Qin, K., Su, B., Sakyi, P.A., Tang, D., Li, X., Sun, H., Xiao, Q., and Liu, P., 2011. SIMS zircon U-Pb geochronology and Sr-Nd isotopes of Ni-Cu-bearing mafic-ultramafic intrusions in Eastern Tianshan and Beishan in correlation with flood basalts in Tarim Basin (NW China): Constraints on a ca. 280 Ma mantle plume; American Journal of Science, v. 311, p. 237–260. doi:10.2475/03.2011.03

Ripley, E.M., Li, C., and Thakurta, J., 2005. Magmatic Cu-Ni-PGE mineralization at a convergent plate boundary: Preliminary mineralogic and isotopic studies of the Duke Island Complex, Alaska, *In:* Mineral Deposit Research, (ed.) P.D.J. Mao, and D.F.P. Bierlein; Meeting the Global Challenge, Springer Berlin Heidelberg, p. 49–51.

Romeo, I., Lunar, R., Capote, R., Quesada, C., Dunning, G.R., Pina, R., and Ortega, L., 2006. U-Pb age constraints on Variscan magmatism and Ni-Cu-PGE metallogeny in the Ossa-Morena Zone (SW Iberia); Journal of the Geological Society of London, v. 163, p. 837–846. doi:10.1144/0016-76492005-065

Saleeby, J.B., 1992. Age and tectonic setting of the Duke Island ultramafic intrusion, southeast Alaska; Canadian Journal of Earth Sciences, v. 29, p. 506–522.

Sappin, A.-A., Constantin, M., Clark, T., and van Breemen, O., 2009. Geochemistry, geochronology, and geodynamic setting of Ni–Cu±PGE mineral prospects hosted by mafic and ultramafic intrusions in the Portneuf–Mauricie Domain, Grenville Province, Quebec; Canadian Journal of Earth Sciences, v. 46, p. 331–353. doi:10.1139/E09-022

Sappin, A.-A., Constantin, M., and Clark, T., 2011. Origin of magmatic sulfides in a Proterozoic island arc—an example from the Portneuf–Mauricie Domain, Grenville Province, Canada; Mineralium Deposita, v. 46, p. 211–237. doi:10.1007/s00126-010-0321-8

Sappin, A.-A., Constantin, M., and Clark, T., 2012. Petrology of mafic and ultramafic intrusions from the Portneuf–Mauricie Domain, Grenville Province, Canada: Implications for plutonic complexes in a Proterozoic island arc; Lithos, v. 154, p. 277–295. doi:10.1016/j.lithos.2012.07.016

Scheel, J.E., 2007. Age and origin of the Turnagain Alaskan-type intrusion and associated Ni-sulphide mineralization, north-central British Columbia, Canada; M.Sc. thesis, The University of British Columbia, Vancouver, British Columbia, 210 p.

Scheel, J.E., Scoates, J.S., and Nixon, G.T., 2009. Chromian spinel in the Turnagain Alaskan-type ultramafic intrusion, northern British Columbia, Canada; The Canadian Mineralogist, v. 47, p. 63–80. doi:10.3749/canmin.47.1.63

Scoates, R.F.J., 1972. Ultramafic rocks and associated copper-nickel sulphide ores, Gordon Lake, Ontario; Ph.D. thesis, University of Manitoba, Winnipeg, Manitoba, 206 p.

Simard, R.-L., Dostal, J., and Roots, C.F., 2003. Development of late Paleozoic volcanic arcs in the Canadian Cordillera: an example from the Klinkit Group, northern British Columbia and southern Yukon; Canadian Journal of Earth Sciences, v. 40, p. 907–924. doi:10.1139/e03-025

Su, B.-X., Qin, K.-Z., Santosh, M., Sun, H., and Tang, D.-M., 2013. The Early Permian mafic–ultramafic complexes in the Beishan Terrane, NW China: Alaskan-type intrusives or rift cumulates?; Journal of Asian Earth Sciences, v. 66, p. 175–187. doi:10.1016/j.jseaes.2012.12.039

Sun, T., Qian, Z.-Z., Deng, Y.-F., Li, C., Song, X.-Y., and Tang, Q., 2013a. PGE and isotope (Hf-Sr-Nd-Pb) constraints on the origin of the Huangshandong magmatic Ni-Cu sulfide deposit in the Central Asian Orogenic Belt, northwestern China; Economic Geology, v. 108, p. 1849–1864. doi:10.2113/econgeo.108.8.1849

Sun, T., Qian, Z.-Z., Li, C., Xia, M.-Z., and Yang, S.-H., 2013b. Petrogenesis and economic potential of the Erhongwa mafic–ultramafic intrusion in the Central Asian Orogenic Belt, NW China: Constraints from olivine chemistry, U–Pb age and Hf isotopes of zircons, and whole-rock Sr–Nd–Pb isotopes; Lithos, v. 182–183, p. 185–199. doi:10.1016/j.lithos.2013.10.004

Taylor, H.P., Jr., and Noble, J.A., 1960. Origin of the ultramafic complexes in southeastern Alaska; Report of the International Geological Congress, Part 13, p. 175–187.

Taylor, H.P., Jr., 1967. The zoned ultramafic complexes of southeastern Alaska, *In:* Ultramafic and Related Rocks, (ed.) P.J. Wyllie; Wiley and Sons, New York, p. 97–121.

Tornos, F., Casquet, C., Galindo, C., Velasco, F., and Canales, A., 2001. A new style of Ni-Cu mineralization related to magmatic breccia pipes in a transpressional magmatic arc, Aguablanca, Spain; Mineralium Deposita, v. 36, p. 700–706.

Tornos, F., Galindo, C., Casquet, C., Rodríguez Pevida, L., Martínez, C., Martínez, E., Velasco, F., and Iriondo, A., 2006. The Aguablanca Ni–(Cu) sulfide deposit, SW Spain: geologic and geochemical controls and the relationship with a midcrustal layered mafic complex; Mineralium Deposita, v. 41, p. 737–769.

Wei, B., Wang, C.Y., Li, C., and Sun, Y., 2013. Origin of PGE-depleted Ni-Cu sulfide mineralization in the Triassic Hongqiling No. 7 orthopyroxenite intrusion, Central Asian Orogenic Belt, northeastern China; Economic Geology, v. 108, p. 1813–1831. doi:10.2113/econgeo.108.8.1813

Weiser, T.W., 2002. Platinum-group minerals (PGM) in placer deposits, *In:* The geology, geochemistry, mineralogy and mineral beneficiation of platinum-group elements, (ed.) L.J. Cabri; Canadian Institute of Mining, Metallurgy and Petroleum, Special Volume 54, p. 721–756.

Wu, F., Wilde, S.A., Zhang, G., and Sun, D., 2004. Geochronology and petrogenesis of the post-orogenic Cu–Ni sulfide-bearing mafic–ultramafic complexes in Jilin Province, NE China; Journal of Asian Earth Sciences, Phanerozoic Continental Growth in Central Asia, v. 23, p. 781–797. doi:10.1016/S1367-9120(03)00114-7

Xia, M.-Z., Jiang, C.-Y., Li, C., and Xia, Z.-D., 2013. Characteristics of a newly discovered Ni-Cu sulfide deposit hosted in the Poyi ultramafic intrusion, Tarim Craton, NW China; Economic Geology, v. 108, p. 1865–1878. doi:10.2113/econgeo.108.8.1865

Xiao, W.-J., Zhang, L.-C., Qin, K.-Z., Sun, S., and Li, J.-L., 2004. Paleozoic accretionary and collisional tectonics of the eastern Tianshan (China): Implications for the continental growth of central Asia; American Journal of Science, v. 304, p. 370–395. doi:10.2475/ajs.304.4.370

Xiao, W.J., Mao, Q.G., Windley, B.F., Han, C.M., Qu, J.F., Zhang, J.E., Ao, S.J., Guo, Q.Q., Cleven, N.R., Lin, S.F., Shan, Y.H., and Li, J.L., 2010. Paleozoic multiple accretionary and collisional processes of the Beishan orogenic collage; American Journal of Science, v. 310, p. 1553–1594. doi:10.2475/10.2010.12

Xie, W., Song, X.-Y., Deng, Y.-F., Wang, Y.-S., Ba, D.-H., Zheng, W.-Q., and Li, X.-B., 2012. Geochemistry and petrogenetic implications of a Late Devonian mafic–ultramafic intrusion at the southern margin of the Central Asian Orogenic Belt; Lithos, v. 144–145, p. 209–230. doi:10.1016/j.lithos.2012.03.010

Xie, W., Song, X.-Y., Chen, L.-M., Deng, Y.-F., Zheng, W.-Q., Wang, Y.-S., Ba, D.-H., Yin, M.-H., and Luan, Y., 2014. Geochemistry insights on the genesis of the subduction-related Heishan magmatic Ni-Cu-(PGE) deposit, Gansu, northwestern China, at the southern margin of the Central Asian Orogenic Belt; Economic Geology, v. 109, p. 1563–1583. doi:10.2113/econgeo.109.6.1563

Zhang, Z., Mao, J., Chai, F., Yan, S., Chen, B., and Pirajno, F., 2009. Geochemistry of the Permian Kalatongke mafic intrusions, northern Xinjiang, northwest China: Implications for the genesis of magmatic Ni-Cu sulfide deposits; Economic Geology, v. 104, p. 185–203. doi:0.2113/gsecongeo.104.2.185

Zhang, C.-L., Li, Z.-X., Li, X.-H., Xu, Y.-G., Zhou, G., and Ye, H.-M., 2010. A Permian large igneous province in Tarim and Central Asian orogenic belt, NW China: Results of a ca. 275 Ma mantle plume?; Geological Society of America Bulletin, v. 122, p. 2020–2040. doi:10.1130/B30007.1

Zhang, M., Li, C., Fu, P., Hu, P., and Ripley, E.M., 2011. The Permian Huangshanxi Cu–Ni deposit in western China: intrusive–extrusive association, ore genesis, and exploration implications; Mineralium Deposita, v. 46, p. 153–170. doi:10.1007/s00126-010-0318-3

GEOLOGICAL SURVEY OF CANADA
OPEN FILE 7856

Targeted Geoscience Initiative 4: Canadian Nickel-Copper-Platinum Group Elements-Chromium Ore Systems — Fertility, Pathfinders, New and Revised Models

Temporal and spatial distribution of magmatic Cr-(PGE), Ni-Cu-(PGE), and Fe-Ti-(V) deposits in the Bird River–Uchi–Oxford-Stull–La Grande Rivière–Eastmain domains: a new metallogenic province within the Superior Craton

Michel G. Houlé[1], C. Michael Lesher[2], Vicki J. McNicoll[3], Riku T. Metsaranta[4], Anne-Aurélie Sappin[1], Jean Goutier[5], Valérie Bécu[1], H. Paul Gilbert[6], and Eric (Xueming) M. Yang[6]

[1]Geological Survey of Canada, Québec, Quebec
[2]Laurentian University, Sudbury, Ontario
[3]Geological Survey of Canada, Ottawa, Ontario
[4]Ontario Geological Survey, Sudbury, Ontario
[5]Ministère de l'Énergie et des Ressources naturelles, Rouyn-Noranda, Quebec
[6]Manitoba Geological Survey, Winnipeg, Manitoba

2015

© Her Majesty the Queen in Right of Canada, as represented by the Minister of Natural Resources Canada, 2015

This publication is available for free download through GEOSCAN (http://geoscan.nrcan.gc.ca/)

Recommended citation

Houlé, M.G., Lesher, C.M., McNicoll, V.J., Metsaranta, R.T., Sappin, A.-A., Goutier, J., Bécu, V., Gilbert, H.P., and Yang, X.M., 2015. Temporal and spatial distribution of magmatic Cr-(PGE), Ni-Cu-(PGE), and Fe-Ti-(V) deposits in the Bird River–Uchi–Oxford-Stull–La Grande Rivière–Eastmain domains: a new metallogenic province within the Superior Craton, *In:* Targeted Geoscience Initiative 4: Canadian Nickel-Copper-Platinum Group Elements-Chromium Ore Systems — Fertility, Pathfinders, New and Revised Models, (ed.) D.E. Ames and M.G. Houlé; Geological Survey of Canada, Open File 7856, p. 35–48.

Publications in this series have not been edited; they are released as submitted by the author.

TABLE OF CONTENTS

Temporal and spatial distribution of magmatic Cr-(PGE), Ni-Cu-(PGE), and Fe-Ti-(V) deposits in the Bird River–Uchi–Oxford-Stull–La Grande Rivière–Eastmain domains: a new metallogenic province within the Superior Craton

Michel G. Houlé[1]*, C. Michael Lesher[2], Vicki J. McNicoll[3], Riku T. Metsaranta[4], Anne-Aurélie Sappin[1], Jean Goutier[5], Valérie Bécu[1], H. Paul Gilbert[6], and Eric (Xueming) M. Yang[6]

[1]Geological Survey of Canada, 490 rue de la Couronne, Québec, Quebec G1K 9A9
[2]Mineral Exploration Research Centre, Department of Earth Sciences, Goodman School of Mines, Laurentian University, 935 Ramsey Lake Road, Sudbury, Ontario P3E 2C6
[3]Geological Survey of Canada, 601 Booth Street, Ottawa, Ontario K1A 0E8
[4]Ontario Geological Survey, 933 Ramsey Lake Road, Sudbury, Ontario P3E 6B5
[5]Ministère de l'Énergie et des Ressources naturelles, 70, avenue Québec, Rouyn-Noranda, Quebec J9X 6R1
[6]Manitoba Geological Survey, 360–1395 Ellice Avenue, Winnipeg, Manitoba R3G 3P2
*Corresponding author's e-mail: michel.houle@rncan-nrcan.gc.ca

ABSTRACT

Chromium and Fe-Ti-(V) mineralization in ultramafic-mafic intrusions is known to occur in several areas of the Superior Province, but was considered to be of marginal significance until the discovery of world-class Cr deposits and potentially significant Fe-Ti-(V) mineralization in the McFaulds Lake greenstone belt ("Ring of Fire") of northern Ontario. Cr-(PGE), Ni-Cu-(PGE), and Fe-Ti-(V) deposits/occurrences in the northern part of the Superior Province occur predominantly within Meso to Neoarchean supracrustal successions along the margins and within the interiors of the Bird River–Uchi–Oxford-Stull–La Grande Rivière–Eastmain domains (i.e. BUOGE domains). These domains define a new metallogenic province within the Superior Province characterized by the presence of major Cr-(PGE) with Ni-Cu-(PGE) and Fe-Ti-(V) metal associations that appear to be fundamentally different from other parts of the Craton, such as the Abitibi greenstone belt or the apparently relatively unmineralized North Caribou core, Island Lake, and Goudalie domains. Despite the fact that only the Cr-(PGE) deposits and Ni-Cu-(PGE) deposits (Eagle's Nest) in the McFaulds Lake greenstone belt appear to be potentially economic, the presence of a significant amount of Cr-(PGE) mineralization across the BUOGE domains highlights the prospectivity of these regions of the Superior Province.

INTRODUCTION

The Superior Province is a well-endowed metallogenic province that contains a variety of mineral deposits, including VMS, lode Au, magmatic Fe-Ni-Cu-(PGE) sulphide, Cr-(PGE), and Fe-Ti-V deposits, and rare-metal deposits. The metallogenic history of the Superior Province has generated interest from the scientific community and exploration for decades. The first attempts to systematically subdivide the Superior Province into metallogenic domains were done in the early 1960s (Lang, 1961). Card and Poulsen (1998a,b) produced an extensive review of the mineral deposits occurring in the Superior Province and proposed seventeen mineral belts across the Superior Province to explain the distribution of these deposits. More recently, an overview of the spatial and the temporal distribution of the mineral deposits in the Superior Province has been conducted by Percival (2007).

The discoveries of world-class Cr-(PGE) deposits, a major Ni-Cu-(PGE) deposit, and numerous significant Fe-Ti-(V) occurrences in the McFaulds Lake greenstone belt (MLGB; also known as "Ring of Fire") of northern Ontario have greatly renewed interest in orthomagmatic mineralization associated with mafic-ultramafic intrusions in the Superior Province. Mafic-ultramafic intrusions and ultramafic volcanic rocks are widespread throughout the Superior Province, but their association with significant Cr-(PGE), Ni-Cu-(PGE), and Fe-Ti-(V) mineralization is not evenly distributed across the craton.

In this study we have focussed primarily on the distribution of the orthomagmatic Cr-(PGE), Ni-Cu-

Houlé, M.G., Lesher, C.M., McNicoll, V.J., Metsaranta, R.T., Sappin, A.-A., Goutier, J., Bécu, V., Gilbert, H.P., and Yang, X.M., 2015. Temporal and spatial distribution of magmatic Cr-(PGE), Ni-Cu-(PGE), and Fe-Ti-(V) deposits in the Bird River–Uchi–Oxford-Stull–La Grande Rivière–Eastmain domains: a new metallogenic province within the Superior Craton, *In:* Targeted Geoscience Initiative 4: Canadian Nickel-Copper-Platinum Group Elements-Chromium Ore Systems — Fertility, Pathfinders, New and Revised Models, (ed.) D.E. Ames and M.G. Houlé; Geological Survey of Canada, Open File 7856, p. 35–48.

(PGE), and Fe-Ti-(V) deposits and to a lesser extent, the significant occurrences. The aim of this contribution is to propose a new Cr-(PGE) metallogenic province (defined as an area characterized by a particular assemblage of mineral deposits, or by one or more characteristic types of mineralization). A metallogenic province may have had more than one episode of mineralization: Jackson, 1997) that also contains Ni-Cu-(PGE) and Fe-Ti-(V) metal associations within the Superior Province based on currently available information and interpretations of the various terrane and domain boundaries within the Superior Province. This study is a part of the High-Magnesium Ultramafic to Mafic Systems subproject under the Targeted Geoscience Initiative 4 of the Geological Survey of Canada (GSC) conducted in collaboration with the Ontario Geological Survey (OGS), the Manitoba Geological Survey (MGS), the ministère de l'Énergie et des Ressources naturelles (MERN: Quebec), several universities across the country, and the mineral industry.

SUPERIOR PROVINCE

The Superior Province is the largest coherent Archean craton in the world, with exceptional mineral endowment reflected in the presence of numerous world-class Au and volcanogenic massive sulphide (VMS) deposits, and significant Ni-Cu-(PGE) deposits (e.g. Poulsen et al., 1992; Card and Poulsen, 1998a,b).

Early investigations of the Superior Province recognized a limited number of subprovinces based on general lithological characteristics and regional structural styles (e.g. Douglas, 1973; Card and Ciesielski, 1986). Subsequently, more detailed lithological and geochronological data were used in an attempt to subdivide the former Sachigo subprovince into terranes (e.g. Thurston et al., 1991) and the western Superior Province was further subdivided into superterranes and terranes by Stott (1997). The eastern Superior Province was subdivided into lithotectonic elements with distinct compositional, mineralogical, and geochronological attributes and aeromagnetic character by Percival et al. (1992). Since then, considerable efforts by the MGS, OGS, MERN, and GSC have been devoted to identifying stratigraphically and tectonically distinct terranes and domains across the Superior Province using high-resolution geochronological, structural, stratigraphic, geochemical, geophysical, and tectonic data that progressively led to a revised tectonic map of terrane and domain boundaries of the Superior Province, which were proposed by Stott et al. (2010) and subsequently revised by Percival et al. (2012).

There is no attempt to describe the overall geology of the Superior Province in this contribution; only a summary of specific relevant aspects are included. The reader is referred to Percival et al. (2012) for a more thorough review of the geology and tectonic evolution of the Superior Province.

The North Caribou Terrane (NCT) is the largest reworked Mesoarchean to Neoarchean crustal block of the western Superior Province. The NCT consists of a central core (North Caribou core) composed of granitoid rocks from the Berens River plutonic complex (2.75 to 2.71 Ga) with remnants of Mesoarchean tonalitic and supracrustal rocks (3.0–2.8 Ga). The North Caribou Terrane is flanked by the Island Lake (ILD) and the Oxford-Stull domains (OSD) to the north and by the Uchi domain (UD) to the south (Fig. 1; Stott et al., 2010; Percival et al., 2012). The ILD consists of older Mesoarchean (2.9–2.85 Ga) with subordinate Neoarchean (2.74 Ga) supracrustal assemblages that appear to have incorporated variable components of older ca. 3.0 Ga crustal sources (e.g. Parks et al., 2014). The OSD, which includes the MLGB, consists largely of Neoarchean volcano-plutonic rocks (2.88–2.73 Ga) with a more juvenile character and it is distinguished from the Island Lake and the Uchi domains by the lack of pre-3.0 Ga supracrustal rocks (e.g. Percival et al., 2012). The UD records more than 300 Ma of tectonostratigraphic evolution and contains several greenstone belts and plutonic complexes that record multiple episodes of rifting, arc-magmatism, deformation, and associated sedimentation from ca. 3.0 to 2.7 Ga (Percival et al., 2006, 2012). Re-examination of the aeromagnetic data of the western Superior Province in Ontario within the OSD and UD led Stott (2008a,b, 2009) to propose that these domains merge under the James Bay Lowland Paleozoic cover on either side of the North Caribou core. Furthermore, it has also been proposed that the OSD and the UD probably extend eastward, along strike with the La Grande Rivière and the Eastmain domains, and could have formed a single domain across the James Bay area (Stott et al., 2010).

Within the Superior Province, another region of interest is the Bird River area located between the English River basin (ERB) and the Winnipeg River terrane (WRT) in southeast Manitoba (Fig. 1). The Bird River greenstone belt and its eastern equivalent, the Separation greenstone belt in Ontario, extend for 150 km from Lac du Bonnet (Manitoba) in the west to Separation Lake (Ontario) in the east and consist of a series of metavolcanic and metasedimentary rocks (Blackburn and Young, 2000; Gilbert et al., 2008). Assignment of the Bird River-Separation Lake greenstone belt to a lithotectonic entity is still under debate and it may be included as part of the Winnipeg River terrane, English River basin, or Uchi domain. Initially, based on its distinct character compared with the surrounding WRT and ERB, Card and Ciesielski (1986) elevated the Bird River-Separation greenstone belt to a

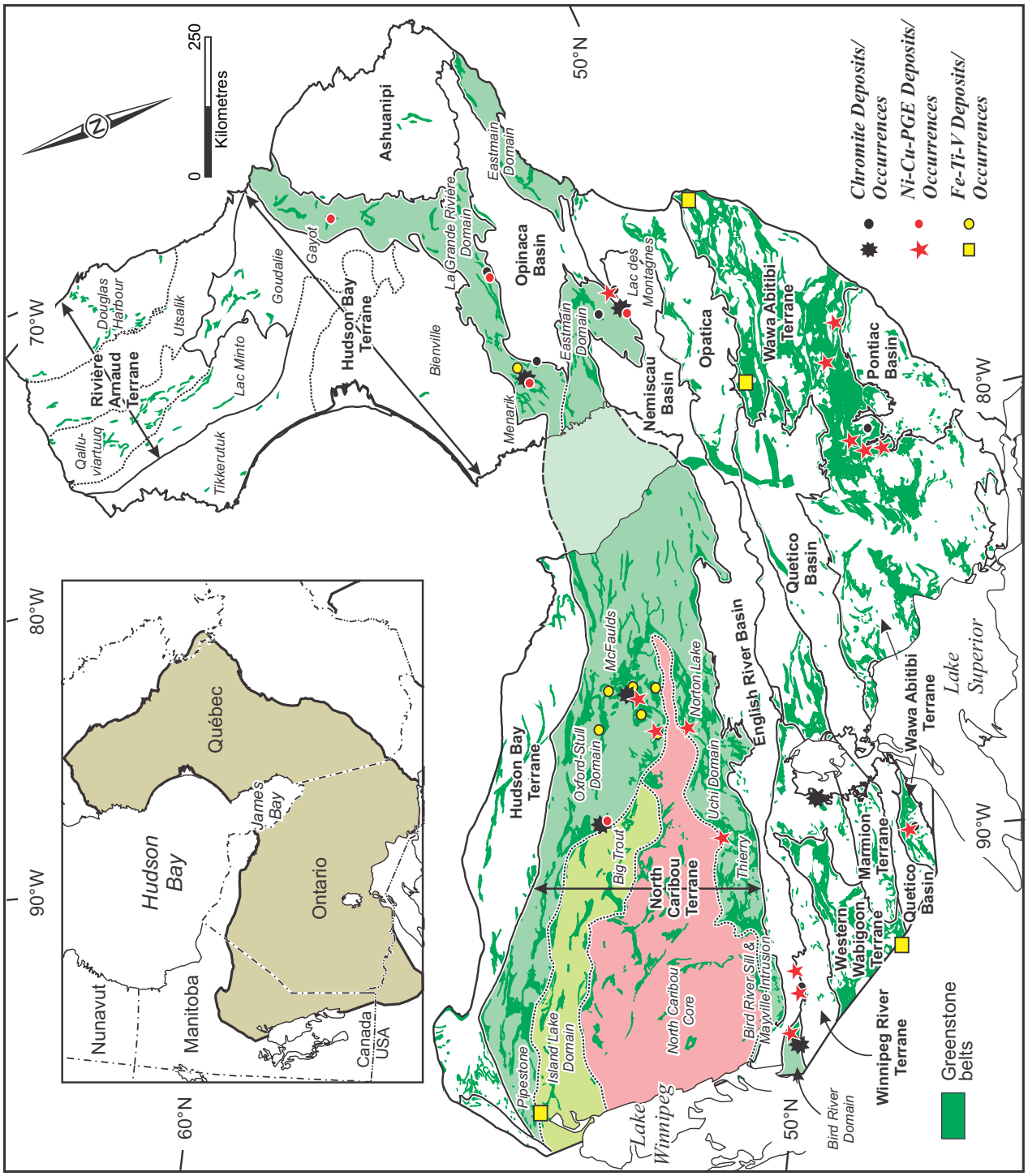

Figure 1. Schematic geological map showing the main Archean Cr-(PGE), Ni-Cu-(PGE), and Fe-Ti-(V) deposits/occurrences within the Superior Province. Terrane and domain boundaries are modified from Stott et al. (2010) and Percival et al. (2012).

subprovince, referred to as the Bird River subprovince (BRS). More recently, Stott et al. (2010) and Percival et al. (2012) have incorporated the BRS into the Winnipeg River terrane. However, recent geological mapping by the MGS in the Bird River greenstone belt and the Rice lake greenstone belt (Uchi domain), located just across the English River basin, has revealed some similarities between these two belts on either side of the English River basin (Anderson, 2005; Gilbert et al., 2008). Early supracrustal assemblages in the Uchi domain have no counterpart in the BRS; however, a possible correlation may be made amongst the younger supracrustal assemblages (Gilbert et al., 2008; Anderson, 2014; Gilbert and Kremer, 2014). Subsequent orogenic sediments in the two belts are interpreted to be correlative (Gilbert et al., 2008; Gilbert and Kremer, 2014) and also stratigraphically equivalent to the epiclastic rocks and metamorphic derivatives of the English River basin, which lies between the Uchi domain and the Bird River subprovince (e.g. Hrabi and Cruden, 2006).

The Uchi–Oxford-Stull-La Grande Rivière–Eastmain domains exhibit similar geochronological, stratigraphic, structural, and tectonic characteristics suggesting that they may represent a similar regional tectonic environment along the margins of the NCT (Stott et al., 2010). These approximately east-west-trending domains appear to have been a favourable region for the emplacement of mafic-ultramafic magmas with significant orthomagmatic mineralization. However, a remaining question is how the Bird River subprovince fits into this picture and further investigation is needed to resolve this issue. In the light of recent geological mapping, many similarities appear to exist between the Bird River and the Rice Lake greenstone belts; therefore it could be postulated that the Bird River subprovince may have a tectonostratigraphic history more similar to the Uchi domain rather than to the Winnipeg River terrane. If this is correct, the Bird River subprovince could be a domain that belongs to the southern margin of the NCT and part of the Uchi–Oxford-Stull-La Grande Rivière–Eastmain domains. These domains have previously been referred to as the BUOGE "superdomain" (Houlé et al., 2013a,b), however, because of uncertainty regarding the Bird River domain, it should be referred to instead as the BUOGE domains (i.e. B: Bird River, U: Uchi, O: Oxford-Stull, G: La Grande Rivière, E: Eastmain) that comprise a broad grouping of domains that appear to share a similar evolution and tectonic history a rather than a strict lithotectonic entity (Fig. 1).

RESULTS

Mafic to ultramafic intrusions occur throughout the BUOGE domains and span a wide range of ages from 2.88 to 2.70 Ga (Table 1; see Houlé et al., 2015a). The vast majority of known Archean Cr-(PGE) deposits and occurrences across the Superior Province have been discovered within Meso- to Neoarchean supracrustal successions along the margins and within the cores of these domains (Fig. 1). Known Archean Ni-Cu-(PGE) deposits occur predominantly within the Wawa-Abitibi terrane, however, the BUOGE domains contain numerous deposits of this type and in some cases the deposits are spatially associated with and/or occur within the same intrusions that hosts Cr-(PGE) deposits (Fig. 1). It is difficult to make generalizations regarding the distribution of the Fe-Ti-(V) deposits, as almost all of them occur within different terranes/domains (e.g. Pipestone deposit in the Island Lake domain – NCT; Bad Vermillion deposit in the western Wabigoon terrane; Rivière Bell and Lac Doré deposits in the Wawa-Abitibi terrane) (Fig. 1). However, numerous Fe-Ti-(V) occurrences, especially in the MLGB, were recently discovered in the vicinity of Cr-(PGE) deposits (Metsaranta et al., 2015). In the course of this study, three main regions across the BUOGE domains, including 1) Bird River greenstone belt (Manitoba), 2) McFaulds Lake greenstone belt (Ontario), and 3) the La Grande Rivière and Eastmain domains, were investigated and are briefly described below.

Bird River Greenstone Belt, Bird River Domain

The Bird River greenstone belt (BRGB) in southeastern Manitoba contains numerous Neoarchean mafic-ultramafic intrusions that host significant Ni-Cu-(PGE) and Cr-(PGE) deposits and occurrences. Nine main intrusions (Table 1) occur over a strike length of 75 km laterally and 20 km across on each side of the Maskwa Lake Batholith.

The internal stratigraphic variations of these intrusions can be characterized by two end members: 1) well layered differentiated mafic-ultramafic intrusions containing variable ultramafic components but preponderant mafic parts (e.g. National-Ledin, Chrome, Page, Maskwa, Bird Lake, Euclid Lake), and 2) poorly layered mafic-dominated intrusions without distinct ultramafic components (e.g. Coppermine, New Manitoba, and Mayville intrusions). The very well layered Chrome mafic-ultramafic intrusion in the Bird River Sill is the type example of the former. It contains a thin lower ultramafic zone composed of dunite and peridotite with lesser chromitite layers overlain by a thicker upper mafic zone composed of gabbro, leucogabbro, and anorthositic gabbro with lesser trondhjemite layers. The less-stratified Mayville intrusion is the type example of the latter. It contains a lower heterolithic intrusive breccia zone with sporadic mafic to ultramafic horizons along the basal contact, overlain by

Table 1. Cr-(PGE), Ni-Cu-(PGE), and Fe-Ti-(V) deposits and main mineral occurrences in the Superior Province with compiled and preliminary age constraints from this study.

Terrane	Greenstone Belt	Intrusive Suite	Intrusions/Volcanics	Age (Ma)		Cr-PGE	Ni-Cu-PGE	Fe-Ti-V	Examples
North Caribou terrane									
Island Lake domain									
	CLGB		Pipestone	A 2760 [1]	CA			X	**Pipestone**
Oxford-Stull domain									
	BTSGB		Big Trout Lake	-	ND	X	X		**Big Trout Lake**
	MLGB	Ring of Fire intrusive suite							
		2733–2734 Ma	Ultramafic-dominated subsuite						
			Black Thor intrusive complex	A 2734	CA	X	X		**Black Thor, Big Daddy, Black Label, Black Creek**
			Double Eagle intrusive complex	-	ND	X	X		**Eagle's Nest; Blackbird, Black Horse**
			Mafic-dominated "ferrogabroic" subsuite						
			Butler West	-	NZ			X	**Butler West**
			Butler East	-	ND			X	**Butler East**
			Thunderbird	A 2734	CA			X	**Thunderbird**
			Big Mac	A 2734	CA			X	
			Croal Lake	A 2733	CA			X	
			Highbank-Fishtrap intrusive complex						
			Highbank	A 2810				X	*Highbank Fe-Ti-(V)*
			Fishtrap	A 2810	CA				
Uchi domain									
	RLGB		Garner Lake intrusive complex	B 2871 [2]	CA				
	PLGB		Thierry	-	ND		X		**Thierry**
			July Falls	A 2749 [3]	CA				
	MFHGB		Norton Lake	-	ND		X		**Norton Lake**
			Oxtoby Lake	A 2717	CA				
			Wabassi intrusive complex						
			Max	A			X		
			Wabassi Main	A 2727	CA			X	*Wabassi Fe-Ti-(V)*
La Grande Rivière domain									
	YGB		Menarik	A 2750	CA	X	X		**Menarik;** *4930N-1; 3700N-1;*
			Lac Ultra		ND				**Menarik**
			Baie Chapus	A 2802	IA			X	*Baie Chapus*
	LGKGB		Lac Guyer komatiite	B 2820 [4]	CA				
	VMGB		Gayot Lake komatiite	B [5]	CA		X		
Eastmain domain									
	BEGB		Lac Fed	B 2739 [6]	CA	X			*Sledgehammer, Dominic*
			Komo formation komatiite	B 2703 [6]	CA				
	NGB		Lac des Montagnes	A 2802	CA		X		**Lac des Montagnes**
			Levack	-	ND	X	X		**Nisk-1**
Winnipeg River terrane									
Bird River domain									
	BRGB								
			Synvolcanic gabbro (Northern MORB fm)	A 2745	CA				
		Bird River intrusive suite							
		2742–2744 Ma	National-Ledin	-	ND	X			
			Chrome	A 2743 [7]	CA	X			**Chrome**
			Page	-	ND	X	X		**Page; Page**
			Maskwa	-	ND	X	X		**Maskwa; Dumbarton**
			Bird Lake	A 2743	CA		X		**Bird Lake**
			Euclid Lake	A 2744	CA	X	X		**Euclid Lake**
			Coppermine	A 2742	CA	X	X		
			New Manitoba	A 2743	CA		X		**New Manitoba**
			Eileen	-	NZ				
			Mayville	A 2743	CA	X	X		**M2**

[1]Corkery et al., 1992; [2]Davis, 1994 and Anderson, 2013; [3]Young et al., 2006; [4]Goutier et al., 2002; [5]David et al., 2009; [6]Moukhsil et al., 2007; [7]Scoates and Scoates, 2013

A = direct age constraint, B = indirect age contraint obtained via a dated crosscutting dykes or subjacent host volcanic rocks; CA = crystallization age; IA = inheritance age; ND = not dated; NZ = not zircon found

Greenstone belt (GB): BRGB = Bird River; BTSLGB = Big Trou Lake–Swan Lake; CLGB = Cross Lake; LGB = Eastmain; LGKGB = Lac Guyer-Keyano; MFHGB = Miminiska–Fort Hope; MLGB = McFaulds Lake; NGB = Nemaska; PLGB = Pickle Lake; VMGB = Venus-Moyer; YGB = Yasinski

Deposits: Black = Chromite deposits; **Red** = Ni-Cu-PGE deposits; **Blue** = Fe-Ti-V = Deposits; *italic* are significant occurrences

a thick mafic zone composed of leucogabbro and megacrystic anorthosite.

Despite their compositional and internal stratigraphic variations, BRGB intrusions are interpreted to have been generated during a single large mafic-ultramafic magmatic event (Houlé et al., 2013c), referred to as the Bird River intrusive suite, emplaced between 2744 and 2742 Ma (Table 1). The footwall of these intrusions, at least within the main part of the BRGB, has been dated during the course of this study and yielded a U-Pb crystallization age of 2745 Ma for a synvolcanic gabbro that occurred within the Northern MORB formation near the Maskwa mine (Table 1). These intrusions also generated significant basal (e.g. Maskwa: Chrome), contact-style Ni-Cu-(PGE) mineralization (e.g. M2: Mayville intrusion), as well as Cr mineralization (e.g. Chrome, Page, Euclid) higher up in the stratigraphy, near the contact between the ultramafic and mafic zones.

McFaulds Lake Greenstone Belt, Oxford-Stull Domain

The McFaulds Lake greenstone belt is an extensive (>200 km long), arcuate-shaped, Meso- to Neoarchean greenstone belt occurring in the central part of the Oxford-Stull domain (Ontario), which is characterized by an unusual endowment of mafic to ultramafic intrusive rocks hosting world-class chromite deposits (e.g. Black Thor, Black Label, Big Daddy, Black Horse, Blackbird), a major Ni-Cu-(PGE) deposit (Eagle's Nest), and several Ni-Cu-(PGE) occurrences (e.g. AT-12, SE-Central-NE Breccia Zones), and significant Fe-Ti-(V) mineralization (e.g. Thunderbird, Butler West, Butler East, Big Mac) (Metsaranta et al., 2015).

At least two generations of mafic-ultramafic intrusions (ca. 2810 and 2734–2733 Ma) appear to host these types of mineralization, although the bulk of significant mineralization appears to be associated with Neoarchean intrusions (see Metsaranta et al., 2015). The Neoarchean intrusions, referred to as the Ring of Fire intrusive suite (RoFIS), can be further subdivided into two main magmatic subsuites: an ultramafic-dominated subsuite (e.g. Black Thor: see Carson et al., 2015) and a mafic-dominated "ferrogabbroic" subsuite (e.g. Thunderbird, Butler and Big Mac: see Kuzmich et al., 2015; Sappin et al., 2015). The RoFIS occurs across the entire MLGB and exhibits incredibly consistent U-Pb crystallization ages at 2.73 Ga, suggesting the presence of a large magmatic mafic-ultramafic event in the MLGB (Table 1).

Thus far, Cr-(PGE) and Ni-Cu-(PGE) mineralization appears to occur essentially within the Neoarchean ultramafic-dominated intrusions of the RoFIS, whereas Fe-Ti-(V) mineralization occurs in both Neoarchean and Mesoarchean mafic-dominated intrusions. However, further investigation currently in progress along the southern margin of the Oxford-Stull domain could reveal that some of the mafic to ultramafic intrusions along this domain boundary may also have the potential to host Cr-(PGE) and Ni-Cu-(PGE) mineralization.

La Grande Rivière and Eastmain Domains

The Yasinski and Nemaska greenstone belts within the La Grande Rivière and Eastmain domains (Quebec), respectively, also contain numerous and widespread Mesoarchean and Neoarchean mafic to ultramafic intrusions, many of which host orthomagmatic Cr-(PGE), Ni-Cu-(PGE), and Fe-Ti-(V) mineralization (Houlé et al., 2015b; Table 1).

Chrome mineralization appears to be one of the most abundant and significant styles of the mineralization in these regions and many chromitite occurrences have been identified over the years. The most significant are associated with the Neoarchean Menarik Complex (MC) and the Mesoarchean Lac des Montagnes intrusion (LMI). Preliminary geochronological data has yielded U-Pb ages of 2750 Ma and 2802 Ma for the Menarik Complex and the Lac des Montagnes intrusion, respectively (Table 1). The LMI intrusion is part of a series of east-northeast-trending ultramafic intrusions, referred to as the Lac des Montagnes intrusive suite, occurring in the Nemaska volcano-sedimentary belt at the margin between the Opinaca basin and the Eastmain domain of the North Caribou terrane. Both intrusions have lower ultramafic zones and upper mafic zones, and contain several laterally continuous chromitite seams, ranging from a few centimetres to 3 metres, within their ultramafic zones. Thus, these chromite deposits in the Eeyou Istchee Baie James region are Meso- and Neoarchean, which differs from those of the RoF area where only Neoarchean chromite deposits have been identified so far. Other intrusions (e.g. Nisk, Gayot) have Ni-Cu-(PGE) mineralization near their bases (Houlé et al., 2015b). Although not as significant as the other mineralization styles, Fe-Ti-(V) mineralization also occurs within some ultramafic to mafic intrusions (e.g. baie Chapus Pyroxenite). This mineralization is characterized by an accumulation of magnetite containing abundant ilmenite exsolutions within a massive to semi-massive magnetite horizon near the upper part of the intrusion.

DISCUSSION

Cr-(PGE) Metallogenic Province

Almost all Cr-(PGE) deposits and significant occurrences in the Superior Province occur within the BUOGE domains and range from Neoarchean to Mesoarchean, with the best examples occurring in the

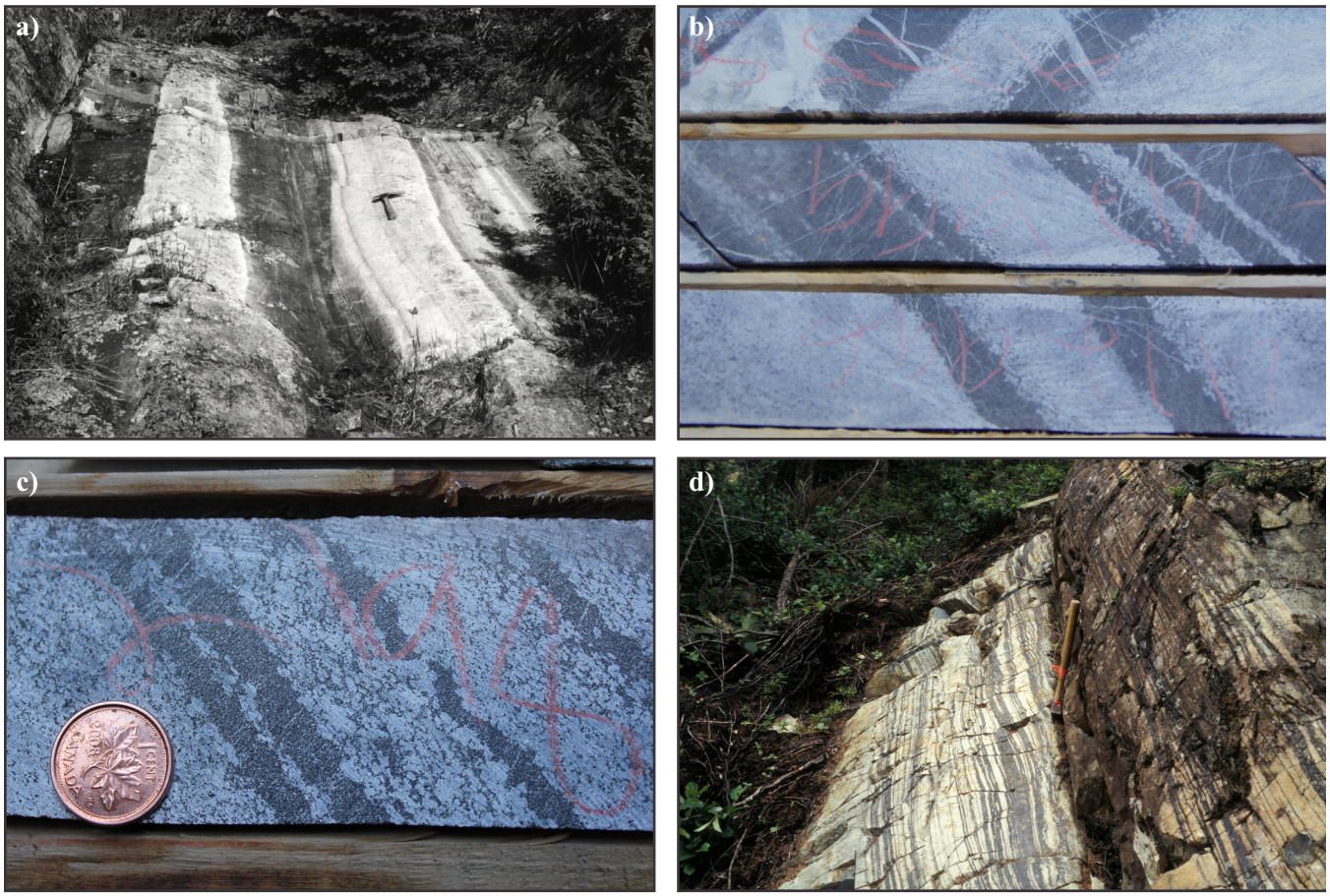

Figure 2. Typical Cr-(PGE) mineralization associated with mafic and ultramafic intrusions in the Bird River–Uchi–Oxford-Stull–La Grande Rivière–Eastmain (BUOGE) domains. **a)** Chromitite layers in the Bird River Sill, southeast Manitoba (after Williamson, 1990). Hammer is 30 cm long. **b)** Chromitite layers at the Black Thor deposit in the Ring of Fire Intrusive Complex, northern Ontario. Diameter of the core is 4.5 cm. **c)** Chromitite layers at the Blackbird deposit in the Ring of Fire Intrusive Complex, northern Ontario. Coin is 1.8 cm in diameter. **d)** Chromitite layers in the Menarik Complex, James Bay area, Quebec. Hammer is 38 cm long.

Bird River (e.g. Chrome - Bird River Sill; Fig. 2a), Oxford-Stull (e.g. Black Thor and Blackbird - Ring of Fire Intrusive Complex; Fig. 2b and 2c, respectively), and La Grande Rivière (e.g. Menarik; Fig. 2d) domains (Table 1). Chromium-(PGE) mineralization is virtually absent in the remainder of the Superior Province except for domains that belong to the North Caribou terrane and for the Bird River domain.

Nickel-Cu-(PGE) deposits are abundant in the Wawa-Abitibi terrane (Houlé and Lesher, 2011) and Bird River domain, but are less abundant in the Uchi, La Grande Rivière, and Eastmain domains, and essentially absent in the remainder of the Superior Province. Nickel-Cu-(PGE) deposits occur across the BUOGE domains and range from Neoarchean to Mesoarchean, with the best examples occurring within the Bird River (e.g. Maskwa – Bird River Sill; Fig. 3a), Uchi (e.g. Norton Lake), Oxford-Stull (e.g. Eagle's Nest - Ring of Fire intrusive suite; Fig. 3b and 3c), Eastmain (e.g. Nisk-1), and La Grande Rivière (e.g. Gayot; Fig. 3d) domains (Table 1).

Iron-Ti-(V) deposits are less abundant and most occur within the southern part of the Superior Province in the Wawa-Abitibi (e.g. Rivière Bell and Lac Doré complexes) and in the western Wabigoon terranes (e.g. Bad Vermillion complex). Another major Fe-Ti-(V) deposit, the Pipestone deposit, is located near the northern margin of the Island Lake domain and the Oxford-Stull domain. Quite significant Fe-Ti-(V) prospects have been discovered recently in the MLGB; but resource estimates have not yet been conducted (Kuzmich et al., 2015; Sappin et al., 2015). A small Fe-Ti-(V) occurrence is also hosted within the baie Chapus Pyroxenite in the La Grande Rivière domain in Quebec (Houlé et al., 2015b).

The overall distribution of the chromite deposits, (essentially restricted to the BUOGE domains) appears to define a craton-scale Cr-PGE metallogenic province within the Superior Province that contains at least two episode of Cr-(PGE) mineralization. The older episode is Mesoarchean age (ca. 2802 Ma; Table 1) that appears, so far, to be restricted to the southern part of

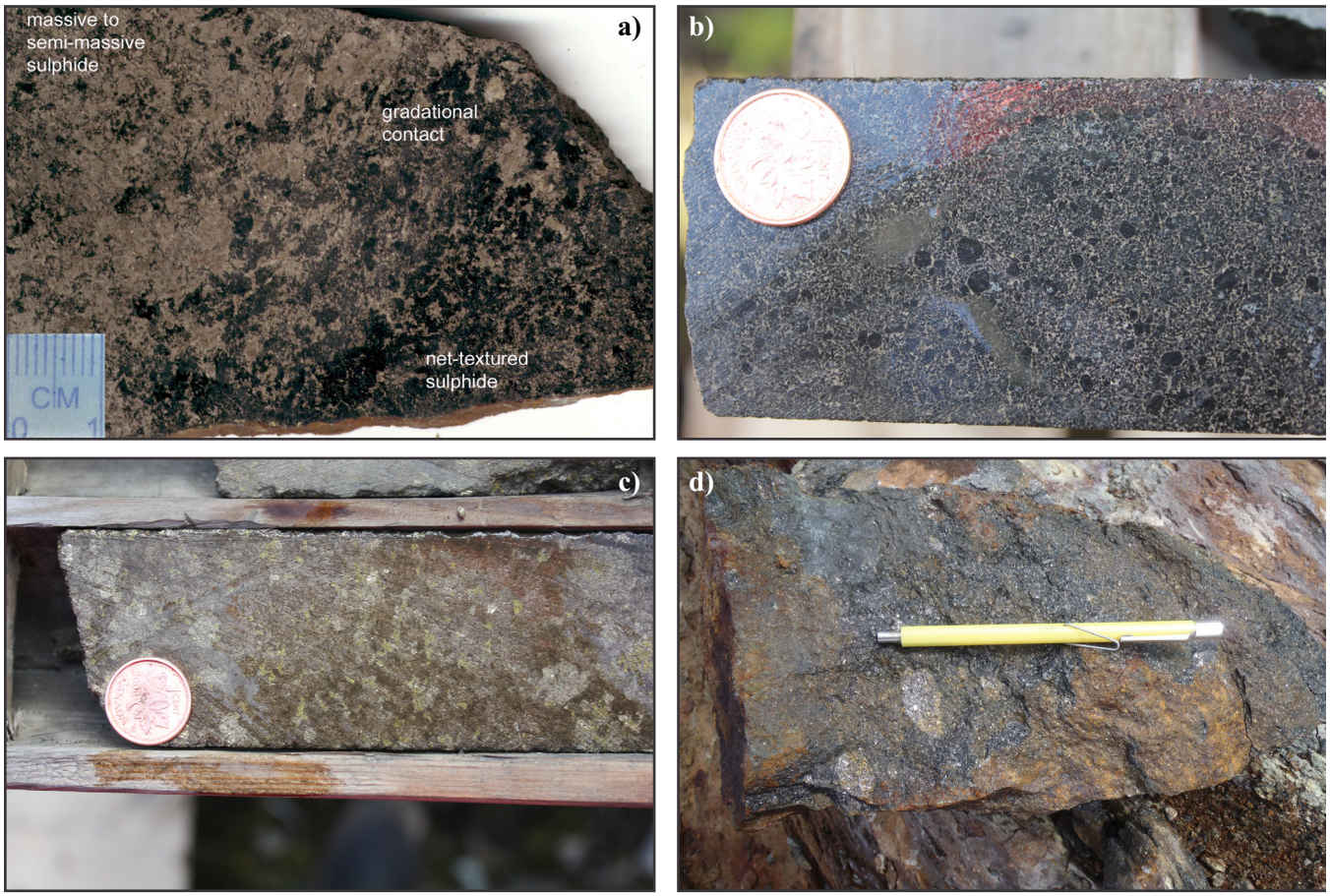

Figure 3. Typical Ni-Cu-(PGE) mineralization associated with mafic and ultramafic intrusions in the Bird River–Uchi–Oxford-Stull–La Grande Rivière–Eastmain (BUOGE) domains. **a)** Gradational contact between semi-massive sulphide and net-textured sulphide at the Maskwa deposit, Bird River Sill, Manitoba (after Stansell, 2006). **b)** Net-textured sulphide at Eagle's Nest in the Ring of Fire Intrusive Complex, Ontario. Coin is 1.8 cm in diameter. **c)** Massive sulphide at Eagle's Nest in the Ring of Fire Intrusive Complex, Ontario. Coin is 1.8 cm in diameter. **d)** Peridotite with disseminated sulphides containing centimetre-scale blebs of massive sulphides from the L occurrence in the Gayot area (courtesy of Mines Virginia). Magnetic pen is 12.3 cm.

the Eastmain domain whereas the second episode is the most significant one, spatially widespread throughout the BUOGE domains (e.g. Bird River, McFaulds Lake, Menarik) and Neoarchean age (ca. 2750–2734 Ma). In contrast to Cr-(PGE) mineralization, Ni-Cu-(PGE) and Fe-Ti-(V) deposits do not show the same spatial restriction with the BUOGE domains. However, within the BUOGE domains, Ni-Cu-(PGE) mineralization is associated with the same ultramafic-dominated intrusive bodies as Cr-(PGE) mineralization and Fe-Ti-(V) occurrences are contained within mafic-dominated intrusions in close vicinity to Cr-bearing intrusions, indicating a strong association of all these metals/mineralization styles. The connection between Cr-(PGE) and Ni-Cu-(PGE) deposits is that both styles of mineralization are formed in dynamic magma conduits.

Potential Remnant of Large Igneous Provinces

The defining features of Large Igneous Provinces (LIPs) include (Bryan and Ernst, 2008; Ernst and Jowitt, 2014) a minimum extrusive/intrusive volume exceeding 0.1 Mkm^3, a minimum areal extent of 0.1 Mkm^2, a short duration of magmatism of less than 50 Ma (but typically less than 10–15 Ma and in many cases a few Ma or less), multiple pulses of magmatism (LIPs with more than 20 Ma age spans typically contain multiple shorter pulses ranging from 1 to 5 Ma), and finally that the magmatism occurred in an intraplate tectonic setting.

Ultramafic to mafic magmatism of various types (e.g. komatiitic, tholeiitic, alkalic) extended over a period of more than 180 Ma within the BUOGE domains, from ca. 2.88 to 2.70 Ga (Table 1). However, four main intervals are recognized to have generated most of the ultramafic to mafic magmatism across these domains: 1) 2.88 to 2.87 Ga, 2) 2.82 to 2.80 Ga, 3) 2.75 to 2.73 Ga, and 4) 2.72 to 2.70 Ga (Fig. 1). In many cases, these age intervals are poorly constrained and might evolve as more precise U-Pb ages are obtained from ultramafic and mafic intrusive rocks. During the course of this study, the focus was placed on the third interval (2.75–2.72 Ga), which includes the

intrusive suites of the Bird River in Manitoba (ca. 2744–42 Ma), the Ring of Fire in Ontario (ca. 2734–33 Ma), and several but more localized ultramafic intrusions within the La Grande domain in Quebec (ca. 2750 Ma). Although limited in size (none of these appear to qualify for the areal extent and volume for a LIP), emplacement of large amounts of ultramafic to mafic magmas over a short period of time, especially in the MLGB and the BRGB, locally combined with komatiite-tholeiite successions, suggest that these intrusions might represent remnants of Archean LIPs. It has been suggested by Mungall et al. (2010) and Ernst and Jowitt (2014) that the mafic-ultramafic intrusions in the BRGB and the MLGB could be part of a single plume-related large igneous province. This hypothesis is plausible, despite the fact that the mafic-ultramafic intrusions in the BRGB, MLGB, and the YGB span over 20 Ma. Scoates and Scoates (2013) have proposed a different scenario in which these intrusions are not related. The mafic-ultramafic intrusions, which were formed by at least three magmatic pulses over 20 Ma (2.75–2.73 Ga), are associated with the emplacement of Cr-(PGE) and Ni-Cu-(PGE) deposits and significant Fe-Ti-(V) occurrences across the BUOGE domains. Furthermore, large amounts of subvolcanic-volcanic ultramafic-mafic rocks and inferred large magma fluxes occur at least in some of these areas (see discussion by Carson et al., 2015) favouring for a plume origin. More detailed investigation is warranted but we suggest that these intrusions may represent remnants of an Archean LIPs and rather than being associated with one single plume-related LIP event, they may be the result of multiple and separate large magmatic events that occurred locally within BUOGE domains and were not physically connected but shared similar geological settings that made these regions highly prospective for Cr-(PGE), Ni-Cu-(PGE), and Fe-Ti-(V) mineralization. At this stage, we cannot rule out completely the single-plume hypothesis, but we suggest that our hypothesis better explains the distribution of the Cr-(PGE) mineralization across the BUOGE domains where it may represent a significant metallogenic province within the Superior Craton.

IMPLICATIONS FOR EXPLORATION

Numerous mafic and ultramafic intrusions in the BUOGE domains appear to define an important Cr-(PGE) metallogenic province, which also contains characteristic Ni-Cu-(PGE) and Fe-Ti-(V) associations across the Superior Craton. These domains also appear to be fundamentally different from adjacent terrains, including the Ni-Cu-(PGE) dominated systems in the Abitibi greenstone belt or the apparently relatively unmineralized North Caribou core, Island Lake domain and Goudalie domain with respect to metal endowment (Cr-(PGE) > other areas with orthomagmatic mineralization), magma composition (low-Mg komatiite/high-Mg tholeiite versus high-Mg komatiite/tholeiite), and volcanic-subvolcanic setting (ultramafic intrusions > lava flows versus ultramafic intrusions < lava flows) (Fig. 1).

It is still unclear which factors might be responsible for this distinctive metal endowment, but some critical features appear to be important and may represent efficient metallotects for Cr-(PGE) mineralization (see also Carson et al., 2015), including the presence of 1) a large magmatic event of primitive mantle-derived magmas emplaced over a short duration, 2) significant nearby crustal discontinuities that could have focussed the passage of magma through the crust, and 3) favourable crustal architecture containing potential sulphur (e.g. sulphide-facies iron formation) and oxide reservoirs (e.g. oxide-facies iron formation) for generating the sulphides and chromitites within these ultramafic to mafic magmatic systems.

Thus far, only the Cr-(PGE) deposits (Black Thor, Black Label, Big Daddy, Black Creek, Black Horse, and Blackbird) and Ni-Cu-(PGE) deposits (Eagle's Nest) in the McFaulds Lake greenstone belt appear to be potentially economic. However, significant Cr-(PGE) mineralization occurs within other ultramafic-mafic intrusions across the BUOGE domains (Table 1) and highlights the prospectivity of these regions of the Superior Province. Ongoing and future work aims to establish geological settings and the main defining characteristics of orthomagmatic deposits in many of these areas. This could help to provide better constraints for the genesis of these orthomagmatic deposits and to evaluate the likelihood of discovering additional mineral resources in the BUOGE domains and also in other parts of the Superior Province or throughout the Canadian Shield.

AVAILABLE PRODUCTS

The preliminary results and interpretations of the BUOGE domains, previously referred to as a "super-domain", have been presented at national and international scientific meetings in Winnipeg (Canada: Houlé et al., 2013a) and in Upsala (Sweden: Houlé et al., 2013b), and at the joint assembly of the AGU-GAC-MAC-CGU to be held in Montréal in May 2015. Further forthcoming contributions from this project are planned within each study area (see Bécu et al., 2015; Houlé et al., 2015b; Metsaranta et al., 2015; and Sappin et al., 2015) also in addition to the BUOGE-scale.

ACKNOWLEDGEMENTS

This work has been supported by the Geological Survey of Canada TGI-4 program, the Natural Sciences and Engineering Research Council of Canada

Collaborative Research and Development Grant and Discovery Grant programs, and numerous mining companies, especially Mustang Minerals Corp., Gossan Resources Ltd., Cliffs Natural Resources Ltd., KWG Resources Inc., MacDonald Mines Ltd., Noront Resources Ltd., Northern Shield Resources Inc., Azimut Exploration Inc., and Monarque Resources Inc.. We would like to express our appreciation to numerous colleagues, including Greg Stott (formerly Ontario Geological Survey), Tim Corkery (formerly Manitoba Geological Survey), Scott Anderson, and Paul Kremer (Manitoba Geological Survey), and Jean-Yves Labbé, Daniel Bandyayera, and Claude Dion (MERN) for valuable discussions on the geology of the Superior Province. We also acknowledge the involvement and participation of numerous researchers, students, and mining company geologists in the high-magnesium ultramafic to mafic system subproject of the Targeted Geoscience Initiative 4 of the Geological Survey of Canada. We are also grateful to Greg Stott for his prompt and constructive reviews that helped us improve the final version of this contribution.

REFERENCES

Anderson, S.D., 2005. Preliminary results and economic significance of geological mapping in the Gem Lake area, southeastern Rice Lake belt, Manitoba (NTS 52L11 and 14), with emphasis on the Neoarchean Gem assemblage; *In:* Report of Activities 2005; Manitoba Industry, Economic Development and Mines, Manitoba Geological Survey, p. 104–116.

Anderson, S.D., 2013. Geology of the Garner–Gem lakes area, Rice Lake greenstone belt, southeastern Manitoba (parts of NTS 52L11, 14). Manitoba Science, Technology, Energy and Mines; Manitoba Geological Survey, Geoscientific Report GR2013-1, 135 p.

Anderson, S.D., 2014. Geological Overview of the Rice Lake Belt, *In:* Short Course: Geology and Mineral Potential of Manitoba's Premier Mineral Belts: Rice Lake/Bird River Belt; Manitoba Minerals and Mining Convention 2014, November 2014, Winnipeg, Manitoba.

Bécu, V., Houlé, M.G., McNicoll, V.J., Yang, X.M., and Gilbert, H.P., 2015. Mafic intrusive rocks from the Bird River intrusive suite, Bird River greenstone belt, southeast Manitoba, *In:* Targeted Geoscience Initiative 4: Canadian Nickel-Copper-Platinum Group Elements-Chromium Ore Systems — Fertility, Pathfinders, New and Revised Models, (ed.) D.E. Ames and M.G. Houlé; Geological Survey of Canada, Open File 7856, p. 49–60.

Bryan, S.E. and Ernst, R.E., 2008. Revised definition of Large Igneous Provinces (LIPs); Earth-Science Reviews, v. 86, p. 175–202.

Blackburn, C.E. and Young, J.B. 2000. Precambrian geology of the Separation Lake area, northwestern Ontario; Ontario Geological Survey, Open File Report 6001, 84 p.

Card, K.D. and Ciesielski, A., 1986. Subdivisions of the Superior Province of the Canadian Shield; Geoscience Canada, v. 13, p. 5–13.

Card, K.D. and Poulsen, K.H., 1998a. Archean and Paleoproterozoic and metallogeny of the southern Canadian Shield; Exploration and Mining Geology, v. 7, p. 181–215.

Card, K.D. and Poulsen, K.H., 1998b. Geology and mineral deposits of the Superior Province of the Canadian Shield, *In:* Geology of the Precambrian Superior and Grenville Provinces and Precambrian Fossils in North America, (ed.) S. Lucas and M.R. St-Onge; Geological Survey of Canada, Geology of Canada, no. 7, p. 13–194.

Carson, H.J.E., Lesher, C.M., and Houlé, M.G., 2015. Geochemistry and petrogenesis of the Black Thor intrusive complex and associated chromite mineralization, McFaulds Lake greenstone belt, Ontario *In:* Targeted Geoscience Initiative 4: Canadian Nickel-Copper-Platinum Group Elements-Chromium Ore Systems — Fertility, Pathfinders, New and Revised Models, (ed.) D.E. Ames and M.G. Houlé; Geological Survey of Canada, Open File 7856, p. 87–102.

Corkery, M.T., Davis, D.W., and Lenton, P.G., 1992. Geochronological constraints on the development of the Cross Lake greenstone belt, northwest Superior Province, Manitoba; Canadian Journal of Earth Sciences, v. 29, p. 2171–2185.

David, J., Maurice, C., and Simard, M., 2009. Datations isotopiques effectuées dans le nord-est de la Province du Supérieur; Travaux de 1998-1999-2000; Ministère des Ressources naturelles du Québec, DV 2008-05, 92 p.

Davis, D.W., 1994. Report on the geochronology of rocks from the Rice Lake belt, Manitoba; Royal Ontario Museum, Geology Department, Toronto, Ontario, unpub. report.

Douglas, R.J.W. 1973. Geological provinces, *In:* The National Atlas of Canada (4th edition); Department of Energy, Mines, and Resources, Ottawa, p. 27-28.

Ernst, R.E. and Jowitt, S.M., 2014. Large Igneous Provinces (LIPs) and metallogeny, *In:* Tectonics, Metallogeny, and Discovery: The North American Cordillera and Similar Accretionary Settings, (ed.) M. Colpron, T. Bissig, B.G. Rusk, and J.F.H. Thompson; Society of Economic Geologists, Special Publication 17, p. 17–51.

Gilbert, H.P. and Kremer, P.D., 2014. Geological Overview of the Bird River Belt, Southeastern Manitoba, *In:* Short Course: Geology and Mineral Potential of Manitoba's Premier Mineral Belts: Rice Lake/Bird River Belt; Manitoba Minerals and Mining Convention 2014, November 2014, Winnipeg, Manitoba.

Gilbert, H.P., Davis, D.W., Duguet, M., Kremer, P.D., Mealin, C.A., and MacDonald, J., 2008. Geology of the Bird River Belt, southeastern Manitoba (parts of NTS 52L5, 6); Manitoba Geological Survey, Geoscientific Map MAP2008-1, scale 1:50 000 (plus notes and appendix).

Goutier, J., Dion, C., Ouellet, M.-C., Davis, D.W., David, J., and Parent, M., 2002. Géologie de la région du lac Guyer (33G/05, 33/G06 et 33G/11); Ministère des Ressources naturelles du Québec, RG 2001-15, 53 p.

Houlé, M.G. and Lesher, C.M., 2011. Komatiite-associated Ni-Cu-(PGE) deposits, Abitibi Greenstone Belt, Superior Province, Canada; Review in Economic Geology, v. 17, p. 89–121.

Houlé, M.G., Lesher, C.M., Metsaranta, R.T., Goutier, J., McNicoll, V.J. and Gilbert, H.P., 2013a. Temporal and spatial distribution of magmatic Ni-Cu-PGE/Cr-PGE/Fe-Ti-V deposits in the Bird River/Uchi/Oxford–Stull/La Grande-Eastmain superdomain*:* A new metallotect within the Superior Province, *In:* Program with Abstracts; Geological Association of Canada–Mineralogical Association of Canada, Joint Annual Meeting, Winnipeg, Manitoba, v. 36, p. 115.

Houlé, M.G., Lesher, C.M., Metsaranta, R.T., Goutier, J., Gilbert, H.P. and McNicoll, V.J., 2013b. Temporal and spatial distribution of magmatic Ni-Cu-PGE, Cr, and Fe-Ti-V deposits in the Bird River–Uchi–Oxford-Stull–La Grande–Eastmain Superdomain*:* A new metallotect within the Superior Province; *In:* Abstracts; Society for Geology Applied to Minerals, 12th SGA Biennial

Meeting, Uppsala, Sweden, August 12–15, 2013, Proceedings, v. 3, p. 1009–1012.

Houlé, M.G., McNicoll, V.J., Bécu, V., Yang, X.M., and Gilbert, H.P., 2013c. New age for the Mayville intrusion: implication for a large mafic-ultramafic event in the Bird River greenstone belt, southeastern Manitoba, *In:* Program with Abstracts; Geological Association of Canada – Mineralogical Association of Canada Joint Annual Meeting, Winnipeg, Manitoba, May 2013, Abstract Volume 36, p. 115.

Houlé, M.G., Lesher, C.M., McNicoll, V., Metsaranta, R.T., Sappin, A.-A., Goutier, J., Bécu, V., and Gilbert, H.P., 2015a. Mafic-ultramafic magmatism in the Bird River/Uchi/Oxford-Stull/La Grande-Eastmain Superdomain*:* potential remnants of Meso- and Neoarchean LIPs in the Northern Superior Province, *In:* Program with Abstracts; American Geophysical Union – Canadian Geophysical Union - Geological Association of Canada–Mineralogical Association of Canada, Joint Annual Meeting, Montréal, Quebec.

Houlé, M.G., Goutier, J., Sappin, A.-A., and McNicoll, V.J., 2015b. Regional characterization of ultramafic to mafic intrusions in the La Grande Rivière and Eastmain domains, Superior Province, Quebec, *In:* Targeted Geoscience Initiative 4: Canadian Nickel-Copper-Platinum Group Elements-Chromium Ore Systems — Fertility, Pathfinders, New and Revised Models, (ed.) D.E. Ames and M.G. Houlé; Geological Survey of Canada, Open File 7856, p. 125–137.

Hrabi, R.B. and Cruden, A.R. 2006. Structure of the Archean English River subprovince: implications for the tectonic evolution of the western Superior Province, Canada; Canadian Journal of Earth Sciences, p. 947–966.

Jackson, J.A., 1997. Glossary of Geology–Fourth Edition; American Geological Institute, Alexandria, Virginia, U.S.A., 769 p.

Kuzmich, B., Hollings, P., and Houlé, M.G., 2015. Petrogenesis of the ferrogabbroic intrusions and associated Fe-Ti-V-(P) mineralization within the McFaulds greenstone belt, Superior Province, northern Ontario, *In:* Targeted Geoscience Initiative 4: Canadian Nickel-Copper-Platinum Group Elements-Chromium Ore Systems — Fertility, Pathfinders, New and Revised Models, (ed.) D.E. Ames and M.G. Houlé; Geological Survey of Canada, Open File 7856, p. 101–109.

Lang, A.H., 1961. A Preliminary Study of Canadian Metallogenic Provinces; Geological Survey of Canada, Paper 60-33, 54 p.

Metsaranta, R.T., Houlé, M.G., McNicoll, V.J., and Kamo, S.L., 2015. Revised geological framework for the McFaulds Lake greenstone belt, Ontario, *In:* Targeted Geoscience Initiative 4: Canadian Nickel-Copper-Platinum Group Elements-Chromium Ore Systems — Fertility, Pathfinders, New and Revised Models, (ed.) D.E. Ames and M.G. Houlé; Geological Survey of Canada, Open File 7856, p. 61–73.

Moukhsil, A., Legault, M., Boily, M., Doyon, J., Sawyer, E., and Davis, D., 2007. Geological and metallogenic synthesis of the Middle and Lower Eastmain greenstone belt (Baie James); ministère des Resources naturelles du Quebec, ET-2007-01, 55 p.

Mungall, J.E., Harvey, J.D., Balch, S.J., Azar, B., Atkinson, J., and Hamilton, M.A., 2010. Eagle's Nest: A magmatic Ni-sulfide deposit in the James Bay Lowlands, Ontario, Canada, *In:* The Challenge of Finding New Mineral Resources: Global Metallogeny, Innovative Exploration, and New Discoveries, Volume I: Gold, Silver, and Copper-Molybdenum, (ed.) R.J. Goldfarb, E.E. Marsh, and T. Monecke; Society of Economic Geologists, Special Publication 15, p. 539–559.

Parks, J., Lin, S., Davis, D., Yang, X.-M., and Corkery, T., 2014. Meso- and Neoarchean evolution of the Island Lake greenstone belt and the northwestern Superior Province: Evidence from lithogeochemistry, Nd isotope data, and U–Pb zircon geochronology; Precambrian Research, v. 246, p. 160–179.

Percival, J.A. 2007. Geology and metallogeny of the Superior Province, Canada, *In:* Mineral Deposits of Canada: A Synthesis of Major Deposit Types, District Metallogeny, the Evolution of Geological Provinces, and Exploration Methods, (ed.) W.D. Goodfellow; Geological Association of Canada, Mineral Deposits Division, Special Publication No. 5, p. 903–928.

Percival, J.A., Mortensen, J.K., Stern, R.A., Card, K.D., and Bégin, N.J., 1992. Giant granulite terranes of northeastern Superior Province; the Ashuanipi Complex and Minto Block; Canadian Journal of Earth Sciences, v. 29, p. 2287–2308.

Percival, J.A., Sanborn-Barrie, M., Stott, G., Helmstaedt, H., Skulski, T., and White, D.J., 2006. Tectonic evolution of the Western Superior Province from NATMAP and LITHOPROBE studies; Canadian Journal of Earth Sciences, p. 1085–1117.

Percival, J.A., Skulski, T., Sanborn-Barrie, M., Stott, G.M., Leclair, A.D., Corkery, M.T., and Boily, M. 2012. Geology and tectonic evolution of the Superior Province, Canada, Chapter 6 *In:* Tectonic Styles in Canada: The LITHOPROBE Perspective, (ed.) J.A. Percival, F.A. Cook, and R.M. Clowes; Geological Association of Canada, Special Paper 49, p. 321–378.

Poulsen, K.H., Card, K.D., and, Franklin, J.M., 1992. Archean tectonic and metallogenic evolution of the Superior Province of the Canadian Shield; Precambrian Research, v. 58, p. 25–54.

Sappin, A.-A., Houlé, M.G., Lesher, C.M., Metsaranta, R.T., and McNicoll, V.J., 2015. Regional characterization of mafic-ultramafic intrusions in the Oxford-Stull and Uchi domains, Superior Province, Ontario, *In:* Targeted Geoscience Initiative 4: Canadian Nickel-Copper-Platinum Group Elements-Chromium Ore Systems — Fertility, Pathfinders, New and Revised Models, (ed.) D.E. Ames and M.G. Houlé; Geological Survey of Canada, Open File 7856, p. 75–85.

Scoates, J.S. and Scoates, R.F.J., 2013. Age of the Bird River Sill, southeastern Manitoba, Canada, with implications for the secular variation of layered intrusion-hosted stratiform chromite mineralization; Economic Geology, v. 108, p. 895–907.

Stansell, A.E., 2006. Sulphide fragments in waste rock at the Maskwa open pit mine, southeastern Manitoba (NTS 52L6 NW): investigations on petrogenesis, potential source rocks and mode of emplacement; B.Sc. thesis, University of Manitoba, Winnipeg, Manitoba, 90 p.

Stott, G.M., 1997. The Superior Province, Canada, *In:* Greenstone Belts, (ed.) M.J. De Wit and L.D. Ashwal; Oxford Monographs on Geology and Geophysics, v. 35, p. 480–507.

Stott, G.M., 2008a. Precambrian geology of the Hudson Bay and James Bay lowlands region interpreted from aeromagnetic data—west sheet; Ontario Geological Survey, Preliminary Map P.3597—Revised, scale 1:500 000.

Stott, G.M., 2008b. Precambrian geology of the Hudson Bay and James Bay lowlands region interpreted from aeromagnetic data—east sheet; Ontario Geological Survey, Preliminary Map P.3598—Revised, scale 1:500 000.

Stott, G.M., 2009. Precambrian geology of the Hudson Bay and James Bay lowlands region interpreted from aeromagnetic data—south sheet; Ontario Geological Survey, Preliminary Map P.3599—Revised, scale 1:500 000

Stott, G.M., Corkery, M.T., Percival, J.A., Simard, M., and Goutier, J., 2010. A revised terrane subdivision of the Superior Province, *In:* Summary of Field Work and Other Activities 2010; Ontario Geological Survey, Open File Report 6260, p. 20-1 to 20-10.

Thurston, P.C., Osmani, I.A., and Stone, D., 1991. Northwestern Superior Province: review and terrane analysis, *In:* Geology of Ontario, (ed.) P.C. Thurston, H.R. Williams, R.H. Sutcliffe, and G.M. Scott; Ontario Geological Survey, Special Volume 4, Part 1, p. 81–142.

Williamson, B., 1990. Geology of the Bird River Sill at the Chrome Property, southeast Manitoba; Geological Survey of Canada, Open File 2067, 44 p.

Young, M.D., McNicoll, V.J., Helmstaedt, H., Skulski, T., Percival, J.A., 2006. The western Superior Province Lithoprobe and NATMAP transects--Les geotraverses des projets CARTNAT et Lithoprobe de la Province du lac Superieur occidentale; Canadian Journal of Earth Sciences, v. 43, p. 821–847.

GEOLOGICAL SURVEY OF CANADA
OPEN FILE 7856

Targeted Geoscience Initiative 4: Canadian Nickel-Copper-Platinum Group Elements-Chromium Ore Systems — Fertility, Pathfinders, New and Revised Models

Mafic intrusive rocks from the Bird River intrusive suite, Bird River greenstone belt, southeast Manitoba

Valérie Bécu[1], Michel G. Houlé[1], Vicki J. McNicoll[2], Eric (Xueming) M. Yang[3], and H. Paul Gilbert[3]

[1]Geological Survey of Canada, Québec, Quebec
[2]Geological Survey of Canada, Ottawa, Ontario
[3]Manitoba Geological Survey, Winnipeg, Manitoba

2015

© Her Majesty the Queen in Right of Canada, as represented by the Minister of Natural Resources Canada, 2015

This publication is available for free download through GEOSCAN (http://geoscan.nrcan.gc.ca/)

Recommended citation

Bécu, V., Houlé, M.G., McNicoll, V.J., Yang, X.M., and Gilbert, H.P., 2015. Mafic intrusive rocks from the Bird River intrusive suite, Bird River greenstone belt, southeast Manitoba, *In:* Targeted Geoscience Initiative 4: Canadian Nickel-Copper-Platinum Group Elements-Chromium Ore Systems — Fertility, Pathfinders, New and Revised Models, (ed.) D.E. Ames and M.G. Houlé; Geological Survey of Canada, Open File 7856, p. 49–60.

Publications in this series have not been edited; they are released as submitted by the author.

Contribution to the Geological Survey of Canada's Targeted Geoscience Initiative 4 (TGI-4) Program (2010–2015)

TABLE OF CONTENTS

Mafic intrusive rocks from the Bird River intrusive suite, Bird River greenstone belt, southeast Manitoba

Valérie Bécu[1*], Michel G. Houlé[1], Vicki J. McNicoll[2], Eric (Xueming) M. Yang[3], and H. Paul Gilbert[3]

[1]Geological Survey of Canada, 490 rue de la Couronne, Québec, Quebec G1K 9A9
[2]Geological Survey of Canada, 601 Booth Street, Ottawa, Ontario K1A 0E8
[3]Manitoba Geological Survey, 360–1395 Ellice Avenue, Winnipeg, Manitoba R3G 3P2
*Corresponding author's e-mail: Valerie.Becu@RNCan-NRCan.gc.ca

ABSTRACT

This study presents new field, petrographic, and geochemical observations for the Coppermine Bay and Euclid Lake intrusions of the Bird River greenstone belt, allowing for comparison with the Mayville and other Bird River sill intrusions in southeast Manitoba. The mafic-dominated Coppermine Bay intrusion, located in the westernmost part of the southern arm of the Bird River greenstone belt, is texturally and petrographically similar to the mafic part of the mafic-ultramafic Euclid Lake intrusion, located 34 km to the northeast, at the northeast margin of the belt's northern arm. The mafic components of the Coppermine Bay and Euclid Lake intrusions possess textural, compositional, and geochemical similarities with the Mayville and with mafic parts of other Bird River sill intrusions. Combined with geochemical and geochronological investigations, a petrogenetic linkage of these mafic-ultramafic intrusions is proposed through a widespread Neaoarchean Bird River magmatic event at ca. 2743 Ma, referred to as the Bird River intrusive suite. TiO_2 and Zr contents, as well as rare earth elements profiles and plagioclase chemistry, may be useful geochemical tools to successfully discriminate and identify potentially fertile intrusions beyond traditionally explored sectors in the Bird River greenstone belt.

INTRODUCTION

In 2011, the Geological Survey of Canada (GSC), through the Targeted Geoscience Initiative 4 (TGI-4) program, in collaboration with the Manitoba Geological Survey (MGS), initiated a multi-year project to characterize mafic and ultramafic intrusions and associated Ni-Cu-(PGE) and Cr-(PGE) orthomagmatic mineralization within the Neoarchean Bird River greenstone belt (BRGB) of southeast Manitoba.

Building on detailed work done in the mid- to late 1980s on the well exposed Chrome property located within the central part of the southern arm of the BRGB (e.g. Scoates, 1983; Scoates et al., 1986, 1989; Williamson, 1990), the current investigation focuses on mafic-ultramafic intrusions located in both the northern and southern arms of the BRGB (Fig. 1) with special emphasis on characterizing the mafic component of intrusive bodies and providing a geological framework for ongoing geochronological work carried out across the belt. More specifically, textural, petrographic, and geochemical results from the less studied Coppermine Bay and the Euclid Lake intrusions, within the southern and northern arms of the BRGB, respectively, are presented and compared with the Mayville intrusion, which is economically the most significant intrusion of the belt's northern arm.

PREVIOUS AND CURRENT WORK

For more than a century the BRGB has been the subject of extensive geological investigations, including regional mapping initiatives and targeted economic mineral studies. Most recently, the MGS carried out regional bedrock mapping initiatives that mainly focussed on the southern (Gilbert et al., 2008) and northern portions (Yang et al., 2012, 2013) of the belt. Readers are referred to Gilbert et al. (2013) for an introduction to the geology and an overview of previous and current work carried out in the belt.

Numerous mafic to ultramafic intrusions containing significant Cr-(PGE) and Ni-Cu-(PGE) mineralization in both arms of the BRGB were recognized early. However, it was not until the discovery of Ni-Cu occurrences east of the Maskwa River in 1917 (Bateman, 1943) that more sustained mineral exploration led to significant discoveries of Ni-Cu and chromite deposits and occurrences hosted in mafic-ultramafic intrusive rocks of the Bird River area (Bird River Sill-BRS), in the southern arm of the BRGB.

Bécu, V., Houlé, M.G., McNicoll, V.J., Yang, X.M., and Gilbert, H.P., 2015. Mafic intrusive rocks from the Bird River intrusive suite, Bird River greenstone belt, southeast Manitoba, *In:* Targeted Geoscience Initiative 4: Canadian Nickel-Copper-Platinum Group Elements-Chromium Ore Systems — Fertility, Pathfinders, New and Revised Models, (ed.) D.E. Ames and M.G. Houlé; Geological Survey of Canada, Open File 7856, p. 49–60.

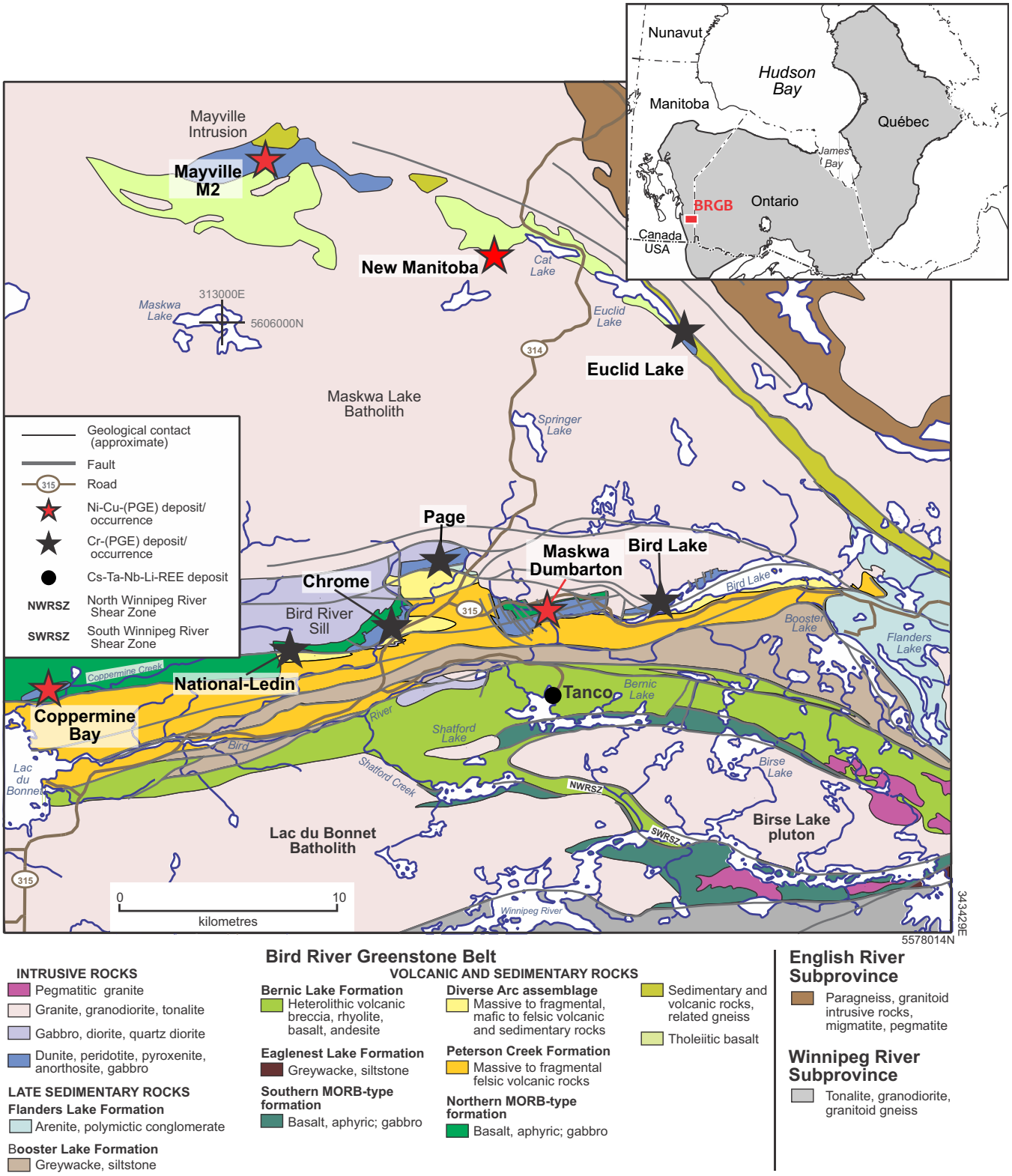

Figure 1. Simplified geology of the northern and southern arms of the Bird River greenstone belt (BRGB) showing the main mafic and ultramafic igneous bodies and associated Ni-Cu-(PGE) and Cr-(PGE) deposits/occurrences, as well as the TANCO Cs-Ta-Nb-Li-REE deposit (modified from Gilbert et al., 2013).

Table 1. Compilation of historical production and resource calculations for nine Ni-Cu-(PGE) and Cr-PGE) deposits/occurrences of the Bird River greenstone belt, southeast Manitoba.

Deposit / Intrusion	District	Ore (Mt)	Ni (%)	Cu (%)	Pt+Pd (g/t)	Cr_2O_3 (%)	Data Source
M2 - Mayville	Northern arm	31.80	0.18	0.45	0.19		Mustang Minerals Corp., 2013
New Manitoba*	Northern arm	0.60	0.24	0.58			Manitoba Inventory File No. 217
Maskwa	Southern arm – BRS	8.27	0.61	0.13	0.42		Coats et al., 1979; Mustang Minerals Corp., 2013
Dumbarton*	Southern arm – BRS	1.54	0.81	0.30			Coats et al., 1979
Page & Ore Fault	Southern arm – BRS	0.55	0.94	0.56	0.35		Marathon PGM Corp., 2008
Euclid Lake*	Northern arm	4.69				6.44	ILAM Associates, 1988
Bird Lake*	Southern arm – BRS	1.12				7.53	ILAM Associates, 1988
Chrome*	Southern arm – BRS	1.34				9.65	ILAM Associates, 1988
Page*	Southern arm – BRS	1.71				7.40	ILAM Associates, 1988

*Not NI 43-101 compliant

Since the initial discoveries, sporadic exploration over the years has led to Ni-Cu and Cr mineral resource estimates (Table 1). Of specific relevance to this contribution, brief overviews of exploration work carried out on the Coppermine Bay, Euclid Lake, and Mayville intrusions are presented herein.

Coppermine Bay Intrusion

Gabbroic rocks of the Coppermine Bay intrusion (Wards claim), in the western extremity of the BRGB's southern arm, were interpreted by Bannatyne and Trueman (1982) and more recently by Gilbert et al. (2008) as a distinct intrusive unit that does not correlate with other BRS intrusions, despite the presence of Cu-Ni-(PGE) and Cr mineralization. The first report of chromite within the Coppermine Bay gabbro dates back to 1929 (Watson, 1982); however, the chromite lenses were interpreted as too small and scattered to be of economic interest (e.g. Bateman, 1943). Since then, Cu-Ni and PGE intersections reported from a single drillhole in 1973 (0.42% Cu, 0.24% Ni, and 2.2 g/t Pt+Pd over 12.2 m; Canex Placer Ltd., 1973) revitalized interest in the economic potential of the intrusion and led Marathon PGM Corporation and Gossan Resources Limited to pursue sporadic exploration in the area between 2004 and 2010. The best results were obtained from a grab sample that graded up to 0.44% Cu%, 0.21% Ni, and 2.6 g/t Pt+Pd (Gossan Resources Ltd., 2007 – reporting Marathon PGM Corporation's initial results).

Euclid Lake Intrusion

The Euclid Lake intrusion, located in the eastern extremity of the BRGB's northern arm, has been interpreted to be an extension of the BRS (e.g. Bateman, 1942; Trueman, 1980). Chromite mineralization was first discovered on the property in 1942 and several chromite resource estimates were subsequently made in the 1980s, mainly based on compilation of historical diamond-drill records (Table 1). Since then, some prospecting activities were carried by Exploratus Elementis Diversis Ltd. in the 1990s and more recently, Mustang Minerals Corporation ("Mustang") carried out geophysical and geological surveys in 2005 and drilled three diamond drillholes in 2011.

Mayville Intrusion

The Mayville intrusion was initially delineated during regional bedrock mapping carried out in the northern arm of the BRGB by the MGS in the late 1940s (Springer 1949, 1950), but it was not until the mid-1980s that the first geological map was published for the western part of the intrusion (Macek, 1985). Ni-Cu sulphide mineralization and chromite occurrences (e.g. Theyer, 1985) led several exploration companies (Exploratus Ltd., Falconbridge Ltd., and TANCO) to conduct detailed geological mapping; other thematic studies were subsequently carried out by the MGS (Peck and Theyer, 1998; Peck et al., 1999, 2002). More recently, Mustang completed detailed geological mapping of the intrusion and updated mineral resource estimates for the M2 Ni-Cu-(PGE) deposit (Table 1). In 2012, the MGS remapped the Mayville intrusion and surrounding area at 1: 12 500 scale, which was updated to 1:10 000 scale in 2014 (Yang, 2014).

PETROGRAPHY AND GEOCHEMISTRY

For simplicity, the prefix "meta" is not used in the following section with the understanding that all rocks have undergone greenschist- to amphibolite-facies metamorphism. Primary minerals have been mostly replaced, but original textures and crystal forms are usually preserved, thus pseudomorphs (e.g. pyroxene) were often used to determine the primary mineralogy.

Coppermine Bay Intrusion

The Coppermine Bay intrusion consists of a series of relatively poorly exposed outcrops distributed along a 2 km long by 400 m wide, northeast-trending corridor in which a Cu-Ni-(PGE) mineralized zone with an 800

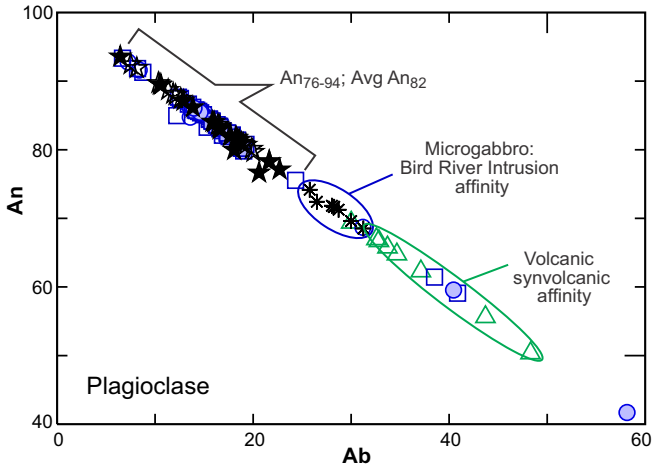

Figure 2. Anorthite (An) versus albite (Ab) components of plagioclase from leuco- to anorthositic gabbro, gabbro, melagabbro, microgabbro, and mafic volcanic units from the Coppermine Bay and Euclid Lake intrusions. Refer to the legend in Figure 4.

m strike length was delineated by Gossan Resources Ltd. (2007). Exposed lithologies include gabbro, leucogabbro, anorthositic gabbro, and rare pyroxenite intercalated with volcanic rocks from the Northern-MORB formation (Gilbert et al., 2008). The Coppermine Bay rocks are medium- to coarse-grained and are composed of calcic plagioclase (Fig. 2) and magnesiohornblende with minor biotite, chlorite, carbonate, and local skeletal ilmenite. Although volumetrically less significant than other lithologies, melagabbroic rocks, which were mainly intersected in drill core, consist of magnesiohornblende and calcic plagioclase (Fig. 2), with variable amounts of biotite, chlorite, and epidote. These units are usually fine- to medium-grained and grain size coarsens generally with increasing plagioclase abundance. The melagabbroic rocks are quite significant as they are the main host-lithology for the Cu-Ni-(PGE) disseminated sulphide mineralization and for the chromite mineralization that grades up to 10.7% Cr_2O_3 locally. Gabbroic, leucogabbroic, and anorthositic rocks of the Coppermine Bay intrusion (Fig. 3a) are texturally similar to other gabbroic rocks of the BRS (Fig. 3b,c,d).

The Coppermine Bay gabbroic rocks display similar contents of MgO, SiO_2, FeO_T, TiO_2, and Zr to those in gabbro and anorthositic gabbro samples obtained by Mealin (2008) from the Chrome property of the BRS (Fig. 4). Rare earth elements (REE) ratios are constant to slightly depleted from La to Nd and REE profiles are relatively flat or show slightly positive slope from Gd to Lu (Fig. 5a). Well defined Eu anomalies are noticeable for most samples and REE profiles exhibit some similarities with the ones obtained at the Chrome property (Fig. 5a).

Mafic volcanic rocks are characteristically dark grey, fine-grained and consist of an amphibole-plagioclase-chlorite assemblage with minor apatite. Altough the MgO and SiO_2 contents are comparable, the FeO_T, TiO_2, and Zr contents are slightly higher than those of the anorthositic to melagabbroic units of the Coppermine Bay intrusion.

Distinct REE profiles, with overall enrichment, positive slope from La to Nd, and minor negative Eu anomalies characterize the volcanic rocks from the intrusion-related gabbroic units (Fig. 5a).

Microgabbro observed in drill core at Coppermine Bay, has sharp to diffuse contacts with bounding gabbroic to leucogabbroic and mafic volcanic units (Fig. 3g). They predominantly consist of fine-grained to aphanitic rocks composed mainly of calcic plagioclase (Fig. 2) and amphibole with minor chlorite. Whereas they possess comparable MgO, SiO_2, FeO_T concentrations to those from coarser gabbroic rock units, two samples exhibit distinctively higher TiO_2 and Zr contents. The higher TiO_2 and Zr contents are comparable to abundances encountered within mafic volcanic units as well as in Northern and Southern MORB-type formations of Gilbert et al. (2008) (Fig. 4). This suggests a volcanic affinity for these rocks, which is also reflected by their REE profiles (Fig. 5a).

Euclid Lake Intrusion

The Euclid Lake intrusion is a poorly exposed mafic to ultramafic intrusion in which Bateman (1943), Springer (1950), and Trueman (1997) reported a few surface exposures of peridotite that contained thin layers of disseminated and dense chromite over a distance of 15 m. Examination of the 2011 drillholes, led Bécu et al. (2013) to propose that the Euclid Lake intrusion consists of an ultramafic zone intercalated between two mafic zones. This differs from the ultramafic sequence overlain by a mafic sequence that is typically observed elsewhere in BRS intrusions.

Medium- to coarse-grained gabbro, leucogabbro, and anorthositic gabbro (Fig. 3e) are the main rock units encountered in a recent cross-section investigation (Bécu et al., 2013). These rocks are texturally sim-

Figure 3 (opposite page). Outcrop and drill-core photographs showing textural similarities between gabbroic units from mafic-ultramafic intrusions in the Bird River greenstone belt. **a)** Medium-grained leucogabbro of the Coppermine Bay intrusion. **b)** Medium-grained leucogabbro of the Chrome intrusion (from Williamson, 1990). **c)** Medium-grained leucogabbroic to anorthositic unit of the Maskwa-Dumbarton intrusion. **d)** Medium- to coarse-grained leucogabbro to anorthosite of the Bird Lake intrusion. **e)** Medium-grained anorthositic to leucogabroic unit of the Euclid Lake intrusion. **f)** Medium- to coarse-grained leucogabbro to anorthosite of the Mayville intrusion. **g)** Fine-grained microgabbro unit of the Coppermine Bay intrusion. **h)** Fine- to medium-grained synvolcanic gabbro of the Euclid Lake intrusion.

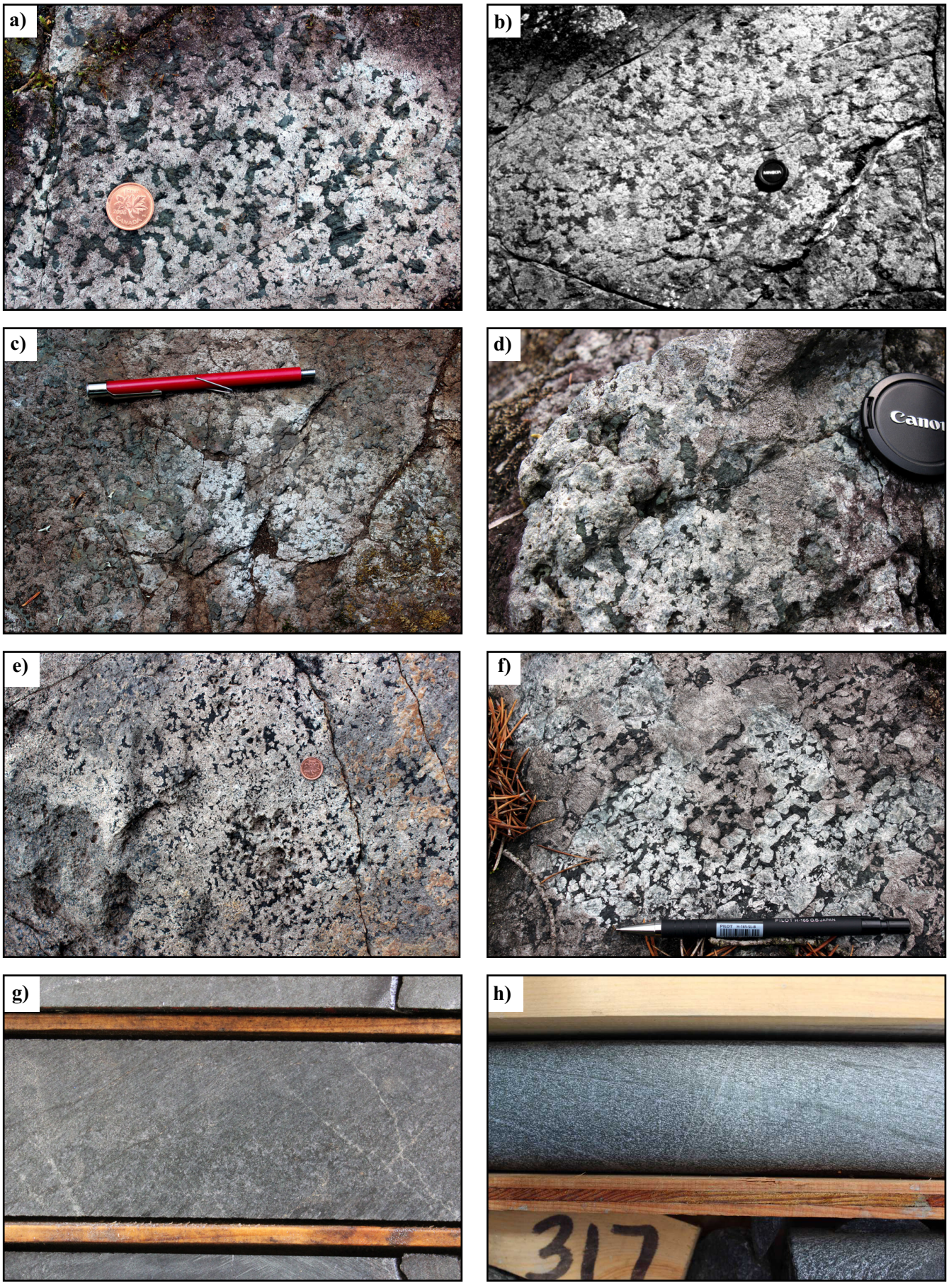
a)
b)
c)
d)
e)
f)
g)
h)
317

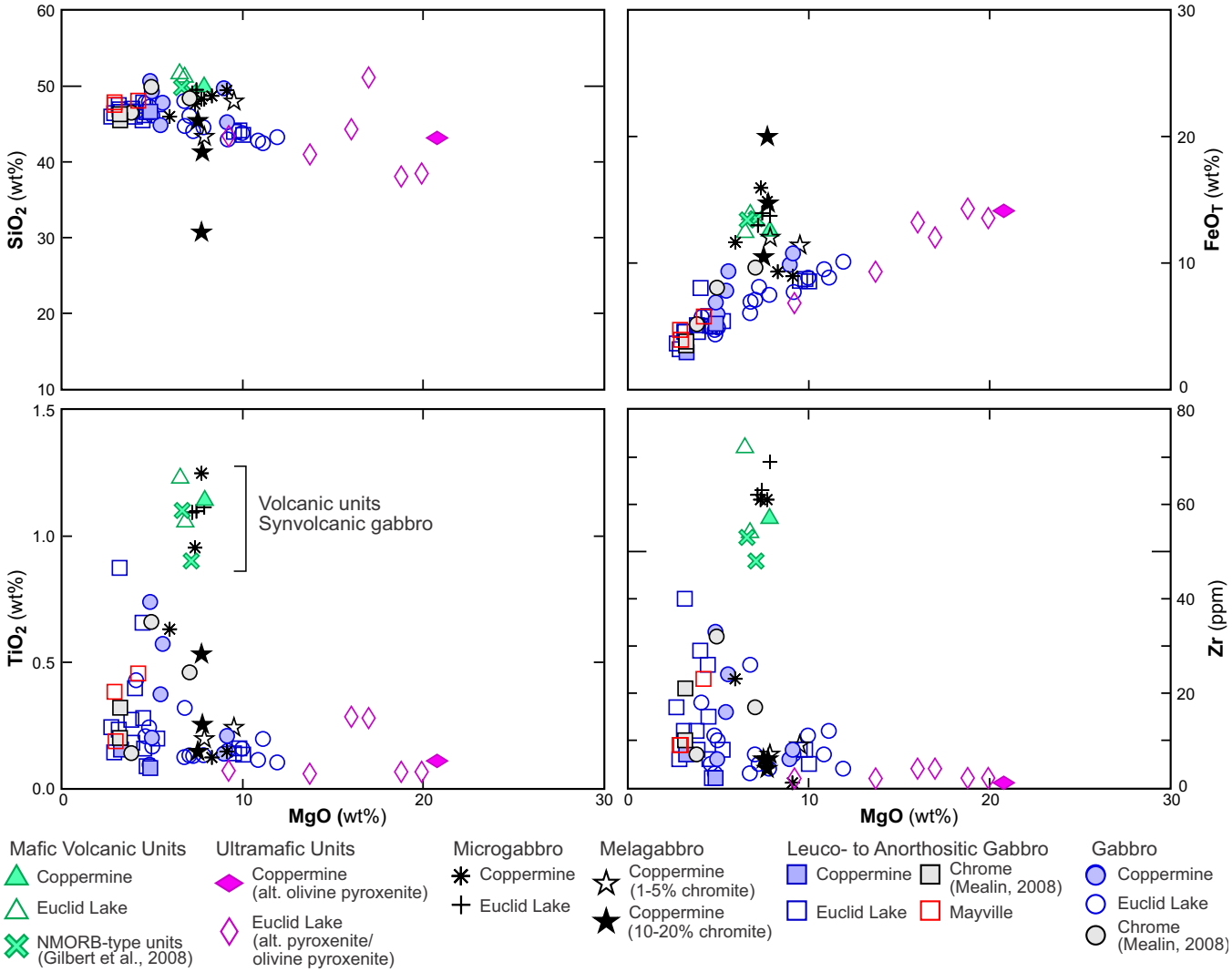

Figure 4. Whole-rock SiO_2, FeO_T, TiO_2, and Zr versus MgO contents for the main rock units from the Coppermine Bay and Euclid Lake intrusions. Chrome property data are from Mealin (2008) and the mean values of the Northern and Southern MORB-type units are from Gilbert et al. (2008).

ilar to gabbroic equivalents in the Coppermine Bay, BRS, and Mayville intrusions (Fig. 3a,d,f, respectively). The units consist mainly of calcic plagioclase (Fig. 2) and magnesiohornblende assemblage with traces of chlorite and ilmenite. The MgO, SiO_2, FeO_T, TiO_2, and Zr contents of these gabbroic phases are quite similar and comparable to those obtained for equivalent rock units from the Coppermine Bay intrusion and the Chrome property (Fig. 4). The REE profiles have a shallow negative slope from La to Nd and are relatively flat from Gd to Lu. Positive Eu anomalies are conspicuous for most samples (Fig. 5b).

Mafic volcanic rocks and subordinate synvolcanic gabbro were recognized at the basal (footwall) contact of the Euclid Lake intrusion (Bécu et al, 2013). The mafic volcanic rocks are typically dark grey and aphanitic to fine-grained, whereas the synvolcanic gabbro unit is fine- to medium-grained, and exhibits a salt-and-pepper texture in drill core in which light-coloured plagioclase (Fig. 2) contrasts with darker magnesiohornblende (Fig. 3h) with traces of apatite and ilmenite. This mineral assemblage is identical to that observed in the mafic volcanic rocks except for grain size and texture. Both the mafic volcanic rocks and synvolcanic gabbro have very similar MgO, SiO_2, FeO_T, TiO_2, and Zr contents (Fig. 4) as well as REE profiles. Their composition is also very similar to the composition of the Northern and Southern MORB-type formations within the BRGB as defined in Gilbert et al. (2008).

Mayville Intrusion

The Mayville intrusion is an east-trending, mafic-ultramafic body, approximately 10.5 km long and up to 1.5 km wide that hosts significant Cu-Ni resources and PGE-Cr occurrences. It is a mafic-dominated body that has been subdivided into a lower heterolithic breccia zone (melagabbro and pyroxenite with anorthosite and

leucogabbro fragments) and an upper leucogabbro to anorthosite zone mainly consisting of leucogabbro, anorthositic gabbro, and anorthosite (e.g. Peck et al., 1999, 2002; Yang et al., 2012). The leucogabbroic to anorthositic rocks are medium-grained and typically contain plagioclase megacrysts (3–5 cm in diameter). These rocks, which are referred to as "golf-ball" leucogabbro/anorthosite, are texturally comparable to leucogabbroic to anorthositic rocks in other BRGB mafic-ultramafic intrusions (Fig. 3f). As observed in the Coppermine Bay and Euclid Lake intrusions, these gabbroic units are composed essentially of a plagioclase and hornblende assemblage with minor chlorite, epidote, and traces of biotite and ilmenite. Representative samples of the Mayville intrusion exhibit similar contents of MgO, SiO_2, FeO_T, TiO_2, and Zr and display similar REE profiles to those of the Chrome property gabbro as well as some of the Coppermine Bay and Euclid Lake intrusions (Figs. 4, 5). They results are also comparable to those obtained by Makie (2003) for gabbroic to anorthositic units from the heterolithic breccia zone.

GEOCHRONOLOGY

Geochronological investigations in this study include dating a leucogabbro xenolith sampled from the heterolithic breccia zone in the Mayville intrusion, which yielded a U-Pb isotope dilution thermal ionization mass spectrometry (ID-TIMS) zircon age of 2742.8 ±0.8 Ma, which is interpreted as the crystallization age for the intrusion (Houlé et al., 2013). This result is identical within error to the 2743.0 ±0.5 Ma age for a BRS leucogabbro from the Chrome property (Scoates and Scoates, 2013). Preliminary U-Pb ID-TIMS zircon ages from Coppermine Bay and Euclid Lake leucogabbroic rocks also suggest crystallization ages of 2743 Ma (McNicoll, unpubl. data).

DISCUSSION

Mafic rocks from mafic-ultramafic intrusions across the BRGB possess similar textural, petrological, and geochemical characteristics. This similarity is especially noticeable in outcrop textures of gabbroic to anorthositic rocks from the Coppermine Bay, Chrome, Maskwa-Dumbarton, Bird Lake, Euclid Lake, and Mayville intrusions (Fig. 3a–f). These units all consist of a calcic plagioclase and magnesiohornblende assemblage with minor chlorite-biotite-ilmenite. Their MgO, SiO_2, FeO_T, TiO_2, and Zr contents, as well as their REE profiles, are similar and suggest a probable magmatic affinity among these intrusions. These observations are in agreement with recently obtained U-Pb geochronological data and support a proposed linkage between mafic-ultramafic intrusions found in both arms of the BRGB. These intrusions are interpreted to have formed as a result of an extensive single Neoarchean magmatic event at ca. 2743 Ma, identified as the Bird River intrusive suite (Houlé et al., 2013, 2015). This also supports previous conclusions of a potential connection between both arms of the BRGB,

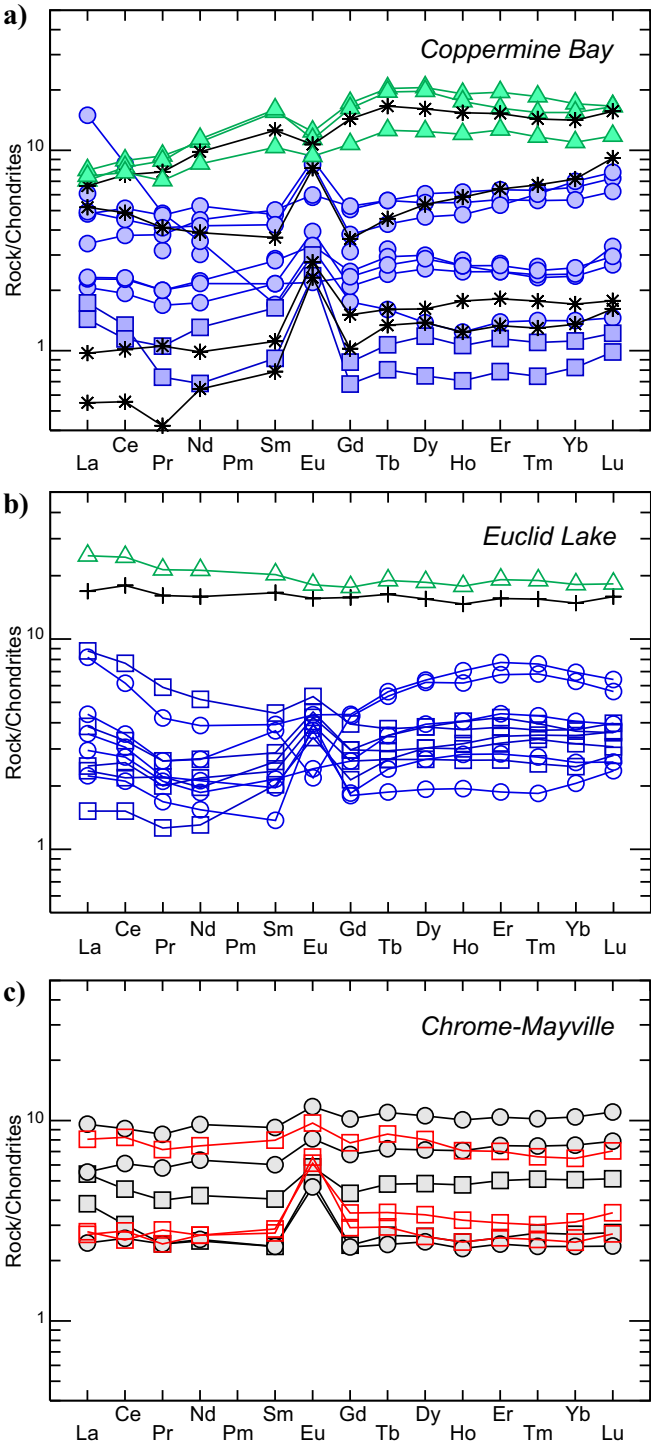

Figure 5. Chondrite-normalized rare earth element diagrams for representative gabbroic and volcanic rock units from **(a)** Coppermine Bay and **(b)** Euclid Lake intrusions. Data presented in **(c)** for the Chrome property (Mealin, 2008) and the Mayville intrusion (this study) are shown for comparison. Normalizing values are from Sun and McDonough (1989).

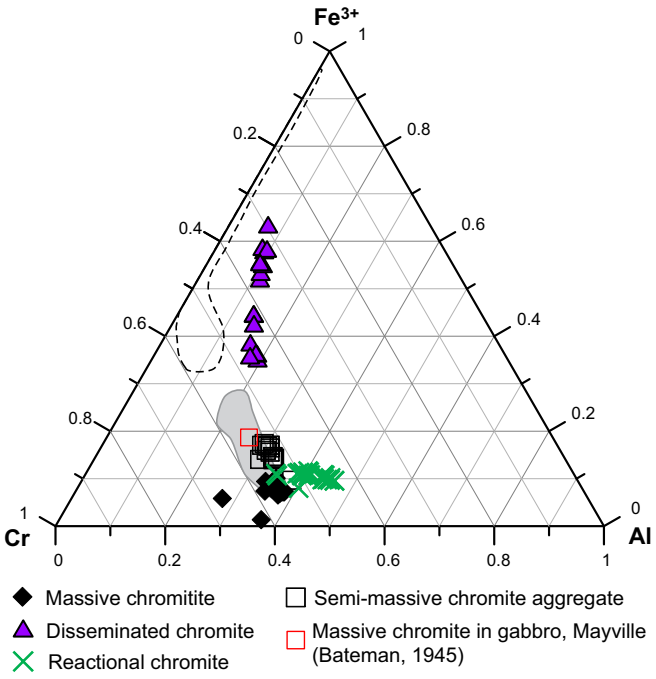

Figure 6. Chromite composition from the Mayville intrusion's E-Ext stripped outcrop, located in the northern arm of the BRGB. Shaded and dashed-line areas correspond to core and rim compositions respectively from Bird River Sill chromite occurrences (data from Barnes and Roeder, 2001; and this study).

and that mineral endowment of mafic-ultramafic intrusions might be linked. For example, a massive chromite sample hosted by gabbro from the Mayville intrusion (Bateman, 1945), as well as massive chromitite and semi-massive chromite aggregates from a chromite-bearing pyroxenite, exhibit mineral compositions similar to BRS-hosted chromite (Fig. 6). These observations support a common magmatic source for the Mayville and BRS intrusions located in the northern and southern arms of the belt, respectively.

The recognition of mafic volcanic rocks in the footwall of the Euclid Lake intrusion and their geochemical similarities with the Northern and Southern MORB-type formations in the southern arm of the BRGB infer an analogous geological setting to BRS. The presence of gabbroic rocks stratigraphically below the pyroxenite unit raises questions as to whether structural and/or complex magmatic process produced the magmatic sequence observed within the Euclid Lake intrusion (Bécu et al., 2013).

Geochemical investigations highlight that TiO_2 and Zr contents for intrusive anorthositic to gabbroic units are noticeably lower than those of mafic volcanic rocks. Similarly REE profiles for intrusive anorthositic to gabbroic units are much less REE enriched than those of mafic volcanic rocks. Although discrimination between these units is usually fairly straightforward in the field, textural criteria are not always adequate for defining microgabbroic units. Geochemistry can thus be used as a tool to help distinguish gabbro potentially related to the Bird River magmatic event from synvolcanic gabbro (Figs. 4, 5). A difference was also noted in the An content of plagioclase for a Coppermine Bay microgabbro (Fig. 3). The sample was interpreted to be of "Bird River magmatic affinity" based on low TiO_2 and Zr contents and a REE profile similar to anorthositic to gabbroic units, as well as distinctive anorthite indexes compared to those of plagioclase from a mafic volcanic unit of the Euclid Lake area. Ongoing investigations indicate that amphibole chemistry could also assist in the distinction between Bird River intrusive and volcanic-related rocks. Despite the relatively small dataset, these observed geochemical distinctions could prove to be useful in discriminating Bird River magmatic event-related mafic units from volcanic-related gabbro.

IMPLICATIONS FOR EXPLORATION

Results from this study suggest that the Coppermine Bay intrusion exhibits textural, petrographic, and geochemical characteristics that are similar to the Euclid Lake intrusion, and furthermore that both intrusions are comparable to the Mayville intrusion, supporting their proposed petrogenetic linkage. These observations, combined with recently obtained U-Pb ages, support the existence of a widespread Bird River magmatic event throughout the BRGB, as proposed by Houlé et al. (2013). Similar mineralization styles among the Coppermine Bay, Mayville, Euclid Lake, and other mafic-ultramafic intrusions, also strongly suggests that the potential for Ni-Cu-PGE-Cr mineralization extends well beyond the traditionally explored areas within the BRS and the Mayville intrusions.

Geochemical signatures, as well as mineral chemistry (plagioclase and amphibole), could be useful discrimination tools between Bird River magmatic event-related units and volcanic units. This could provide exploration tools to vector towards more prospective and fertile intrusions in the BRGB, especially in volcanic-dominated areas such as the Cat Creek area south of the Mayville intrusion.

ACKNOWLEDGEMENTS

We would like to acknowledge Mustang Minerals Corp., Gossan Resources Ltd., Stillwater Canada Inc., and Clifton Star Inc. for providing access to their properties, drill core, and geological databases. We are especially grateful to C. Galeschuk (Mustang Minerals Corp.) for general technical support, insights, and always constructive discussions. Thanks are extended to P. Brouillette and A. Morin for thorough GIS support and to M. Choquette (Université Laval) for providing support during electron microprobe analysis.

C. Boudreau, M.-P. Bédard, and C. Brind'Amour-Côté are acknowledged for field and technical assistance. The authors would like to sincerely thank R.F.J. Scoates for constructive reviews that genuinely helped to improve the final version of the document.

REFERENCES

Bannatyne, B.B. and Trueman, D.L., 1982. Chromite reserves and geology of the Bird River Sill, Manitoba; Manitoba Department of Energy and Mines, Mineral Resources Division, Open File Report 82-1, 73 p.

Barnes, S.J. and Roeder, P.L., 2001. The range of spinel compositions in terrestrial mafic and ultramafic rocks; Journal of Petrology, v. 42, p. 2279–2302.

Bateman, J.D., 1942. Chromite: Manitoba's gift to war industry; extent of deposits and their value in warfare; Precambrian Magazine, v. 15, p. 2, 5–7, 23.

Bateman, J.D., 1943. Bird River chromite deposits, Manitoba; Transactions of the Canadian Institute of Mining and Metallurgy, v. 46, p. 154–183.

Bateman, J.D., 1945. Composition of the Bird River chromite, Manitoba; American Mineralogist, v. 30, p. 596–600.

Bécu, V., Houlé, M.G., Yang, X.M., and Gilbert, H.P., 2013. Euclid Lake intrusion: a revisited cross-section through a historical chrome deposit of the Bird River greenstone belt, southeastern Manitoba, *In:* Report of Activities 2013; Manitoba Mineral Resources, Manitoba Geological Survey, p. 85–94.

Canex Placer Ltd., 1973. Geology of the Macroy-ZIYone options, Coppermine Bay area, Lac Du Bonnet, Manitoba; Manitoba Department of Energy and Mines, Assessment File 91382, 39 p.

Coats, C.J.A, Stockford, H.R., and Buchan, R., 1979. Geology of the Maskwa West Nickel Deposit, Manitoba; The Canadian Mineralogist, v. 17, p. 309–318.

Gilbert, H.P., Houlé, M.G., Yang, X.M., Scoates, J.S., Scoates, R.F.J., Mealin, C.A., Bécu, V., McNicoll, V.J., and Galeschuk, C.R., 2013. Mafic and ultramafic intrusive rocks and associated Ni-Cu-(PGE) and Cr-(PGE) mineralization in the Bird River greenstone belt, southeast Manitoba; Geological Association of Canada – Mineralogical Association of Canada Joint Annual Meeting, Winnipeg, Manitoba, May 2013, Field Trip Guidebook FT-C2 (also Manitoba Innovation, Energy and Mines, Manitoba Geological Survey, Open File OF2013-7), p. 17–22.

Gilbert, H.P., Davis, D.W., Duguet, M., Kremer, P.D., Mealin, C.A., and MacDonald, J., 2008. Geology of the Bird River Belt, southeastern Manitoba (parts of NTS 52L5, 6); Manitoba Science, Technology, Energy and Mines, Manitoba Geological Survey, Geoscientific Map MAP2008-1, scale 1:50 000 (plus notes and appendix).

Gossan Resources Ltd., 2007. Marathon PGM enthused by initial results at Gossan's Bird River Property; News Release, August 30, 2007. http://www.gossan.ca/news/news.html

Houlé, M.G., McNicoll, V.J., Bécu, V., Yang, X.M., and Gilbert, H.P., 2013. New age for the Mayville intrusion: implication for a large mafic-ultramafic event in the Bird River greenstone belt, southeastern Manitoba, *In:* Program with Abstracts; Geological Association of Canada – Mineralogical Association of Canada Joint Annual Meeting, Winnipeg, Manitoba, May 2013, Abstract Volume 36, p. 115.

Houlé, M.G., Lesher, C.M., McNicoll, V.J., Metsaranta, R.T., Sappin, A.-A., Goutier, J., Bécu, V., Gilbert, H.P., and Yang, X.M., 2015. Temporal and spatial distribution of magmatic Cr-(PGE), Ni-Cu-(PGE), and Fe-Ti-(V) deposits in the Bird River–Uchi–Oxford-Stull–La Grande Rivière–Eastmain domains: a new metallogenic province within the Superior Craton, *In:* Targeted Geoscience Initiative 4: Canadian Nickel-Copper-Platinum Group Elements-Chromium Ore Systems — Fertility, Pathfinders, New and Revised Models, (ed.) D.E. Ames and M.G. Houlé; Geological Survey of Canada, Open File 7856, p. 35–47.

Ilam and Associates Ltd., 1988. An evaluation of the chromite reserves in the Bird River Sill southeastern Manitoba; Manitoba Department of Energy and Mines, Assessment File 74747, 158 p.

Macek, J.J., 1985. Cat Creek; Manitoba Energy and Mines, Preliminary Map 1985C-1, scale 1:10 000.

Marathon PGM Corp., 2008. Technical report and resource estimate on the Ore Fault, Galaxy and Page zones of the Marathon PGM / Gossan Resources Ltd. JV, Bird River property, southeast Manitoba; P&E Mining Consultants Inc., NI-43-101 & 43-101F1 Technical Report No 154, 112 p.

Mackie, R., 2003. Emplacement history and PGE-enriched sulphide mineralization of the heterolithic breccia zone in the Mayville intrusion; B.Sc. thesis, University of Manitoba, Winnipeg, Manitoba, 131 p.

Mealin, C.A., 2008. Geology, geochemistry and Cr-Ni-Cu-PGE mineralization of the Bird River Sill: evidence for a multiple intrusion model; M.Sc. thesis, University of Waterloo, Waterloo, Ontario, 155 p., 1 folded colour map.

Mustang Minerals Corp., 2013, Mayville Makwa project webpage http://www.mustangminerals.com/projects/mayville-makwa/

Peck, D.C. and Theyer, P., 1998. PGE-copper-nickel potential of mafic-ultramafic intrusions in the Bird River greenstone belt (parts of NTS 52L), *In:* Report of Activities 1998; Manitoba Energy and Mines, Manitoba Geological Services, p. 151–160.

Peck, D.C., Theyer, P., Bailes, A.H., and Chornoby, J., 1999. Field and lithogeochemical investigations of mafic and ultramafic rocks and associated Cu-Ni-PGE mineralization in the Bird River greenstone belt (parts of NTS 52L), *In:* Report of Activities 1999; Manitoba Industry, Trade and Mines, Geological Services, p. 106–110.

Peck, D.C., Scoates, R.F.J., Theyer, P., Desharnais, G., Hulbert, L.J., and Huminicki, M.A.E., 2002. Stratiform and contact-type PGE-Cu-Ni mineralization in the Fox River Sill and the Bird River Belt, Manitoba, *In:* The Geology, Geochemistry, Mineralogy and Mineral Beneficiation of Platinum-Group Elements, (ed.) L.J. Cabri; Canadian Institute of Mining and Metallurgy, Special Volume 54, p. 367–387.

Scoates, J.S. and Scoates, R.F.J., 2013. Age of the Bird River Sill, southeastern Manitoba, Canada, with implications for the secular variation of layered intrusion-hosted stratiform chromite mineralization; Economic Geology, v. 108, p. 895–907.

Scoates, R.F.J., 1983. A preliminary stratigraphic examination of the ultramafic zone of the Bird River Sill, southeastern Manitoba, *In:* Report of Field Activities 1983; Manitoba Department of Energy and Mines, Mineral Resources Division, p. 70–83.

Scoates, R.F.J., Williamson, B.L., and Duke, J.M., 1986. Igneous layering in the ultramafic series, Bird River Sill, *In:* Layered Intrusions of Southeastern Manitoba and Northwestern Ontario, (ed.) R.F.J. Scoates, B.L. Williamson, J.M. Duke, W. Mandziuk, W.C. Brisbin, and R.H. Sutcliffe; Geological Association of Canada, Field Trip 13 Guidebook, p. 1–19.

Scoates, R.F.J., Williamson, B.L., Eckstrand, O.R., and Duke, J.M., 1989. Stratigraphy of the Bird River Sill and its chromitiferous zone, and preliminary geochemistry of the chromitite layers and PGE-bearing units, Chrome property, Manitoba, *In:* Investigations by the Geological Survey of Canada in Manitoba and Saskatchewan during the 1984-1989 Mineral Development

Agreements, (ed.) A.G. Galley; Geological Survey of Canada, Open File 2133, p. 69–82.

Springer, G.D., 1949. Geology of the Cat Lake–Winnipeg River area: Manitoba Mines and Natural Resources, Mines Branch, Preliminary Report 48-7, 15 p., 1 map, scale 1:63 360.

Springer, G.D., 1950. Geology of the Cat Lake – Winnipeg River area, Manitoba; Manitoba Mines and Natural Resources, Mines Branch, Publication 49-7, 14 p.

Sun, S.S. and McDonough, W.F. 1989. Chemical and isotopic systematics of oceanic basalts: implications for mantle composition and processes, *In:* Magmatism in the Ocean Basins, (ed.) A.D. Saunders and M.J. Norry; Geological Society, Special Publication 42, p. 313–345.

Theyer, P., 1985. Platinum-palladium distribution in ultramafic rocks of the Bird River complex, southeastern Manitoba; Manitoba Department of Energy and Mines, Open File Report OF 85-4, 64 p.

Trueman, D.L., 1980. Stratigraphy, structure and metamorphic petrology of the Archean greenstone belt at Bird River Manitoba; Ph.D. thesis, University of Manitoba, Winnipeg, Manitoba, 150 p.

Trueman, D.L., 1997. Report on the chromite, nickel-copper, and platinum group metal holdings in the Bird River area, southeastern Manitoba; Manitoba Department of Energy and Mines, Assessment File 73385, 107 p.

Watson, D.M., 1982. Chromite resources of the Bird River area; *In:* Report of Field Activities 1982; Manitoba Department of Energy and Mines, Mineral Resources Division, Report GS-11, p. 60–63.

Williamson, B.L., 1990. Geology of the Bird River Sill at the Chrome Property, southeast Manitoba; Geological Survey of Canada Open File 2067, 44 p.

Yang, X.M., 2014. Bedrock geology of the Cat Creek area, Bird River greenstone belt, southeastern Manitoba (part of NTS 52L12); Manitoba Mineral Resources, Manitoba Geological Survey, Preliminary Map PMAP2014-3, scale 1:10 000.

Yang, X.M., Gilbert, H.P., and Houlé, M.G., 2012. Geological investigations of the Cat Creek area in the Neoarchean Bird River greenstone belt, southeastern Manitoba (part of NTS 52L12): new insights into PGE-Ni-Cu-Cr mineralization, *In:* Report of Activities 2012; Manitoba Innovation, Energy and Mines, Manitoba Geological Survey, p. 32–53.

Yang, X.M., Gilbert, H.P., and Houlé, M.G., 2013. Cat Lake–Euclid Lake area in the Neoarchean Bird River greenstone belt, southeastern Manitoba (parts of NTS 52L11, 12): preliminary results of bedrock geological mapping and their implications for geodynamic evolution and metallogeny, *In:* Report of Activities 2013; Manitoba Mineral Resources, Manitoba Geological Survey, p. 70–84.

GEOLOGICAL SURVEY OF CANADA
OPEN FILE 7856

Targeted Geoscience Initiative 4: Canadian Nickel-Copper-Platinum Group Elements-Chromium Ore Systems — Fertility, Pathfinders, New and Revised Models

Revised geological framework for the McFaulds Lake greenstone belt, Ontario

Riku T. Metsaranta[1], Michel G. Houlé[2], Vicki J. McNicoll[3], and Sandra L. Kamo[4]

[1]Ontario Geological Survey, Sudbury, Ontario
[2]Geological Survey of Canada, Québec, Quebec
[3]Geological Survey of Canada, Ottawa, Ontario
[4]University of Toronto, Toronto, Ontario

2015

© Her Majesty the Queen in Right of Canada, as represented by the Minister of Natural Resources Canada, 2015

This publication is available for free download through GEOSCAN (http://geoscan.nrcan.gc.ca/)

Recommended citation

Metsaranta, R.T., Houlé, M.G., McNicoll, V.J., and Kamo, S.L., 2015. Revised geological framework for the McFaulds Lake greenstone belt, Ontario, *In:* Targeted Geoscience Initiative 4: Canadian Nickel-Copper-Platinum Group Elements-Chromium Ore Systems — Fertility, Pathfinders, New and Revised Models, (ed.) D.E. Ames and M.G. Houlé; Geological Survey of Canada, Open File 7856, p. 61–73.

Publications in this series have not been edited; they are released as submitted by the author.

Contribution to the Geological Survey of Canada's Targeted Geoscience Initiative 4 (TGI-4) Program (2010–2015)

TABLE OF CONTENTS

Revised geological framework for the McFaulds Lake greenstone belt, Ontario

Riku T. Metsaranta[1]*, Michel G. Houlé[2], Vicki J. McNicoll[3], and Sandra L. Kamo[4]

[1]Ontario Geological Survey, 933 Ramsey Lake Road, Sudbury, Ontario P3E 6B5
[2]Geological Survey of Canada, 490 rue de la Couronne, Québec, Quebec G1K 9A9
[3]Geological Survey of Canada, 601 Booth Street, Ottawa, Ontario K1A 0E8
[4]Department of Earth Sciences, University of Toronto, 22 Russell Street, Toronto, Ontario M5S 3B1
*Corresponding author's e-mail: riku.metsaranta@ontario.ca

ABSTRACT

The McFaulds Lake greenstone belt (MLGB) is an extensive (>200 km long), arcuate-shaped, Meso- to Neoarchean, greenstone belt located in the central part of the Oxford-Stull domain of northern Ontario. The MLGB records a history of episodic volcanism, sedimentation, ultramafic-felsic intrusive activity and tectonism spanning from at least 2.83 to 2.66 Ga. Supracrustal rocks are tentatively subdivided into 7 tectonostratigraphic assemblages based on mapping, U-Pb geochronology, and geophysical interpretation. Mafic and ultramafic intrusive rocks comprise at least two distinct suites: a mafic-dominated, large layered intrusive suite represented by the Highbank-Fishtrap intrusive complex that was emplaced at ca. 2810 Ma, and an ultramafic to mafic intrusive suite termed the Ring of Fire intrusive suite. The latter comprises an ultramafic-dominated subsuite with significant Cr-Ni-Cu-PGE mineralization, and a mafic-dominated subsuite that contains significant Fe-Ti-V-(P) mineralization that was emplaced at ca. 2734 Ma.

INTRODUCTION

Regional bedrock mapping and diamond-drill core relogging has been carried out in the "Ring of Fire" (RoF) region by the Ontario Geological Survey and the Geological Survey of Canada since 2010 through a cooperative research program (Targeted Geoscience Initiative, TGI-4). A primary focus of this work was to improve our understanding of the geology of the McFaulds Lake greenstone belt (MLGB) and to investigate the mafic-ultramafic intrusions that host the Cr-Ni-Cu-PGE-Fe-Ti-V-P orthomagmatic mineralization in the region. Mapping in the RoF region is hampered by extensive overburden, as well as flat-lying Paleozoic cover in its eastern portions. However, the discovery of numerous mineral deposits and occurrences in the RoF region has generated a significant new source of geoscience information through the diamond drilling conducted over the past several years. This contribution highlights the most recent advances in our understanding of the geology and the stratigraphy of the McFaulds Lake greenstone belt (MLGB) based on compilation of data from more than 1500 cored diamond drillholes, relogging of core, outcrop mapping, and new results of U-Pb geochronology.

TECTONOSTRATIGRAPHIC FRAMEWORK FOR THE McFAULDS LAKE GREENSTONE BELT

The MLGB has been tentatively subdivided into 7 distinct tectonostratigraphic assemblages based on their main lithological characteristics, new U-Pb zircon age constraints (new high-precision magmatic ages were generally determined by ID-TIMS; detrital zircon from metasedimentary rocks were determined by LA-ICP-MS) and geophysical interpretation (Figs. 1, 2). The geology of these assemblages is briefly reviewed, from oldest to youngest in the following section. Examples of typical rock types are shown in Figure 3.

Butler Assemblage (ca. 2828 Ma)

The supracrustal successions in the Butler assemblage (BA) can be divided into a western and an eastern part, which are separated by a large tonalitic intrusion. The western part comprises a succession dominated by felsic to intermediate metavolcanic rocks characterized by intense hydrothermal alteration. Metamorphosed mineral assemblages commonly contain garnet, muscovite, orthoamphibole, staurolite, and cordierite. Volcanogenic massive sulphide (VMS) occurrences are a conspicu-

Metsaranta, R.T., Houlé, M.G., McNicoll, V.J., and Kamo, S.L., 2015. Revised geological framework for the McFaulds Lake greenstone belt, Ontario, *In:* Targeted Geoscience Initiative 4: Canadian Nickel-Copper-Platinum Group Elements-Chromium Ore Systems — Fertility, Pathfinders, New and Revised Models, (ed.) D.E. Ames and M.G. Houlé; Geological Survey of Canada, Open File 7856, p. 61–73.

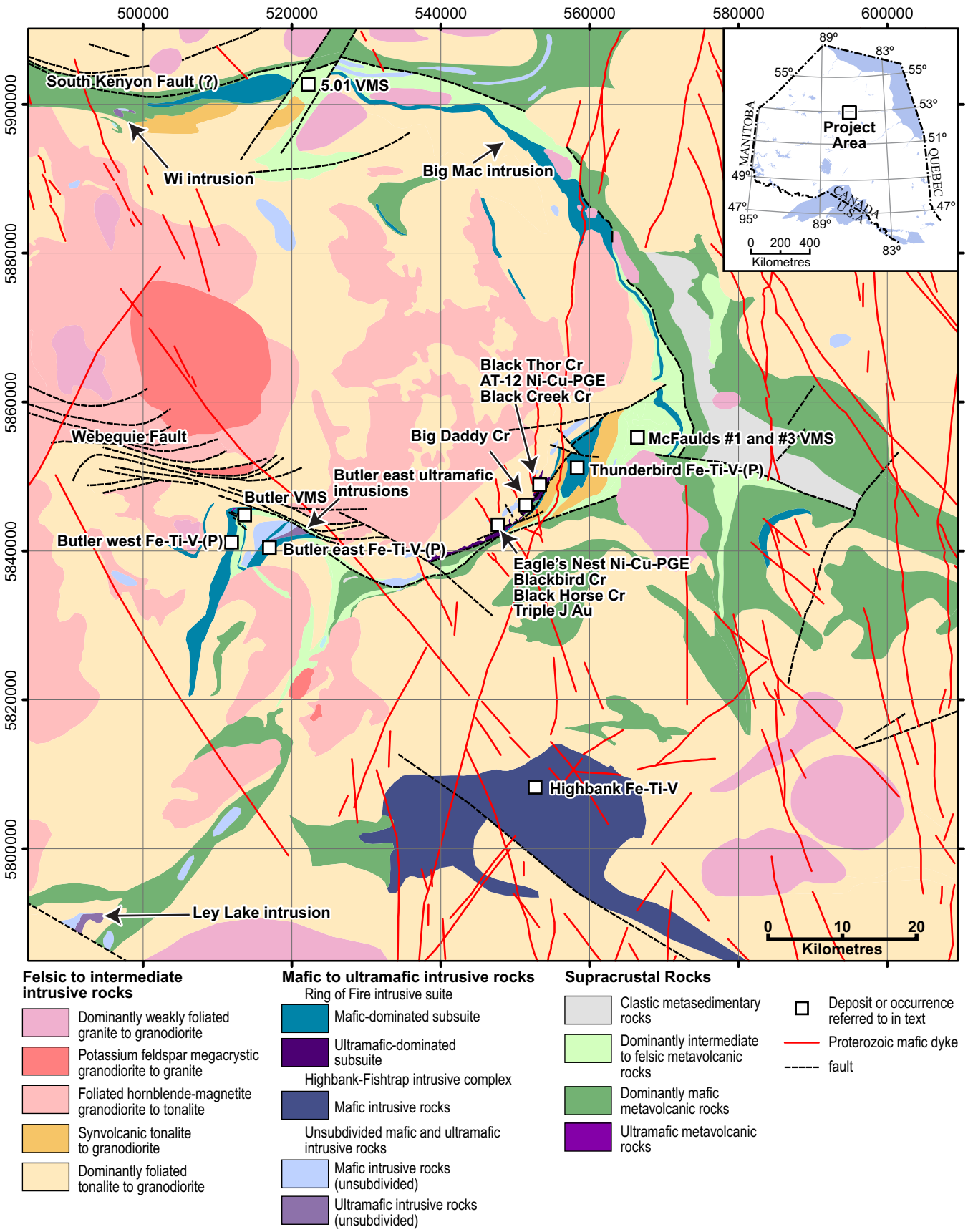

Figure 1. Simplified geological map of the McFaulds Lake greenstone belt showing the location of mineral deposits in the "Ring of Fire" region.

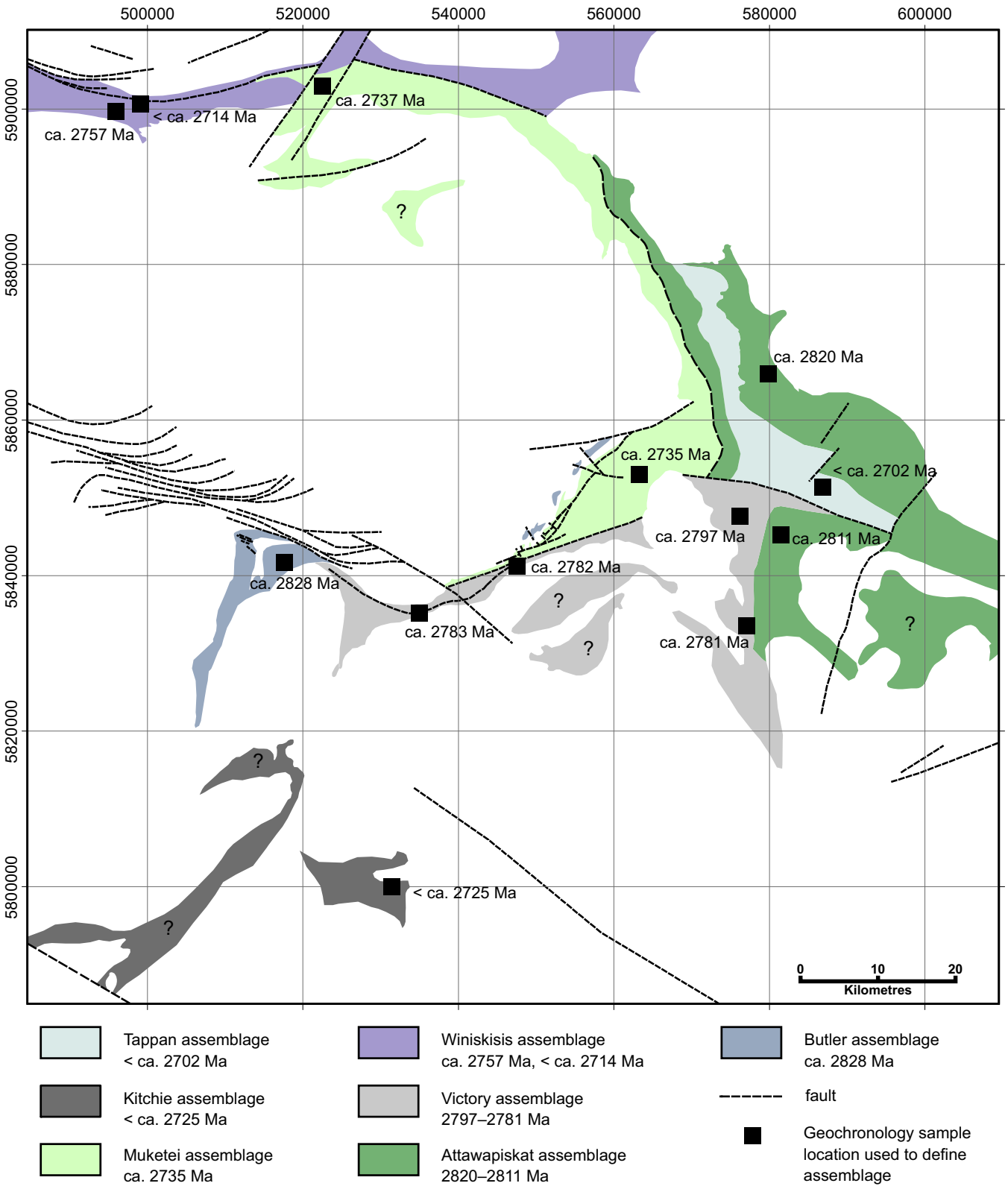

Figure 2. Simplified tectonostratigraphic framework of the McFaulds Lake greenstone belt.


A
C-GONT
B
C
D
E
inch
NOTES
ONTARIO
F
G
11RM300
H

ous component of this part of the BA. The eastern part of the BA comprises mafic metavolcanic rocks with lesser magnetite-chert iron formation and minor felsic metavolcanic rocks with an age of ca. 2828 Ma, based on new data from this study. Mafic-ultramafic intrusions are also abundant in this area. This unit may correlate with similar rocks present in the footwall of Cr-Ni-Cu-PGE mineralized intrusions in the central part of the RoF. The BA is folded and strongly deformed by the Webequie fault zone, but in general, appears to face to the east-southeast.

Attawapiskat Assemblage (2820–2811 Ma)

The Attawapiskat assemblage (AA) forms a broadly northwest-striking unit in the eastern part of the MLGB and was previously subdivided by Metsaranta and Houlé (2012, 2013) into three parts: a felsic to mafic metavolcanic succession to the west, a clastic metasedimentary succession in the central part, and a mafic metavolcanic succession to the east. However, this interpretation is revised based on new U-Pb ages obtained from a felsic metavolcanic horizon in the eastern part of the AA that yielded an age of ca. 2820 Ma for the eastern metavolcanic succession. The central metasedimentary unit has been renamed the Tappan assemblage (described below), which contains zircon grains as young as 2702 Ma and is now considered a separate assemblage that may unconformably overlie or be tectonically interleaved with the AA. Rare primary flow features in mafic metavolcanic rocks suggest that the overall stratigraphy faces broadly to the northeast but only a few reliable younging indicators have been observed. In addition, some oxide-facies iron formation, sulphidic-graphitic argillite, chloritized clastic metasedimentary intervals, and feldspar-phyric intermediate intrusions have been reported by Polk (2009) in the northern part of the AA, which suggests a far more complex geological history. Anomalous Cu and Zn concentrations associated with graphitic argillite units were also reported in this area (Polk, 2009).

Victory Assemblage (2797–2780 Ma)

The Victory assemblage (VA) comprises a bimodal sequence of mafic and felsic metavolcanic rocks with minor metasedimentary rocks, including rare oxide-facies iron formation. Subconcordant gabbroic to pyroxenitic sills also occur within this assemblage. The spatial extent of the VA is inferred from geophysical and geochronological signatures. In the central part of the RoF it is bounded on the north side by a regionally extensive shear zone that structurally juxtaposes younger rocks of the Muketei assemblage (described below). East of McFaulds Lake, supracrustal rocks of the VA and AA appear to form a north-south-trending synform, however, the nature of the boundary between these assemblages remains unclear.

Winiskisis Assemblage (ca. 2757 Ma, younger sedimentary component <2714 Ma)

The east-striking Winiskisis assemblage (WA) forms the northern part of the MLGB but its characteristics are poorly constrained, as exposures are limited to a few outcrops and drill-core intersections. A felsic metavolcanic rock from the western part of this assemblage has an age of ca. 2757 Ma, but the assemblage also contains younger <2714 Ma (maximum age based on detrital zircon analyses) sheared, metasedimentary, or metavolcanic rocks based on sampling and geochronology reported by Buse et al. (2009). Relogging a series of diamond-drill cores in the western part of the assemblage revealed the presence of schistose to gneissic, felsic to intermediate rocks (quartz-plagioclase-biotite-garnet schist and gneiss) interpreted as tuffaceous metasedimentary or metavolcanic rocks, and fine- to medium-grained amphibolite interpreted as mafic metavolcanic rocks. In less deformed and metamorphosed areas, supracrustal rocks including interbedded grey wacke and black siltstone/shale, massive and locally normally graded felsic tuffaceous sandstone, aphyric and quartz-phyric felsic metavolcanic rocks, and less commonly mafic flows. Sporadic, thin, silicified zones with pyrite-pyrrhotite mineralization and chert-magnetite iron formation are also present within this succession. The eastern part of the WA is also poorly exposed but appears to be dominated by variably deformed, pillowed mafic metavolcanic rocks with rare local northeast younging indicators. Geophysical data for this unit typically shows a low magnetic signature coupled with an anomalous

Figure 3 (opposite page). Typical rock types from the McFaulds Lake greenstone belt and related mafic-ultramafic intrusions. **a)** Layered hornblende-gabbro and anorthosite of the Highbank-Fishtrap complex. Hammer is 40 cm long. **b)** Magmatic breccia displaying clasts of massive and layered chromitite in a serpentinized peridotite. Pencil is 15 cm long. **c)** Weakly deformed, pillowed mafic metavolcanic rocks from the eastern part of the Winiskisis assemblage exposed near the Ekwan River. Pencil is 15 cm long. **d)** Deformed, pillowed mafic metavolcanic rocks exposed along strike from the Attawapiskat assemblage, a few kilometres to the east of the Ring of Fire map area. Hammer is 40 cm long. **e)** Folded chert-magnetite iron formation interlayered with mafic metavolcanic rocks from the eastern Butler assemblage. **f)** Strong orthoamphibole-garnet alteration of metavolcanic rocks near the Bulter 3 VMS occurrence. Hammer is 40 cm long. **g)** Interbedded sandstone and grey siltstone typical of the Tappan assemblage. Sandstone beds commonly display normal graded bedding. The core in the photo is 3.7 cm in diameter. **h)** Felsic tuff breccia near the 5.01 VMS occurrence, Muketei assemblage. The core diameter is 4.8 cm.

high gravity signature similar to the mafic metavolcanic succession of the AA. Thus, with existing age constraints, it cannot be ruled out that the eastern part of the WA and the AA are correlative based on similar rock types and geophysical signatures.

Muketei Assemblage (ca. 2735 Ma)

The Muketei assemblage (MA) comprises a dominantly felsic to intermediate metavolcanic succession in the central and northern parts of the MLGB. Volcanic rocks in this area were reported to be ca. 2737 Ma (Rayner and Stott, 2005). However, geochronology from this study provides a more precise age constraint age of ca. 2735 Ma. The assemblage contains a number of small VMS occurrences including the McFaulds #1 and #3 deposits. VMS occurrences in the area display strong talc-chlorite-magnetite alteration zones proximal to mineralization and broader distal sericite alteration halos. In the vicinity of VMS occurrences, the assemblage comprises dominantly felsic to intermediate flows and tuffs with minor mafic metavolcanic rocks and oxide-facies iron formation. Stratigraphically above ultramafic to mafic intrusions in the central RoF, a bimodal succession of normal to high-Mg mafic metavolcanic rocks with minor felsic tuffaceous horizons is present (based on scarce drilling). The northern extension of the MA is dominated by felsic to intermediate metavolcanic rocks, based on a series of diamond-drill cores (e.g. Kilbourne 2009, 2010). These units are typically moderately to strongly deformed quartz-biotite ± garnet ± amphibole schist, likely derived from felsic to intermediate tuff, lapilli tuff, quartz-phyric flows and coarse tuff breccia. Subordinate fine-grained amphibolite, which probably represents mafic metavolcanic rocks, are interlayered with these units. Sulphide-mineralized zones, up to several metres thick, were encountered in drill core (e.g. the 5.01 occurrence). Reliable regional younging indicators for this assemblage were not recognized.

Kitchie Assemblage (in part <2725 Ma)

The Kitchie assemblage (KA) is a poorly exposed sequence of supracrustal rocks observed in the vicinity of the Highbank-Fishtrap Lake intrusive complex (HFIC) in the southern part of the RoF area. In outcrop it consists of deformed amphibolitized mafic metavolcanic rocks and metasandstone cut by foliated mafic dykes. A metasedimentary outcrop in this area contains detrital zircon grains as young as ca. 2725 Ma. Reconnaissance logging revealed that the KA is composed primarily of fine- to medium-grained amphibole-plagioclase-biotite ± garnet schist interpreted as mafic metavolcanic rocks, and grey, quartz-plagioclase-biotite ± garnet ± muscovite schist interpreted as felsic to intermediate metavolcanic rocks. Pillow selvages are present locally within mafic metavolcanic rocks. Rare fine-grained, bedded quartz-biotite-plagioclase-garnet schist is also present and is interpreted as metasedimentary rocks. Rare, foliated metagabbroic to metapyroxenitic intrusions crosscut supracrustal rocks of the KA.

Tappan Assemblage (<2702 Ma)

The Tappan assemblage (TA) is a poorly exposed west-northwest striking metasedimentary unit located in the eastern part of the MLGB. Unconformable or fault contacts between the TA and enclosing metavolcanic successions of the AA are inferred as supported by age differences shown by these supracrustal packages. The TA consists primarily of grey, fine- to coarse-grained sandstone interbedded with grey siltstone and black sulphidic mudstone. The overall fine-grain size and occurrences of sedimentary structures (e.g. graded bedding, load features, and rare cross-lamination) are consistent with deposition in a deep-water environment. Detrital zircon geochronology by LA-ICP-MS from a sample of interbedded sandstone and siltstone yielded individual zircon ages as young as 2702 Ma, which provides a maximum age for this assemblage. It is the youngest supracrustal unit to have been identified in the MLGB.

MAFIC AND ULTRAMAFIC INTRUSIONS

Mafic and ultramafic intrusions in the RoF region occur in at least two main age intervals, at ca. 2810 Ma and ca. 2734 Ma. Thus far, the best known Mesoarchean intrusion is the Highbank-Fishtrap Lake intrusive complex (HFIC), which consists of gabbro, anorthositic gabbro, magnetite-bearing gabbro, and rare pyroxenite units (Sappin et al., 2015). It is unclear what it was emplaced into, as existing geochronology for the adjacent KA suggests that it postdates the HFIC and no geochronology exists for surrounding granitoid rocks, although it is crosscut by a ca. 2728 Ma inter-

Figure 4 (opposite page). Examples of different mineralization styles and host rocks in the McFaulds Lake greenstone belt. **a)** Massive sulphide, Eagle's Nest deposit. Coin is 1.8 cm. **b)** Net-textured sulphide mineralization, Eagle's Nest deposit. Coin is 1.8 cm. **c)** Massive chromite, Big Daddy deposit. Core is 4.8 cm in diameter. **d)** Massive and peridotite-clast-rich chromite mineralization, Black Horse deposit. Lense cap is 5.5 cm in diameter. **e)** Massive magnetite mineralization, Thunderbird prospect. Coin is 1.8 cm.**f)** Plagioclase with interstitial magnetite, typical of lower grade Fe-Ti-V mineralized gabbroic intrusions. Pencil is 15 cm long. **g)** Massive pyrite with interbedded, altered, and sulphide-mineralized, black mudstone clast breccia, Bulter 3 VMS occurrence. Pencil is 15 cm long. **h)** Sheared ultramafic and rocks with silicification and quartz-carbonate veining along a Au-barren section of the Triple J shear zone. Pencil is 15 cm long.


A
B
C
D
Nikon
E
F
G
H

Table 1. Summary of mineral deposits in the "Ring of Fire" region.

Deposit	Mineral Resources/ Reserves		Tonnage (Mt)	Grade of Mineralization				
Chromite Deposits	*Mineral Resources*			**Cr_2O_3 (%)**			**Cr/Fe**	
Black Thor[1]	Inferred		121.9	27.8				
		Total	**121.9**	**27.8**				
Big Daddy[2]	Measured		23.3	32.1				
	Indicated		5.8	30.1				
	Inferred		3.4	28.1				
		Total	**32.5**	**31.3**				
Black Horse[3]	Inferred		77.2	35.1				
		Total	**77.2**	**35.1**				
Black Creek[4]	Measured		5.3	37.0			1.80	
	Indicated		3.4	38.0			1.80	
	Inferred		1.6	37.8			1.70	
		Total	**10.3**	**37.5**				
Blackbird[5]	Measured		9.3	37.4			2.00	
	Indicated		11.2	34.4			1.95	
	Inferred		23.5	33.1			1.97	
		Total	**43.9**	**34.4**				
Total Mineral Resources in the MLGB			**285.8**	**31.5**				
Magmatic Ni-Cu-PGE Deposits				**Ni** (%)	**Cu** (%)	**Pt** (g/t)	**Pd** (g/t)	**Au** (g/t)
Eagle's Nest[6]	*Mineral Reserves*							
	Proven		5.3	2.0	1.04	1.01	3.45	0.19
	Probable		5.9	1.4	0.72	0.78	2.76	0.18
		Total	**11.1**	**1.7**	**0.9**	**0.9**	**3.1**	**0.2**
	Mineral Resources							
	Inferred		9.0	1.1	1.14	1.16	3.49	0.3
Total Resources & Reserves			**20.1**	**1.4**	**1.0**	**1.0**	**3.3**	**0.2**
Volcanogenic Massive Sulphide Deposits				**Cu** (%)	**Zn** (%)			
	Mineral Resources							
McFaulds #1[7]	Inferred		0.8	3.8	1.10			
		Total	**0.8**	**3.8**	**1.10**			
McFaulds #3[7]	Inferred		0.3	2.1	0.58			
		Total	**0.3**	**2.1**	**0.58**			
Total Mineral Resources in the MLGB			**1.1**	**3.4**	**1.0**			

Sources: [1]Aubut (2010); [2]Aubut (2014a); [3]Aubut (2014b); [4]Murahwi et al. (2011); [5]Murahwi et al. (2012); [6]Burgess et al. (2012); [7]Lahti (2008)

mediate dyke. In contrast, the Neoarchean mafic-ultramafic intrusions, defined as the Ring of Fire intrusive suite (RoFIS), are subdivided into two main magmatic subsuites, an ultramafic-dominated subsuite (see Carson et al., 2015) and a mafic-dominated "ferrogabbro" subsuite (Kuzmich et al. 2015; Sappin et al., 2015) that is more regionally widespread. The ultramafic-dominated subsuite comprises variably serpentinized and/or talc carbonate-altered, dunite, peridotite, chromitite, pyroxenite, and gabbro, whereas the mafic-dominated subsuite comprises variably magnetite-bearing, layered gabbro, anorthosite, anorthositic gabbro, and rare pyroxenite.

Ultramafic-dominated intrusions are also present in other parts of the MLGB. The Wi intrusion occurs in the western part of the WA, crosscuts deformed supracrustal rocks that are interpreted to be ca. 2757 Ma based on new geochronology, and therefore could be similar in age to the RoFIS. It consists principally of undifferentiated, serpentinized, foliated, poorly layered, dunite and peridotite with a variable amount of disseminated chromite. An outcrop of gabbro to pyroxenite on the Winiskisis Channel could be a more evolved part of the intrusion. The Ley Lake intrusion, in the far southwest part of the area, consists primarily of green, foliated, serpentinized dunite and peridotite, in places with disseminated chromite. An outcrop of foliated gabbro is also present nearby. Varieties of mafic and ultramafic rocks are also present in the eastern Butler Lake area and may be correlative with the RoFIS.

MINERALIZATION STYLES

The MLGB and RoF region contain a wide variety of mineralization styles (Fig. 4), which are summarized in Tables 1 and 2. The most economically prospective deposit types are orthomagmatic Cr-(PGE) deposits (e.g. Black Thor) and Ni-Cu-PGE sulphide deposits (e.g. Eagle's Nest). Defined mineral resources and reserves in the area and significant occurrences, such as

Table 2. Select mineral occurrences and example drill core intersections in the "Ring of Fire" region.

Occurrence Name	Primary Commodity	Example of Intersections from Drill Core
Fe-Ti-V Occurrences		
Thunderbird[1]	V	164.9 m of 0.36% V_2O_5, including 45.9 m 0.51% V_2O_5 241.4 m of 0.37% V_2O_5, including 59.8 m averaging 0.54% V_2O_5
Butler[2]	V	36 m of 0.54% V_2O_5, 0.46% TiO_2 and 23.78% Fe 4.2 m of 1.17% V_2O_5, 7.97% TiO_2, and 40.73% Fe
Highbank[3]		0.75% V_2O_5 over 5.2 m, including a higher grade interval of 0.98% V_2O_5 over 2.2 m
Lode Gold Occurrences		
Triple J[4]	Au	1.1 m averaging 12.65 grams per tonne gold 10.0 m of 1.72 grams per tonne gold, including 4.4 m of 3.43 g/t gold
VMS Occurrences		
Butler VMS[5]	Cu-Zn	41.5 m of 0.4 Cu, 3.26% Zn and 6 g/t Ag 14.0 m of 0.56% Cu, 1.83% Zn and 11.31 g/t Ag 167 m of 0.39% Cu and 1.13% Zn 17 m of 1.0% Cu and 0.12 g/T Au 26.7 m of 0.6% Cu and 0.35% Zn 8 m of 4.68% Zn, 0.46% Cu and 7.7 g/t Ag
5.01 occurrence[6]	Cu-Zn	102 m of 6.5% Zn, 0.44% Cu, 0.19% Pb, and 3 g/t Ag, including 26 m 13.8% Zn, 0.50% Cu, 0.05%Pb, and 2 g/t Ag

[1]Noront resources press release dated July 29, 2009 - http://norontresources.com/?p=802 (assessed Dec 31 2014)

[2]MacDonald Mines Exploration Ltd., news release, May 11, 2011 - http://www.macdonaldmines.com/news/2011/79-macdonald-mines-announces-vanadium-assays-from-butler-lake-project-in-the-ring-of-fire (accessed Jan 2, 2015)

[3]Northern Shield Resources Inc., Highbank Lake property, www.northern-shield.com/properties/highbank [accessed September 27, 2012]

[4]Noront Resources Ltd. News release dated Oct 27 2009 - http://norontresources.com/?p=785 (accessed Dec 31, 2014)

[5]MacDonald Mines Ltd. News release dated May 11, 2011 www.macdonaldmines.com/news/2011/79-macdonald-mines-announces-vanadium-assays-from-butler-lake-project-in-the-ring-of-fire assessed January 2, 2015

[6]Metalex Ventures Ltd., www.metalexventures.com/html/james_bay.html accessed January 2, 2015

AT-12 (Ni-Cu-PGE), are restricted to the ultramafic-dominated RoFIS intrusions (Table 1). Fe-Ti-V-(P) mineralization is more widespread within mafic-dominated intrusions (e.g. HFIC, Butler, and Thunderbird intrusions) that belong to both the ca. 2810 Ma and ca. 2734 Ma suites. Fe-Ti-V-(P) mineralization (Table 2) occurs generally as thin layers of semi-massive to massive oxides and/or thicker zones of heavily disseminated oxide-rich gabbroic rocks.

VMS occurrences are quite common in the MLGB, although only two deposits have been defined (Table 1). These occurrences are present in most of the identified tectonostratigraphic assemblages in the area, and their distribution is broadly comparable to other large greenstone belts (e.g. Abitibi) where VMS-style base metal mineralization is widespread spatially and temporally.

The MLGB is not well known for its potential for lode gold mineralization. However, a number of gold occurrences are localized along the Triple J fault zone in the central part of the RoF. The Triple J fault, a southwest-striking structure that appears to dip ~55° towards the northwest, separates ultramafic-dominated intrusions from tonalitic basement between the Blackbird and the Black Horse chromite deposits. This deformation zone is generally characterized by variably thick, highly altered ultramafic rocks (i.e. talc-carbonate schist) with abundant quartz-carbonate veining.

A number of kimberlitic intrusions occur beneath Paleozoic cover, mainly in the eastern part of the area, which indicates the potential to host economic concentrations of diamond. These kimberlite intrusions are Mesoproterozoic (1.1 Ga) based on geochronology reported in Heaman et al. (2004).

IMPLICATIONS FOR REGIONAL EXPLORATION

The prospectivity of ultramafic- and mafic-dominated intrusions of the RoFIS to host a variety of orthomagmatic Cr-(PGE), Ni-Cu-PGE, Fe-Ti-V-(P) deposit types has been well established by recent discoveries. However, the spatial and temporal distribution of these intrusions is not fully understood and further characterization should be undertaken. For example, additional ultramafic intrusions, such as the Wi intrusion, Ley Lake intrusion, and a few intrusions in the Butler Lake area, are poorly exposed and not well characterized. These intrusions, which appear to have crystallized from Cr-rich magmas based on the presence of disseminated visible chromite, may be correlative with the ultramafic-dominated intrusion of the RoFIS and therefore are prospective to host Ni-Cu-PGE and Cr mineralization. Furthermore, the presences of numerous Ni-Cu-(PGE) occurrences (e.g. AT-12 occurrence) within

the ultramafic-dominated intrusions of the RoFIS highlight the potential for this type of mineralization, especially in the central area. Large areas of gabbroic intrusions prospective for Fe-Ti-V-(P) mineralization have been identified based on limited drilling and geophysical interpretation and remain attractive for additional Fe-Ti-V-(P) discoveries.

Prospectivity for VMS-style mineralization is high in many areas of the MLGB, as suggested by the presence of significant alteration systems, synvolcanic intrusions, and the number of occurrences occurs across the belt. Further investigation in the Butler Lake area and in the vicinity of the McFaulds #1 and #3 deposits is needed to characterize the detailed stratigraphy and alteration systems associated with these volcanic successions, as well as their structural setting, and to better target future exploration programs for this style of mineralization. Much more exploration and drilling are required to fully assess and effectively target additional VMS-style discoveries in these areas, particularly at depth, as the lack of exposure makes targeting more challenging.

Only limited gold exploration has been conducted in the RoF region. Further investigation is warranted to better understand the distribution and controlling factors on gold distribution in the Triple J shear zone. In addition, a number of large-scale regional faults (e.g. Webequie fault zone, and the extension of the South Kenyon Fault zone in the northern part of MLGB) have yet not been significantly explored for gold.

FORTHCOMING WORK

This contribution is offered as an interim summary of our current geological knowledge in the RoF region. Several regional-scale geological maps (1:100 000 scale) for the entire RoF region complemented with more detailed geological maps in the vicinity of known deposits and in the Butler area are also forthcoming. In conjunction with maps, compilations of field and drill-core data, whole rock geochemistry, and a summary of U-Pb geochronological data will be also released. New geological knowledge acquired by the OGS and the GSC in the RoF area highlights knowledge gaps in our understanding of the architecture and evolution of the MLGB, therefore further investigations are still warranted.

ACKNOWLEDGEMENTS

Thanks are extended to all mining companies involved in the RoF area. In particular we would like to thank: Richard Fink and Michael Orobona (Cliffs Natural Resources), Andrew Mitchell, David Shinkle, Ryan Weston, Daron Slaney and Randy Abraham (formerly Cliffs Natural Resources), Don Hoy and Martin Tuscherer (formerly Freewest Resources/Cliffs Natural Resources), Ralph MacNally, Eric Mosley, Matt Downey (Noront Resources), Mike Flanagan and Peter Smith (Fancamp Exploration), Moe Lavigne (KWG Resources), Quentin Yarie, Jacob McKinnon, Craig Sherba, Craig Hunt, and James Masters (MacDonald Mines), David Palmer (Probe Mines), Jim Voisin (UC Resources), David Clarke (Canterra Minerals), Nathalie Hansen, Éric Hébert and Ian Lawyer (Melkior Resources), and Christine Vaillancourt and Ian Bliss (Northern Shield Resources) for their generous assistance, numerous discussions, permission to access properties/diamond-drill cores, and corporate geological databases.

Jim Franklin, Larry Hulbert, Jim Mungall, and Greg Stott are thanked for valuable discussions and insight into the geology of the RoF area. Thanks also to Mike Lesher, Heather Carson, Kaveh Merhmanesh, Naghmeh Farhangi, Jack Spath, Pete Hollings, Ben Kuzmich, Anne-Aurélie Sappin, Jordan Laarman, Desmond Rainsford, Pierre Keating, and Mark Pilkington. Mike Hamilton, and Don Davis (U. of Toronto), and Robert Lodge, and Joe Petrus (Laurentian U.) are thanked for preliminary geochronological analyses. Hearst Air Service, Leuenberger Air Service, Thunder Airlines, Nakina Air Service, and the Ministry of Natural Resources are thanked for float plane and helicopter services. Elijah Jacob, Jonas Whitehead, Travis Spence, Leah Wabasse, and Chris McKay are thanked for assisting with various aspects of our work in Webequie. Jean-François Beausoleil, Cedric Mayer, and James Nopper provided excellent field assistance. We are also grateful to Jack Parker (OGS) and Léopold Nadeau (GSC) for timely and comprehensive reviews that helped us improve the final version of this contribution.

REFERENCES

Aubut, A., 2010. National Instrument 43-101 Technical Report, McFauld's Lake Area, Ontario, Canada, Black Thor Chromite Deposit Mineral Resource Estimation Technical Report; Freewest Resources Canada Ltd. internal report, 65 p.

Aubut, A., 2014a. National Instrument 43-101 Technical Report, Big Daddy chromite deposit McFaulds Lake Area, Ontario, Canada, Porcupine Mining Division, NTS 43D16, Updated Mineral Resource Estimation Technical Report; KWG Resources Canada Ltd. internal report, 66 p.

Aubut, A., 2014b. National Instrument 43-101 Technical Report, Koper Lake Project Chromite Deposit, McFauld's Lake Area, Ontario, Canada, Porcupine Mining Division, NTS 43D16, Updated Mineral Resource Estimation Technical Report; KWG Resources Canada Ltd. internal report, 75 p.

Burgess, H., Gowans, R., Jacobs, C., Murahwi, C. and Damjanovic, B. 2012. NI 43-101 Technical Report Feasibility Study McFaulds Lake Property Eagle's Nest Project James Bay Lowlands Ontario, Canada; Noront Resources Ltd. internal report, 210 p.

Buse, S., Smar, L., Stott, G.M., and McIlraith, S.J., 2009. Precambrian geology of the Winisk Lake area; Ontario Geological Survey, Preliminary Map P.3607, scale 1:100 000.

Carson, H.J.E., Lesher, C.M., and Houlé, M.G., 2015. Geochemistry and petrogenesis of the Black Thor intrusive complex and associated chromite mineralization, McFaulds Lake greenstone belt, Ontario *In:* Targeted Geoscience Initiative 4: Canadian Nickel-Copper-Platinum Group Elements-Chromium Ore Systems — Fertility, Pathfinders, New and Revised Models, (ed.) D.E. Ames and M.G. Houlé; Geological Survey of Canada, Open File 7856, p. 87–102.

Heaman, L.M., Kjarsgaard, B.A., and Creaser, R.A., 2004. The temporal evolution of North American kimberlites; Lithos, v. 76, p. 377– 397.

Houlé, M.G. and Metsaranta, R.T., 2013. An update of the high-magnesium ultramafic to mafic systems subproject under the Targeted Geoscience Initiative 4, *In:* Summary of Field Work and Other Activities 2013; Ontario Geological Survey, Open File Report 6290, p. 49-1 to 49-7.

Houlé, M.G., Lesher, C.M., and Metsaranta, R.T., 2012. Overview of the high-magnesium ultramafic to mafic systems subproject under the Targeted Geoscience Initiative 4: an Ontario perspective, *In:* Summary of Field Work and Other Activities 2012; Ontario Geological Survey, Open File Report 6280, p. 42-1 to 42-9.

Kilbourne, M., 2009. White Pine Resources–Noront Resources–Golden Valley Mines, Luc Bourdon Project, James Bay Lowlands 2009 drill summary report; Thunder Bay North Resident Geologist's Office, assessment file AFRO# 2.4442, 123 p.

Kilbourne, M., 2010. White Pine Resources-Noront Resources-Golden Valley Mines, Luc Bourdon Project, James Bay Lowlands, 2010 drill summary report; Thunder Bay North Resident Geologist's Office, assessment file AFRO# 2.48443 (AFRI# 20000006907), 27 p.

Kuzmich, B., Hollings, P., and Houlé, M.G., 2015. Petrogenesis of the ferrogabbroic intrusions and associated Fe-Ti-V-(P) mineralization within the McFaulds greenstone belt, Superior Province, northern Ontario, *In:* Targeted Geoscience Initiative 4: Canadian Nickel-Copper-Platinum Group Elements-Chromium Ore Systems — Fertility, Pathfinders, New and Revised Models, (ed.) D.E. Ames and M.G. Houlé; Geological Survey of Canada, Open File 7856, p. 101–109.

Lahti, H.R., 2008. Updated technical report on the McFaulds Lake project, Porcupine Mining Division, James Bay Lowland, Ontario, Canada, for UC Resources Limited and Spider Resources Inc. by Deep Search Exploration Technologies Inc., August 30, 2008; Technical Report under NI 43-101, filed September 4, 2008, with SEDAR®, 96 p.

Metsaranta, R.T. and Houlé, M.G., 2012. Progress on the McFaulds Lake ("Ring of Fire") region data compilation and bedrock geology mapping project, *In:* Summary of Field Work and Other Activities 2012; Ontario Geological Survey, Open File Report 6280, p.43-1 to 43-12.

Metsaranta, R.T. and Houlé, M.G., 2013. An update on regional bedrock geology mapping in the McFaulds Lake ("Ring of Fire") Region, *In:* Summary of Field Work and Other Activities 2013; Ontario Geological Survey, Open File Report 6290, p. 50-1 to 50-12.

Murahwi, C.Z., San Martin, A.J., and Spooner, J., 2011. Technical report on the updated mineral resource estimate for the Black Creek chrome deposit, McFaulds Lake area, James Bay Lowlands, northern Ontario, Canada, for Probe Mines Limited by Micon International Ltd. February 2, 2011; Technical Report under NI 43-101, filed February 4, 2011, with SEDAR®, 135 p.

Murahwi, C., San Martin, A.J., Gowans, R.M., and Spooner, J., 2012. Technical report on the updated mineral resource estimate for the Blackbird Chrome Deposits, McFaulds Lake project, James Bay Lowlands, Ontario, Canada, for Noront Resources Ltd. by Micon International Ltd., April 18, 2011; NI 43-101 report.

Polk, B.K., 2009. Assessment report on ground geophysical work for blocks 2, 2.25, 33, 41 and 92 and diamond drilling on Block 2, BMAs 527862, 527864, 528854, 531854, 531861, 532862, Porcupine Mining Division, Thunder Bay Mining Division, Metalex Ventures Ltd. and White Pine Resources Inc; Thunder Bay North Resident Geologist's Office, assessment file AFRO# 2.43025, 121 p.

Rayner, N. and Stott, G.M., 2005. Discrimination of Archean domains in the Sachigo Subprovince: a progress report on the geochronology, *In:* Summary of Field Work and Other Activities 2005; Ontario Geological Survey, Open File Report 6172, p.10-1–10-21.

Sappin, A.-A., Houlé, M.G., Lesher, C.M., Metsaranta, R.T., and McNicoll, V.J., 2015. Regional characterization of mafic-ultramafic intrusions in the Oxford-Stull and Uchi domains, Superior Province, Ontario, *In:* Targeted Geoscience Initiative 4: Canadian Nickel-Copper-Platinum Group Elements-Chromium Ore Systems — Fertility, Pathfinders, New and Revised Models, (ed.) D.E. Ames and M.G. Houlé; Geological Survey of Canada, Open File 7856, p. 75–85.

GEOLOGICAL SURVEY OF CANADA
OPEN FILE 7856

Targeted Geoscience Initiative 4: Canadian Nickel-Copper-Platinum Group Elements-Chromium Ore Systems — Fertility, Pathfinders, New and Revised Models

Regional characterization of mafic-ultramafic intrusions in the Oxford-Stull and Uchi domains, Superior Province, Ontario

Anne-Aurélie Sappin[1], Michel G. Houlé[1], C. Michael Lesher[2], Riku T. Metsaranta[3], and Vicki J. McNicoll[4]

[1]Geological Survey of Canada, Québec, Quebec
[2]Laurentian University, Sudbury, Ontario
[3]Ontario Geological Survey, Sudbury, Ontario
[4]Geological Survey of Canada, Ottawa, Ontario

© Her Majesty the Queen in Right of Canada, as represented by the Minister of Natural Resources Canada, 2015

This publication is available for free download through GEOSCAN (http://geoscan.nrcan.gc.ca/)

Recommended citation

Sappin, A.-A., Houlé, M.G., Lesher, C.M., Metsaranta, R.T., and McNicoll, V.J., 2015. Regional characterization of mafic-ultramafic intrusions in the Oxford-Stull and Uchi domains, Superior Province, Ontario, *In:* Targeted Geoscience Initiative 4: Canadian Nickel-Copper-Platinum Group Elements-Chromium Ore Systems — Fertility, Pathfinders, New and Revised Models, (ed.) D.E. Ames and M.G. Houlé; Geological Survey of Canada, Open File 7856, p. 75–85.

Publications in this series have not been edited; they are released as submitted by the author.

Contribution to the Geological Survey of Canada's Targeted Geoscience Initiative 4 (TGI-4) Program (2010–2015)

TABLE OF CONTENTS

Regional characterization of mafic-ultramafic intrusions in the Oxford-Stull and Uchi domains, Superior Province, Ontario

Anne-Aurélie Sappin[1]*, Michel G. Houlé[1], C. Michael Lesher[2], Riku T. Metsaranta[3], and Vicki J. McNicoll[4]

[1]Geological Survey of Canada, 490 rue de la Couronne, Québec, Quebec G1K 9A9
[2]Mineral Exploration Research Centre, Department of Earth Sciences, Goodman School of Mines, Laurentian University, 935 Ramsey Lake Road, Sudbury, Ontario P3E 2C6
[3]Ontario Geological Survey, 933 Ramsey Lake Road, Sudbury, Ontario P3E 2C6
[4]Geological Survey of Canada, 601 Booth Street, Ottawa, Ontario K1A 0E8
*Corresponding author's e-mail: asappin@nrcan.gc.ca

ABSTRACT

The mafic-dominated Big Mac, Fishtrap Lake, Highbank Lake, and Oxtoby Lake, the ultramafic-dominated Max, and the mafic-ultramafic Wabassi Main intrusions in the Oxford-Stull and Uchi domains of the Superior Province show significant potential for Fe-Ti-V-(P), Ni-Cu-(PGE), and/or Cr-(PGE) mineralization. The broadly layered Big Mac intrusion appears to have crystallized from an evolved high Fe-Ti basaltic parental magma that was injected from a feeder conduit below the northern part of the intrusion. The Fishtrap Lake and Highbank Lake intrusions represent parts of a large layered mafic-dominated igneous complex that formed from the injection of several pulses of basaltic magma. The genetically associated Max and Wabassi Main intrusions have crystallized from more primitive, basaltic parental magmas that were injected from a feeder conduit below the northwestern part of the Wabassi Main layered intrusion. In this magmatic system, the Max intrusion represents a magmatic conduit. The Oxtoby Lake intrusion appears to have crystallized from a differentiated basaltic parental magma and may represent an isolated intrusion.

INTRODUCTION

The eastern part of the Oxford-Stull and Uchi domains (Superior Province) hosts numerous mafic and ultramafic intrusions with great potential to host orthomagmatic mineralization, as attested by the occurrence of world-class Cr deposits (e.g. Black Thor), significant Ni-Cu-(platinum-group element (PGE)) deposits (e.g. Eagle's Nest), and Fe-Ti-V-(P) occurrences (e.g. Thunderbird).

This study is part of the high-magnesium ultramafic to mafic systems subproject under the Targeted Geoscience Initiative 4 (TGI-4; Houlé et al., 2012; Houlé and Metsaranta, 2013) of the Geological Survey of Canada (GSC). The main purpose of this research is to characterize mafic and ultramafic intrusions within the McFaulds Lake and Miminiska-Fort Hope greenstone belts (Fig. 1) in order to assess their economic potential and identify the most prospective intrusions. In this contribution, we present the main petrological, geochemical, mineralogical, and geochronological characteristics of some of these intrusions and discuss their internal structure, the nature of their parental magmas, the sulphide and oxide saturation history, their emplacement processes, and the implications for exploration.

RESULTS

Methodology

The studied intrusions are mostly covered by surficial deposits and are exposed only in scarce outcrops. For each intrusion, several representative samples were selected from diamond-drilled cores and rare outcrops for detailed petrographic, geochemical, and mineralogical studies (Table 1). The main characteristics for each intrusion are presented in Table 2.

All samples from the Big Mac intrusion and a few samples from the Fishtrap Lake, Oxtoby Lake (formerly Wabassi North), and Wabassi Main intrusions were analyzed for whole-rock geochemistry at the Ontario Geoscience Laboratories (Sudbury, Canada); the bulk of the samples from Fishtrap Lake, Highbank Lake, Max, Oxtoby Lake, and Wabassi Main intrusions were analyzed at ALS Minerals (Vancouver, Canada). Major elements have been recalculated to a 100% volatile-free basis and full analytical details are provided in Sappin et al. (in prep.).

Major element contents of silicates and Fe-Ti oxides, and minor and trace element contents of Fe-Ti oxides were determined using a CAMECA SX-100 five-spectrometer electron microprobe at Université

Sappin, A.-A., Houlé, M.G., Lesher, C.M., Metsaranta, R.T., and McNicoll, V.J., 2015. Regional characterization of mafic-ultramafic intrusions in the Oxford-Stull and Uchi domains, Superior Province, Ontario, *In:* Targeted Geoscience Initiative 4: Canadian Nickel-Copper-Platinum Group Elements-Chromium Ore Systems — Fertility, Pathfinders, New and Revised Models, (ed.) D.E. Ames and M.G. Houlé; Geological Survey of Canada, Open File 7856, p. 75–85.

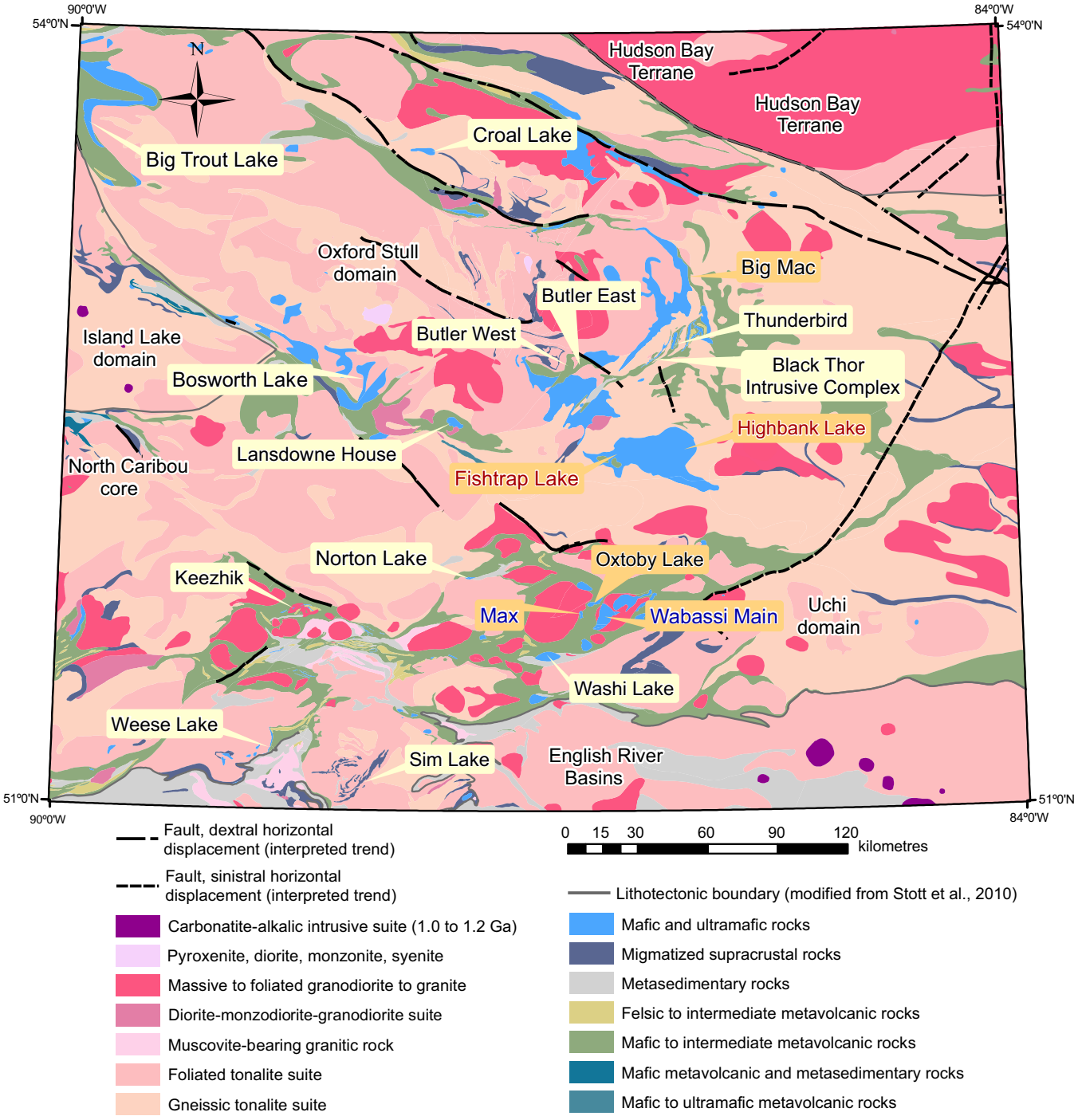

Figure. 1. Simplified geological map of the eastern Oxford-Stull and Uchi domains and general location of the main mafic and ultramafic intrusions in the area, including the studied (orange) intrusions (modified from Houlé and Metsaranta, 2013). The intrusions with their name in red and those with their name in blue are, respectively, genetically related. Geology modified from Stott and Josey (2009).

Laval (Québec, Canada). Analytical conditions are provided in Sappin et al. (in prep.).

Petrography

All mafic and ultramafic rocks have been metamorphosed to greenschist-amphibolite facies (Metsaranta and Houlé, 2012), but igneous textures are often preserved and igneous minerals are sometimes preserved, so the prefix "meta" has been omitted for simplicity.

Big Mac Intrusion

The 120 km^2 Big Mac intrusion is composed of gabbroic rocks (Fig. 2a), minor anorthosite, and rare pyroxenite. It also contains a few decimetre- to metre-thick semi-massive to massive magnetite-ilmenite layers (Fig. 2b). The pyroxenite and the oxide layers are

Table 1. Type and number of samples from each intrusion that were characterized through this study.

		Big Mac	Fishtrap Lake	Highbank Lake	Max	Oxtoby Lake	Wabassi Main
Petrographic study							
	Core	40 (5 ddhs)	-	113 (14 ddhs)	29 (7 ddhs)	6 (1 ddh)	75 (15 ddhs)
	Surface	-	9	3	-	-	29
Geochemistry							
Whole rock	*Core*	57	-	83	23	6	50
	Surface	-	6	1	-	-	22
Mineral	*Core*	20	-	40	8	3	13
	Surface	-	6	1	-	-	6

Note: 40 (5 ddhs) = 40 samples from 5 diamond drillholes

restricted to the northern part of the intrusion. The gabbroic rocks, anorthosite, and pyroxenite mostly contain plagioclase and amphibole, with rare preserved clinopyroxene and up to 35% Fe-Ti oxides. They display relict cumulate textures with cumulus plagioclase. Semi-massive oxides (40–80% Fe-Ti oxides) and massive oxides (>80% Fe-Ti oxides) mostly contain large magnetite crystals with ilmenite exsolutions, rare silicate phases, and up to 20% disseminated to net-textured Fe-Ni-Cu sulphides.

Fishtrap Lake and Highbank Lake Intrusions

The 270 km^2 Fishtrap Lake intrusion is composed of layers of gabbroic rocks interbedded with layers of anorthosite (Fig. 2c). They mostly contain plagioclase and amphibole. The gabbroic rocks and anorthosite are likely former plagioclase cumulates.

The 420 km^2 Highbank Lake intrusion is composed of layers of gabbroic rocks interlayered with layers of anorthosite and pyroxenite (Fig. 2d) and a few decimetre-thick semi-massive magnetite-ilmenite layers restricted to the north-central part of the intrusion. The gabbroic rocks, anorthosite, and pyroxenite commonly contain plagioclase and amphibole, with up to 40% Fe-Ti oxides and up to 40% disseminated to net-textured Fe-Cu-Ni sulphides. The gabbroic rocks and pyroxenite are likely former pyroxene-plagioclase cumulates. The anorthosite is likely former plagioclase cumulates. Semi-massive oxides (60–75% Fe-Ti oxides) mostly contain large magnetite crystals with ilmenite exsolutions and rare silicate phases.

Max, Oxtoby Lake, and Wabassi Main Intrusions

The 4 km^2 Max intrusion is composed of peridotite (Fig. 2e), minor olivine pyroxenite, pyroxenite, plagioclase-bearing pyroxenite, and rare gabbroic rocks. The peridotite and olivine pyroxenite mostly contain olivine and pyroxene, with up to 15% disseminated to net-textured Fe-Ni-Cu sulphides. They display cumulate textures with cumulus olivine-plagioclase± chromite and poikilitic pyroxene. The pyroxenite, plagioclase-bearing pyroxenite, and gabbroic rocks primarily contain amphibole and plagioclase.

The 12 km^2 Oxtoby Lake intrusion is composed of gabbroic rocks (Fig. 2f). They mostly contain plagioclase and amphibole.

The 42 km^2 Wabassi Main intrusion is composed of gabbroic rocks, olivine gabbroic rocks, local anorthosite, minor feldspathic peridotite (Fig. 2g) and Fe-Ti oxide-rich ferrogabbroic rocks, and subordinate hornblende-bearing gabbroic rocks (Fig. 2h). The olivine gabbroic rocks and the peridotite are mainly restricted to the western and northern parts of the intrusion, the ferrogabbroic rocks to the southeastern part, and the hornblende-bearing gabbroic rocks near the western margin and in the central and the southeastern parts. The gabbroic rocks, olivine gabbroic rocks, anorthosite, and peridotite mostly comprise pyroxene, plagioclase, olivine, and a few centimetre- to decimetre-thick intervals with up to 75% pyrrhotite-dominated disseminated, net-textured, and semi-massive Fe-Cu-Ni sulphides. The gabbroic rocks, olivine gabbroic rocks, and anorthosite display cumulate textures with cumulus pyroxene-plagioclase±olivine±Fe-Ti oxides and, locally, poikilitic pyroxene; the peridotite displays cumulate textures with with cumulus olivine-plagioclase±chromite and poikilitic pyroxene. The hornblende-bearing gabbroic rocks mainly contain amphibole, plagioclase, and quartz.

Whole-Rock Chemistry

Big Mac Intrusion

Big Mac mafic and ultramafic rocks commonly have low to intermediate SiO_2 contents, low MgO contents, and locally high FeO_t contents (Fig. 3, Table 2).

Big Mac mafic rocks are enriched in highly incompatible lithophile elements (HILE) relative to moderately incompatible lithophile elements (MILE) but enriched to depleted in Nb-Ta relative to HILE of similar compatibility, enriched to depleted in Hf-Zr relative to MILE of similar compatibility, and enriched in Ti relative to MILE of similar compatibility (Table 2). Big Mac pyroxenite is depleted in HILE relative to MILE but their profiles show weak negative anomalies in Zr and Hf and pronounced positive anomalies in Ti compared with the rare earth elements (Table 2).

Fishtrap Lake and Highbank Lake Intrusions

Fishtrap Lake mafic rocks have intermediate SiO_2 contents and low MgO and FeO_t contents (Fig. 3, Table 2). Highbank Lake mafic and ultramafic rocks have generally low to intermediate SiO_2 contents, low to high MgO contents, and locally high FeO_t contents (Fig. 3, Table 2). Overall, the composition of the mafic rocks from the Fishtrap Lake intrusion follows the same compositional trends defined by the mafic and ultramafic rocks of the Highbank Lake intrusion (Fig. 3).

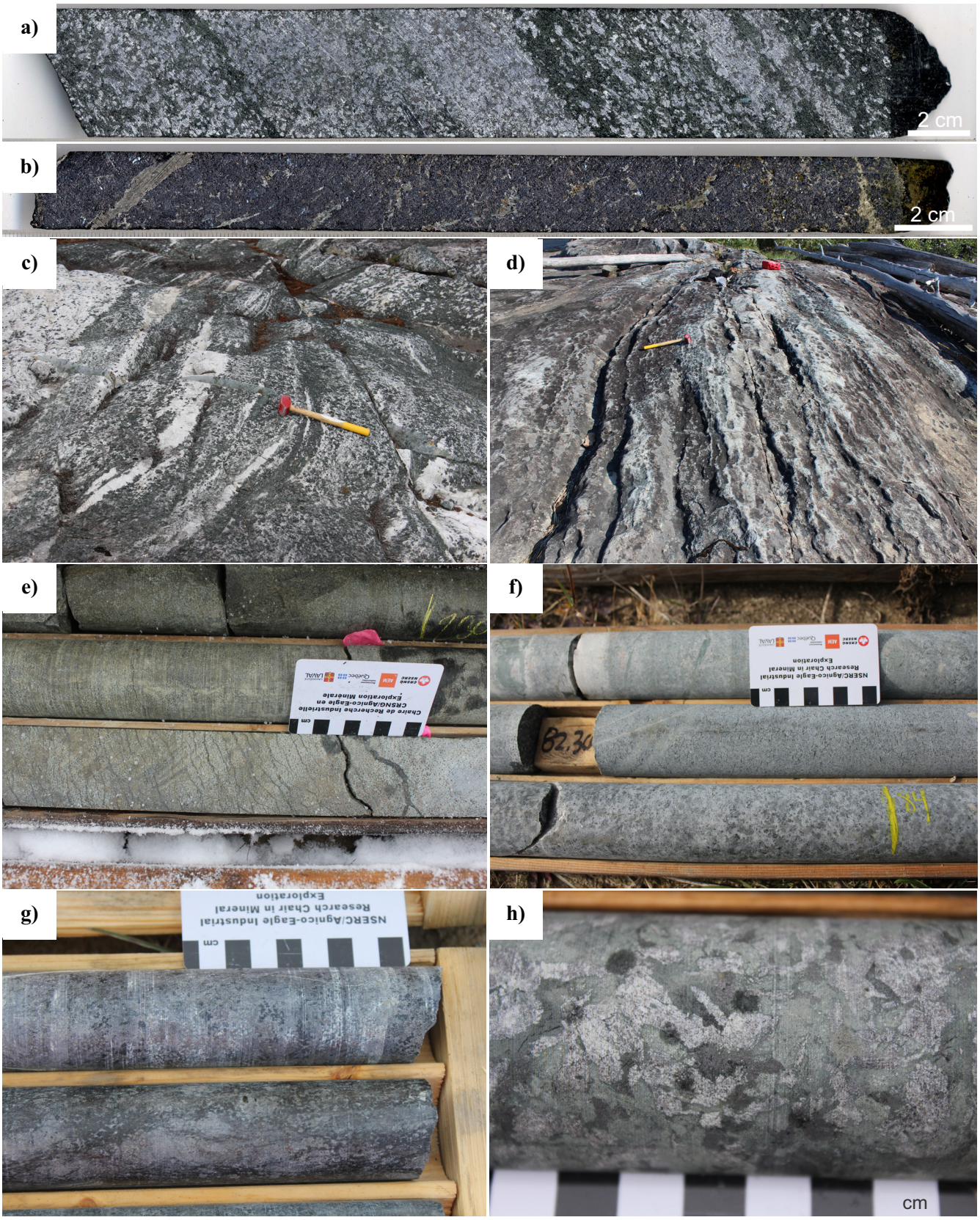

Figure 2. Photographs of outcrop and drill core. **a)** Gabbroic rocks from the Big Mac intrusion (BM09-04, 43.28 m). **b)** Massive Fe-Ti oxides from the Big Mac intrusion (BM09-04, 23.70 m). **c and d)** Modal magmatic layering in the Fishtrap Lake and Highbank Lake intrusions. The hammer is ~38 cm long. **e)** Peridotite from the Max intrusion (08MX-02, 282.84 m). **f)** Hornblende-bearing gabbroic rocks from the Oxtoby Lake intrusion (08WA-02, 82.30 m). **g)** Peridotite from the Wabassi Main intrusion (10WA-05, 240.48 m). **h)** Hornblende-bearing gabbroic rocks from the Wabassi Main intrusion (11WA-18, 30.71 m).

Table 2. Summary of the main petrological, geochemical, and mineralogical characteristics of the studied intrusions.

	Big Mac		Fishtrap Lake	Highbank Lake		Max		Oxtoby Lake	Wabassi Main	
Location	McFaulds Lake greenstone belt					Miminiska-Fort Hope greenstone belt				
Mafic/Um ratio	Mafic >>> Um		Mafic	Mafic > Um		Um >>> Mafic		Mafic	Mafic > Um	
Internal structure	Broadly layered		Layered	Layered		-		-	Layered	
Size	1–4 km x 60 km 120 km^2		27 km x 16 km 270 km^2	21 km x 35 km 420 km^2		1.5 km x 3 km 4 km^2		7 km x 2 km 12 km^2	9 km x 11 km 42 km^2	
Lithology	Gabbroic rocks, minor anorthosite, pyroxenite, and semi-massive to massive Fe-Ti oxides		Gabbroic rocks, anorthosite	Gabbroic rocks, anorthosite, pyroxenite, and minor semi-massive Fe-Ti oxides		Peridotite, minor olivine pyroxenite, pyroxenite, plagioclase-bearing pyroxenite, and gabbroic rocks		Gabbroic rocks	Gabbroic rocks (± olivine), anorthosite, minor peridotite	
Igneous mineralogy	Pl, Cpx, Opx?, Mag, Ilm, Ap		Pl, Opx, Cpx?, Ilm, Ap	Pl, Px?, Ilm, Mag, Ap		Ol, Opx, Cpx?, Pl, Chr		Pl, Px?, Mag, Ilm, Ap	Cpx, Opx, Pl, Ol, Ilm, Mag, Chr, Ap	
Mineralization	Fe-Ti-V-(P) 76% FeO_t, 19% TiO_2, 0.58% V_2O_5		- -	Fe-Ti-V, Cr-(PGE) 64% FeO_t, 17% TiO_2, 0.98% V_2O_5 (www.northernshield.com/properties/highbank)		Ni-Cu-(PGE) 0.31% Ni, 0.18% Cu, 0.32 ppm Pt+Pd (Vaillancourt and Bliss, 2010)		- -	Ni-Cu-(PGE) 3.5% Cu, 0.24% Ni (Vaillancourt et al., 2011)	
Geochemistry	**Mafic**	**Um**	**Mafic**	**Mafic**	**Um**	**Mafic**	**Um**	**Mafic**	**Mafic**	**Um**
Major elements										
SiO_2 (wt.%)	32–55	38	50–52	28–52	40–53	51–52	41–49	47–50	44–59	44–49
MgO (wt.%)	0–11	10	0–7	1–12	6–24	9–12	23–38	4–6	2–16	24–28
FeO_t (wt.%)	2–36	35	1–8	3–37	11–27	6	10–18	9–13	4–20	13–16
Trace Elements										
HILE/MILE ratio	HILE>MILE	HILE<MILE	HILE<MILE to HILE>MILE	HILE<MILE to HILE>MILE	HILE<MILE to HILE>MILE	HILE>MILE	HILE>MILE	HILE>MILE	HILE≈MILE to HILE>MILE	HILE≈MILE to HILE>MILE
Nb/Th	0.9–60.8	14.68	6.3–7.3	0.5–61.4	0.4–6.7	3.4–3.8	2.3–7.5	2.3–7.1	0.7–158.3	1.8–5.5
Ta/Th	0.1–4.5	1.0	nd	0.0–6.7	0.0–0.6	0.3–0.5	0.2–0.8	0.1–0.3	0.1–10.0	0.1–0.5
Hf/Y	0.0–0.5	0.0	0.1–0.2	0.0–0.3	0.1–2.0	0.1	0.1–0.2	0.1–0.2	0.0–0.4	0.1–0.2
Zr/Y	0.8–13.4	1.5	1.5–6.0	0.3–15.0	2.0–81.9	2.8–6.3	3.6–6.2	2.9–6.9	0.8–15.0	5.3–9.5
Ti/Y	138–26834	2209	397–1093	219–19709	143–4914	321–404	197–612	470–949	52–5965	276–660
Mineral Composition	**Mafic**	**Um**	**Mafic**	**Mafic**	**Um**	**Mafic**	**Um**	**Mafic**	**Mafic**	**Um**
Olivine	-		-	-		-	$Mg\#_{80–67}$	-	$Mg\#_{78–19}$	$Mg\#_{78–73}$
Orthopyroxene	-		$Mg\#_{53}$	-		-	$Mg\#_{84–82}$	-	$Mg\#_{84–44}$	$Mg\#_{84–77}$
Clinopyroxene	-	$Mg\#_{68-60}$	-	-		-		-	$Mg\#_{80–56}$	$Mg\#_{95–91}$
Plagioclase	$An_{90–20}$	-	$An_{71–31}$	$An_{99–24}$	$An_{86–36}$	-		$An_{68–47}$	$An_{96–31}$	$An_{100–61}$
Magnetite	V ≤ 9319 Ni ≤ 230 Cr ≤ 11077 Ti ≤ 14090	V ≤ 2830 Ni ≤ 100 Cr ≤ 9530 Ti ≤ 1190	-	V ≤ 10726 Ni ≤ 731 Cr ≤ 21900 Ti ≤ 65330	V ≤ 7749 Ni ≤ 786 Cr ≤ 13869 Ti ≤ 28790	-	No primary Mag	V ≤ 3380 Ni ≤ 1290 Cr ≤ 2020 Ti ≤ 53938	V ≤ 12380 Ni ≤ 1713 Cr ≤ 30714 Ti ≤ 123685	No primary Mag
Ilmenite	V ≤ 5308 Ni ≤ 130 Cr ≤ 766 Mn ≤ 22304	V = 0 Ni ≤ 134 Cr ≤ 360 Mn ≤ 16040	V = nd Ni ≤ 120 Cr ≤ 1530 Mn ≤ 20090	V ≤ 3881 Ni ≤ 180 Cr ≤ 2853 Mn ≤ 30498	V = 0 Ni ≤ 100 Cr ≤ 790 Mn ≤ 38610	-	No primary Ilm	V ≤ 3710 Ni = 0 Cr ≤ 710 Mn ≤ 12990	V ≤ 5 290 Ni ≤ 680 Cr ≤ 4 190 Mn ≤ 14610	No primary Ilm
Mag/Ilm ratio	Mag > Ilm	Mag > Ilm	Ilm >>> Mag	Ilm > Mag	Ilm > Mag	-	-	Mag > Ilm	Ilm > Mag	-
Parental magma	Basaltic with high-Fe and Ti contents		Basaltic	Basaltic with high-Fe and Ti contents		Basaltic		Basaltic	Basaltic	

Abbreviations: Ap = appatite, Chr = chromite, Cpx = clinopyroxene, HILE = highly incompatible lithophile elements (e.g. Th, Nb, Ta, light rare earth elements), Ilm = ilmenite, Mag = magnetite, MILE = moderately incompatible lithophile elements (e.g. Zr, Hf, Ti, middle rare earth elements, Y), nd = not determined, Ol = olivine, Opx = orthopyroxene, PGE = platinum-group element, Pl = plagioclase, Px = pyroxene, Um = ultramafic

Note: Mg# (Mg number) = 100×Mg/(Mg+Fe^{2+}) in atomic proportions, An (anorthite content) = 100×Ca/(Na+K+Ca) in atomic proportions.
V, Ni, Cr, Ti, Mn concentrations in magnetite and ilmenite are in ppm.

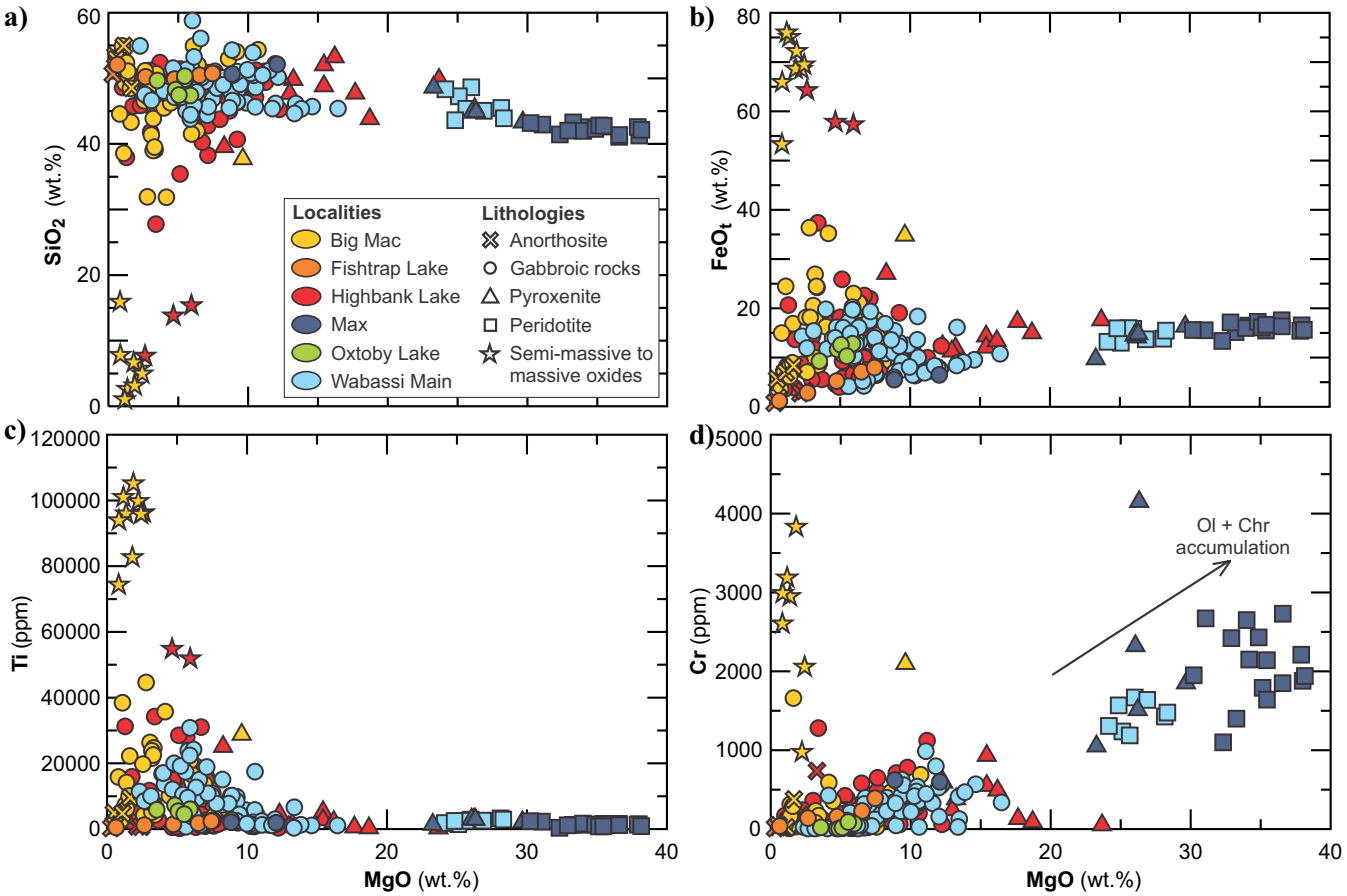

Figure 3. Binary plots showing **(a)** SiO_2 versus MgO, **(b)** FeO_t versus MgO, **(c)** Ti versus MgO, and **(d)** Cr versus MgO. Abbreviations: Chr = chromite, Ol = olivine.

Fishtrap Lake and Highbank Lake mafic and ultramafic rocks are slightly depleted to enriched in HILE relative to MILE but less enriched in Nb relative to HILE of similar compatibility, and depleted in Hf-Zr relative to MILE of similar compatibility (Table 2). Highbank Lake mafic and ultramafic rocks may also be enriched to depleted in Ta relative to Nb and in Hf-Zr-Ti relative to MILE of similar compatibility (Table 2).

Max, Oxtoby Lake, and Wabassi Main Intrusions

Max mafic and ultramafic rocks have intermediate SiO_2 contents, low to high MgO contents, and low to intermediate FeO_t contents (Fig. 3, Table 2). Oxtoby Lake mafic rocks have intermediate SiO_2 and FeO_t contents and low MgO contents (Fig. 3, Table 2). Wabassi Main mafic and ultramafic rocks have intermediate SiO_2 contents, low to high MgO contents, and low to intermediate FeO_t contents (Fig. 3, Table 2). The composition of the intrusive rocks of the three intrusions shows well correlated trends (Fig. 3).

Max mafic and ultramafic rocks are enriched in HILE relative to MILE but less enriched in Nb and, locally, Ta relative to HILE of similar compatibility (Table 2). Oxtoby Lake mafic rocks are enriched in HILE relative to MILE but less enriched in Nb-Ta relative to HILE of similar compatibility and less enriched in Zr-Hf relative to MILE of similar compatibility (Table 2). Wabassi Main mafic and ultramafic rocks are unenriched to enriched in HILE relative to MILE but less enriched in Nb relative to HILE of similar compatibility and enriched to depleted in Ta relative to Nb and, locally, in Hf-Zr-Ti relative to MILE of similar compatibility (Table 2).

Mineral Chemistry

Big Mac Intrusion

Big Mac intrusive rocks contain plagioclase (An_{90-20}, where An=100×Ca/(Na+K+Ca)) and rare clinopyroxene ($Mg\#_{68-60}$, where Mg#=100×Mg/(Mg+Fe^{2+})) with mostly evolved compositions (Table 2). Big Mac intrusive rocks contain magnetite and ilmenite with wide compositional variations (Table 2).

Composition of the Big Mac intrusive rocks varies with location. To the north, plagioclase has the most primitive composition (up to An_{84}) and magnetite and ilmenite are richest in compatible elements in mafic magmas such Al-Mg-V-Ni-Cr. To the south, plagioclase has the most evolved composition (up to An_{49})

and magnetite and ilmenite are poor in Al-Mg-V-Ni-Cr and locally rich in Ti-Mn-Zn.

Fishtrap Lake and Highbank Lake Intrusions

Fishtrap Lake intrusive rocks contain plagioclase (An_{71-31}) and rare relicts of orthopyroxene ($Mg_{\#53}$) with relatively evolved compositions (Table 2). Highbank Lake intrusive rocks contain plagioclase (An_{99-24}) with wide compositional variations (Table 2). Fishtrap Lake and Highbank Lake intrusive rocks contain magnetite and ilmenite with wide compositional variations (Table 2).

Max, Oxtoby Lake, and Wabassi Main Intrusions

Max ultramafic cumulates contain olivine ($Mg\#_{80–67}$) and orthopyroxene ($Mg\#_{84–82}$) with intermediate compositions (Table 2). Oxtoby Lake hornblende-bearing gabbroic rocks contain plagioclase ($An_{68–47}$) with evolved compositions (Table 2). Wabassi Main ultramafic cumulates contain olivine ($Mg\#_{78–73}$), orthopyroxene ($Mg\#_{84–77}$), clinopyroxene ($Mg\#_{95–91}$), and plagioclase ($An_{100–61}$) with intermediate compositions. Wabassi Main gabbroic rocks (± olivine) and anorthosite contain olivine ($Mg\#_{78–19}$), orthopyroxene ($Mg\#_{84–44}$), clinopyroxene ($Mg\#_{80–56}$), and plagioclase ($An_{96–37}$) with evolved to intermediate compositions. Wabassi Main hornblende-bearing gabbroic rocks contain plagioclase ($An_{66–31}$) with evolved compositions.

Composition of the Wabassi Main intrusive rocks varies with location. Near the western contact, olivine (up to $Mg\#_{78}$), orthopyroxene (up to $Mg\#_{84}$), clinopyroxene (up to $Mg\#_{95}$), and plagioclase (up to An_{100}) have the most primitive composition. In the southeastern area, olivine is absent and orthopyroxene (up to $Mg\#_{57}$), clinopyroxene (up to $Mg\#_{73}$), and plagioclase (up to An_{71}) have more evolved composition.

Geochronology

The Highbank Lake intrusion has a U-Pb zircon age of ca. 2808 Ma (Stott, 2008). Preliminary U-Pb isotope dilution thermal ionization mass spectrometry (ID-TIMS) zircon data from hornblende-plagioclase-bearing gabbroic rock suggest crystallization ages of 2810 Ma, 2717 Ma, and 2727 Ma (McNicoll, unpublished data) for the Fishtrap Lake, Oxtoby Lake, and Wabassi Main intrusions, respectively.

DISCUSSION

Internal Structure

The internal structure of the broadly layered Big Mac intrusion is not well constrained. Based on the presence of more primitive whole-rock and mineral chemical signatures in the northern part and more evolved signatures in the southern part, and assuming that it fractionated upwards, the intrusion appears to young to the south.

The Fishtrap Lake and Highbank Lake intrusions are layered, but their internal structure is thus far poorly constrained. Preliminary mineral chemical data suggest that these intrusions are not systematically fractionated and therefore formed from multiple magma replenishments.

The Max and Oxtoby Lake intrusions do not exhibit any internal structural variations. The Max intrusion is composed primarily of cumulate rocks, which suggests that it represents a magmatic conduit in which cumulus olivine ± pyroxenes accumulated. The Oxtoby Lake intrusion is composed primarily of gabbroic rocks and likely represents an undifferentiated intrusion.

The Wabassi Main intrusion is layered with an interpreted stratigraphic top to the southeast based on geochemistry and mineral chemistry.

Parental Magmas

The whole-rock major element, whole-rock trace element, and mineral chemical characteristics of the studied intrusions (Table 2) suggest that they are mantle-derived rather than crustally derived magmas. The $Mg\#_{80}$ and $Mg\#_{78}$ maximum Mg numbers of olivine and $Mg\#_{84}$ maximum Mg numbers of orthopyroxene in the Max and Wabassi Main intrusions suggest that they crystallized from basaltic rather than picritic or komatiitic parental magmas. The Big Mac, Fishtrap Lake, Highbank Lake, and Oxtoby Lake intrusions do not contain any relict igneous olivine but the composition of the whole rocks, orthopyroxene, clinopyroxene, and plagioclase suggests they are more evolved. This suggests that they are part of a larger magmatic system, the lower parts in which crystal fractionation occurred.

Sulphide and Oxide Saturation History

Platinum group element data are needed to better constrain the sulphide saturation history of the intrusions, but the higher Ni contents of olivine in peridotite of the Wabassi Main intrusion suggest that the parental magma did not segregate significant amounts of sulphide and was therefore fertile; the lower Ni contents of olivine in other lithologies of the Wabassi Main intrusion and in the Max intrusion suggest that those rocks formed from magmas that had segregated sulphides. The variations from undepleted to depleted suggest that this occurred at higher levels (perhaps locally) rather than at lower levels (which would have left all of the rocks depleted).

All of cumulate rocks in the Max and Wabassi Main intrusions are enriched in Cr relative to the non-cumulate rocks, suggesting that all of the magmas were sat-

urated in chromite (Fig. 3d). This is consistent with the relatively evolved inferred compositions of the parental magmas.

Form and Emplacement

The Big Mac intrusion appears to have the form of a subconcordant sill. The rocks in the northern part of the intrusion are more primitive and may represent a more vent-proximal facies, whereas the rocks in the southern part are more evolved and may represent a more distal facies.

The Fishtrap Lake and Highbank Lake intrusions are interpreted to be genetically related because of their geographic proximity and their petrographic, mineralogical, geochemical, and geochronological similarities. They represent the largest known mafic intrusive complex in the McFaulds Lake area, which we have called the Highbank-Fishtrap intrusive complex (HFIC).

The Max and Wabassi Main intrusions appear to be genetically related based on similarities in ultramafic cumulate textures, geochemical signatures, and silicate mineral compositions. However, the smaller Max intrusion contains primarily olivine-rich cumulate rocks and cumulate rocks have higher olivine contents, suggesting that it represents a magmatic conduit in which more olivine accumulated and less fractionation occurred. In contrast, the larger Wabassi Main intrusion contains a wider range of cumulate and non-cumulate rocks and the cumulate rocks contain less olivine, suggesting that it represents a magma chamber in which less olivine accumulated and more fractionation occurred.

Despite its proximity to the Max and Wabassi Main intrusions, the Oxtoby Lake intrusion is different in terms of petrography, whole-rock chemistry, mineral chemistry, and geochronology. Its homogeneous non-cumulate composition is consistent with a magmatic conduit that did not experience any olivine accumulation or fractional crystallization.

IMPLICATIONS FOR EXPLORATION

The intrusions studied in the eastern part of the Oxford-Stull and Uchi domains, with the exception perhaps of the Oxtoby Lake intrusion, exhibit some prospectivity to host Fe-Ti-V-(P), Cr-(PGE), and/or Ni-Cu-(PGE) mineralization.

The presence of semi-massive to massive oxide layers with high Fe-Ti-V-P contents within the Big Mac intrusion and the HFIC clearly demonstrates their potential to host those styles of mineralization, but it is not yet clear if these represent closed-system fractional crystallization products or whether the systems were open enough for long enough to contain large amounts of mineralization.

The potential for Cr-(PGE) mineralization in these intrusions is less clear. However, as noted above, the magmas that formed the Max and Wabassi Main intrusions were saturated in chromite, and the occurrence of chromite-rich boulders in the vicinity of the HFIC highlights the potential for this type of mineralization within their ultramafic parts.

The potential for Ni-Cu-(PGE) mineralization is uncertain. The Max intrusion contains some Ni-Cu-(PGE) mineralization and most likely represents an open and dynamic magmatic system that has interacted with the surrounding rocks (Sappin et al., 2013). However, the Oxtoby Lake intrusion appears to have been a closed system and the Wabassi Main intrusion also appears to have been relatively closed, so are much less prospective.

Work in progress will further evaluate the economic potential of these intrusions.

FORTHCOMING PRODUCTS

The preliminary results and interpretations presented in this contribution will be used in three upcoming referred journal publications. Each paper will focus on understanding the formation of one of these three magmatic systems — such as the Big Mac intrusion, the HFIC, and the Max, Oxtoby Lake, and Wabassi Main intrusions — and also to evaluate their potential for orthomagmatic mineralization.

ACKNOWLEDGEMENTS

We would like to thank Northern Shield Resources Inc. (C. Vaillancourt, I. Bliss, R.-L. Simard, and G. Budulan), MacDonald Mines Exploration Ltd. (Q. Yarie), and INV metals (R.C. Bell) for their assistance, permission to access diamond-drill cores, samples, drill logs, drill-core pictures, thin sections, and geoscience data sets. Thanks are also extended to Bronwyn Azar from the Ontario Geological Survey and to Hearst Air Service (A. Lemieux, M. Veilleux) for the support and the help during the field investigation in 2013. The authors thank M. Choquette (Université Laval) for providing essential support during our work with the electron microprobe. We are also grateful to V. Bécu (GSC) for reviews that helped us improve the final version of this contribution. This study is supported by the Ni-Cu-PGE-Cr Project under the Targeted Geoscience Initiative 4 (TGI-4) of the GSC. A.-A. Sappin acknowledged the support of the Visiting Fellowships in Canadian Government Laboratories Program from the Natural Sciences and Engineering Research Council of Canada (NSERC) and the GSC.

REFERENCES

Houlé, M.G. and Metsaranta, R.T., 2013. An update of the high-magnesium ultramafic to mafic systems subproject under the

Targeted Geoscience Initiative 4; Ontario Geological Survey, Open File Report 6290, p. 49.1–49.7.

Houlé, M.G., Lesher, C.M., and Metsaranta, R.T., 2012. Overview of the high-magnesium ultramafic to mafic systems subproject under the Targeted Geoscience Initiative 4: an Ontario perspective; Ontario Geological Survey, Open File Report 6280, p. 42.1–42.9.

Metsaranta, R.T. and Houlé, M.G., 2012. Progress on the McFaulds Lake ("Ring of Fire") region data compilation and bedrock geology mapping project; Ontario Geological Survey, Open File Report 6280, p. 43.1–43.12.

Sappin, A.-A., Houlé, M.G., Lesher, C.M., and McNicoll, V.J., 2013. Overview of the mafic and ultramafic intrusions in the eastern Uchi domain of the Superior Province, Northern Ontario; Ontario Geological Survey, Open File Report 6290, p. 51.1–51.16.

Stott, G.M., 2008. Superior Province: terranes, domains and autochthons; Northwestern Ontario Mines and Minerals Symposium, Sudbury, Canada, 2008.

Stott, G.M. and Josey, S.D., 2009. Regional geology and mineral deposits of northern Ontario, north of latitude 49º30′; Ontario Geological Survey, Miscellaneous Release – Data 265.

Stott, G.M., Corkery, M.T., Percival, J.A., Simard, M., and Goutier, J., 2010. A revised terrane subdivision of the Superior Province; Ontario Geological Survey, Open File Report 6260, p. 20.1–20.10.

Vaillancourt, C. and Bliss, I., 2010. Technical report - Exploration of the Wabassi, Wabassi North and Max mafic-ultramafic intrusions, Oxtoby Lake, Venton Lake, Sherlock Lake, Wowchuk Lake and Saarimaki Lake townships, Northern Ontario, Canada; Northern Shield Resources Ltd., 55 p.

Vaillancourt, C., Bliss, I., and Budulan, G., 2011. Technical report - Wabassi property, Northern Ontario, Canada. Drill programs 2010 & 2011, Discovery Harbour Option, 77 p.

GEOLOGICAL SURVEY OF CANADA
OPEN FILE 7856

Targeted Geoscience Initiative 4: Canadian Nickel-Copper-Platinum Group Elements-Chromium Ore Systems — Fertility, Pathfinders, New and Revised Models

Geochemistry and petrogenesis of the Black Thor intrusive complex and associated chromite mineralization, McFaulds Lake greenstone belt, Ontario

Heather J.E. Carson[1], C. Michael Lesher[1], and Michel G. Houlé[2]

[1]Laurentian University, Sudbury, Ontario
[2]Geological Survey of Canada, Québec, Quebec

2015

© Her Majesty the Queen in Right of Canada, as represented by the Minister of Natural Resources Canada, 2015

This publication is available for free download through GEOSCAN (http://geoscan.nrcan.gc.ca/)

Recommended citation

Carson, H.J.E., Lesher, C.M., and Houlé, M.G., 2015. Geochemistry and petrogenesis of the Black Thor intrusive complex and associated chromite mineralization, McFaulds Lake greenstone belt, Ontario, *In:* Targeted Geoscience Initiative 4: Canadian Nickel-Copper-Platinum Group Elements-Chromium Ore Systems — Fertility, Pathfinders, New and Revised Models, (ed.) D.E. Ames and M.G. Houlé; Geological Survey of Canada, Open File 7856, p. 87–102.

Publications in this series have not been edited; they are released as submitted by the author.

Contribution to the Geological Survey of Canada's Targeted Geoscience Initiative 4 (TGI-4) Program (2010–2015)

TABLE OF CONTENTS

Geochemistry and petrogenesis of the Black Thor intrusive complex and associated chromite mineralization, McFaulds Lake greenstone belt, Ontario

Heather J.E. Carson[1*], C. Michael Lesher[1], and Michel G. Houlé[2]

[1]Mineral Exploration Research Centre, Department of Earth Sciences, Goodman School of Mines, Laurentian University, 935 Ramsey Lake Road, Sudbury, Ontario P3E 2C6
[2]Geological Survey of Canada, 490 rue de la Couronne, Québec, Quebec G1K 9A9
*Corresponding author's e-mail: hcarson@laurentian.ca

ABSTRACT

The Black Thor intrusive complex (BTIC) contains a conduit-hosted, stratiform Cr-Ni-Cu-(PGE) deposit with a very large amount of chromite for an intrusion of its size. Most conduit-hosted stratiform deposits are Archean, formed from komatiitic magmas containing approximately 3000 ppm Cr_2O_3, and are typically saturated in chromite. The fundamental problem in understanding the genesis of the BTIC deposit and other deposits of this type is explaining how such large quantities of chromite crystalized from a magma that normally crystallizes only small amounts chromite and normally have a chromite:olivine abundance ratio of ~1:60. Current genetic models, such as in situ crystallization (by oxidation, pressure increase, magma mixing, and/or wholesale assimilation of felsic rocks or iron formation) or physical transportation of chromite slurries do not provide a wholly satisfactory explanation for the high abundance of chromite in this type of deposit. We are testing an alternative model: partial assimilation (as opposed to wholesale assimilation) of local oxide-silicate-facies iron formation by a Cr-rich magma. As low-Mg komatiite is saturated in chromite, the magma may dissolve the silicate component (quartz/chert and Fe-silicate minerals) of the iron formation, but would be unable to dissolve the oxide component (magnetite). Through interaction with the high-temperature (1400°C) Cr-rich magma, the fine-grained magnetite could be upgraded via diffusion to chromite during transportation within the conduit. This upgrading is similar to the upgrading of barren sulphide xenomelts that has been proposed for Ni-Cu-(PGE) deposits.

INTRODUCTION

The Black Thor intrusive complex (BTIC) is part of the Neoarchean "Ring of Fire" Intrusive Suite (RoFIS) located within the 2.7–2.8 Ga McFaulds Lake greenstone belt (MLGB) in the James Bay Lowlands of northern Ontario. The Black Thor chromite deposit, discovered in 2006, is one of the largest and best-preserved chromite deposits in the world. It contains ~102 Mt of chromite-mineralized material in a zone measuring up to 3 km in strike length and likely extends ~15 km to the Big Daddy, Black Creek, Black Horse, and Blackbird deposits. The bulk ore of the Black Thor deposit has an aggregate thickness of up to 100 m and an average grade of 31% Cr_2O_3 (Weston and Shinkle, 2013).

Previous work in the area includes a M.Sc. thesis on the nearby Blackbird chromite deposit (Azar, 2010), a paper on the Eagle's Nest Ni-Cu-(PGE) deposit (Mungall et al., 2010), and a Ph.D. thesis on the chemistry of chromite from the Black Thor, Black Label, and Big Daddy chromite deposits in the MLGB Black Thor chromitite layers (Laarman, 2014). However, the BTIC as a whole has not been studied in detail and is characterized only by airborne and ground geophysics and exploration-scale core logs (Tuchscherer et al., 2010). The main objective of this research is to establish the stratigraphy, geochemistry, and petrogenesis of the BTIC and associated chromium and nickel-copper-platinum group element (PGE) mineralization.

METHODOLOGY

Core logging and sampling were completed in May-June 2012 and June-July 2013 (Fig. 1). One hundred and twenty-three finely ground slabs from drillhole BT-11-196 were studied using a binocular microscope; 178 polished thin sections were studied in transmitted and reflected light using a compound petrographic microscope. Three hundred and twenty-four whole-rock samples were analyzed for major, minor, and trace elements by a combination of wavelength-dispersive X-ray fluorescence spectrometry, inductively coupled plasma (ICP) atomic emission spectrometry, and ICP

Carson, H.J.E., Lesher, C.M., and Houlé, M.G., 2015. Geochemistry and petrogenesis of the Black Thor intrusive complex and associated chromite mineralization, McFaulds Lake greenstone belt, Ontario *In:* Targeted Geoscience Initiative 4: Canadian Nickel-Copper-Platinum Group Elements-Chromium Ore Systems — Fertility, Pathfinders, New and Revised Models, (ed.) D.E. Ames and M.G. Houlé; Geological Survey of Canada, Open File 7856, p. 87–102.

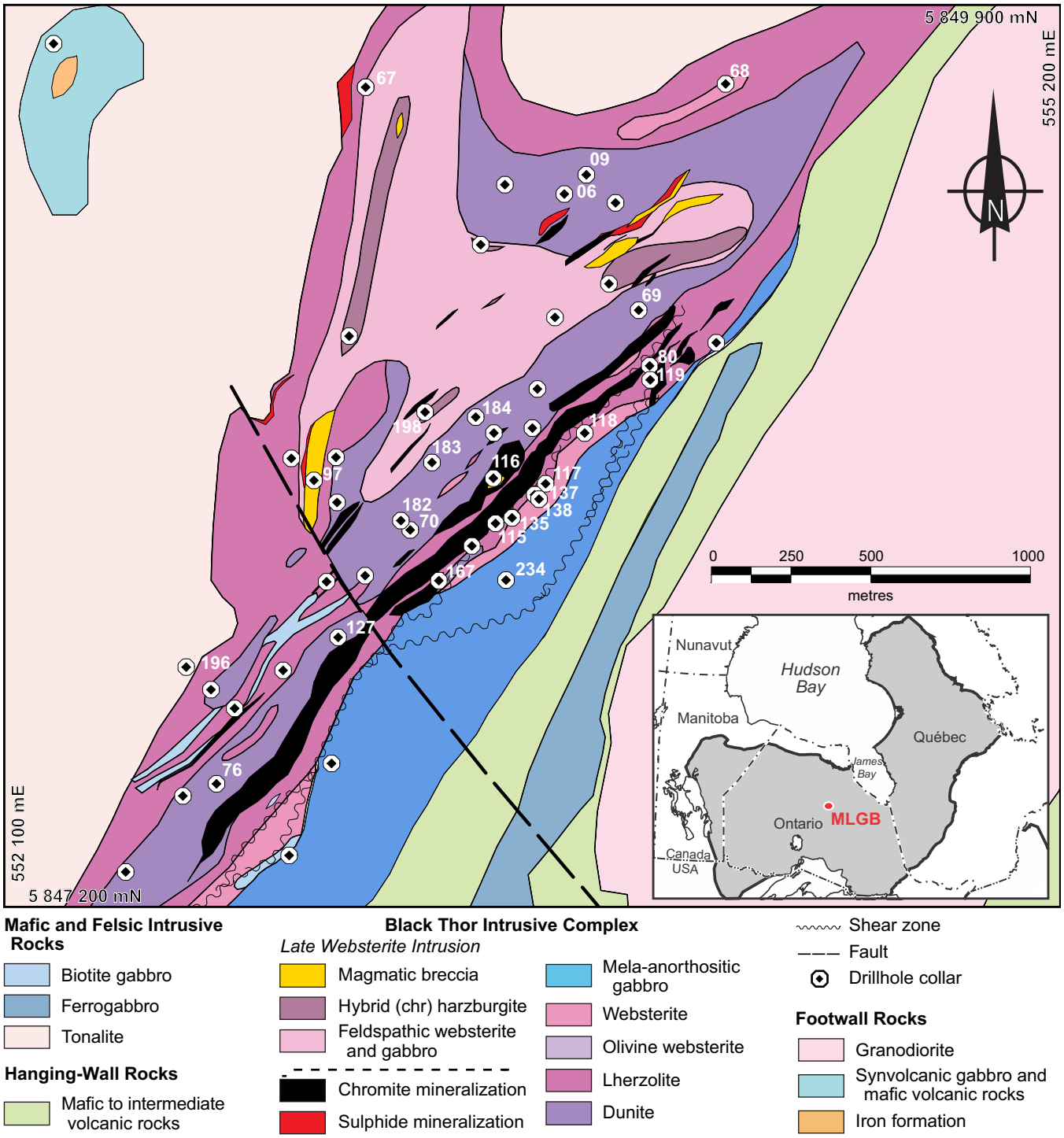

Figure 1. Geological map of the Black Thor intrusive complex showing the locations of diamond drillholes (DDH) that were logged and sampled in the course of this study (modified from Weston and Shinkle, 2013). Diamond drillhole identifications are given for those mentioned in the text. The first parts of the DDH identifications have been omitted for simplicity, DDH identifications: BT-08-06, 09; BT-09-67, 68, 69, 70, 76, 80; BT-10-115, 116, 117, 118, 119, 127, 135, 137, 138, 167; BT-11-182, 183, 184, 198, 196; and BT-12-234. MLGB: McFaulds Lake greenstone belt.

mass spectrometry. Chromite and associated melt inclusions and silicate minerals from 13 samples have been analyzed thus far by a combination of energy-dispersive X-ray emission spectrometry (XRES) using a scanning electron microscope, wavelength-dispersive XRES using an electron probe microanalyzer, and laser-ablation ICP-MS. Three-dimensional X-ray tomographic studies, O, S, Cr-Ni-Fe, Nd, Hf, and Os isotope analyses, and computer models of the miner-

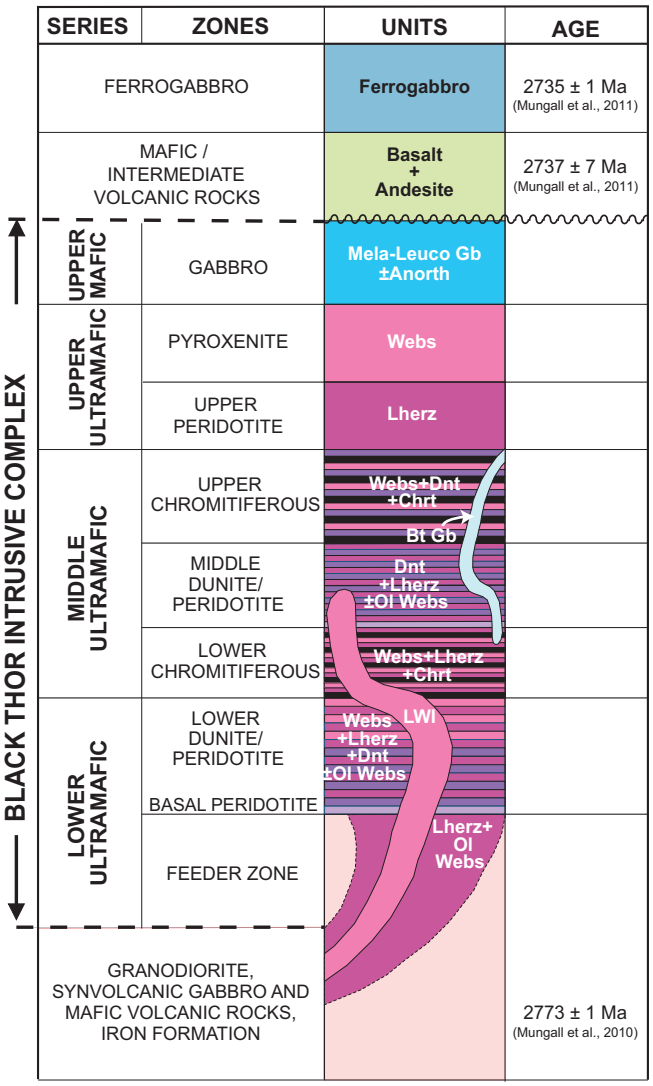

Figure 2. Schematic cross-section through the Black Thor intrusive complex (modified from Carson et al., 2013). Abbreviations: Anorth = anorthosite, Bt Gb = biotite gabbro, Chrt = chromitite, Dnt = dunite, Lherz = lherzolite, LWI = late websterite intrusion, Mela-Leuco Gb = mela- to leucogabbro, Ol Webs = olivine websterite, Webs = websterite.

alogical and geochemical data will be done later in 2015.

RESULTS

Geology of the Black Thor Intrusive Complex

The BTIC is a semi-conformable, funnel-shaped intrusion that has been structurally rotated into a subvertical orientation (Fig. 1). It is subdivided into four series (from stratigraphic base to top; Fig. 2): 1) a lower ultramafic series of interlayered dunite and lherzolite and minor olivine websterite (Fig. 3a–e); 2) a middle ultramafic series of interlayered dunite, lherzolite, and websterite with a thin lower chromitite zone (Black Label horizon; Fig. 4a–d) and a thick upper chromitite zone (Black Thor horizon; Fig. 4e–l); 3) an upper ultramafic

Table 1. Primary and hydrated mineralogy of the main rock type of the Black Thor intrusive complex.

Lithology	Igneous Mineralogy	Hydrated Mineralogy
Dunite	Ol-(Chr)	Atg/Lz-Mag-(Chl)-(Iow)-Tc
Lherzolite	Ol-Opx-(Chr)	Atg/Lz-Mag-Tr-Chl-Act-Tc
Chromitite	Chr-Ol	Atg/Lz-Mag-(Chl) -(Käm)-Tc
Ol Websterite	Opx-Ol-Chr	Act-MgHb-Käm±NiClc-Chl
Websterite	Opx-Cpx	Act-Chl-Tc
Melagabbro	Cpx-Plag	Act-Chl-(Czo)
Mesogabbro	Plag-Cpx	Ab-Chl-Czo-Act
Leucogabbro	Plag-Cpx-Ilm	Ab-Chl-Czo-Act-Ms-Ttn

Abbreviations: Ab = albite; Act = actinolite; Atg/Lz = antigorite/lizardite; Chl = chlorite; Chr = chromite; Cpx = clinopyroxene; Czo = clinozoisite; Ilm = ilmenite; Iow = iowite; Käm = kämmererite; Mag = magnetite; MgHb = magnesiohornblende; Ms = Muscovite; NiClc = Ni-clinochlore; Ol = olivine; Opx = orthopyroxene; Plag = plagioclase; Tc = Talc; Tr = tremolite; Ttn = titanite.

series composed of lherzolite, websterite, feldspathic websterite, and olivine websterite (Fig. 3f–h); and 4) a mafic series consisting of mela-, meso-, and leucogabbro with lesser anorthosite (Fig. 3i–l). It was originally not clear whether the upper mafic series was part of the BTIC, but gradational contacts with the underlying ultramafic rocks indicate that it is part of the intrusion. In places these rocks interfinger with (and are interpreted to intrude) overlying mafic volcanic rocks of the MLGB.

After accumulation and partial solidification of the BTIC, a late websterite intrusion (LWI) was emplaced into the lower and middle ultramafic series rocks and locally brecciated the Black Label chromitite horizon. The BTIC was later metamorphosed to lower-greenschist facies, but most of the rocks contain well preserved igneous textures, and relict igneous chromite, pyroxene, and olivine are variably preserved (Table 1). The term "meta" will be omitted for simplicity in this contribution.

Cr and Ni-Cu-(PGE) Mineralization

Chromite mineralization displays a range of textures that are distinguished based on chromite content: massive (>90%), semi-massive (90–75%), matrix (75–50%), net-textured (50–30%), heavily disseminated (30–10%), and lightly disseminated (<10%). Chromite is uniformly fine grained (0.1–0.2 mm) and forms networks between coarse-grained (<2 cm) altered pyroxene oikocrysts and between fine-grained (~5 mm) serpentinized olivine grains (Fig. 4). The Black Thor chromitite horizon (this study) and the undisrupted parts of the Black Label chromitite horizon (Mehrmanesh et al., 2013) contain thinly laminated to thickly bedded massive chromitite layers that alternate with partially continuous layers of serpentinized dunite. Brecciated parts of Black Label (Spath et al., 2015) contain angular to amoeboid clasts of chromitite,

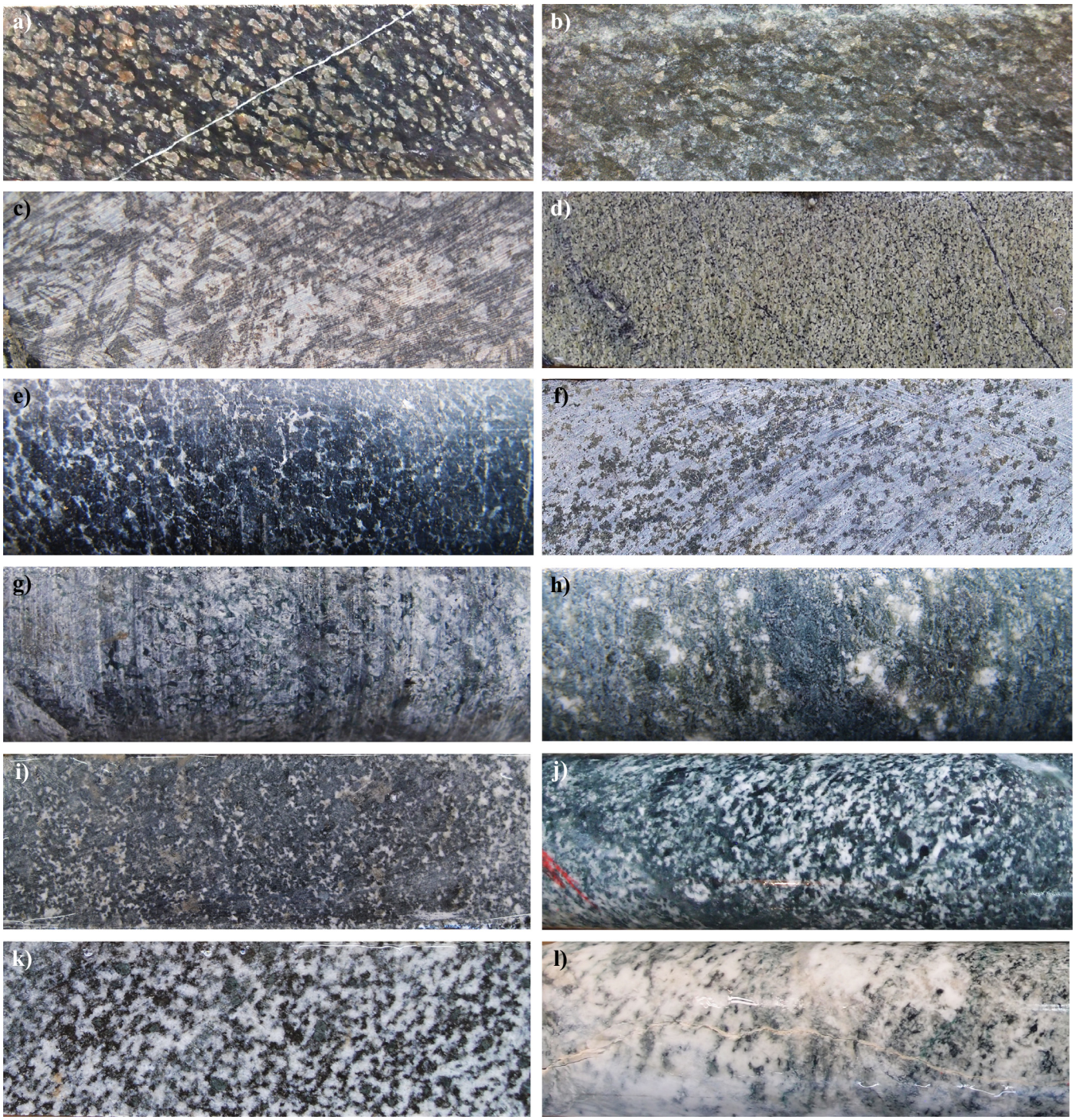

Figure 3. Photographs of drill cores showing typical rock types of the lower ultramafic series (a to e), the upper ultramafic series (f to h), and the mafic series (i to l) of the Black Thor intrusive complex. **a)** Basal peridotite (harzburgite); BT-09-70/37.70 m. **b)** Late pyroxenite; BT-11-198/42.00 m. **c)** Olivine spinifex-textured olivine, BT-09-97/136.09 m. **d)** Heavily serpentinized dunite; BT-09-70/98.11 m. **e)** Serpentinized peridotite, BT-11-196/180.10 m. **f)** Olivine pyroxenite; BT-10-115/83.85 m. **g)** Pyroxenite; BT-12-234/38.05 m. **h)** Feldspathic pyroxenite; BT-11-194/165.92 m. **i)** Melagabbro; BT-09-70/244.05 m. **j)** Mesogabbro; BT-12-234/211.33 m. **k)** Leucogabbro; BT-09-80/245.65 m. *l)* Anorthosite; BT-12-234/198.20 m. Younging direction in all photos is to the right. For the core shown in (d), (f), (i), (j), (k), and (l), the height (top to bottom) of the photo represents a core width of 4.7 cm; for all other photos, the height (top to bottom) of the photo represents a core width of 2.35 cm.

chromite-harzburgite, dunite, chromite, and olivine within a websterite matrix, forming a range of hybridized lithologies.

The Black Thor and Black Label chromitite horizons extend over a strike length of more than 3 km and 1.5 km, respectively. However, individual chromitite layers, particularly in Black Thor and the central parts of Black Label, are very difficult to follow along strike;

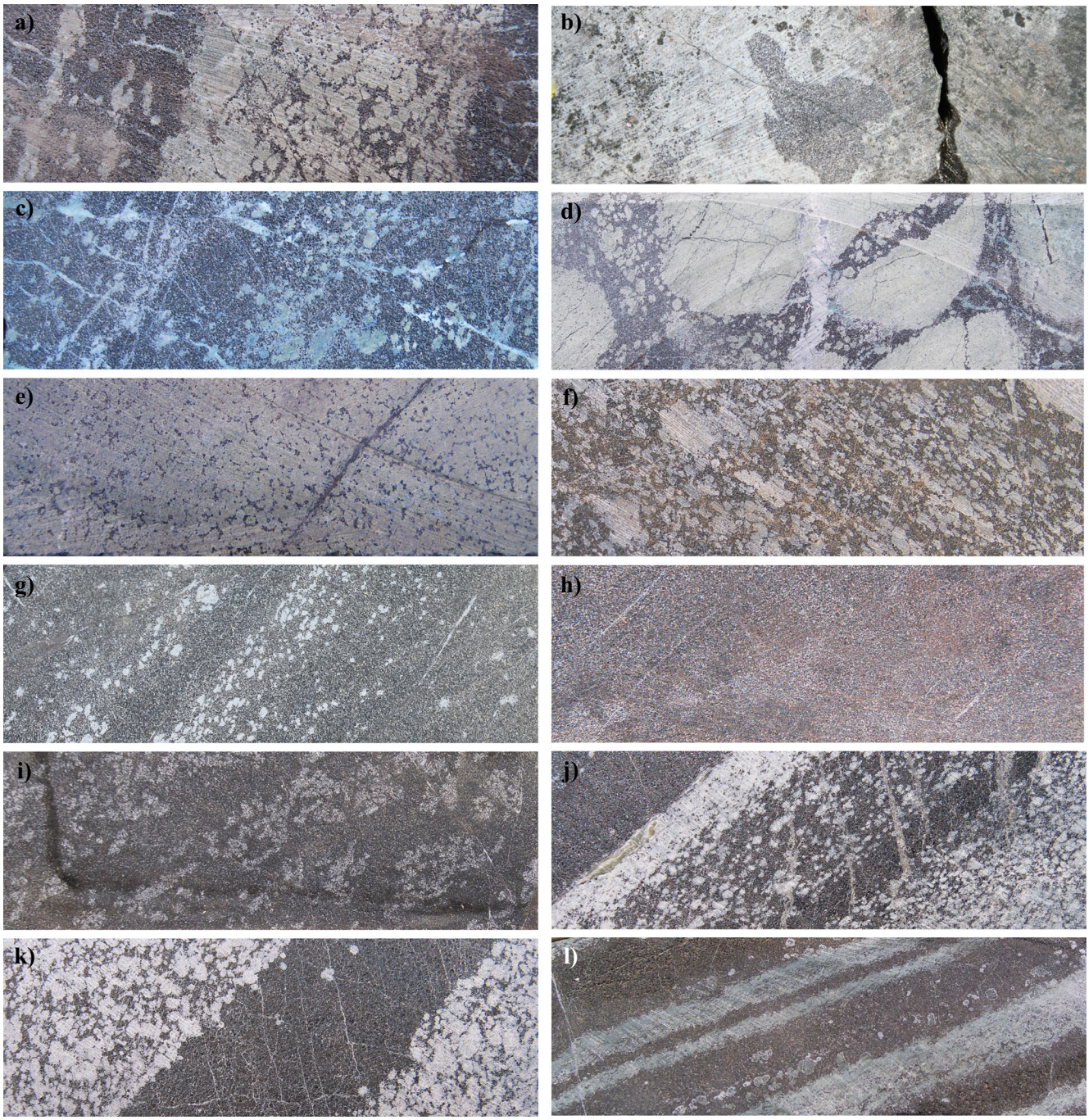

Figure 4. Photographs showing chromite textures of the Black Label chromitite horizon (a to d) and the Black Thor chromitite horizon (e to l) of the middle ultramafic series of the Black Thor intrusive complex. **a)** Massive chromitite layer with wavy, undulating upper contact against the matrix chromitite layer in serpentinized dunite, grading upwards into a massive chromitite layer; drill core BT-11-198/198.40 m. **b)** Blebby, co-mingling chromitite "clasts" hosted within late pyroxenite matrix; dril lcore BT-08-06/291.50 m. **c)** Semi-massive chromitite layer; drill core BT-11-198/195.07 m. **d)** Brecciated, matrix chromitite layer; drill core BT-11-198/199.00 m. **e)** Patchy net-textured chromitite, drill core BT-11-198/260.20 m. **f)** Matrix chromitite; drill core BT-11-196/548.74 m. **g)** Semi-massive chromitite; drill core BT-08-09/143.95 m. **h)** Massive chromitite; drill core BT-10-117/99.40 m. **i)** Mottled, semi-massive chromitite with "floating or suspended" serpentinized and/or pseudomorphed olivine grains; drill core BT-09-70/177.47 m. **j)** Massive chromitite layer with sharp upper contact against talc-tremolite-chlorite rock and serpentinized, pseudomorphed olivine, grading into semi-massive chromitite with a sharp upper contact against matrix chromitite layer; drill core BT-11-196/538.30 m. **k)** Matrix chromitite layer containing talc-tremolite-chlorite silicate minerals and serpentinized pseudomorphed olivine, with a sutured upper contact against a massive chromitite layer, in turn with a wavy, undulating upper contact against a matrix chromitite layer; drill core BT-11-196/559.30 m. **l)** Semi-massive chromitite layers alternating with continuous and semi-continuous serpentinized pseudomorphed olivine grain layers; drill core BT-10-113/172.17 m. Younging direction in all photographs is to the right. For the core shown in photographs (b), (d), (i), and (l), the height (top to bottom) of the photo represents a core width of 4.7 cm; for all other photographs, the height (top to bottom) of the photo represents a core width of 2.35 cm.

they are thicker and lenticular in the central part of the intrusion near and above the feeder zone and thinner and sheet-like away from the feeder zone. Pyroxene oikocrysts are more abundant in the central part of Black Thor horizon, where massive and semi-massive chromitite is common. Layers exhibiting normal modal grading (chromite-rich base and silicate-rich top) are more abundant in the lateral parts where matrix, net-textured, and disseminated chromitite is common. Layers containing intrafolial folds are only rarely observed.

Ni-Cu-(PGE) mineralization occurs dominantly in the lower ultramafic series of the BTIC. It includes multiple types and generations of mineralization (Farhangi et al., 2013): 1) early-magmatic mineralization along the basal contact of the intrusion; 2) intermediate-magmatic, sulphide-poor, PGE-rich, reef-style mineralization in the chromitite horizons; 3) intermediate-late-magmatic, sulphide-rich, PGE-poor, reef-style mineralization in fractionated gabbroic rocks of the mafic series; 4) late-magmatic, sulphide-rich mineralization associated with brecciation of the BTIC by the late websterite intrusion; and 5) tectonically/hydrothermally mobilized sulphide-rich mineralization within shear zones in the transition zone between the upper ultramafic and mafic series.

Whole-rock Geochemistry

The major element geochemical results reported here were obtained from drill core BT-11-196, which cuts through a part of the intrusion undisturbed by the LWI, and additional drill cores from the feeder zone (BT-09-67, BT-09-68, BT-09-69, BT-09-76, BT-10-115, BT-10-116, BT-10-117, BT-10-118, BT-10-119, BT-10-127, BT-10-135, BT-10-137, BT-10-138, BT-10-167, BT-1-182, BT-11-183, BT-11-184); these results are compared with the Cliffs XRF assay results of the entire deposit (Fig. 5). Three major trends are evident in MgO variation diagrams:

1. Mixing trends between olivine (~40% SiO_2, 45% MgO, and 8% FeO_t, with minor to negligible abundances of other elements — based on mineral analyzes and stoichiometry) and chromite (10–45% Cr_2O_3, 8% Al_2O_3, ~15% FeO_t, and 20–30% MgO, with minor to negligible abundances of other elements).
2. Mixing trends between olivine and orthopyroxene (~52% SiO_2, 3% Al_2O_3, ~10% FeO_t, ~30% MgO, and <5% CaO, with minor to negligible abundances of other elements).
3. Fractionation trends from the inferred parental magma (~46% SiO_2, ~9% Al_2O_3%, ~11% FeO_t, ~22% MgO, and ~8% CaO, with minor to negligible abundances of other elements — based on observed mineral assemblages and consistent with that proposed for Blackbird by Mungall et al., 2010) toward the leuco-, meso-, and melanogabbro in the upper part of the BTIC.

The majority of low-Cr samples on the loss-on-ignition (LOI) versus MgO diagram plot between hydrated websterite (30–35% MgO and 5–20% LOI) and serpentinized lherzolite/dunite ± chromitite (up to 25% LOI). The majority of high-Cr samples plot at lower MgO and/or higher LOI, reflecting higher degrees of carbonatization of the silicate components in chromitite. The cluster at low MgO and LOI represents least-altered mafic rocks of the upper series, whereas the cluster at 25–30% MgO and low LOI represents late websterite samples, which are the least altered rocks within the BTIC.

Low-Cr late websterite samples have low Ca and Al contents, indicating that they are composed primarily of orthopyroxene with only minor clinopyroxene or plagioclase (see Spath et al., 2015). High-Cr late websterite samples contain xenolithic and xenocrystic chromite incorporated from Black Label during emplacement.

The increase in Cr with decreasing Mg (Fig. 5) reflects accumulation of chromite with a chromite: olivine ratio well above the cotectic proportion of ~1:60 (e.g. Lesher and Stone, 1996; Barnes and Roeder, 2001); only a few samples lie on the cotectic (Fig. 6). This means that superimposed on the very small background abundance defined by the cotectic, chromite has been added through either (1) supersaturation (i.e. consistently precipitating extra chromite beyond the amount defined by the cotectic), (2) modifying the location of the cotectic (i.e. consistently precipitating more chromite with olivine than under normal conditions), or (3) mechanical accumulation of chromite in addition to that crystallized with olivine.

Chemostratigraphy

Lithogeochemistry has been plotted against depth and correlated with digitized stratigraphic logs to give an indication of the geochemical changes through the complex (Fig. 7). The overall trend within the ultramafic portion of the BTIC is one of decreasing Si-Fe-Mg and increasing Cr-Al-Ti-V. However, superimposed on this overall trend are (1) at the base of the complex, a reversal from Mg-poor olivine websterite to Mg-rich dunite that is interpreted to reflect more rapid cooling along the lower contact, which resulted in lower rates of accumulation of olivine at the base of the body; (2) many small reversals in the overall trend associated with chromite horizons and interlayering of dunite, lherzolite, and websterite; and (3) an abrupt decrease in Cr-Fe-Al-(Ti)-V and increase in Si-(Na-K) above the Black Thor chromite horizon, reflecting the upper mafic portion of the BTIC. Based on petro-

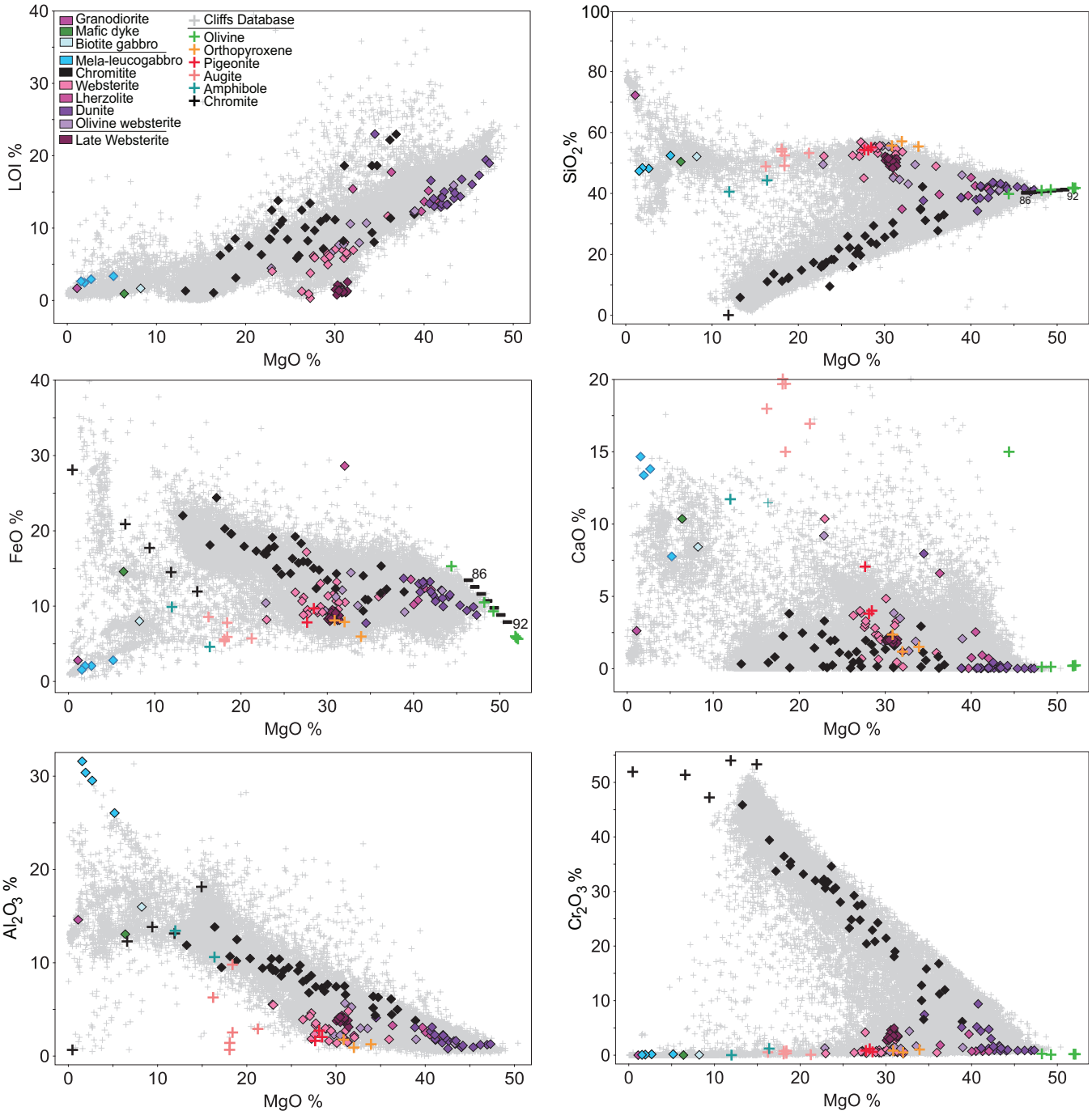

Figure 5. Major oxide versus MgO variation diagrams for samples from drillhole BT-11-196 (solid symbols). Also shown are compositions from a suite of samples from Cliffs Natural Resources database (pale grey crosses) and mineral compositions from Arndt et al. (2008; compiled from various sources, crossed symbols). In the MgO-SiO_2 and FeO-SiO_2 diagrams, 86 and 92 are mole percent forsterite contents in olivine, shown for reference. Abbreviations: FeO = total iron, LOI = loss on ignition.

graphic observations, this is interpreted to reflect a decreasing abundance of olivine and an increasing abundance of chromite with increasing stratigraphic height.

Trace Element Geochemistry

Most rock types exhibit negative Nb-Ta and variable Sr anomalies relative to Th, La, and LREEs, which is interpreted to represent addition of an upper continental crust component. U is enriched in some dunite and websterite samples, which is interpreted to reflect U mobility in metamorphic fluids. Positive Sr anomalies in chromite- and plagioclase-rich samples presumably reflect mobility of Sr and accumulation of plagioclase, respectively. Positive Ti anomalies in Cr-rich samples reflect enrichment in Ti in the minor ulvöspinel com-

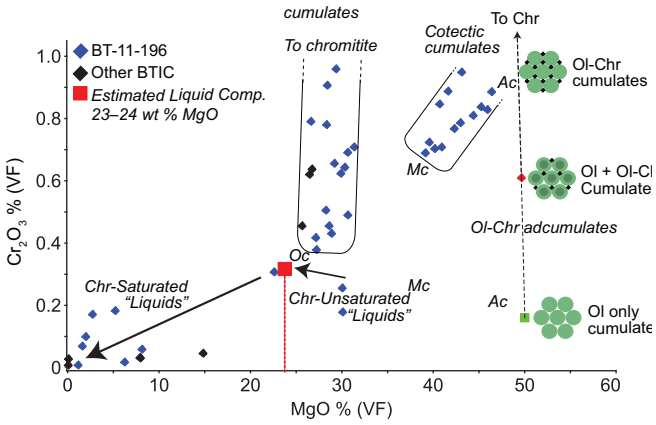

Figure 6. Mg-Cr diagram (note scale at 1% Cr_2O_3) highlighting samples that lie on the olivine:chromite cotectic (cotectic cumulates) and those that do not (non-cotectic cumulates), suggesting chromite has been added through supersaturation, modification of the cotectic, or mechanical accumulation (see text). Dashed line is the proportion of olivine:chromite from 100% olivine (green), 99:1 olivine:chromite (red square) along a mixing line to 100% chromite (not shown). No samples fall within the field for adcumulate at 100% olivine, indicating the liquid was already saturated in chromite during crystallization. Abbreviations: Ac = adcumulate, Chr = chromite; Mc = mesocumulate, Oc = orthocumulate textures; Ol = olivine.

ponent of chromite. Variable MREE/HREE ratios are interpreted to represent variable degrees of accumulation of olivine and orthopyroxene (Fig. 8).

Websterite (Fig. 8) also exhibits negative Nb-Ta anomalies relative to Th, La, and LREEs, but has negative Sr anomalies in Cr-poor samples and positive Sr and Ti anomalies in Cr-rich samples. Late websterite has systematically lower REE abundances and displays flatter MREE-HREE patterns, whereas BTIC websterite has systematically higher REE abundances, is more enriched in HILE-LREE relative to MILE, and displays steeper MREE-HREE patterns.

Gabbroic rocks exhibit the same negative Nb-Ta anomalies relative to Th, La, and LREEs, but exhibit large positive Sr and (for 2 of 3 samples) Eu anomalies, reflecting accumulation of plagioclase. The similarities of the trace element patterns of the mafic rocks with the ultramafic rocks provide further evidence to support the interpretation that they are co-magmatic.

Chromite Petrography and Chemistry

The BTIC chromite can be homogenous, or contain large (0.5–2 mm) spherical inclusions or abundant fine inclusions. Preliminary ED-XRES analyses of the coarse and fine inclusions indicate that they are composed of a serpentine-amphibole-chlorite-carbonate assemblage that, based on their similarity to the mineralogy of the interstitial liquid, likely represent melt inclusions that have been altered during serpentinization.

LA-ICP-MS maps (not shown) indicate that (1) homogenous chromite displays little or no chemical variation, however some grains show outward increases in Ti-V and decreases in Al-Cr, which is interpreted to represent re-equilibration with trapped silicate melt; (2) zoned chromite displays outer rims enriched in Mn-Fe-Co-Ni-Zn, which are interpreted to be associated with metamorphic overgrowth and mag-

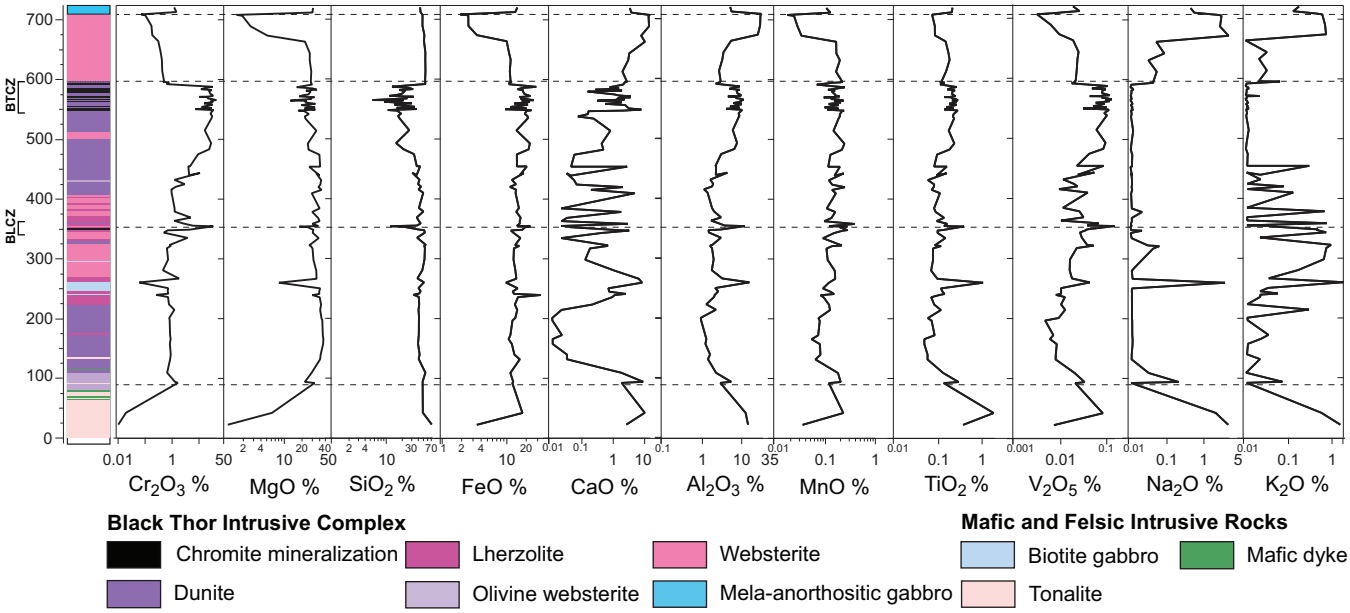

Figure 7. Whole-rock analytical results are plotted against depth in drillhole BT-11-196 and correlated with the stratigraphic log to illustrate the geochemical changes through the intrusive complex. The overall trend in the Black Thor intrusive complex (i.e. except for a basal reversal and small-scale variations) is one of decreasing Mg-Si with increasing Cr-Fe-Mn-Al-Ti-V. Abbreviations: BLCZ = Black Label (lower) chromitiferous zone; BTCZ = Black Thor (upper) chromitiferous zone.

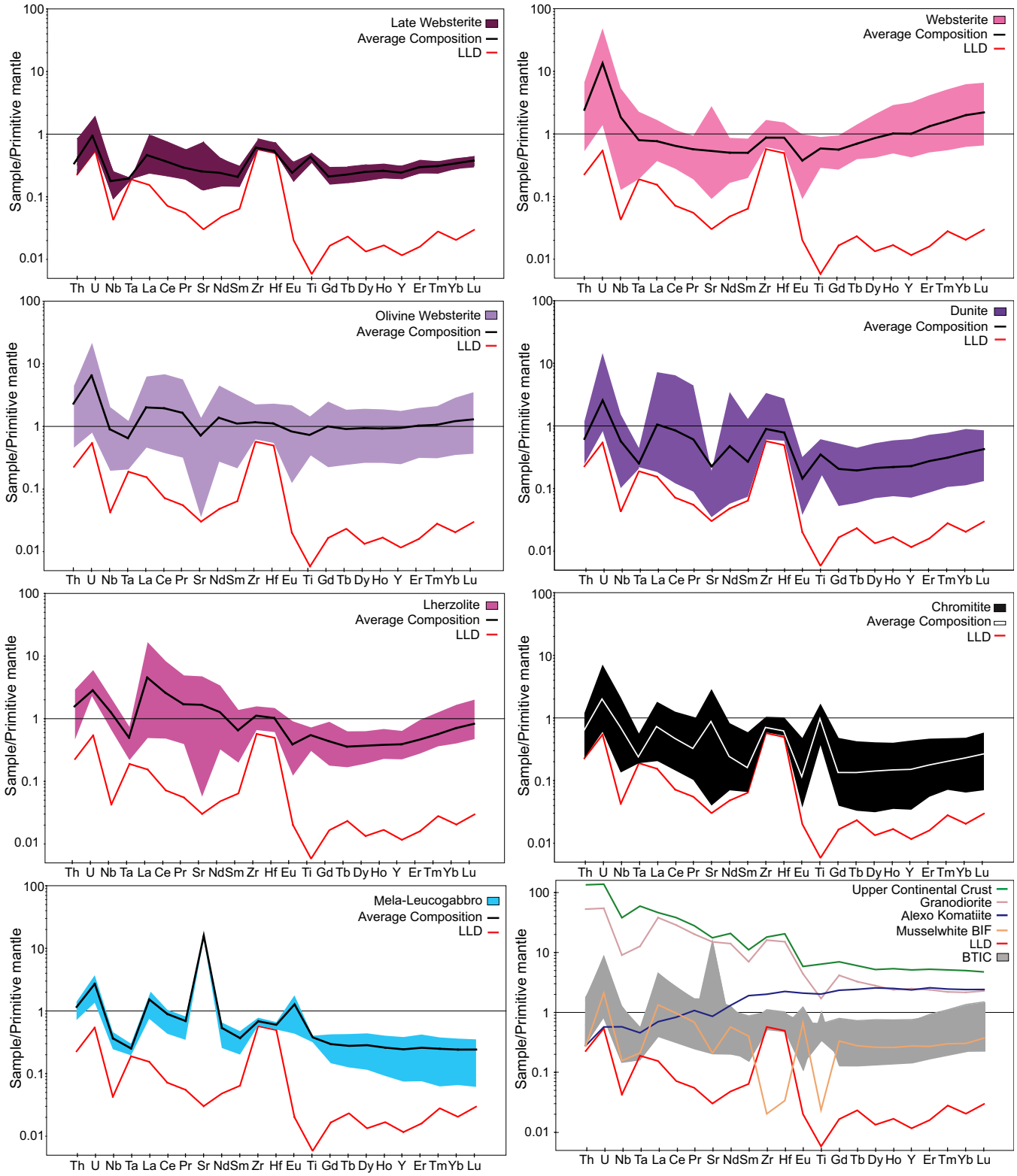

Figure 8. Rare earth element and trace element geochemistry from drillhole BT-11-196 and from reference data: Upper continental crust (Taylor and McLennan, 1985), Alexo komatiite (KAX-1 geochemical analysis by GeoLabs, Sudbury, ON), and Musselwhite banded iron formation (Gourcerol et al., 2013). Primitive mantle normalizing values are from McDonough and Sun (1995). Abbreviations: BIF = banded iron formation; BTIC = Black Thor intrusive complex; LLD = lower limit of detection.

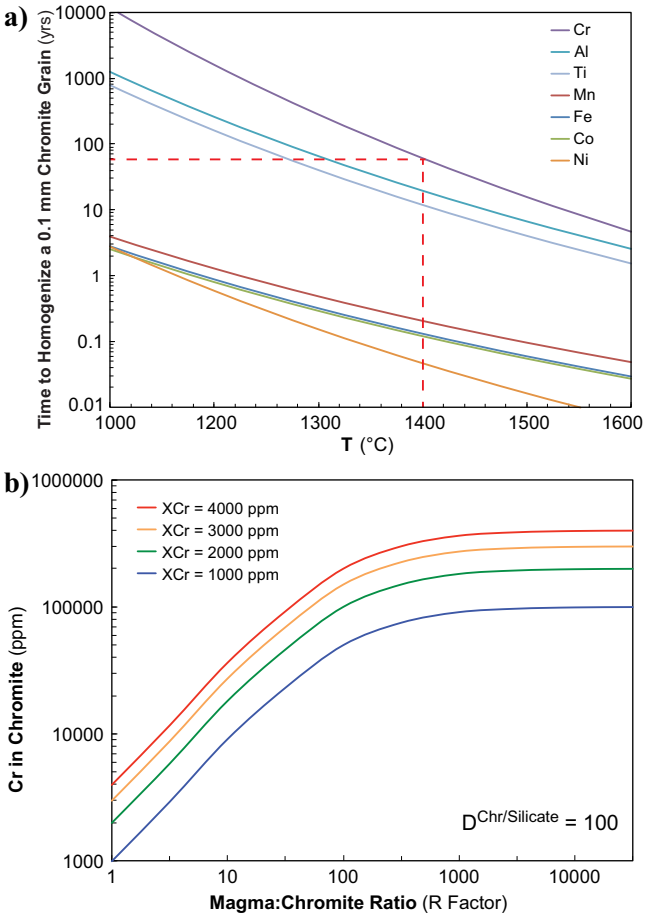

Figure 9. Magnetite diffusion and mass balance models. **a)** At 1400°C it would take approximately 50 years for Cr to diffuse through a 0.1 mm magnetite grain and transform it to chromite (diffusion constants from Dieckmann and Schmalzried, 1977; Dieckmann et al., 1978; Aggarwal and Dieckmann, 2002). **b)** Mass balance calculations estimate a komatiitic magma at ~3000 ppm Cr with chromite/magma partition coefficients of 100–200 for Cr, indicate a minimum magma:chromite ratio (R Factor) of 200 will upgrade magnetite to chromite.

netite alteration; and (3) inclusions in chromite layers are composed of serpentine ± chlorite ± amphibole ± calcite, which are interpreted to be serpentinized melt inclusions.

GENETIC MODEL

The fundamental problem in the understanding of the genesis of the BTIC is in inability to explain how such large quantities of chromite could accumulate from a magma that would normally crystallize chromite in only accessory abundances.

Most stratiform chromite deposits are hosted by large layered complexes that are interpreted to represent periodically replenished magma chambers (e.g. Bushveld Complex, South Africa; Stillwater Complex, USA). Genetic models for these deposits include (1) in situ crystallization associated with oxidation (Ulmer, 1969) or pressure increase (Lipin, 1993); (2) contamination and wholesale assimilation of felsic rocks or iron formation (Irvine, 1975; Rollinson, 1997); (3) magma mixing (e.g. Irvine, 1977; Campbell and Murck, 1993); and (4) physical transportation of fine-grained chromite in magmatic slurries (e.g. Eales, 2000; Mondal and Mathez, 2007; Maier et al., 2013). However, the Black Thor and Black Label chromitite deposits as well as several others (e.g. Kemi, Finland; Inyala and Railway Block, Zimbabwe; Ipueira-Medrado, Brazil; Sukinda, India; Nkomati, South Africa) are hosted by smaller intrusions that are interpreted to represents flow-through feeder sills and magma conduits that are stratiform in structure but lenticular in shape.

The much higher abundances of chromite in the latter deposits are not easily explained by the above processes, which has stimulated the development of a new model that involves partial melting of oxide-silicate-facies iron formation (OXIF) of the type observed in the footwall rocks (Fig. 1). Complete melting of OXIF is excluded due to the absence of Fe enrichment in the host rocks (Azar, 2010; Mungall et al., 2010). In the new model, silicate components (chert/quartz and Fe-silicate minerals) are melted and incorporated into the magma, accounting for the anomalous abundance of orthopyroxene in systems that should crystallize only very small amounts of orthopyroxene. However, magnetite cannot melt, because low-Mg komatiitic magmas, like the one in the BTIC, are saturated in chromite and therefore cannot incorporate any additional oxide. Very fine-grained disaggregated xenocrystic magnetite could be upgraded to chromite during transport, in the same way that barren sulphide xenomelts are interpreted to have been upgraded to form Ni-Cu-(PGE) deposits via interaction with komatiitic magma (see Lesher and Campbell, 1993).

Cr is one of the slower elements to diffuse in magnetite (Fig. 9a). Preliminary calculations indicate that at 1400°C (assuming komatiitic basalt magma composition) it would take approximately only 50 years to homogenize a 0.1 mm diameter magnetite grain and transform it into chromite. Considering that this is a dynamic flow-through system and that large mafic magmatic systems are typically active for 1–5 million years (e.g. continental flood basalt provinces and other large igneous provinces), this is more than enough time to completely re-equilibrate xenocrystic magnetite, especially if it started out as very fine grains. Mass balance calculations, using 2500–3500 ppm Cr in the magma and chromite/magma partition coefficients for Cr of 100–200, indicate that a magma:chromite ratio (R factor) as low as 200 is enough to transform magnetite into chromite (Fig. 9b). This range of R is well within the range estimated for many komatiite-associated Ni-

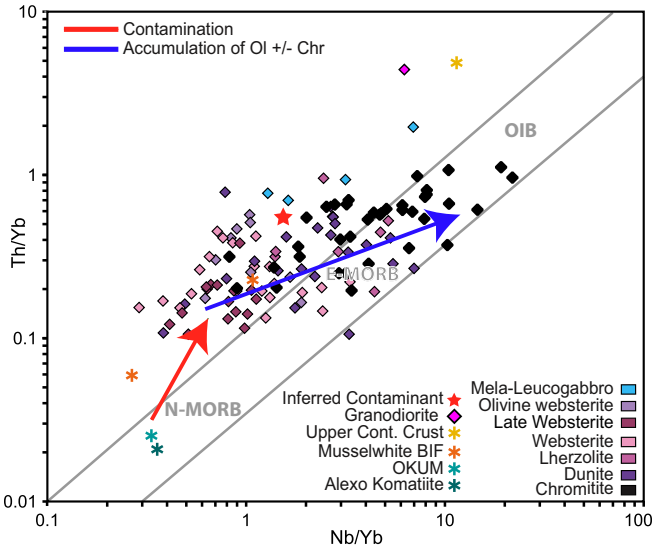

Figure 10. Nb-Th proxy diagram (designed for oceanic basalts but valid for olivine-pyroxene cumulates, assuming that Th-Nb-Yb are housed in the interstitial liquids rather than the cumulus minerals) highlighting the contamination evolution of Black Thor intrusion complex rocks, from an N-MORB source (KAX-1 Alexo komatiite and OKUM komatiite reference material from the GeoLabs, Sudbury, Ontario) towards an inferred contaminant (star, indicated by red line) based on mixing average upper continental crust (Taylor and McLennan, 1985) and granodiorite from the Black Thor intrusive complex (1330501, drill core BT-11-196/22.50 m) with oxide-facies iron formation (Musselwhite banded iron formation (BIF); Gourcerol et al., 2015), resulting in a higher Th/Yb ratio. Accumulation of olivine and chromite is highlighted by a large spread in the Nb/Yb ratio (indicated by the blue line). Abbreviations: Chr = chromite; Ol = olivine.

Cu-(PGE) systems (e.g. Kambalda, Perseverance, Raglan: Lesher and Keays, 2002).

The trace element geochemical data exhibit considerable scatter because of the very low abundances (near the detection limits) of such elements in olivine ± chromite ± pyroxene cumulates, but they suggest contamination by rocks of the upper continental crust. Iron formations contain low abundances of trace elements (Figs. 7. 9), indicating that although considerable amounts of iron formation could be present as a contaminant, it cannot be the source of the pronounced HILE enrichment relative to MILE and HREE. Rocks of the upper continental crust, such as the footwall tonalite-granodiorite, are sufficiently enriched in HILE (relative to MILE-HREE) to be the source of the pronounced enrichment in BTIC rocks, but they are too enriched in Th relative to Yb and too enriched in Nb relative to Yb to produce the geochemical signatures of the olivine – chromite-poor samples. So, a combination of contaminants is required. The presence of these signatures in all of the rocks suggests contamination at depth, not in the BTIC itself.

Partial assimilation of OXIF and the upgrading of magnetite to chromite, in conjunction with contamination by rocks of the upper continental crust, could be key to the formation of the BTIC mineralization (and other conduit-hosted stratiform deposits). In order for this mechanism to be feasible (Fig. 10), the following are required: (1) a Cr-rich komatiitic magma, (2) the presence of sufficient oxide-facies iron formation near or below the stratigraphic level of the intrusion, and (3) a flow-through magmatic system with sufficient flux to transport fine magnetite grains and allow them to interact with the Cr-rich magma. Additional work is planned to further evaluate this process.

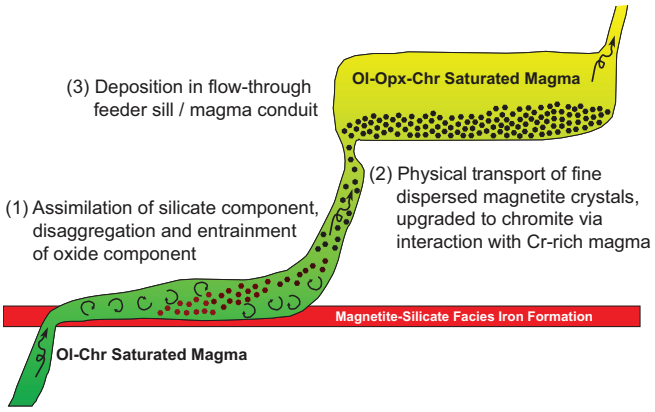

Figure 11. Preliminary schematic model of the partial-assimilation and magnetite-upgrading process proposed in this study. (1) Magma saturated in olivine and chromite is intruded into magnetite-bearing oxide-silicate-facies iron formation, partially assimilating it by dissolving the silicate component (chert, quartz, and Fe-silicate minerals) but not the oxide component; (2) fine-grained magnetite grains are disaggregated and transported within the magma conduit, where they interact with the Cr-rich magma and, via diffusion, are enriched in Cr and upgraded to chromite; (3) lastly, the chromite is deposited in the feeder sill / magma conduit. Abbreviations: Chr = chromite; Ol = olivine; Opx = orthopyroxene.

IMPLICATIONS FOR EXPLORATION

The new genetic model proposed in this study has many important implications that could help target mineral exploration for this type of chromite deposit.

- Exploration should focus on areas where high-Cr, low-Mg komatiitic magma is present. Higher Mg komatiitic magma may be less prospective, as they are not saturated in chromite. Some prospective magma is Archean but many are early Proterozoic.
- Exploration should focus on areas where oxide-facies (rather than sulphide-facies) iron formation is present.
- Exploration should focus on areas where olivine ± orthopyroxene cumulates are present (rather than olivine-only cumulates).

This study highlights the proposition that small, Archean, ultramafic-dominated intrusions like the

BTIC can not only host large chromite deposits but also contain significant Ni-Cu-(PGE) mineralization.

ACKNOWLEDGEMENTS

We would like to thank R. Metsaranta and B. Azar (Ontario Geological Survey), and R. Weston, D. Shinkle, and Bryan Maciag (Cliffs Natural Resources Inc.) for their help and insightful discussions. We are very grateful to R. Fink and A. Mitchell (Cliffs Natural Resources Inc.) for logistical support and access to the property and geological databases, and to the team in Esker Camp for their assistance during the 2012 and 2013 field seasons. Financial support is being provided by the NSERC-CRD, NSERC Discovery, and Geological Survey of Canada TGI-4 programs, the Ontario Geological Survey, and the Society of Economic Geologists Student Research Grant program. Joe Petrus (LU), Dave Crabtree, and Sandra Clarke (GeoLabs) provided assistance in LA-ICP-MS analysis and EMPA/SEM/XRD analysis, respectively. We are also grateful to T. Clark (MERNQ) for many helpful editorial suggestions that significantly improved this contribution.

REFERENCES

Aggarwal, S. and Dieckmann, R., 2002. Point defects and cation tracer diffusion in $(Ti_xFe_{1-x})_{3-\delta}O_4$. II. Cation tracer diffusion; Physics and Chemistry of Minerals, v. 29, p. 707–718.

Arndt, N., Lesher, C.M., and Barnes, S.J., 2008. Komatiite, 1st edition; Cambridge University Press, Cambridge, United Kingdom, 467 p.

Azar, B., 2010. The Blackbird chromite deposit, James Bay Lowlands of Ontario, Canada: Implications for chromitite genesis in ultramafic conduits and open magmatic systems; M.Sc. thesis, University of Toronto, Toronto, Ontario, 154 p.

Barnes, S.J. and Roeder, P.L., 2001. The range of spinel compositions in terrestrial mafic and ultramafic rocks; Journal of Petrology, v. 42, p. 2279–2302.

Campbell, I.H. and Murck, B.W., 1993. Petrology of the G and H chromitite zones in the Mountain View area of the Stillwater complex, Montana; Journal of Petrology, v. 34, p. 291–316.

Carson, H.J.E., Lesher, C.M., Houlé, M.G., Weston, R.J., Metsaranta, R.T., and Shinkle, D.A. 2013. Komatiite-associated Cr and Ni-Cu-(PGE) mineralization in the Black Thor–Black Label ultramafic intrusive complex, McFaulds Lake greenstone belt, *In:* Proceedings; 12th Biennial SGA Meeting, Uppsala, Sweden, August 12-15, 2013, p. 960–963.

Dieckmann, R. and Schmalzried, H., 1977. Defects and cation diffusion in magnetite; Reports of the Bunsen Society for Physical Chemistry, v. 81, p. 344–347.

Dieckmann, R., Mason., T.O., Hodge, J.D., and Schmalzried, H., 1978. Defects and cation diffusion in magnetite (III.) Tracer diffusion of foreign tracer cations as a function of temperature and oxygen potential; Reports of the Bunsen Society for Physical Chemistry, v. 82, p. 778–783.

Eales, H.V., 2000. Implications of the Cr budget of the western limb of the Bushveld Complex; South Africa Journal Geology, v. 103, p. 141–150

Farhangi, N., Lesher, C.M., and Houlé, M.G., 2013. Mineralogy, Geochemistry and Petrogenesis of Nickel-Copper-Platinum Group Element Mineralization in the Black Thor Intrusive Complex, McFaulds Lake Greenstone Belt, Ontario, *In:* Summary of Field Work and Other Activities 2013; Ontario Geological Survey, Open File Report 6290, p. 55-1 to 55-7.

Gourcerol, B., Thurston, P.C., Kontak, D.J., Côté-Mantha, O., and Biczok, J., 2015. Distinguishing primary and mineralization-related signatures of chert from the banded iron-formation-hosted gold deposits at Musselwhite, Ontario and Meadowbank, Nunavut; Geological Survey of Canada, Current Research 2015-1, 21 p.

Irvine, T.N., 1975. Crystallization sequences in the Muskox Intrusion and other layered intrusions II. Origin of chromite layers and similar deposits of other magmatic ores; Geochimica et Cosmochimica Acta, v. 39, p. 991–1020.

Irvine, T.N., 1977. Origin of the chromite layers in the Muskox Intrusion and other stratiform intrusions: A new interpretation; Geology, v. 5, p. 273–277.

Laarman, J.E., 2014. A detailed metallogenic study of the McFaulds Lake chromite deposits, northern Ontario; Ph.D. thesis, University of Western Ontario, London, Ontario, 529 p.

Lesher, C.M. and Campbell, I.H., 1993. Geochemical and fluid dynamic modeling of compositional variations in Archean komatiite-hosted nickel sulfide ores in Western Australia; Economic Geology, v. 88, p. 804–816.

Lesher, C.M. and Keays, R.R., 2002. Komatiite-associated Ni-Cu-(PGE) deposits: mineralogy, geochemistry, and genesis, *In:* The Geology, Geochemistry, Mineralogy, and Mineral Beneficiation of the Platinum-Group Elements, (ed.) L.J. Cabri; Canadian Institute of Mining, Metallurgy and Petroleum, Special Volume 54, p. 579–617.

Lesher, C.M. and Stone, W.E., 1996. Exploration geochemistry of komatiites, *In:* Igneous Trace Element Geochemistry: Applications for Massive Sulphide Exploration; Geological Association of Canada, Short Course, v. 12, p. 153–204.

Lipin, B.R., 1993. Pressure increases, the formation of chromite seams, and the development of the Ultramafic Series in the Stillwater Complex, Montana; Journal of Petrology, v. 34, p. 955–976.

Maier, W.D., Barnes, S.-J., and Groves, D.I., 2013. Bushveld formation of Pt-Pd, Cr, V-rich layers via hydrodynamic sorting of mobilised cumulate slurry in a large, relatively slowly cooling, subsiding magma chamber; Mineralium Deposita, v. 48, p. 1–56.

McDonough, W.F. and Sun, S.-S., 1995. Composition of the Earth; Chemical Geology, v. 120, p. 223–253. doi:10.1016/0009-2541(94)00140-4

Mehrmanesh, K., Carson, H.J.E., Lesher, C.M., and Houlé, M.G., 2013. Stratigraphy, geochemistry and petrogenesis of the Black Label chromitite horizon, Black Thor Intrusive Complex, McFaulds Lake Greenstone Belt, Ontario, *In:* Summary of Field Work and Other Activities 2013; Ontario Geological Survey, Open File Report 6290, p. 53-1 to 53-6.

Mondal, S.K. and Mathez, E.A., 2007. Origin of the UG2 chromitite layer, Bushveld Complex; Journal of Petrology, v. 48, p. 495–510.

Mungall, J.E., Harvey, J.D., Balch, S.J., Azar, B., Atkinson, J., and Hamilton, M.A., 2010. Eagle's Nest: A magmatic Ni-sulfide deposit in the James Bay Lowlands, Ontario, Canada, *In:* The Challenge of Finding New Mineral Resources: Global Metallogeny, Innovative Exploration, and New Discoveries, Volume I: Gold, Silver, and Copper-Molybdenum, (ed.) R.J. Goldfarb, E.E. Marsh, and T. Monecke; Society of Economic Geologists, Special Publication 15, p. 539–559.

Mungall, J.E., Azar, B., and Hamilton, M., 2011. Ni-Cu-PGE-Cr-Fe-Ti-V and VMS mineralization of the Ring of Fire intrusive suite, Ontario, *In:* Program with Abstracts; Geological Association of Canada-Mineralogical Association of Canada-Society of Economic Geologists-Society for Geology Applied

to Mineral Deposits (GAC-MAC-SEG-SGA) joint meeting, Ottawa, May 25-27, 2011, v. 34, p. 148.

Rollinson, H., 1997. The Archean komatiite-related Inyala chromitite, southern Zimbabwe; Economic Geology, v. 92, p. 98–107.

Spath, C.S. III, Lesher, C.M., and Houlé, M.G., 2015. Hybridized ultramafic rocks in the Black Label hybrid zone of the Black Thor intrusive complex, McFaulds Lake greenstone belt, Ontario, *In:* Targeted Geoscience Initiative 4: Canadian Nickel-Copper-Platinum Group Elements-Chromium Ore Systems — Fertility, Pathfinders, New and Revised Models, (ed.) D.E. Ames and M.G. Houlé; Geological Survey of Canada, Open File 7856, p. 103–114.

Taylor, S.R. and McLennan, S.M., 1985. The Continental Crust: It's Composition and Evolution, An Examination of the Geochemical Record Preserved in Sedimentary Rocks; Blackwell Scientific Publication Inc., Palo Alto, California, 328 p.

Tuchscherer, M.G., Hoy, D., Johnson, M., Shinkle, D., and Holmes, M., 2010. Fall 2008 to winter 2009 technical drill report on the Black Thor chromite deposit-Black Label chromite zone and associated Ni-Cu-PGEs, McFaulds Lake property, James Bay Lowlands, Northern Ontario; Internal technical report, Freewest Resources Canada Inc., filed February 2010, 57 p.

Ulmer, G.C., 1969. Experimental investigations of chromite spinels, *In:* Magmatic Ore Deposits, (ed.) H.D.B. Wilson; Society of Economic Geologists, Monograph 4, p. 114–131.

Weston, R. and Shinkle, D.A., 2013. Geology and stratigraphy of the Black Thor and Black Label chromite deposits, James Bay Lowlands, Ontario, Canada, *In:* Proceedings; 12th Biennial SGA Meeting, Uppsala, Sweden, August 12–15, 2013, p. 1069–1071.

GEOLOGICAL SURVEY OF CANADA
OPEN FILE 7856

Targeted Geoscience Initiative 4: Canadian Nickel-Copper-Platinum Group Elements-Chromium Ore Systems — Fertility, Pathfinders, New and Revised Models

Hybridized ultramafic rocks in the Black Label hybrid zone of the Black Thor intrusive complex, McFaulds Lake greenstone belt, Ontario

Charles S. Spath III[1], **C. Michael Lesher**[1], **and Michel G. Houlé**[2]

[1]Laurentian University, Sudbury, Ontario
[2]Geological Survey of Canada, Québec, Quebec

2015

© Her Majesty the Queen in Right of Canada, as represented by the Minister of Natural Resources Canada, 2015

This publication is available for free download through GEOSCAN (http://geoscan.nrcan.gc.ca/)

Recommended citation

Spath, C.S. III, Lesher, C.M., and Houlé, M.G., 2015. Hybridized ultramafic rocks in the Black Label hybrid zone of the Black Thor intrusive complex, McFaulds Lake greenstone belt, Ontario, *In:* Targeted Geoscience Initiative 4: Canadian Nickel-Copper-Platinum Group Elements-Chromium Ore Systems — Fertility, Pathfinders, New and Revised Models, (ed.) D.E. Ames and M.G. Houlé; Geological Survey of Canada, Open File 7856, p. 103–114.

Publications in this series have not been edited; they are released as submitted by the author.

Contribution to the Geological Survey of Canada's Targeted Geoscience Initiative 4 (TGI-4) Program (2010–2015)

TABLE OF CONTENTS

Hybridized ultramafic rocks in the Black Label hybrid zone of the Black Thor intrusive complex, McFaulds Lake greenstone belt, Ontario

Charles S. Spath III[1]*, C. Michael Lesher[1], Michel G. Houlé[2]

[1]Mineral Exploration Research Centre, Department of Earth Sciences, Goodman School of Mines, Laurentian University, 935 Ramsey Lake Road, Sudbury, Ontario P3E 2C6
[2]Geological Survey of Canada, 490 rue de la Couronne, Québec, Quebec G1K 9A9
*Corresponding author's e-mail: CSpath@laurentian.ca

ABSTRACT

The ca. 2.7 Ga Black Thor intrusive complex (BTIC) is an ultramafic to mafic, layered intrusion composed primarily of dunite, peridotite, pyroxenite, and chromitite overlain by lesser gabbroic rocks and rare anorthosite. After emplacement but before complete crystallization, a late websterite intrusion (LWI) reactivated the feeder conduit and transected the basal part of the BTIC, including the Black Label chromitite zone (BLCZ). All rocks have been metamorphosed to lower greenschist facies, but igneous minerals are preserved in some parts (particularly in the LWI) and relict igneous textures are well preserved in most parts. Logging of selected parts of 39 drill cores shows that semi-concordant intrusion of LWI magma and incorporation of inclusions produced a 1 to 10 m thick marginal zone of heterogeneous, interfingering brecciation defined as the Black Label hybrid zone (BLHZ). The BLHZ contains variably sized (1–50 cm) dunite/lherzolite/ chromitite inclusions with subangular to amoeboidal geometries, sharp to diffuse contacts, and locally significant amounts of patchy disseminated to patchy net-textured Fe-Ni-Cu-(PGE) sulphide mineralization. The core of the LWI is typically an inclusion-free, medium-grained, orthopyroxene-rich adcumulate with accessory chromite or olivine; however, inclusion-rich intervals of the LWI contain more olivine and chromite produced by disaggregation and partial assimilation of BTIC ultramafic rocks. There are two types of hybrid groundmass: one containing xenocrystic olivine and one containing xenocrystic chromite and olivine in varying proportions. Geochemical signatures of the hybrid rocks reflect the partial assimilation and brecciation of chromitite/lherzolite/dunite sequences. Similar Th-U-Nb-Ta-light rare earth element LREE patterns suggest that the LWI is related to the BTIC, presumably representing a more fractionated magma from deeper in the system. Further characterization of the hybrid rocks and inclusion variability is in progress and will help to establish the range and variability of processes within the BTIC, and their influence on the genesis of associated Fe-Ni-Cu-PGE sulphide mineralization in the BLHZ.

INTRODUCTION

The ca. 2.7 Ga Black Thor intrusive complex (BTIC) is a funnel-shaped, semi-conformable, layered intrusion composed primarily of dunite, lherzolite, olivine websterite, websterite, and chromitite overlain by lesser melagabbro to leucogabbro, and rare anorthosite. It is part of the "Ring of Fire" intrusive suite (RoFIS) located within the McFaulds Lake greenstone belt (MLGB) in the Oxford-Stull domain, James Bay Lowlands of northern Ontario. After emplacement and before complete crystallization of the BTIC, a late websterite intrusion (LWI) transgressed the semi-consolidated lower and middle ultramafic parts of the complex, including the Black Label chromitite zone (BLCZ), producing a variety of breccia and hybrid rock types, referred to as the Black Label hybrid zone (BLHZ). The BLHZ contains variably sized (1–50 cm) dunite/lherzolite/chromitite inclusions with subangular to amoeboidal geometries and sharp to diffuse contacts. The BLHZ is localized in marginal zones and in discrete pods within the LWI, and is locally associated with synmagmatic patchy disseminated to patchy net-textured Fe-Ni-Cu-(PGE) sulphide mineralization.

The objectives of this project are to (1) characterize all rock types and lithofacies associated with the BLHZ, including the ultramafic precursors of the BTIC and the LWI; (2) establish the textural variability of the inclusions (e.g. heterolithic versus homolithic compositions, rounded versus subangular forms, sharp versus diffuse contacts); and (3) constrain the mechanism(s) of emplacement and hybridization. The purpose of this contribution is to present the main objectives, research

Spath, C.S. III, Lesher, C.M., and Houlé, M.G., 2015. Hybridized ultramafic rocks in the Black Label hybrid zone of the Black Thor intrusive complex, McFaulds Lake greenstone belt, Ontario, *In:* Targeted Geoscience Initiative 4: Canadian Nickel-Copper-Platinum Group Elements-Chromium Ore Systems — Fertility, Pathfinders, New and Revised Models, (ed.) D.E. Ames and M.G. Houlé; Geological Survey of Canada, Open File 7856, p. 103–114.

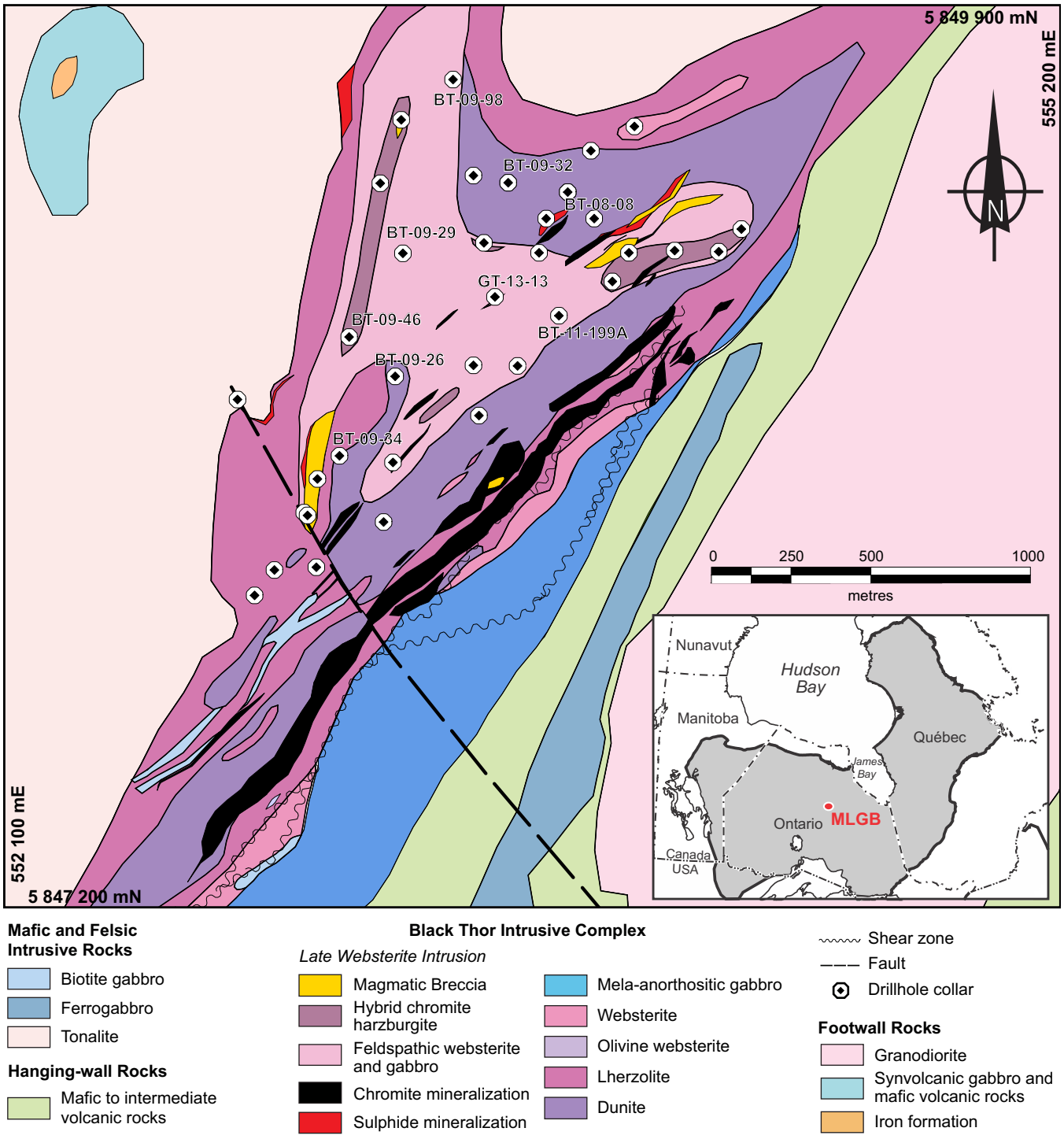

Figure 1. Simplified geological map at 100 m depth showing the locations of diamond drillholes that were logged and sampled in the course of this study (modified from Weston and Shinkle, 2013). Abbreviation: MLGB = McFaulds Lake greenstone belt.

methods, preliminary results, and some exploration implications of an M.Sc. project undertaken by the senior author at Laurentian University under the supervision of Drs. Lesher and Houlé.

METHODOLOGY

Fieldwork for this project was completed in June and July 2013 at the Cliffs Natural Resources "Esker Camp" in the James Bay Lowland. Detailed core logging was conducted to record rock types and textural variations within each rock unit (LWI, BLHZ, BTIC, BLCZ) and to collect homogeneous representative samples for petrographic study, mineral analyses, and whole-rock geochemical analyses. Selected parts of 39 drill cores (Fig. 1) were re-logged, from which 314 representative samples were taken including 123 samples

of the LWI websterite, 19 samples of LWI feldspathic websterite and gabbro, 139 samples of the BLHZ rocks, 10 samples of BTIC dunite and peridotite, and 23 samples of the BLCZ. Thus far, 150 representative NQ core samples (48 mm in diameter) have been halved, ground to remove saw marks, scanned, and examined using binocular microscopy to establish relevant mesoscopic textures. One hundred and twenty-four of these samples were examined in thin section (81 standard polished, 17 standard, 21 large, and 5 extra-large thin sections) using transmitted and reflected light to establish mineralogy and microscopic textures relevant to the petrogenesis of the BLHZ, and also to select representative least altered samples for whole-rock geochemistry. Thirty-three samples have been analyzed thus far for major, minor, and trace elements by a combination of wavelength dispersive X-ray fluorescence spectrometry (WDS-XRFS) and inductively coupled plasma mass spectrometry (ICP-MS) at the Ontario Geoscience Laboratories in Sudbury. Results for another 55 samples are pending. The data received have been interpreted in combination with data collected by Carson et al. (2015). Five polished thin sections have been studied/analyzed using a scanning electron microscope (SEM) and energy dispersive-X-ray emission spectrometry (ED-XRES) methods to establish the nature of zoning of silicate and oxide minerals associated with the BLHZ. Twelve polished thin sections (399 total spots) have been analyzed using an electron probe micro-analyzer (EPMA) and wavelength dispersive XRES methods to determine the compositions of relict pyroxene, olivine, plagioclase, and chromite.

RESULTS

Geology and Petrography of the Late Websterite Intrusion

The late websterite intrusion (LWI) is defined as a distinct intrusion comprising websterite, feldspathic websterite, and gabbro that transgresses the basal portions of the BTIC, which is spatially, texturally, mineralogically, and genetically different from websterite present in the upper parts of the BTIC. It is distinguished from BTIC pyroxenite by (1) a much greyer colour; (2) a low degree of alteration; (3) the presence of much more orthopyroxene, which is characterized by an adcumulate texture; (4) abundant inclusions in the parts bordering the earlier phases of the BTIC; and (5) restriction to the lower 2/3 of the BTIC. The LWI is ~1.8 km long and ~1 km thick and has been intersected in drill core in the feeder, basal, and central parts of the BTIC (Fig. 1).

Websterite

The dominant rock type in the LWI, which composes ~85% of the intrusion, is an orthopyroxene-rich, pinkish grey, generally medium-grained, meso- to adcumulate websterite with varying proportions of pyroxene (95:5 to 80:20 orthopyroxene:clinopyroxene) with lesser plagioclase (up to 10 modal%; An_{77}), accessory chromite and olivine (Figs. 2a and 3a). Orthopyroxene is always a cumulus phase, clinopyroxene is most commonly an intercumulus phase, and feldspar is almost always an intercumulus phase. The late websterite is crosscut by gabbroic dykes and sulphide/magnetite/talc-serpentine veinlets, but remains relatively unaltered. However, both pyroxene and olivine contained within the inclusion-rich phases of the LWI are more commonly serpentinized or amphibolitized.

Feldspathic Websterite and Gabbro

Feldspathic websterite and gabbro that compose 15% of the LWI occur most commonly in the central portion of the LWI and contain no inclusions. These rocks appear to represent the residual liquid of the crystallizing LWI cumulates. The LWI feldspathic websterite and LWI gabbro are enriched in Al-Ca-P-K-Ti-Sr-Zr-REE and other incompatible lithophile elements, are depleted in Mg-Fe, and have higher abundances of plagioclase (up to 60 modal%; ~An_{85}) and clinopyroxene relative to LWI websterite (Fig. 3b). Late websterite intrusion feldspathic websterite and LWI gabbro comprise three varieties, all of which are blue-grey and coarse-grained to pegmatitic: 1) orthocumulate feldspathic websterite, which occurs in small (5–50 cm) stringers within websterite (Fig. 2b); 2) melagabbro; and 3) rare meso-leucogabbro, which occurs in both large (0.5–5 m) discrete pods, and crosscutting pegmatitic dykes (5–30 cm), respectively. Fe-Ni-Cu-(PGE) sulphide (5–10%) mineralization is present as small blebs along the margins of small pods and dykes of meso-leucogabbro that transgress BTIC lithologies and LWI websterite.

Geology and Petrography of the Black Label Hybrid Zone

The LWI is transgressive to layering in the lower parts of the BTIC, but semi-concordant along the lateral margins, especially in the BLCZ, where fine, distinct olivine- and chromite-rich bedding exists. The amoeboidal shapes of some of the chromite inclusions suggest that the Black Label hybrid zone (BLHZ) formed by injection of the late websterite melt into semi-consolidated dunite-lherzolite-chromitite horizons of the BTIC. Within inclusion-rich intervals, interclastic groundmass has been locally hybridized through the disaggregation of partially consolidated ultramafic intervals (i.e. incorporation of xenocrystic olivine and chromite; Fig. 2c,d). Black Label hybrid zone intervals are localized in marginal zones (1–10s m thick) and in discrete pods (1–15 m) and within the LWI. Websterite

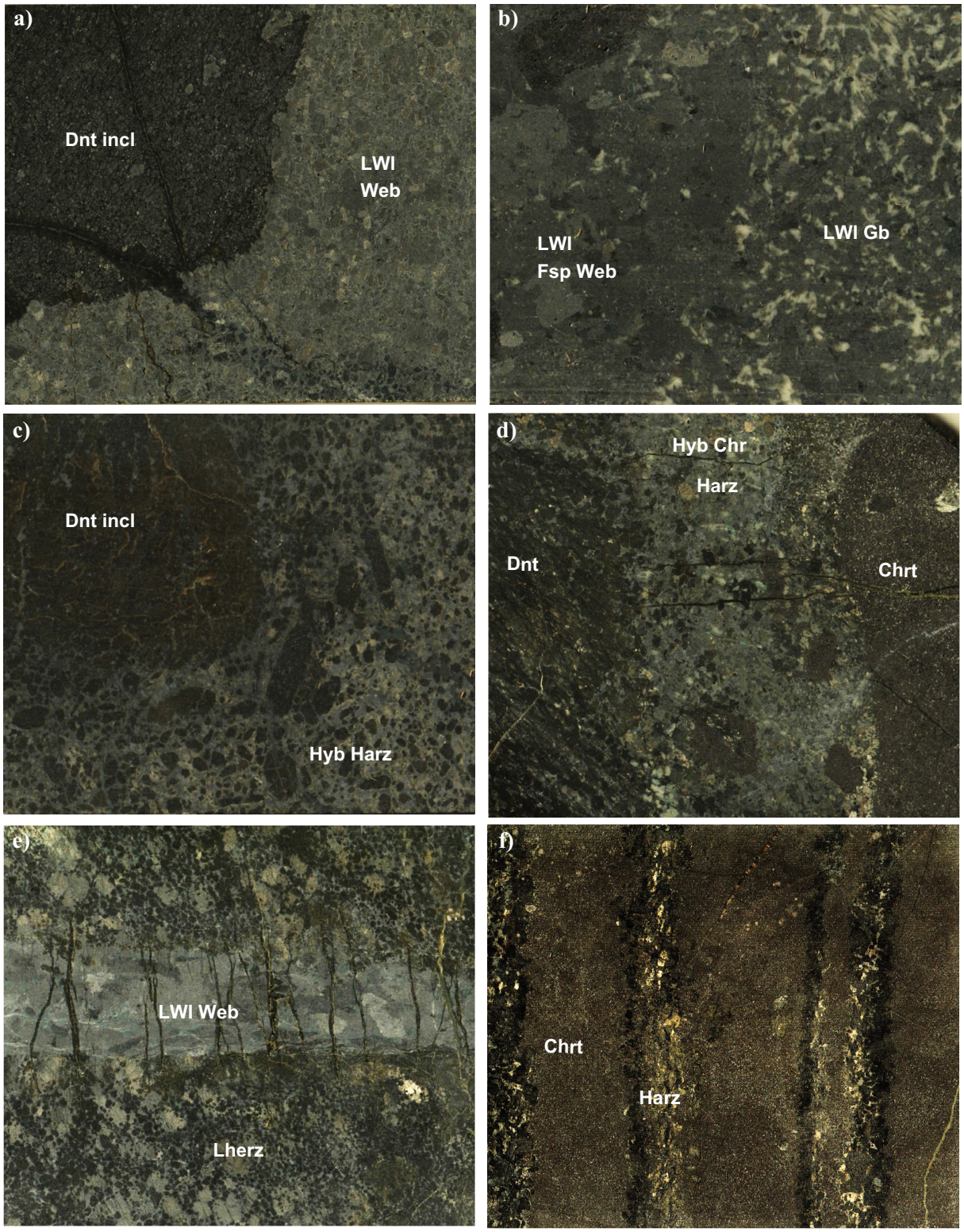

Figure 2. Representative scans of NQ (48 mm diameter) and HQ (64 mm diameter) drill core (younging direction to the right). **a)** Dunite inclusion (Dnt incl) contained within the late websterite intrusion (LWI Web); note vein of alteration (serpentinization and amphibolization), sample BT-11-199A/34.2 m, HQ core. **b)** Pegmatitic LWI feldspathic websterite (LWI Fsp Web) with more evolved LWI gabbro (LWI Gb) at right, sample BT-09-98/211.4 m, NQ core. **c)** Dunite inclusion (Dnt inc) within hybrid harzburgite (Hyb Harz); note the bimodal xenocrystic olivine, sample BT-09-46/212 m, NQ core. **d)** Concordant injection of late websterite (now hybrid chromite harzburgite: Hyb Chrt Harz) between chromitite (Chrt) and dunite (Dnt) beds, focusing disaggregation; note the presence of smaller (<1 cm) inclusions and xenocrysts, sample GT-13-13/251.3 m, HQ core. **e)** BTIC lherzolite (Lherz) discordantly injected by late websterite (LWI Web), note crosscutting serpentinite veinlets, sample GT-13-13/43.5 m, HQ core. **f)** Bedded chromitite (Chrt) with alternating massive chromite-harzburgite (Harz) intervals, sample GT-13-13/247.5 m, HQ core.

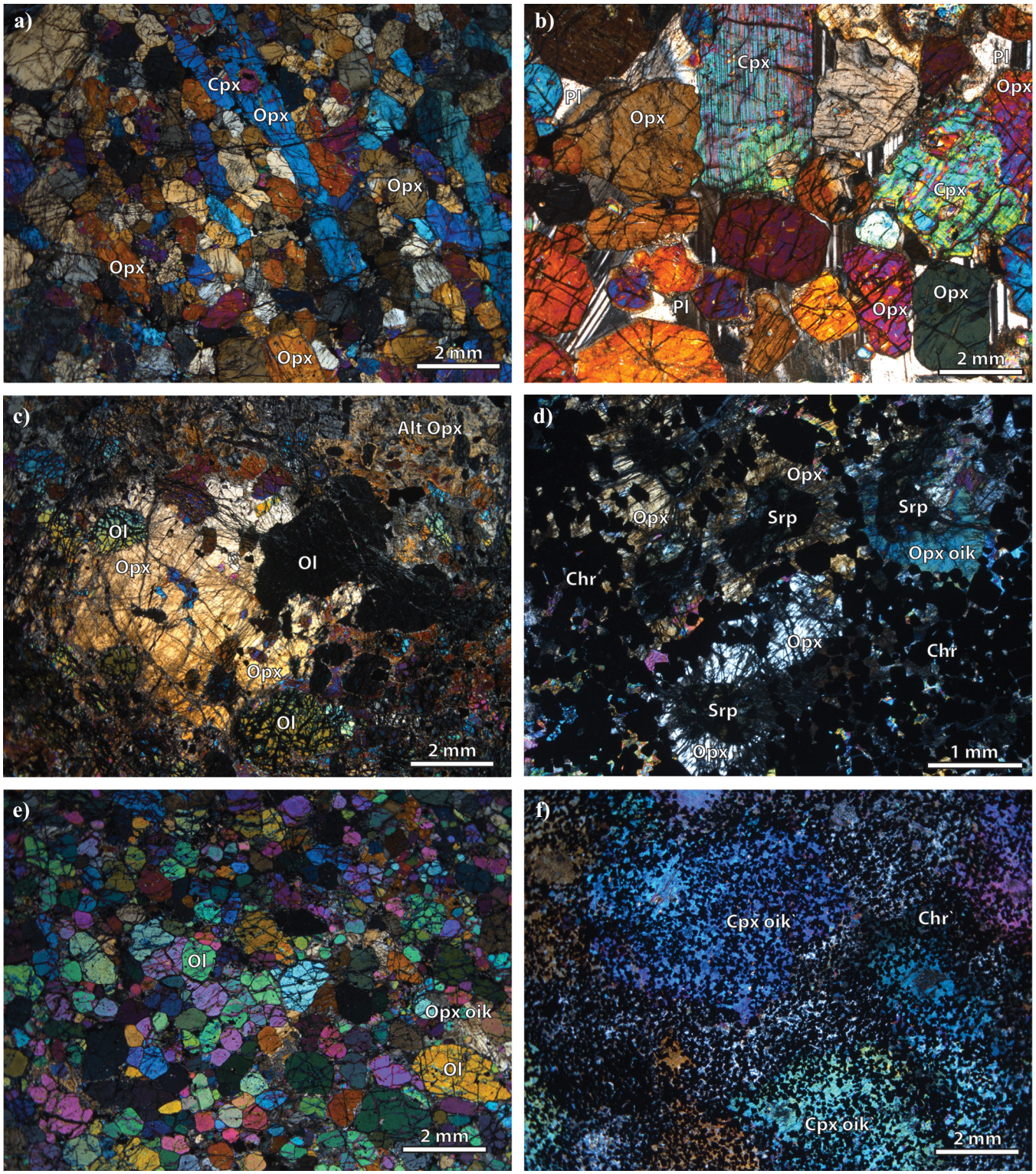

Figure 3. Photomicrographs of representative polished thin sections in cross-polarized light. **a)** Adcumulate late websterite intrusion (LWI) with a hypidiomorphic texture; note clinopyroxene (Cpx) oikocryst (oik) and atypical elongate crystals of orthopyroxene (Opx), sample BT-09-98 @ 249 m. **b)** Heteradcumulate LWI feldspathic websterite with oikocrystic plagioclase (Pl) and both euhedral clinopyroxene and orthopyroxene, sample BT-09-34 @ 120.5 m. **c)** Poikilitic hybrid harzburgite adjacent to dunite inclusion (lower right); note blebby olivine (Ol) with corroded margins and altered orthopyroxene (Alt Opx), sample BT-09-98 @ 361 m. **d)** Heteradcumulate hybrid chromite harzburgite; note blebby, irregular serpentinized olivine (Srp) enclosed with orthopyroxene that is devoid of chromite (Chr), sample BT-09-29 @ 313.7 m. **e)** Adcumulate dunite with inequigranular and panidiomorphic texture, sample BT-09-32 @ 129 m. **f)** Net-textured chromitite, with oikocrystic clinopyroxene (Cpx oik) enveloping fine-grained chromite between oikocrysts chromite, is locally more abundant giving a patchy texture, sample BT-08-08 @ 217 m.

that contains inclusions, *but* not hybrid groundmass, is considered part of the LWI; whereas websterite that has a locally hybridized matrix and/or inclusions is considered part of the BLHZ. The greater abundance of xenocrystic olivine and inclusions in the BLHZ results in a more pervasive alteration signature than in the LWI.

Hybrid Harzburgite

The most abundant hybrid rock type is localized in dunite-lherzolite inclusion-rich intervals and comprises varying proportions of orthopyroxene (40–70%), olivine (5–50%), and clinopyroxene (5–20%). Accessory chromite, plagioclase, and sulphide are present, with some intervals containing up to 10% disseminated to patchy net-textured Fe-Ni-Cu-(PGE) sulphides. Olivine is a cumulus phase and ranges from 2 to 9 mm in diameter (Fig. 3c). It is localized along inclusion margins and appears to have been produced by disaggregation of lherzolite and dunite inclusions. The abundance of olivine varies, forming olivine websterite or harzburgite. Orthopyroxene is euhedral and a cumulus phase, but when present with olivine exhibits an oikocrystic texture. Olivine xenocrysts are corroded along the margins and blebby and irregular in shape within orthopyroxene oikocrysts (derived from LWI melt) (Fig. 3c). Clinopyroxene is an anhedral intercumulus phase. Distinguishing between rock types at a map-scale is difficult, as they vary on the decimetre to metre scale within the BLHZ, thus for simplicity this component is termed the "hybrid harzburgite".

Hybrid Chromite Harzburgite

This rock type is less abundant and occurs in brecciated BLCZ intervals; it comprises varying proportions of orthopyroxene (20–70%), olivine (5–40%), chromite (10–40%), and clinopyroxene (5–20%). Accessory plagioclase and sulphide are present, with some intervals containing up to 10% disseminated to patchy net-textured Fe-Ni-Cu-(PGE) sulphides. Olivine, orthopyroxene, and clinopyroxene exhibit the same textures as in hybrid harzburgite, but are fine- to very fine-grained; euhedral chromite chadacrysts exhibit no corrosive features and were apparently refractory during hybridization.

Textural relationships in heavily disseminated to net-textured chromite harzburgite (10–50% chromite) indicate selective replacement of olivine by orthopyroxene, where the margins of originally larger olivine grains have been replaced by orthopyroxene, leaving smaller corroded olivine surrounded by chromite-free halos (Fig. 3c). Olivine and chromite xenocrysts are localized around inclusion margins and therefore are interpreted to represent disaggregation of banded chromitite-dunite and heavily disseminated to semi-massive chromitite. The abundance of olivine varies, forming chromite websterite, chromite olivine-websterite, or chromite harzburgite. Similar to the hybrid harzburgite, distinguishing between rock types on a map-scale is difficult, so for simplicity this component is termed the "hybrid chromite harzburgite".

Ni-Cu-(PGE) Mineralization

Significant sulphide mineralization is present in the SW breccia, Central breccia, and NE breccia zones of the BLHZ (Farhangi et al., 2013) and always occurs interstitially to the silicate and oxide constituents of the BLHZ, indicating that it formed during the hybridization process. It forms low interfacial angles (15–70°) with olivine and chromite, indicating that it "wetted" olivine, but high interfacial angles (65–105°) with pyroxene, indicating that it did not wet pyroxene, resulting in patchy disseminated to patchy net textures.

Inclusion Variability

Inclusions are ubiquitous in the BLHZ and in the adjacent LWI (within ~5 m), and range from homo- to heterolithic (Table 1). The Black Label hybrid zone typically contains 10 to 50% inclusions, whereas the adjacent LWI websterite contains 5 to 10% inclusions. Only the core of the LWI contains extensive (>100 m) inclusion-free intervals. Inclusions vary in geometry (subangular to amoeboidal), contact style (sharp to diffuse), and size (1–50 cm, rarely >1 m). The lithological variability of the inclusions depends on the scale of layering in adjacent BTIC intervals: heterolithic inclusions occur adjacent to thinly layered chromitite-dunite intervals, whereas homolithic inclusions are more abundant adjacent to more thickly layered chromitite-dunite intervals. Inclusion geometries vary systematically in the LWI. Subangular to subrounded inclusions are dominant along the basal contact, and rounded to amoeboidal inclusions are dominant in the core and upper margin of the LWI. The size of inclusions and the sharpness of their contacts vary, but show no regular distribution.

Mineral Chemistry

Major and selected minor-element compositions of the olivine, pyroxene, plagioclase, and chromite minerals in the LWI, adjacent BTIC, and BTIC inclusions are presented in Table 2.

Olivine compositions determined from the LWI, BLHZ, and BTIC are Fo_{75-70}, Fo_{81-76}, and Fo_{85-78}, respectively. It is apparent from trends in MgO variation plots of dunite-lherzolite that the most magnesian olivine in the BTIC is not represented in the suite of samples analysed so far, which is expected given that the analyzed samples were in the central, more evolved part of the BTIC and not in the lower, most primitive part (Fig. 4a).

Table 1. Petrographic features of the main types of inclusions in the Black Thor intrusive complex.

Lithology	Colour	Chromite (modal %)	Texture	Grain Size	Mineralogy	Description
Dunite	dark grey, green	0-10%	Oac	fg-cg	Ol (90-98%)-Opx-Chr	Cumulus Ol±Chr with intercumulus Opx; fg-mg Ol but rarely cg (up to 9 mm), fg-mg Opx, and vfg-fg Chr (Fig. 2a,c, 3e); most common inclusion in BLHZ and typically exhibits less angular shapes than chromite inclusions
Lherzolite	dark grey-green	0-10%	Omc to Ooc	fg-cg	Ol (75-90%) Opx (10-20%) -Cpx-Chr	Cumulus Ol and Chr with intercumulus Opx/Cpx; fg-mg Ol, mg-cg Opx; locally oikocrystic lherzolite with >30% cg lensoidal Opx (Fig. 2e)
Heavily disseminated to net-textured chromitite	dark grey-green	10-50%	OChac to OCoc	bi	1) Chr-Ol/Opx 2) Chr-Cpx± Ol/Opx	Ol, Chr, Opx cumulus with Cpx intercumulus; fg Chr, mg Ol and Opx, and cg-vcg Cpx; refractory chromitite inclusions typically exhibits more angular shapes. Chr occurs either: 1) locally within interstices of cumulus Ol and/or Opx (i.e. chain-texture); 2) patchy disseminated within oikocrystic Cpx with minor cumulus Ol/Opx (Fig. 3f)
Matrix & semimassive chromitite	dark grey	50-90%	OChac to OCoc	bi	1) Chr-Ol/Opx 2) Chr-Cpx± Ol/Opx	Same description as heavy disseminated to net-textured Chr; most common chromitite inclusion in BLHZ
Massive chromitite	black	90-98%	OChac	vfg-fg	Chr±(Ol/ Opx/Cpx)	Cumulus Chr, with minor cumulus Ol, Opx, and intercumulus Cpx; fg Chr, mg Ol and Opx, and cg-vcg Cpx; Massive chromitite occurs with either: a) round aggregates of Ol/Opx; b) mono- to polymineralic layering (<1 cm thickness) of Ol/Opx (Fig. 2f); c) negligible intercumulus Cpx phase

Minerals: Chr = chromite; Cpx = clinopyroxene; Ol = olivine; Opx = orthopyroxene; Pl = plagioclase. Cumulate phase: O, C = olivine, chromite, respectively
Cumulate texture: ac = adcumulate; hac = heteradcumulate; mc = mesocumulate; oc = orthocumulate. Grain size: vfg, fg, mg, cg, vcg = very fine- fine-, medium-, coarse-, very coarse-grained; bi = bimodal.

Table 2. Representative results of electron microanalyses of minerals from the late websterite intrusion (LWI), Black Label hybrid zone (BLHZ), and Black Thor intrusive complex (BTIC) inclusions within the BLHZ.

	LWI Websterite				LWI Gabbro			BLHZ Harzburgite			BLHZ Chromite Harzburgite				BTIC Chromitite Inclusion				BTIC Dunite Inclusion	
	Ol	Opx	Cpx	Pl	Opx	Cpx	Pl	Ol	Opx	Cpx	Chr	Ol	Opx	Cpx	Chr	Ol	Opx	Cpx	Ol	Opx
SiO_2	38.8	55.5	52.0	49.4	55.6	52.4	47.1	39.5	55.9	52.7	0.11	40.0	54.9	52.2	<0.01	40.5	56.2	53.2	40.4	55.5
TiO_2	<0.01	0.05	0.24	0.03	0.07	0.39	0.02	<0.01	0.09	0.22	0.89	<0.01	0.10	0.22	0.8	<0.01	0.08	0.14	<0.01	0.06
Al_2O_3	<0.01	1.13	2.83	31.8	1.50	2.30	33.3	<0.01	1.53	2.69	17.6	<0.01	1.64	2.69	15.9	0.01	1.59	1.99	<0.01	2.12
V_2O_3	N/A	N/A	N/A	N/A	N/A	N/A	N/A	N/A	N/A	N/A	0.23	N/A	N/A	N/A	0.2	N/A	N/A	N/A	N/A	N/A
Cr_2O_3	<0.01	0.28	0.89	N/A	0.46	0.63	N/A	0.01	0.41	0.90	41.0	<0.01	0.46	1.05	45.7	0.02	0.57	1.07	0.02	0.75
Fe_2O_3	N/A	N/A	N/A	0.24	N/A	N/A	0.06	N/A	N/A	N/A	8.64	N/A	N/A	N/A	6.85	N/A	N/A	N/A	N/A	N/A
FeO	20.4	12.4	5.46	0.22	9.92	4.47	0.06	14.0	9.45	4.16	24.8	13.7	10.3	4.57	20.2	11.7	8.19	3.18	13.0	8.63
MnO	0.27	0.28	0.17	<0.01	0.24	0.15	0.02	0.23	0.25	0.15	0.33	0.21	0.25	0.16	0.3	0.18	0.22	0.11	0.21	0.22
CoO	0.03	0.01	0.01	N/A	0.02	0.01	N/A	0.03	0.01	0.01	0.03	0.02	<0.01	<0.01	0.03	0.03	0.01	<0.01	0.02	0.01
NiO	0.22	0.06	0.03	N/A	0.07	0.03	N/A	0.19	0.05	0.03	0.03	0.17	0.05	0.02	0.04	0.27	0.06	0.03	0.26	0.06
ZnO	N/A	N/A	N/A	N/A	N/A	N/A	N/A	N/A	N/A	N/A	0.09	N/A	N/A	N/A	0.07	N/A	N/A	N/A	N/A	N/A
MgO	40.5	29.8	15.9	0.01	31.3	16.4	0.01	44.6	31.4	16.4	6.96	45.7	30.7	16.8	9.43	47.7	32.2	17.5	46.5	31.1
CaO	0.03	0.65	22.0	15.0	0.85	22.4	17.0	0.02	1.00	22.5	N/A	0.02	1.29	22.0	N/A	0.03	1.41	22.3	0.01	1.98
SrO	N/A	N/A	N/A	0.01	N/A	N/A	<0.01	N/A	N/A	N/A	N/A	N/A	N/A	N/A	N/A	N/A	N/A	N/A	N/A	N/A
Na_2O	<0.01	0.01	0.39	3.12	0.01	0.36	1.94	<0.01	0.03	0.41	N/A	<0.01	0.01	0.3	N/A	<0.01	0.03	0.31	<0.01	0.03
K_2O	<0.01	<0.01	0.01	0.02	<0.01	<0.01	0.01	<0.01	0.01	<0.01	N/A	<0.01	<0.01	<0.01	N/A	<0.01	<0.01	<0.01	<0.01	<0.01
Total	100.26	100.13	99.98	99.54	100.1	99.53	99.52	99.3	100.1	100.12	99.82	99.73	99.73	99.93	99.57	100.41	100.48	99.82	100.28	100.42

Abbreviations are same as Table 1; N/A = not analyzed. Sample locations: LWI Websterite from BT-11-180/171 m; LWI Gabbro from BT-09-32/119 m; BLHZ Harzburgite from BT-11-179/86.7 m; BLHZ Chromite Harzburgite from BT-11-177/107.6 m; BTIC Chromitite Inclusion from BT-11-182/275.8 m; and BTIC Dunite Inclusion from BT-11-199A/46.2 m.

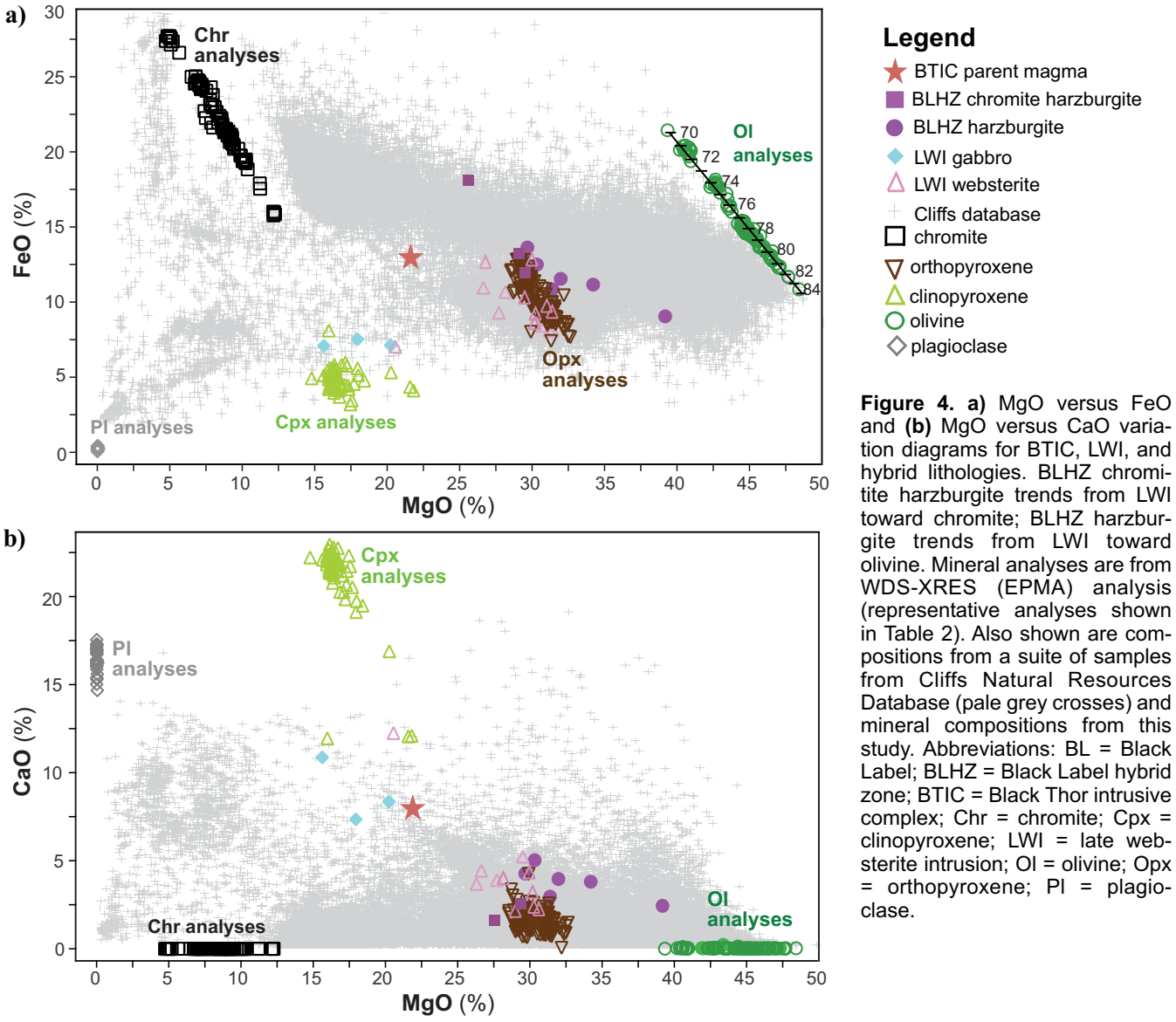

Figure 4. a) MgO versus FeO and **(b)** MgO versus CaO variation diagrams for BTIC, LWI, and hybrid lithologies. BLHZ chromitite harzburgite trends from LWI toward chromite; BLHZ harzburgite trends from LWI toward olivine. Mineral analyses are from WDS-XRES (EPMA) analysis (representative analyses shown in Table 2). Also shown are compositions from a suite of samples from Cliffs Natural Resources Database (pale grey crosses) and mineral compositions from this study. Abbreviations: BL = Black Label; BLHZ = Black Label hybrid zone; BTIC = Black Thor intrusive complex; Chr = chromite; Cpx = clinopyroxene; LWI = late websterite intrusion; Ol = olivine; Opx = orthopyroxene; Pl = plagioclase.

Orthopyroxene in the LWI (in both websterite and gabbro) ranges from En_{78} to En_{84} and clinopyroxene ranges from Wo_{47} En_{48} Fs_5 to Wo_{41} En_{52} Fs_7 in composition. Orthopyroxene in BTIC inclusions (dunite and net-textured chromitite lithologies) ranges from En_{83} to En_{87} and clinopyroxene ranges Wo_{47} En_{48} Fs_5 to Wo_{45} En_{51} Fs_4 in composition. Orthopyroxene in BLHZ (both hybrid lithologies) ranges from En_{82} to En_{85} and clinopyroxene ranges from Wo_{46} En_{49} Fs_5 to Wo_{40} En_{52} Fs_8 in composition. Plagioclase in the LWI gabbro is significantly more calcic compared to plagioclase in LWI websterite and ranges from An_{87} to An_{83} in gabbro and from An_{83} to An_{78} in websterite.

Whole-Rock Geochemistry

The majority of the rocks in the BTIC are olivine ± chromite ± orthopyroxene ± (clinopyroxene) adcumulate to mesocumulate rocks, that define three broad trends on MgO variation plots (Fig. 4; see also Carson et al., 2015):

1. A mixing trend between olivine-rich and chromite-rich cumulate rocks;
2. A mixing trend between olivine-rich and orthopyroxene-rich cumulate rocks;
3. A fractionation trend between pyroxenite and gabbro.

The compositions of BLHZ chromite harzburgites (purple circles in Fig. 4), trend from LWI toward chromite, and BLHZ harzburgites (purple squares in Fig. 4), trend from LWI toward olivine. Trace element geochemistry (Fig. 5) of the LWI websterite shows a relatively flat pattern with positive U and light rare earth element anomalies and negative Th, Nb-Ta, and Sr anomalies. The negative Nb-Ta anomalies suggest incorporation of an upper crustal component; the negative Sr anomalies probably reflects greater mobility

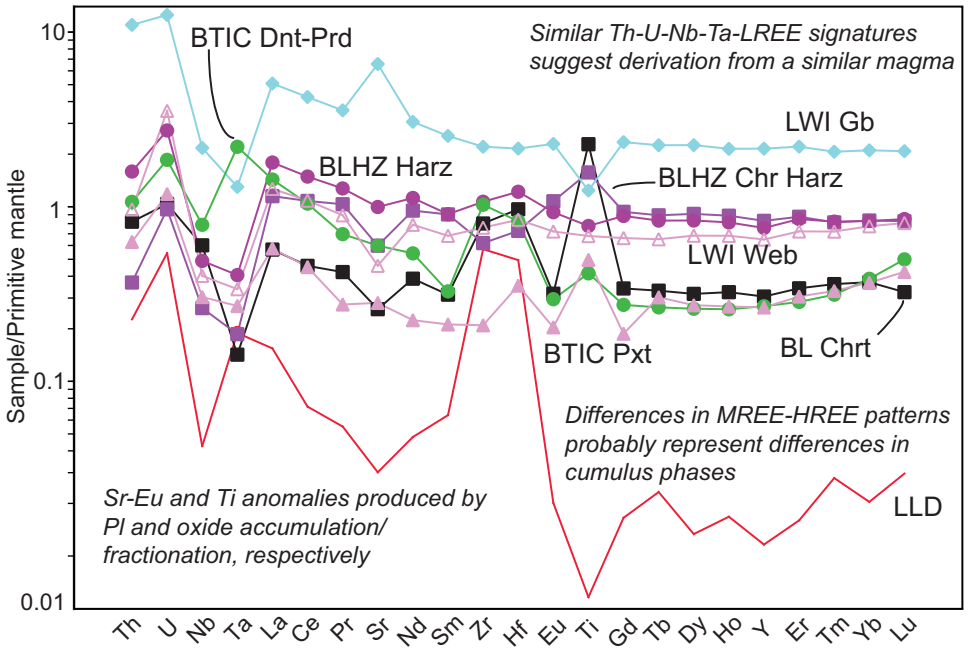

Figure 5. Trace element spider plot of representative samples of LWI, BTIC, and hybrid rock types. Signatures are labeled and symbols correspond to the legend in Figure 4. Normalizing values after McDonough and Sun (1995). Abbreviations: BL = Black Label; BLHZ = Black Label hybrid zone; BTIC = Black Thor intrusive complex; Chrt = chromitite; Dnt = dunite; Gb = gabbro; Harz = harzburgite; LLD = lower limit of detection; LWI = late websterite intrusion; Prd = peridotite; Pxt = pyroxenite; Web = websterite.

during alteration. The hybrid rocks posses Th-U-Nb-Ta-Ti-REE signatures similar to BTIC and LWI.

DISCUSSION

Hybridization Processes

Formation of the BLHZ appears to have involved three main processes: 1) mechanical disaggregation of BTIC rocks by LWI magma, 2) partial melting of BTIC inclusions by LWI magma, and 3) chemical re-equilibration of the remaining material of the BTIC inclusions with LWI magma.

Mechanical Disaggregation

The physical injection of LWI melt into the lower and middle ultramafic parts of the BTIC mechanically brecciated adjacent rocks, forming inclusions that were incorporated into LWI melt. Inclusions were disaggregated along their margins into smaller inclusions or individual xenocrysts of olivine and chromite (Figs. 2, 3). Mixing of the inclusions and xenocrysts with the LWI magma likely formed most of the hybrid lithologies. The semi-consolidated nature of the inclusions, forceful injections of the late melt, and other hybridization processes (e.g. partial melting of interstitial phases) may have facilitated this disaggregation.

Partial Melting

Partial melting of lower temperature phases in BTIC inclusions locally left only rounded olivine and euhedral chromite as xenocrysts, suggesting that the remainder of the original minerals in the BTIC inclusions (clinopyroxene ± orthopyroxene ± interstitial melt) were melted. This process would have weakened the olivine ± chromite cumulate framework and facilitated disaggregation. Experimental studies (see review in Arndt et al., 2008) indicate that lower temperature phases will disappear at temperatures above 1190°C at 1 atm, so the temperature of the LWI magma can be inferred to have been higher than 1190°C.

Chemical Re-equilibration

Chemical re-equilibration also appears to have occurred between the silica-rich hybrid melt and remaining olivine xenocrysts. This re-equilibration is supported by the presence of irregular, blebby geometries and corrosive margins of olivine chadacrysts and xenocrysts, indicating that they have reacted with LWI melt. This process is especially apparent in net-textured chromitite, where LWI melt invaded and chemically reacted with olivine to form a chromite-free orthopyroxene halo around a residual core of olivine (Fig. 3d). The inferred reaction is

$$(Mg,Fe)_2SiO_{4\ (Ol)} + SiO_{2\ (LWI\ melt)} \rightarrow 2(Mg,Fe)SiO_{3\ (Opx)}$$

Inclusion Variability

Megascopic and microscopic observations suggest that the sizes, shapes, sharpness of margins, and compositions of inclusions are controlled by the thickness, initial temperature, and the layered rock types present in the source rock (BTIC), as well as the degree of thermal equilibration between the wall rock and the intruding magma:

1. The LWI commonly intrudes bedding within the BTIC, so the thickness of the bedding and the nature of the original contacts (sharp versus irregular versus diffuse: Fig. 2) influences the rock types

(homolithic versus heterolithic), sizes, and shapes (subspherical versus tabular) of inclusions (Fig. 2).

2. Inclusions are subangular to subrounded at the basal contact, and rounded to amoeboidal in the core and at the top margin of LWI, indicating that the BTIC was incompletely crystallized with a hotter, semi-solid core and cooler peripheries adjacent to the granodiorite footwall. Hotter, less consolidated wall rocks are more likely to form inclusions with irregular shapes, whereas cooler, more consolidated wall rocks are more likely to form angular inclusions.
3. More refractory chromitite inclusions tend to have more angular geometries than less refractory dunite-lherzolite inclusions. However, all inclusion rock types exhibit a range of shapes, indicating that the initial temperature and degree of consolidation varied in the system. Where rounded to amoeboidal geometries are present, the precursor rock was hotter and less consolidated, and where subangular to subrounded geometries are present, the precursor rock was cooler and more consolidated.
4. Inclusions that were incorporated earlier in the process are more likely to have irregular shapes than inclusions incorporated later in the process, due to thermal equilibration (e.g. partial melting of lower temperature phases).

Petrogenesis

Trends of increasing Ni-Mg and decreasing Al-Ti in hybrid harzburgite reflect variable degrees of incorporation of olivine into LWI magma, whereas increasing Ni-Mg-Cr and decreasing Al-Ti in hybrid chromite harzburgite reflect variable degrees of incorporation of olivine and chromite into LWI magma. The similar Th-U-Nb-Ta-LREE signatures of LWI and BTIC suggest derivation from similar sources.

IMPLICATIONS FOR EXPLORATION

The intrusion of LWI magma does not appear to have consumed BLCZ, but it has diluted the grade of the chromite mineralization by dispersing it within the LWI magma. The Fe-Ni-Cu-(PGE) sulphide mineralization associated with LWI hybrid rocks is texturally, mineralogically, and geochemically slightly different from Fe-Ni-Cu-(PGE) sulphide mineralization along the basal contact of the BTIC. Both are clearly magmatic, but the mineralization associated with BLHZ breccia clearly formed during the magma interaction process. Further characterization of the hybrid rocks and inclusion-variability is in progress and will help to establish the range and variability of processes within the BTIC, and their influence on the genesis of associated Fe-Ni-Cu-(PGE) sulphide mineralization in the BLHZ.

ACKNOWLEDGEMENTS

This ongoing project is being supported by grants from Cliffs Natural Resources, the Natural Sciences and Engineering Research Council of Canada (NSERC) Collaborative Research and Development Program, the Ontario Geological Survey (OGS), the Society of Economic Geologists (SEG) Fellowship Program, the Ontario Graduate Scholarship Program, and the Targeted Geoscience Initiative 4 (TGI-4) of the Geological Survey of Canada (GSC). We are also grateful to R. Metsaranta (OGS) for comprehensive reviews that helped us improve the final version of this contribution.

REFERENCES

Arndt, N., Lesher, C.M., and Barnes, S.J., 2008. Komatiite; Cambridge, UK, University Press, 467 p.

Carson, H.J.E., Lesher, C.M., and Houlé, M.G., 2015. Geochemistry and petrogenesis of the Black Thor intrusive complex and associated chromite mineralization, McFaulds Lake greenstone belt, Ontario *In:* Targeted Geoscience Initiative 4: Canadian Nickel-Copper-Platinum Group Elements-Chromium Ore Systems — Fertility, Pathfinders, New and Revised Models, (ed.) D.E. Ames and M.G. Houlé; Geological Survey of Canada, Open File 7856, p. 87–102.

Farhangi, N., Lesher, C.M., and Houlé, M.G., 2013. Mineralogy, geochemistry and petrogenesis of nickel-copper-platinum group element mineralization in the Black Thor intrusive complex, McFaulds Lake greenstone belt, Ontario, *In:* Summary of Field Work and Other Activities, 2013; Ontario Geological Survey, Open File Report 6290, p. 55-1 to 55-7.

McDonough, W.F. and Sun, S.-S., 1995. Composition of the Earth; Chemical Geology, v. 120, p. 223–253. doi: 10.1016/0009-2541(94)00140-4

Mungall, J.E., Harvey, J.D., Balch, S.J., Azar, B., Atkinson, J., and Hamilton, M.A., 2010. Eagle's Nest: A magmatic Ni-sulfide deposit in the James Bay Lowlands, Ontario, Canada, *In:* The Challenge of Finding New Mineral Resources: Global Metallogeny, Innovative Exploration, and New Discoveries, Volume I: Gold, Silver, and Copper-Molybdenum, (ed.) R.J. Goldfarb, E.E. Marsh, and T. Monecke; Society of Economic Geologists, Special Publication 15, p. 539–559.

Weston, R. and Shinkle, D.A., 2013. Geology and stratigraphy of the Black Thor and Black Label chromite deposits, James Bay Lowlands, Ontario, Canada, *In:* Abstracts; Society for Geology Applied to Minerals, 12th SGA Biennial Meeting, Uppsala, Sweden, August 12–15, 2013, Proceedings, v. 3, p. 1069–1071.

GEOLOGICAL SURVEY OF CANADA
OPEN FILE 7856

Targeted Geoscience Initiative 4: Canadian Nickel-Copper-Platinum Group Elements-Chromium Ore Systems — Fertility, Pathfinders, New and Revised Models

Petrogenesis of the ferrogabbroic intrusions and associated Fe-Ti-V-(P) mineralization within the McFaulds greenstone belt, Superior Province, northern Ontario

Benjamin Kuzmich[1], Peter Hollings[1], and Michel G. Houlé[2]

[1]Lakehead University, Thunder Bay, Ontario
[2]Geological Survey of Canada, Québec, Quebec

2015

© Her Majesty the Queen in Right of Canada, as represented by the Minister of Natural Resources Canada, 2015

This publication is available for free download through GEOSCAN (http://geoscan.nrcan.gc.ca/)

Recommended citation

Kuzmich, B., Hollings, P., and Houlé, M.G., 2015. Petrogenesis of the ferrogabbroic intrusions and associated Fe-Ti-V-(P) mineralization within the McFaulds greenstone belt, Superior Province, northern Ontario, *In:* Targeted Geoscience Initiative 4: Canadian Nickel-Copper-Platinum Group Elements-Chromium Ore Systems — Fertility, Pathfinders, New and Revised Models, (ed.) D.E. Ames and M.G. Houlé; Geological Survey of Canada, Open File 7856, p. 115–123.

Publications in this series have not been edited; they are released as submitted by the author.

Contribution to the Geological Survey of Canada's Targeted Geoscience Initiative 4 (TGI-4) Program (2010–2015)

TABLE OF CONTENTS

Petrogenesis of the ferrogabbroic intrusions and associated Fe-Ti-V-(P) mineralization within the McFaulds greenstone belt, Superior Province, northern Ontario

Benjamin Kuzmich[1*], Peter Hollings[1], and Michel G. Houlé[2]

[1]Department of Geology, Lakehead University, 955 Oliver Road, Thunder Bay, Ontario P7B 5E1
[2]Geological Survey of Canada, 490 rue de la Couronne, Québec, Quebec G1K 9A9
*Corresponding author's e-mail: bnkuzmic@lakeheadu.ca

ABSTRACT

The Thunderbird and Butler intrusions of the McFaulds Lake greenstone belt ("Ring of Fire") were studied to determine petrogenesis and associated Fe-Ti-V-(P) mineralization. These intrusions are characterized by variably well layered gabbro-anorthosite intrusions with abundant Fe-Ti oxides, broadly termed ferrogabbro. The layers are composed of partial to complete cycles that comprise basal massive oxide (magnetite-ilmenite), which grade into semi-massive oxide units, followed by oxide-rich pyroxenite/melagabbro/gabbro, oxide-poor melagabbro/gabbro/leucogabbro, and topped with oxide-free leucogabbro/anorthosite. The cycles range from centimetres to metres in thickness and define the well layered portions of the intrusions that typically exhibit sharp upper and lower contacts with gradational internal contacts. Conversely, the intrusions contain broad intervals of disseminated magnetite-ilmenite (2–5%) hosted in melagabbro/gabbro/leucogabbro/anorthosite, which range in thickness from metres to tens of metres. The layering and textures observed within the ferrogabbro units are thought to be dominantly produced by convection currents with intermittent periods of quiescence.

The ferrogabbro intrusions are characterized by gently sloping LREE and flat HREE patterns. This geochemical signature most closely corresponds to an E-MORB source that is thought to have been the result of interaction of a mnalte plume with MORB-like mantle under the McFaulds Lake area. This plume-related magma is thought to have undergone differentiation, resulting in the abundant Cr-Ni-Cu-PGE-bearing ultramafic and evolved Fe-Ti-rich mafic suites in the McFaulds area. Additionally, the plume may have resulted in a thinned lithosphere and produced the coeval VMS occurrences.

Also studied is the potential application of the TiO_2/V_2O_5 ratio for the identification of prospective vanadium mineralization and to aid in the determination of magmatic stratigraphy.

INTRODUCTION

The McFaulds Lake greenstone belt (MLGB), commonly known as the "Ring of Fire", has been the site of base and precious metal exploration over the past decade. This region, located in Ontario's far north, was recognized as an underexplored greenstone belt with the discovery of the McFaulds Lake VMS occurrences in 2002 (Metsaranta and Houlé, 2011, 2012). Exploration in the area quickly resulted in the discovery of numerous chromite deposits (e.g. Black Thor, Black Label, Big Daddy, Black Creek, Black Horse, and Blackbirds), one Ni-Cu-PGE deposit (Eagle's Nest), and numerous Fe-Ti-V-(P) occurrence (Metsaranta et al., 2015).

Although most of the emphasis has been placed on Cr and Ni-Cu-PGE deposits, the Fe-Ti-V-(P) mineralized intrusions have received little attention and this study was initiated in response to this lack of knowledge on the mafic-dominated intrusions that host this style of mineralization. The main goal of this research project was to investigate the petrogenesis of the Fe-Ti-V-(P) mineralization within the Thunderbird, Butler West, and Butler East intrusions in the McFaulds Lake greenstone belt (Fig. 1).

RESEARCH METHODS

In the course of this project, several weeks of fieldwork was completed on the Butler Lake and the Thunderbird properties. Fifteen diamond drillholes were selected and characterized to produce detailed stratigraphic logs (10 drillholes at Butler and 5 drillholes at Thunderbird) of the intrusions. Petrographic work was conducted on 143 samples, 68 from the Thunderbird intrusion and 75 from the Butler (East and West) intrusions, to investigate their textural and lithological characteristics. Further characterization of the silicate and oxide minerals was conducted using a CAMECA SX-100 elec-

Kuzmich, B., Hollings, P., and Houlé, M.G., 2015. Petrogenesis of the ferrogabbroic intrusions and associated Fe-Ti-V-(P) mineralization within the McFaulds greenstone belt, Superior Province, northern Ontario, *In:* Targeted Geoscience Initiative 4: Canadian Nickel-Copper-Platinum Group Elements-Chromium Ore Systems — Fertility, Pathfinders, New and Revised Models, (ed.) D.E. Ames and M.G. Houlé; Geological Survey of Canada, Open File 7856, p. 115–123.

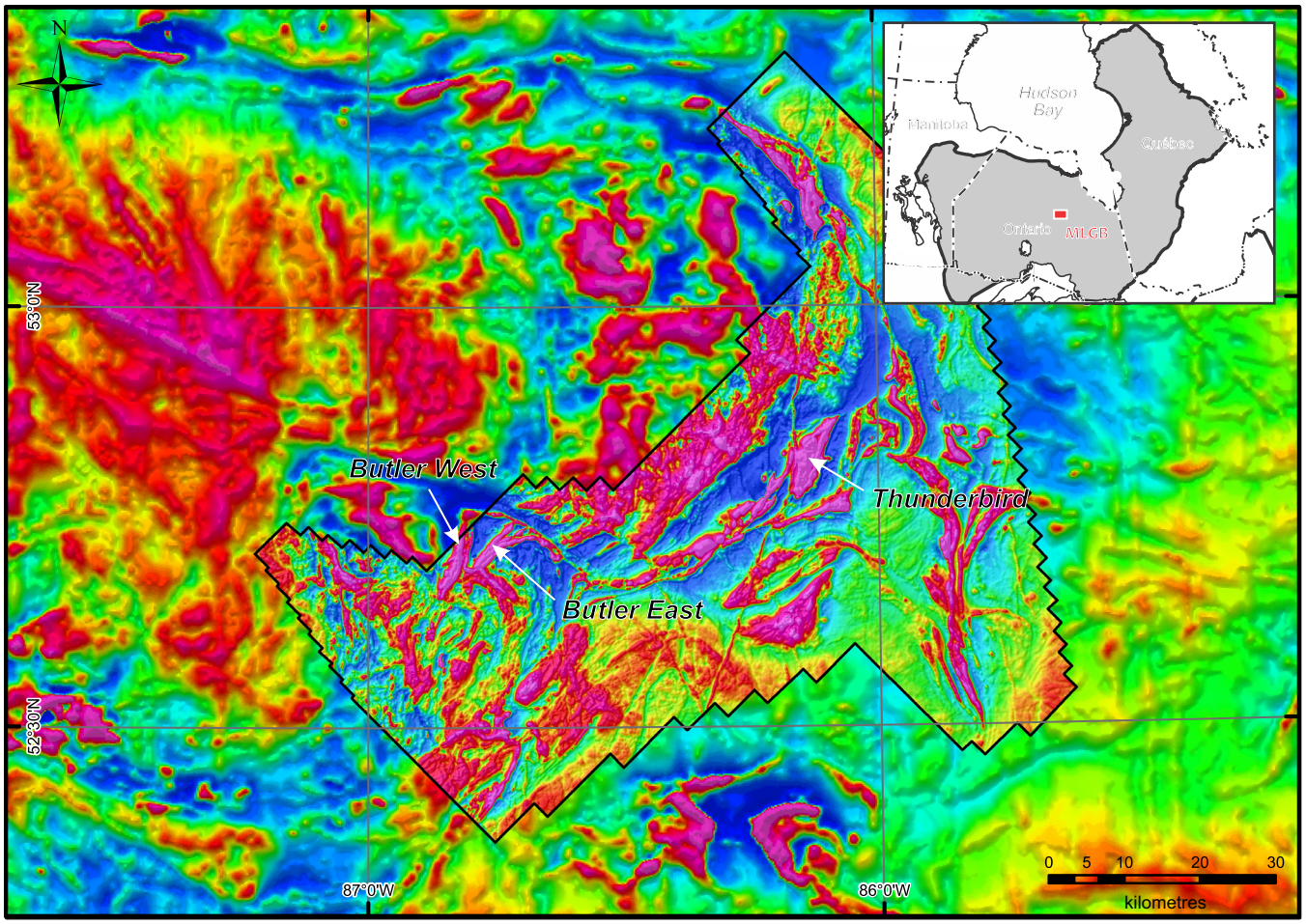

Figure 1. Total residual magnetic field showing the location of the Butler West, Butler East, and Thunderbird intrusions in the McFaulds Lake area. Detailed magnetic data are from the Ontario Geological Survey–Geological Survey of Canada (2011) and the regional data are from the Geoscience Data Repository for geophysical data of Natural Resources Canada, which can be access at http://gdr.agg.nrcan.gc.ca/gdrdap/dap/search-eng.php.

tron microprobe analyzer (EMPA) at the Ontario Geoscience Laboratories (Geo Labs). A total of 100 samples of representative drill core were selected for whole-rock and trace element geochemistry, 46 samples from Thunderbird intrusion and 54 from the Butler intrusions, to characterize the lithologies and determine possible magmatic stratigraphy (Kuzmich et al., 2015). The reader is also referred to Kuzmich et al. (2013) and Kuzmich (2014) for more detailed aspects of this project, including the analytical parameters and procedures used in this study.

RESULTS

Lithofacies

The Butler and Thunderbird intrusions are part of a mafic-dominated "ferrogabbro" subsuite of the Neoarchean Ring of Fire Intrusive Suite (RoFIS) and represent some of the best defined ferrogabbroic intrusions within the McFaulds Lake greenstone belt. The the ferrogabbroic subsuite are described as mafic-dominated intrusions that exhibit an excess of iron oxides and/or an iron and titanium geochemical enrichment (Metsaranta and Houlé, 2011; Metsaranta et al., 2015). These intrusions are characterized by a suite of well layered magnetite-ilmenite-rich rocks that are dominantly composed of gabbroic to anorthositic (Fig. 2a,b) units with lesser stratigraphically conformable units composed of massive magnetite-ilmenite (Fig. 2c). Rare pegmatitic units have been also observed within these intrusions but are better exposed in the Butler East intrusion (Fig. 2d). These pegmatitic units are bound by gradational contacts and are composed of mineralogy identical to the ferrogabbro units but with plagioclase and pyroxene grains in excess of 3 cm. The Fe-Ti oxides are variably mineralized with vanadium but generally contain low chromium contents (magnetite up to 2.45 wt% V_2O_5 and 0.99 wt% Cr_2O_3; ilmenite up to 0.57 wt% V_2O_5). The massive and semi-massive oxide layers range in thickness from centimetres to metres (Fig. 2e) and occur typically as basal members of repeated cycles characterized by sharp lower contacts that grade upwards into oxide-rich

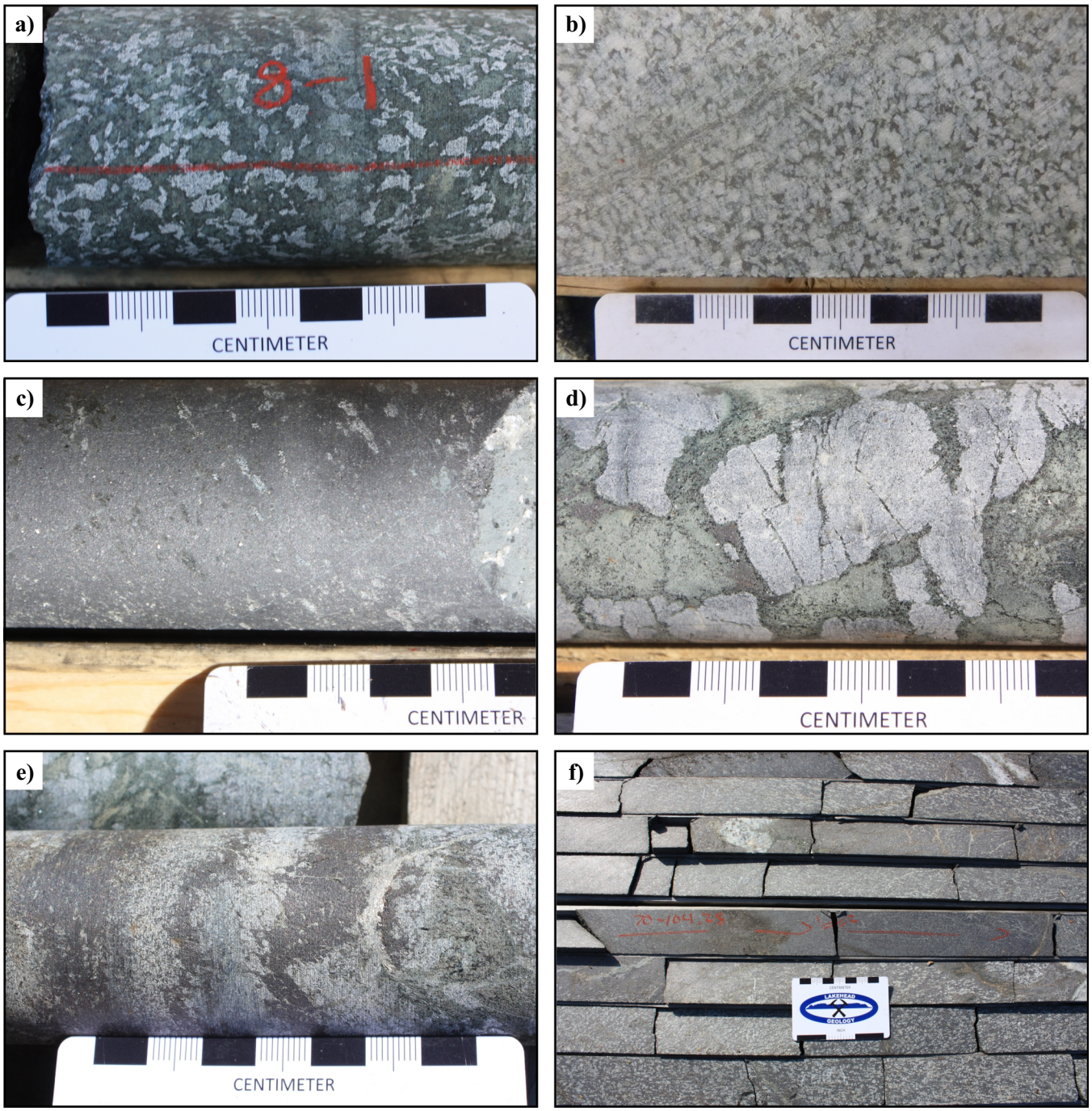

Figure 2. Representative lithofacies within the ferrograbroic subsuite in the McFaulds Lake greenstone belt. **a)** Medium-grained gabbro from the Butler West intrusion (sample BP11-V08). **b)** Medium-grained anorthosite from the Thunderbird intrusion (sample NOT-11-2G25). **c)** Fine-grained massive oxide unit from the Butler West intrusion (sample BP11-V08). **d)** Pegmatitic gabbro with fractured plagioclase from Butler West intrusion (sample MN08-117). **e)** Thinly layered massive oxides and anorthosite from the Butler West intrusion (sample MN08-117). **f)** Semi-massive to massive oxide layers from the Butler East intrusion (sample MN08-70).

pyroxenite, followed by oxide-bearing leucogabbro and/or anorthosite (Fig. 2f).

Petrography

The majority of the ferrogabbroic intrusions are variably composed of medium-grained pyroxene, amphibole, plagioclase, magnetite, and ilmenite. However, the primary silicate mineralogy of these intrusions has largely been replaced by secondary Fe-rich and Fe-poor chlorite, amphibole, clinozoisite, and epidote with accessory titanite, garnet, quartz, and/or potassium feldspar. Primary plagioclase often exhibits strong deformation features (e.g. deformation twins, subgrain boundaries) and as a result the anorthite content, deter-

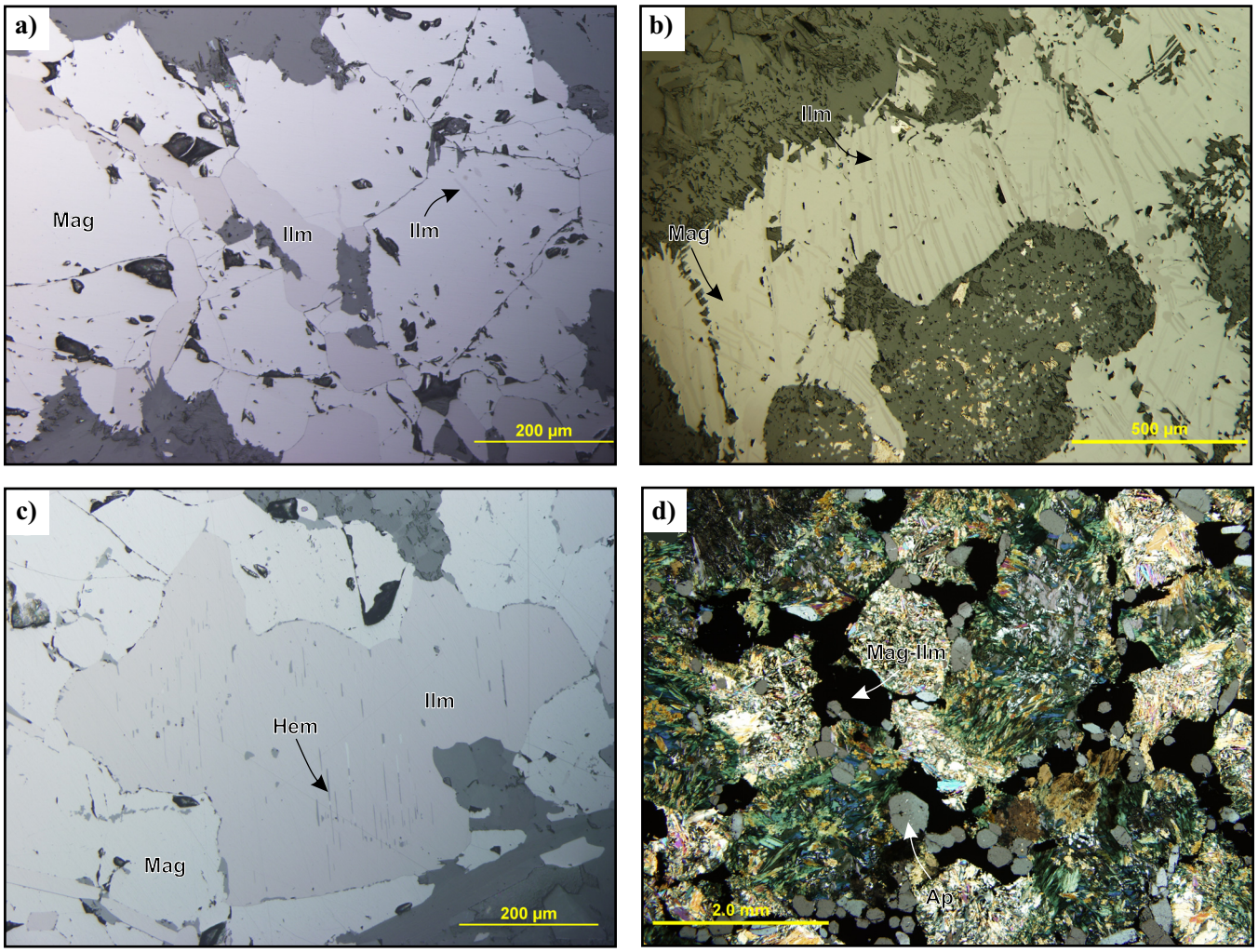

Figure 3. Representative photomicrographs displaying Fe-Ti-V-(P) mineralization textures. **a)** Granular ilmenite with minor ilmenite exsolution within magnetite (reflected light, XPL: sample MN10-117, Butler West intrusion). **b)** Ilmenite exsolution within evolved magnetite (reflected light, XPL: sample NOT-11-2G46, Thunderbird intrusion). **c)** Hematite exsolution within primary ilmenite (reflected light, XPL: sample BP11-V01, Butler West intrusion). **d)** Apatite-oxide mineralization within melagabbro (transmitted light, XPL: sample NOT-11-2G46, Thunderbird intrusion). Abbreviation: Ap = apatite; Hem = hematite; Ilm = ilmenite; Mag = magnetite; XPL = cross-polarized.

minations using the Michel-Lévy method are generally unreliable. Pyroxene grains, when present, are typically clinopyroxene with rare orthopyroxene and are partially to completely replaced by blue/green amphibole grains, which rim the pyroxene. Magnetite grains are typically fine- to medium-grained and display variable abundances of ilmenite exsolution and textures. Magnetite, which is interpreted to have crystallized within the basal portion of these intrusions, generally contains only minor (0–5%), thin (<3 µm) ilmenite lamellae and/or very fine-grained granular ilmenite (Fig. 3a), in stark contrast to the magnetite within the highly evolved upper member of these intrusions, which is characterized by the presence of thick (5–15 µm), abundant (20–30%) ilmenite lamella (Fig. 3b). Primary ilmenite (i.e. not a product of oxy-exsolution) displays less variation than the ilmenite that has exsolved from magnetite. Primary ilmenite generally occurs as subhedral to euhedral tabular fine- to medium-grained crystals with trace amounts of very fine-grained (<2 µm) hematite exsolutions, which is only observed within the upper portions of the intrusions (Fig. 3c). Apatite is a rare mineral and only occurs in significant concentrations (1–4.5%) in the most evolved portion of the Thunderbird intrusion. Apatite occurs as fine-grained euhedral clear prismatic grains associated with disseminated to net-textured fine-grained anhedral magnetite-ilmenite (Fig. 3d).

Mineral Geochemistry

Magnetite and ilmenite grains lack any apparent compositional zoning. Magnetite grains are V_2O_3-rich (<2.46%) but poor in TiO_2 (<1.42%) and Cr_2O_3 (<0.99%) and display patterns of increasing TiO_2, V_2O_5, Al_2O_3, and Cr_2O_3 with decreasing Fe_2O_3/FeO contents. Magnetite has very low concentrations of

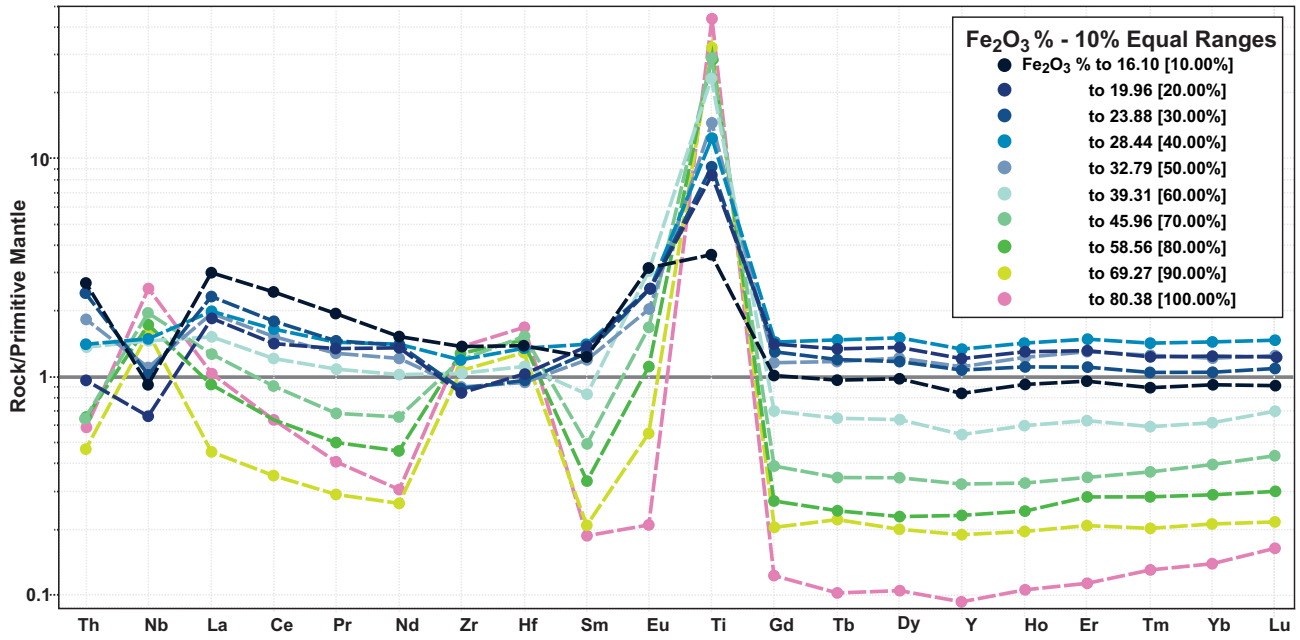

Figure 4. Primitive-mantle normalized plot for the Butler West, Butler East, and Thunderbird intrusions grouped according to weight % Fe_2O_3. Normalizing values are from Sun and McDonough (1989).

SiO_2, Al_2O_3, MgO, MnO, CoO, NiO, CuO, and ZnO. Ilmenite grains contain significant MnO (<1.82%), V_2O_5 (<0.57%), and MgO (<0.41%) with only minor SiO_2, Al_2O_3, Cr_2O_3, Nb_2O_3, CoO, NiO, CuO, and ZnO. Primary magnetite-ilmenite pairs have been used to calculate the conditions of crystallization based on the method proposed by Spencer and Lindsley (1981), although large variations in data were observed, the approximate temperature of crystallization has been calculated as 400–500°C (Kuzmich, 2014). However, the calculated temperatures obtained are too low to represent crystallization of a gabbroic melt, which is suggested to be ~1100°C (Toplis and Carroll, 1995), and are interpreted instead to represent the conditions of oxy-exsolution from a primary ulvöspinel-magnetite solid solution (Kuzmich, 2014). Magnetite and ilmenite grains also display lower concentrations of highly compatible elements (e.g. V, Cr) with increasing stratigraphic height.

The study of silicate minerals was focused on the identification of end-member minerals. Pyroxene grains were largely composed of augite and pigeonite with lesser ferrosilite, enstatite, and/or wollastonite. Pyroxene grains have been partially to completely replaced by amphibole, which is dominantly composed of hornblende and actinolite with lesser pargasite. Plagioclase compositions display a trend of decreasing anorthite content with increased stratigraphic height. Basal plagioclase generally ranges from 53 to 67% An (labradorite) with a few analysis as high as 86% An (bytownite), whereas more evolved units contain plagioclase that is generally restricted to 37–52% An (andesine dominate).

Whole-Rock and Trace Element Geochemistry

The ferrogabbroic rocks display a large range of major element compositions due to the large variability in modal mineralogy. However, the major elements display positive trends of increasing SiO_2 contents with increasing Al_2O_3, CaO, MgO, and Na_2O and decreasing Fe_2O_3, MnO, V_2O_5, and TiO_2. Additionally, higher Fe_2O_3 contents (which may be used to estimate the amount of magnetite in the sample) correlate with increased TiO_2, V_2O_5, Cr, Ni, Co, and Zn contents.

Trace element diagrams display similar patterns between the Thunderbird and Butler intrusions (Fig. 4). The plots are characterized by slightly depleted LREE, flat HREE patterns, and positive Ti and weak negative Y anomalies. These patterns display a strong dependence on the concentration of magnetite-ilmenite within each sample (Fig. 4). Samples with high concentrations of Fe-Ti oxides (e.g. massive oxides) generally exhibit positive Nb, Zr, Hf, and Ti anomalies, whereas the oxide-free samples (e.g. gabbro) display negative Nb, Zr, and Hf anomalies. Additionally, oxide-rich samples contain lower trace element contents by an order of magnitude on average than the oxide-free samples but contain similar high field strength element (HFSE) contents. Apatite-bearing units display distinctly different trace element patterns that are characterized by one to two orders of magnitude higher concentrations of trace elements than the average ferrogabbroic rocks.

DISCUSSION

Formation of Layering

Igneous layering within the ferrogabbroic rocks is a

distinct feature observed throughout each intrusion. The most pronounced form of layering within these intrusions is composed of repeated partial to complete sequences characterized by sharp lower and upper contacts with gradational internal contacts. These cycles are composed of basal massive oxides that grade upwards into semi-massive oxides, followed by oxide-rich pyroxenite/melagabbro/gabbro, oxide-poor melagabbro/gabbro/leucogabbro/anorthosite, and topped with oxide-free gabbro/leucogabbro/anorthosite. These layers are interpreted to have formed through intermittent convection currents (Kuzmich, 2014) similar to what it has been proposed by Naslund et al. (1991) for the Skaergaard intrusion. Each convective cycle supplied the crystallizing front with dense, Fe-Ti oxides and in periods of quiescence the magma deposited crystals/minerals in order of decreasing density.

Layers of stratigraphically conformable pegmatitic units composed of oxide-bearing ferrogabbro occur within all intrusions, but are most prevalent within the Butler West intrusion. These units display gradational contacts and are mineralogically identical to the surrounding medium-grained ferrogabbro. These layers are thought to have formed in the presences of relatively volatile-rich phases and possibly reflect introduced fluids from the country rocks or from the migration of fluid dissolves in the intercumulus melt during the cooling of the cumulate pile within the intrusion (e.g. Nicholson and Mathez, 1991; Boudreau, 1999).

Petrogenesis of Butler and Thunderbird Intrusions

The Butler and Thunderbird intrusions represent three of numerous gabbroic intrusions currently recognized within the McFaulds Lake area that are characterized by extreme degrees of iron enrichment (Metsaranta et al., 2015). These intrusions are proposed by Kuzmich (2014) to have originated from a mantle plume source that underplated the McFaulds Lake greenstone belt. The plume-related magmas likely differentiated into a primitive ultramafic portion and an evolved mafic portion, similar to what has been proposed for the Emeishan plume (Zhou et al., 2008). The evolved mafic magma would exist as a reduced, anhydrous melt that was variably contaminated by the depleted mantle, as suggested by enriched mid-ocean ridge basalt (E-MORB) trace element patterns.

The plume-sourced mafic melt underwent a two-stage evolution, the first of which is characterized by a system that was closed to oxygen, anhydrous, reduced, and underwent crystallization of Fe-poor mineral phases (e.g. olivine, plagioclase), which resulted in an Fe-rich residual magma. The second stage is characterized by shallow emplacement within a system partially open to oxygen, which allowed the magma to initiate

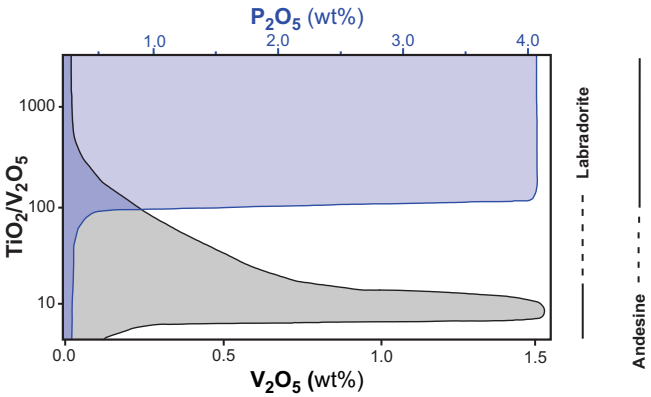

Figure 5. Binary plot of TiO_2/V_2O_5 ratio versus V_2O_5 (bottom axis) and versus P_2O_5 (top axis), which is use as proxy for V-rich magnetite and for apatite, respectively, in the Butler and Thunderbird intrusions (Kuzmich, 2014).

the crystallization of Fe-Ti oxides. The onset of magnetite-ilmenite crystallization would reverse the evolution from Fe-Ti enrichment to a system that would follow an anorthositic-granitic evolutionary trend. Kuzmich (2014) suggested the same mantle plume that generated the ferrogabbroic intrusions also produced the voluminous Cr-Ni-PGE-mineralized ultramafic intrusion (e.g. Eagle's Nest, Black Thor) and resulted in a thinned lithosphere that facilitated the coeval Cu-Zn VMS occurrences at ca. 2735 Ma (Mungall et al., 2010).

IMPLICATIONS FOR EXPLORATION

Through this study on the Fe-Ti-V-(P) mineralized ferrogabbroic intrusions in the McFaulds Lake greenstone belt, variations in the TiO_2/V_2O_5 whole rock ratio have demonstrated the potential to be a useful tool in the interpretation of stratigraphy and to aid in the determination of prospective vanadium and/or possible phosphorous horizons (Fig. 5). The ratio is interpreted to increase during magmatic evolution and, with large datasets, can be used to interpret stratigraphic way-up. The use of the TiO_2/V_2O_5 ratio is particularly of interest due to the resistant nature of the host oxide minerals (magnetite and ilmenite) to metamorphism and the minerals can be analysed at relatively low cost (e.g. X-ray fluorescence) and are independent of the bulk silicate composition.

The maximum vanadium potential for the Butler and Thunderbird intrusions, based on a data set of >2600 samples (data provided by from MacDonald Mines Ltd. and Noront Resources Ltd.), can be estimated using Figure 5. Samples that have TiO_2/V_2O_5 values of ~8 to 12 display the richest vanadium-bearing magnetite and therefore the highest potential for economic concentrations in massive and semi-massive oxide layers. The vanadium potential exponentially decreases as the TiO_2/V_2O_5 ratio increases; for example, a ratio of ~40 is proposed to represent one third of the potential

as values in the ~8 to 12 range, and ratios of >500 display no potential for vanadium mineralization, even within massive oxide units. Conversely, all apatite mineralization (<4 wt% P_2O_5) is associated with higher TiO_2/V_2O_5 ratios (>100), which may represent Fe-Ti-P-rich melts (nelsonite).

ACKNOWLEDGEMENTS

We would like to acknowledge the efforts of Riku Metsaranta of the Ontario Geological Survey (OGS) for his insights during the field investigation and also many discussions regarding the McFaulds greenstone belt. We would also like to thank MacDonald Mines Exploration Ltd. and Noront Resources Ltd. for sharing their geological datasets and allowing us to sample their drill core from the Butler and Thunderbird properties, respectively. We are grateful to the Geological Survey of Canada, under the TGI-4 program, and the OGS for providing financial and analytical supports that permitted this project to become a reality. We also extend our acknowledgements to Anne Hammond and Kristy Tavener at Lakehead University for their excellent lapidary work. We also thank Sarah Dare for timely and comprehensive reviews that improved the final version of this contribution.

REFERENCES

Boudreau, A.E., 1999. Fluid fluxing of cumulates: the J-M Reef and associated rocks of the Stillwater Complex, Montana; Journal of Petrology, v. 40, p. 755–772.

Kuzmich, B., 2014. Petrogenesis of the Ferrogabbroic Intrusions and Associated Fe-Ti-V-P Mineralization within the McFaulds Greenstone belt, Superior Province, Northern Ontario, Canada; M.Sc. thesis, Lakehead University, Thunder Bay, Ontario, 496 p.

Kuzmich, B., Hollings, P., and Houlé, M.G., 2013. Petrogenesis of ferrogabbroic intrusions and associated iron titanium-vanadium-phosphorus mineralization within the McFaulds Lake greenstone belt, Superior Province, northern Ontario; *In:* Summary of Field Work and Other Activities 2013; Ontario Geological Survey, Open File Report 6290, p. 56-1 to 56-9.

Kuzmich, B., Hollings, P., and Houlé, M.G., 2015. Lithogeochemistry of iron titanium-vanadium-phosphorus mineralized mafic intrusions in the McFaulds Lake area, northern Ontario; Ontario Geological Survey, Miscellaneous Release, Data 318.

Metsaranta, R.T. and Houlé, M.G., 2011. McFaulds Lake area regional compilation and bedrock mapping project update, *In:* Summary of Field Work and Other Activities 2011; Ontario Geological Survey, Open File Report 6270, p. 12-1 to 12-12.

Metsaranta, R.T. and Houlé, M.G., 2012. Progress on the McFaulds Lake ("Ring of Fire") region data compilation and bedrock geology mapping project, *In:* Summary of Field Work and Other Activities 2012; Ontario Geological Survey, Open File Report 6280, p. 43-1 to 43-12.

Metsaranta, R.T., Houlé, M.G., McNicoll, V.J., and Kamo, S.L., 2015. Revised geological framework for the McFaulds Lake greenstone belt, Ontario, *In:* Targeted Geoscience Initiative 4: Canadian Nickel-Copper Platinum Group Elements-Chromium Ore Systems — Fertility, Pathfinders, New and Revised Models, (ed.) D.E. Ames and M.G. Houlé; Geological Survey of Canada, Open File 7856, p. 61–73.

Mungall, J.E., Harvey, J.D., Balch, S.J., Azar, B., Atkinson, J., and Hamilton, M.A., 2010. Eagle's Nest: A magmatic Ni-sulfide deposit in the James Bay Lowlands, Ontario, Canada, *In:* The Challenge of Finding New Mineral Resources: Global Metallogeny, Innovative Exploration, and New Discoveries, Volume I: Gold, Silver, and Copper-Molybdenum, (ed.) R.J. Goldfarb, E.E. Marsh, and T. Monecke; Society of Economic Geologists, Special Publication 15, p. 539–559.

Naslund, H., Turner, P., and Keith, D., 1991. Crystallization and layered formation in the Middle zone of the Skaergaard intrusion; Bulletin of Geologic Society Denmark, v. 38, p. 359–367.

Nicholson, D.M. and Mathez, E.A., 1991. Petrogenesis of the Merensky Reef in the Rustenburg section of the Bushveld Complex; Contributions to Mineralogy and Petrology, v. 107, p. 293–309.

Ontario Geological Survey–Geological Survey of Canada, 2011. Ontario airborne geophysical surveys, gravity gradiometer and magnetic data, grid and profile data (ASCII and Geosoft® formats) and vector data, McFaulds Lake area; Ontario Geological Survey, Geophysical Data Set 1068.

Spencer, K. and Linsley, D., 1981. A solution model for coexisting iron-titanium oxides; American Mineralogist, v. 66, p. 1189–1291.

Sun, S.S. and McDonough, W.F., 1989. Chemical and isotopic systematics of oceanic basalts: implications for mantle composition and processes, *In:* Magmatism in the Ocean Basins, (ed.) A.D. Saunders and M.J. Norry; Geological Society, Special Publication 42, p. 313–345.

Toplis, M. and Carroll, M., 1995. An experimental study of the influence of oxygen fugacity on Fe-Ti-oxide stability, phase relations, and mineral-melt equilibrium in ferro-basaltic systems; Journal of Petrology, v. 36, p. 1137–1170.

Zhou, M.-F., Arndt, N., Malpas, J., Wang, C., and Kennedy, A., 2008. Two magma series and associated ore deposit types in the Permian Emeishan large igneous province, SW China; Lithos, v. 103, p. 352–368.

GEOLOGICAL SURVEY OF CANADA
OPEN FILE 7856

Targeted Geoscience Initiative 4: Canadian Nickel-Copper-Platinum Group Elements-Chromium Ore Systems — Fertility, Pathfinders, New and Revised Models

Regional characterization of ultramafic to mafic intrusions in the La Grande Rivière and Eastmain domains, Superior Province, Quebec

Michel G. Houlé[1], Jean Goutier[2], Anne-Aurélie Sappin[1], and Vicki J. McNicoll[3]

[1]Geological Survey of Canada, Québec, Quebec
[2]Ministère de l'Énergie et des Ressources naturelles, Rouyn-Noranda, Quebec
[3]Geological Survey of Canada, Ottawa, Ontario

2015

© Her Majesty the Queen in Right of Canada, as represented by the Minister of Natural Resources Canada, 2015

This publication is available for free download through GEOSCAN (http://geoscan.nrcan.gc.ca/)

Recommended citation

Houlé, M.G., Goutier, J., Sappin, A.-A., and McNicoll, V.J., 2015. Regional characterization of ultramafic to mafic intrusions in the La Grande Rivière and Eastmain domains, Superior Province, Quebec, *In:* Targeted Geoscience Initiative 4: Canadian Nickel-Copper-Platinum Group Elements-Chromium Ore Systems — Fertility, Pathfinders, New and Revised Models, (ed.) D.E. Ames and M.G. Houlé; Geological Survey of Canada, Open File 7856, p. 125–137.

Publications in this series have not been edited; they are released as submitted by the author.

Contribution to the Geological Survey of Canada's Targeted Geoscience Initiative 4 (TGI-4) Program (2010–2015)

TABLE OF CONTENTS

Regional characterization of ultramafic to mafic intrusions in the La Grande Rivière and Eastmain domains, Superior Province, Quebec

Michel G. Houlé[1]*, Jean Goutier[2], Anne-Aurélie Sappin[1], and Vicki J. McNicoll[3]

[1]Geological Survey of Canada, 490 rue de la Couronne, Québec, Quebec G1K 9A9
[2]Ministère de l'Énergie et des Ressources naturelles, 70, avenue Québec, Rouyn-Noranda, Quebec J9X 6R1
[3]Geological Survey of Canada, 601 Booth Street, Ottawa, Ontario K1A 0E8
*Corresponding author's e-mail: michel.houle@rncan-nrcan.gc.ca

ABSTRACT

The Eeyou Istchee Baie-James region is dominantly underlain by Archean rocks belonging to the Superior Province, which is mainly composed of juxtaposed sequences of predominantly sedimentary, volcano-plutonic and plutonic rocks. The distribution of mafic to ultramafic intrusions and ultramafic volcanism reveals a general abundance at the regional scale, with the greatest volume in the La Grande Rivière and Eastmain domains of the La Grande Subprovince in the central-eastern part of the Superior Province flanked by the Opinaca Subprovince to the south, the Ashuanipi Subprovince to the east, and the Minto Subprovince to the north.

Preliminary geochronological results in the Eeyou Istchee Baie-James region indicate that the ultramafic-mafic magmatism extended over a period of more than 200 Ma, from ca. 2.88 Ga to 2.63 Ga. Various types of ultramafic to mafic magmatism have been documented in the La Grande Rivière and Eastmain domains and their vicinity: 1) ultramafic lavas and ultramafic intrusions of komatiitic affinity; 2) dominantly ultramafic intrusions; 3) dominantly mafic intrusions; 4) ultramafic to mafic intrusions of alkaline affinity; and 5) lesser volumes of ultramafic lamprophyres. Several of these ultramafic to mafic intrusion types also contain Cr-(PGE), Ni-Cu-(PGE), and Fe-Ti-(V) mineralization. The most important examples of these types of mineralization include the Menarik Complex (Cr-(PGE)), the Lac des Montagnes intrusions (Cr-(PGE)), the Lac Gayot intrusions (Ni-Cu-(PGE)), the Nisk intrusion (Ni-Cu-(PGE)), and the baie Chapus Pyroxenite (Fe-Ti-(V)).

As part of the Targeted Geoscience Initiative – Phase 4 (TGI-4), the Geological Survey of Canada and the Ministère de l'Énergie et des Ressources naturelles (MERN) have undertaken reconnaissance work to better characterize these types of intrusions in terms of their distribution, geochemical and mineralogical characteristics, and prospectivity for the above-mentioned mineralization types. Studies are ongoing for intrusions in the Lac Yasinski, Lac Pelletan, Lac Gayot, Lac des Montagnes, and Lac Fed areas, in addition to a more regional study underway in the area south of the La Grande 4 Reservoir (Lac Richardie). New geochronological work is also in progress, which will allow us to better understand the temporal distribution of the ultramafic to mafic magmatism in this portion of the Superior Province. A better understanding of these ultramafic and mafic intrusions will also reveal whether they demonstrate similar characteristics to ultramafic to mafic intrusions recently discovered in the McFaulds Lake area of Ontario (a.k.a. "Ring of Fire"), which contains major Cr-(PGE) and Ni-Cu-(PGE) deposits.

INTRODUCTION

Mafic and ultramafic intrusions and ultramafic volcanic rocks are widely distributed throughout the Superior Province, many of which host significant Cr-platinum-group element (PGE), Ni-Cu-(PGE) and Fe-Ti-(V) orthomagmatic mineralization (see Fig. 1 in Houlé et al., 2015). Recent discoveries of world-class chromite deposits (e.g. Black Thor, Big Daddy), Ni-Cu-(PGE) deposits (e.g. Eagle's Nest), and Fe-Ti-(V) occurrences (e.g. Thunderbird) in the McFaulds Lake greenstone belt (MLGB) in northern Ontario (see Metsaranta et al., 2015) highlight the mineral potential of this region, in addition to possible correlative areas eastward across the Superior Province, such as the La Grande Rivière and Eastmain domains within the Eeyou Istchee Baie-James region in northern Quebec (Houlé et al., 2015).

As part of the High-Mg Ultramafic to Mafic Ore Systems subproject under the Targeted Geoscience Initiative 4 (TGI-4), the Geological Survey of Canada

Houlé, M.G., Goutier, J., Sappin, A.-A., and McNicoll, V.J., 2015. Regional characterization of ultramafic to mafic intrusions in the La Grande Rivière and Eastmain domains, Superior Province, Quebec, *In:* Targeted Geoscience Initiative 4: Canadian Nickel-Copper-Platinum Group Elements-Chromium Ore Systems — Fertility, Pathfinders, New and Revised Models, (ed.) D.E. Ames and M.G. Houlé; Geological Survey of Canada, Open File 7856, p. 125–137.

and the Ministère de l'Énergie et des Ressources naturelles (MERN) undertook a reconnaissance study to better characterize some of the numerous ultramafic to mafic intrusions within the La Grande Rivière and the Eastmain domains within the La Grande Subprovince in the Eeyou Istchee Baie-James region (Fig. 1). The main goal of this contribution are to present the spatial and temporal distribution of these ultramafic to mafic intrusions including the main geological findings from local-scale studies conducted across these domains over the past couple of years in the Lac Yasinski, Lac Pelletan, Lac Richardie, and Lac Gayot areas within the La Grande Rivière domain and the Lac des Montagnes and Lac Fed areas within the Eastmain domain (Fig. 1). Some economic implications at the regional scale will be also briefly discussed.

GEOLOGICAL SETTING

The Eeyou Istchee Baie-James region is dominantly underlain by Archean rocks of the Superior Province, which are mainly composed of juxtaposed sequences of predominantly sedimentary, volcano-plutonic and plutonic rocks. The distribution of ultramafic to mafic intrusions and ultramafic volcanism reveals a general abundance at the regional scale, with the greatest volume in the La Grande Rivière and Eastmain domains (La Grande Subprovince) in the central-east part of the Superior Province, flanked by the Opinaca Subprovince to the south, the Ashuanipi Subprovince to the east, and the Minto Subprovince to the north (Fig. 2).

RESULTS

Spatial and Temporal Distribution of Ultramafic and Mafic Intrusions

Various types of ultramafic to mafic magmatism have been documented in the La Grande Rivière and Eastmain domains and vicinity including (1) ultramafic lavas and ultramafic intrusions of komatiitic affinity, (2) ultramafic-dominated intrusions, (3) mafic-dominated intrusions, (4) ultramafic to mafic intrusions of alkaline affinity, and (5) ultramafic lamprophyres. To date, the komatiitic rocks have been recognized essentially within the La Grande Rivière domain but also occur sporadically within the Eastmain domain. The main occurrences of komatiitic rocks are recognized in the Guyer Group within the Lac Guyer-Keyano greenstone belt, in the Dalmas Formation within the Escale-Trieste greenstone belt, and in the Gayot Complex within the Vénus-Moyer greenstone belt but some have been also reported in the Laforge-Aquilon and Coulon greenstone belts (Figs. 1, 2). The presence of komatiitic rocks in the Eastmain domain is more restricted; they occur mostly in the Komo and Natal formations within the Basse Eastmain greenstone belt and at the base of the Haute Eastmain greenstone belts in the Lac Lépante area (Figs. 1, 2). The ultramafic-dominated and mafic-dominated intrusions are widespread across these domains and commonly coexist. However, they appear to be locally grouped and form ultramafic-dominated areas and mafic-dominated areas, which broadly alternate from north to south and trend east-west in the Eeyou Istchee Baie-James area (Fig. 2). The ultramafic to mafic alkaline intrusions are much more restricted and occur predominantly in the Lac Pelletan and Lac Richardie areas of the La Grande Rivière domain and in its vicinity within the Opinaca Subprovince near the boundary of between these two lithotectonic entities. Ultramafic lamprophyre is relatively widespread throughout the area but extremely marginal in abundance.

Preliminary geochronological results indicate that the ultramafic-mafic magmatism in the La Grande Rivière and Eastmain domains may have extended over a period of more than 200 Ma, from ca. 2.88 to 2.63 Ga. The upper age constraint is provided by a felsic volcanic rock in the Lac Gayot area within the Vénus-Moyer greenstone belt that yielded an U-Pb age of ca. 2880 Ma (David et al., 2009), which would constrained the komatiite lava flows in that greenstone belt the oldest recognized manifestation of the ultramafic magmatism in the La Grande Rivière domain. The lower age constraint is defined by a maximum age of ca. 2630 Ma (U-Pb), which was obtained in the course of this study from an alkaline gabbroic rock in the Lac Pelletan area within the Opinaca Subprovince at the margin of the La Grande Rivière domain (see below).

Local-Scale Studies – La Grande Rivière Domain

Lac Yasinski Area

Regional bedrock mapping has been conducted in the Lac Yasinski area by the ministère de l'Énergie et des Ressources naturelles (MERN) in the late 1990s, where a series of ultramafic to mafic intrusions (e.g. Menarik Complex, baie Chapus Pyroxenite) was recognized and further characterized by Cimon et al. (1997), Houlé (2000), Houlé et al. (2002), and Houlé and Goutier (unpub. data). However, during the course of this study, reassessment of the baie Chapus Pyroxenite has been undertaken by Sappin et al. (2015) and new geochronological work has been carried out on this intrusion and also on the Menarik Complex (MC) to better understand their temporal relationship.

The MC (~2 x 3 km; Fig. 1) is one of the largest layered ultramafic-mafic intrusions found in the La Grande Rivière domain. It consist of a lower Ultramafic Zone composed of peridotite, poikilitic

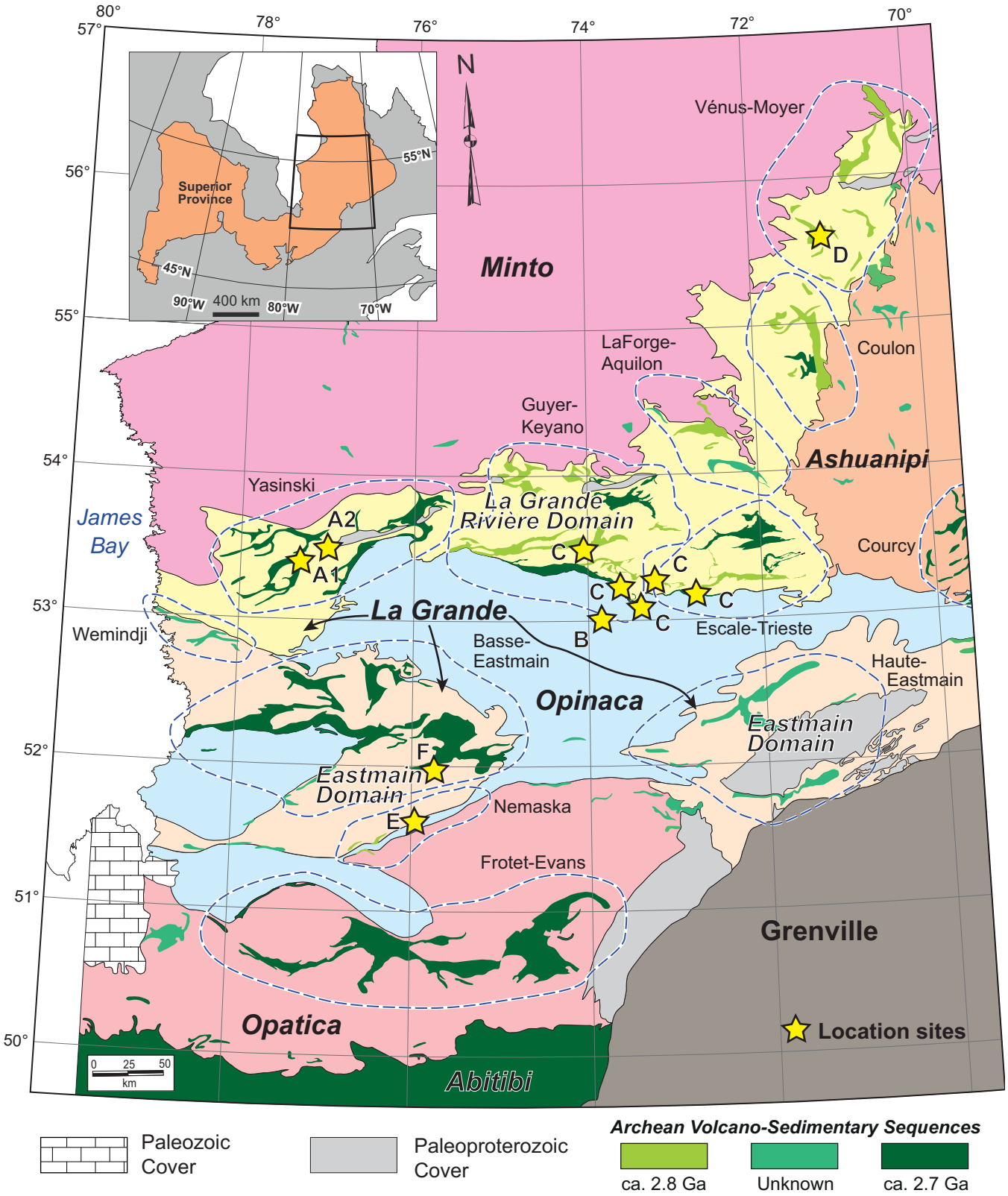

Figure 1. Simplified geological map of the eastern part of the Superior Province showing the distribution of the main Archean volcano-sedimentary sequences within the La Grande Rivière and Eastmain domains of the La Grande Subprovince (modified from Thériault and Beauséjour, 2012). Yellow stars indicate the location sites: A = Lac Yasinski (A1 = Menarik Complex, A2 = baie Chapus Pyroxenite); B = Lac Pelletan; C = Lac Richardie; D = Lac Gayot; E = Lac des Montagnes; and F = Lac Fed. Dashed blue outlines highlight the greenstone belts.

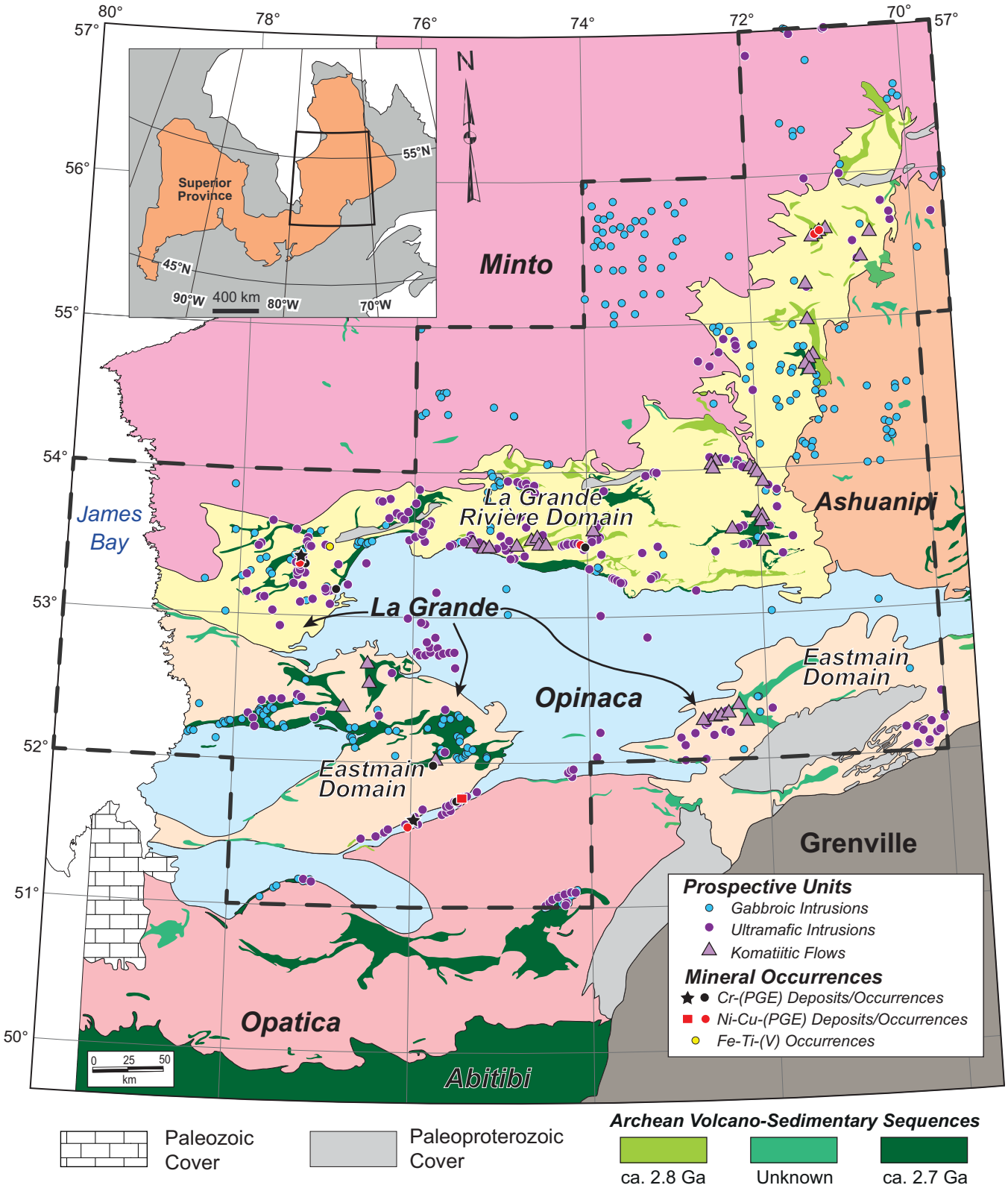

Figure 2. Simplified geological map of the eastern part of the Superior Province showing the distribution of the prospective units (ultramafic and mafic intrusions and komatiitic flows) and the main Cr-(PGE), Ni-Cu-(PGE), and Fe-Ti-(V) deposits and occurrences within the La Grande Rivière and Eastmain domains of the La Grande Subprovince (modified from Thériault and Beauséjour, 2012). Dashed black outline referred to the area where prospective units have been extracted from the SIGEOM.

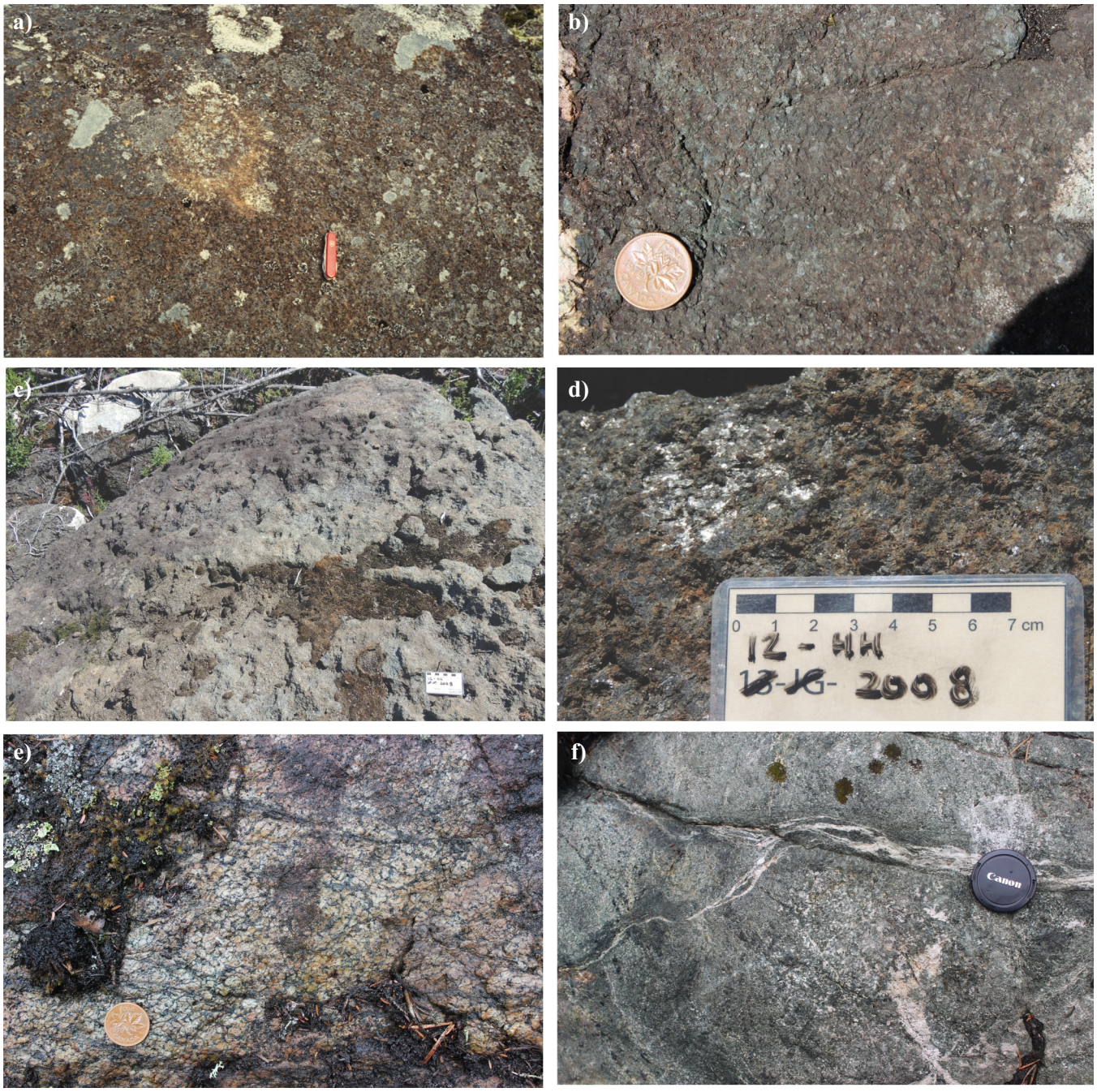

Figure 3. Typical lithologies associated with the ultramafic-dominated intrusion within the La Grande Rivière and Eastmain domains. **a)** Typical poikilitic peridotite from the Menarik Complex. **b)** Typical pyroxenite from the baie Chapus Pyroxenite. **c)** Phlogopite pyroxenite from an alkaline intrusion in the La Grande Rivière domain. **d)** Close-up of the phlogopite pyroxenite showing in (c) with a pyroxene porphyroblast of 4 cm in diameter. **e)** Chromite-bearing peridotite from the Lac des Montagnes intrusions. **f)** Varitextured gabbro from the Lac des Montagnes intrusions.

peridotite (Fig. 3a) with lesser pyroxenite and chromite-rich horizons and an overlying Mafic Zone composed of gabbroic rocks. The intrusive rocks mostly have high Cr_2O_3 contents and flat rare earth elements (REE) profiles but their mineral compositions are unknown as almost all primary mineralogy has been replaced except for chromite. The composition of the chromite cores plot in a limited range of Cr# (100*Cr/(Cr+Al)), from 69 to 58, but exhibit a much wider range of Mg# ($100*Mg^{2+}/(Mg^{2+}+Fe^{2+})$), from 61 to 2, that are interpreted to reflect the primary composition of the parental magma and the subsolidus reequilibration with the silicates, respectively (Fig. 4a). A pegmatitic gabbroic rock has been sampled and yields a crystallization age of ca. 2750 Ma.

The baie Chapus Pyroxenite (~1 x 3 km; Fig. 1) is a broadly layered intrusion, composed mainly of pyroxenite (Fig. 3b), plagioclase pyroxenite, and olivine

pyroxenite, in addition to mesocratic gabbro and lesser peridotite and dunite. Significant accumulations of magnetite were found near the summit of the intrusion. The intrusive rocks have locally high-FeO_t content and are enriched in light REE compared with heavy REE and contain preserved clinopyroxene with relatively primitive composition ($Mg\#_{92–73}$). Near the top of the intrusion, a pegmatitic phase composed of chlorite, hornblende, plagioclase with lesser ilmenite and apatite, yielded an age of ca. 2802 Ma, which is significantly older than the age obtained from the MC. However, this age is interpreted to represent an inherited zircon age based on the presence of numerous tonalitic enclaves and trace element signature that appeared to be the result of mixing between the uncontaminated pyroxenite of the intrusion and the adjacent tonalitic rocks or underlying Mesoarchean basement.

Lac Pelletan Area

Regional bedrock mapping conducted by the MERN in the Lac Pelletan area during the summer 2012 led to the discovery of an ultramafic intrusion (Fig. 1) characterized by an uncommon metamorphic mineralogical assemblage (e.g. anthophyllite, hornblende) and texture (Chartier-Montreuil, 2013) in the Eeyou Istchee Baie-James region.

This ultramafic-mafic intrusion (~90 x 240 m) has been metamorphosed to upper amphibolite facies but is relatively undeformed. It consists primarily of an olivine pyroxenite unit that contains typically large orthopyroxene porphyroblasts (from mm to 5 cm-scale, but locally up to 10 cm in diameter) and a minor gabbroic unit. The presence of phlogopite and generally high K_2O contents of these intrusive rocks suggest an alkalic affinity for this intrusion. These rocks are also enriched in light REE compared with heavy REE and the ultramafic unit contains relicts of olivine of intermediate composition ($Mg\#_{79–73}$). U-Pb geochronology on the gabbroic unit of this intrusion yielded an age of ≤2630 Ma.

Lac Richardie Area

Several ultramafic intrusions were inventoried during a mapping program conducted in the summer 2013 by the MERN in the Lac Richardie area (Fig. 1) within the La Grande Rivière domain and Opinaca subprovince and were further characterized by Grzela et al. (2014).

These ultramafic intrusions (<10 km length) were subdivided into two main types, based on field observations, petrographic work, and geochemical analysis. Type I intrusions are composed mainly of peridotite with minor layers of chromite. The intrusions are generally enriched in Cr_2O_3 and PGE and exhibit flat REE profiles. Type II intrusions are composed mainly of olivine pyroxenite and pyroxenite with localized peridotite and they exhibit light REE enrichment profiles. Several subtypes have been defined for the type II intrusions: (1) a subtype characterized by the presence of phlogopite and enrichment in K_2O suggesting an alkalic affinity (Fig. 3c,d), (2) a subtype characterized by the lack of phlogopite and a depletion in K_2O, and (3) a subtype characterized by an enrichment in FeO. The mineral composition and ages of these ultramafic intrusions have not been studied.

Lac Gayot Area

A komatiitic succession, including lava flows and intrusions, has been discovered within the Vénus-Moyer greenstone belt (Fig. 1) during bedrock regional mapping by the MERN and prospecting by Virginia Mines in 1998. This area has not been revisited by the authors but new petrographic work and geochemical analysis has been conducted during the course of this study (Huot et al., 2015).

The komatiitic succession is subdivided into a lower and upper komatiitic unit. The lower unit consists of peridotite, with local harrisite, pyroxenite, and gabbro, which are interpreted to be intrusive in origin based on the lack of volcanic features and local discordant relationships with the country rocks exhibiting metamorphism and metasomatism contacts. The upper unit is composed of very fine-grained ultramafic rocks that are likely extrusive, as suggested by poorly developed pillowed flows and volcanic breccias (Huot et al., 2015).

Local-Scale Studies – Eastmain Domain

Lac des Montagnes

The Lac des Montagnes ultramafic-dominated intrusion (LMI) is part of a series of east-northeast-trending ultramafic intrusions found in the Nemaska volcano-sedimentary belt (Fig. 1) and referred as the Lac des Montagnes intrusive suite (Fig. 2). A reconnaissance study was conducted by Bédard et al. (2014, 2015) to better characterize this intrusion.

This ultramafic-dominated intrusion (~185 x 1100 m) is mainly composed of peridotite (Fig. 3e), olivine pyroxenite and pyroxenite with lesser chromite-rich layers and is overlain by a mafic sequence composed of mesocratic to melanocratic gabbroic rocks (Fig. 3f). Geochemical analysis of this intrusion is in progress. The core compositions of the chromite have a wider range of Cr# than other intrusions, from 98 to 62, but some of these extreme values might be related to a loss of aluminum during the alteration. However, the range exhibit a of Mg#, which range from 49 to 9, are similar to the other intrusions in the area (Fig. 4b). The intrusion is interpreted to possess komatiitic affinities, based on the occurrence of randomly-oriented olivine

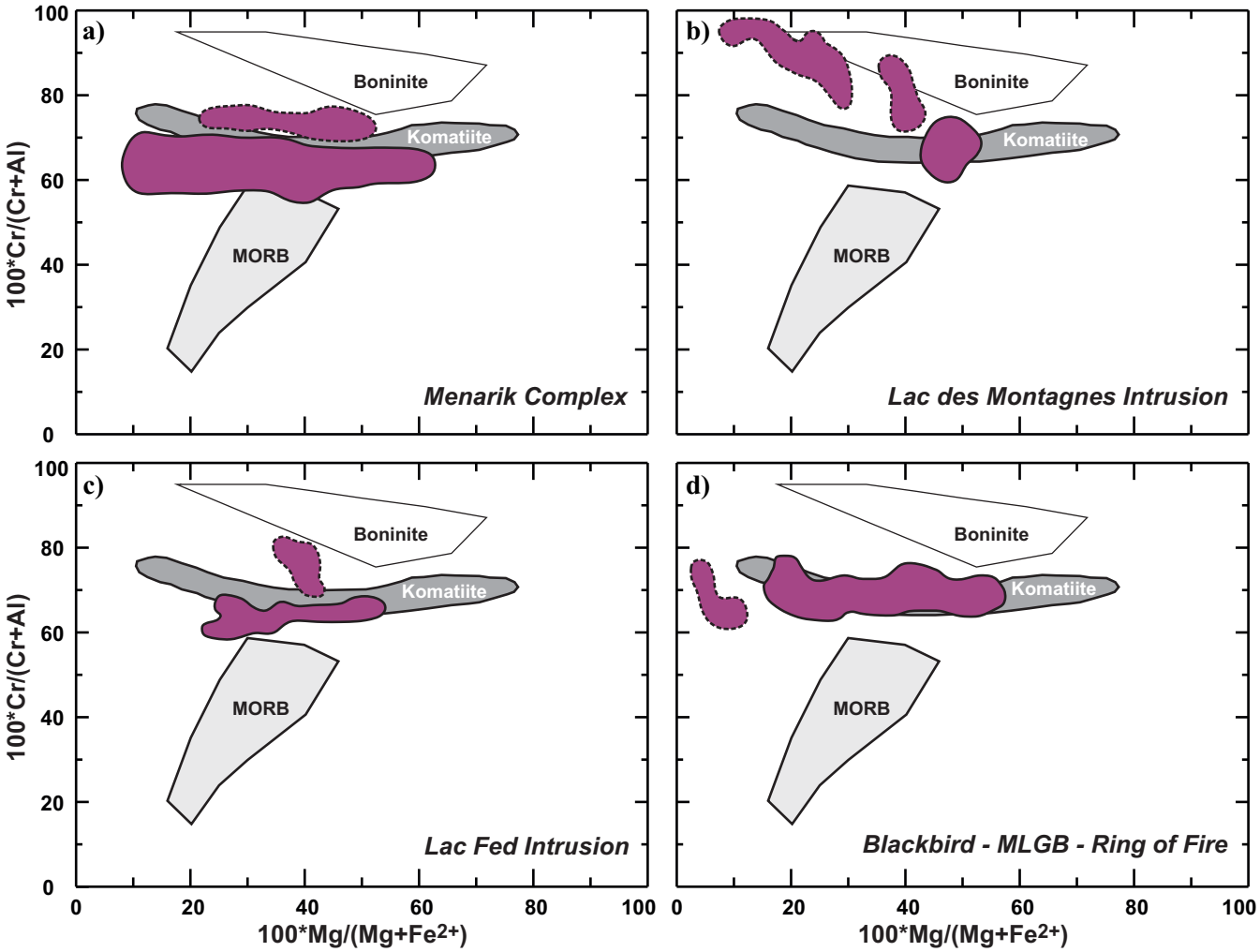

Figure 4. Typical compositions of chromite cores obtained by electron microprobe analysis (in purple) associated with some of the ultramafic-dominated intrusions in the La Grande Rivière and Eastmain domains. **a, b, c, d)** Cr# (100*Cr/(Cr+Al)) versus Mg# (100*Mg 2+/(Mg 2+ + Fe 2+)), for the Menarik Complex (a), the Lac des Montagnes intrusions (b), the Lac Fed intrusion (c), and the Blackbird deposit (d) in the McFaulds Lake greenstone belt (MLGB) (data from Azar, 2010). Fields for MORB and the boninites are from Bédard and Hébert (1996) and field for the komatiites is from Liipo et al. (1995). Dashed outlines on a, b, c, and d represent chromite core compositions that might have been modified by subsequent alteration.

spinifex texture near the base of the intrusion, chromite composition that is similar to typical chromite composition of komatiites, and the presence of olivine with high Mg number ($Mg\#_{91–89}$). A pegmatitic gabbroic rock was sampled for geochronological work and yielded an age of ca. 2802 Ma, which is interpreted as the crystallization age.

Lac Fed Area

The Lac Fed intrusion (Fig. 1) has been recognized by Labbé and Grant (1998) during a bedrock geological mapping conducted by the MERN. This site was not visited during the course of this study; however, a suite of samples for geochemical analysis was provided by Azimut Exploration Inc. and characterized by Fecteau (2013).

This ultramafic intrusion (~1 x 3 km) is composed mainly of peridotite and chromite-bearing peridotite that includes chromitite layers. Komatiite lava flows containing spinifex textures have also been recognized in the vicinity of the intrusion by Labbé and Grant (1998) and are interpreted to be located in its stratigraphic hanging wall. The intrusive rocks have high Cr_2O_3 contents. The core compositions of the chromite have a limited range of Cr#, from 80 to 64, but exhibit a much wider range of Mg#, from 53 to 35 (Fig. 4c). However, despite all composition reported are from the cores of the chromite grains, not all appear to represent a primary composition and may reflect some subsolidus re-equilibration with the silicates and post-magmatic alteration, as suggested for chromite from the LMI. The chromite composition, similar to the composition of chromite from komatiites, coupled with the presence of komatiite nearby suggests a komatiitic affinity for this ultramafic intrusion. The REE contents and age of the Lac Fed intrusion are unknown.

Mineralization Styles

The La Grande Rivière and Eastmain domains host a diversity of mineralization styles (e.g. lode gold, iron ore, Li-Ta bearing pegmatite), including several ultramafic to mafic intrusions that contain Cr-(PGE), Ni-Cu-(PGE) or Fe-Ti-(V) orthomagmatic mineralization (Fig. 2).

Cr-(PGE) Mineralization

Numerous Cr-(PGE) deposits and occurrences have been identified within the La Grande Rivière and Eastmain domains but the MC and LMI within the Yasinski and the Nemaska greenstone belts, respectively, are the most important (Fig. 2).

The MC contains more 30 silicate-chromitite and chromitite seams distributed throughout the Ultramafic Zone. These chromite-rich horizons were divided into 3 types: (1) chromitite and silicate chromitite (Fig. 5a) are present in massive layers ranging from 30 cm to 1 m thick (>50% chromite), (2) homogeneous chromite-rich peridotite layers range from 5 to 30 cm (<50% chromite), and (3) olivine-rich peridotite interlayered with chromitite seams or chromite-rich peridotites that reach 2 m thick (Houlé, 2000). Two styles of PGE mineralization are also present in the MC with early PGE mineralization associated with chromitite seams and later PGE mineralization associated with Fe-Ni-Cu sulphide veins (Houlé et al., 2002).

The LMI occur has three main chromite-rich zones that are hosted within the ultramafic sequence (Williams, 1965; Bédard et al., 2014). The lower and upper chromitite zones are several cm-thick layers with up to 30% net-textured chromite, alternating with serpentinized peridotite with a cumulative thickness averaging ~10s m. The 10 m thick middle chromitite zone is the most important and consists of several massive to semi-massive chromitite (75–85% chromite) layers ranging from about 10 cm to 3 m thick alternating with serpentinized peridotite with well-preserved cumulate textures (Fig. 5b).

Other significant occurrences of Cr-(PGE) mineralization occur in the Lac Long intrusion (Fig. 5c) and in the Lac Fed intrusion (Fig. 5d) within the Guyer-Keyano and the Basse Eastmain greenstone belts, respectively (Fig. 1).

Ni-Cu-(PGE) Mineralization

Numerous Ni-Cu-(PGE) occurrences are present within the La Grande Rivière and Eastmain domains, the most of which are located within the komatiitic sequences in the Vénus-Moyer greenstone belt and within the Nisk intrusion in the Nemaska greenstone belt (Figs. 1, 2).

Several of these were found in the Mesoarchean subvolcanic to volcanic komatiitic sequences in the Lac Gayot area (Huot et al., 2015). Ni-Cu-(PGE) mineralization occurs as disseminated, blebby (Fig. 5g), net-textured, and massive sulphides hosted within komatiitic units and locally within the country rocks. Despite the presence of intrusive and extrusive komatiitic rocks in this area, the mineralization has only been recognized in only the intrusive component, which is interpreted as a magmatic feeder and subconcordant sills (Huot et al., 2015).

Several Ni-Cu-(PGE) mineral occurrences have been recognized in the Nemaska area and the Nisk-1 deposit is the most significant one. It occurs within a composite peridotitic sill at the contact between the lower and upper peridotite zones and is interpreted to have a komatiitic affinity (Vallée, 2012). The sulphide mineralization exhibits several sulphide facies (e.g. Fig. 5e). The most common are massive (Fig. 5f), net-textured, and disseminated sulphides, typical of what it is observed in komatiite-associated Ni-Cu-(PGE) deposits.

Fe-Ti-(V) Mineralization

Fe-Ti-(V) mineralization is relatively uncommon in the La Grande Rivière and the Eastmain domains. The only known example is found within the baie Chapus Pyroxenite where the mineralization is several metres wide and composed of a massive to semi-massive magnetite (55–90 % magnetite) layer that and extends more than 70 m (Fig. 5h). This layer of titaniferous and vanadiferous magnetitite layer, grades up to 66% Fe_2O_{3t}, 9.2% TiO_2 and 0.7 % V_2O_5 and is composed of magnetite enriched in Ti (340–49 860 ppm) and V (1310–7440 ppm), and low in Cr (<300 ppm), Al (<140 ppm) and Ni (<620 ppm) (Fig. 6; Sappin et al., 2015).

DISCUSSION

The spatial and temporal distribution of the ultramafic to mafic intrusions is still poorly constrained across the Eeyou Istchee Baie-James region despite our new TGI-4 investigations at several localities within the La Grande Rivière and Eastmain domains.

The ultramafic-mafic magmatism that occurred broadly between ca. 2.88 Ga and 2.63 Ga (this study) generated various types of ultramafic to mafic intrusions/lavas including komatiitic ultramafic units, ultramafic-dominated intrusions, mafic-dominated intrusions, alkaline ultramafic to mafic intrusions, and ultramafic lamprophyre. These intrusions/lavas have different levels of prospectivity to host Cr-(PGE), Ni-Cu-(PGE), and Fe-Ti-(V) orthomagmatic mineralization. Preliminary results suggest that the most prospective units are associated with ultramafic bodies that are enriched in olivine and exhibit a komatiitic affinity.

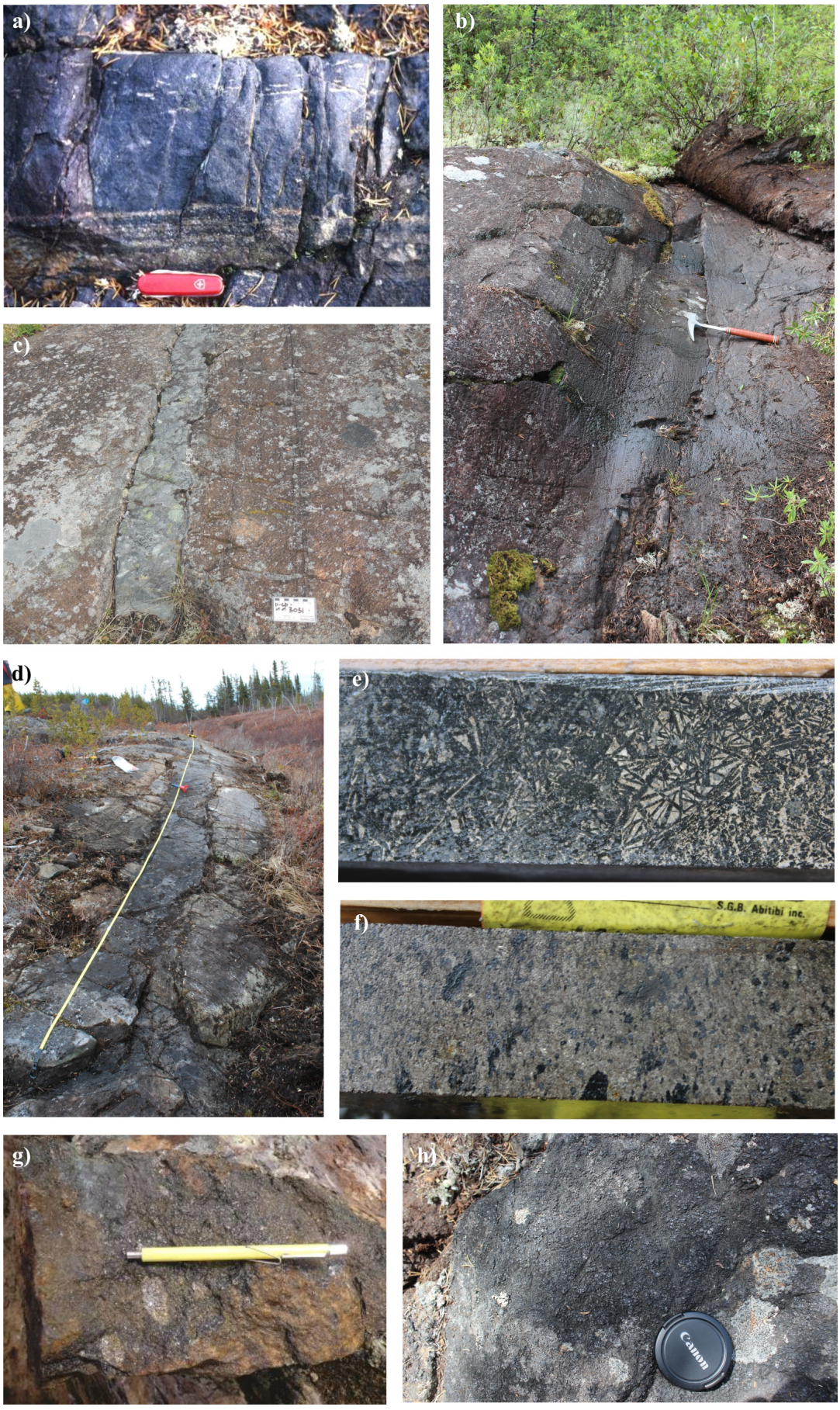

Figure 5. Typical examples of Cr-(PGE), Ni-Cu-(PGE), and Fe-Ti-(V) orthomagmatic mineralization observed in the La Grande Rivière and Eastmain domains. **a)** Chromitite and silicate chromitite seam from the Menarik Complex. Knife is 9 cm long. **b)** Massive and semi-massive chromitite seams from the Lac des Montagnes intrusions. Hammer is 30 cm. **c)** Thin massive chromite seam from the Lac Long intrusion. **d)** Massive chromite seam from the Lac Fed intrusion. Chisel is 24 cm long. **e)** Jack-straw-textured ore from the Nisk-1 deposit. Core is 4.5 cm in diameter. **f)** Massive to semi-massive sulphides from the Nisk-1 deposit. Core is 4.5 cm in diameter. **g)** Peridotite with disseminated sulphides containing cm-scale blebs of massive sulphides from the L occurrence in the Gayot area (courtesy of Mines Virginia). Magnetic pen is 12.5 cm long. **h)** Massive magnetitite from the Baie Chapus Pyroxenite. Lens cap is 4 cm.

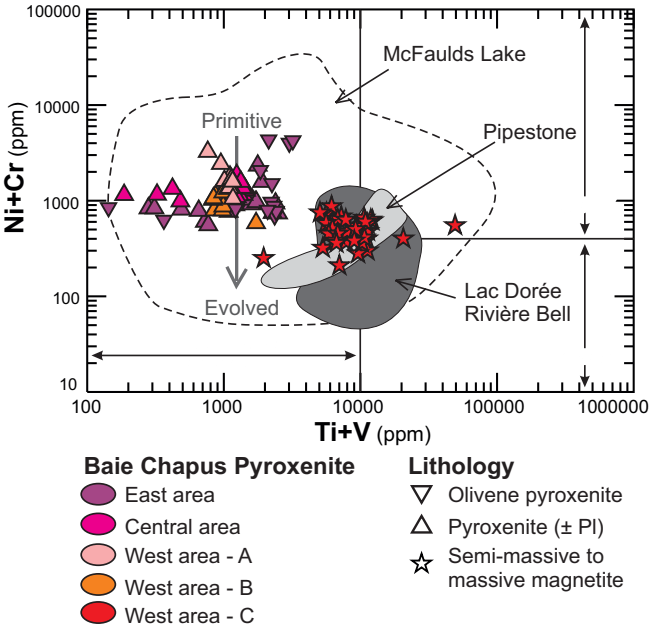

Figure 6. Ni+Cr versus Ti+V discriminant diagram from Méric (2011) for magnetite from Fe-Ti-V-P deposits and hydrothermal deposits. The data represent individual magnetite analyses from the baie Chapus Pyroxenite. The main geographic subdivisions of the baie Chapus Pyroxenite are shown on Fig. 2b in Sappin et al. (2015). The compositional field of magnetite are from TGI-4 study.

IMPLICATIONS FOR EXPLORATION

Numerous ultramafic to mafic intrusions and ultramafic volcanic rocks occur in the La Grande Rivière and Eastmain domains of the La Grande Subprovince, however, none are known to host world-class or very large Cr-(PGE), Ni-Cu-(PGE), and Fe-Ti-(V) concentrations of orthomagmatic mineralization. Although, preliminary observations suggest the Cr-(PGE), Ni-Cu-(PGE), and Fe-Ti-(V) mineralization is relatively modest, the composition of the analyzed chromite (MC, LMI, Lac Fed) (Fig. 4) and magnetite (baie Chapus) (Fig. 6) are similar to those from the McFaulds Lake area (Ring of Fire: Ontario). In light of these results, we suggest that the entire area, but more specifically the area where the ultramafic intrusions are the most abundant (Fig. 2), has potential for these styles of mineralization, which should be taken into account when planning exploration programs related to mafic and ultramafic intrusions in the Eeyou Istchee Baie-James region.

ACKNOWLEDGEMENTS

We express our sincere thanks to numerous colleagues from academia and students for their contribution to the High-Mg Ultramafic-Mafic Ore Systems: Marie-Pier Bédard, William Chartier-Montreuil, Antoine Fecteau, as well as Dr. Réjean Hébert and Dr. François Huot from Université Laval; Donald Grzela and Dr. Jonathan O'Neil from the University of Ottawa. We would like to thank Monarques Resources (Jonathan Lalancette et Jean-Marc Lacoste) and Azimut Exploration Ltd. (François Bissonnette, Jean-Marc Lulin) for their assistance, permission to access diamond-drill cores, grab samples, drill logs, drill-core pictures, thin sections, and geoscience data sets. The authors thank M. Choquette (Université Laval) for providing essential support during our work with the electron microprobe. We are also grateful to James Moorhead (MERN) for reviews that helped us improve the final version of this contribution. This study is supported by the Ni-Cu-PGE-Cr Project under the Targeted Geoscience Initiative 4 (TGI-4) of the Geological Survey of Canada (GSC). A.-A. Sappin acknowledged the support of the Visiting Fellowships in Canadian Government Laboratories Program from the Natural Sciences and Engineering Research Council of Canada (NSERC) and the GSC.

REFERENCES

Azar, B., 2010. The Blackbird chromite deposit, James Bay Lowlands of Ontario, Canada: Implications for chromitite genesis in ultramafic conduits and open magmatic systems; M.Sc. thesis, University of Toronto, Toronto, Canada, 154 p.

Bédard, J.H. and Hébert, R., 1996. The lower crust of the Bay of Islands ophiolite, Canada: Petrology, mineralogy, and the importance of syntexis in the magmatic differentiation in ophiolites and at the ocean ridges; Journal of Geophysical Research, v. 101, p. 25101–25124.

Bédard, M.-P., Houlé, M.G., Hébert, R., and Goutier, J., 2014. Étude pétrographique de l'intrusion ultramafique chromifère du lac des Montagnes, Baie James, Québec, *In:* Résumés des conférences et des photoprésentations, Québec Mines 2013; Ministère des Ressources naturelles du Québec, DV 2014-03, p. 55.

Bédard, M.-P., Houlé, M.G., Hébert, R., and Goutier, J., 2015. Étude pétrographique de l'intrusion ultramafique chromifère du lac des Montagnes, Baie James, Québec; Geological Survey of Canada, Open File 7563, 1 poster.

Chartier-Montreuil, W., 2013. Minéralogie et géochimie d'une intrusion ultramafique du Laguiche, Baie James; Thèse B.Sc., Université Laval, Québec, 64 p.

Cimon, J., Goutier, J., and Houlé, M.G., 1997. Caractérisation de corps ultramafiques dans la région du lac Yasinski, Baie-James. *In:* Programme with abstract; Séminaire d'information sur la recherche géologique, 1997, Ministère des Ressources naturelles du Québec, DV 97-03, p. 42.

David, J., Maurice, C., and Simard, M., 2009. Datations isotopiques effectuées dans le nord-est de la Province du Supérieur; Travaux de 1998-1999-2000; Ministère des Ressources naturelles du Québec, DV 2008-05, 92 p.

Fecteau, A., 2013. Pétrographie et géochimie des roches du Complexe mafique et ultramafique du lac Fed; Thèse B.Sc., Université Laval, Québec, 61 p.

Grzela, D., Goutier, J., O'Neil, J., and Houlé, M.G., 2014. Étude des intrusions ultramafiques de la région du lac Richardie, Baie-James, Québec; Geological Survey of Canada, Open File 7564, 1 poster.

Houlé, M.G., 2000. Pétrologie et métallogénie du Complexe de Menarik, Baie-James, Québec, Canada; Thèse M.Sc., Université Laval, Québec, 515 p.

Houlé, M.G., LaFlèche, M.R., Hébert, R., Beaudoin, G., and

Goutier, J., 2002. PGE mineralization in the Archean Menarik Igneous Complex, James Bay, Québec, Canada, *In:* Proceedings; 9th International Platinum Symposium, Billings, Montana, 2002, p. 185–187.

Houlé, M.G., Lesher, M.J., McNicoll, V.J., Metsaranta, R.T., Sappin, A.-A., Goutier, J., Bécu, V., Gilbert, H.P., and Yang, X.M., 2015. Temporal and spatial distribution of magmatic Cr-(PGE), Ni-Cu-(PGE), and Fe-Ti-(V) deposits in the Bird River–Uchi–Oxford-Stull–La Grande Rivière–Eastmain domains: a new metallogenic province within the Superior Craton, *In:* Targeted Geoscience Initiative 4: Canadian Nickel-Copper-Platinum Group Elements-Chromium Ore Systems — Fertility, Pathfinders, New and Revised Models, (ed.) D.E. Ames and M.G. Houlé; Geological Survey of Canada, Open File 7856, p. 35–47.

Huot, F., Houlé, M.G., Pearson, V., and Archer, P., 2015. Ni-Cu-PGE Mineralizations within a Komatiitic Subvolcanic and Volcanic Succession in the Mesoarchean Venus Greenstone Belt, Superior Province, Northern Québec, Canada, *In:* Program with Abstract; Joint Assembly Annual Meeting AGU-GAC-MAC-CGU, , Montréal, Quebec, May 2015.

Labbé, J.-Y. and Grant, M., 1998. Géologie de la région de Lac Natel (33B/04); Ministère des Ressources naturelles du Québec, RG 98-14, 28 p.

Liipo, J.P., Vuollo, J.I., Nykänen, V.M., and Piirainen, T.A., 1995. Zoned Zn-rich chromite from the Näätäniemi Serpentine Massif, Kuhmo greenstone belt, Finland; The Canadian Mineralogist, v. 33, p. 537–545.

Méric, J., 2011. Caractérisation géochimique des magnétites de la zone critique de l'intrusion magmatique de Sept-Îles (Québec, Canada) et intégration à une base de données utilisant la signature géochimique des oxydes de fer comme outil d'exploration; Rapport de stage non-publié, Université du Québec à Chicoutimi, Saguenay, 48 p.

Metsaranta, R.T., Houlé, M.G., McNicoll, V.J., and Kamo, S.L., 2015. Revised geological framework for the McFaulds Lake greenstone belt, Ontario, *In:* Targeted Geoscience Initiative 4: Canadian Nickel-Copper-Platinum Group Elements-Chromium Ore Systems — Fertility, Pathfinders, New and Revised Models, (ed.) D.E. Ames and M.G. Houlé; Geological Survey of Canada, Open File 7856, p. 61–73.

Sappin, A.-A., Houlé, M.G., Goutier, J., and McNicoll, V., 2015. Caractérisation pétrographique et géochimique de la Pyroxénite de baie Chapus, Baie-James: Un exemple de minéralisation en Fe-Ti-V dans la Province du Supérieur; Geological Survey of Canada, Open File 7745, 1 poster.

Thériault, R. and Beauséjour, S., 2012. Geological map of Quebec, 2012 edition; Ministère de l'Énergie et des Ressources naturelles du Québec, DV 2012-06, Map and digital data, 8 p.

Vallée, M., 2012. Description métallogénique, métamorphique et morphologique du gîte magmatique de nickel, cuivre, cobalt, platine et palladium Nisk-1, situé dans la bande du Lac des Montagnes; M.Sc. thesis, Université du Québec à Montréal, Montréal, Canada, 165 p.

Williams, D., 1965. Mountain Lake Chromite Deposits, Mistassini Territory; M.Sc. thesis, Université Laval, Québec, 37 p.

GEOLOGICAL SURVEY OF CANADA
OPEN FILE 7856

Targeted Geoscience Initiative 4: Canadian Nickel-Copper-Platinum Group Elements-Chromium Ore Systems — Fertility, Pathfinders, New and Revised Models

The petrology, mineralization, and regional context of the Thunder mafic to ultramafic intrusion, Midcontinent Rift, Thunder Bay, Ontario

Brent E. Trevisan[1], Peter Hollings[1], Doreen E. Ames[2], and Nicole M. Rayner[2]

[1]Lakehead University, Thunder Bay, Ontario
[2]Geological Survey of Canada, Ottawa, Ontario

2015

© Her Majesty the Queen in Right of Canada, as represented by the Minister of Natural Resources Canada, 2015

This publication is available for free download through GEOSCAN (http://geoscan.nrcan.gc.ca/)

Recommended citation

Trevisan, B.E., Hollings, P., Ames, D.E., and Rayner, N.M., 2015. The petrology, mineralization, and regional context of the Thunder mafic to ultramafic intrusion, Midcontinent Rift, Thunder Bay, Ontario, *In:* Targeted Geoscience Initiative 4: Canadian Nickel-Copper-Platinum Group Elements-Chromium Ore Systems — Fertility, Pathfinders, New and Revised Models, (ed.) D.E. Ames and M.G. Houlé; Geological Survey of Canada, Open File 7856, p. 139–149.

Publications in this series have not been edited; they are released as submitted by the author.

Contribution to the Geological Survey of Canada's Targeted Geoscience Initiative 4 (TGI-4) Program (2010–2015)

TABLE OF CONTENTS

The petrology, mineralization and regional context of the Thunder mafic to ultramafic intrusion, Midcontinent Rift, Thunder Bay, Ontario

Brent E. Trevisan[1*], Peter Hollings[1], Doreen E. Ames[2], and Nicole M. Rayner[2]

[1]Department of Geology, Lakehead University, 955 Oliver Road, Thunder Bay, Ontario P7B 5E1
[2]Geological Survey of Canada, 601 Booth Street, Ottawa, Ontario K1A 0E8
*Corresponding author's e-mail: btrevisa@lakeheadu.ca

ABSTRACT

The 1108 Ma Thunder mafic to ultramafic intrusion is a small, 800 x 100 x 500 m, Cu-PGE mineralized body, located on the outskirts of Thunder Bay, Ontario. It is associated with the early magmatic stages of the Midcontinent Rift based on geochemical similarities to mafic and ultramafic rocks of the Nipigon Embayment and a $^{207}Pb/^{206}Pb$ zircon age of 1108.0 ± 1.0 Ma. The Thunder intrusion is similar to other known mineralized early-rift Midcontinent Rift intrusions; however, it is the only known occurrence of the Midcontinent Rift hosted in an Archean greenstone belt (Shebandowan). Major textural and geochemical differences can be used to subdivide the intrusion into a lower mafic to ultramafic unit and an upper gabbroic unit; the similar trace and rare earth element ratios of the two units suggest a single magmatic pulse that has undergone subsequent fractional crystallization and related cumulate phase layering. The estimated parental composition of the Thunder intrusion has a Mg# ($MgO/(MgO+FeO_{Tot})$, mole%) of 57, which represents a more evolved magma than other early-rift mafic to ultramafic intrusions and may indicate multiple staging chambers during the ascent of the parent magma.

Trace and rare earth element patterns are consistent with a mantle plume ocean island basalt-like source but with high-Th concentrations and a negative Nb anomaly. The εNd_t values of the intrusion range between -0.7 and +1.0, with no trends indicative of progressive wall-rock contamination, whereas the $^{87}Sr/^{86}Sr_i$ ratios range from 0.70288 to 0.70611 and trend towards wall-rock values of between 0.70712 and 0.70873. The radiogenic Sm-Nd and Rb-Sr isotope signature is similar to the contamination trends of the Nipigon sills, which is interpreted to represent contamination by shallow-basin-filling sedimentary rocks.

Ni-Cu-PGE sulphide mineralization (20 m of 0.22 wt% Cu, 0.06 wt% Ni, 0.25 ppm Pt, and 0.29 ppm Pd) is hosted by feldspathic peridotite in the lower mafic to ultramafic unit adjacent to the footwall rock of the Thunder intrusion. Sulphides typically comprise 1 to 5 modal%, rarely up to 30 modal%, with textures ranging from medium- to fine-grained, disseminated, globular, and rarely net-textured. Pyrrhotite, chalcopyrite, and rare pentlandite, with common secondary marcasite-pyrite replacement, occur together with trace michenerite, kotulskite, merenskyite, sperrylite, hessite, electrum, and argentian pentlandite. Whole-rock geochemical data display fractionated Ni-Cu-PGE patterns with depletion of iridium subgroup relative to the platinum subgroup.

Sulphide $\delta^{34}S$ values from the Thunder intrusion range from -2.0 to +3.8‰ and are similar to values for the metavolcanic host rock, which range from -3.1 to +2.3‰. Two samples of the basal mineralization zone sulphides yield $\Delta^{33}S$ values of 0.066 and 0.122‰ and one sample of the metavolcanic wall rock yields 0.149‰. The $\delta^{34}S$ and $\Delta^{33}S$ values for the Thunder intrusion fall within range for rocks of typical upper mantle composition. The sulphur source is difficult to resolve. It appears to be of mantle origin as the wall-rock S isotope values and S/Se_{Tot} signature are similar to that of upper mantle; however, assimilation of crustal sulphur is also a possibility.

INTRODUCTION

The recent discovery (2002) of the high-grade Ni-Cu-PGE Eagle deposit in the Midcontinent Rift (MCR) in Michigan has stimulated exploration for small mafic to ultramafic intrusions hosting "conduit-type" mineralization across the Canada-United States border. More than six poorly exposed mineralized early-rift mafic to ultramafic intrusion have been discovered within the Lake Superior region, leading to considerable petrological research (e.g. Heggie, 2005; Hollings et al., 2007a,b; Ding et al., 2010; Foley, 2011; Goldner, 2011) and re-evaluation of the current MCR tectono-magmatic model (Heaman et al., 2007; Hollings et al., 2010; Miller and Nicholson, 2013). However, the small

Trevisan, B.E., Hollings, P., Ames, D.E., and Rayner, N.M., 2015. The petrology, mineralization, and regional context of the Thunder mafic to ultramafic intrusion, Midcontinent Rift, Thunder Bay, Ontario, *In:* Targeted Geoscience Initiative 4: Canadian Nickel-Copper-Platinum Group Elements-Chromium Ore Systems — Fertility, Pathfinders, New and Revised Models, (ed.) D.E. Ames and M.G. Houlé; Geological Survey of Canada, Open File 7856, p. 139–149.

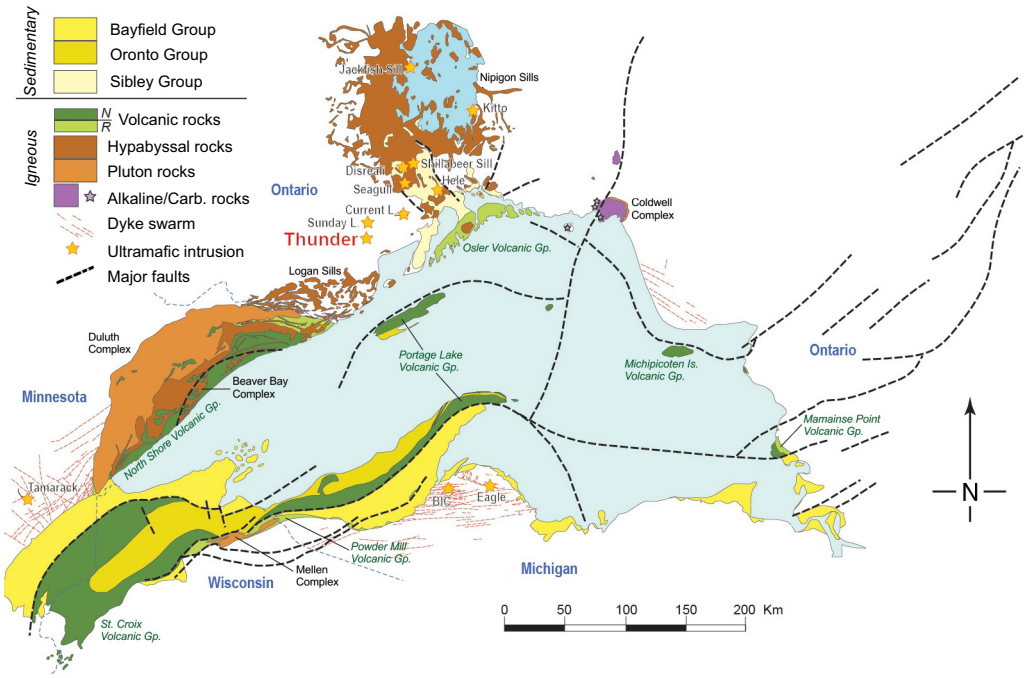

Figure 1. Present-day exposure of the Midcontinent Rift geology in the Lake Superior region. Labelled are the major volcanic and intrusive units. Indicated by the yellow stars are locations of the known ultramafic intrusions associated with the early magmatic stages of Midcontinent Rift evolution. Figure modified after Miller and Nicholson (2013).

size of these buried mineralized ultramafic intrusions makes them hard to detect, both on the ground and from regional magnetic survey maps.

The Thunder intrusion is a small, mineralized, mafic to ultramafic intrusion, which is located on the outskirts of the City of Thunder Bay (Fig. 1) and was explored by Rio Tinto (formerly Kennecott Canada Exploration Inc.) in 2005 and 2007 (Bidwell and Marino, 2007). Early investigations interpreted this intrusive body to be an early-rift occurrence based on geochemical similarities with the mafic to ultramafic intrusive units of the Nipigon Embayment (e.g. Hele intrusion and Shillabeer sill; Hollings et al., 2007a; D. Rossell, pers. comm., 2012). The Thunder intrusion is distinct from other mineralized early-rift intrusions in that it is the only known occurrence hosted by the metavolcanic and metasedimentary rocks of the Archean Shebandowan greenstone belt (Ames et al., 2012). Other early-rift intrusions north of the Canada-United States border, including Current Lake and Seagull, intrude the Archean Quetico metasedimentary subprovince and/or Mesoproterozoic Sibley Group sedimentary rocks (Heggie, 2005; MacTavish et al., 2013). South of the Canada-United States border, the Paleoproterozoic sedimentary rocks of the Animikie and Baraga basins (Ding et al., 2010; Foley, 2011; Goldner, 2011) host a number intrusions, such as Eagle, Bovine Igneous Complex, and Tamarack.

This report highlights the first author's (B.E. Trevisan) M.Sc. study (2014), which was a collaborative project between Lakehead University (LU), the Geological Survey of Canada (GSC), and the Ontario Geological Survey (OGS) as part of the Ni-Cu-PGE-Cr project, Targeted Geoscience Initiative-4 program (TGI-4; Ames et al., 2012). The main objective is to characterize the petrology, mineralization, and alteration footprint of the Thunder intrusion within the context of the MCR as a whole, in order to identify criteria for targeting buried mineralization (Fig. 1).

METHODOLOGY

Field work included geological mapping and re-logging of the seven diamond drillholes (DDH) intersecting the mineralized Thunder intrusion. A suite of 104 samples of representative lithology, mineralization, and alteration types were analysed for whole-rock geochemistry (OGS, in-kind contribution; Trevisan et al., 2015). A subset of samples was studied and analyzed using SEM (LU and GSC), electron microprobe (GSC), radiogenic Rb-Sr and Sm-Nd isotopes (Carleton University), S-isotopes (Indiana University), and geochronology (GSC). Most of the samples used for the analytical investigations were from DDH 07TH004, as it was determined to be the most stratigraphically complete representation of the Thunder intrusion and its wall rocks.

A 5 kg sample of a coarse (grain size ~1 cm) gabbroic phase of Thunder intrusion was prepared using standard methods of crushing and grinding, followed by density separations using a Wilfley table and heavy liquids (methylene iodide) to concentrate heavy minerals. Zircon and baddeleyite grains were selected after examination under a binocular microscope. The sample was analyzed by the isotope dilution-thermal ionization mass spectrometry (ID-TIMS) technique. Zircon grains were treated with the chemical abrasion method

(Mattinson, 2005) before being submitted for U-Pb chemical analysis. Baddleyeite grains were not subjected to any pre-dissolution treatment (neither chemical nor physical abrasion). Dissolution of both zircon and baddeleyite in a concentrated heavy fraction, extraction of U and Pb, and mass spectrometry followed the methods described in Parrish et al. (1987). Data reduction and numerical propagation of analytical uncertainties follow Roddick (1987). Analytical blanks for Pb were 1 pg. Results are presented in Table 1 with uncertainties reported at the 2σ level. The computer profram Isoplot v. 3.00 (Ludwig, 2003) was used to generate concordia plots and calculate weighted means. All ages quoted in the text and error ellipses on all concordia diagrams represent 2σ uncertainty level.

RESULTS AND SUMMARY

Geology of the Thunder Mafic to Ultramafic Intrusion

Field mapping showed the Thunder intrusion to be a mafic to ultramafic intrusion with a surface area of 800 x 1000 m (Fig. 2). The intrusion can be divided into two major lithological units: a lower mafic to ultramafic unit and an upper gabbroic unit. The country rocks include mafic to intermediate metavolcanic rocks of the Shebandowan greenstone belt. In addition, outcrops of a north-trending gabbroic dyke were identified east of the Thunder intrusion. The magnetic signature of an iron formation horizon can be traced with the aid of airborne geophysical data (OGS, 2003). No major structures were observed in the field surrounding the Thunder intrusion. Contact relationships between the Thunder intrusion and surrounding country rock were only rarely observed. The geological boundary of the Thunder intrusion was defined with the aid of airborne geophysical data, as there was generally a gap between outcrops of the Thunder intrusion and country rock (Fig. 2). A geological field guide is available for the area (Trevisan et al., 2013).

A simplified lithological cross-section of the Thunder intrusion was constructed along five drillholes that lie along a similar azimuth. This section suggests that the Thunder intrusion is <600 m total thickness with a steep southward dip (Fig. 3). Only the intrusion and the footwall rocks were intersected by drilling.

Petrology of the Thunder Intrusion

Primitive mantle-normalized profiles of the Thunder intrusion are characterized by light rare earth element enrichment and fractionated heavy rare earth element. The similar slope of the upper gabbroic unit and lower mafic to ultramafic unit primitive mantle-normalized profiles are consistent with a single magmatic pulse that has undergone subsequent fractional crystallization and related cumulate phase layering (Trevisan, 2014).

Table 1. U-Pb TIMS analytical data .

Fraction[1]	Description[2]	Wt. µg	U ppm	Pb[3] ppm	$^{206}Pb/^{204}Pb$	Pb[5] pg	$^{208}Pb/^{206}Pb$	Isotopic Ratios[6] $^{207}Pb/^{235}U$	±1SE Abs	$^{206}Pb/^{238}U$	±1SE Abs	Corr.[7] Coeff.	$^{207}Pb/^{206}Pb$	±1SE Abs	Ages[8] (Ma) $^{206}Pb/^{238}U$	±2SE	$^{207}Pb/^{235}U$	±2SE	$^{207}Pb/^{206}Pb$	±2SE	% Disc
12AV-BT130 (Z11000)																					
B1 (11)	Br, El, Str, NM10	19	96	17	7404	3	0.01	1.96998	0.00228	0.18651	0.00017	0.928726048	0.07661	0.00004	1102.4	1.8	1105.3	1.6	1110.9	1.9	0.8
B2 (10)	Br, El, Str, NM10	21	92	16	5961	4	0.01	1.97198	0.0023	0.18672	0.00016	0.928578322	0.0766	0.00004	1103.6	1.8	1106.0	1.6	1110.7	1.9	0.7
B4 (5)	Br, El, Str, NM10	12	157	27	7197	3	0.01	1.96863	0.00237	0.18647	0.00018	0.924354866	0.07657	0.00004	1102.2	1.9	1104.8	1.6	1110.0	1.9	0.8
B5 (6)	Br, El, Str, NM10	14	203	35	9227	4	0.01	1.95946	0.00225	0.18562	0.00016	0.936024354	0.07656	0.00003	1097.6	1.8	1101.7	1.5	1109.8	1.8	1.2
Z1A (1)	Co, Clr, An, Frac, M10	11	224	48	10694.3	3	0.30	1.92427	0.00231	0.18245	0.00017	0.943328099	0.07649	0.00003	1080.3	1.9	1089.6	1.6	1108.0	1.8	2.7
Z1B (1)	Co, Clr, An, Frac, M10	14	544	115	18397.4	5	0.23	1.97189	0.00236	0.18702	0.00018	0.944364682	0.07647	0.00003	1105.2	1.9	1106.0	1.6	1107.4	1.7	0.2
Z1C (1)	Co, Clr, An, Frac, M10	15	210	47	14608.9	2	0.31	1.97760	0.00232	0.18743	0.00017	0.938764663	0.07652	0.00003	1107.4	1.9	1107.9	1.6	1108.8	1.8	0.1

Notes:

[1]Fraction name abbreviations: B=baddeleyite, Z=zircon; number of grains making up each fraction shown in parentheses; all zircon fractions were chemically abraded using a modified procedure from Mattinson (2005)

[2]Zircon/baddeleyite descriptions: An=anhedral, Clr=clear, Co=colourless, Br=brown, El=elongate, Frac=fractured, M10=magnetic@1.8A 10°SS, NM10=nonmagnetic@1.8A 10°SS, Str=striated

[3]Radiogenic Pb

[4]Measured ratio, corrected for spike and fractionation

[5]Total common Pb in analysis corrected for fractionation and spike

[6]Corrected for blank Pb and U and common Pb, errors quoted are 1 standard error (absolute); procedural blank values for this study are 0.1 pg U and 1 pg Pb; Pb blank isotopic composition is based on the analysis of procedural blanks; corrections for common Pb were made using Stacey and Kramers (1975) compositions

[7]Correlation coefficient

[8]Corrected for blank and common Pb; errors quoted are 2 standard error in Ma

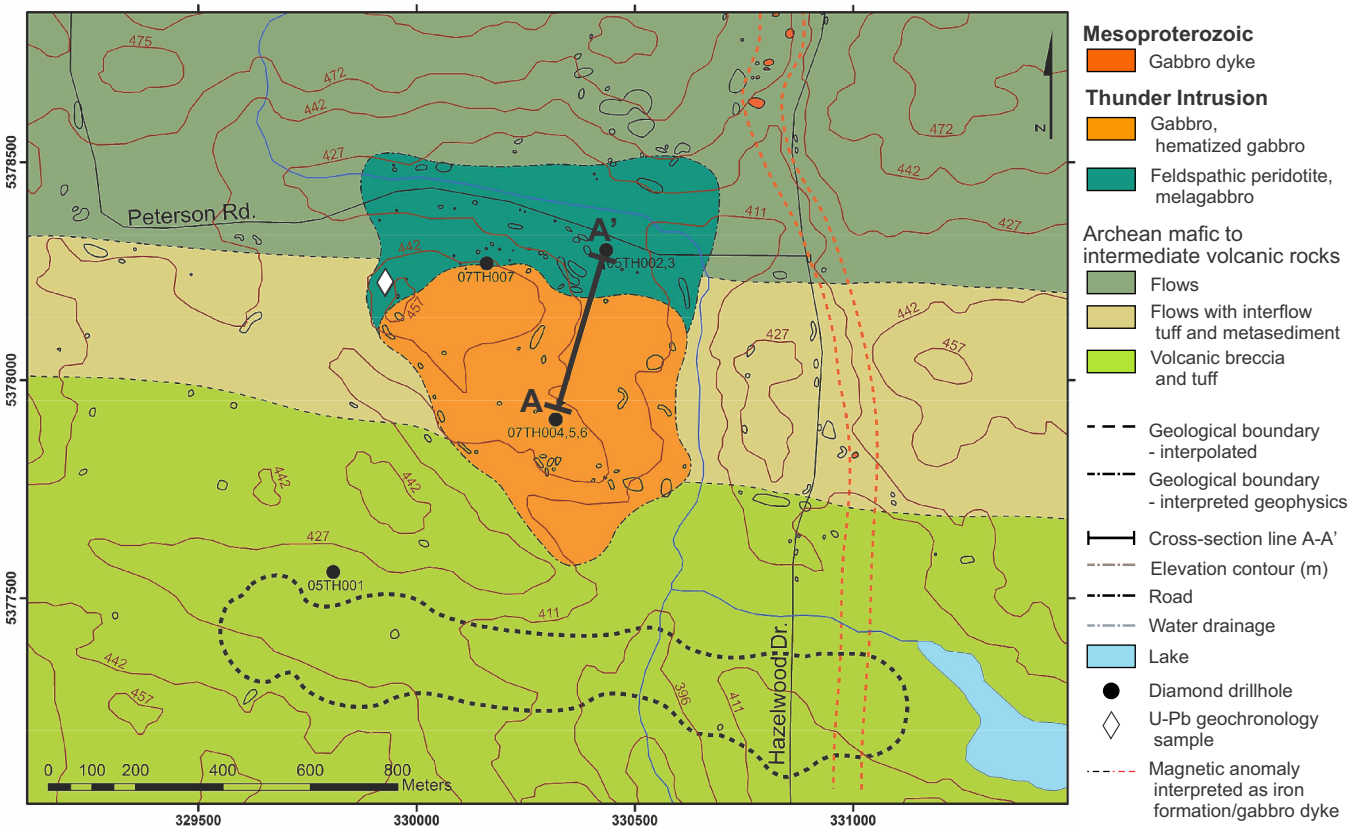

Figure 2. Geological map of the Thunder intrusion and vicinity at 1:9000 scale. Included on the map are the locations of the diamond drillholes, cross-section line, and geochronology samples. Geophysical interpretations are from OGS (2003).

Correlating petrographic observations, whole-rock geochemistry, and magnetic susceptibility defines a four-stage cumulate mineral paragenetic sequence: clinopyroxene + olivine, clinopyroxene + olivine + Fe-Ti oxide, plagioclase + clinopyroxene + Fe-Ti oxide, and plagioclase + clinopyroxene + Fe-Ti oxide + apatite (Trevisan, 2014).

Olivine analyses focused on a suite of samples collected from the lower mafic to ultramafic unit of DDH 07TH004 (n = 10). The coarser and least altered olivine crystals enclosed by plagioclase were preferred for analysis as they should have avoided potential exchange with adjacent sulphide minerals (Donoghue et al., 2014). No fresh olivine was found in the upper gabbroic unit. Both core and rim were analysed for multiple olivine grains from each sample. The full dataset is available in Trevisan (2014). Olivine forsterite compositions range from 56.3 to 86.9 mol% Fo, with an average of ~65 mol% Fo. There is little variation between core and rim measurements (typically <0.5 mol% Fo), indicating that cumulus olivine was not overly modified by sub-solidus re-equilibration with trapped silicate liquid (i.e. the trapped liquid shift; Barnes, 1986). Sample RTTC-BT-089 showed a wide range in mol% Fo values, from ~69 to 86, indicating disequilibrium along the basal contact of the lower mafic to ultramafic unit.

A sample of the lower mafic to ultramafic unit collected 20 cm from the wall-rock contact (sample RTTC-BT-089) was selected as being representative of a "quenched" parental liquid. With 10 modal% of olivine in sample RTTC-BT-089, it was assumed that the parental magma also contained 10 modal% of Fo_{86}

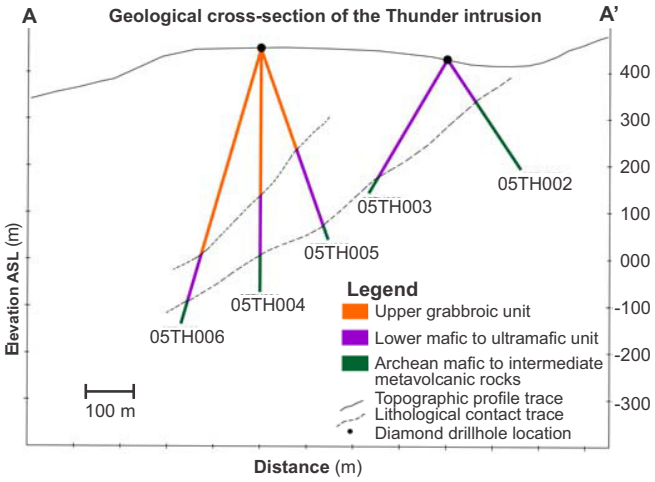

Figure 3. Geological cross-section of the Thunder intrusion looking towards 290°. For the location of the section line, see Figure 2.

olivine; both the Fo_{86} olivine and whole-rock composition were used in the mass balance equation of Roeder and Emslie (1970). The Mg# calculated using the estimate parent magma composition yielded ~57.

Radiogenic Sm-Nd and Rb-Sr Isotopes

Rb-Sr and Sm-Nd isotope analyses focused on ten samples from the upper gabbroic unit, lower mafic to ultramafic unit, and the metavolcanic wall rocks from DDH 07TH004. Values of $^{87}Sr/^{86}Sr_i$ ratios and εNd_t were calculated at time t = 1100 Ma and represent the 2σ uncertainty level. The upper gabbroic unit (n = 4) is characterized by $^{87}Sr/^{86}Sr_i$ ranging from 0.7031 to 0.7061, $^{143}Nd/^{144}Nd$ ranging from 0.511992 to 0.512127, and εNd_t ranging from -0.7 to 1.0. The lower mafic to ultramafic unit (n = 4) is characterized by 87Sr/86Sri ranging from 0.7288 to 0.7034, $^{143}Nd/^{144}Nd$ ranging from 0.512065 to 0.512298, and εNd_t ranging from 0.5 to 1.0. The metavolcanic wall rocks (n = 2) are characterized by $^{87}Sr/^{86}Sr_i$ ranging from 0.7071 to 0.7087, $^{143}Nd/^{144}Nd$ ranging from 0.511047 to 0.51186, and εNd_t ranging from -16.8 to -15.8.

Sulphur Isotopes and Se/S Ratios

Twenty samples from surface and DDH 07TH004 were analysed for $\delta^{34}S$ isotopes, including the upper gabbroic unit, the lower mafic to ultramafic unit, and the metavolcanic wall rocks. Values of $\delta^{34}S$ for the upper gabbroic unit (n = 10) range from -2.0 to 4.9‰; from -1.3 to 2.9‰ for the lower mafic to ultramafic unit (n = 6); and from -3.1 to 2.3‰ for the metavolcanic rocks (n = 10). In addition, three samples were analysed for $\delta^{33}S$ to investigate the involvement of crustal sulphur during mineralization. Values are presented in delta cap notation (where $\Delta^{33}S = \ln(\delta^{33}S+1)-0.515*\ln(\delta^{34}S+1)$; Ono et al., 2012): a surface and a drill-core sample of the lower mafic to ultramafic unit yielded values of 0.122 and 0.066‰, respectively, and a drill-core sample of the metavolcanic wall rock yielded a value of 0.149‰.

The samples used for the S-isotope analyses were also analysed for whole-rock Se concentrations. Ratios of $Se/S_{Tot} \times 10^6$ range from 400 to 2000 for the upper gabbroic unit (n = 5); from 180 to 3000 for the lower mafic to ultramafic unit (n = 6); and from 40 to 1000 for the metavolcanic rocks (n = 6). Anomalously high Se/S_{Tot} ratios were determined to be the result of some samples having S concentrations at or near the lower detection limit.

Sulphide and Platinum-Group Element Mineralogy

The basal mineralization zone, which is hosted by feldspathic peridotite of the lower mafic to ultramafic unit, is the primary mineralization in the Thunder intrusion and is interpreted to be the accumulation of immiscible sulphide droplets via gravitational settling. The upper gabbroic unit exhibits weak to no mineralization. Ni-Cu-PGE grades are highest in DDHs 07TH004, 005, and 05TH003, but are low in DDHs 07TH006 and 05TH002. Sulphides in the basal mineralization zone rarely comprise up to 30 modal% and are typically 1 to 5 modal%. Sulphide textures range from medium- to fine-grained disseminated, coarse-grained globular, and rarely net-textured. The primary sulphide mineralogy mainly consists of composite textured pyrrhotite and chalcopyrite (pyrrhotite > chalcopyrite) intergrown with minor Fe-Ti oxide. Rare inclusions of very fine-grained pentlandite, siegenite, sphalerite, cobaltite, cubanite. and galena are hosted by pyrrhotite and chalcopyrite. In addition, extensive secondary graphic and nickeliferous marcasite-pyrite-magnetite intergrowths occur replacing the primary sulphides.

Table 2. Summary of platinum-group minerals, precious-metal minerals identified in representative samples of the various styles of mineralization observed in the Thunder intrusion and footwall.

Intrusion-hosted		Footwall-hosted	
Mineral	Formula	Mineral	Formula
Upper zone		*Pyrrhotite-rich massive sulphide veinlet*	
Kotulskite	Pd(Te,Bi)	Naldrettite	Pd_2Sb
Basal zone		Stibiopalladinite	Pd_5Sb_2
Argentian pentlandite	$(Fe,Ni,Ag)_9S_8$		
Electrum	(Au,Ag)	*Chalcopyrite-rich massive sulphide veinlets*	
Hessite	Ag_2Te		
Kotulskite	Pd(Te,Bi)	Electrum	(Au,Ag)
Merenskyite	$(Pd,Pt)(Te,Bi)_2$	Native silver	Ag
Michenerite	(Pd,Pt)BiTe		
Sperrylite	$PtAs_2$		
unknown mineral	Pd_3Pt_3Sn		

Platinum-group minerals and precious-metal minerals that were identified by electron microprobe are summarized in Table 2 with the majority being Pd-rich telluride and bismuthide with minor Pt-rich arsenide.

Geochronology

Three single grain fractions of zircon and four multi-grain fractions of baddeleyite were analyzed and are shown in Figure 4. Two of the three zircon fractions are concordant, but all have consistent $^{207}Pb/^{206}Pb$ ages with a weighted mean of 1108.0 ± 1.0 Ma. All four baddeleyite fractions are slightly discordant, and three of them overlap within error. The weighted mean $^{207}Pb/^{206}Pb$ age of the baddeleyite fractions is 1110.3 ± 0.9 Ma. As observed in this study, others have noted a consistent discordance problem (and consequent shift to older $^{207}Pb/^{206}Pb$ ages) for baddeleyite relative to zircon (Paces and Miller, 1993 ; Heaman et al., 2007). The reason for this discordance is poorly understood

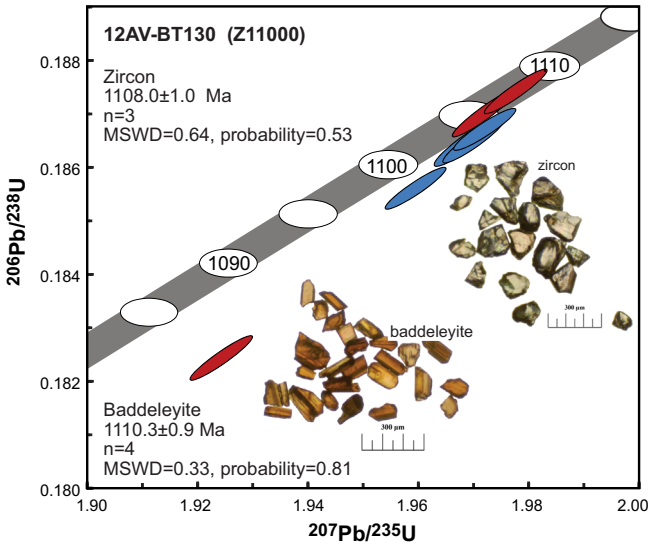

Figure 4. Concordia diagram illustrating geochronology results for zircon (red ellipses) and baddeleyite (blue ellipses) from the Thunder intrusion. The concordia curve is shown as a band incorporating uncertainties in the decay constant. Error ellipses and uncertainties in the weighted mean $^{207}Pb/^{206}Pb$ ages are given at 2σ. Inset photomicrographs illustrate a selection of grains that is representative of those analysed (300 μm scale bar).

but needs to be taken into account when comparing high-precision results of other samples. In order to permit the comparison of this age with earlier studies, the best estimate of the crystallization of the Thunder intrusion is the zircon weighted mean $^{207}Pb/^{206}Pb$ age of 1108.0 ± 1.0 Ma. Considering the recently proposed tectono-magmatic model of Miller and Nicholson (2013) the Thunder intrusion fits between the initial (1115–1110 Ma) to early (1110–1105 Ma) magmatic stages of the MCR evolution and falls within range of other fertile early-rift mafic to ultramafic intrusions, such as the Eagle at 1107.20 ± 5.7 Ma (Ding et al., 2010), Tamarack at 1105.6 ± 1.2 Ma (Goldner, 2011), and Seagull at 1112.80 ± 1.4 Ma (Heaman et al., 2007).

DISCUSSION

Petrology

The geochemical signature of the Thunder intrusion is broadly comparable to Sun and McDonough's (1989) modern plume-derived ocean island basalt (OIB). A negative Nb anomaly for the upper most section of the upper gabbroic unit, assimilation features (e.g. irregular quartz-rich fragments surrounded by pods of granophyre), and an up-hole increase in Th concentrations are all consistent with contamination by older crustal material. The radiogenic Sm-Nd and Rb-Sr isotope signature is similar to the contamination trends of the Nipigon sills, which are interpreted to be the result of contamination by shallow basin-filling sedimentary rocks (Fig. 5; Hollings et al., 2007b; Trevisan, 2014).

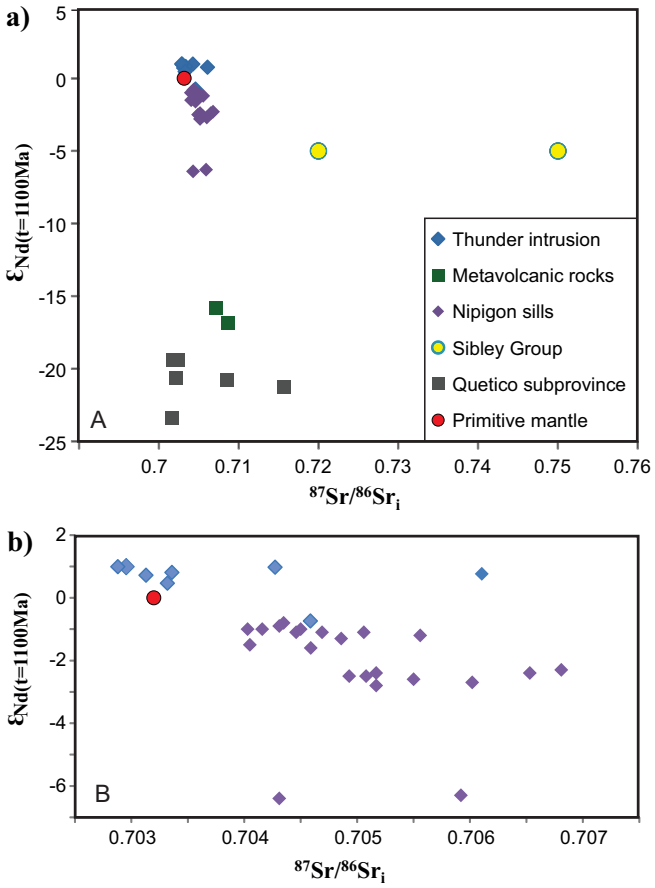

Figure 5. Plots of εNd_t versus $^{87}Sr/^{86}Sr_i$ at 1100 Ma for the host rocks and units of the **(a)** Thunder intrusion (diamond drillhole 07TH004), the Nipigon sills, Quetico subprovince metasedimentary rocks, and Sibley Group sedimentary rocks; and **(b)** Close-up of the Thunder intrusion and Nipigon sill dataset relative to primitive mantle. Data sources include primitive mantle values from Nicholson and Shirey (1990), Nipigon sill data from Hollings et al. (2007b), Quetico subprovince data from Pan et al. (1999), and Sibley Group data from Metasaranta et al. (pers. comm., 2005).

The lack of correlation between Sr_i and in εNd_t (r = -0.28) implies that the metavolcanic rocks that immediately underlie the Thunder intrusion were not a likely contaminant to the magma. Expansion of the radiogenic isotope study is required to investigate other possible contaminants.

On a plot of Gd/Yb_n versus La/Sm_n, both intrusive units of the Thunder intrusion plot slightly above the field of the mafic to ultramafic intrusions and sills of the Nipigon Embayment (e.g. Hele intrusion and Shillabeer sill, respectively; Fig. 6). The high Gd/Yb_n values are consistent with the interpretation of Hollings et al. (2007a) that the parent magmas of the mafic to ultramafic intrusions of the Nipigon Embayment were derived from a deeper source than the diabase sills (e.g. Nipigon sills). Regardless of Archean host rock, the Thunder intrusion's geochemical signature is consistent with other known early-rift mafic to ultramafic intrusions, including relatively high Gd/Yb_n values that

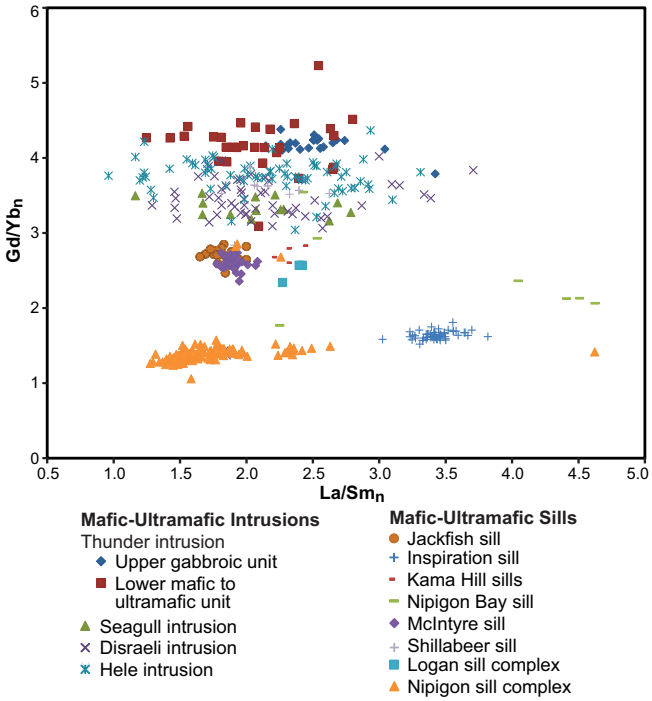

Figure 6. Plot of Gd/Yb_n versus La/Sm_n for the upper gabbroic unit and lower mafic to ultramafic unit of the Thunder intrusion and other intrusions of the Nipigon Embayment. Chondrite-normalized rare earth element ratios calculated from the values of Sun and McDonough (1989). Nipigon Embayment data from Cundari et al. (2013).

are similar to mafic to ultramafic intrusions in the Nipigon Embayment (Hollings, 2007a), and has OIB-like characteristics that suggest crustal contamination (e.g. Heggie, 2005; Hollings et al., 2007b).

The Wawa and Quetico subprovince boundary is roughly outlined by granitoid bodies of the Dog Lake Granite Chain and Nipigon Bay granite. These granitoid bodies are interpreted to have been emplaced along crustal-scale faults that formed the terrane boundaries as "stitching plutons" (e.g. Hollings and Kuzmich, 2014). The spatial proximity of early-rift mafic to ultramafic intrusions, such as Thunder, Sunday Lake, and Current Lake, and the Dog Lake Granite Chain suggests a possible structural control on the distribution of mafic to ultramafic intrusions containing Ni-Cu-PGE sulphide mineralization in the northern Lake Superior region north of the Canada-United States border. The Thunder parent magma likely travelled along the deep-seated structure represented by the Wawa and Quetico subprovince boundary, which was reactivated during the Mesoproterozoic rifting event (Trevisan, 2014). The structural control on the primary distribution of mafic to ultramafic intrusions containing Ni-Cu-PGE sulphide mineralization in the roots of large igneous provinces has been observed elsewhere, such as in the Huangshandong, Huanshang, and Jinchuan intrusions in China (Lightfoot and Evans-Lamswood, 2014). The low Mg# (~57) estimate for the parent magma likely represents a more evolved magma than the other early-rift mafic to ultramafic intrusions in the MCR. The involvement of multiple staging chambers during the ascent of the Thunder intrusion may account for the evolved composition, possibly reflecting a conduit system similar to the one proposed for the Noril'sk-Talnakh deposits (Arndt, 2005).

Mineralization

As this intrusion is hosted by metavolcanic rocks bearing Ag and Au mineralization (MacDonald, 1939; Thomson, 1989), it is possible that wall-rock assimilation could account for the precious metal mineralogy observed in the basal mineralization zone. Whole-rock geochemistry indicates fractionated Ni-Cu-PGE patterns with depletion in iridium-subgroup PGEs relative to platinum-subgroup PGEs for the disseminated sulphide mineralization hosted by the Thunder intrusion's lower mafic to ultramafic unit. The Thunder intrusion's Ni-Cu-PGE patterns are similar to the upper massive sulphide zone, semi-massive sulphide zone, and chalcopyrite-rich veins of the Eagle deposit (Ding et al., 2011). This similarity is consistent with an early sulphide liquid-phase forming deeper in the system, which has concentrated the iridium-subgroup PGEs. The sulphur source appears to be of mantle origin, however, the assimilation of crustal sulphur is a possibility that is hard to resolve as the wall-rock S isotope and S/Se_{Tot} signature is similar to that of upper mantle.

IMPLICATIONS FOR EXPLORATION

This study has improved the emplacement model for the Thunder intrusion and has provided key insights into early-rift mafic to ultramafic magmatism, revealing a single, differentiated, Cu-(Ni)-PGE mineralization magmatic body that has undergone fractionation and cumulate processes. Regardless of host rock, the Thunder intrusion's geochemical signature is consistent with the other known early-rift mafic to ultramafic intrusions, including relatively high Gd/Yb_n values that are similar to mafic to ultramafic intrusions in the Nipigon Embayment (Hollings, 2007a), and has OIB-like characteristics with indications of crustal contamination (e.g. Heggie, 2005; Hollings et al., 2007b). Based on whole-rock geochemistry and olivine chemistry (e.g. Ding et al., 2010; Foley, 2011; Goldner, 2011), the parental magma that formed the Thunder intrusion is relatively more evolved than other mineralized early-rift mafic to ultramafic intrusions, such as BIC, Tamarack, and Eagle. Our research on the Thunder Cu-(Ni)-PGE-bearing intrusion, reflects the possible involvement of multiple staging chambers during the ascent of a more primitive parent magma.

The Thunder parent magma likely travelled along a conduit through reactivated deep-seated structures during the Mesoproterozoic rifting event (Trevisan, 2014). The relative proximity of the Dog Lake Granite Chain and early-rift mafic to ultramafic intrusions, such as Thunder, Sunday Lake, and Current Lake, indicates a possible structural conduit along the Wawa and Quetico subprovince boundary.

ACKNOWLEDGEMENTS

This study was a collaborative project as part of the Ni-Cu-PGE-Cr project, Targeted Geoscience Initiative-4 program, including funding to the first author under the Research Affiliate Program, Natural Resources Canada, with in-kind geochemical support from the Ontario Geological Survey Geoscience Laboratories in Sudbury. We thank Dean Rossell, Rio Tinto, for guidance initiating this study and providing access. Expert analytical work in the Geological Survey of Canada's Geochronology Laboratories was carried out by Julie Peressini, Linda Cataldo, and Carole Lafontaine. Anne Hammond and Kristi Tavener of Lakehead University are thanked for the manufacture of thin sections.

REFERENCES

Ames, D.E., Dare, S.A.S., Hanley, J.J., Hollings, P., Jackson, S.E., Jugo, P.J., Kontak, D.J., Linnen, R.L., and Samson, I.M., 2012. Update on research activities in the Targeted Geoscience Initiative 4 magmatic-hydrothermal nickel-copper-platinum group elements ore system subproject: system fertility and ore vectors, *In:* Summary of Field Work and Other Activities, 2012; Ontario Geological Survey, Open File Report 6280, p. 41-1 to 41-11.

Arndt, N.T., 2005. The conduits of magmatic ore deposits, *In:* Exploration for Platinum-Group Element Deposits; Mineralogical Association of Canada. Short Course, v. 35, p. 181–201.

Barnes, S.J., 1986. The effect of trapped liquid shift crystallization on cumulus mineral compositions in layered intrusions; Contributions to Mineralogy and Petrology, v. 93, p. 524–531.

Bidwell, G.E. and Marino, F., 2007. Thunder Project: 2007 Field program diamond drilling on the 1245457 claim; Ontario Geologic Survey, Assessment File 2.34638.

Cundari, R.M., Carl, C.F.J., Hollings, P., and Smyk, M.C. 2013, New and compiled whole-rock geochemical and isotope data of Midcontinent Rift-related rocks, Thunder Bay area; Ontario Geological Survey, Miscellaneous Release Data 308.

Ding, X., Li, C., Ripley, E.M., Rossell, D., and Kamo, S., 2010. The Eagle and East Eagle sulfide ore-bearing mafic-ultramafic intrusions in the Midcontinent Rift System, upper Michigan: geochronology and petrologic evolution; Geochemistry Geophysics Geosystems, v. 11, p. 1–22.

Ding, X., Ripley, E.M., and Li, C., 2011. PGE geochemistry of the Eagle Ni-Cu-(PGE) deposit, upper Michigan: constraints on ore genesis in a dynamic magma conduit; Mineral Deposita, v. 47, p. 89–104.

Donoghue, K.A., Ripley, E.M., and Li, C., 2014. Sulfur isotope and mineralogical studies of Ni-Cu sulfide mineralization in the Bovine Igneous Complex (BIC Intrusion), Baraga Basin, northern Michigan; Economic Geology, v. 109, p. 325–341.

Foley, D.J., 2011. Petrology and Cu-Ni-PGE Mineralization of the Bovine Igneous Complex, Baraga County, Northern Michigan; M.Sc. thesis, University of Minnesota, Duluth, Minnesota, 211 p.

Goldner, B.D., 2011. Igneous Petrology of the Ni-Cu-PGE Mineralized Tamarack Intrusion, Aitkin and Carlton Counties, Minnesota; M.Sc. thesis, University of Minnesota, Duluth, Minnesota, 166 p.

Heaman, L.M., Easton, M., Hart, T.R., Hollings, P., MacDonald, C.A., and Smyk, M., 2007. Further refinement to the timing of Mesoproterozoic magmatism, Lake Nipigon Region, Ontario; Canadian Journal of Earth Sciences, v. 44, p. 1055–1086.

Heggie, G.J., 2005. Whole rock geochemistry, mineral chemistry, petrology and Pt, Pd mineralization of the Seagull intrusion, Northwestern Ontario; M.Sc. thesis, Lakehead University, Thunder Bay, Ontario, 364 p.

Hollings. P. and Kuzmich, B., 2014. Preliminary geochemical analysis of the Nipigon Bay granites, northern Lake Superior, *In:* Program with Abstracts; Geological Association of Canada-Mineralogical Association of Canada, v. 37, p. 119–120.

Hollings, P., Hart, T., Richardson, A., and MacDonald, C.A., 2007a. Geochemistry of the Mesoproterozoic intrusive rocks of the Nipigon Embayment, northwestern Ontario: evaluating the earliest phases of rift development; Canadian Journal of Earth Sciences, v. 44, p. 1087–1110.

Hollings, P., Richardson, A., Creaser, R.A., and Franklin, J.M., 2007b. Radiogenic isotope characteristics of the Mesoproterozoic intrusive rocks of the Nipigon Embayment, northwestern Ontario; Canadian Journal of Earth Sciences, v. 44, p. 1111–1129.

Hollings, P., Smyk, M., Heaman, L.M., and Halls, H., 2010. The geochemistry, geochronology, and paleomagnetism of dikes and sills associated with the Mesoproterozoic Midcontinent Rift near Thunder Bay, Ontario, Canada; Precambrian Research, v. 183, p. 553–571.

Lightfoot, P.C. and Evans-Lamswood, D., 2014. Structural controls on the primary distribution of mafic-ultramafic intrusions containing Ni-Cu-Co-(PGE) sulfide mineralization in the roots of large igneous provinces; Ore Geology Reviews, v. 64, p. 354–386.

Ludwig, K.R., 2003. User's manual for Isoplot/Ex rev. 3.00: A Geochronological Toolkit for Microsoft Excel; Berkeley Geochronology Center, Special Publication 4, Berkeley, 70 p.

MacDonald, R.D., 1939. Geology of Gorham Township and Vicinity; Ontario Geological Survey, Annual Report, Part 3, v. 49, p. 1–8.

MacTavish, A.D., Heggie, G.J., and Johnson, J.R., 2013. The Thunder Bay North Pt-Pd-Cu-Ni Deposits, *In:* Proceedings of the 2013 Workshop on Ni-Cu-PGE Deposits of the Lake Superior Region; Precambrian Research Center, Short Course v. 13-01, p. 177–179.

Mattinson, J.M., 2005. Zircon U–Pb chemical abrasion ("CA-TIMS") method: combined annealing and multi-step partial dissolution analysis for improved precision and accuracy of zircon ages; Chemical Geology, v. 220, p. 47–66.

Miller, J. and Nicholson, S., 2013. Geology and mineral deposits of the1.1 Ga Midcontinent Rift in the Lake Superior region: an overview, in field guide to copper-nickel-platinum group element deposits of the Lake Superior region; Precambrian Research Center, Guidebook v. 13-01, p. 1–50.

Nicholson, S.W. and Shirey, S.B., 1990. Midcontinent Rift volcanism in the Lake Superior Region: Sr, Nd and Pb isotopic evidence for a mantle plume origin; Journal of Geophysical Research, v. 95, p. 10851–10868.

Ono, S., Keller, N.S., Rouxel, O., and Alt, J.C., 2012. Sulfur-33 constraints on the origin of secondary pyrite in altered oceanic

Ontario Geological Survey, 2003. Shebandowan area, Ontario airborne magnetic and electromagnetic surveys; Ontario Geological Survey, Geophysical Data Set 1021 - Revised.

Paces, J.B. and Miller, J.D., Jr., 1993. Precise U-Pb ages of Duluth Complex and related mafic intrusions, northeastern Minnesota: New insights for physical, petrogenetic, paleomagnetic and tectono-magmatic processes associated with the 1.1 Ga Midcontinent Rift system; Journal of Geophysical Research, v. 98, no. B8, p. 13,997–14, 013

Pan, Y., Fleet, M.E., and Longstaffe, F.J., 1999, Melt-related metasomatism in mafic granulites of the Quetico Subprovince, Ontario: constraints from O–Sr–Nd isotopic and fluid inclusion data; Canadian Journal of Earth Sciences, v. 36, p. 1449–1462.

Parrish, R.R., Roddick, J.C., Loveridge, W.D., and Sullivan, R.W., 1987. Uranium-lead analytical techniques at the geochronology laboratory, Geological Survey of Canada; *In:* Radiogenic Age and Isotopic Studies: Report 1; Geological Survey of Canada, Paper No. 87-2, p. 3–7.

Roddick, J.C., 1987. Generalized numerical error analysis with application to geochronology and thermodynamics; Geochimica et Cosmochimica Acta, v. 51, p. 359–362.

Roeder, P.L. and Emslie, R.F., 1970, Olivine-liquid equilibrium; Contributions to Mineralogy and Petrology, v. 29, p. 275–289.

Stacey, J.S. and Kramers, J.D., 1975. Approximation of Terrestrial Lead Isotope Evolution by a 2-Stage Model; Earth and Planetary Science Letters, v. 26, p. 207–221.

Sun, S.S. and McDonough, W.F., 1989. Chemical and isotopic systematics of oceanic basalts: implications for mantle composition and processes, in magmatism in the ocean basins, *In:* Magmatism in the Ocean Basins, (ed.) A.D. Saunders and M.J. Norry; Geological Society, Special Publication, v. 42, p. 313– 345.

Thomson, K., 1989. Noranda Exploration Company Limited, report of Gorham Township properties; Ontario Geologic Survey, Assessment File 2.12687.

Trevisan, B.E., 2014. The petrology, mineralization and regional context of the Thunder mafic to ultramafic intrusion, Midcontinent Rift, Thunder Bay, Ontario; M.Sc. Thesis, Lakehead University, Thunder Bay, Ontario, 299 p.

Trevisan, B., Hollings, P., and Ames, D.E., 2013. Field Trip 10: Geology and mineralization of the Thunder Intrusion, Thunder Bay, Ontario, *In:* Field Guide to Copper-Nickel-Platinum Group Element Deposits of the Lake Superior Region; Precambrian Research, Center Guidebook 13-01, p. 231–247.

Trevisan, B.E., Hollings, P., and Ames, D.E., 2015. Geochemistry of the Thunder mafic to ultramafic intrusion, Midcontinent Rift, Thunder Bay, Ontario; Ontario Geological Survey, Miscellaneous Release Data 305, 8 p.

GEOLOGICAL SURVEY OF CANADA
OPEN FILE 7856

Targeted Geoscience Initiative 4: Canadian Nickel-Copper-Platinum Group Elements-Chromium Ore Systems — Fertility, Pathfinders, New and Revised Models

New field observations and U-Pb ages in the Sudbury area: toward a detailed cross-section through the deformed Sudbury Structure

Wouter Bleeker[1], Sandra L. Kamo[2], Doreen E. Ames[1], and Don Davis[2]

[1]Geological Survey of Canada, Ottawa, Ontario
[2]University of Toronto, Toronto, Ontario

2015

© Her Majesty the Queen in Right of Canada, as represented by the Minister of Natural Resources Canada, 2015

This publication is available for free download through GEOSCAN (http://geoscan.nrcan.gc.ca/)

Recommended citation

Bleeker, W., Kamo, S.L., Ames, D.E., and Davis, D., 2015. New field observations and U-Pb ages in the Sudbury area: toward a detailed cross-section through the deformed Sudbury Structure, *In:* Targeted Geoscience Initiative 4: Canadian Nickel-Copper-Platinum Group Elements-Chromium Ore Systems — Fertility, Pathfinders, New and Revised Models, (ed.) D.E. Ames and M.G. Houlé; Geological Survey of Canada, Open File 7856, p. 151–166.

Publications in this series have not been edited; they are released as submitted by the authors.

Contribution to the Geological Survey of Canada's Targeted Geoscience Initiative 4 (TGI-4) Program (2010–2015)

TABLE OF CONTENTS

New field observations and U-Pb ages in the Sudbury area: toward a detailed cross-section through the deformed Sudbury Structure

Wouter Bleeker[1*], Sandra L. Kamo[2], Doreen E. Ames[1], and Don Davis[2]

[1]Geological Survey of Canada, 601 Booth Street, Ottawa, Ontario K1A 0E8
[2]Jack Satterly Geochronology Laboratory, University of Toronto, 22 Fussell Street, Toronto, Ontario M5S 3B1
*Corresponding author's e-mail: wbleeker@nrcan.gc.ca

ABSTRACT

The Sudbury area straddles the transition from the Archean Superior structural province to the Paleoproterozoic Southern province. To the south it is flanked by younger Proterozoic belts and finally the ca. 1 Ga Grenville Front. It is unique in that it also hosts the deformed remnants of one of the largest and oldest preserved impact structures in the geological record, the ~300 km diameter Sudbury Structure. This structure is characterized by a differentiated melt sheet, commonly referred to as the Sudbury Igneous Complex (SIC), which at or near its base hosts one of the largest concentrations of Ni-Cu-PGE sulphides on the planet. These metal-rich sulphides have formed the basis for an extensive mining industry since nickel was first discovered during railway construction in 1883. Despite more than a century of research, many geological questions remain unresolved in this fascinating area.

Here we present new field observations and preliminary U-Pb zircon and baddeleyite ID-TIMS results on a suite of about 20 critical samples that help resolve some long-standing geological questions. Many rock units in the Sudbury area have experienced significant shock metamorphism, which has increased the complexity of the Pb-loss patterns of their zircon crystals. Therefore, a key rationale for the present study was to apply "chemical abrasion" pre-treatment to single best-preserved zircon crystals, or fragments thereof, to reduce or eliminate young Pb loss and allow us to see through the shock-induced Pb loss.

We show that the Joe Lake Gabbro below the North Range is an Archean metagabbro, consistent with observed field relationships. Foliated granite on the Southeast Range is also Archean, requiring that metavolcanic rocks it intruded are Archean as well and not part of the basal Huronian rift succession. We present the first robust age on the Creighton Granite, showing it to be a folded subvolcanic sill and the magma chamber to the overlying Copper Cliff Rhyolite. Together, the Creighton Granite and Copper Cliff Rhyolite represent a single felsic magmatic system 2455–2460 Ma in age, which developed in the immediate aftermath of the main pulse of Matachewan mafic magmatism at ca. 2460 Ma. Magma mingling structures near the base of the Creighton Granite sill demonstrate the intimate relationship with Matachewan mafic magmas.

We have dated a number of mafic dyke swarms in the area, both pre- and post-dating the SIC. Among these is the first recognition of a ca. 2507 Ma dyke swarm in the Sudbury area. Furthermore, we present several ages on the SIC and its offset dykes, including a weighted mean $^{207}Pb/^{206}Pb$ age of 1849.7 ±0.2 Ma for a high-MgO norite in the South Range, and a precise concordant baddeleyite age of 1848.5 ±0.8 Ma for the radial Pele dyke on the North Range. The latter likely represents the youngest and final dyke injection of the offset dyke system into the fractured footwall of the SIC.

INTRODUCTION: NEW GEOCHRONOLOGY OF THE SUDBURY AREA

About 20 samples from across the wider Sudbury area were selected for U-Pb geochronology (Table 1, Fig. 1). These samples address a number of critical rock units and geological relationships. Some units, such as the Joe Lake Gabbro, North Range, had not been previously dated and their origin was subject to debate (e.g. Archean versus an early intrusive pulse of the Matachewan event). Others had poorly resolved ages (e.g. Creighton Granite), or were known to be artificial groupings based on varied field relationships (e.g. the "Trap dykes").

We also aimed to tackle, at the highest precision, the time scale of igneous crystallization and cooling of the Sudbury Igneous Complex (SIC), and to resolve some of the controversies surrounding which dykes are part

Bleeker, W., Kamo, S.L., Ames, D.E., and Davis, D., 2015. New field observations and U-Pb ages in the Sudbury area: toward a detailed cross-section through the deformed Sudbury Structure, *In:* Targeted Geoscience Initiative 4: Canadian Nickel-Copper-Platinum Group Elements-Chromium Ore Systems — Fertility, Pathfinders, New and Revised Models, (ed.) D.E. Ames and M.G. Houlé; Geological Survey of Canada, Open File 7856, p. 151–166.

Table 1. Preliminary results on samples from the Sudbury area.

#	Rock Unit	Sample No.	Easting (mE)	Northing (mN)	Description	New U-Pb Age (Ma)	Comment	Method[1]	Event	References
1	Joe Lake Gabbro	BNB-12-094	497330	5178808	Foliated metagabbro in footwall of SIC, cut by Sudbury Breccia	**ca. 2660**	Minimum; age of metamorphism	U-Pb, zircon	Levack Gneiss Complex	This study
2	Crosscutting pegmatite	BNB-12-095	497323	5178800	Pink granitic pegmatite dyke, shallow dipping and undeformed, cuts metagabbro	**2648 ±9**		U-Pb, zircon	Cartier Granite suite	This study
3	Late Archean granite	BNB-13-052	518496	5161806	Archean granite, moderately foliated, cuts mafic volcanic rocks	**2676 ±7***	Minimum: 2653 ±7	U-Pb, zircon	Late Archean granite, pre-Cartier	This study
4	"Pyroxenite dyke"	BNB-13-087A	453291	5162853	Mafic dyke, cutting Cartier Granite, and itself cut by megacrystic Matachewan diabase dyke	**2507 ±4***	Minimum: 2479 ±3	U-Pb, baddeleyite	Early Matachewan or Mistassini?	This study
5	"Tailings Pond Gneiss"	BNB-13-058	490094	5147118	Migmatitic gneiss, relict compositional banding in paleosome, probably paragneiss	*Not yet analyzed*	Detrital zircon population		Basal Huronian clastics	See Petrus (2014) for LA-ICP-MS data on zircons from a similar sample
6	Falconbridge Twp Intrusion	BNB-13-051	517882	5162308	Coarse anorthositic gabbro, steeply dipping layering, cuts Archean granite		No datable minerals recovered		Matachewan LIP, East Bull Lake suite?	This study; see Prevec & Baadsgaard (2005)
7	Gabbro sill enclave	BNB-13-093	485966	5144629	Coarse metagabbro enclave in brecciated Creighton Granite, along Lively regional road	**2476 ±7***	Both zircon and baddeleyite	U-Pb, zircon	Early Matachewan sills	This study
8	Matachewan dykes	BNB-08-130	452847	5289123	Large mafic dykes, north-northwest-trending, near Gogama	2460 ±2		U-Pb, baddeleyite	Matachewan LIP, main pulse	Bleeker et al. (2012); Halls et al. (2005)
9a	Creighton Granite	BNB-12-058	490094	5147118	Coarse-grained porphyritic granite/granodiorite, from approximate middle of granite sill	**2464 ±35***	Minimum: 2437 ±2	U-Pb, zircon	Matachewan LIP, felsic pulse	This study; see also Frarey et al. (1982) and Smith (2002)
9b	Creighton Granite	BNB-12-060A	486067	5141778	Second sample of Creighton Granite, west side of Hwy 144 Bypass, near top of sill	2433 ±4	Minimum	U-Pb, zircon	Matachewan LIP, felsic pulse	This study
10	Murray Granite	BNB-12-059	496735	5150992	Pink biotite granite, homogeneous, along railway cut	**2460 ±6***	Minimum: 2448 ±3	U-Pb, zircon	Matachewan LIP, felsic pulse	This study; see also Krogh et al. (1996)
11a	Copper Cliff Rhyolite	BNB-12-064	488430	5141367	Rhyolite tuff, crudely bedded, Lively area, large outcrops north of Hwy 17	2465 ±14* (2455-2460)	Minimum: 2455 ±3	U-Pb, zircon	Matachewan LIP, felsic pulse	This study; see also Krogh et al. (1984); Ketchum et al. (2013)
11b	Copper Cliff Rhyolite	BNB-12-098	489311	5141660	Massive flow-banded rhyolite near top of unit, Lively area, outcrop north of Hwy 17	2426 ±3	Minimum	U-Pb, zircon	Matachewan LIP, felsic pulse	This study
	Creighton & Copper Cliff	BNB-12-058, 060A, 064			Combined regression through Creighton Granite (4) and Copper Cliff (3) data	2464 ±12*	Combined (n=7, MSWD=3.1)	U-Pb, zircon	Matachewan LIP, felsic pulse	This study
	Creighton & Copper Cliff	BNB-12-058, 060A, 064			Combined regression through Creighton Granite (3) and Copper Cliff (3) data	**2459 ±7***	Combined (n=6, MSWD=1.9)	U-Pb, zircon	Matachewan LIP, felsic pulse	This study
12	Nipissing Sill	BNB-13-048A	502367	5142640	Large, more magnetic late-stage pegmatoidal melt pod in Nipissing Diabase	2215 ±1	Minimum	U-Pb, zircon & baddeleyite	Nipissing (Senneterre, Ungava)	This study; see also Corfu & Andrews (1986); Noble & Lightfoot (1992)
13a	Pre-SIC mafic dykes (Ia)	BNB-12-022	358234	5128148	Large mafic dyke cutting Huronian Supergroup	2116 ±5	Preliminary	U-Pb, baddeleyite	Marathon LIP	Bleeker & Chamberlain, unpublished data; see also Halls et al. (2008)
13b	Pre-SIC mafic dykes (Ib)	BNB-12-028B	331657	5135079	Large mafic dyke cutting Huronian Supergroup	2105 ±5	Preliminary	U-Pb, baddeleyite	Marathon LIP	Bleeker & Chamberlain, unpublished data
14	Pre-SIC mafic dykes (II)	BNB-12-025	353644	5122629	Large mafic dyke cutting Huronian Supergroup	ca. 1930	Preliminary	U-Pb, baddeleyite	New event for southern Superior	Bleeker & Chamberlain, unpublished data
15	Mafic norite	BNB-13-007	484226	5146795	Black Norite with high MgO, higher up in "norite stratigraphy", along Hwy 144 Bypass	**1849.7 ±0.2**	Weighted mean (n=4, MSWD=1.2)	U-Pb, evaporation & ID-TIMS	SIC meltsheet, early	This study; see also Davis (2008), Krogh et al. (1984)
16	"Crowfoot" granophyre	BNB-14-010	484495	5150103	Coarse latest crystallizing granophyre, South Range, along Hwy 144 Bypass	*in progress*		U-Pb, zircon	SIC meltsheet, final crystallization	
17	Hess Offset, quartz diorite	BNB-13-088A	449037	5160679	Outer main phase of quartz diorite, trench across Hess Offset dyke, no sulphides	**1849.1 ±0.9**	Upper intercept	U-Pb, baddeleyite	Early offset dyke injection into footwall	This study; see also Corfu & Lightfoot (1996)
18	Cascaden Offset, quartz diorite	BNB-13-089	458169	5162474	Quartz diorite dyke, fine- to medium-grained, ~10–12 m wide, northwest of SIC	*in progress*		U-Pb, baddeleyite	Offset dyke injection into footwall	Dave Smith, Wallbridge Mining Inc., pers. comm. (2013)
19	Pele Offset, evolved diorite	BNB-13-090B	477219	5178116	Evolved more felsic diorite, with plagioclase phenocrysts, from centre of dyke	1848.5 ±0.8	One concordant precise analysis	U-Pb, baddeleyite	Final, cooler offset dyke injection	This study
20	Trap dykes (III)	BNB-13-047E	502530	5142589	Late-stage granophyric melt pod in ~10 m-wide "Trap dyke"	1748 ±5	Preliminary	U-Pb, zircon	Trap dyke swarm	This study
21	Felsite dyke, undeformed	BNB-13-049	502340	5142616	Crosscutting felsic dyke, fine-grained matrix, small feldspar, biotite and quartz phenocrysts	**1766 ±9**	Youngest single zircon grain	U-Pb, zircon	Cutler Batholith suite?	This study; see also Davidson et al. (1992)

Notes:
1: CA-ID-TIMS on single zircons or small fragments thereof, unless otherwise noted.
*: Upper intercept based on discordant array with 1850 Ma lower intercept.
Ages noted in bold font are preferred interpretations of the data.

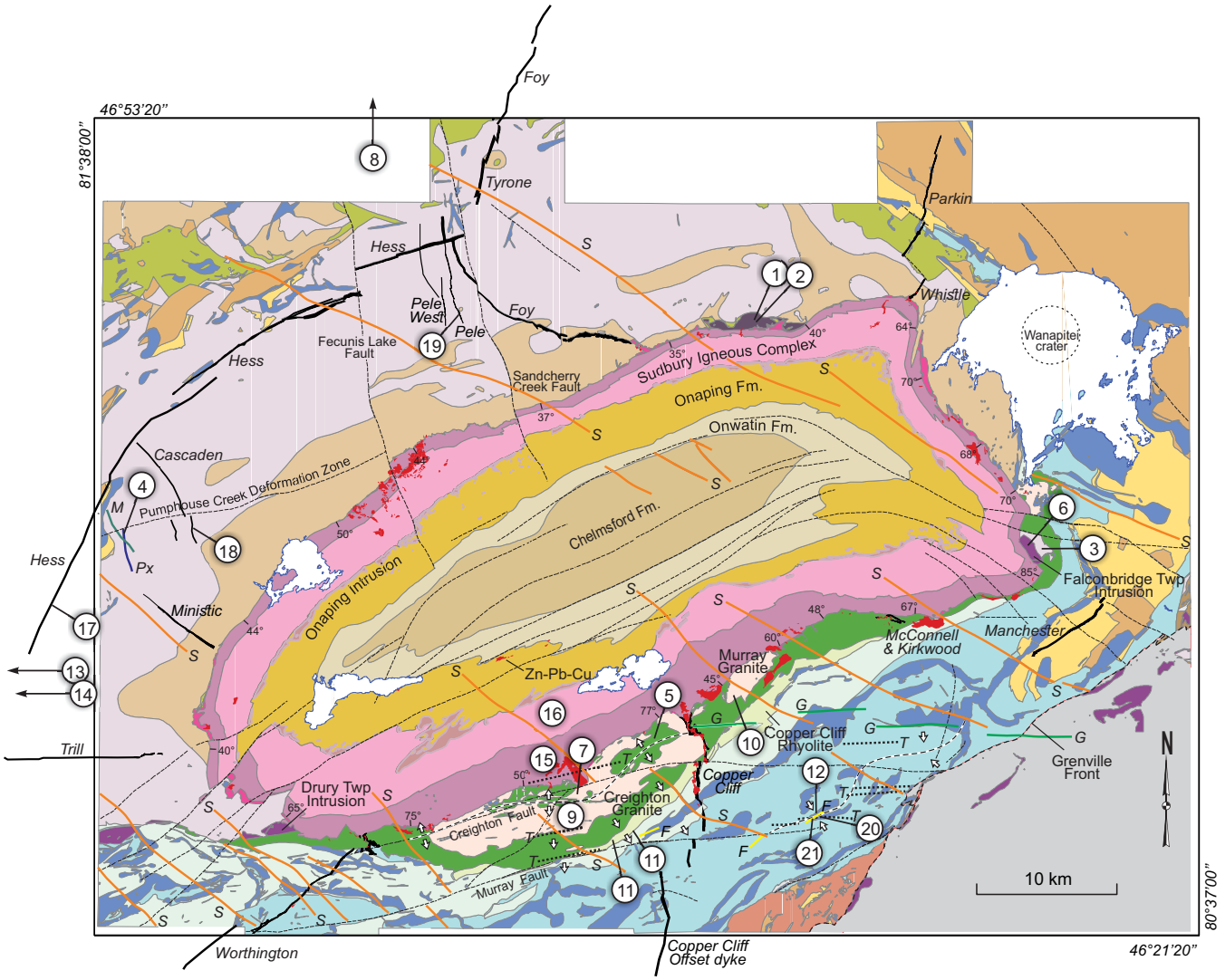

GRENVILLE PROVINCE
- Undifferentiated gneiss

YOUNGER PROTEROZOIC BELTS
- Chief Lake Complex, Cutler Batholith, other Paleo- to Mesoproterozoic rocks

WHITEWATER GROUP (ca. 1850–1830 Ma)
- Chelmsford Formation, turbidite
- Onwatin Formation, slate
- Onaping Formation, fallback breccia

SUDBURY IGNEOUS COMPLEX (1850 Ma)
- Offset dykes
- Onaping Intrusions
- Granophyre
- Norite
- Sublayer
- Ni-Cu-PGE sulphide orebodies

NIPISSING DIABASE (ca. 2220–2210 Ma)
- Diabase sills and sheets, gabbro

HURONIAN SUPERGROUP (ca. 2500–2300 Ma)
- Cobalt Group
- Quirke Lake Group
- Hough Lake Group
- McKim Formation turbidite (Elliot Lake Group)
- Mafic and felsic volcanic rocks (Elliot Lake Group)

PALEOPROTEROZOIC INTRUSIVE ROCKS (ca. 2480–2450 Ma)
- Creighton and Murray granite, and undiff.
- East Bull Lake Suite mafic intrusions

OTHER
- Antiform in Creighton Granite sill
- Faults and shear zones
- (#) U-Pb sample locality (see Table 1)

ARCHEAN BASEMENT OF THE SUPERIOR CRATON
- Cartier Granite Suite
- Metavolcanic rocks
- Levack Gneiss Complex
- Joe Lake Gabbro

SELECTED DYKES
- Px "Pyroxenite dyke" (ca. 2507 Ma)
- M Matachewan dykes (2460 Ma)
- Hess SIC Offset dykes (1849–1850 Ma)
- T Trap dykes (ca. 1750 Ma)
- F Felsite dykes (ca. 1766 Ma)
- S Sudbury dykes (1240 Ma)
- G Grenville dykes (590 Ma)

Figure 1. Map of the Sudbury area (adapted from Ames and Farrow, 2007), with locations of samples marked. Numbers 1 to 21 correlate with Table 1.

of the "offset dyke" system of the SIC versus unrelated older dyke sets.

Collectively, these ages will help to sharpen the geological framework for this unique area, and they will be incorporated into an updated and expanded version of the digital map compilation for the area (Ames et al., 2006; 2008a,b). Furthermore, they help constrain a detailed regional geological cross-section that will accompany an updated version of this map (Bleeker et al., 2013, 2014a,b).

RATIONALE

With several important geochronological questions unresolved in this area, a key rationale for the present study was to apply some critical innovations in high-precision ID-TIMS U-Pb geochronology. These include micro-sampling of complex zircon crystals, made possible by low-Pb blank levels of ~0.2–0.5 pg, and "chemical abrasion" pre-treatment of the selected single zircon fragments (Mattinson, 2005, 2011), to reduce or eliminate young Pb loss and thereby allowing us to see through the shock-induced Pb loss.

Obtaining precise ages on some of the pre-SIC target rocks has proven difficult due to most zircons having experienced substantial Pb loss at multiple times, notably at 1850 Ma or shortly thereafter, in response to the impact event (Dietz, 1964; Dietz and Butler, 1964; Bray et al., 1966; Pye et al., 1984; Faggart et al., 1985; Grieve et al., 1991; Spray et al., 2004) and the associated shock metamorphism (e.g. Krogh et al., 1996), but also at younger times (e.g. multiple Proterozoic events). Discordance patterns are further complicated by variable degrees of recent Pb loss, making many upper intercept age interpretations uncertain and non-unique. An important example is the age of the Creighton Granite, a major unit in the footwall of the South Range of the SIC (Fig. 1) that, despite several previous U-Pb studies (Frarey et al., 1982; Smith, 2002), has remained controversial due to variably discordant and scattered data points. Does this granite represent a relatively unique magmatic event in this part of the Superior craton at ca. 2330 Ma (Frarey et al., 1982), or at ca. 2375 Ma (Smith, 2002)? Or are these ages merely a function of unresolved Pb-loss complexity from damaged zircons?

A definitive answer to questions like these will only come from more concordant data on single zircons, avoiding mixing of discordant ages and minimizing projection to the concordia curve. Thus, the ever increasing ability to analyse smaller and better preserved single zircon grains, or only highest quality fragments thereof, and to improve their concordance through chemical abrasion, may finally resolve some of the long-standing age questions. By applying these techniques we have now resolved the age of the Creighton Granite to ca. 2460 Ma, consistent with this intrusion being a high-level subvolcanic sill and magma chamber of the Copper Cliff Rhyolite Formation, for which we have obtained a similar age.

On another level, the time scale of igneous crystallization and cooling of the ~3–5 km-thick Sudbury melt sheet represents another important question. We are tackling this by selecting first and last crystallizing phases of the SIC and subjecting their igneous zircons to an evaporative pre-treatment (similar to Davis, 2008) prior to high-precision ID-TIMS analysis of the annealed and most robust remnants of the crystals. This method holds the potential to resolve crystallization ages of distinct phases of the SIC down to an uncertainty level of ca. 0.1–0.2 Ma (2σ). Resolving this question of the time scale of cooling will inform advanced modeling studies of the dynamic and igneous evolution of the melt sheet.

SAMPLES, PRELIMINARY RESULTS, AND INTERPRETATION

Below we discuss preliminary results obtained on our U-Pb sample suite. Some samples are still in progress, whereas the odd sample failed to produce a suitable mineral separate or was otherwise aborted or temporarily set aside. In general, the samples and resulting ages will be discussed from oldest to youngest and with reference to Table 1. Locations of all samples are shown in Figure 1, with precise GPS coordinates (±4 m) given in the table.

In terms of interpretation, in some cases fully concordant results were obtained and interpretation of a final age is straightforward, with the uncertainty reflecting 95% confidence limits of the data. In other cases, where discordance was improved upon (relative to previous studies) but not fully eliminated, the data can be discussed in terms of a "minimum age" and a "preferred upper intercept age". The minimum age is provided by the $^{207}Pb/^{206}Pb$ age of the least discordant zircon analysis (barring inheritance). In some cases, for instance the new 2437 ±2 Ma minimum age for the Creighton Granite, such ages already provide a strong guide toward the final answer and eliminate previously proposed age interpretations.

In a number of samples, multiple discordant data points require some judgement in the choice of regression and a corresponding upper intercept calculation. Such discordant data commonly fit a discordia line with an 1850 Ma lower intercept (e.g. Krogh, 1984; Krogh et al., 1996), i.e., the age of impact and shock-induced Pb loss. Where appropriate, we thus calculate an upper intercept based on such a model. In some samples, however, alternative regressions and upper intercepts are suggested by the data.

1. Joe Lake Gabbro, Immediate Footwall to Part of the North Range

Many small rounded and clear zircon crystals were separated from the Joe Lake Gabbro. Field observations showed this gabbro to be a variably foliated metagabbro (Fig. 2a), with a foliation that merged with that of the surrounding Levack Gneiss Complex (Card, 1994). We thus interpret the Joe Lake Gabbro as an Archean metagabbro and the zircons most likely represent metamorphic zircon growth during deformation. Concordant and near concordant data indicate an age of high-grade metamorphism and zircon growth at ca. 2660 Ma. Interestingly, the zircons did not show any obvious shock damage (fracturing, pervasive cloudiness). The Joe Lake Gabbro is an Archean metagabbro and not part of the Paleoproterozoic East Bull Lake suite.

2. Crosscutting Pegmatite Dykes, Joe Lake Area

The Joe Lake metagabbro is crosscut by several parallel, shallow dipping, and essentially undeformed pink granite pegmatite dykes (Fig. 2b). These dykes postdate the penetrative fabric of the host metagabbro and represent a late (latest?) granitic phase intruding the Levack Gneiss Complex. Data for four zircon grains are variably discordant but collinear, yielding an upper intercept age of 2648 ±9 Ma, which is interpreted as the crystallization age of this late granite pegmatite, in agreement with the slightly older metamorphic age of the host metagabbro. The data allow some latitude in the choice of lower intercept, but they do not strongly project to a lower intercept of 1850 Ma; i.e., there is no overriding control from shock-induced Pb loss. This duplicates observations in the previous sample. These pegmatite dykes, in a broad sense, are probably part of the ca. 2642 Ma Cartier Granite complex (Card, 1994; Meldrum et al., 1997) that dominates the area north of the SIC, and they post-date essentially all of the penetrative Archean deformation in the Levack Gneiss Complex. Wodicka (1997) reported similar age constraints on deformation as part of a larger geochronological data set on the northern footwall of the SIC.

3. Late Archean Granite, Southeast Range, Falconbridge Township

In Falconbridge Township, near the southeastern apex of the folded SIC, we dated a foliated biotite granite (Fig. 2c). This granite intrudes metavolcanic rocks, and is itself intruded by the crudely layered anorthositic gabbro body of the "Falconbridge Township Intrusion" (Thomson, 1957; Dressler, 1984; see also section 6, *Falconbridge Township Intrusion,* below). On the present compilation map of the Sudbury Structure (Ames et al., 2006, 2008b), volcanic rocks surrounding the foliated granite body are identified as lower Huronian mafic volcanic rocks (Stobie Formation). However, multiple single zircon analyses indicate a late Archean age for this granite, with a minimum age of ca. 2653 Ma. The near concordant data fit a discordia line to an 1850 Ma lower intercept and, using this model, provide a 2676 ±7 Ma upper intercept age. Clearly this granite is part of the Archean basement below the Huronian rift succession and the mafic volcanic rocks it intruded must also be Archean, rather than early Huronian. Remapping of this area is required to redefine the Archean-Huronian unconformity. In contrast to the North Range samples discussed above (1 and 2), the zircon data of this late Archean granite indicate strong shock metamorphism, in agreement with the presence of major bodies of Sudbury Breccia in the immediate area. This can be interpreted, qualitatively, in terms of an order of magnitude stronger shock intensity in this area compared to that in the northern footwall of the SIC near Joe Lake. In other words, the Falconbridge Township area must be significantly closer to the centre of the impact than the Joe Lake area.

4. "Pyroxenite Dyke", North Range: A Sudbury Igneous Complex-Related Offset Dyke?

This unit is a ~50 m-wide mafic dyke of melanocratic gabbro to pyroxenite that intrudes the Cartier Granite complex, ~10 km northwest of the northwestern flank of the SIC (Fig. 2d; see Fig. 1 for location). There was some question whether this dyke might represent a radially oriented "offset dyke" (D. Smith, Wallbridge Mining, pers. comm., 2013). Field investigation by the first author uncovered the crosscutting contact of a plagioclase megacrystic Matachewan dyke, with the latter dyke chilled against the "pyroxenite dyke". Hence the "pyroxenite dyke" is older than ca. 2460 Ma. Baddeleyite crystals separated from this dyke indicate a minimum age of 2479 ±3 Ma. Several of the discordant fractions show a linear array that is consistent with an 1850 Ma lower intercept. Using this model, the upper intercept age is 2507 ±4 Ma. This allows the possibility that ca. 2510 Ma dykes (e.g. Mistassini event; Fahrig and West, 1986; Ernst and Bleeker, 2010) are present in this part of the Superior craton. Alternatively, this dyke may represent a primitive early pulse of the Matachewan event (cf. Heaman, 1997). It is interesting to note that a detrital zircon of similar age (2497 ±10 Ma) has been reported from basal Huronian sediments further west (a quartz wacke of the Livingstone Creek Formation; see Craddock et al., 2013), providing additional evidence for a zircon source, and thus magmatic activity, predating the Matachewan event in the southern Superior craton.

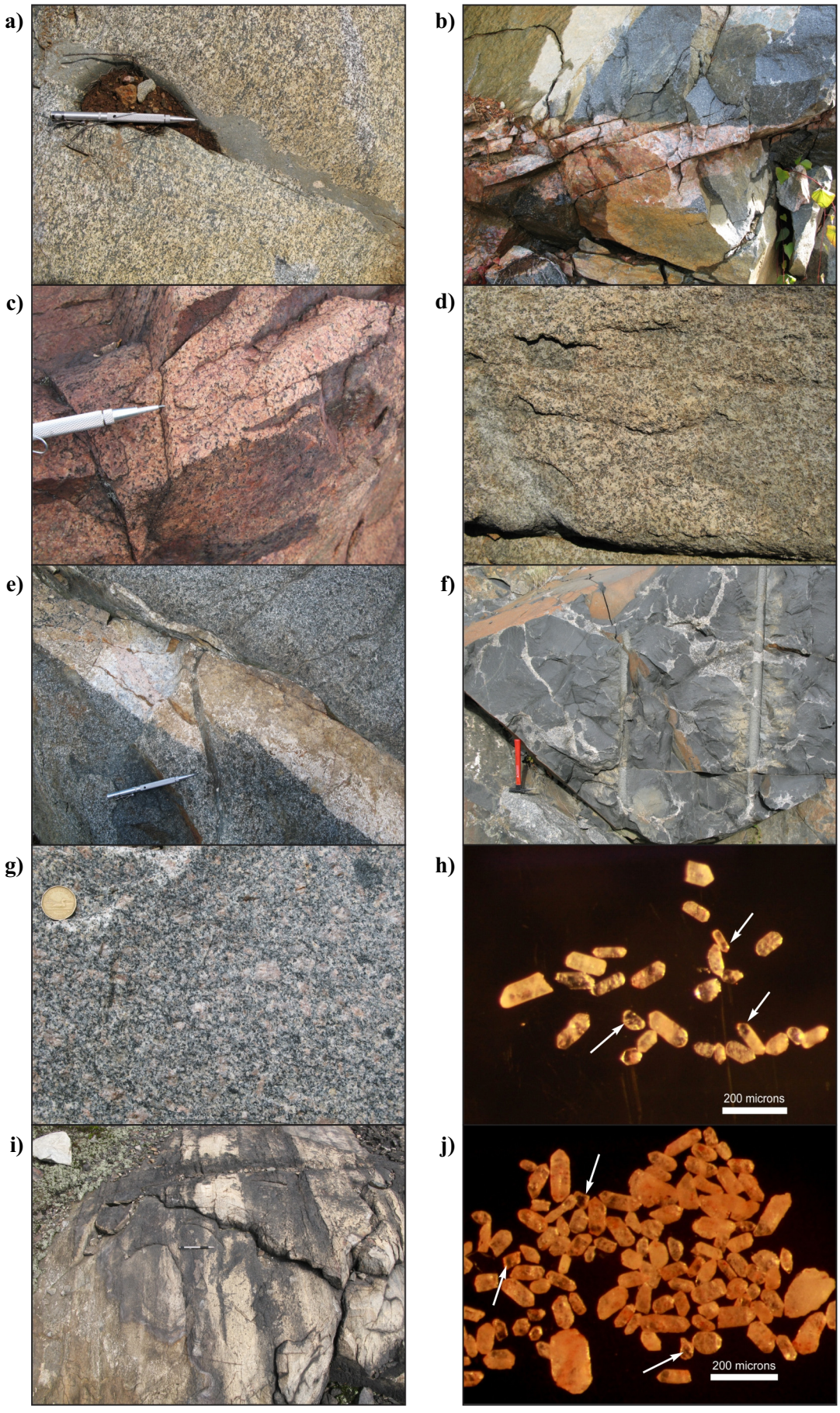
a)
b)
c)
d)
e)
f)
g)
h)
200 microns
i)
j)
200 microns

5. "Tailings Pond Gneiss"

A migmatitic gneiss, intruded by granitic leucosome veins, occurs in an outcrop in the middle of the large tailings pond west of the Copper Cliff smelter complex. The question was whether this gneissic rock represents an Archean basement inlier on the South Range. On closer inspection and after slabbing of the samples, it was revealed that this gneiss represents a high-grade metasandstone or wacke with relict graded bedding, and not an Archean orthogneiss. Its overall character suggests a high-grade metamorphic lower Huronian rift sandstone that is part of the migmatitic envelope to the Creighton Granite sill (near the inferred hot base of this large sill). A heterogeneous detrital zircon population separated from this sample supports this interpretation. We have not yet analyzed any of these zircons, which likely represent a varied Archean provenance. Any provenance interpretation is likely to be complicated by "smearing" of $^{207}Pb/^{206}Pb$ ages due to varied degrees of 1850 Ma Pb loss, even if chemical abrasion is successful in eliminating most of the young Pb loss. Additional data on this "gneiss" can be found in Petrus (2014).

6. Falconbridge Township Intrusion

This is one of two intrusions (Falconbridge and Drury) thought to be of early Huronian age. They are dominated by layered anorthositic gabbro. Their ages are currently not well constrained but Prevec and Baadsgaard (2005) suggested an age of ca. 2441 Ma for the Falconbridge intrusion based on complexly discordant zircon data. Unfortunately, our sample of the Falconbridge intrusion did not yield any datable minerals. We may revisit these intrusions in the near future. However, we are aware of at least one independent study aiming to date the Drury Township Intrusion.

7. Coarse Gabbro Enclave in Creighton Granite

The Creighton Granite intruded the lower Huronian succession. The granite includes rafts of metamorphosed siltstone, graded wacke, and arenite, as well as mafic sills of probable Matachewan age. Near the Creighton Mine, in what we infer is the base of the folded Creighton Granite sill (Fig. 1), a large gabbro inclusion or enclave is surrounded by Creighton Granite (Fig. 2e). From the various mafic rocks in this area, this gabbro was the coarsest grained and thus most likely to yield datable minerals. Mineral separation of a ~10 kg sample yielded both skeletal primary zircon grains and baddeleyite. The latter mineral showed overgrowths of polycrystalline zircon and produced complex data. Chemically abraded skeletal zircons are somewhat discordant, defining a linear array consistent with an 1850 Ma lower intercept. Based on this model, the data indicate an upper intercept age of 2476 ±7 Ma, in agreement with recently published ages for other early Huronian intrusions, such as the River Valley intrusion (James et al., 2002 and references therein).

8. Matachewan Dykes, Main Pulse

As part of a separate study, the timing of the main pulse of Matachewan dykes north of Sudbury has been refined. Ages show a tight clustering around 2460 Ma. (Bleeker et al., 2012; see also Halls et al., 2005; cf. Heaman, 1997). Dykes of this age typically carry ubiquitous calcic plagioclase megacrysts, indicating some residence time of the magma in a large lower or mid-crustal magma chamber. They are clearly younger than the ca. 2480 Ma early pulse of the Matachewan event (e.g. Krogh et al., 1984; James et al., 2002) that led to the East Bull Lake Suite of layered intrusions. We include this age here in Table 1 because it is important for the age interpretation of other units along the South Range of the SIC. Main pulse Matachewan dykes are ubiquitous in basement to the north of the SIC but are not known to crosscut the Creighton Granite and lower Huronian formations such as the Copper Cliff Rhyolite. Crosscutting northerly trending mafic dykes would be immediately apparent in these felsic units. Their absence thus constrains Huronian felsic magmatism to younger than 2460 Ma.

9. Creighton Granite

We sampled the main phase of the Creighton Granite (Fig. 2g), a coarse-grained, variably K-feldspar porphyritic granite to granodiorite (e.g. Dutch, 1979;

Figure 2 (opposite page). Photographs of selected samples. **a)** Foliated metagabbro of the ca. 2660 Ma Joe Lake Gabbro, immediate footwall to parts of the North Range of the Sudbury Igneous Complex (SIC) and host to the WD16 deposit. The foliation in the metagabbro is cut by a Sudbury Breccia dykelet. **b)** Shallow-dipping pink pegmatite that cuts across the foliation of the Joe Lake metagabbro, dated at ca. 2648 ±9 Ma. **c)** Late Archean foliated biotite granite, Falconbridge Township, dated at ca. 2676 ±7 Ma. **d)** Close-up of the "pyroxenite dyke" north of the SIC, dated at ca. 2507 Ma. **e)** Metagabbro enclave in Creighton Granite, dated at ca. 2476±7 Ma. Gabbro is cut by granitic dykelet. **f)** Magma mingling and hybridization between ca. 2460 Ma mafic magma and Creighton Granite felsic magma. **g)** Porphyritic Creighton Granite, main phase, dated at ca. 2460 Ma. **h)** Examples of zircons from the Creighton Granite, after annealing. Small clear grain fragments that were analyzed are highlighted (see arrows). **i)** Bedded crystal tuff of the Copper Cliff Rhyolite Formation, with a minimum age of 2455 ±3 Ma. **j)** Example of zircons from the Copper Cliff crystal tuff, with clear fragments that were analyzed highlighted. Combined age for the Creighton Granite and Copper Cliff Rhyolite is 2455–2460 Ma.

Table 2. U-Pb data for Creighton Granite and Copper Cliff Rhyolite samples.

Sample Number	Weight (µg)	U (ppm)	Th/U	PbC (pg)	$^{206}Pb/^{204}Pb$ measured	$^{207}Pb/^{235}U$	2 σ	$^{206}Pb/^{238}U$	2 σ	Error Corr	$^{207}Pb/^{206}Pb$	2 σ	$^{206}Pb/^{238}U$ Age (Ma)	2 σ	$^{207}Pb/^{235}U$ Age (Ma)	2 σ	$^{207}Pb/^{206}Pb$ Age (Ma)	2 σ	Disc (%)
BNB-12-058 *Creighton Granite (K-feldspar porphyritic granodiorite; GPS#2093: 46°26'23.04"N, 81°11'15.65"W)*																			
z1	0.2	377	0.47	0.5	4594	9.904	0.030	0.4540	0.0012	0.897	0.15823	0.00021	2412.8	5.3	2425.9	2.8	2436.9	2.3	1.2
z2	0.8	100	0.47	0.5	4811	9.484	0.030	0.4437	0.0013	0.851	0.15501	0.00026	2367.3	5.9	2386.0	2.9	2401.9	2.9	1.7
z3	0.2	675	0.51	0.4	9284	8.848	0.022	0.4279	0.0009	0.925	0.14998	0.00015	2296.2	4.0	2322.5	2.3	2345.7	1.7	2.5
BNB-12-060A *Creighton Granite (K-feldspar porphyritic granodiorite; GPS#2107: 46°25'45.96"N, 81°10'52.85"W)*																			
z1	na	na	0.58	8.0	376	9.175	0.108	0.4353	0.0014	0.787	0.15289	0.00144	2329.4	6.2	2355.7	10.8	2378.5	16.1	2.5
z2	na	na	0.44	3.1	1631	9.630	0.036	0.4424	0.0011	0.761	0.15785	0.00038	2361.6	5.1	2400.0	3.4	2432.8	4.1	3.5
BNB12-064 *Copper Cliff Rhyolite Formation (crystal tuff; GPS#2131: 46°25'32.80"N, 81°09'02.09"W)*																			
z1	0.3	28	0.68	0.3	727	9.902	0.144	0.4576	0.0060	0.923	0.15694	0.00088	2429	27	2426	13	2422.9	9.5	-0.3
z2	0.8	45	0.45	0.2	4834	10.008	0.046	0.4569	0.0020	0.956	0.15884	0.00021	2426.1	8.8	2435.5	4.2	2443.4	2.3	0.9
z3	0.3	125	0.63	0.2	6059	10.067	0.049	0.4564	0.0020	0.938	0.15995	0.00027	2423.9	8.9	2440.9	4.5	2455.2	2.8	1.5
z4	1.0	13	0.77	0.5	751	10.148	0.103	0.4617	0.0039	0.896	0.15942	0.00073	2447	17	2448	9	2449.5	7.7	0.1
BNB12-098 *Copper Cliff Rhyolite Formation (flow-banded rhyolite: GPS#2205: 46°25'42.34"N, 81°08'20.83"W)*																			
z1	1.0	14	0.30	0.8	389	4.589	0.127	0.3161	0.0029	0.603	0.10531	0.00245	1771	14	1747	23	1720.0	43.0	-3.4
z2	na	na	0.53	3.4	450	8.296	0.025	0.3828	0.0009	0.841	0.15718	0.00026	2089	4	2264	3	2425.6	2.8	16.2
z3	na	na	0.45	10	1369	9.607	0.302	0.4386	0.0027	0.952	0.15886	0.00407	2344	12	2398	29	2443.6	43.6	4.8

Notes:
All zircon grains have been thermally annealed and etched in HF (Mattinson, 2005).
Th/U calculated from radiogenic $^{208}Pb/^{206}Pb$ ratio and $^{207}Pb/^{206}Pb$ age assuming concordance.
PbC is total common Pb assuming the isotopic composition of laboratory blank.
$^{206}Pb/^{204}Pb$ corrected for fractionation and common Pb in spike.
Pb/U ratio corrected for fractionation, common Pb in the spike, and blank.
Error Corr is correllation coefficients of X-Y error on the concordia plot.
Correction for ^{230}Th disequilibrium in $^{206}Pb/^{238}U$ and $^{207}Pb/^{206}Pb$ assuming Th/U of 4.2 in the magma.
Disc is percent discordance for the given $^{207}Pb/^{206}Pb$ age.

Frarey et al., 1982; Smith, 2002), in two places along Highway 144, west of Lively. Although zircon is relatively abundant, it is poorly preserved, in part due to fracturing as a result of the shock metamorphism and subsequent alteration. Previous studies have shown that it is difficult to obtain concordant data from this unit (e.g. Smith, 2002). We dated rare, small, unaltered crystal fragments (Fig. 2h) that were chemically abraded prior to U-Pb analysis. This strategy indeed produced more concordant results than previous studies but none of the data are fully concordant (Table 2, Fig. 3). However, the data define a linear array consistent with an 1850 Ma lower intercept. The least-discordant grain indicates a minimum age of 2437 ±2 Ma, eliminating the possibility that this granite might be younger than 2400 Ma (cf. Frarey et al., 1982; Smith, 2002; Raharimahefa et al., 2014). Collectively, the data suggest an upper intercept age of ca. 2460 Ma, an age that is similar to that of the nearby Murray Granite (see below, and Krogh et al., 1996). It allows a simple interpretation of the field relationships in which the Creighton Granite is a subvolcanic sill and the magma chamber to the overlying and chemically similar Copper Cliff Rhyolite Formation. Magma-mingling structures and hybridization with mafic magmas were observed near the base of the sill (Fig. 2f) and indicate a close and essentially contemporaneous relationship with mafic magmas low in the Huronian rift succession. South of the Creighton Granite and evidently part of the felsic magmatic system, intrusive bodies of finer grained granite porphyry were observed at an intermediate stratigraphic level between the top of the Creighton Granite sill and the overlying Copper Cliff Rhyolite.

10. Murray Granite

A similar approach as above applied to the Murray Granite yielded three new analyses that are more concordant than but collinear with previously reported results (Krogh et al., 1996). One of our analyses overlaps the concordia curve and indicates a minimum age of 2448 ±3 Ma. An upper intercept age calculated including these new data is 2460 ±6 Ma, consistent with the field relationships described above (i.e. absence of Matachewan dykes). The more discordant data indicate the strong control imparted by 1850 Ma Pb loss, i.e., further evidence for the intense shock-induced Pb loss in this part of the South Range, as documented and described in detail by Krogh et al. (1996).

11. Copper Cliff Rhyolite

We separated zircons from two different samples of the Copper Cliff Rhyolite Formation, a layered crystal-rich tuff from near the middle of the formation (Fig. 2i) and a massive flow-banded rhyolite near the top of the formation, both from the Lively area. Although zircons were abundant, nearly all are of poor quality (Fig. 2j). Three small fragments from the crystal tuff nevertheless plot toward the upper end of the discordant array (Fig. 3). The most precise of these is 1.5% discordant and yields a minimum age of 2455 ±3 Ma. A regression of all the data (Copper Cliff plus Creighton, n=7), from 1850 Ma, yields an upper intercept age of 2464 ±12 Ma with a mean square weighted deviation (MSWD) of 3.1. Eliminating one point from this regression (n=6) yields a better fit (MSWD<2.0) and more precise upper intercept age of 2459 ±7 Ma. This regression also fits the least discordant data from earlier studies of the

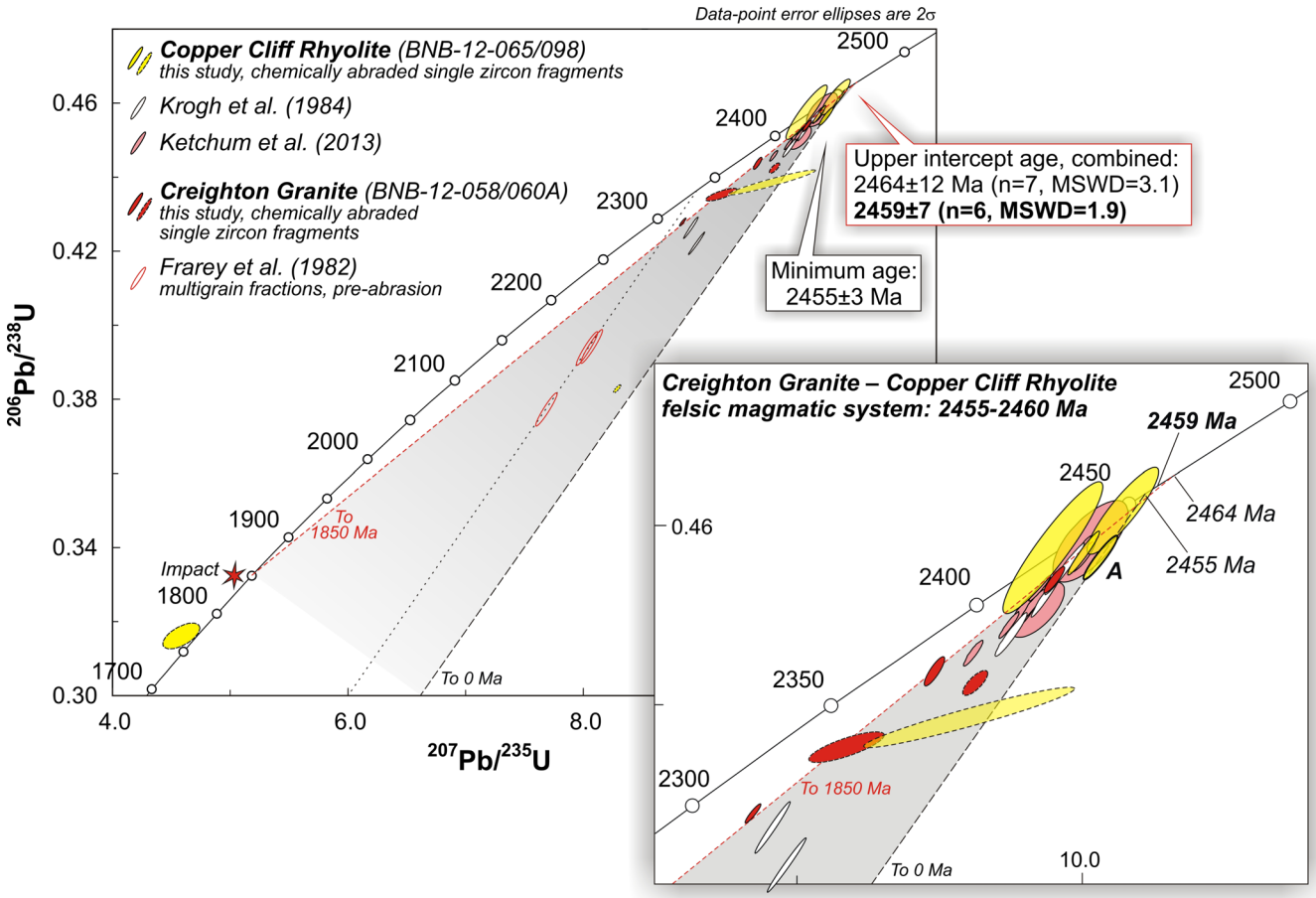

Figure 3. U-Pb concordia diagram of Creighton Granite (red ellipses) and Copper Cliff Rhyolite (yellow and other ellipses) zircon data. Data from Krogh et al. (1984; open ellipses) and Ketchum et al. (2013; pink ellipses) are also shown. The various data sample the complex Pb-loss field (shaded grey) bounded by the shock metamorphism-induced discordia line (red dashed line) to 1850 Ma and various younger episodes of Pb loss, and finally the chord to the origin defined by recent Pb loss. Large multi-grain zircon fractions of Frarey et al. (1982), from an early pre-air abrasion study on the Creighton Granite (open red ellipses), sample the middle of this field, averaging various degrees of Pb loss and processes. Due to the severity of the Pb loss, only the clearest grain fragments pre-treated by chemical abrasion get close to the apex of the Pb-loss field and approach the primary crystallization age. The $^{207}Pb/^{206}Pb$ age of our most precise and least discordant datum from the Copper Cliff crystal tuff sample (A in inset) constrains a minimum age of 2455 ±3 Ma. The majority of the chemically abraded zircon data plot on or near the discordia with the 1850 Ma lower intercept, the age of shock-induced Pb loss. The upper intercept of this discordia is 2464 ±12 Ma or 2459 ±7 Ma if one analysis is eliminated from the regression. Together with field relationships, the age of the combined Creighton Granite and Copper Cliff Rhyolite magmatic system can be constrained to 2455–2460 Ma, immediately following the main pulse of Matachewan mafic magma input at ca. 2460 Ma.

Copper Cliff Rhyolite (Krogh et al., 1984; Ketchum et al., 2013) and is the most precise age estimate that can be interpreted from our data. Together with the constraint from the Matachewan dykes, and also considering the new age of the nearby Murray Granite, 2460 ±6 Ma, we suggest that the age of the Copper Cliff Rhyolite and Creighton Granite magmatic system is 2455–2460 Ma. This is slightly older and more precise than previous estimates for the age of the Copper Cliff Rhyolite (Krogh et al., 1984; see also Ketchum et al., 2013). All our results are consistent with a sharply timed peak of felsic magmatism at ca. 2455–2460 Ma, immediately following the main pulse of Matachewan mafic magma input at ca. 2460 Ma. One zircon from the flow-banded rhyolite gave a younger age near the time of impact. This analysis is reversely discordant and plots at the young end of the mixing line from 2464 to 1850 Ma. This small equant grain (~50 μm) appears to have recrystallized as a consequence of the impact event, which would have reset its U-Pb systems at 1850 Ma.

12. Nipissing Diabase Sill, South of the Sudbury Igneous Complex, Conformable in Mississagi Formation Quartzite

We sampled one of the main Nipissing Diabase sills south of the SIC (Fig. 1). The sill is conformable with layering (i.e. bedding) in the surrounding Mississagi Formation quartzite, and both are folded into a tight east-plunging syncline. These observations are inconsistent with suggestions of a pre-Nipissing folding event in the area, the so-called "Blezardian orogeny"

(Frarey et al., 1982; Stockwell, 1982). The diabase sill hosts several late-stage pegmatoidal pods from which baddeleyite and skeletal zircon were extracted. U-Pb data for both minerals define a 2215 ±1 Ma upper intercept age with a lower intercept anchored at 0 Ma, which we interpret as a minimum age for the time of intrusion. If the grains were affected by some earlier Pb loss, a slightly older upper intercept in the 2215–2220 Ma range is possible. This new result is in agreement with previous age estimates on Nipissing Diabase (Corfu and Andrews, 1986; Noble and Lightfoot, 1992; see also Buchan et al., 1993).

13. Pre-Sudbury Igneous Complex Mafic Dykes, I

Rocks along the South Range are intruded by a variety of mafic dykes that post-date the Creighton Granite. Apart from the much younger and unmetamorphosed "Sudbury" olivine diabase dykes (e.g. Krogh et al., 1987), all of these are metamorphosed, in broad terms allowing an age range from ca. 2450 Ma to ca. 1600 Ma. On closer inspection, some of these metadiabase dykes are affected by Sudbury Breccia formation, whereas others post-date Sudbury Breccia and crosscut all SIC units. Trends of the metadiabase dykes vary from 040 to 100°, also suggesting more than one event. Many of these dykes have been referred to as "Trap dykes". The older of these dykes are difficult to date because they are typically less than 15 m wide and fully recrystallized. In a separate study, we have dated approximately east-west-trending diabase dykes well to the west of the SIC, and these were shown to be ca. 2105–2116 Ma (Bleeker and Chamberlain, in prep.), i.e., they belong to the Marathon large igneous province (Fahrig and West, 1986; Halls et al., 2008). We therefore suggest that dykes of this age likely extend into the Sudbury area and represent some of the pre-SIC dykes.

14. Pre-Sudbury Igneous Complex Mafic Dykes, II

Similar to the mafic dykes described above, and again well west of the SIC, a more northwesterly trending set of mafic dykes was also dated, yielding a preliminary baddeleyite age of ca. 1900–1950 Ma (Bleeker and Chamberlain, in prep.). Again, we suspect this event to be represented in the Sudbury area.

15. Mafic High-MgO Norite, Sudbury Igneous Complex

This unit consists of a dark, MgO-rich norite high in the norite "stratigraphy" of the South Range (Lightfoot and Zotov, 2005). It contains both baddeleyite and newly formed skeletal zircons. Zircon grains were pretreated by evaporating off labile Pb at high temperature, in vacuum within a mass spectrometer. The remainder of the grains were then dissolved and subjected to standard ID-TIMS analysis. Geological discordance cannot be determined by this method because of the Pb evaporation step but this does not disturb $^{207}Pb/^{206}Pb$ ages, which may represent the magmatic age if disturbed Pb was completely eliminated. Four analyses, each involving multiple zircons pretreated by evaporation, fully overlap and yield a precise weighted mean of 1849.7 ±0.2 Ma, with an MSWD of 1.16, representing the zircon crystallization age in this part of the norite stratigraphy. This age is comparable to ages obtained by Davis (2008).

16. Last Crystallizing Granophyre Phase, the "Crowfoot" Granophyre, Sudbury Igneous Complex

We consider the very coarse "Crowfoot" granophyre as a likely candidate for the last water- and incompatible element-enriched residual melt phase of the SIC. Using a similar strategy as described above for the norite, we hope to obtain a highly precise age for this stage of the crystallization history, thus constraining the overall time span of igneous crystallization and cooling of the SIC. Only crosscutting granitic dykes represent potentially younger melt phases (derived from melting of the footwall?), and could potentially add further insights. Work on these units is in progress.

17. Hess Offset Dyke, Outer Inclusion-Free Quartz Diorite ("QD")

As part of on-going efforts to date some of the recently uncovered offset dykes, we dated a homogeneous outer quartz diorite phase of the concentric Hess Offset dyke (Wood and Spray, 1998), in a new exploration trench northwest of the SIC. This particular sample was partly meant as a benchmark for other offset dyke data sets. The sample contained fresh unaltered baddeleyite. Four nearly concordant fractions define an age of 1849.1 ±0.9 Ma (regression through 0 Ma). This age is in agreement with the high-precision age on the norite (see section 15, *Mafic High-MgO Norite, Sudbury Igneous Complex,* above), and with previous U-Pb zircon and baddeleyite ages on offset dykes (Corfu and Lightfoot, 1996; Osterman et al., 1996).

18. Cascaden Offset Dyke, Northwest of the Sudbury Igneous Complex

The Cascaden dyke, which is also located to the northwest of the SIC, is a suspected radial offset dyke. It was discovered by Wallbridge Mining geologists. It is ~10–12 m wide and trends ~330º, with a subvertical attitude. It consists of fine-grained, somewhat more evolved, quartz diorite with a field appearance similar to that of other offset dykes. We have identified badde-

leyite in thin section and U-Pb dating of this dyke is in progress.

19. Pele Offset Dyke, North of the Sudbury Igneous Complex

This interesting ~28 m-wide dyke is more evolved than typical South Range quartz diorite dykes. It is radial, essentially vertical, and clearly chilled against granitic country rocks. It contains small platy plagioclase phenocrysts, which near the margin are aligned in the magmatic flow. Evidently this dyke, if part of the SIC offset dyke system, was injected late and no longer was superheated, with plagioclase on the liquidus during emplacement and phenocrysts having grown to ~5 mm. A sample from the medium-grained centre of this dyke yielded baddeleyite, one fraction of which is fully concordant with a precise age of 1848.5 ±0.8 Ma. From this we conclude that this dyke is indeed part of the offset dyke system and one of the last dykes to be injected into the footwall. The precise age of this more evolved dyke provides a hint of the young end of the SIC crystallization time scale, with an overall duration on the order of ~0.5 to 1.0 Myr, from 1849.7 ±0.2 Ma to 1848.8 ±0.8 Ma. This estimate of the overall time scale of the high-temperature part of the thermal evolution is consistent with, but more precise than, that provided by hydrothermal titanite from overlying Onaping Formation breccia (1848.4 +3.80/-1.8 Ma, see Ames et al., 1998).

20. Post-Sudbury Igneous Complex "Trap Dykes", III, South Range of the Sudbury Igneous Complex

Metadiabase dykes, with sheared margins but otherwise essentially undeformed, form a distinct swarm of approximately east-west-trending diabase dykes across the South Range (Fig. 1). They cut across the SIC, the offset dykes, and some of the Ni-sulphide orebodies (P. Lightfoot, pers. comm.), and they also post-date most if not all of the folding in the SIC and Huronian Supergroup. Yet they are fully metamorphic in character, i.e., characterized by fully recrystallized metamorphic mineral assemblages. They must be significantly younger than 1850 Ma, yet old enough to see the regional metamorphism across the South Range. We have identified both micro-baddeleyite and late-stage zircon in these typically 5–15 m-wide dykes and dating is in progress. Our preliminary age, based on chemically abraded zircons, is 1748 ±5 Ma. We suggest that the name "Trap dykes" or "Trap dyke swarm" be reserved for these post-SIC dykes. They most likely relate to a post-Penokean rifting event in the evolving margin of southeastern Laurentia.

21. Northeast-trending Felsite Dykes

A distinct suite of very fine-grained, weakly porphyritic felsic dykes intrudes across the South Range. (Fig. 1). They are granitic in composition, with small phenocrysts of quartz, feldspar, and black biotite in a very fine-grained quartzofeldspathic matrix. They are near vertical, with a northeasterly trend, and are essentially undeformed, showing only minor faulting with quartz vein development. They post-date the Trap dyke swarm. Dating of these dykes is complicated by inheritance, as demonstrated by one of our samples, but a single concordant zircon analysis indicates a maximum age of intrusion at 1766 ±9 Ma. If confirmed, this would represent the onset of the post-Penokean granitoid events documented further south (e.g. Davidson et al., 1992; Sullivan and Davidson, 1993; Davidson and van Breemen, 1994; see also Corfu and Easton, 2001). The relatively undeformed character of these dykes near the SIC indicates that essentially all deformation of the South Range was in place by ca. 1766 Ma.

CONCLUSIONS

New U-Pb ages are presented on a suite of ~20 samples from the Sudbury area, together with new field observations. Some of the age data are preliminary or still in progress.

On the North Range of the SIC, our field observations and age data show that the Joe Lake Gabbro is a metagabbro unit within the Levack Gneiss Complex. It is not part of the East Bull Lake suite of early Huronian layered intrusions. As the latter intrusions were emplaced along the Archean-Paleoproterozoic unconformity, an early Huronian age for the Joe Lake Gabbro would severely limit the possible amount of impact excavation along the North Range. Now that the Joe Lake Gabbro is shown to be an Archean metagabbro, this constraint is removed, allowing significant differential uplift of the high-grade Levack Gneiss Complex to be part of the impact process.

Levels of shock metamorphism in zircons from the North Range footwall are much lower than on the South Range, suggesting that "ground zero" of the impact was well to the south, most likely in the Frood-Stobie to Copper Cliff area, just south of the (preserved) SIC proper. A preliminary analysis of all shatter cone data (e.g. Bray et al., 1996) also points to this area as the centre of the impact (W. Bleeker, unpubl. data). This suggests that all of the preserved SIC melt sheet merely represents an erosional remnant of one flank of a much larger melt sheet (Bleeker et al., 2014a). This has important implications for how to best interpret the overall "stratigraphy" of the SIC, for interpretation of the seismic section (Milkereit and Green, 1992; Wu et al., 1995), and for the final size of the impact structure (e.g. Spray et al., 2004). Nearly all

previous studies have implicitly assumed that the centre of the impact is within in the preserved extent of the SIC.

On the southeastern limb of the SIC, we have dated a foliated granite as late Archean. The mafic volcanic rocks it intruded must therefore also be Archean, rather than basal Huronian (cf. compilation maps of the area: Dressler, 1984; Ames et al., 2006). A similar conclusion probably also applies to the Skead pluton somewhat further north. These findings require remapping of the area to better define the Archean–Paleoproterozoic unconformity. The layered anorthositic gabbro of the Falconbridge Township intrusion did not yield datable minerals and remains relatively poorly dated (Prevec and Baadsgaard, 2005).

Using chemical abrasion, the age of the Murray Granite has been refined to 2460 ±6 Ma, slightly younger and more precise than the previous estimate of 2477 ±9 Ma (Krogh et al., 1996), and in better agreement with field relationships.We also present the first robust and relatively precise age on the Creighton Granite, at 2455–2460 Ma, based on combined U-Pb data and field relationships. Analysis of six chemically abraded zircon crystal fragments from both the Creighton Granite and the Copper Cliff Rhyolite yield a combined upper intercept age of 2459 ±7 Ma. Our observations show that the Creighton Granite is a folded sill-like body that likely acted as the high-level magma chamber to the Copper Cliff Rhyolite Formation. Tight folding and tilting of this sill and the surrounding Huronian rift succession predated the impact and subsequent emplacement of the SIC. Magma-mingling structures show that the Creighton Granite interacted with mafic magmas, low in the Huronian rift structure, during and following the main pulse of Matachewan magmatism at 2460 Ma.

A tightly folded Nipissing Diabase sill has been dated at 2215 ±1 Ma. It is fully conformable with surrounding Huronian strata on the South Range, inconsistent with the concept of a pre-Nipissing "Blezardian orogeny". The main rationale for the Blezardian orogeny was the idea that deformation and intrusion of granite plutons, such as the Creighton Granite, thought to be ca. 2.3 Ga in age, terminated the depositional history of the Huronian succession (Frarey et al., 1982; Stockwell, 1982). None of these ideas are supported by present evidence. The Creighton Granite is an early Huronian 2455–2460 Ma rift-related granite, not an orogenic granite pluton; folding of the Huronian succession did not commence until well after emplacement of Nipissing Diabase sills and sheets with the onset of Penokean accretion and collision events at ca. 1860 Ma. Other observations that have contributed to the concept of a Blezardian orogeny can all be explained without a significant pre-Nipissing deformation event. For instance, saucer-shaped Nipissing sills locally may appear to crosscut Huronian strata and, after superimposed Penokean deformation, could easily lead to confusing field relationships.

Several new ages on "offset dykes" have been obtained (Hess, Pele), resolving that the radial Pele dyke is indeed part of the offset dyke system. The Pele dyke likely represents the youngest and last phase of SIC offset dyke injection. It carries phenocrysts, hence it was no longer superheated, and it was injected as a regular magmatic dyke, with chilled and relatively straight contacts. Its age of 1848.5 ±0.8 Ma provides a hint of the overall time scale of melt-sheet evolution and crystallization on the order of 0.5–1.0 Myr. A new highly precise $^{207}Pb/^{206}Pb$ age, obtained by a hybrid technique (see also Davis, 2008), dates zircon crystallization in South Range high-MgO norite at 1849.7 ±0.2 Ma.

Other dykes have been shown to be part of unrelated older dyke sets. We present the first evidence of a ca. 2507 Ma swarm in this part of the Superior craton, an age similar to that of the Mistassini swarm farther to the northeast. Other dykes west of Sudbury have been dated at ca. 2105–2116 Ma and ca. 1900–1950 Ma (Bleeker and Chamberlain, in prep.). The former, which we call the Blind River dykes, are part of the Marathon large igneous province. The latter define a new event in the southern Superior craton. Continental breakup along the southern margin of the Superior craton only occurred after most of these dyke swarms were emplaced, making the entire Huronian Supergroup an intra-continental rift and sag succession (Bleeker and Ernst, 2006; Ernst and Bleeker, 2010) and not a long-lived passive margin succession as commonly portrayed (e.g. Bennett et al., 1991; Young et al., 2001).

Trap dykes, a name we restrict to ~east-west-trending post-SIC dykes across the South Range, have a preliminary zircon age of 1750 Ma. Having identified both baddeleyite and zircon in these dykes, their U-Pb dating is in progress. They post-date most if not all of the folding of Huronian strata (and SIC) across the South Range and must be related to a post-Penokean rifting event in the evolving margin of southeastern Laurentia. Nevertheless, they are fully metamorphic and (statically) recrystallized. They are cut by a younger suite of essentially undeformed felsite dykes that have a preliminary age of 1766 ±9 Ma.

ACKNOWLEDGEMENTS

We thank Dave Smith and Joshua Bailey, from Wallbridge Mining Company, and Peter Lightfoot, from Vale, Sudbury, for helpful discussions and sharing some of their knowledge of the Sudbury Structure. Dave Smith guided us to some of their properties and pointed out possible offset dykes of interest. Peter

Lightfoot provided the sample of the MgO-rich norite. Mike Easton of the Ontario Geological Survey is thanked for discussion and critical reading of the manuscript. Proof reading of the final manuscript by Tony LeCheminant is also gratefully acknowledged. Elizabeth Ambrose handled the final editing and lay-out of the manuscript.

REFERENCES

Ames, D.E. and Farrow, C.E.G., 2007. Metallogeny of the Sudbury Mining Camp, Ontario. *In:* Mineral Deposits of Canada: A Synthesis of Major Deposit Types, District Metallogeny, the Evolution of Geological Provinces, and Exploration Methods, (ed.) W.D. Goodfellow; Geological Association of Canada, Mineral Deposits Division, Special Publication No. 5, p. 329–350.

Ames, D.E., Watkinson, D.H., and Parrish, R.R., 1998. Dating of a regional hydrothermal system induced by the 1850 Ma Sudbury impact event; Geology, v. 26, p. 447–450.

Ames, D.E., Singhroy, V., Buckle, J., Davidson, A., and Molch, K., 2006. Integrated bedrock geology – Radarsat – Digital elevation data of Sudbury, Ontario. Geological Survey of Canada Open File 4571. Scale 1: 75,000.

Ames, D.E., Davidson, A., and Wodicka, N., 2008a. Geology of the giant Sudbury polymetallic mining camp, Ontario, Canada; Economic Geology, v. 103, p. 1057–1077.

Ames, D.E., Card, K., Wodicka, N., and Davidson, A., 2008b. 100K Geological map of the Sudbury mining camp and Surrounding area, Ontario, Canada; Supplement to Ames, D.E. and Wodicka, N., 2008, Geology of the Giant Sudbury Polymetallic Mining Camp, Ontario, Canada; Economic Geology, v. 103, p. 1057–077.

Bennett, G., Dressler, B.O., and Robertson, J.A., 1991. The Huronian Supergroup and associated intrusive rocks. *In:* Geology of Ontario; Ontario Geological Survey, Special Volume 4, Part 1, p. 549–592.

Bleeker, W. and Ernst, R.E., 2006. Short-lived mantle generated magmatic events and their dyke swarms: The key unlocking Earth's palaeogeographic record back to 2.6 Ga. *In:* Dyke Swarms—Time Markers of Crustal Evolution: Selected Papers of the Fifth International Dyke Conference, Rovaniemi, Finland, 31 July – 3 August, 2005 (also Fourth International Dyke Conference, Kwazulu-Natal, South Africa 26–29 June, 2001) (ed.) E. Hanski, S. Mertanen, T. Rämö, J. Vuollo; A.A. Balkema, Rotterdam, p. 3–26.

Bleeker, W., Hamilton, M.A., Ernst, R.E., and Söderlund, U., 2012. Resolving the age structure of the Matachewan event: Magmatic pulses at ca. 2445–2452 Ma, 2458–2461 Ma, and 2475–2480 Ma; unpublished CAMIRO Reports A96, A97, and A98, 17 p.

Bleeker, W., Kamo, S., and Ames, D.E., 2013. New field observations and U-Pb age data for footwall (target) rocks at Sudbury: Towards a detailed cross-section through the Sudbury Structure, *In:* Extended Abstracts; Large Meteorite Impacts and Planetary Evolution V Meeting, 5-8 August, Sudbury, Ontario, Lunar Planetary Institute contribution No. 1737, p. 13.

Bleeker, W., Kamo, S., Ames, D.E., 2014a. Towards a detailed geological cross-section of the deformed Sudbury impact basins: New observations and new geochronology (Presentation); Ontario Exploration and Geoscience Symposium, November 3-4, 2014, Sudbury.

Bleeker, W., Kamo, S., Ames, D., and Smith, D., 2014b. New U-Pb ages for some key events in the Sudbury area, including the Creighton Granite and Joe Lake metagabbro, *In:* Abstracts; Geological Association of Canada, Annual Meeting, May 21-23, Fredericton, New Brunswick, Abstract Volume 37, p. 32–33.

Bray, J.G, and Geological Staff, 1966. Shatter cones at Sudbury; The Journal of Geology, v. 74, p. 243–245.

Buchan, K.L., Mortensen, J.K., and Card, K.D., 1993. Northeast-trending Early Proterozoic dykes of southern Superior Province: multiple episodes of emplacement recognized from integrated paleomagnetism and U-Pb geochronology; Canadian Journal of Earth Sciences, v. 30, p. 1286–1296.

Card, K.D., 1994. Geology of the Levack gneiss complex, the northern footwall of the Sudbury structure, Ontario, *In:* Canadian Shield; Geological Survey of Canada, Current Research 1994-C, p. 269–278. doi:10.4095/193807

Corfu, F. and Andrews, A.J., 1986. A U-Pb age for mineralized Nipissing diabase, Gowganda; Canadian Journal of Earth Sciences, v. 23, p. 107–109.

Corfu, F. and Easton, R.M., 2001. U-Pb evidence for polymetamorphic history of Huronian rocks underlying the Grenville Front tectonic zone east of Sudbury, Ontario; Chemical Geology, v. 172, p. 149–171.

Corfu, F. and Lightfoot, P.C., 1996. U-Pb geochronology of the sublayer environment, Sudbury igneous complex, Ontario; Economic Geology, v. 91, p. 1263–1269.

Craddock, J.P., Rainbird, R.H., Davis, W.J., Davidson, C., Vervoort, J.D., Konstantinou, A., Boerboom, T., Vorhies, S., Kerber, L., and Lundquist, B., 2013. Detrital zircon geochronology and provenance of the Paleoproterozoic Huron (~2.4–2.2 Ga) and Animikie (~2.2–1.8 Ga) basins, southern Superior Province; The Journal of Geology, v. 121, p. 623–644. doi:10.1086/673265

Davidson, A. and van Breemen, O., 1994. U-Pb ages of granites near the Grenville Front, Ontario, *In:* Radiogenic Age and Isotopic Studies: Report 8; Geological Survey of Canada, Current Research 1994-F, p. 107–114.

Davidson, A., van Breemen, O., and Sullivan, R.W., 1992. Circa 1.75 Ga ages for plutonic rocks from the Southern province and adjacent Grenville Province: what is the expression of the Penokean orogeny? *In:* Radiogenic Age and Isotopic Studies, Report 6; Geological Survey of Canada, Paper 92-2, p. 107–107.

Davis, D.W., 2008. Sub-million-year age resolution of Precambrian igneous events by thermal extraction–thermal ionization mass spectrometer Pb dating of zircon: Application to crystallization of the Sudbury impact melt sheet; Geology, v. 36, p. 383–386.

Dietz, R.S., 1964. Sudbury structure as an astrobleme; Journal of Geology, v. 72, p. 412–434.

Dietz, R.S. and Butler, L.W., 1964. Shatter-cone orientation at Sudbury, Canada; Nature, v. 204, p. 280–281.

Dressler, B.O., 1984. Sudbury geological compilation; Ontario Geological Survey, Precambrian Geology Series, Map 2491, scale 1:50,000.

Dutch, S.I., 1979. The Creighton pluton, Ontario: an unusual example of a forcefully emplaced intrusion; Canadian Journal of Earth Sciences, v. 16, p. 333–349.

Ernst, R.E. and Bleeker, W., 2010. Large igneous provinces (LIPs), giant dyke swarms, and mantle plumes: Significance for breakup events within Canada and adjacent regions from 2.5 Ga to the Present. *In:* Special Issue on the theme LITHOPROBE—parameters, Processes, and the Evolution of a Continent. LITHOPROBE Contribution 1482 and Geological Survey of Canada Contribution 20100072; Canadian Journal of Earth Sciences, v. 47, p. 695–739, doi:10.1139/E10-025

Fahrig, W.F. and West, T.D., 1986. Diabase dyke swarms of the Canadian Shield; Geological Survey of Canada, Map 1627A, scale 1:4,973,900.

Faggart, B.E., Basu, A.R., and Tatsumoto, M., 1985. Origin of the Sudbury complex by meteoritic impact: Neodymium isotopic evidence; Science, v. 230, p. 436–439.

Frarey, M.J., Loveridge, W.D., and Sullivan, R.W., 1982. A U-Pb zircon age for the Creighton Granite, Ontario, *In:* Current Research, Part C; Geological Survey of Canada, Paper 82-1C, p. 129–132.

Grieve, R.A., Stöffler, D., and Deutsch, A., 1991. The Sudbury Structure: Controversial or misunderstood?; Journal of Geophysical Research: Planets (1991–2012), v. 96, p. 22753–22764.

Halls, H.C., Stott, G.M. and Davis, D.W., 2005. Paleomagnetism, geochronology and geochemistry of several Proterozoic mafic dike swarms in northwestern Ontario; Ontario Geological Survey, Open File Report 6171, 59 p.

Halls, H.C., Davis, D.W., Stott, G.M., Ernst, R.E., and Hamilton, M.A., 2008. The Paleoproterozoic Marathon large igneous province: new evidence for a 2.1 Ga long-lived mantle plume event along the southern margin of the North American Superior Province; Precambrian Research, v. 162, p. 327–353.

Heaman, L.M., 1997. Global mafic magmatism at 2.45 Ga: Remnants of an ancient large igneous province?; Geology, v. 25, p. 299–302.

James, R.S., Easton, R.M., Peck, D.C., and Hrominchuk, J.L., 2002. The East Bull Lake intrusive suite: Remnants of a ~2.48 Ga large igneous and metallogenic province in the Sudbury area of the Canadian Shield; Economic Geology, v. 97, p. 1577–1606.

Ketchum, K.Y., Heaman, L.M., Bennett, G., and Hughes, D.J., 2013. Age, petrogenesis and tectonic setting of the Thessalon volcanic rocks, Huronian Supergroup, Canada; Precambrian Research, v. 233, p. 144–172.

Krogh, T.E., Davis, D.W., and Corfu, F., 1984. Precise U-Pb zircon and baddeleyite ages for the Sudbury area, *In:* The Geology and Ore Deposits of the Sudbury Structure (ed.) E.G. Pye, A.J. Naldrett, and P.E. Giblin; Ontario Geological Survey, Special Volume 1, p. 431–447.

Krogh, T.E., Corfu, F., Davis, D.W., Dunning, G.R., Heaman, L.M., Kamo, S.L., Machado, N., Greenhough, J.D., and Nakamura, N., 1987. Precise U-Pb isotopic ages of diabase dikes and mafic to ultramafic rocks using trace amounts of baddeleyite and zircon, *In:* Mafic dyke swarms, (ed.) H.C. Halls and W.F. Fahrig; Geological Association of Canada, Special Paper 34, p. 147–152.

Krogh, T.E., Kamo, S.L, and Bohor, B.F., 1996. Shock metamorphosed zircons with correlated U-Pb discordance and melt rocks with concordant protolith ages indicate an impact origin for the Sudbury structure, *In:* Earth Processes: Reading the Isotopic Code (ed.) A. Basu and S. Hart; American Geophysical Union, Geophysical Monograph 95, p. 343–353.

Lightfoot, P.C. and Zotov, I.A., 2005. Geology and geochemistry of the Sudbury Igneous Complex, Ontario, Canada: Origin of nickel sulfide mineralization associated with an impact-generated melt sheet; Geology of Ore Deposits, v. 47, p. 387–420.

Mattinson, J.M., 2005. Zircon U–Pb chemical abrasion ("CA-TIMS") method: combined annealing and multi-step partial dissolution analysis for improved precision and accuracy of zircon ages; Chemical Geology, v. 220, p. 47–66.

Mattinson, J.M., 2011. Extending the Krogh legacy: development of the CA-TIMS method for zircon U-Pb geochronology; Canadian Journal of Earth Sciences, v. 48, p. 95–105.

Meldrum, A., Abdel-Rahman, A.F., Martin, R.F., and Wodicka, N., 1997. The nature, age and petrogenesis of the Cartier Batholith, northern flank of the Sudbury Structure, Ontario, Canada; Precambrian Research, v. 82, p. 265–285.

Milkereit, B. and Green, A., 1992. Deep geometry of the Sudbury structure from seismic reflection profiling; Geology, v. 20, p. 807–811.

Noble, S.R. and Lightfoot, P.C., 1992. U-Pb baddeleyite ages for the Kerns and Triangle Mountain intrusions, Nipissing Diabase, Ontario; Canadian Journal of Earth Sciences, v. 29, p. 1424–1429.

Osterman, M., Schärer, U., and Deutsch, A., 1996. Impact melt dikes in the Sudbury multi-ring basin (Canada): Implications from uranium-lead geochronology on the Foy Offset Dike; Meteoritics & Planetary Science, v. 31, p. 494–501.

Petrus, J., 2014. Mineralogical, chemical and isotopic evolution of impact bombarded rocks and minerals; Ph.D. thesis, Laurentian University, Sudbury, Ontario, 269 p.

Prevec, S.A. and Baadsgaard, H.B., 2005. Evolution of Paleoproterozoic mafic intrusions located within the SIC thermal aureole: Isotopic, geochronological and geochemical evidence; Geochimica et Cosmochimica Acta, v. 69, p. 3653–3669.

Pye, E.G., Naldrett, A.J., Giblin, P.E. (ed.), 1984. The geology and ore deposits of the Sudbury Structure; Ontario Geological Survey, Special Volume 1, 603 p.

Raharimahefa, T., Lafrance, B., and Tinkham, D.K., 2014. New structural, metamorphic, and U–Pb geochronological constraints on the Blezardian Orogeny and Yavapai Orogeny in the Southern Province, Sudbury, Canada; Canadian Journal of Earth Sciences, v. 51, p. 750–774.

Smith, M.D., 2002. The timing and petrogenesis of the Creighton pluton, Ontario: An example of felsic magmatism associated with Matachewan igneous events; M.Sc. thesis, University of Alberta, Edmonton, Alberta, 123 p.

Spray, J.G., Butler, H.R., and Thompson, L.M., 2004. Tectonic influences on the morphometry of the Sudbury impact structure: Implications for terrestrial cratering and modeling; Meteoritics & Planetary Science, v. 39, p. 287–301.

Stockwell, C.H., 1982. Proposals for time classification and correlation of Precambrian rocks and events in Canada and adjacent areas of the Canadian Shield, Part 1: A time classification of Precambrian rocks and events; Geological Survey of Canada, Paper 80-19, 135 p.

Sullivan, R.W. and Davidson, A., 1993. Monazite age of 1747 Ma confirms post-Penokean age for the Eden Lake complex, Southern Province, Ontario, *In:* Radiogenic Age and Isotopic Studies: Report 7; Geological Survey of Canada, Paper 93-2, p. 45–48.

Thomson J.E., 1957. Geology of Falconbridge Township. Ontario; Department of Mines Annual Report, v. 66, 36 p.

Young, G.M., Long, D.G., Fedo, C.M., and Nesbitt, H.W., 2001. Paleoproterozoic Huronian basin: product of a Wilson cycle punctuated by glaciations and a meteorite impact; Sedimentary Geology, v. 141, p. 233–254.

Wodicka, N., 1997. Sudbury structure: Northern footwall rocks and Sudbury Igneous Complex. *In:* Timmins to Sudbury transect: New Insights into the Regional Geology and the Setting of Ore Deposits, (ed.) D.E. Ames, W. Bleeker, K.B. Heather, and N. Wodicka; Geological Association of Canada–Mineralogical Association of Canada, Joint Annual Meeting, Ottawa '97, Field Trip Guidebook B6, 133 p.

Wood, C.R. and Spray, J.G., 1998. Origin and emplacement of offset dikes in the Sudbury impact structure: Constraints from Hess; Meteoritics & Planetary Sciences, v. 33, p. 337–347.

Wu, J., Milkereit, B., and Boerner, D.E., 1995. Seismic imaging of the enigmatic Sudbury Structure; Journal of Geophysical Research, v. 100, p. 4117–4130.

GEOLOGICAL SURVEY OF CANADA
OPEN FILE 7856

Targeted Geoscience Initiative 4: Canadian Nickel-Copper-Platinum Group Elements-Chromium Ore Systems — Fertility, Pathfinders, New and Revised Models

Gravity gradiometer data analysis in mineral exploration

Mark Pilkington and Pierre Keating

Geological Survey of Canada, Ottawa, Ontario

2015

© Her Majesty the Queen in Right of Canada, as represented by the Minister of Natural Resources Canada, 2015

This publication is available for free download through GEOSCAN (http://geoscan.nrcan.gc.ca/)

Recommended citation

Pilkington, M. and Keating, P., 2015. Gravity gradiometer data analysis in mineral exploration, *In:* Targeted Geoscience Initiative 4: Canadian Nickel-Copper-Platinum Group Elements-Chromium Ore Systems — Fertility, Pathfinders, New and Revised Models, (ed.) D.E. Ames and M.G. Houlé; Geological Survey of Canada, Open File 7856, p. 167–173.

Publications in this series have not been edited; they are released as submitted by the author.

Contribution to the Geological Survey of Canada's Targeted Geoscience Initiative 4 (TGI-4) Program (2010–2015)

TABLE OF CONTENTS

Gravity gradiometer data analysis in mineral exploration

Mark Pilkington* and Pierre Keating

Geological Survey of Canada, 615 Booth Street, Ottawa, Ontario K1A 0E9
*Corresponding author's e-mail: mpilking@NRCan.gc.ca

ABSTRACT

Gravity gradiometer surveys are becoming increasingly important in the search for and characterization of mineral deposits. Measurement of the full gravity gradient tensor provides the opportunity for processing and interpretation of single tensor components or combinations of components. To effectively use these components and combinations thereof, it is necessary to characterize the information content in order to interpret the gradiometer data correctly. We use linear inverse theory to evaluate different components and their combinations and find that which concatenated components produce the smallest modelling errors. Of the single tensor components, the Tzz component was found to provide the best performance overall. Since airborne gradiometer data are collected in a highly dynamic environment, noise is ever-present and must be compensated for to produce a clean signal for interpretation. Two approaches were investigated for removing noise: kriging and directional filtering. The kriging and directional filtering results show a similar level of smoothness, the main difference being the increased smoothing along strike of the directionally filtered data. Since kriging is a data-driven procedure, it provides an objective estimate of the data noise level and degree of smoothness. Based on the kriging results, processing parameters can be chosen to give a similar level of smoothness and noise suppression for directional filtering, that more effectively delineates geological trends in the data.

INTRODUCTION

Unlike gravity data, gravity gradiometer (GG) data comprise measurements of all components of the gravity field and provide greater sensitivity at shorter wavelengths, making them well suited for small-scale mineral exploration studies. Recently, the Geological Survey of Canada has collected GG data over several mineral prospects in Canada. To understand and effectively utilize these data, our studies had two main goals: (1) to quantify the information content in the different gravity gradient tensor components and (2) to suppress the noise in the measured data.

Methods of interpretation for GG data parallel those developed for gravity and magnetic data due to their similarities but gradiometer systems measure components that do not have an equivalent counterpart in gravity and magnetic interpretation. Qualitative methods, such as a simple visual inspection of all tensor components, are hindered by the complicated form of the non-Tzz components. Consequently, Tzz is usually the component of choice, especially for qualitative interpretation. Quantitative methods have been developed for GG data that use either single tensor components or combinations thereof (Vasco and Taylor, 1991; Zhang et al., 2000; Zhdanov et al., 2004; Beiki and Pedersen, 2010; Martinez et al., 2013). A quantitative comparison of tensor components and their combinations was made by Pilkington (2012), who utilized GG data to determine the densities within a three-dimensional (3-D) subsurface volume. Using a measure of information content commonly used in optimal survey design to rate different components (and some component combinations), Pilkington (2012) concluded that Tzz was the most useful single tensor component and that results could be improved by adding more components to the data vector. However, Pilkington (2012) did not consider data errors and the geometry of the model employed did not allow for investigation of individual model parameters and their effects on the components. Therefore, we used parametric inversion to evaluate tensor components and their combinations through inversions using models with only a small number of parameters. By analyzing the parametric errors generated by inversion of different tensor components and combinations, we evaluated the relative information content of the different data types.

Collecting gravity data in a dynamic environment, such as an aircraft, leads inevitably to the presence of noise in the measurements. The sources and approaches to treatment of noise in airborne gravity gradiometer systems are numerous and have been discussed extensively (e.g. Dransfield and Christensen,

Pilkington, M. and Keating, P., 2015. Gravity gradiometer data analysis in mineral exploration, *In:* Targeted Geoscience Initiative 4: Canadian Nickel-Copper-Platinum Group Elements-Chromium Ore Systems — Fertility, Pathfinders, New and Revised Models, (ed.) D.E. Ames and M.G. Houlé; Geological Survey of Canada, Open File 7856, p. 167–173.

Table 1. Tensor components and component combinations used in this paper (notation *Tuv* | *Txy* means that, for example, data vectors *Tuv* and *Txy* both with length *n* are concatenated to form an augmented vector with length 2*n*).

No.	Description
1	Txx = Gradient in x direction of x-component of gravity field
2	Txy = Gradient in y direction of x-component of gravity field
3	Txz = Gradient in z direction of x-component of gravity field
4	Tyy = Gradient in y direction of y-component of gravity field
5	Tyz = Gradient in z direction of y-component of gravity field
6	Tzz = Gradient in z direction of z-component of gravity field
7	Tuv = = 0.5*(Txx-Tyy)
8	I1 = TxxTyy+TyyTzz+TxxTzz-Txy^2-Tyz^2-Txz^2
9	I2 = Txx(TyyTzz-Tyz^2)+Txy(TyzTxz-TxyTzz)+Txz(TxyTyz-TxzTyy)
10	H1 = sqrt(Txz^2+Tyz^2)
11	H2 = sqrt(Txy^2+0.25*(Tyy-Txx)^2)
12	C1 = Tuv | Txy
13	C2 = Txz | Tyz | Tzz
14	C3 = Txy | Tyz | Txz
15	C4 = Txx | Tyy | Txy
16	C5 = Tzz | Tyz | Txz | Txy | Txx
17	C6 = Tyy | Tyz | Txz | Txy | Txx

2013). Standard processing of GG data is designed to suppress the unwanted noise and emphasize the geological signals. Nonetheless, currently produced GG data often still contain high enough levels of noise to interfere with both qualitative and quantitative interpretations. Our approach was to explore several noise-reduction methods to determine their applicability and effectiveness in removing unwanted noise in GG data.

RESULTS

Evaluating Tensor Component Utility

The aim of this study was to use the estimated parameter errors resulting from inversions of single and multiple tensor components to quantitatively rate their information content. Table 1 gives a list of 17 different component quantities consisting of single tensor components (1 to 6), combinations of components (7 to 11), and concatenations of components (12 to 17); Figure 1 shows quantities 1 through 11 calculated for a prismatic model.

Linear inverse theory provides all the tools to examine the relationship between the different data types and the model parameters (Inman, 1975). A simple prism model (Fig. 1) was used, which was characterized by just seven parameters: xc and yc - the x and y coordinates of the prism centre; w and b - the prism width (in x) and breadth (in y); ρ - the density; z - the depth to the top surface; and t - the vertical thickness.

Once an inversion is completed, the errors in the model parameters can be estimated (Pilkington, 2014). A range of models was tested to determine how different component quantities affected parameter errors (see Table 2 for a list of parameter values). Varying parameters t, w, b, and z simulates shallow to deep prisms, and thin to thick plates and dykes. For each model, the

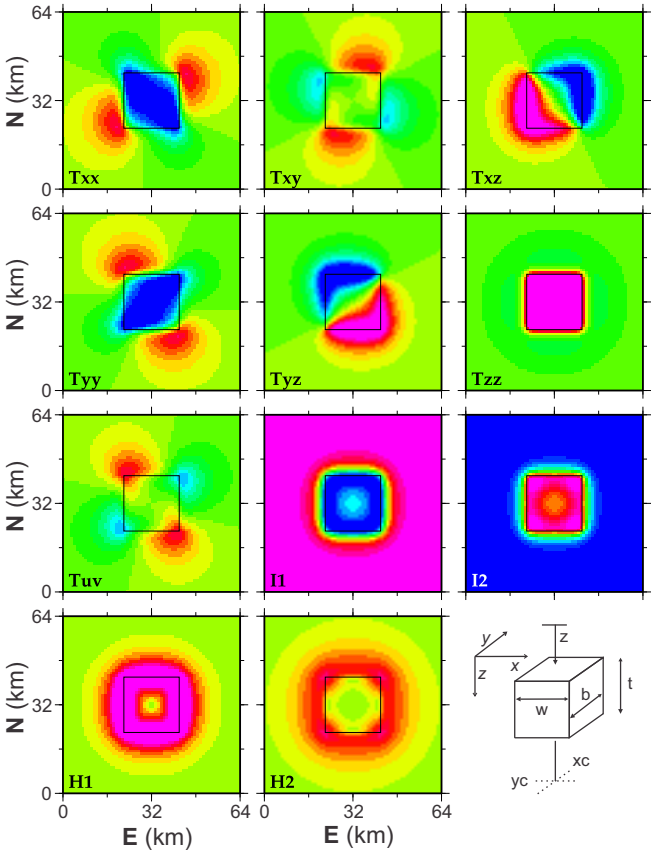

Figure 1. Component quantities from Table 1 (1 to 11) calculated over a single prism, with the measurement coordinate system rotated by 30º, which simulates a flight direction of N60ºE. Prism model parameters are z = 2 km, t = 8 km, w = 20 km, b = 20 km, ρ = 0.2 gcm^{-3}.

standard deviations of the parameter errors were calculated. The resulting standard deviations were then ranked for each parameter by component quantity (Table 1), with a value of 1 assigned to the smallest parameter error and a value of 17 to the largest. Figure 2 illustrates the summing of the rank values for the 29 models (a high-ranking value is indicative of large parameter errors). Seven points are plotted for each component quantity, each corresponding to a single model parameter.

Figure 2 shows that most of the 17 component quantities have parameter rankings clustered fairly close together, i.e., none of the parameters are much more reliably estimated than the others. Tzz shows a lower ranking (lower error) than the other single components (Fig. 2). Some individual parameters are estimated to have lower errors than those generated using Tzz but these are limited to a few cases where parameters benefit from directional strengths in some of the single tensor components. The mainly horizontal component combinations H1 and C1 (Tuv | Txy, Table 1) are ranked at a similar level as Tzz. In contrast, the purely horizontal quantities H2, Tuv, and Txy have higher errors. These three components comprise just Txx, Tyy, and/or

Table 2. Values of the parameters used in the 29 models shown in Figure 2. Note: xc and yc are the x and y coordinates of the prism centre; w and b are the prism width (in x) and breadth (in y); ρ represents the density; z is the depth to the top surface; and t is the vertical thickness.

xc (km)	xc (km)	z (km)	t (km)	w (km)	b (km)	ρ (g/cm^3)
32	32	4	1,3,6,13,43	12	12	0.2
32	32	4	13	0.1,0.5,2,6,9	12	0.2
32	32	0.1,1,3,6,12	40	12	12	0.2
32	32	2	1	1	1	0.2
32	32	2	4	4	4	0.2
32	32	2	8	8	8	0.2
32	32	0.5,1,2	4	1	1	0.2
32	32	0.5,1,2,4	1	8	8	0.2
32	32	0.5,1,2,4	2	2	2	0.2

Txy. The invariants I1 and I2 are ranked between the lower ranked concatenated combinations and those discussed above. Both I1 and I2 have tightly clustered parameter rankings and have the lowest errors of the combined component quantities.

In agreement with Pilkington (2012), Figure 2 shows that the concatenated components have the lowest ranking, producing the smallest parameter error estimates. This demonstrates that when components are combined into a single quantity through multiplication and addition, it does not perform as well as if the same components are simply concatenated. For example, comparing H2 and C4 (Txx | Tyy | Txy combination, Table 1), they both contain the same (purely horizontal) components but provide very different error estimates, the latter having much lower errors. Component quantity C1 (Tuv | Txy, Table 1) is a mix of combination and concatenation, and has a ranking between H2 and C4 (Txx | Tyy | Txy, Table 1).

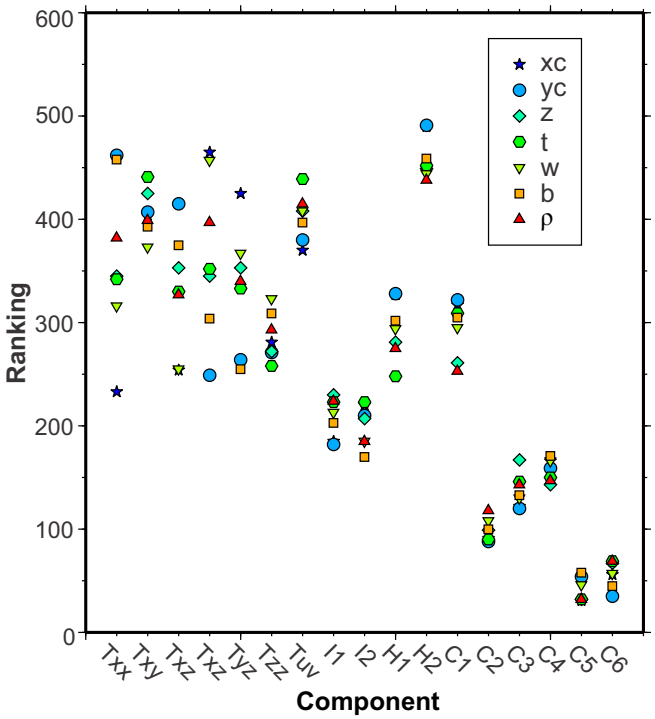

Figure 2. Parameter rankings versus component type based on 29 model inversions. For each inversion, the parameter standard deviations were ranked by component quantity (see Table 1), with a value of 1 assigned to the smallest parameter error and a value of 17 to the largest. Plotted values are the sums of the ranked values. High-ranking values are equivalent to large parameter errors.

Noise Suppression for Gradiometer Data

Two approaches were considered for noise removal in GG data: kriging and directional filtering. Kriging is an estimation procedure commonly used in geostatistics for the interpolation of spatial data (Matheron, 1963) and provides the best linear unbiased estimator. A more detailed description of the method can be found in Keating and Pilkington (2013) and Pilkington and Shamsipour (2014). For the simple case of signal (gravity effects of geology) and uncorrelated noise, ordinary kriging provides an unbiased estimate of a noise-free signal and hence was chosen for use with the GG data.

Figure 3a shows a portion of the Tzz component from a GG data survey, illustrating the noisy character of this kind of data. The kriged data (Fig. 3b) shows a significant reduction in uncorrelated noise level, resulting in the appearance of more coherent gradient features throughout the area. With the suppression of shorter wavelength components, the kriged data are generally smoother than the gridded (minimum curvature) flight-line data (Fig. 3a). The kriged values are, nonetheless, optimal in the sense of being estimated from an interpolator based on the data themselves, and not from an arbitrary interpolator such as the minimum curvature operator. The difference between standard minimum curvature gridding (Fig. 3a) and kriging (Fig. 3b) is illustrated in Figure 3c, which shows the mostly uncorrelated noise components removed by the kriging method.

The type of anomaly in GG data that is most useful for geological mapping is two-dimensional (2-D). Quasi-linear (2-D) features in the data may correspond to lithological contacts, but even if this is not the case, such trends can help in distinguishing structural regimes, and deformation styles and trends. Since a 2-D feature varies more smoothly along strike than perpendicular to strike, low-pass filtering to remove noise can be tuned to take this into account. Short-wavelength features can be removed preferentially along strike but preserved in the cross-strike direction. In this fashion, short-wavelength components that provide the detailed definition of the 2-D features are unaffected, whereas the short-wavelength noise that overprints and

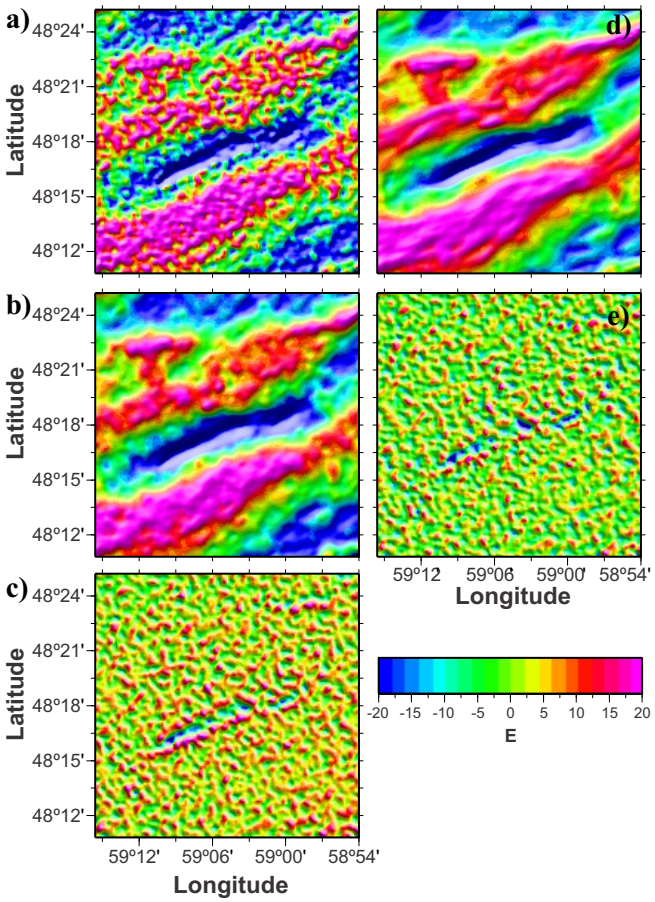

Figure 3. a) Original Tzz data from St. Georges Bay, Newfoundland and Labrador. **b)** Kriged data for the same area as (a). **c)** Difference between grids (a) and (b). **d)** Data from (a) directionally filtered. **e)** Difference between grids in (a) and (d).

disrupts along-strike trends is suppressed. This is the essence of directional filtering (e.g. Brewster, 2013). A directional filter requires the orientation or strike of the filter to be known at each grid point, which can be found from the two orthogonal horizontal gradients of the component.

Figure 3d shows the results of directionally filtering the data in Figure 3a. There is likely still some residual short-wavelength noise in the filtered grid, but through the smoothing effect of the directional filter the signal-to-noise ratio of the data is increased. Also, because the directional filtering uses the long-wavelength portion (assumed noise-free) of the input data to orient the smoothing, the short-wavelength trends are likely more reliable. Figure 3e shows the difference between the original (Fig. 3a) and directionally filtered data (Fig. 3d) for the Tzz component. The difference grid appears predominantly random, except for some coherent signals related to the strong ENE-WSW negative anomaly in the centre of the area. The kriging (Fig. 3b) and directional-filtering results (Fig. 3d) are not grossly different in appearance. The level of smoothness is similar and the main contrast between the two is the extra smoothing along strike for the directionally filtered data.

Kriging is computationally intensive, but almost completely data driven. On the other hand, directional filtering requires several user-defined parameters. A practical approach for noise reduction is to use kriging first and use the results to guide the choice of the parameters required in directional filtering. Kriging gives an estimate of how much noise is present and also specifies the correlation character of the data. The directional filtering can then be tuned to give a similar level of smoothness and noise suppression as the kriging results, but with the advantage of keeping more short-wavelength information in the cross-strike direction for better trend definition.

DISCUSSION

Using estimated parameter errors from parametric inversions allows for a quantitative ranking of single tensor components, combinations of components, and concatenations of components. Furthermore, linear inverse theory allows incorporation of the appropriate relative noise levels of the tensor components. Ranking of the estimated model errors from a range of model types shows that data sets consisting of concatenated components produce the smallest parameter standard deviations. Combinations of the purely horizontal components Txx and Tyy perform the poorest. Of the single tensor components, Tzz gives the best performance overall, but single components with strong directional sensitivity (e.g. Txx, Tyy) can produce some individual parameter estimates with smaller errors.

Both ordinary kriging and directional filtering are shown to be viable options for noise suppression in gravity gradiometer data. Kriging is based on the statistical character of the data and produces estimates with a commensurate level of smoothness and noise reduction. For directional filtering, the degree of smoothing is user-defined but has the advantage of being sensitive to strike information derived from the data. Both approaches successfully reduce noise levels so that coherent, geologically meaningful anomaly patterns are revealed.

IMPLICATIONS FOR EXPLORATION

The utility of gravity gradiometer data is dependent on both the quality of the data and also our understanding of what information the data contain. The development of practical ways of suppressing noise in GG data allows more effective presentations of the data for qualitative interpretation and provides more accurate input values into quantitative interpretation methods such as modelling and inversion. Determining the information content in the individual tensor compo-

nents and their combinations can be a guide when selecting which tensor components should be used in an interpretation. GG data can provide a high-resolution gravity signal that, combined with co-located magnetic data, can provide an essential tool in Ni-Cu-PGE, Cr-PGE, and Fe-Ti-V exploration by identifying mafic and ultramafic prospective units within poorly exposed regions and also constitute important constraints in the modelling of individual geophysical anomalies directly related to magmatic ore deposits.

ACKNOWLEDGEMENTS

We thank Mike Thomas and Michel Houlé for timely and comprehensive reviews. This study was conducted as part of phase IV of the Natural Resources Canada's Targeted Geoscience Initiative (TGI-4). In addition to this study, several other GG surveys were completed as part of this initiative: Blatchford Lake, Northwest Territories; Strange Lake, Québec and Newfoundland and Labrador; and, in collaboration with the Ontario Geological Survey, McFaulds Lake, Ontario.

REFERENCE

Beiki, M. and Pedersen, L.B., 2010. Eigenvector analysis of gravity gradient tensor to locate geologic bodies; Geophysics, v. 75, p. I37–I49.

Brewster, J., 2013. Directional filter for processing full tensor gradiometer data; Bell Geospace Inc., US Patent application 13/966722.

Dransfield, M. and Christensen, A., 2013. Performance of airborne gravity gradiometers; The Leading Edge, v. 32, p. 908–922.

Inman, J.R., 1975. Resistivity inversion with ridge regression; Geophysics, v. 40, p. 798–817.

Keating, P. and Pilkington, M., 2013. Analysis and reprocessing of airborne gravity gradiometer data over the Strange Lake rare-earth deposit, Quebec-Labrador: The Leading Edge, v. 32, p. 940–947.

Martinez, C., Li, Y., Krahenbuhl, R., and Braga, M., 2013. 3D inversion of airborne gravity gradiometry data in mineral exploration: A case study in the Quadrilátero Ferrífero, Brazil; Geophysics, v. 78, p. B1–B11.

Matheron, G.F., 1963. Principles of geostatistics; Economic Geology, v. 58, p. 1246–1266.

Pilkington, M., 2012. Analysis of gravity gradiometer inverse problems using optimal design measures; Geophysics, v. 77, p. G25–G31.

Pilkington, M., 2014. Evaluating the utility of gravity gradient tensor components; Geophysics, v. 79, p. G1-G14.

Pilkington, M. and Shamsipour, P., 2014. Noise reduction procedures for gravity gradiometer data; Geophysics, v. 79, p. G69–G78.

Vasco, D.W. and Taylor, C., 1991. Inversion of airborne gravity gradient data, southwestern Oklahoma; Geophysics, v. 56, p. 90–101.

Zhang, C., Mushayandebvu, M.F., Reid, A.B. Fairhead, J.D., and Odegard, M.E., 2000. Euler deconvolution of gravity tensor gradient data; Geophysics, v. 65, p. 512–520.

Zhdanov, M.S., Ellis, R., and Mukherjee, S., 2004. Three-dimensional regularized focusing inversion of gravity gradient tensor component data; Geophysics, v. 69, p. 925–937.

GEOLOGICAL SURVEY OF CANADA
OPEN FILE 7856

Targeted Geoscience Initiative 4: Canadian Nickel-Copper-Platinum Group Elements-Chromium Ore Systems — Fertility, Pathfinders, New and Revised Models

Trace elements in Fe-oxide minerals from fertile and barren igneous complexes: Investigating their use as a vectoring tool for Ni-Cu-PGE sulphide mineralization

Sarah A.S. Dare[1], Doreen E. Ames[2], Peter C. Lightfoot[3], Sarah-Jane Barnes[1], and Georges Beaudoin[4]

[1]Université du Québec à Chicoutimi, Saguenay, Quebec
[2]Geological Survey of Canada, Ottawa, Ontario
[3]Vale Brownfield Exploration, Sudbury, Ontario
[4]Université Laval, Québec, Quebec

2015

© Her Majesty the Queen in Right of Canada, as represented by the Minister of Natural Resources Canada, 2015

This publication is available for free download through GEOSCAN (http://geoscan.nrcan.gc.ca/)

Recommended citation

Dare, S.A.S., Ames, D.E., Lightfoot, P.C., Barnes, S.-J., and Beaudoin, G., 2015. Trace elements in Fe-oxide minerals from fertile and barren igneous complexes: Investigating their use as a vectoring tool for Ni-Cu-PGE sulphide mineralization, *In:* Targeted Geoscience Initiative 4: Canadian Nickel-Copper-Platinum Group Elements-Chromium Ore Systems — Fertility, Pathfinders, New and Revised Models, (ed.) D.E. Ames and M.G. Houlé; Geological Survey of Canada, Open File 7856, p. 175–185.

Publications in this series have not been edited; they are released as submitted by the author.

Contribution to the Geological Survey of Canada's Targeted Geoscience Initiative 4 (TGI-4) Program (2010–2015)

TABLE OF CONTENTS

Trace elements in Fe-oxide minerals from fertile and barren igneous complexes: Investigating their use as a vectoring tool for Ni-Cu-PGE sulphide mineralization

Sarah A.S. Dare[1]*, Doreen E. Ames[2], Peter C. Lightfoot[3], Sarah-Jane Barnes[1], and Georges Beaudoin[4]

[1]Canada Research Chair in Magmatic Ore Deposits, D.S.A. Sciences de la Terre, 555, boulevard de l'Université, Université du Québec à Chicoutimi, Saguenay, Quebec G7H 2B1
[2]Geological Survey of Canada, 601 Booth Street, Ottawa, Ontario K1A 0E8
[3]Vale Brownfield Exploration, 18 Rink Street, Copper Cliff, Ontario P0M 1N0
[4]Département de géologie et de génie géologique, Université Laval, 1065 avenue de la Médecine, Québec, Quebec G1V 0A6
*Corresponding author's e-mail: sdare@uOttawa.ca

ABSTRACT

The aim of this study was to develop a new technique to determine the fertility of mafic intrusions for Ni-Cu-PGE sulphide mineralization using the mineral chemistry of Fe oxides in the silicate host rocks. A suite of 25 trace elements was determined in magnetite and ilmenite, by laser ablation ICP-MS at LabMaTer (UQAC), from a variety of barren and fertile igneous complexes. Two of Canada's largest Ni deposits, the 1.85 Ga Sudbury Igneous Complex and its vast Ni-Cu-PGE mineral district (Ontario) and the 1.34 Ga Eastern Deeps Intrusion-hosting Ni-Cu-Co sulphide mineralization at Voisey's Bay (Newfoundland), were selected for study. Samples chosen from igneous complexes that are barren of significant Ni sulphide mineralization comprise layered mafic intrusions (Bushveld Complex, South Africa and Sept Iles, Quebec) and anorthosite suites (Saguenay-Lac-St.-Jean, Quebec) that host Fe-Ti-V-P oxide deposits, some of which contain trace amounts of Ni-Cu-PGE sulphides. Mafic rocks of the 1.33 Ga Newark Island layered intrusion (Labrador) were also studied as they are similar in composition and setting to Voisey's Bay but devoid of significant Ni sulphide mineralization.

In sulphide-undersaturated magmas, Cu, Sn, Mo, and Zn are incompatible during fractionation and thus increase in concentration in late-crystallizing magnetite and ilmenite. Upon sulphide saturation and the formation of a trace amount of sulphide, only Cu is depleted in the silicate magma relative to the incompatible elements. Copper depletion, as recorded by Fe oxides, is a sensitive indicator of sulphide saturation and can be diagnostic of whether a Ni-bearing sulphide deposit will have formed if the Cu depletion occurred early during fractionation. In contrast, Ni and Co are compatible during fractionation, partitioning into olivine, orthopyroxene, and, where present, sulphide, and their concentrations steadily decrease in the Fe oxides, together with Cr, as crystallization proceeds. Iron oxides from barren igneous complexes plot on a single Ni-Cr trend but Fe oxides from fertile complexes (those hosting Ni sulphide deposits) plot on a parallel Ni-Cr trend displaced to lower Ni concentration. Nickel depletion is therefore recorded in Fe oxides and has the potential to identify intrusions with buried Ni-sulphide mineralization. The advantages of using Fe oxides as an exploration tool include their resistance to post-magmatic processes, such as alteration, and their preservation and easy recovery from glacial till and heavy mineral separates.

INTRODUCTION

Magmatic Ni-Cu-PGE sulphide deposits are hosted towards the base of ultramafic and mafic igneous complexes and formed by efficient accumulation of immiscible sulphide liquids that scavenged chalcophile metals from the host silicate magma (Naldrett, 2004). Exploration work undertaken to identify Ni-Cu-PGE sulphide mineralization benefits from an understanding of whether the intrusions are anomalously depleted or enriched in highly chalcophile metals (PGE, Cu, and Ni). At present, this comprises bulk rock geochemical ratios, such as Ni/Ni* (Lightfoot et al., 2001, 2011; Darling et al., 2010: where Ni* is the expected Ni concentration for a given MgO content of a S-undersaturated within-plate basalt. Thus a low Ni/Ni* value indicates Ni depletion due to S-saturation and segregation), Cu/Zr (Lightfoot and Hawkesworth, 1997; Li et al., 2000; Darling et al., 2010) and Cu/Pd (Keays, 1995; Barnes and Lightfoot, 2005), and Ni depletion in olivine (Li et al., 2000). Magmatic Fe oxides (magnetite and/or ilmenite) commonly crystallize in the middle to upper parts of mafic-ultramafic intrusions,

Dare, S.A.S., Ames, D.E., Lightfoot, P.C., Barnes, S.-J., and Beaudoin, G., 2015. Trace elements in Fe-oxide minerals from fertile and barren igneous complexes: Investigating their use as a vectoring tool for Ni-Cu-PGE sulphide mineralization, *In:* Targeted Geoscience Initiative 4: Canadian Nickel-Copper-Platinum Group Elements-Chromium Ore Systems — Fertility, Pathfinders, New and Revised Models, (ed.) D.E. Ames and M.G. Houlé; Geological Survey of Canada, Open File 7856, p. 175–185.

which may or may not host Ni or PGE mineralization at their bases. Recent studies on the trace element composition of Fe oxides in massive sulphide from Ni-Cu-PGE deposits (Dare et al., 2012; Boutroy et al., 2014) and massive oxides from Ti-V-P deposits (Dare et al., 2014b) demonstrate that Fe-oxide trace element chemistry is sensitive to fractionation of sulphide and silicate liquids and to the presence of sulphide minerals. The purpose of this mineralogical study was to investigate whether 1) the composition of Fe oxides, found in mafic intrusions that host world-class Ni deposits, records sulphide saturation and segregation via chalcophile depletion, and 2) whether this signature can be used as a fertility indicator to distinguish fertile from barren intrusions and help vector towards a Ni sulphide deposit at the base or in the footwall of prospective intrusions.

SAMPLING AND METHODOLOGY

Samples

The study focused on two well known fertile igneous complexes that contain some of Canada's largest Ni-deposits: the 1.85 Ga Sudbury Igneous Complex, Ontario (total of 69 samples, 450 Fe-oxide grains), and the 1.34 Ga Voisey's Bay intrusion of Eastern Deeps (total of 19 samples, 192 Fe-oxide grains) within the Nain Plutonic Suite of Labrador. The 1.33 Ga Newark Island layered intrusion (total of 18 samples, 76 Fe-oxide grains), also within the Nain Plutonic Suite, was chosen to represent a 'barren' mafic intrusion of similar age, composition, and setting to Voisey's Bay but without any significant Ni-mineralization. Details of the geological background, sample locations, and geochemical databases (both mineral and whole rock) for these 3 intrusions are presented in Dare et al. (2014a). This mineral database was compared to a background data set of Fe oxides (total of 54 samples, ~340 Fe-oxide grains) from Ti-V-P deposits (Méric, 2011; Néron, 2012; Dare et al., 2014b) hosted in igneous complexes that are barren of significant nickel sulphide mineralization. These comprise samples of massive Fe oxides from layered mafic intrusions, such as the Bushveld Complex (South Africa), Sept Iles (Canada), and Rio Jacaré (Brazil), as well as from the anorthosite massif of Saguenay-Lac-St.-Jean (Quebec, Canada). Although these igneous complexes are barren of massive Ni-rich sulphide mineralization, most had some history of sulphide saturation; trace amounts of magmatic sulphides, some of which are enriched in PGE, formed either in the lower parts of some of the complexes, such as the world-class Merensky Reef of the Bushveld Complex, and in the upper part with the massive oxide layers in the Rio Jacaré Complex (Sá et al., 2005).

Methodology

In situ determination of trace elements in the magnetite and ilmenite were carried out on 107 polished thin sections using 1) electron microprobe (EMP) at Université Laval, Quebec City, following normal protocol (see details in Dare et al. (2012)); and 2) laser ablation-ICP-MS at LabMaTer, Université du Québec à Chicoutimi (UQAC) for Mg, Al, Si, P, Ca, S, Sc, Ti, V, Cr, Mn, Fe, Co, Ni, Cu, Zn, Ga, Ge, Y, Zr, Nb, Mo, Ru, Pd, Sn, La, Sm, Yb, Hf, Ta, W, Re, Ir, Pt, Au, Pb, and Bi. The laser system at UQAC comprises a RESOlution M-50 (Excimer 193 nm) coupled to an Agilent 7700x ICP-MS. Beam size varied from 33 to 75 μm with a laser frequency of 10 to 15 Hz. ^{57}Fe was used as the internal standard. USGS synthetic basaltic glass, GSE-1g, was used to calibrate and GSD-1g and an in-house standard (Bushveld magnetite) were used to monitor the results. Analytical protocol and full data sets are given in Dare et al. (2014a, b). Detection limits are typically sub-ppm, e.g., <0.1 ppm for Cu and Mo (see Dare et al., 2014a). Sulphur, Re, Ir, Ru, Pt, Pd, and Au were below detection in the Fe oxides and were thus not quantified using GSE-1g. The relatively large spot size used during LA-ICP-MS analysis homogenizes the magnetite and any subsolidus exsolutions, such as ilmenite or spinel. Thus the data represent the initial composition of the magmatic magnetite that crystallized from the silicate melt before subsolidus processes took place. The raw data signals were screened to avoid inclusions of silicates and sulphides in analysis.

RESULTS AND DISCUSSION

Data analysis: Barren Intrusions

Chalcophile elements commonly present at concentrations above detection limits in igneous Fe oxides are Ni, Cu, Co, Mo, Zn, Sn, and Pb whereas the PGE are typically below detection limits (Dare et al., 2012, 2014b). However, of these elements that can be measured in Fe oxides, only Cu and Ni record chalcophile depletion of the silicate magma upon S-saturation, due to their high partition coefficients (D) into sulphide melt (D ~1000 and ~500, respectively, see review in Barnes and Lightfoot (2005)). Iron-oxide data from mafic intrusions that are barren of significant Ni sulphide mineralization demonstrate the behaviour of chalcophile elements during fractionation of mafic magmas (Fig. 1a). Nickel and Co are compatible and thus decrease during fractionation, as they readily partition into silicate minerals (e.g. olivine and pyroxene). This evolution of silicate melt composition is recorded by both magnetite and ilmenite: the Ni, Co, Cr, and V contents of Fe oxides systematically decrease up sequence in layered intrusions with highest values in Fe oxides from the lowermost (Ti-V deposits) magnetite layers and lowest values in those from the upper-

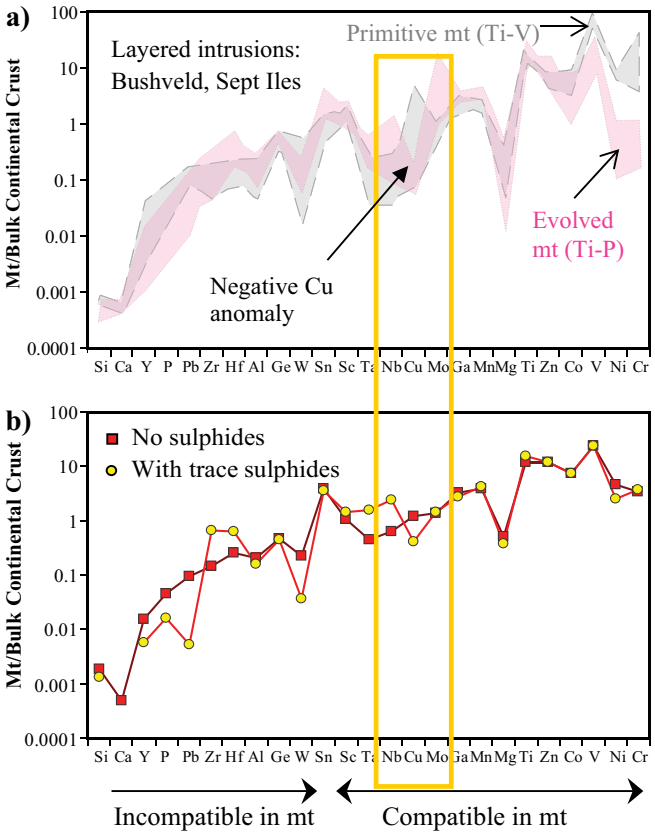

Figure 1. Multi-element diagrams for magnetite, normalized to bulk continental crust, from **(a)** layered intrusions barren of Ni deposits and **(b)** andesite lavas. Modified from Dare et al. (2014b).

most (Ti-P deposits) magnetite layers (Méric, 2011; Dare et al., 2014b). In contrast, elements incompatible during fractionation, such as Sn, Mo, and Zn, increase in Fe oxides, together with Nb, Ta, and Mn, even when trace amounts of immiscible sulphides formed (Méric, 2011; Dare et al., 2014b). This is because their partition coefficients into sulphide melt are not high enough (D~10–20) to deplete the silicate magma upon the crystallization of a small amount of sulphides. In the absence of sulphides, Cu is also incompatible and increases in the silicate melt during fractionation, whereas upon sulphide-saturation Cu becomes compatible and is depleted (Li et al., 2000). Recent experimental studies indicate that Cu should partition into Ti-rich magnetite (Simon et al., 2008). Analysis of Ti-rich magnetite in andesite lavas from Chile confirms that Cu can be present in solid solution in magnetite (30–100 ppm: Dare et al., 2014b). These andesite samples are sulphide-undersaturated due to the oxidized nature of magmas developed in a continental arc setting, which was calculated as +2 QFM (quartz-fayalite-magnetite buffer) for these samples (Dare et al., 2014b). On the multi-element diagram (Fig. 1b), Cu is positioned between Nb and Mo because these three elements have similar partition coefficients into magnetite from silicate melt (Dare et al., 2014b). For magnetite that crystallized from sulphide-undersaturated andesitic magma, the Cu, Nb, and Mo content of magnetite on the multi-element diagram define a flat line, i.e., there is no Cu anomaly. However, crystallization of magnetite may locally reduce andesitic magma and trigger formation of small amounts of sulphide droplets (Chiaradia et al., 2011). In this study, one of the andesite samples has small Cu sulphide inclusions in magnetite and as a result the magnetite has a small negative Cu anomaly (Fig. 1b). This is because the sulphide droplet has preferentially taken Cu from the silicate melt and thus depleted the magnetite in Cu (11 ppm). A large Cu anomaly is present in magnetite from the uppermost layers of the Sept Iles and Bushveld layered intrusions (Fig. 1a), which supports the observation that small amounts of immiscible sulphide formed in the lower parts of these intrusions. Thus a negative Cu anomaly is indicative of the formation of a small amount (cotectic proportions: 0.3 wt% S) of sulphide liquid in barren intrusions.

Ni and Cu Content of Fe-Oxide Minerals as Indicators of Fertility of Mafic Magmas

This study proposes that the most useful elements/element ratios to monitor the amount and timing of chalcophile depletion of mafic magmas, from which the history of sulphide saturation can be obtained, are the Cu anomaly ($Cu/Cu^*_N = 2Cu_N/(Nb_N + Mo_N)$) and Ni content of Fe oxides (both magnetite and ilmenite) plotted against Cr, which is used to monitor the degree of fractionation (Fig. 2). Fe oxides from all igneous complexes that are barren of significant Ni sulphide mineralization, but contain small amounts of sulphides, are plotted on these diagrams to define the field of barren intrusions (Fig. 2). During fractionation, the Cr content of magnetite and ilmenite decreases 4 orders of magnitude. However, there is a slight tendency for the negative Cu anomaly to increase, i.e., the value gets smaller during fractionation (Fig. 2a, b). This is most evident for magnetite from magnetite-rich intrusions (Fig. 2a). This is because Cu is depleted in the melt (and in the Fe oxides) upon sulphide saturation and therefore does not increase during fractionation, unlike Nb and Mo. Both Ni and Cr in magnetite and ilmenite decrease with fractionation with or without a small amount of sulphide removal (Fig. 2c, d).

The effect of the crystallization of different amounts of sulphide on the behaviour of chalcophile elements during fractionation is modelled in Figure 3. The cotectic proportion (0.3%) of sulphide was chosen to represent the maximum amount of sulphides forming in igneous complexes that are barren of significant Ni sulphide mineralization. A larger amount of sulphides (1%) was chosen for fertile igneous complexes with

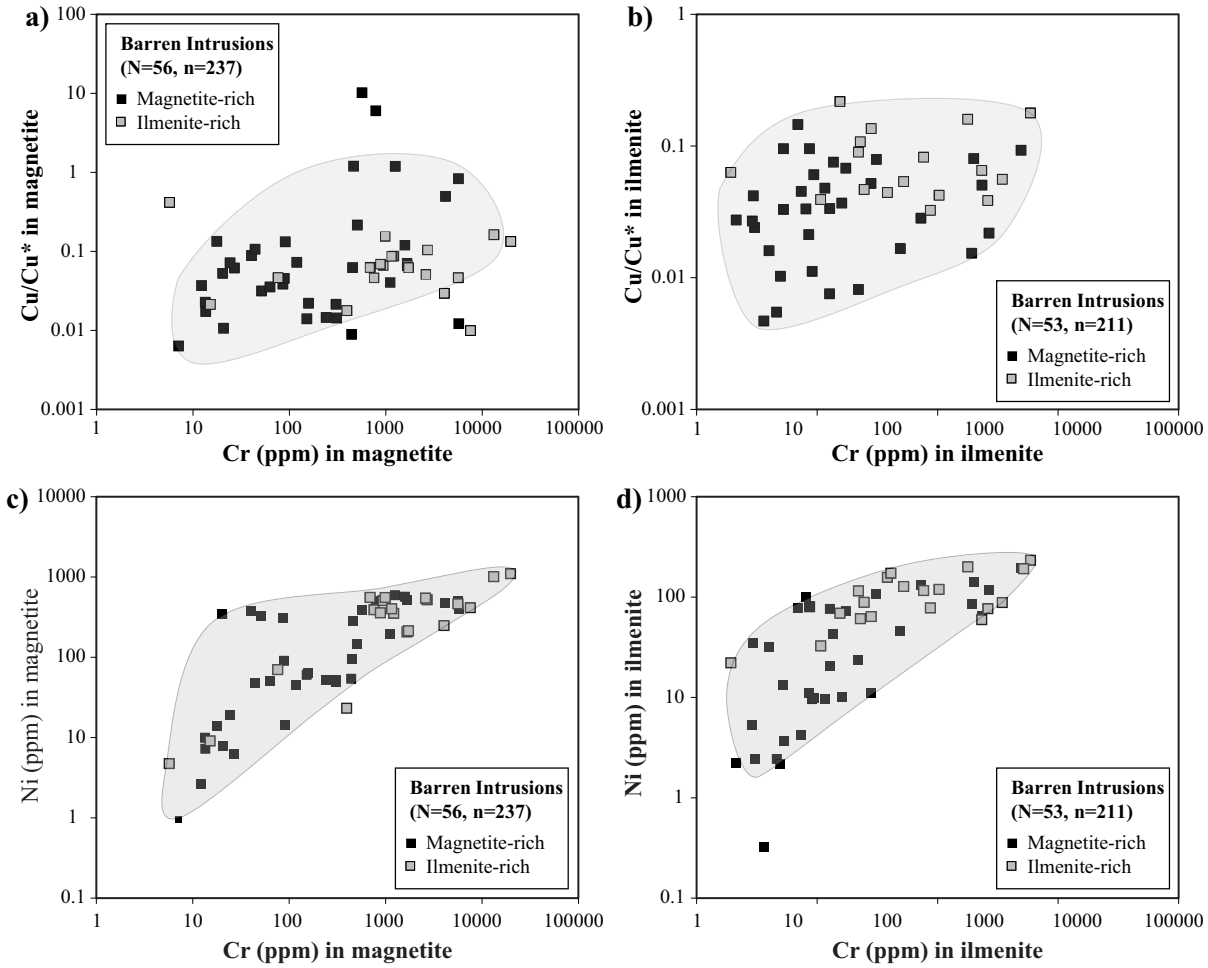

Figure 2. Fe-oxide data for Cu, Ni, and Cr in intrusions that are barren of significant Ni sulphide mineralization: the Cu anomaly (Cu/Cu*) versus Cr content of **(a)** magnetite and **(b)** ilmenite. Nickel versus Cr content of **(c)** magnetite and **(d)** ilmenite. Sources of data: Méric (2011), Néron (2012), Dare et al. (2014b), and Dare (unpublished).

significant Ni sulphide mineralization. Figure 3 indicates that the size and timing of Ni and Cu depletion should be different for barren and fertile magmas. As indicated above, the size and rate of metal depletion depends on the partition coefficient between sulphide and silicate magmas. In both models, the PGEs ($D \approx 10000$) are the most rapidly depleted, followed by Cu ($D \approx 1000$), then Ni ($D \approx 500$). The remaining chalcophile elements ($D \approx 10$ for Mo, Co, Pb, Sn, and Zn) show no significant depletion in the melt due to sulphide crystallization. As the crystallization of Fe oxides typically occurs late, after 40 to 70% of fractionation, they are ideal minerals to record significant depletion of Ni and Cu in the magma. Only a mineral that crystallizes early, such as chromite, is able to record depletion of PGE upon sulphide saturation (Locmelis et al., 2013; Pagé et al., 2015). Figure 3b illustrates that for fertile magmas, which either crystallized (or interacted with) a large proportion of sulphide, the depletion of Ni and Cu occurs earlier than in barren intrusions. Fe oxides that crystallize from a fertile magma after the same degree (40–70%) of fractionation (i.e. same Cr value) should therefore display significant depletion in Ni and Cu. Magnetite and ilmenite from fertile igneous complexes at Voisey's Bay and Sudbury were plotted on these new Fe-oxide diagrams to test this hypothesis (Figs. 4, 5).

Voisey's Bay

Ilmenite is the dominant Fe oxide in the troctolite and olivine gabbro units of the Eastern Deep Intrusion, which is host to part of the Voisey's Bay Ni sulphide deposit. Some samples are weakly mineralized but the majority are devoid of sulphide mineralization. Massive sulphide mineralization occurs towards the base of the intrusion and in the feeder dyke (Lightfoot et al., 2012). Ilmenite occurs as an intercumulus mineral in these primitive rocks and is thus Cr-rich (2000–100 ppm); however, magnetite is rare. Ilmenite displays an early Cu depletion (at high Cr values) and most of the data plot outside the barren field on the Cu/Cu* versus Cr plot (Fig. 4a), indicating a large and early depletion of Cu in the magma due to the formation of significant amounts of sulphide mineralization

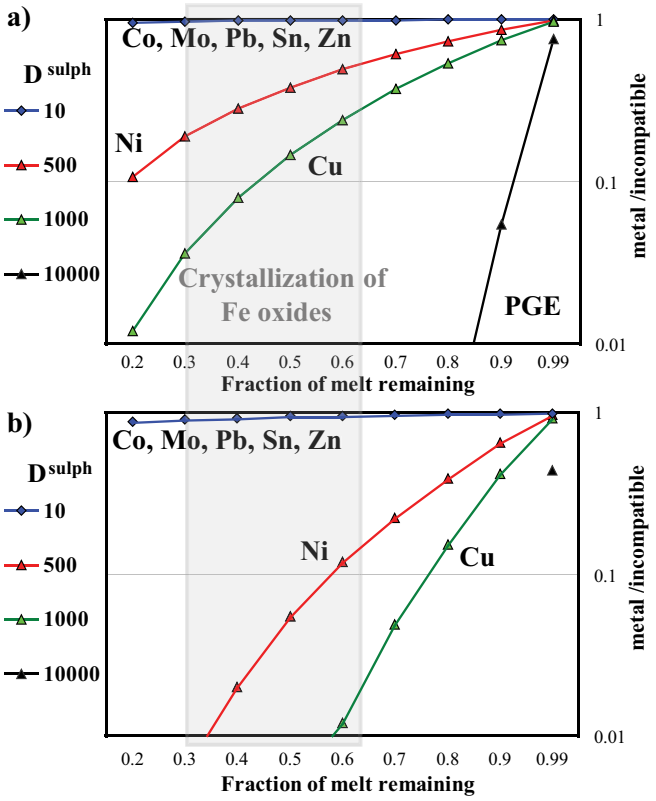

Figure 3. Element modelling of chalcophile depletion during fractionation of mafic magma with different amounts of sulphides. **a)** Crystallization of cotectic proportion of sulphide (0.3%), common in intrusions barren of Ni deposits. **b)** Crystallization of larger amounts of sulphide (1%), to simulate chalcophile depletion in fertile intrusions. The grey box indicates the typical 'window' of crystallization of cumulus Fe oxides (40–70% fractionation).

at depth. This result is supportive of the whole rock Cu/Zr geochemistry results of Li et al. (2000). On the Ni-Cr diagram, however, most of the ilmenite data plots within the barren field, with only a few plotting at lower Ni values, indicating that there was no significant Ni depletion (Fig. 4b) of the magma. This is also in agreement with the whole rock data (Lightfoot et al., 2012). For primitive rocks, that crystallize after 15 to 20% fractionation (Li et al., 2000), the model in Figure 4c indicates that there will be significant Cu depletion (1 order of magnitude difference) but less significant Ni depletion (only half order of magnitude difference).

Sudbury Igneous Complex

Both ilmenite and magnetite are present as cumulus and intercumulus minerals in the oxide-rich gabbro and underlying norite, respectively, of the Sudbury Igneous Complex. Samples were selected both above and away from known massive sulphide mineralization. Darling et al. (2010) showed that samples above mineralization are the most depleted in Ni and Cu (~65%) whereas samples away from mineralization are still significantly depleted (~45%). Both magnetite and ilmenite

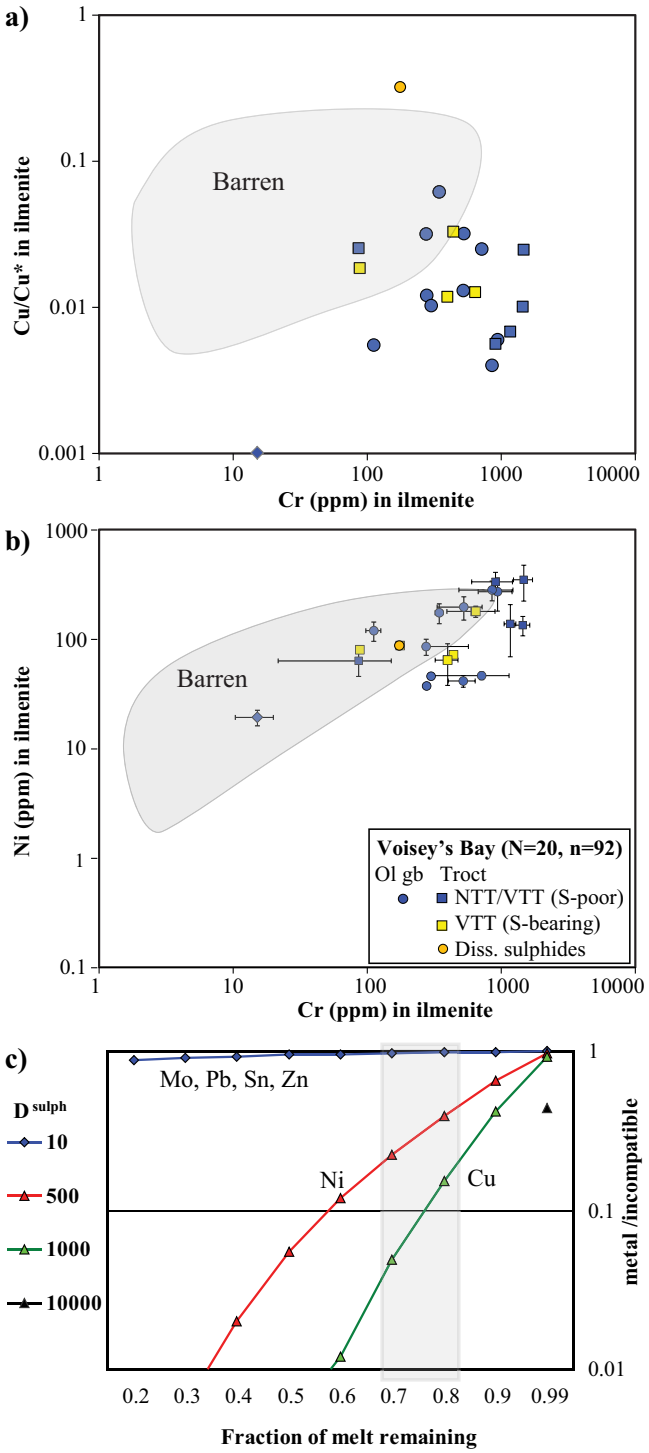

Figure 4. Results for ilmenite in troctolite (troct) and olivine gabbro (ol gb) from the fertile intrusion of Voisey's Bay Ni-Co deposit: **a)** Cu anomaly (Cu/Cu*) versus Cr; **b)** Ni versus Cr; **c)** model of the behaviour of the chalcophile depletion for fertile intrusion (same as in Fig. 3b). Legend for the rock types are given in (b), where NTT = normal-textured troctolite; VTT = variable-textured troctolite; and diss. sulphides = disseminate sulphides. The grey box in (c) indicates that the low degree of fractionation (15–20%) of the samples may explain the lack of Ni depletion recorded by ilmenite. N = number of samples; n = number of grains analysed.

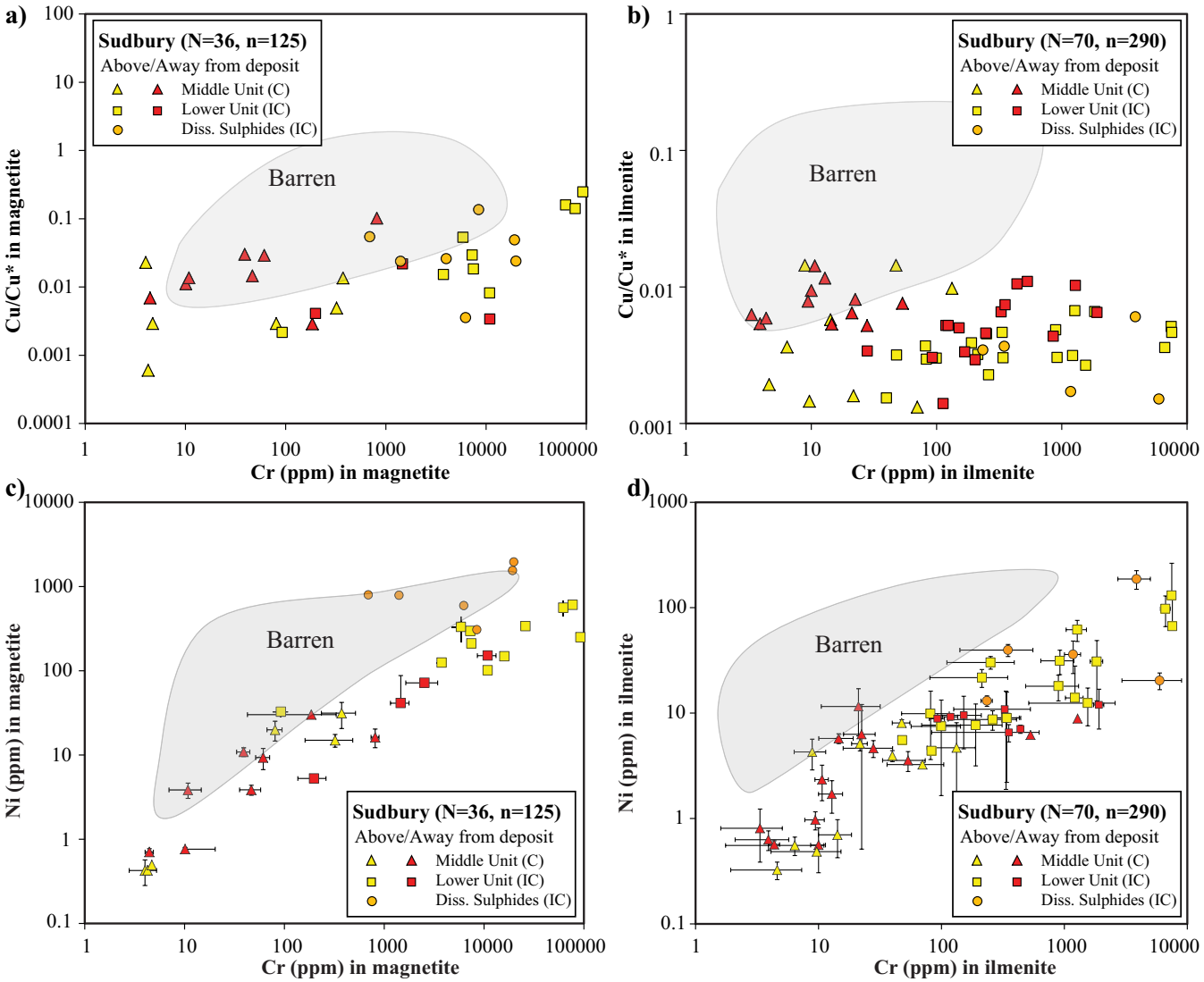

Figure 5. Results for Fe oxides from the Sudbury Igneous Complex, which is the world's largest Ni mining camp: **(a and b)** Cu anomaly versus Cr content of magnetite and ilmenite and **(c and d)** Ni versus Cr content of magnetite and ilmenite. Note that magnetite from disseminated sulphide samples have unusually high Ni contents, probably due to subsolidus re-equilibration with Ni-rich sulphide. N = number of samples; n = number of grains analysed.

have large negative Cu anomalies and as such most plot at lower values of Cu/Cu*, outside of the barren field (Fig. 5a, b), with the exception of a few more evolved samples collected away from known deposits. This indicates that the Fe oxides in the Sudbury Igneous Complex record a large and extensive Cu depletion of the magma that was present at the start of fractionation. Compared to ilmenite from Voisey's Bay, the depletion in Cu at Sudbury is an order of magnitude larger. On the Ni-Cr diagrams (Fig. 5c, d), all ilmenite data, and most of the magnetite data plot off the barren trend, at much lower Ni values. Thus the widespread Cu and Ni depletion recorded by the Fe oxides is in agreement with the whole rock geochemical data (Cu/Zr and Ni/Ni*: Lightfoot et al., 2001; Darling et al., 2010) and indicates that a large volume of sulphides efficiently collected the chalcophile metals from the overlying silicate melt. However, there is no significant difference in the chemistry of the Fe oxides in samples from directly above or away from mineralization.

Newark Island Layered Intrusion: Barren or Fertile?

This intrusion is part of the same Nain Plutonic Suite as Voisey's Bay; it was considered on a whole to be barren of significant Ni mineralization, based on whole rock data and past exploration (Lightfoot et al., 2012). Mafic samples were selected from the Newark Island intrusion specifically for this study to compare with those from the Eastern Deeps Intrusion at Voisey's Bay. They range in composition from olivine gabbro to gabbro but are slightly more evolved than the mafic-ultramafic samples from Voisey's Bay. As such, the Fe oxides are mainly cumulus phases: ilmenite is domi-

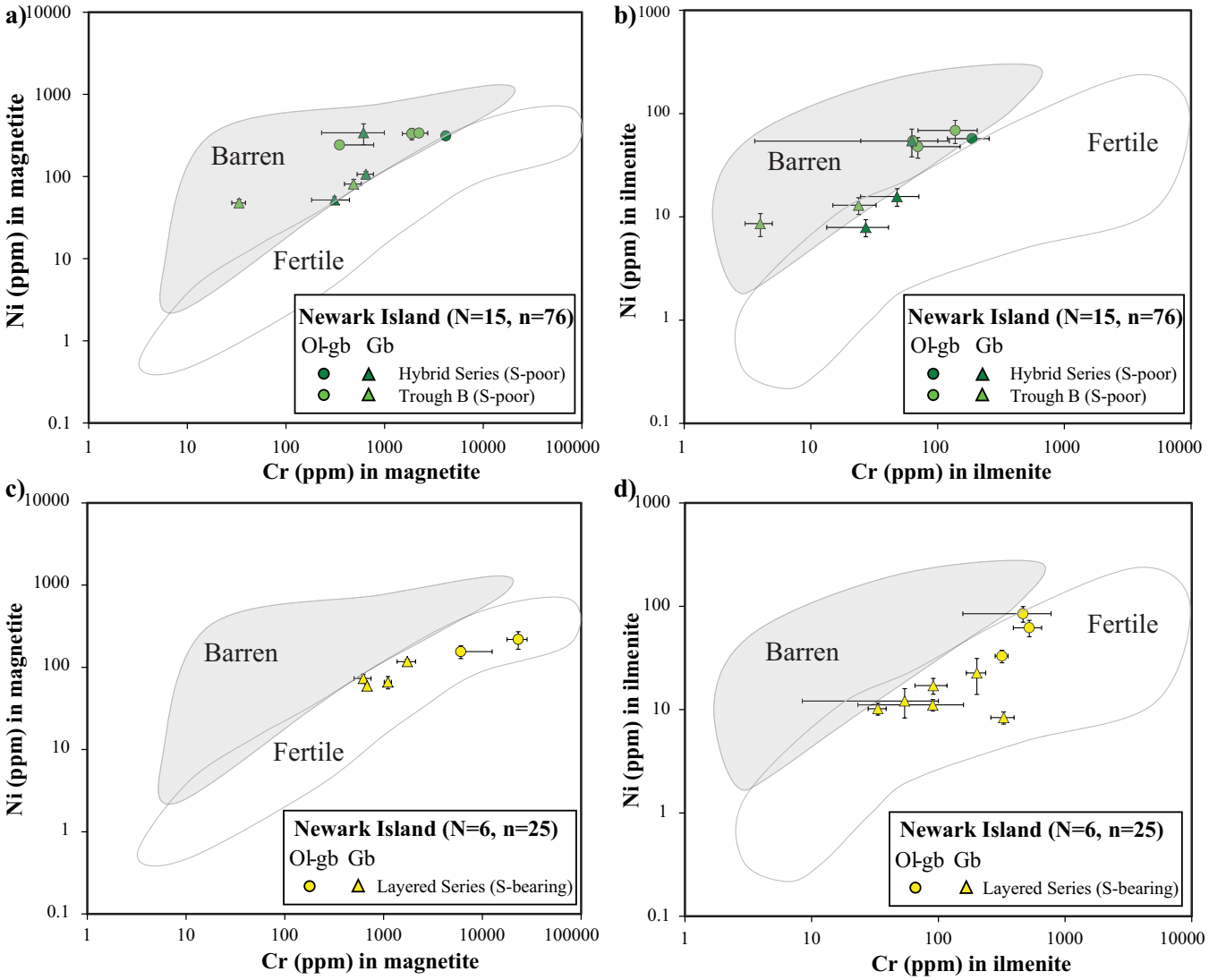

Figure 6. Results for Fe oxides from the supposedly barren Newark Island layered intrusion using Ni versus Cr diagrams. **a and b)** Magnetite and ilmenite from the upper part of the intrusion (Hybrid Series and Trough B) plot in barren field. **c and d)** Magnetite and ilmenite from the lower part of the intrusion (Layered Series) plot in the fertile field. N = number of samples; n = number of grains analysed.

nant but some magnetite crystallized shortly afterwards, followed by pyrrhotite (Wiebe and Snyder, 1993). Iron oxides from the upper part of the layered intrusion (Hybrid and Trough series) plot entirely in the barren field on the Ni-Cr diagram for magnetite and mostly in the barren field for ilmenite (Fig. 6a, b). In contrast, samples from the lower part of the intrusion (Layered Series) are relatively depleted in Ni and plot entirely in the fertile field defined by Sudbury Igneous Complex Fe oxides. A close inspection of the Ni-MgO whole rock data of Lightfoot et al. (2012) for these two series agrees with the results from the Fe oxides, showing no Ni depletion for the Hybrid Series and some Ni depletion for the Layered Series (Fig. 7). This indicates that the lower part of the intrusion is potentially fertile. However, this cannot yet be determined as the lower part of the intrusion is not exposed onshore. It is noteworthy to highlight that the fertile field for Fe oxides, although defined by Sudbury Igneous Complex samples that were formed by melting of the continental crust, can also be applied to evaluate the fertility of mantle-derived melts.

IMPLICATIONS FOR EXPLORATION

The examination of Fe-oxide geochemistry in fertile Ni-Cu-PGE environments, compared to barren environments, provides critical knowledge on the sulphide saturation and segregation history of the intrusion. We have shown that sulphide saturation is recorded by Ni and Cu depletion in Fe oxides. Significantly, fertile intrusions can be distinguished from barren intrusions by the size and timing of Ni and Cu depletion in relation to fractionation of the silicate magma. The mineral chemistry results are in agreement with whole-rock

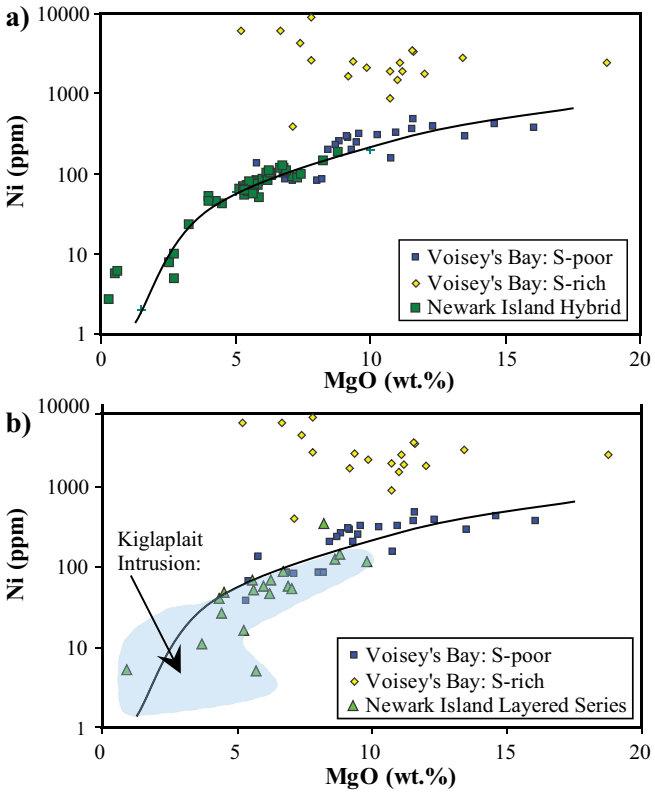

Figure 7. Whole rock Ni versus MgO plots for Nain plutonic suite rocks: a) Voisey's Bay (fertile) and Newark Island Hybrid Series (barren) both show no Ni depletion; b) Newark Island Layered Series shows similar Ni depletion to that from the nearby Kiglaplait intrusion. Data from Lightfoot et al. (2012) and Dare et al. (2014a).

data. The advantages of using Fe-oxide chemistry are that they are resistant to alteration and are commonly preserved and easily recovered from till and sediments. This new mineral technique provides a novel approach for determining the potential fertility of an intrusion for Ni-Cu-PGE deposits in support of exploration targeting.

ACKNOWLEDGEMENTS

This work was funded by the Targeted Geoscience Initiative 4 (TGI-4) "Magmatic-Hydrothermal Nickel-Copper-Platinum Group Elements Ore System Subproject: System Fertility and Ore Vectors" project of the Geological Survey of Canada (GSC). We wish to thank Sadia Medhi (UQAC) and Marc Choquette (Université Laval) for their assistance with LA-ICP-MS and EMP analyses, respectively. We also thank Simon Jackson (GSC) for his thorough review of this manuscript. The study is part of a Vale-sponsored research project on oxide geochemistry funded through the University of Laval.

REFERENCES

Barnes, S.-J. and Lightfoot, P.C., 2005. Formation of magmatic nickel-sulfide ore deposits and processes affecting their copper and platinum-group element contents, *In:* One Hundredth Anniversary Volume, (ed..) J.W. Hedenquist, J.F.H. Thompson, R.J. Goldfarb, and J.P. Richards; Economic Geology, p. 179–213.

Barnes, S.-J. and Lightfoot, P.C., 2005. Formation of magmatic nickel-sulfide ore deposits and processes affecting their copper and platinum-group element contents, *In:* One Hundredth Anniversary Volume, (ed..) J.W. Hedenquist, J.F.H. Thompson, R.J. Goldfarb, and J.P. Richards; Economic Geology, p. 179–213.

Boutroy, E., Dare, S.A.S., Beaudoin, G., Barnes, S.-J., and Lightfoot, P.C., 2014. Magnetite composition in Ni-Cu-PGE deposits worldwide and its application to mineral exploration; Journal of Geochemical Exploration, v. 145, p. 64–81.

Chiaradia, M., Müntener, O., and Beate, B., 2011. Enriched basaltic andesites from mid-crustal fractional crystallization, recharge, and assimilation (Pilavo Volcano, Western Cordillera of Ecuador); Journal of Petrology, v. 52, p. 1107–1141.

Dare, S.A.S., Barnes, S.-J., and Beaudoin, G., 2012. Variation in trace element content of magnetite crystallized from a fractionating sulfide liquid, Sudbury, Canada: Implications for provenance discrimination; Geochimica et Cosmochimica Acta, v. 88, p. 27–50.

Dare, S.A.S., Ames, D.E., Lightfoot, P.C., Barnes, S.-J., and Beaudoin, G., 2014a. Mineral chemistry and supporting databases for TGI4 project on 'Trace elements in Fe-oxides from fertile and barren igneous complexes: Investigating their use as a vectoring tool in the intrusions that host Ni-Cu-PGE deposits"; Geological Survey of Canada, Open File Report, 7538. doi:10.4095/293640

Dare, S.A.S., Barnes, S.-J., Beaudoin, G., Méric, J., Boutroy, E., and Potvin-Doucet, C., 2014b. Trace elements in magnetite as petrogenetic indicators; Mineralium Deposita, v. 49, p. 785–796.

Darling, J.R., Hawkesworth, C.J., Lightfoot, P.C., Storey, C.D., and Tremblay, E., 2010. Isotopic heterogeneity in the Sudbury impact melt sheet; Earth and Planetary Science Letters, v. 289, p. 347–356.

Keays, R., 1995, The role of komatiitic and picritic magmatism and S-saturation in the formation of ore deposits; Lithos, v. 34, p. 1–18.

Li, C., Lightfoot, P.C., Amelin, Y., and Naldrett, A.J., 2000. Contrasting petrological and geochemical relationships in the Voisey's Bay and Mushuau intrusions, Labrador, Canada: implications for ore genesis; Economic Geology, v. 95, p. 771–799.

Lightfoot, P.C. and Hawkesworth, C.J., 1997, Flood basalts and magmatic Ni, Cu, and PGE sulphide mineralization: Comparative geochemistry of the Noril'sk (Siberian Traps) and West Greenland sequences, *In:* Large Igneous Provinces: Continental, Oceanic and Planetary Flood Volcanism, (ed.) J. Mahoney and M.F. Coffin; American Geophysical Union, Monograph 100, p. 357–380.

Lightfoot, P.C., Keays, R.R., and Doherty, W., 2001. Chemical evolution and origin of nickel sulfide mineralization in the Sudbury Igneous Complex, Ontario, Canada; Economic Geology, v. 96, p. 1855–1875.

Lightfoot, P.C., Keays, R.R., Evans-Lamswood, D., and Wheeler, R., 2012. S saturation history of Nain Plutonic Suite mafic intrusions: origin of the Voisey's Bay Ni–Cu–Co sulfide deposit, Labrador, Canada; Mineralium Deposita, v. 47, p. 23–50.

Locmelis, M., Fiorentini, M.L., Barnes, S.-J., and Pearson, N.J., 2013. Ruthenium variation in chromite from komatiites and komatiitic basalts—a potential mineralogical indicator for nickel sulfide mineralization; Economic Geology, v. 108, p. 355–364.

Méric, J., 2011. Caractérisation géochimiques des magnétites de la zone critique de l'intrusion magmatique de Sept-Iles (Québec, Canada) et intégration a une base de données utilisant la signa-

ture géochimique des oxydes de fer comme outil d'exploration; Université du Québec à Chicoutimi, 48 p.

Naldrett, A. J., 2004. Magmatic Sulfide Deposits: Geology, Geochemistry and Exploration; Springer, 728 p.

Néron, A., 2012. Caractérisation géochimiques des oxydes de Fe-Ti dans un dépôt de Fe-Ti-P associe à la suite anorthositique de Lac Saint Jean, Québec, Canada (secteur Lac à Paul) et intégration des données du secteur Lac à La Mine; Université du Québec à Chicoutimi, 39 p.

Pagé, P., Barnes, S.-J., Méric, J., and Houlé, M.G., 2015. Geochemical composition of chromite from Alexo komatiite in the western Abitibi greenstone belt: Implications for mineral exploration, *In:* Targeted Geoscience Initiative 4: Canadian Nickel-Copper-Platinum Group Elements-Chromium Ore Systems — Fertility, Pathfinders, New and Revised Models, (ed.) D.E. Ames and M.G. Houlé; Geological Survey of Canada, Open File 7856, p. 187–195.

Sá, J.H.S., Barnes, S.-J., Prichard, H.M., and Fisher, P.C., 2005. The distribution of base metals and platinum-group elements in magnetitite and its host rocks in the Rio Jacaré Intrusion, northeastern Brazil; Economic Geology, v. 100, p. 333–348.

Simon, A.C., Candela, P.A., Piccoli, P.M., Mengason, M., and Englander, L., 2008. The effect of crystal-melt partitioning on the budgets of Cu, Au, and Ag; American Mineralogist, v. 93, p. 1437–1448.

Wiebe, R.A. and Snyder, D., 1993, Slow, dense replenishments of a basic magma chamber: the layered series of the Newark Island layered intrusion, Nain, Labrador; Contributions to Mineralogy and Petrology, v. 113, p. 59–72.

GEOLOGICAL SURVEY OF CANADA
OPEN FILE 7856

Targeted Geoscience Initiative 4: Canadian Nickel-Copper-Platinum Group Elements-Chromium Ore Systems — Fertility, Pathfinders, New and Revised Models

Geochemical composition of chromite from Alexo komatiite in the western Abitibi greenstone belt: Implications for mineral exploration

Philippe Pagé[1], Sarah-Jane Barnes[1], Julien Méric[1], and Michel G. Houlé[2]

[1]Université du Québec à Chicoutimi, Saguenay, Quebec
[2]Geological Survey of Canada, Québec, Quebec

2015

© Her Majesty the Queen in Right of Canada, as represented by the Minister of Natural Resources Canada, 2015

This publication is available for free download through GEOSCAN (http://geoscan.nrcan.gc.ca/)

Recommended citation

Pagé, P., Barnes, S.-J., Méric, J., and Houlé, M.G., 2015. Geochemical composition of chromite from Alexo komatiite in the western Abitibi greenstone belt: Implications for mineral exploration, *In:* Targeted Geoscience Initiative 4: Canadian Nickel-Copper-Platinum Group Elements-Chromium Ore Systems — Fertility, Pathfinders, New and Revised Models, (ed.) D.E. Ames and M.G. Houlé; Geological Survey of Canada, Open File 7856, p. 187–195.

Publications in this series have not been edited; they are released as submitted by the author.

Contribution to the Geological Survey of Canada's Targeted Geoscience Initiative 4 (TGI-4) Program (2010–2015)

TABLE OF CONTENTS

Geochemical composition of chromite from Alexo komatiite in the western Abitibi greenstone belt: implications for mineral exploration

Philippe Pagé[1*] , Sarah-Jane Barnes[1], Julien Méric[1], and Michel G. Houlé[2]

[1]Canada Research Chair in Magmatic Ore Deposits, D.S.A. Sciences de la Terre, 555, boulevard de l'Université, Université du Québec à Chicoutimi, Saguenay, Quebec G7H 2B1
[2]Geological Survey of Canada, 490 rue de la Couronne,Québec, Quebec G1K 9A9
*Corresponding author's e-mail: Philippe_Page@uqac.ca

ABSTRACT

This study, which focuses on the composition of chromite from mineralized and unmineralized komatiitic flows and sills from the Alexo Mine area in Dundonald Township, within the western Abitibi greenstone belt, aims to develop new exploration tools for poorly exposed mineralized komatiitic systems. It is possible to clearly identify chromite derived from massive sulphide (having very high Cr# and depleted Ru content) from chromite derived from barren and poorly mineralized samples based on its composition. LA-ICP-MS analyses show that chromite from massive sulphide are depleted in Al, Ni, and Mg, and are enriched in Ti, Zn, Mn, Fe and V compared to chromite from barren samples; however, alteration can also modify chromite chemistry. Samples from the Hart deposit are pervasively altered and their chromite compositions are enriched in Fe, Zn, Co, and Mn, and are depleted in Mg. We propose a binary diagram of Ni/Mn versus Ni/Cr ratios which can be used to clearly discriminate between sulphide segregation prior to chromite crystallization and later superimposed alteration. Mass balance calculations show that chromite does fractionate and concentrate Ir-group platinum-group elements (IPGE: Os, Ir, Ru) and Rh but that chromite contribution to the whole-rock IPGE and Rh budget is rather limited, and for mineralized samples, this contribution is even smaller. From these results, it is clear that IPGE+Rh-rich phases (nano- to micro- platinum-group minerals) are needed to account for the IPGE and Rh contents in whole-rock geochemistry.

INTRODUCTION

This study, part of the Targeted Geoscience Initiative 4 (TGI-4) program, focuses on the chromite composition from mineralized and unmineralized komatiitic flows and sills at the Alexo Mine area in Dundonald Township, within the western Abitibi greenstone belt (WAGB). There were several goals of the present work. (1) Develop a method to use chromite as an indicator mineral for ore-forming processes related to Ni-Cu-(PGE) mineralization associated with komatiite. (2) Explore whether chromite composition can be used to constrain magmatic to post-magmatic processes involved in the generation and the evolution of komatiitic rocks, such as the order of crystallization, sulphide segregation, metamorphism, and alteration. (3) Define a typical signature associated with Ni-Cu-(PGE) sulphide mineralization that can be used targeting prospective regions in exploration campaigns within poorly exposed and/or extensively overburden-covered areas.

Experimental studies of sulphide-undersaturated melts have suggested that chromium-rich spinel fractionates platinum-group elements (PGE) and preferentially incorporates osmium, iridium, ruthenium, and rhodium, which are found to be compatible; platinum and palladium stay in the magma during fractional crystallization as they are incompatible in chromite (e.g. Righter et al., 2004; Brenan et al., 2012). Recently, Locmelis et al. (2011, 2013), Pagé et al. (2012), Park et al. (2012) and Arguin et al. (2014) demonstrated from natural samples that ruthenium in particular, but also osmium, iridium, and rhodium, are incorporated into chromite in the absence of an immiscible sulphide melt, and are, on the other hand, expected to partition into sulphide when droplets of sulphide liquid are present (Fig. 1). Therefore, it has been suggested that a better understanding of Ir-group platinum-group elements (IPGE: Os, Ir, Ru) and Rh behaviour during chromite crystallization in komatiitic systems might lead to new exploration tools (i.e. IPGE+Rh-rich chromite = barren komatiite while IPGE+Rh-poor chromite = mineralized komatiite) that could vector toward Ni-Cu-(PGE) sulphide mineralization in komatiitic systems.

Pagé, P., Barnes, S.-J., Méric, J., and Houlé, M.G., 2015. Geochemical composition of chromite from Alexo komatiite in the western Abitibi greenstone belt: Implications for mineral exploration, *In:* Targeted Geoscience Initiative 4: Canadian Nickel-Copper-Platinum Group Elements-Chromium Ore Systems — Fertility, Pathfinders, New and Revised Models, (ed.) D.E. Ames and M.G. Houlé; Geological Survey of Canada, Open File 7856, p. 187–195.

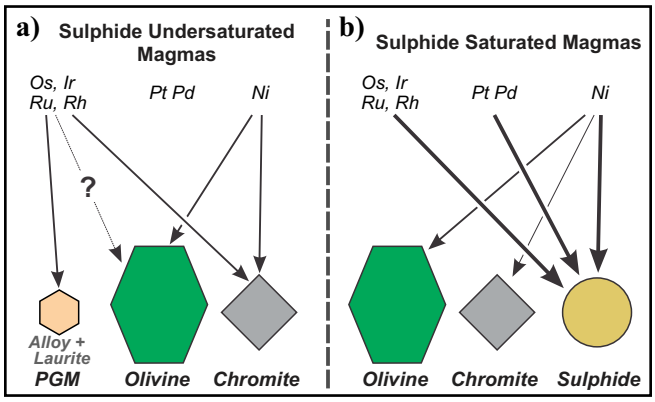

Figure 1. Illustration showing the behaviour of Ir-group platinum-group elements (Os, Ir, Ru) and Rh during the crystallization of **(a)** sulphide-undersaturated magma and **(b)** sulphide-saturated magma. Abbreviations: PGM = platinum-group minerals.

METHODOLOGY

Sample Selection

Samples used in this study must meet three criteria: i) low metamorphic grade (prehnite-pumpellyite up to lower greenschist metamorphic facies; Arndt, 1986), ii) well preserved primary volcanic textures and structures with localized and non-penetrative deformation (Houlé et al., 2012), and iii) large number of samples must be available from a well characterized geological setting. A suite of 47 well preserved samples, which many contains relics of olivine, from the Alexo Mine area were selected as they had been well described by Barnes (1983) and Houlé (2008) in their Ph.D. studies (24 samples from Barnes (1983); 23 samples from Houlé (2008)). Another 6 samples were selected to investigate the effect of alteration on the composition of komatiitic chromite from the komatiite-associated Ni-Cu-(PGE) Hart deposit in the Shaw Dome area in the WAGB, which is pervasively serpentinized and affected by talc-carbonate alteration. The reader is also referred to Barnes et al. (1983), Houlé et al. (2012), and Méric et al. (2012) for detailed geology of the study area.

Analytical Methods

Detailed petrographic work has been conducted on the selected samples to characterize their mineralogy, texture, and degree of alteration. Chromite grains selected were subsequently analyzed with the electron microprobe at Laval University and the LA-ICP-MS at Université du Québec à Chicoutimi. Samples were also analyzed for whole-rock and PGE geochemistry. Detailed analytical parameters and procedures will be presented in a forthcoming dissertation by J. Méric.

RESULTS

Chromite Chemistry

The composition of chromite from the Alexo Mine and

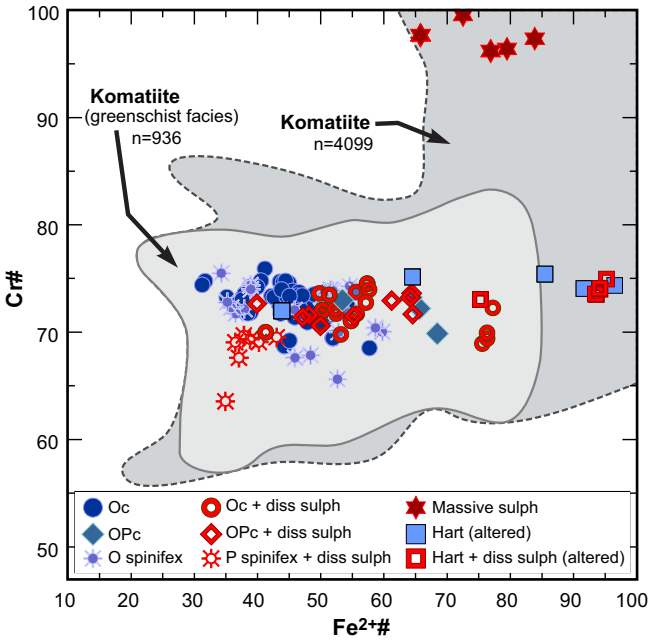

Figure 2. Cr# (100Cr/(Cr+Al)) versus Fe^{2+}# (100Fe^{2+}/(Fe^{2+}+Mg)) diagram of chromite from komatiite from the Alexo Mine area and the Hart deposit. Fields are compiled from Barnes and Roeder (2001). Medium-grey field outlines the composition of chromite in komatiite of various facies, metamorphic grades, and alteration degrees; light-grey field outlines the composition of chromite from komatiite that has undergone greenschist or lower grade metamorphism. Abbreviations: Oc = olivine cumulate; OPc = olivine + pyroxene cumulate; O spinifex = olivine spinifex; diss sulph = disseminated sulphide; P spinifex = pyroxene spinifex; sulph = sulphide.

Hart deposit plot in a limited range of Cr# (100Cr/(Cr+Al)), from ~65 to ~75, but exhibit a much wider range of Fe^{2+}# (100Fe^{2+}/(Fe^{2+}+Mg)), from ~35 to ~75 at Alexo Mine and from ~45 to ~95 at Hart deposit (Fig. 2). However, a group of chromite from massive sulphide samples from Alexo exhibits a very distinctive chemistry with very high Cr# (~97.5) and a range of Fe^{2+}# from ~66 to ~84 (Fig. 2). The distinction between barren samples and those containing traces of disseminated sulphides is not clearly defined based on major elements, even though the latter tend to have higher Fe^{2+}#. However, results of trace elements obtained from LA-ICP-MS do show significant differences between mineralized and barren samples (Fig. 3). Chromite from olivine cumulates and olivine-spinifex samples have very similar patterns, which are representative of typical signatures of well preserved and unmineralized samples (Fig. 3). Compared to these samples, chromite from the sulphide-rich samples are enriched in Ti, Mn, FeO*, and V, and are depleted in Al_2O_3, Ni, and MgO (Fig. 3a). To explore alteration effects, chromite from highly altered samples of the Hart deposit was also compared to the chromite from the fresh and unmineralized olivine cumulates and olivine-spinifex komatiite samples (Fig. 3b). The

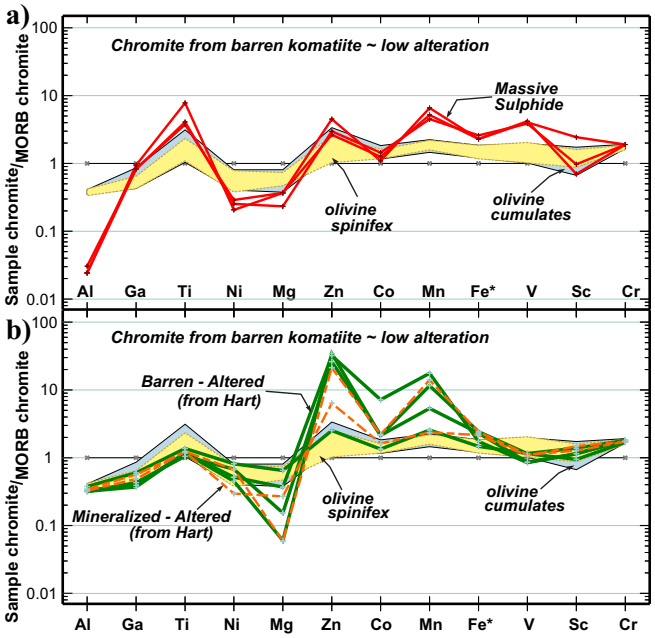

Figure 3. Multi-element profiles of chromite from barren olivine cumulates and olivine-spinifex compared to chromite from **(a)** massive sulphide samples and from **(b)** pervasively altered samples from the Hart deposit. Normalized to the composition of chromite in mid-ocean ridge basalt (MORB) from Pagé and Barnes (2009).

mobility of some element during alteration is strongly supported on this diagram by an increase in Zn, Co, Mn, and a decrease in Mg contents (Fig. 3b). However, the alteration seems to have little effect on elements having higher valencies (≥3+), with the possible exception of Fe^{3+}. Based on these observations, elemental ratios were identified to that would distinguish between the main magmatic processes (e.g. fractional crystallization versus sulphide segregation), and also evaluate alteration effects (Fig. 4). The plot of Ni/Ti ratios versus Ni/Cr ratios illustrates the combined effect of fractional crystallization and possible sulphide segregation on the chromite composition during the evolution of the komatiitic magma (Fig. 4a). These two ratios do not appeared to be greatly influenced by alteration. Other processes are discernible by plotting Ni/Mn versus Ni/Cr ratios (Fig. 4b): (1) alteration processes are suggested by a decrease in the Ni/Mn ratio (very low values because of high Mn content), and (2) the presence of sulphide phases in the paragenesis are indicated by the change in the slope at Ni/Mn < 0.4 (Fig. 4b).

Osmium, Iridium, Ruthenium, and Rhodium in Chromite

Ruthenium has the highest concentrations of the IPGE and Rh, ranging from <10 to 450 ppb (Fig. 5); Os, Ir, and Rh have a more limited range of <1–5 to 75 ppb (not shown). Despite the very high affinities of IPGE and Rh for sulphides compared to chromite ($D^{sulph/melt}$ / $D^{chr/melt} \approx 1000$), the data presented here for Ru cannot be readily interpreted as Locmelis et al. (2013) proposed. These authors concluded that the presence of Ru-rich chromite indicates a barren system and conversely that Ru-poor chromite indicates a mineralized system. From the distribution observed in Figure 5, chromite that crystallized from sulphide liquid is effectively depleted in IPGE and Rh and chromite from barren samples usually contain >150 ppb Ru. However, it

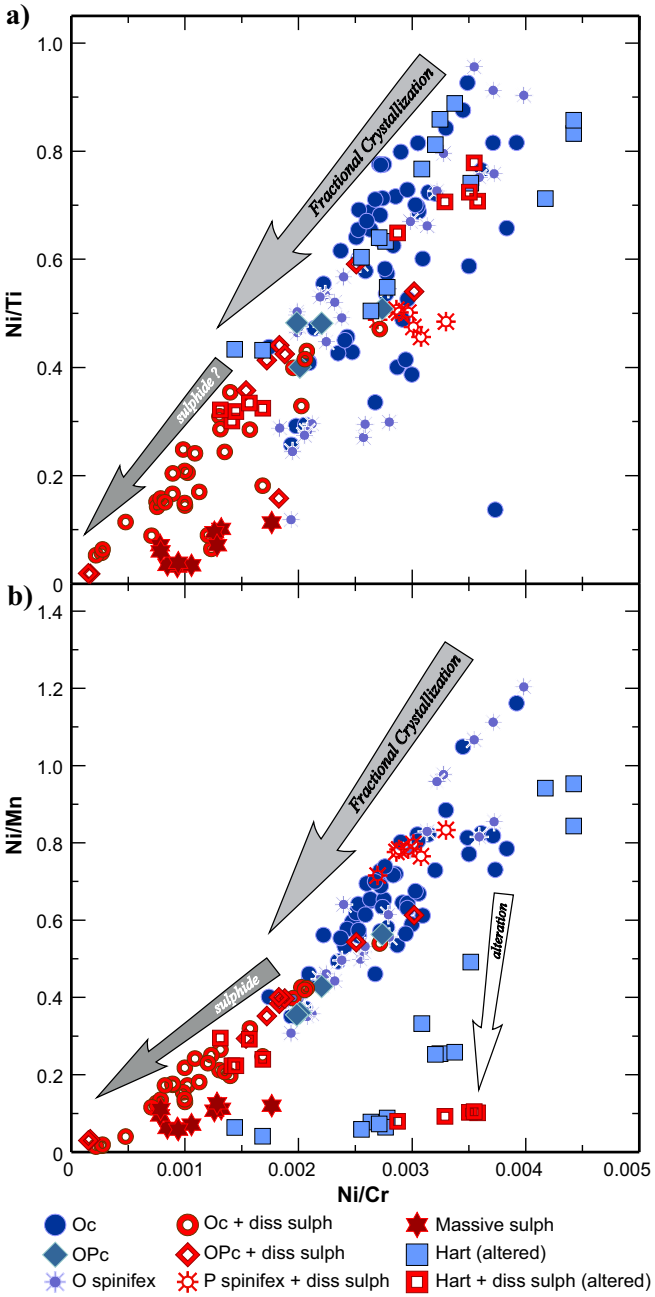

Figure 4. Binary plots of metal ratios **(a)** Ni/Ti versus Ni/Cr and **(b)** Ni/Mn versus Ni/Cr for chromite from komatiite from the Alexo Mine area and the Hart deposit. Abbreviations: Oc = olivine cumulate; OPc = olivine + pyroxene cumulate; O spinifex = olivine spinifex; diss sulph = disseminated sulphide; P spinifex = pyroxene spinifex; sulph = sulphide.

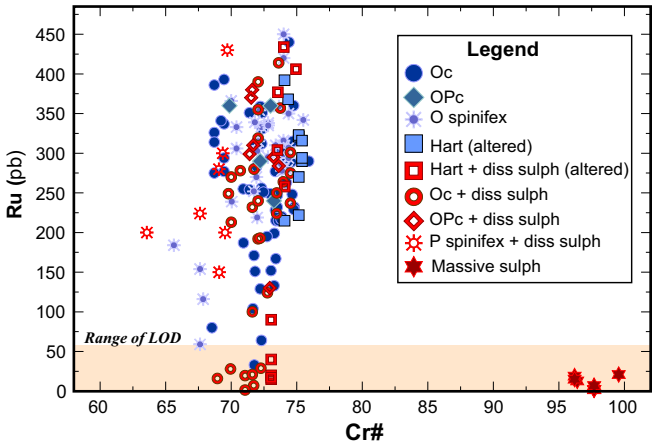

Figure 5. Diagram showing the concentration of Ru in chromite versus its Cr# (100Cr/(Cr+Al)). Chromite is from komatiites from the Alexo Mine area and the Hart deposit. Abbreviations: Oc = olivine cumulate; OPc = olivine + pyroxene cumulate; O spinifex = olivine spinifex; diss sulph = disseminated sulphide; P spinifex = pyroxene spinifex; sulph = sulphide.

is not as clear for sulphide-bearing samples as these cover the entire range of Ru concentrations, with a group of depleted chromite, which is expected when sulphide segregates before chromite crystallization (Fig. 5). These observations strongly suggest that the timing of chromite crystallization versus sulphide segregation is a critical factor to consider during interpretation of the results.

To constrain the effects of sulphides and, if possible alteration, a primitive mantle normalized (PM_N) profile was generated to compare the IPGE and Rh contents of chromite from samples of sulphide-bearing (disseminated to massive) and from the Hart deposit with chromite from samples of fresh and barren olivine cumulate and olivine-spinifex from the Alexo Mine (Fig. 6, see also Table 1). Chromite from the barren Alexo komatiite has PM_N IPGE and Rh profiles enriched in all four elements, a positive Ru anomaly

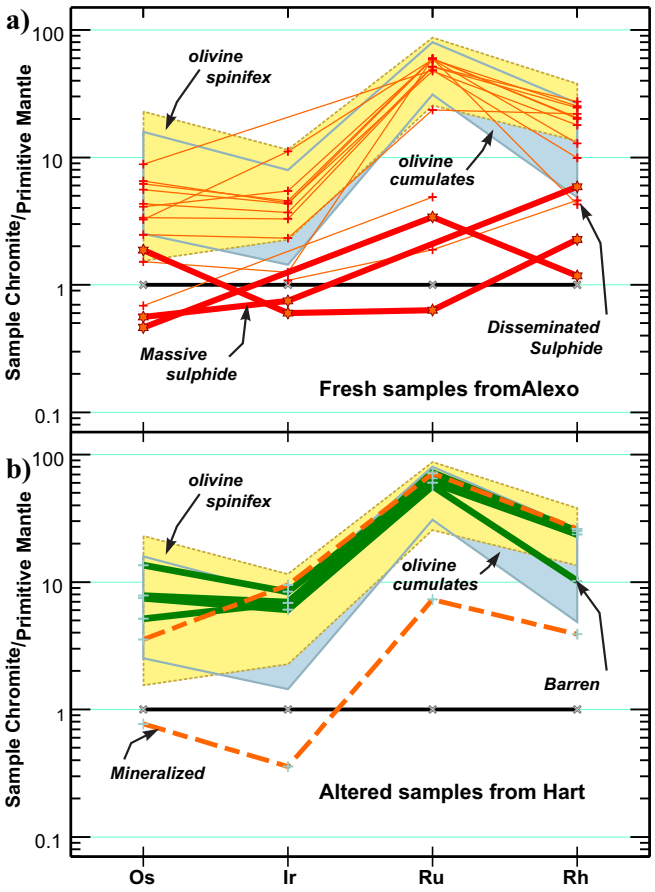

Figure 6. Primitive mantle normalized Ir-group platinum-group elements (Os, Ir, Ru) and Rh profiles for chromite from olivine cumulates and olivine-spinifex compared to chromite from **(a)** the sulphide-bearing samples, and **(b)** the pervasively altered Hart deposit samples. Normalizing values are from McDonough and Sun (1995).

(Ru_N/Ir_N ~14 - 15; Ru_N/Rh_N ~ 3 - 4), and displays no significant differences between chromite from samples of olivine cumulate or spinifex. When compared to chromite from the sulphide-bearing samples, the first thing to note is the depleted PM_N IPGE and Rh profiles

Table 1. Osmium, iridium, ruthenium, and rhodium content of chromite.

	Os (ppb)			**Ir** (ppb)			**Ru** (ppb)			**Rh** (ppb)		
	min	avg	max	min	avg	max	min	avg	max	min	avg	max
Alexo Mine Komatiite												
Barren	5.3	20.8	77.5	4.6	14.3	37	128	277	435	4.4	13.9	23.5
mantle value	1.6x	6.1x	22.8x	1.4x	4.5x	11.6x	25.6x	55.5x	87x	4.9x	15.4x	26.1x
Diss. Sulphides	2.33	12.9	30	bdl	10.8	35.6	9.4	217.1	299.2	bdl	15.4	24.6
mantle value	0.7x	3.8x	8.8x	-	3.4x	11.1x	1.9x	43.4x	59.8x	-	17.1x	27.3x
Mass. Sulphides	bdl	3.3	6.35	bdl	~2	2.4	bdl	10.1	17	bdl	2.8	5.3
mantle value	-	1.0x	1.9x	-	0.6x	0.75x	-	2.0x	3.4x	-	3.1x	5.9x
Hart Deposit Komatiite												
Barren	17.5	28.9	46	19.4	22.6	26.8	284	317.9	362.4	9.2	18.6	22.6
mantle value	5.2x	8.5x	13.5x	6.1x	7.1x	8.4x	56.8x	63.6x	72.5x	10.2x	20.6x	25.1x
Diss. Sulphides	2.6	7.3	12	bdl	~12	30.3	36.4	196.1	355.8	3.5	13.5	23.5
mantle value	0.8x	2.2x	3.5x	-	3.8x	9.5x	7.3x	39.2x	71.2x	3.9x	15.0x	26.1

Abbreviations: avg = average; bdl = below detection level; Diss = disseminated; Mass. = massive; max = maximum; min = minimum
Note: (6.1x) = 6.1 times the mantle value

of the chromite from the massive sulphide samples, essentially less than the detection limits. The Os, Ir, and Rh contents of chromite from most of the samples containing sulphides include the range of chromite from barren samples down to the limits of detection. On the other hand, Ru content does not show the same spread; it tends to cluster around ~55x mantle (~275 ppb), with only few analyses at lower Ru concentrations (Fig. 6a). Chromite from the Hart deposit is also mostly enriched in all four elements and has a positive Ru anomaly (Ru_N/Ir_N ~8.8; Ru_N/Rh_N ~ 3.3), similar to the enriched part of the fields of chromite from barren Alexo samples (Fig. 6b). The fact that chromites are still enriched in IPGE and Rh despite their pervasive alteration suggests an immobile behaviour of IPGE and Rh until upper greenschist grade, and preservation of IPGE and Rh signatures. One sample from Hart contains IPGE+Rh-poor chromite that probably crystallized from an already sulphide-saturated magma (Fig. 6b).

The LA-ICP-MS results in this study strongly support the presence of IPGE and Rh in solid-solution within chromite, even though its total contribution to the whole-rock IPGE and Rh budgets is unknown. Mass balance calculations have been conducted to investigate the overall contribution of chromite to the whole-rock IPGE and Rh contents using the following formula:

$$F_{Chr}^{PGE} = 100x(C_{Chr}^{PGE}x(C_{WR}^{Cr}/C_{Chr}^{Cr}))/C_{WR}^{PGE} \quad (1)$$

Where:

F_{Chr}^{PGE} = whole-rock fraction of IPGE and Rh accounted by chromite
C_{Chr}^{PGE} = IPGE and Rh concentration in chromite
C_{WR}^{Cr} = Cr_2O_3 concentration in whole rock
C_{Chr}^{Cr}) = Cr_2O_3 concentration in chromite
C_{WR}^{PGE} = IPGE and Rh concentration in whole rock

The results show that chromite does have a real effect on the fractionation and concentration of IPGE and Rh, and that although its contribution to the whole-rock budgets is relatively minor for Os, Ir, and Rh, it is significant for Ru (up to 90% of whole-rock budget, Fig. 7). Indeed, chromite from the barren samples on average account for ≤10% of the whole-rock Os, Ir, and Rh budgets, and for 45% of the whole-rock Ru budget, with the exception of 1/5 of the samples in which chromite accounts for >75% of the whole-rock Ru budget (Fig. 7). For the sulphide-bearing samples, chromite contributes even less to the whole-rock IPGE and Rh budgets; it accounts, on average, for ≤5% of the whole-rock Os, Ir, and Rh budgets, and for ~15% of the whole-rock Ru budget, not reaching a contribution of higher than 37%.

DISCUSSION

Our results show that chromite from the Alexo Mine and the Hart deposit have typical komatiitic composition, with limited variations in Cr# but a larger spread of Fe^{2+}#. Some of the variations observed in the Fe^{2+}# appeared to be related to alteration of the samples. However, it is difficult to adequately discriminate chromite composition based solely on the major elements, with the exception of chromite from massive sulphides, which are easily recognizable as being depleted in Al, resulting in very high Cr# values. Systematic differences in minor element compositions observed in chromite from massive sulphide and highly altered samples, compared to chromite from fresh and barren komatiite samples, allowed us to propose elemental ratios that underline the effects of fractional crystallization and sulphide segregation, but that also underpin alteration. These two diagrams (Ni/Ti versus Ni/Cr and Ni/Mn versus Ni/Cr) are new geochemical tools that can be used to determine the evolution of the komatiitic magma or its degree of alteration. Contrary to our working hypothesis, samples containing IPGE+Rh-rich chromite are not necessary indicative of the absence of trace or disseminated sulphides, as most of these sulphide-bearing samples contained chromite with high concentrations of Ru. However, sulphide-rich samples (i.e. samples of massive sulphide) were found to contain chromite that is highly depleted in IPGE and Rh. These observations highlight the importance of the

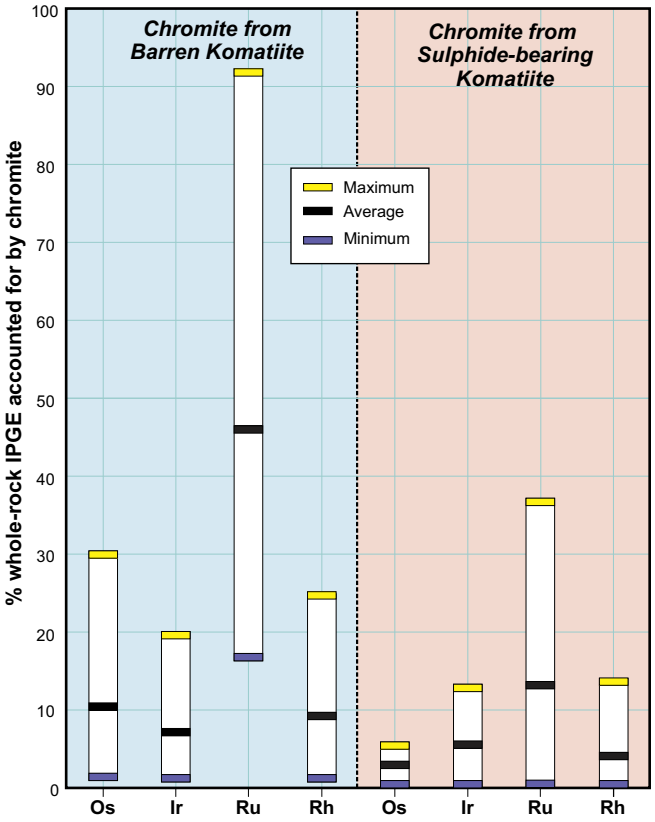

Figure 7. Mass balance calculations showing the contribution of chromite to the whole-rock Ir-group platinum-group elements (Os, Ir, Ru) and Rh budgets for **(a)** barren komatiite and **(b)** sulphide-bearing samples.

timing between chromite and sulphide saturation as a critical factor controlling the IPGE and Rh content of the chromite. In this study, many samples appeared to reach chromite saturation before reaching sulphide saturation. This is supported by the PM_N IPGE and Rh profiles of the chromite from samples containing disseminated sulphides which shows similarities in abundances and shapes with chromite from the fresh and barren komatiite samples. However, a few samples contain chromite that is partly to strongly affected by sulphide segregation, and the PM_N IPGE and Rh profiles for chromite from these samples are similarly depleted in IPGE and Rh as the chromite found in massive sulphide samples. Our results also show that alteration has limited effect on the chromite IPGE and Rh content. Furthermore, mass balance calculations support the knowledge that chromite partitions and concentrates IPGE and Rh, but chromite's total contribution to the whole-rock content is insufficient to account for the overall IPGE and Rh budget, which suggests that even when sulphides are not present, other IPGE+Rh-rich phases are needed to explain the entire IPGE and Rh abundances of whole-rock analysis.

IMPLICATIONS FOR EXPLORATION

It has been proposed by Locmelis et al. (2011, 2013) that the depleted Ru content in chromite is indicative of chromite that crystallized in equilibrium with a sulphide liquid, and that Ru-depleted chromite can be used as an effective exploration tool to vector toward mineralized komatiitic sequences. Despite the fact that in our study, chromite from massive sulphide samples (which were extremely depleted in Ru) strongly support this interpretation, our results from less mineralized samples show the coexistence of chromite with both depleted and enriched Ru content suggesting a more complex evolution of the komatiitic systems. These results are best explained by a mixing of chromite that crystallized from a sulphide-undersaturated magma (Ru-enriched chromite) and a sulphide-saturated magma (Ru-depleted chromite) supporting the flow-through komatiitic system at Alexo as proposed by Houlé et al. (2012). Indeed, the use of metal ratios (Ni/Mn versus Ni/Cr) has allowed us to discriminate barren from mineralized samples, but also to illustrate alteration effects. So far, in terms of chromite composition, it seems that the combination of Ru versus Cr# and Ni/Mn versus Ni/Cr diagrams constitutes good exploration tools for identifying chromite derived from mineralized versus barren lithologies within komatiitic successions. However, further investigations are needed to fully characterize and understand the behaviour of IPGE and Rh in order to use them as a more efficient tool for targeting the most prospective units in komatiitic systems.

ACKNOWLEDGEMENTS

The project has been funded by the Geological Survey of Canada under the Targeted Geoscience Initiative 4 (TGI-4) and the Canada Research Chair in Magmatic Ore Deposits (UQAC). We also thank Céline Dupuis (GSC) for careful review that helped us improve this contribution.

REFERENCES

Arguin, J.-P., Pagé, P., Barnes, S.-J., Yu, S.-Y., and Song, X.-Y., 2014. Osmium, Ir, Ru and Rh whole-rock concentrations controlled by crystallizing chromites from sulphide-poor picritic magma from the Emeishan Large Igneous Province, southwestern China; Geological Association of Canada – Mineralogical Association of Canada (GAC-MAC) Meeting, May 21–23rd, Fredericton, New Brunswick.

Arndt, N.T., 1986. Differentiation of komatiite flows; Journal of Petrology, v. 27, p. 279–301.

Barnes, S.-J., 1983. The origin of the fractionation of platinum group elements in Archean komatiites of the Abitibi greenstone belt, northern Ontario, Canada; Ph.D. thesis, University of Toronto, Toronto, Ontario, 231 p.

Barnes, S.J. and Roeder, P.L., 2001. The range of spinel compositions in terrestrial mafic and ultramafic rocks; Journal of Petrology, v. 42(12), p. 2279–2302.

Barnes, S.-J., Gorton, M.P., and Naldrett, A.J., 1983. A comparative study of olivine and clinopyroxene spinifex flows from Alexo, Abitibi greenstone belt, Ontario, Canada; Contributions to Mineralogy and Petrology, v. 83, p. 293–308.

Brenan, J.M., Finnigan, C.S., McDonough, W.F. and Homolova, V., 2012. Experimental constraints on the partitioning of Ru, Rh, Ir, Pt and Pd between chromite and silicate melt: the importance of ferric iron; Chemical Geology, v. 302-303, p. 16-32.

Houlé, M.G., 2008. Physical volcanology and metallogenesis of komatiitic rocks in the Abitibi greenstone belt, Superior Province, Ontario, Canada; Ph.D. thesis, University of Ottawa, Ottawa, Ontario, 211 p.

Houlé, M.G., Lesher, C.M., and Davis, P.C., 2012. Thermomechanical erosion at the Alexo Mine, Abitibi greenstone belt: implications for the genesis of komatiite-associated Ni-Cu-(PGE) mineralization; Mineralium Deposita, v. 47, p. 105–128.

Locmelis, M., Pearson, N.J., Barnes, S.J., and Fiorentini, M.L., 2011. Ruthenium in komatiitic chromite; Geochimica et Cosmochimica Acta, v. 75, p. 3645–3661.

Locmelis, M., Fiorentini, M.L., Barnes, S.J., and Pearson, N.J., 2013. Ruthenium variation in chromite from komatiites and komatiitic basalts - A potential mineralogical indicator for nickel sulfide mineralization; Economic Geology, v. 108, p. 355–364.

McDonough, W.F. and Sun, S., 1995. The composition of the Earth; Chemical Geology, v. 120, p. 223–253.

Méric, J., Pagé, P., Barnes, S.-J., and Houlé, M.G., 2012. Geochemistry of chromite from the Alexo komatiite, Dundonald Township: preliminary results from electron microprobe and laser ablation inductively coupled plasma mass spectrometric analyses, *In:* Summary of Field Work and Other Activities 2012; Ontario Geological Survey, Open File Report 6280, p. 46-1 – 46-12.

Pagé, P. and Barnes, S.-J., 2009. Using trace elements in chromites to constrain the origin of podiform chromitites in the Thetford Mines ophiolite, Québec, Canada; Economic Geology, v. 104, p. 997–1018.

Pagé, P., Barnes, S.-J., Bedard, J.H., and Zientek, M.L., 2012. In situ determination of Os, Ir and Ru in chromites formed from komatiite, tholeiite and boninite magmas: implications for chromite control of Os, Ir and Ru during partial melting and crystal fractionation; Chemical Geology, v. 302-303, p. 3–15.

Park, J.-W., Campbell, I.H., and Eggins, S.M., 2012. Enrichment of Rh, Ru, Ir and Os in Cr spinels from oxidized magmas: Evidence from the Ambae volcano, Vanuatu; Geochimica et Cosmochimica Acta, v. 78, p. 28–50.

Righter, K., Campbell, A.J., Humayun, M., and Hervig, R.L., 2004. Partitioning of Ru, Rh, Pd, Re, Ir, and Au between Cr-bearing spinel, olivine, pyroxene and silicate melts; Geochimica et Cosmochimica Acta, v. 68, p. 867–880.

GEOLOGICAL SURVEY OF CANADA
OPEN FILE 7856

Targeted Geoscience Initiative 4: Canadian Nickel-Copper-Platinum Group Elements-Chromium Ore Systems — Fertility, Pathfinders, New and Revised Models

Identifying and tracing crustal contamination in the Hart komatiite-associated Ni-Cu-(PGE) deposit using multiple S and Fe isotopes: Abitibi greenstone belt, Ontario

Russel S. Hiebert[1], Andrey Bekker[2,1], Michel G. Houlé[3], Olivier J. Rouxel[4], and Boswell A. Wing[5]

[1]University of Manitoba, Winnipeg, Manitoba, Canada
[2]University of California, Riverside, California, U.S.A.
[3]Geological Survey of Canada, Québec, Quebec, Canada
[4]Unité Géosciences Marines, Plouzané, France
[5]McGill University, Montréal, Quebec, Canada

2015

© Her Majesty the Queen in Right of Canada, as represented by the Minister of Natural Resources Canada, 2015

This publication is available for free download through GEOSCAN (http://geoscan.nrcan.gc.ca/)

Recommended citation

Hiebert, R.S., Bekker, A., Houlé, M.G., Rouxel, O.J., and Wing, B.A., 2015. Identifying and tracing crustal contamination in the Hart komatiite-associated Ni-Cu-(PGE) deposit using multiple S and Fe isotopes: Abitibi greenstone belt, Ontario, *In:* Targeted Geoscience Initiative 4: Canadian Nickel-Copper-Platinum Group Elements-Chromium Ore Systems — Fertility, Pathfinders, New and Revised Models, (ed.) D.E. Ames and M.G. Houlé; Geological Survey of Canada, Open File 7856, p. 197–207.

Publications in this series have not been edited; they are released as submitted by the author.

Contribution to the Geological Survey of Canada's Targeted Geoscience Initiative 4 (TGI-4) Program (2010–2015)

TABLE OF CONTENTS

Identifying and tracing crustal contamination in the Hart komatiite-associated Ni-Cu-(PGE) deposit using multiple S and Fe isotopes: Abitibi greenstone belt, Ontario

Russel S. Hiebert[1*], Andrey Bekker[2,1], Michel G. Houlé[3], Olivier J. Rouxel[4], and Boswell A. Wing[5]

[1]Department of Geological Sciences, University of Manitoba, 125 Dysart Road, Winnipeg, Manitoba R3T 2N2, Canada
[2]Department of Earth Sciences, University of California, 900 University Avenue, Riverside, California 92521, U.S.A.
[3]Geological Survey of Canada, 490 rue de la Couronne, Québec, Quebec G1K 9A9, Canada
[4]IFREMER, Centre de Brest, Unité Géosciences Marines, 29280, Plouzané, France
[5]Department of Earth and Planetary Sciences, McGill University, 3450 University Street, Montréal, Quebec H3A 0E8, Canada
*Corresponding author's e-mail: umhieb11@cc.umanitoba.ca

ABSTRACT

Assimilation by mafic/ultramafic magmas of sulphur-bearing country rocks, typically of sedimentary origin, is commonly considered a critical factor for the genesis of magmatic sulphide deposits. Mass-independent fractionation of sulphur isotopes in the Archean atmosphere produced isotopically distinct pools of S that are recorded in Archean sediments, and can be differentiated easily from mantle sulphur. Likewise, low-temperature processing of iron, potentially including biological and abiotic redox cycling, is also expected to produce Fe isotope values in sediments distinct from the mantle.

The Hart deposit is composed of two mineralized zones; the main zone, a type-I komatiite-associated Ni-Cu-(PGE) sulphide deposit at the base of the basal flow, and the eastern extension, a zone of semi-massive sulphides 12 to 25 m above the base of the second flow within the komatiite sequence. Isotopic characterization, using multiple S and Fe isotopes, of exhalite and graphitic argillite present in the footwall of the mineralization allows tracing the extent of contamination and the degree of mixing within, and adjacent to, the deposit with these potential S sources. This method identifies the exhalite and graphitic argillite as the dominant contaminants for the main zone and the eastern extension mineralization of the Hart deposit, respectively. Additionally, the contamination signature is greatest within the deposit and decreases away from it in the komatiite flow and could potentially be used as a vector towards mineralization. This pattern points also to a local source for crustal contamination of the mantle-derived komatiitic melt and a low degree of homogenization between the mineralization and the surrounding lava flow.

INTRODUCTION

Exploration models for magmatic Ni-Cu-(PGE) sulphide deposits are relatively well established, and most deposits are thought to have been formed by segregation of a sulphide xenomelt at the base of the magma chamber or lava flow as a result of melting of sulphur-bearing country rocks by mafic or ultramafic magmas (Lesher and Campbell, 1993; Lesher and Burnham, 2001). Recently, multiple sulphur isotopes have been used to link nickel sulphide mineralization to sedimentary sulphur sources in Archean komatiite-associated deposits because the link is not always unequivocal based on $\delta^{34}S$ values alone, due to near mantle values in many of these deposits and in adjacent sedimentary rocks (e.g. Bekker et al., 2009; Fiorentini et al., 2012).

This study intends to expand on these previous efforts by examining the link between magmatic nickel sulphide mineralization and sedimentary sulphur source rocks at the Hart deposit, and also investigating the lateral and vertical variations of the stable isotope signatures within the komatiite flows at and away from the mineralized ore zones. Stable isotopes, including $\delta^{34}S$, $\Delta^{33}S$, and $\delta^{56}Fe$ data, are used to identify the most likely sulphur sources for the genesis of the Hart komatiite-associated Ni-Cu-(PGE) deposit within the Shaw Dome area in the western Abitibi greenstone belt (AGB) in Ontario (Fig. 1).

Background

Under present terrestrial conditions, sulphur isotope fractionation is controlled strictly by relative isotope mass differences and, therefore, is a mass-dependent process. However, as a result of photochemical reactions in the anoxic Archean atmosphere, atmospherically processed Archean sulphur exhibits mass-inde-

Hiebert, R.S., Bekker, A., Houlé, M.G., Rouxel, O.J., and Wing, B.A., 2015. Identifying and tracing crustal contamination in the Hart komatiite-associated Ni-Cu-(PGE) deposit using multiple S and Fe isotopes: Abitibi greenstone belt, Ontario, *In:* Targeted Geoscience Initiative 4: Canadian Nickel-Copper-Platinum Group Elements-Chromium Ore Systems — Fertility, Pathfinders, New and Revised Models, (ed.) D.E. Ames and M.G. Houlé; Geological Survey of Canada, Open File 7856, p. 197–207.

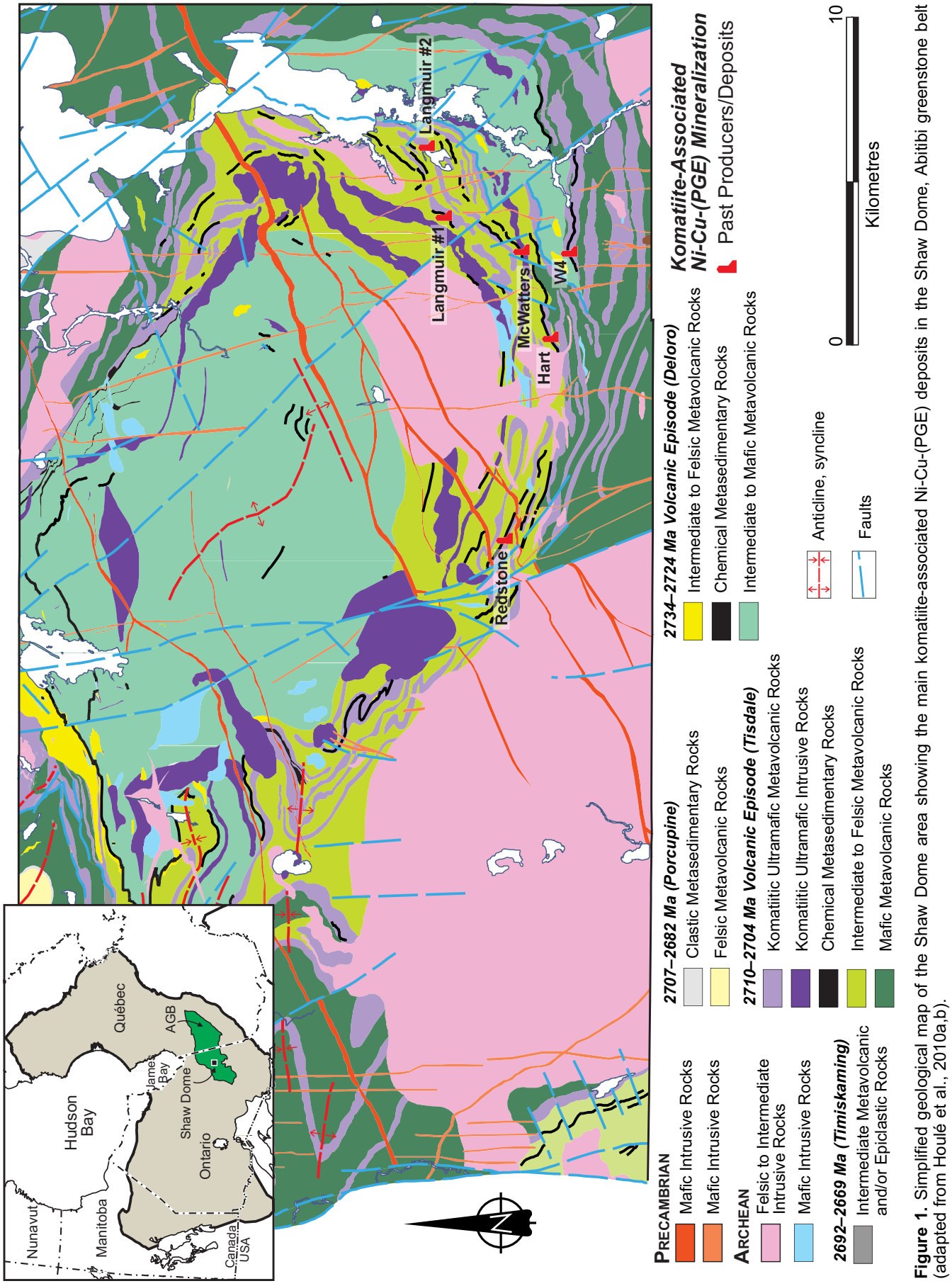

Figure 1. Simplified geological map of the Shaw Dome area showing the main komatiite-associated Ni-Cu-(PGE) deposits in the Shaw Dome, Abitibi greenstone belt (adapted from Houlé et al., 2010a,b).

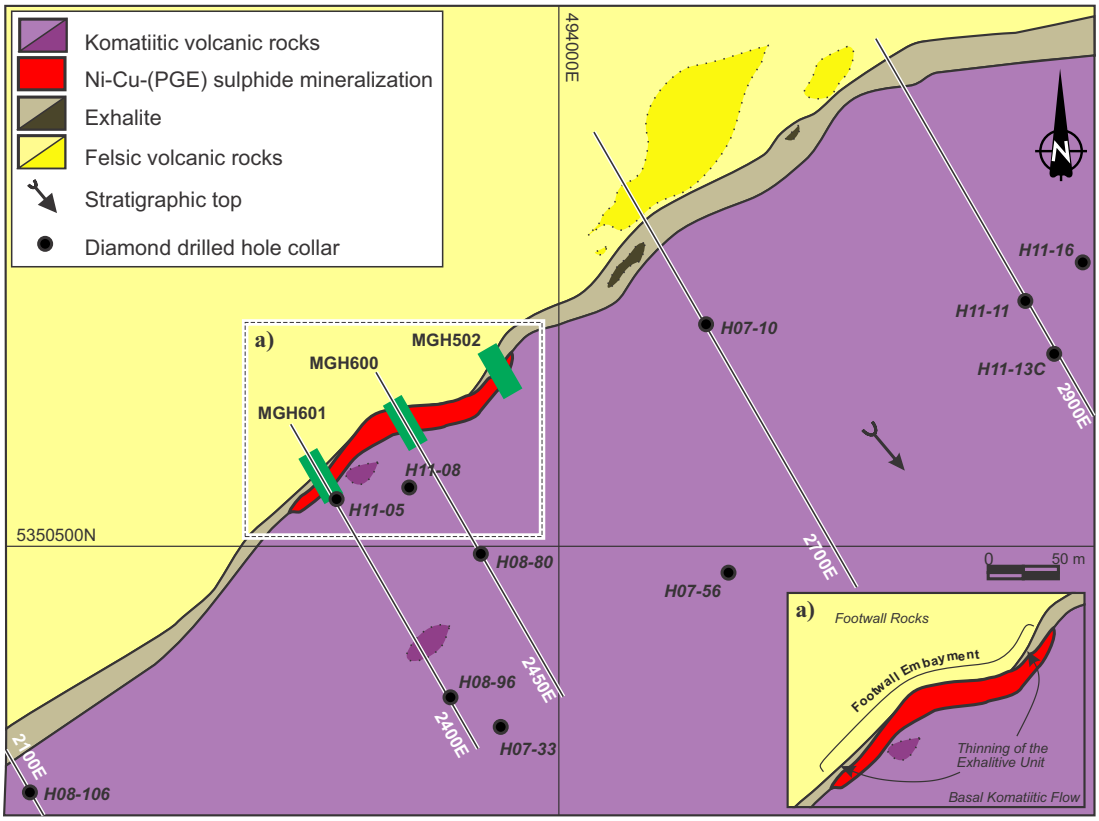

Figure 2. Geological map of the Hart deposit area (modified from Houlé et al., 2010b and Brereton, 2004). Drillhole collar locations and section lines for composite isotope data traverses through the deposit are indicated. Locations of sampled surface trenches are indicated by the green bars. The UTM grid is in NAD 83, Zone 17.

pendent fractionation that can be characterized by the difference between the $\delta^{33}S$ value expected from normal mass-dependent fractionation and the measured $\delta^{33}S$ value (Farquhar et al., 2000; Farquhar and Wing, 2003; Bekker et al., 2009). It can be calculated from the measured values as

$$\Delta^{33}S = \delta^{33}S - 0.515*\delta^{34}S$$

Where δ values are defined as

$$\delta^{XX}Z = \frac{\left({}^{XX}Z \Big/ {}^{YY}Z_{sample} - {}^{XX}Z \Big/ {}^{YY}Z_{standard} \right)}{{}^{XX}Z \Big/ {}^{YY}Z_{standard}}$$

Where XX and YY are the minor and major isotope masses of element Z (e.g. masses 56 and 54 of Fe), and is presented in per mil (‰).

The photochemically fractionated sulphur was delivered to Archean seawater and ultimately preserved in sediments. Additionally, for several Archean lithologies, such as ferruginous sediments and organic matter-rich shales, the $\delta^{56}Fe$ values have been shown to exhibit significant variability (e.g. Rouxel et al., 2005), which can be used to complement multiple S isotope data to constrain the extent of country rock assimilation and the mechanisms that led to the formation of the mineralization.

Once the signature of contamination by the sedimentary source is known, tracing the contamination in the komatiite can provide insights into the flow regime and cooling history of the komatiite (Lesher and Arndt, 1995). Utilization of both S and Fe isotopes provides two tracers of contamination that are sensitive to different degrees of contamination.

Local Geology

The volcano-sedimentary succession in the Shaw Dome comprises massive to pillowed intermediate volcanic rocks with thin, but laterally extensive, banded iron formations of the 2734–2724 Ma Deloro Volcanic Episode overlain by felsic to intermediate volcaniclastic rocks and massive to pillowed mafic volcanic rocks of the 2710–2704 Ma Tisdale Volcanic Episode (Fig. 1). Komatiitic dykes, sills, and lavas with lesser and more discontinuous banded iron formations are interspersed within the lower part of the episode, whereas only komatiitic flows are interspersed within the upper part of the episode (Houlé et al., 2010a).

The main mineralized zone of the Hart deposit is hosted in the basal flow of several stacked komatiite flows that overly the felsic to intermediate volcanic and sedimentary rocks (Figs. 2, 3). The eastern extension of the Hart deposit is hosted within the second komatiite flow of this succession. The main mineralized zone is typical stratiform basal mineralization (Type I) hosted by thick olivine ortho- to mesocumulate komatiite units in which the sulphides are localized at the base of a

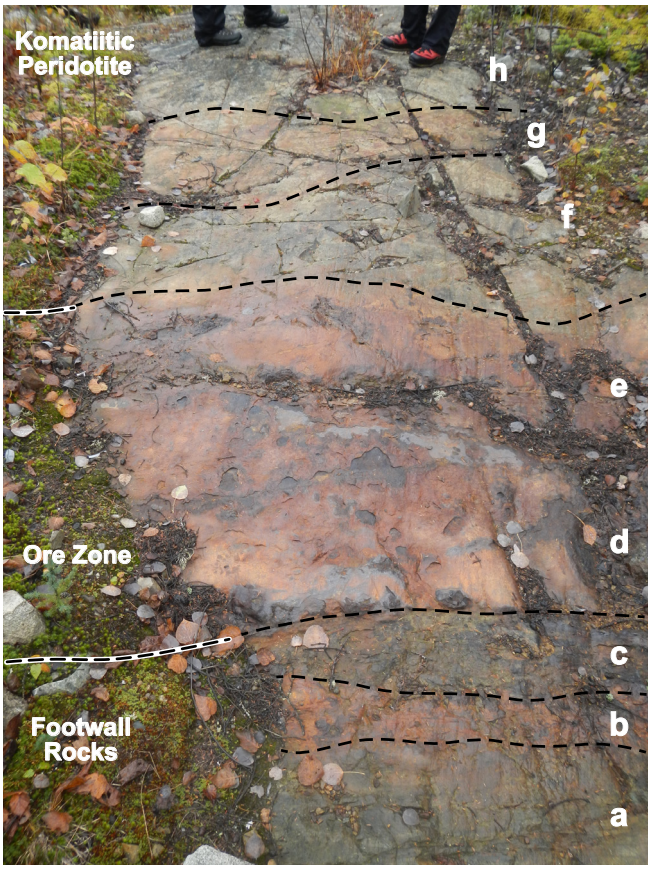

Figure 3. Field photograph of trench MGH600 showing the Hart mineralized zone, from stratigraphic base to top, **(a)** felsic volcanic rocks, **(b)** exhalite, **(c)** felsic volcanic rocks, **(d)** massive sulphide, **(e)** net-textured sulphide in komatiitic peridotite, **(f)** barren komatiitic peridotite, **(g)** disseminated sulphides in komatiitic peridotite, and back **(h)** into barren komatiitic peridotite.

wide (>200 m) footwall embayment, interpreted to have been produced by thermo-mechanical erosion of the underlying substrate by the komatiite lava flows (Houlé et al., 2010b). The exhalative unit becomes thinner at the edge and disappears completely within the thickest part of the embayment (Fig. 2, inset a). In addition, the eastern extension consists of a zone of semi-massive, net-textured, and disseminated sulphide located 12 to 25 m above the base of the second flow (Hiebert et al., 2013a). No significant mineralization is known to occur higher into the succession.

The footwall rocks are composed of felsic to intermediate volcanic and volcaniclastic rocks with lesser banded iron formation with variable content of oxide-rich layers, chert-rich unit, and massive sulphides, and minor graphitic argillite. In the vicinity of the Hart deposit, some of the iron formation has been reclassified under the broader term exhalite due to the predominance of chert and chert-rich lithologies (Hiebert et al., 2013a). The graphitic argillite is composed predominantly of graphite with pyrite nodules and bands up to 1 cm in diameter and was observed only in drill core in the eastern part of the property.

METHODOLOGY

Ninety-three samples were selected for this project from diamond drill cores and mechanically stripped trenches made available by Northern Sun Mining Corporation. Several transects were selected within and away from the main mineralized zone at the Hart deposit, and sampling was performed to include all footwall lithologies (felsic volcanic rocks, exhalite, and graphitic argillite), the mineralization (massive, semi-massive, net-textured, and disseminated sulphides), and the hosting komatiite flow for each deposit immediately above the mineralization and upward into barren komatiitic flows. Additionally, one sample of the third flow was taken to represent true barren komatiite that likely never produced significant sulphide mineralization. Crushed whole-rock samples were then analysed for S and Fe isotope analysis using the method described by Hiebert et al. (2013b).

RESULTS

Isotope data for lithologies present in the footwall to the komatiite and those associated with komatiitic flows (Table 1) have been treated separately; the latter have been further subdivided, based on the visual estimate of the abundance of sulphide, into barren komatiite (<5% sulphide minerals by volume), disseminated or blebby (5–30%), net-textured and semi-massive (30–70%), and massive sulphides (>70%).

Footwall Lithologies

The exhalite shows the largest S isotope variability of any lithology in the area, whereas the graphitic argillite shows the least variability (Table 1, Fig. 4a). Exhalite and graphitic argillite have overlapping ranges of $\delta^{34}S$, $\Delta^{33}S$, and $\delta^{56}Fe$ (Table 1, Fig. 4a,b). Felsic volcanic rocks have overlapping ranges of $\delta^{34}S$ and $\Delta^{33}S$ with the iron formation and the argillite but distinct values of $\delta^{56}Fe$ (Fig. 4a,b).

Mineralized and Barren Komatiite

S isotope ($\delta^{34}S$ and $\Delta^{33}S$) variability in komatiite samples can be related to the abundance of sulphide mineralization present in each sample (Table 1, Fig. 4c). In general, massive sulphides have the most negative $\delta^{34}S$ and $\Delta^{33}S$ values and disseminated mineralization the least negative. Barren komatiite has generally higher values (Fig. 4c). In barren komatiite, there is a narrow range of $\delta^{56}Fe$ values near 0.0‰, consistent with a mantle-derived magma (0.09 ±0.1‰; Beard et al., 2003). However, mineralized komatiite has $\delta^{56}Fe$ values significantly different from mantle values (-1.5 to +0.2‰), showing a continuum that spans the range

Table 1. Range of isotopic signatures of footwall rocks and komatiite flows at the Hart deposit.

	$\delta^{33}S_{V\text{-}CDT}$	$\delta^{34}S_{V\text{-}CDT}$	$\Delta^{33}S$	$\delta^{56/54}Fe_{IRMM\text{-}14}$
Footwall Rocks				
Felsic volcanic rocks	**-3.4 to +0.7**	**-5.7 to 1.9**	**-0.5 to -0.2**	**-0.9 to -0.1**
with sulphides	-3.4 to -0.9	-5.7 to -0.7	-0.5	-0.9 to -0.7
without sulphides	-0.3 to +0.7	+0.2 to +1.9	-0.5 to -0.2	-0.5 to -0.1
Exhalite	**-6.3 to +3.2**	**-11.4 to +7.6**	**-1.4 to -0.3**	**-2.1 to -0.9**
Silicate facies iron formation	+0.6	+2.6	-0.8	-1.7
Oxide facies iron formation	-5.2 to +3.2	-9.0 to +7.6	-0.7 to -0.3	-2.1 to -1.2
Chert (with minor Fe-oxide laminae)	-6.2 to +0.6	-11.0 to +2.4	-0.8 to -0.4	-1.9 to -0.9
Massive sulphides	-6.3 to +0.1	-11.4 to +3.0	-1.4 to -0.5	-2.0 to -1.6
Graphitic argillite	**+0.6 to +2.3**	**+1.6 to +5.0**	**-0.9 to -0.2**	**-2.0 to -1.7**
Komatiite Flows				
Barren komatiitic peridotite				
No sulphides	**-3.5 to +2.1**	**-5.8 to +3.3**	**-0.7 to +0.6**	**-0.6 to +0.1**
Mineralized komatiitic peridotite	**-2.6 to +0.2**	**-3.8 to +1.7**	**-0.7 to -0.4**	**-1.5 to +0.2**
Traces of sulphides	-2.6 to -0.1	-3.8 to +1.0	-0.7 to -0.4	-1.1 to +0.1
Disseminated and blebby sulphides	-2.1 to -0.1	-2.9 to +1.2	-0.7 to -0.6	-1.0 to +0.1
Net-textured and semi-massive sulphides	-2.5 to +0.2	-3.7 to +1.7	-0.7 to -0.6	-1.4 to +0.1
Massive sulphides	-2.4 to -0.5	-3.4 to +0.3	-0.7 to -0.6	-1.5 to +0.2

Abbreviations: V-CDT = Vienna Cañon Diablo troilite; IRMM-14 = Institute for Reference Materials and Measurements – Fe metal

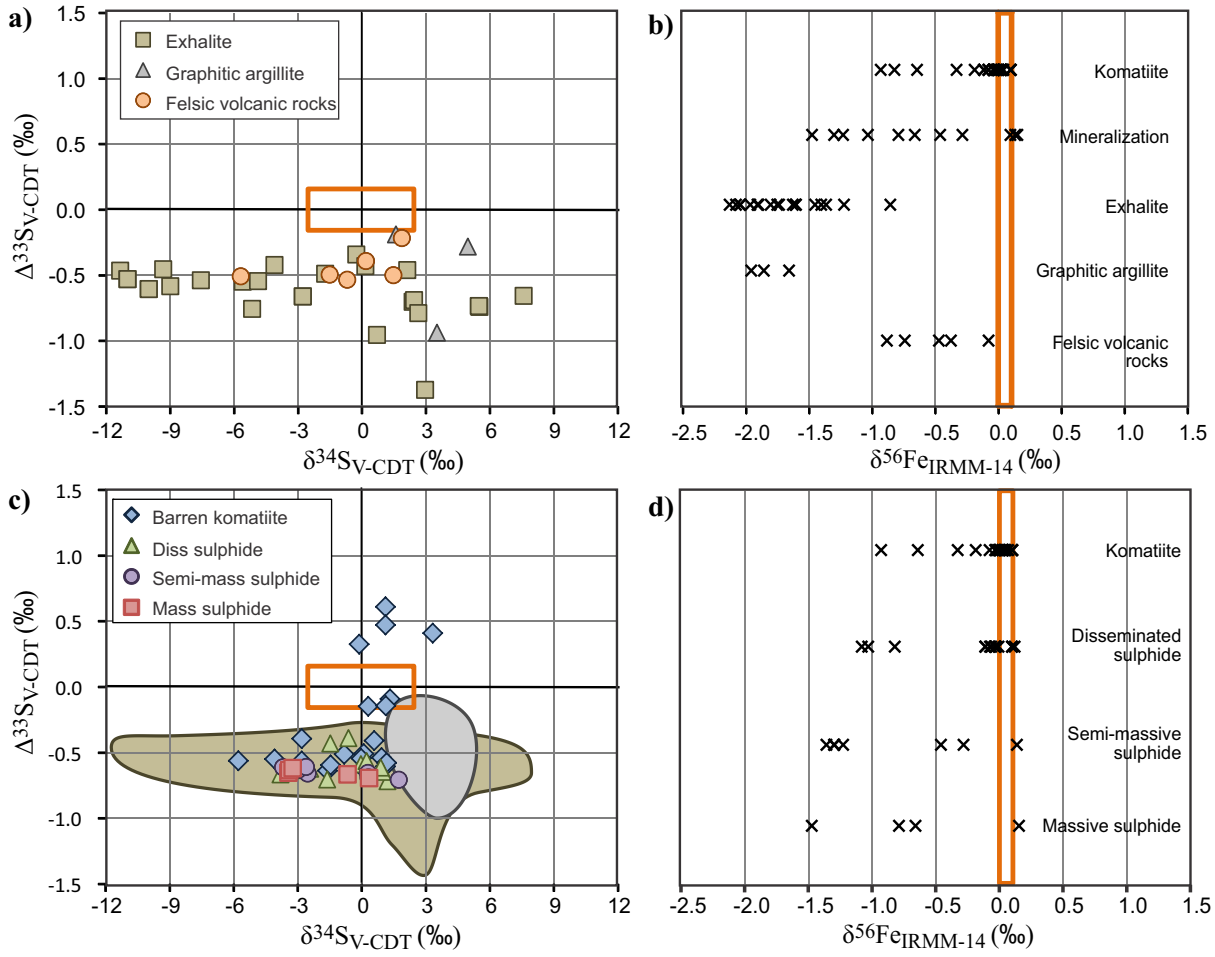

Figure 4. Plots of $\Delta^{33}S$, $\delta^{34}S$, and $\delta^{56}Fe$ for the Hart deposit. **a)** Plot of $\Delta^{33}S$ versus $\delta^{34}S$ values showing the variations in S isotope composition of potential sulphur source rocks. **b)** Plot of $\delta^{56}Fe$ variations for the lithologies present. **c)** Plot of $\Delta^{33}S$ versus $\delta^{34}S$ values showing variations of barren and mineralized komatiite units. Exhalite and graphitic argillite data are represented by the brown field and the grey field, respectively. **d)** Plot of $\delta^{56}Fe$ variations for barren and mineralized komatiite units. Orange boxes represent the mantle range (Bekker et al., 2009).

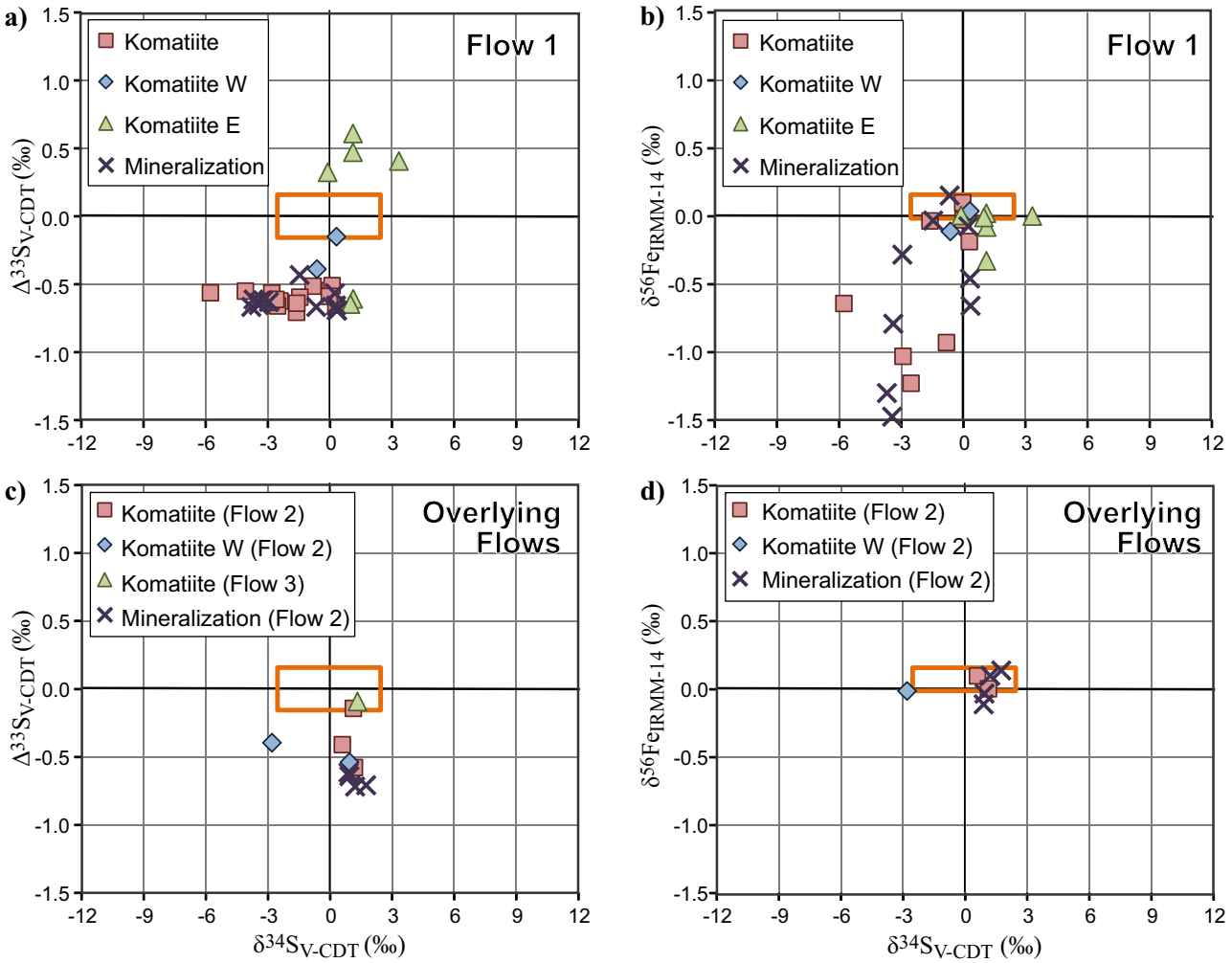

Figure 5. Plots of $\Delta^{33}S$ versus $\delta^{34}S$ **(a, c)** and $\delta^{56}Fe$ versus $\delta^{34}S$ **(b, d)** showing the isotope signatures at different location within komatiitic flows (above, east, and west of mineralization) at the Hart deposit. Flow 1 (a, b): mineralization and komatiite data from sections 2400E and 2450E; Komatiite E: from sections 2700E and 2900E; and Komatiite W: from section 2100E. Overlying flows (c, d): mineralization and komatiite data from section 2900E, Komatiite W from sections 2450E and 2700E. Orange boxes represent mantle range (as in Fig. 4).

between those of barren komatiite and exhalite or graphitic argillite from the footwall. Similar to S isotopes, the most negative $\delta^{56}Fe$ values are generally found in heavily mineralized samples (massive and semi-massive sulphides), and the least negative $\delta^{56}Fe$ values are in disseminated sulphides (Fig. 4d).

The basal flow, host of the main mineralized zone, shows isotopic values ($\delta^{34}S$, $\Delta^{33}S$, and $\delta^{56}Fe$) that are most negative within and near the mineralized zone but increase towards mantle values away from it, both laterally to the west, and also towards the top of the flow. To the east of the deposit, $\delta^{34}S$ values are slightly positive and $\Delta^{33}S$ values exhibit a bimodal distribution, with some samples showing similar values to the main zone (approximately -0.5 to -0.6‰), and others showing positive $\Delta^{33}S$ values (Fig. 5a,b).

In the second flow, mineralization at the eastern extension exhibits positive $\delta^{34}S$ and negative $\Delta^{33}S$ values. These values trend to mantle values laterally, to the west, and vertically, both above and below the mineralization (Fig. 5c). In the third flow, $\delta^{34}S$ and $\Delta^{33}S$ values are within the mantle range. Little variability exists in $\delta^{56}Fe$ values for samples from the second flow, all values lying within or near the mantle range (Fig. 5d).

DISCUSSION

Identifying the Source of Contamination

Many authors have discussed the need for the incorporation of external sulphur by komatiitic melts for the genesis of komatiite-associated Fe-Ni-Cu sulphide deposits and the application of isotope data to identify this contaminant (e.g. Lesher and Burnham, 2001; Bekker et al., 2009 and references therein). The potential contaminant that could have acted as the dominant source of sulphur for the Hart deposit has previously been interpreted to be the exhalite unit (Houlé et al., 2010b). However, the recent discovery of significant

concentrations of sulphide in the graphitic argillite unit provides another viable sulphur source for the genesis of this deposit.

Distinguishing between Footwall Lithologies

Two isotopically distinct S pools were formed by the photochemical reactions in the Archean atmosphere: 1) a reduced pool with positive $\Delta^{33}S$ values, and 2) an oxidized pool with negative $\Delta^{33}S$ values (e.g. Farquhar et al., 2002; Ono et al., 2003). The reduced pool is inferred to have been delivered to the Archean ocean, reacted with Fe^{2+} dissolved in the anoxic seawater and precipitated as disseminated Fe-sulphide in sediments (Ono et al., 2009; Maynard et al., 2013), whereas the oxidized pool is thought to have been reduced and incorporated into paleosols on the continents (Maynard et al., 2013), or been added to the oceans as dissolved sulfate (Farquhar et al., 2002). These S pools could be distinguished by different $\delta^{34}S$ and $\Delta^{33}S$ values, with positive values typical for the reduced pool and negative values for the oxidized pool (e.g. Ono et al., 2003). However, the $\delta^{34}S$ values of the dissolved sulfate could be modified by mass-dependent fractionation; for example via bacterial or thermogenic seawater sulfate reduction, nodules or layers of sulphides in sediments with highly variable $\delta^{34}S$ values with consistently negative $\Delta^{33}S$ values can be produced (Ono et al., 2003; 2009), as seen in the data from the exhalite and graphitic argillite. The consistently negative $\Delta^{33}S$ values of both the exhalite and graphitic argillite at the Hart deposit suggest that sulphides in both lithologies formed as a result of bacterial sulphate reduction of the Archean seawater sulphate, and their $\Delta^{33}S$ values do not provide an adequate means of distinguishing between these two potential sulphur sources. However, the average $\delta^{34}S$ values of the exhalite (-2.1‰) and graphitic argillite (+3.4‰) are quite different, although the range of values for the exhalite (-11.4 to +7.6‰) overlaps with those from the graphitic argillite (+1.6 to +5.0‰).

On the other hand, Fe isotope fractionation is thought to be dominantly controlled by redox reactions, with igneous rocks generally having values of ~0.1‰. Redox reactions in surface conditions fractionate oxidized Fe-species towards positive $\delta^{56}Fe$ values, and reduced Fe-species towards negative $\delta^{56}Fe$ values (e.g. Beard et al., 2003; Rouxel et al., 2005). Alteration of oceanic crust by hydrothermal fluids leads to the preferential removal of reduced Fe, leaving the altered oceanic crust with $\delta^{56}Fe$ values above 0‰, and the fluids having $\delta^{56}Fe$ values of ≤0‰ (Rouxel et al., 2005). Therefore, Fe delivered to the oceans by hydrothermal fluids, and any Fe-sulphides deposited from these fluids, will have negative $\delta^{56}Fe$ values. Oxidized Fe minerals that precipitate with Fe delivered by hydrothermal fluids form iron formations that tend to have positive $\delta^{56}Fe$ values (Planavsky et al., 2012). The residual reduced Fe could then precipitate as sulphides with $\delta^{56}Fe < 0$‰. Similar to the $\Delta^{33}S$ values at Hart, negative values of $\delta^{56}Fe$ in exhalite and graphitic argillite cannot differentiate these lithologies.

Each isotope alone is not capable of discriminating between the footwall lithologies but the combination of these three isotopic tracers provides an isotopic signature that helps identify the dominant contaminant that might have been responsible for the sulphur saturation in the komatiite at the Hart deposit. In most of the mineralized samples, $\Delta^{34}S$ or $\delta^{56}Fe$ values are required to distinguish whether S was derived from the mantle or the footwall lithologies, as $\delta^{34}S$ values of mineralization largely overlap with the mantle range. However, trends in $\delta^{34}S$ values towards average values of the exhalite and graphitic argillite can suggest the more likely sulphur source for the mineralized zones, making the use of multiple isotope systems necessary for confident identification of sulphur source in the Hart deposit mineralization.

Isotopic Variations within Komatiitic Flows

The mineralization and associated isotopic signatures observed within the komatiite and at the Hart deposit can be divided into three main groups, each with distinct physical characteristics and unique isotopic signatures. The main zone of mineralization is characterized by negative $\Delta^{33}S$, $\delta^{34}S$, and $\delta^{56}Fe$ values. These values are most negative where mineralization is most abundant, gradually shifting towards 0‰ above the mineralization and laterally away from the main zone (Fig. 6). This isotopic signature is most consistent with the dominant sulphur source for the main zone being the exhalite.

In comparison, sulphide mineralization at the eastern extension is characterized by negative $\Delta^{33}S$ values, positive $\delta^{34}S$ values, and slightly negative to near zero $\delta^{56}Fe$ values. This isotopic signature is generally more characteristic of the graphitic argillite, as the range of values in mineralized samples spans the range between barren komatiite and average graphitic argillite values. The absence of graphitic argillite at the contact between the basal and the second komatiite flows suggests that the komatiite flow has either completely consumed an interflow graphitic argillite unit through thermomechanical erosion, or it was in direct contact with this unit upstream from the actual location of the mineralization.

IMPLICATIONS FOR EXPLORATION

Using multiple stable isotope systems provides an opportunity to assess magma contamination by crustal rocks, a critical factor involved in the genesis of mag-

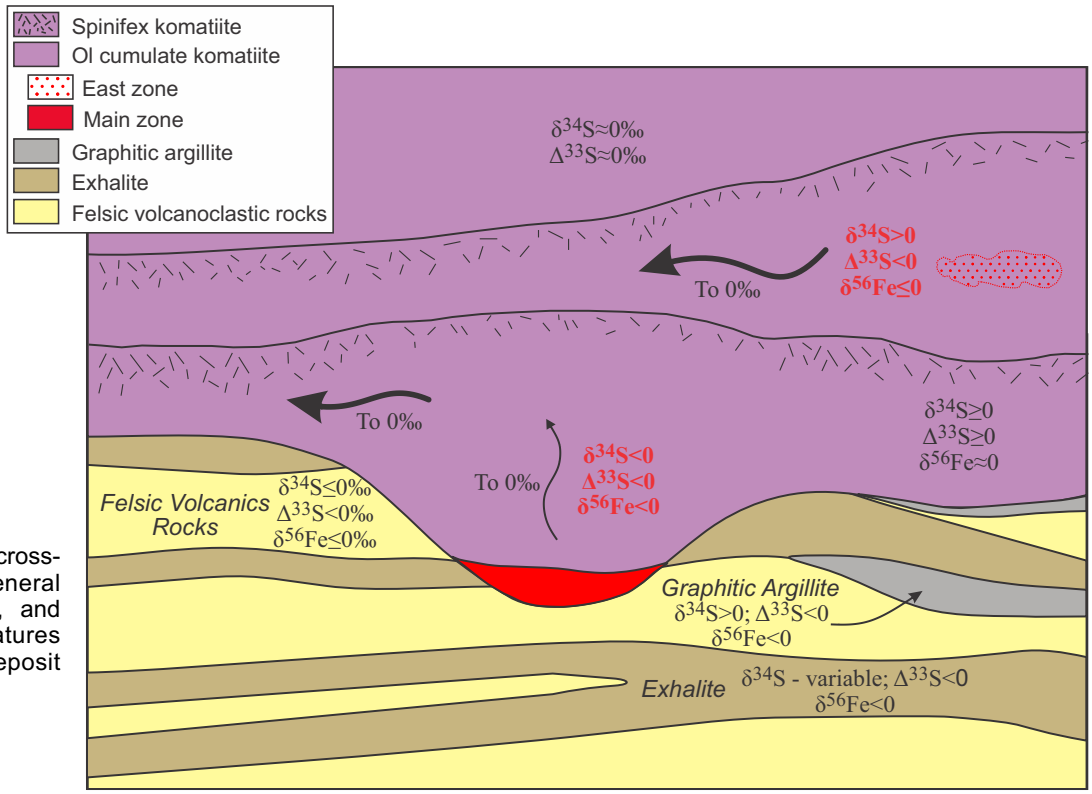

Figure 6. Schematic cross-section showing general trends of $\Delta^{33}S$, $\delta^{34}S$, and $\delta^{56}Fe$ isotopic signatures through the Hart deposit (looking north).

matic sulphide deposits. In the case of the Hart deposit, none of these isotopic systems alone ($\delta^{34}S$, $\Delta^{33}S$, or $\delta^{56}Fe$) could distinguish unequivocally between the possible sulphur sources in these mineralized environments. However, used in conjunction, these systems can help fingerprint the degree of contamination and also the sulphur sources. In many mineralized samples, $\delta^{34}S$ values are indistinguishable from mantle values, but $\Delta^{33}S$ and $\delta^{56}Fe$ indicated the komatiitic magma had been contaminated by footwall rocks. However, despite some overlapping, $\delta^{34}S$ values allow for discrimination between the two possible sulphur sources in this deposit. More importantly, these isotope systems all trend toward mantle values away from the deposit, but the $\Delta^{33}S$ contamination signature can still be identified several hundreds of metres away, allowing these techniques to be used to determine the potential fertility of the magma, and to successfully vector towards mineralization (Fig. 6).

ACKNOWLEDGEMENTS

We would like to express our appreciation to Northern Sun Mining Corp. and more specifically Todd Mathieu and Peter Calbick for their logistical support, access to their geological database, and discussions throughout this project. Discussion with, and advice from, Dr. Michael Lesher (Laurentian University) was also greatly appreciated during the course of this study. Financial support for this project has been provided by the Targeted Geoscience Initiative 4 of the Geological Survey of Canada and a Natural Sciences and Engineering Research Council of Canada (NSERC) Discovery and Accelerator Grant to AB. We would like to thank S. Jackson for constructive reviews that helped to improve the final version of this contribution.

REFERENCES

Beard, B.L., Johnson, C.M., Skulan, J.L., Nealson, K.H., Cox, L., and Sun, H., 2003. Application of Fe isotopes to tracing the geochemical and biological cycling of Fe; Chemical Geology, v. 195, p. 87–117.

Bekker, A., Barley, M.E., Fiorentini, M.L., Rouxel, O.J., Rumble, D., and Beresford, S.W., 2009. Atmospheric sulphur in Archean komatiite-hosted nickel deposits; Science, v. 326, p. 1086–1089.

Brereton, W.E., 2004. A report to NI 43-101 standards on the Timmins area nickel properties of the Legendary Ore Mining Corporation to be acquired by Canadian Arrow Mines Ltd., Ontario, Canada; MPH Consulting Ltd., Technical Report under NI 43-101, filed February 17, 2004, with SEDAR®, 70 p.

Farquhar, J., Bao, H., and Thiemens, M., 2000. Atmospheric influence of Earth's earliest sulphur cycle; Science, v. 289; p. 756–758.

Farquhar, J. and Wing, B.A., 2003. Multiple sulphur isotopes and the evolution of the atmosphere; Earth and Planetary Science Letters, v. 213, p. 1–13.

Farquhar, J., Wing, B.A., McKeegan, K.D., Harris, J.W., Cartigny, P., and Thiemens, M.H., 2002. Mass-independent sulphur of inclusions in diamond and sulphur recycling on early earth; Science, v. 298, p. 2369–2372.

Fiorentini, M., Beresford, S., Barley, M., Duuring, P., Bekker, A., Rosengren, N., Cas, R., and Hronsky, J., 2012. Distrinct to camp controls on the genesis of komatiite-hosted nickel sulfide deposits, Agnew-Wiluna greenstone belt, Western Australia:

Insights from the multiple sulphur isotopes; Economic Geology, v. 107, p. 781–796.

Hiebert, R.S., Bekker, A., Houlé, M.G., Lesher, C.M., and Wing, B.A., 2013a. Multiple sulphur isotopes and the Hart komatiite-hosted Ni-deposit, Abitibi greenstone belt, Ontario: Evaluating and tracing the signature of contamination in komatiite, *In:* Program with Abstracts; Geological Association of Canada – Mineralogical Association of Canada Joint Annual Meeting, Winnipeg, Manitoba, May 2013, Abstract Volume 36, p. 112.

Hiebert, R.S., Bekker, A., Wing, B.A., and Rouxel, O.J., 2013b. The role of paragneiss assimilation in the origin of the Voisey's Bay Ni-Cu sulphide deposit, Labrador: multiple S and Fe isotope evidence; Economic Geology, v. 108, p. 1459–1469.

Houlé, M.G., Lesher, C.M., Gibson, H.L., Ayer, J.A., and Hall, L.A.F., 2010a. Localization of komatiite-associated Ni-Cu-(PGE) deposits in the Shaw Dome, Abitibi greenstone belt, Superior Province; In: Abstracts; 11th International Platinum Symposium, June 21–24, 2010, Sudbury, Ontario, Canada; Ontario Geological Survey, Miscellaneous Release, Data 269.

Houlé, M.G., Lesher, C.M., Préfontaine, S., Ayer, J.A., Berger, B.R., Taranovic, V., Davis, P.C., and Atkinson, B., 2010b. Stratigraphy and physical volcanology of komatiites and associated Ni-Cu-(PGE) mineralization in the western Abitibi greenstone belt, Timmins area, Ontario: a field trip for the 11th International Platinum Symposium; Ontario Geological Survey, Open File Report 6255, 99 p.

Lesher, C.M. and Arndt, N.T., 1995. REE and Nd isotope geochemistry, petrogenesis and volcanic evolution of contaminated komatiites at Kambalda, Western Australia; Lithos, v. 34, p. 127–157.

Lesher, C.M. and Burnham, O.M., 2001. Multicomponent elemental and isotopic mixing in Ni-Cu-(PGE) ores at Kambalda, Western Australia; The Canadian Mineralogist, v. 39, p. 421–446.

Lesher, C.M. and Campbell, I.H., 1993. Geochemical and fluid dynamic modeling of compositional variations in Archean komatiite-hosted nickel sulphide ores in Western Australia; Economic Geology, v. 88, p. 804–816.

Maynard, J.B., Sutton, S.J., Rumble III, D., and Bekker, A., 2013. Mass-independently fractionated sulphur in Archean paleosols: a large reservoir of negative $\Delta^{33}S$ anomaly on the early Earth; Chemical Geology, v. 362, p. 74–81.

Ono, S., Eigenbrode, J.L., Pavlov, A.A., Kharecha, P., Rumble III, D., Kasting, J.F., and Freeman, K.H., 2003. New insights into Archean sulphur cycle from mass-independent sulphur isotope records from the Hamersley Basin, Australia; Earth and Planetary Science Letters, v. 213, p. 15–30.

Ono, S., Beukes, N.J., and Rumble, D., 2009. Origin of two distinct multiple-sulphur isotope compositions of pyrite in the 2.5 Ga Klein Naute Formation, Griqualand West Basin, South Africa; Precambrian Research, v. 169, p. 48–57.

Planavsky, N., Rouxel, O.J., Bekker, A., Hofmann, A., Little, C.T.S., and Lyons, T.W., 2012. Iron isotope composition of some Archean and Proterozoic iron formations; Geochimica et Cosmochimica Acta, v. 80, p. 158–169.

Rouxel, O.J., Bekker, A., and Edwards, K.J., 2005. Iron isotope constraints of the Archean and Paleoproterozoic ocean redox state; Science, v. 307, p. 1088–1091.

GEOLOGICAL SURVEY OF CANADA
OPEN FILE 7856

Targeted Geoscience Initiative 4: Canadian Nickel-Copper-Platinum Group Elements-Chromium Ore Systems — Fertility, Pathfinders, New and Revised Models

Recent advances in fluid and melt inclusion and applied mineralogical research in the Sudbury mining camp: improving ore genesis models and exploration success

Jacob J. Hanley[1], Matthew A. MacMillan[1], Mitchell J. Kerr[1], Kathleen M. Watts[1], Michael R. Warren[1], and Doreen E. Ames[2]

[1]Saint Mary's University, Halifax, Nova Scotia
[2]Geological Survey of Canada, Ottawa, Ontario

2015

© Her Majesty the Queen in Right of Canada, as represented by the Minister of Natural Resources Canada, 2015

This publication is available for free download through GEOSCAN (http://geoscan.nrcan.gc.ca/)

Recommended citation

Hanley J.J., MacMillan, M.A., Kerr, M.J., Watts, K.M., Warren, M.R., and Ames, D.E., 2015. Recent advances in fluid and melt inclusion and applied mineralogical research in the Sudbury mining camp: improving ore genesis models and exploration success, *In:* Targeted Geoscience Initiative 4: Canadian Nickel-Copper-Platinum Group Elements-Chromium Ore Systems — Fertility, Pathfinders, New and Revised Models, (ed.) D.E. Ames and M.G. Houlé; Geological Survey of Canada, Open File 7856, p. 209–231.

Publications in this series have not been edited; they are released as submitted by the author.

Contribution to the Geological Survey of Canada's Targeted Geoscience Initiative 4 (TGI-4) Program (2010–2015)

TABLE OF CONTENTS

Recent advances in fluid and melt inclusion and applied mineralogical research in the Sudbury mining camp: improving ore genesis models and exploration success

Jacob J. Hanley[1]*, Matthew A. MacMillan[2], Mitchell J. Kerr[1], Kathleen M. Watts[1], Michael R. Warren[1], and Doreen E. Ames[2]

[1]Department of Geology, Saint Mary's University, 923 Robie Street, Halifax, Nova Scotia B3H 3C3
[2]Geological Survey of Canada, 601 Booth Street, Ottawa, Ontario K1A 0E8
*Corresponding author's e-mail: Jacob.Hanley@smu.ca

ABSTRACT

A variety of microanalytical techniques (LA-ICP-MS, microthermometry, SIMS) were applied to resolve uncertainties about the chemical evolution of the Sudbury Igneous Complex (SIC) melt sheet and its associated hydrothermal systems. In the SIC sublayer and main mass, silicate melt inclusions in early apatite cumulate grains preserve evidence for high-temperature (>1100°C) immiscibility between Fe-rich and Si-rich liquids. Melt inclusions record the base metal (Ni, Cu, Co) endowment of the melt sheet prior to and after sulphide saturation and allow quantification of trace element partitioning at various stages during melt-sheet evolution, and prediction of the likelihood that an offset dyke contains or does not contain sulphide ore deposits locally. Melt inclusions were deemed unaffected by post-cumulus processes, providing an opportunity to characterize primary magmatic processes otherwise obscured by 1.85 Ga of metamorphism, deformation, and hydrothermal alteration. In the sublayer, analysis of the trace element chemistry of alteration, metamorphic and igneous biotite identified the chemical signature of biotites associated with the host inclusion-rich quartz diorite offset-style Ni-Cu-platinum-group element (PGE) sulphide orebodies, characterized by elevated Ni, Cu, and Ni/Cr ratios. Trace metal analysis of biotite allows differentiation between this key rock type and barren quartz diorite that is otherwise compositionally and texturally comparable. In footwall Cu-Ni-PGE ore deposits, alteration, fluid inclusion, and stable isotope studies provide a systematic description of "low-sulphide" deposit style. Hydrothermal sulphide precipitation, a process recorded in alteration vein styles, was associated with mixing of oxidized, ^{18}O-enriched, high salinity metal-rich fluids with cooler, reduced, ^{18}O-depleted, high-Ca groundwaters. Recognition of this mixing process through isotope mapping, fluid inclusion microthermometry, and alteration mineral chemistry provides a means to identify metal-precipitation fronts within the complex footwall environment.

INTRODUCTION

Improving exploration models for base metal and PGE deposits using advanced microanalytical research techniques aims to increase Canada's long-term resource base of these essential commodities. The research described here improves exploration models for deposits of Ni, Cu, and the platinum-group elements (PGE) in mafic-ultramafic igneous intrusions. The world-class Sudbury Igneous Complex (SIC) is one such intrusion associated with abundant magmatic-hydrothermal Ni-Cu-PGE sulphide deposits. Understanding the processes that led to the formation of these deposits is limited by significant knowledge gaps, some of which are outlined below, and addressed through the current research.

The study of melt inclusions (i.e. trapped Sudbury magma droplets hosted in minerals that grew from the magma) is key in understanding the evolution of the SIC, the origin of its associated nickel and PGE deposits, and, defining robust criteria that can be used to discriminate between barren and mineralized regions of the Sudbury margin. Since its formation, the SIC has undergone intense deformation and hydrothermal alteration. These processes have modified the composition of the rocks, making it difficult to use the current chemical composition of the intrusion as a proxy for ore-forming processes that occurred 1.85 billion years ago when the deposits were forming. For example, a major limitation of mass balance exercises, which are focused at determining the amount of magma needed to generate the sulphide deposits, is knowledge of the metal and S content of the magma before the deposits formed and *before* the intrusion was subjected to deformation and alteration. Modelling the crystallization of

Hanley J.J., MacMillan, M.A., Kerr, M.J., Watts, K.M., Warren, M.R., and Ames, D.E., 2015. Recent advances in fluid and melt inclusion and applied mineralogical research in the Sudbury mining camp: improving ore genesis models and exploration success, *In:* Targeted Geoscience Initiative 4: Canadian Nickel-Copper-Platinum Group Elements-Chromium Ore Systems — Fertility, Pathfinders, New and Revised Models, (ed.) D.E. Ames and M.G. Houlé; Geological Survey of Canada, Open File 7856, p. 209–231.

the SIC melt evolution has been equally problematic; the controversy stems from conflicting models pertaining to the source of the melt sheet and its differentiation history (Peredery and Naldrett, 1975; Kuo and Crocket, 1979; Faggart et al., 1985; Grieve et al., 1991; Chai and Eckstrand 1994; Lightfoot et al., 1997a,b, 2001; Ariskin et al., 1999; Dicken et al., 1999; Ames et al., 2002; Therriault et al., 2002; Pope et al., 2004; Zieg and Marsh, 2005). In such environments where post-magmatic processes have reduced the effectiveness of routine whole rock geochemistry, the analysis of melt inclusion chemistry, could significantly enhance exploration success and address genetic uncertainties masked by post-cumulus processes.

The study of fluid inclusion, alteration, and stable isotope systematics of the footwall ore-forming systems contributes further to extensive fluid inclusion, O and H isotope, and petrographic evidence in high-sulphide systems, suggesting that high-salinity volatiles played a role in the precipitation and redistribution of base and precious metals, the compositional modification of the magmatic sulphides, and the generation of halogen-enriched haloes encompassing the orebodies (Li, 1992; Farrow, 1994; Jago et al., 1994; Farrow and Watkinson, 1997, Molnár et al., 2001; Hanley and Mungall, 2003; Hanley et al., 2004, 2005, 2011; Ames and Farrow 2007; Péntek et al., 2008; Hanley and Bray, 2009; Tuba et al., 2010). Evidence from these studies that lends support to a hydrothermal origin for low-sulphide footwall ore deposits include (i) the occurrence of ore metal-bearing, saline fluid inclusions in sulphide and silicate alteration minerals; (ii) the occurrence of co-precipitated metal halide minerals (e.g. Pd-Bi-chloride) in PGE-Au-rich sulphide vein assemblages; (iii) the occurrence of primary, low-temperature Pt- and Pd-bearing minerals hosted in Cl-rich, hydroxysilicate mineral assemblages; and (iv) the presence of altered, oxidized, Cu-, Au-, and PGE-depleted ore zones, ("epidote zone") interpreted to be contact-style ores that were leached by hydrothermal fluids. Investigations of deposit-scale mineralogy and spatial relationships among different ore zones within the footwall (e.g. Farrow et al., 2005) show that low-sulphide footwall-style deposits possess a largely fluid-derived metal component and were emplaced in the footwall prior to the emplacement of the sharp-walled high-sulphide deposits. Previous research has suggested that ore fluids associated with footwall-style deposits were mixtures of deeply sourced saline groundwaters and high-temperature "magmatic" fluids derived from the mineralized contact region or the main igneous mass of the SIC (Marshall et al., 1999; Hanley et al., 2005; Péntek et al., 2008; Tuba et al., 2010; Hanley et al., 2011). Areas of intense alteration and areas showing evidence of metal precipitation and/or remobilization appear to be spatially associated with zones of partial melting within the footwall (Péntek et al., 2013) and injection of residual silicate liquids from the SIC into the surrounding footwall (Hanley et al., 2011). In addition to saline aqueous fluids in the North Range of the SIC, carbonic fluid phases (CO_2, hydrocarbons) have also been reported (Farrow, 1994; Molnár et al., 2001; Hanley et al., 2005). Recent studies of the low-sulphide footwall deposits illustrate the importance of PGE-enriched volatile phases and the existence of brittle structures in the Archean footwall as conduits for fluid migration and a chemical trap for metal precipitation (Tuba et al., 2014); however, the exact mechanism of metal precipitation and the source of volatiles remain unconstrained.

The study of metal chemistry of common alteration and igneous hydroxysilicate silicate minerals is justified based on the lack of such descriptions in unweathered, fresh, or hydrothermally altered (at non-surficial conditions) mafic-ultramafic settings. The majority of these studies have focused on magmatic Ni-Cu-PGE ore styles and associated alteration assemblages at Sudbury, Ontario, Canada where elevated concentrations of Ni (as structural substitutions) have been reported in biotite, amphibole, and chlorite in proximity to sulphide deposits (Li and Naldrett, 1993; Farrow, 1994; Magyarosi et al., 2002; Hanley and Mungall, 2003; Stewart, 2011; Tuba, 2012; Ames and Kjarsgaard, 2013 and references therein). Of these minerals, biotite is the most appropriate mineral for study as a pathfinder/indicator mineral because it is ubiquitous throughout both the SIC and all surrounding country rocks, having grown in association with specific and easily discernible magmatic, metamorphic, and hydrothermal events that are well documented in the literature (e.g. Coats and Snajdr, 1984; Thomson et al., 1985; Corfu and Andrews, 1986; Noble and Lightfoot, 1992; Li and Naldrett, 1993; Farrow, 1994; Farrow and Watkinson, 1997; Magyarosi, 1998; Magyarosi et al., 2002; Stewart, 2002; Hanley and Mungall 2003; Tuba, 2012; Ames and Kjarsgaard, 2013). However, there have been no robust evaluations of the factors controlling the Ni enrichment in biotite or its reliability as a routine exploration tool for Ni-Cu-PGE sulphide ore deposits at Sudbury, or any other mafic-ultramafic-associated sulphide deposit.

ANALYTICAL METHODS

Optical and Scanning Electron Microscopy

Optical petrography was completed using a Nikon Eclipse H550L microscope and major/minor element compositions for homogenized silicate melt inclusions, silicates, phosphates, carbonates, sulphides, and discrete metal-bearing phases were obtained using a LEO 1450VP scanning electron microscope (SEM) at Saint

Mary's University, Halifax, Nova Scotia. An energy dispersive X-ray (EDS) Oxford INCA 80 mm^2 silicon drift detector (SDD; attached to the SEM) was operated at a working distance of 20 mm, beam current of 40 μA, and accelerating voltage of 20–25 kV for analyses of all mineral types.

Laser Ablation ICP-MS Analysis of Trace Elements in Garnet

Trace element mapping and analysis of garnet was done at the University of New Brunswick, Fredericton, New Brunswick (quantified offline using *lolite* software) using a Resonetics S-155-LR 193 nm excimer laser coupled to an Agilent 7700x quadrupole inductively coupled plasma mass spectrometer (ICP-MS). The standards NIST 612 and BCR-2G were measured to calibrate analyte sensitivities as well as monitor instrumental bias and internal standardization was completed using Ca determined from microprobe and quantitative SEM-EDS analyses. The laser conditions used for all raster sequences were a spot size of 124 μm, scan speed between 12 to 25 μm/s, and pulse rate of 10 Hz.

Laser Ablation ICP-MS Analysis of Trace Elements in Apatite and Melt Inclusions

Trace elements in apatite and homogenized and non-homogenized melt inclusions were determined using a Resonetics RESOlution M50 laser probe (Ar-F Excimer laser) operated in dual detector mode at Laurentian University, Sudbury, Ontario, at a repetition rate of 5 Hz and a fluence of 6 J/cm^2. Data reduction for melt inclusions analysed by LA-ICP-MS was done using SILLS (Guillong et al., 2008). Evaluation of analytical accuracy and precision for transient LA-ICP-MS signals is challenging since no certified synthetic melt inclusion reference standards are available. However, some statements can be made concerning the quality of the data. The accuracy of trace element analyses in melt inclusions, repeated analyses of synthetic glass standards at the Laurentian University laser ablation ICP-MS facility as secondary quality control (QC) standards (BHV02 from US Geological Survey; ATHO from MPI-DING), quantified using NIST610, routinely yield concentrations better than within 15% relative of expected concentrations (J. Petrus, pers. comm., 2013). Analytical precision cannot be readily evaluated since the method is destructive, however, two possible strategies are considered. First, when different integration windows through homogenized (glassy) melt inclusions are quantified, adjacent intervals of inclusion yield analytical reproducibility better than 5% relative. Similarly, when melt inclusion results from a single sample are compared (and assumed to contain the same liquid, for melt end-member compositions) reproducibility of melt compositions within single samples is high. However, these results are measures of melt homogeneity at various scales rather than true (external) precision. With respect to the accuracy of major element analyses in melt inclusions, comparison of analytical results yielded from SEM/EMP for homogenized inclusions with data from LA-ICP-MS shows that all major elements (with the exception of FeO, MgO, and MnO) yield concentrations within 25% (relative) of each respective method. For reasons that are unclear at this time, and likely related to the low concentrations in the standard NIST610 glass, FeO, MgO, and MnO are up to 70% higher in the LA-ICP-MS analyses of equivalent inclusions analysed by SEM/EMP. For these reasons, it is our preference to utilize the SEM/EMP data for major elements and the LA-ICP-MS data for trace elements. For precision of major element analyses, only a similar approach as that stated above for trace elements can be employed for the LA-ICP-MS method. For SEM/EMP analyses, repeated analyses of single points within homogenized melt inclusions yielded reproducibilities in the quantified EDS spectra of better than 2% relative. Analytical uncertainties in the SEM/EMP analyses (in the total wt% oxides excluding H_2O, the CaO composition of the host apatite) and uncertainty introduced by assuming La to be the matrix-only tracer also impact the overall uncertainty in major and trace element analyses. Uncertainties in the host composition (which was selected for all data reduction as a constant value of CaO for each respective sample by SEM/EMP) are no larger than a few %, which would impact the resulting melt inclusion data reduced in SILLS proportionally. With respect to La as the matrix-only tracer, the actual ratio of $La_{host}/La_{inclusion}$ is on the order of ~100 (i.e. 0.2 wt% La in apatite versus 20 ppm expected for felsic liquids; not quantifiable). Uncertainties in melt composition resulting from this unmixing procedure will be larger for elements that show less compatibility in the melt phase.

Laser Ablation ICP-MS Analysis of Trace Elements in Biotite

Trace elements in biotite were determined by LA-ICP-MS at the Geological Survey of Canada, Ottawa using polished thick sections (200 um thick). The instrumentation used comprised a Photon Machines Analyte.193 Excimer laser for sample introduction and an Agilent 7700x quadrupole ICP-MS for isotope measurements. Details of the conditions for the analyses (including laser ablation parameters, ICP-MS settings, oxide production rates, etc.) are summarized in Warren et al. (2015). For single grain analyses, 1–3 spots per biotite grain and 4–20 grains per sample were obtained. Grain boundaries, cleavage planes, and grains that contained

visible inclusions were avoided to reduce contamination. The isotopes ^{42}Ca (count rate increases when amphibole and plagioclase are encountered) and ^{39}K (count rate decreases when chlorite is encountered) were monitored visually and during data reduction to identify and avoid contamination from other hydroxysilicate minerals. Data reduction was done using Glitter™ software (Macquarie University), which allowed selection of portions of each signal that have consistent count rates, eliminating localized contamination in the signal (see discussion below). Calibration of analyte sensitivities was done using the standard basalt glass GSE-1G (USGS). Quality control standards BCR-2G (USGS), and SRM612 (NIST) were analyzed to evaluate the accuracy of results (which are in agreement with accept values to within ~10% relative for major and trace elements, with the exception of Cr, Zn, Ag, Cd, Sn, Sb, and Cu that were to within ~10–30% relative). The internal standard used for quantification was the average wt% Al_2O_3 determined independently by quantitative SEM-EDS. The same population of grains was analyzed by SEM-EDS prior to LA-ICP-MS. Inter- and intra-grain variations in Al concentrations within single samples were very small and the results were comparable EMP analysis of biotite populations in the Worthington area by Magyarosi (1998). Uncertainties in determined trace element concentrations resulting from the use of average biotite Al_2O_3 values in a single sample are ± 2% (relative; i.e. 400 ppm Cr ± 8 ppm). Element maps of biotite grains were also generated by LA-ICP-MS spot analyses over square gridded areas. The software Glitter™ was used for spot quantification and an in-house (Geological Survey of Canada) program was used to generate logarithmic and percentile-scaled maps of major and trace element concentration. Concentrations were calculated using GSE-1G for external standardization and normalizing to 100% total element abundance; this approach does not account for the OH^- content of biotite, and therefore, mapped element concentrations are overestimated by approximately 5% (relative). Minimum detection limits (MDL) for analytes are calculated by Glitter™ software at the 99% confidence level, based on Poisson counting statistics (MDL = $2.3x\sqrt{2B}$; where B is the total counts in the background interval), converted to a concentration based on sensitivity determined using the external standard, and corrected for ablation yield.

Electron Microprobe Analysis

Electron microprobe analyses of silicate and phosphate minerals and homogenized silicate melt inclusions were obtained at Dalhousie University using a JEOL 8200 Superprobe. The operating conditions for all analyses were an accelerating voltage of 15.0 kV, beam diameter of 1 μm, and 20 seconds/10 seconds for mineral measurements/background measurements on each element, respectively. Standards and crystals used to measure each element of interest were K (Sanidine, PETJ), Cr (Cr_metal_CH2P, PETJ), Na (Jadeite_Naonly, TAPH), Si (Sanidine, TAP), Mn (PyrolusiteCH5L, LIFH), Ca (K_KaersCaTiMg, PETJ), Ti (K_KaersCaTiMg, PETJ), Mg (K_KaersCaTiMg, TAPH), Al (Sanidine, TAP), Fe (Garnet12442Fe5, LIFH), Ba (Barite_BaCH2P, PETJ), Ni (Ni_metal_CH5L, LIFH), and Zn (Gahnite, LIFH).

Fluid and Melt Inclusion Microthermometry

Microthermometric analyses on fluid inclusions were carried out at Saint Mary's University using a Linkam FTIR 600 heating-freezing stage mounted on an Olympus BX51 microscope. Stage calibration was carried out using synthetic fluid inclusion standards containing pure CO_2 (melting at -56.6°C) and pure, critical density H_2O (melting at 0°C and homogenizing at 374.1°C). Absolute uncertainties associated with the fluid inclusion measurements (based on measurement precision of the instrumentation and measurement reproducibility on standards) range from ±2–3°C for output temperatures around the extremes of working conditions for the heating-freezing stages (-190°C and 560°C) to better than ±0.2°C for output temperatures near 0°C. Eutectic (first) ice-melting temperatures (T_e^{ice}) were observed to help identify major cation compositions of the respective inclusions and final ice-melting temperatures were used to calculate NaCl and $CaCl_2$ weight percent equivalency values (i.e. bulk salinity). Microthermometric determination of melt inclusion first melting, final melting, and bubble closure (providing minimum $T_{trapping}$) was conducted using a Linkam TS1500 heating stage with sapphire plates for heating. The stage was mounted on a BX53 microscope with a Q imaging colour video camera. Heating rates varied between 10 and 100°C/min, and a flow rate of 40 ml/min of argon gas was used to prevent oxidation of melt inclusions and their apatite host during heating. The error associated with the absolute temperature is ±2°C, based on monitoring of fixed temperature stability. Pure Ag, Au, and Cu metals were used as standards to calibrate the stage by measuring their melting points and comparing them against accepted values.

Secondary Ion Mass Spectrometry

Oxygen isotope compositions in garnet and calcite were measured at the University of Manitoba, Winnipeg, Manitoba, using a Cameca IMS 7f secondary ion mass spectrometer (SIMS). Hand-picked garnet crystals were mounted in epoxy resin then polished using diamond paste to ensure even surfaces with exposed mineral grains. Samples were cleaned and

coated with a thin layer of gold to provide a conductive surface (then held in SIMS sample holders and kept under vacuum overnight). During all analyses, a cesium (Cs^+) primary beam with an ~2 nA current was accelerated at 8.75 kV towards the sample surface with a sputtering diameter of ~15–20 μm and the instrument was operated at a 250 V offset, -9 kV negative secondary accelerating voltage, and mass resolving power of 347. An intrinsic mass-dependent bias was introduced during SIMS analyses that favours the low-mass isotope and is known as "instrumental mass fractionation" (IMF). The ionization process is the most relevant contributor to IMF and depends most strongly on the chemical composition of the sample. IMF is also commonly referred to as "compositionally dependent fractionation" or "matrix effects" (e.g. Riciputi et al. 1998). Accurate SIMS isotope analyses require that IMF be corrected using mineral standards that are compositionally similar to the unknown. Isotopic measurements from the standard are compared against its accepted isotopic composition to calculate correction factors, which are applied to the unknowns that are measured during the same analysis session (e.g. Holliger and Cathelineau, 1988). The standard Joplin Calcite, ($\delta^{18}O_{V\text{-}SMOW}$ = 5.7‰; where $\delta^{18}O_{V\text{-}SMOW}$ = 1.03086*$\delta^{18}O_{PDB}$ + 30.86) was used for analyses of calcite; UWG-2 ($\delta^{18}O_{V\text{-}SMOW}$ = 5.8‰; Valley et al., 1995) was used for analyses of both garnet cores and garnet rims. However, the composition of UWG-2 ($Alm_{45}Prp_{40}Grs_{14}Sps_1$) is not closely matched to the compositions of the cores or rims analyzed in this study. The most closely matched garnet standards reported in the literature for the cores and rims of the Sudbury footwall garnets are 92LEW7 ($Adr_{89}Grs_6Alm_4Prp_1$) and 92LEW10 ($Adr_{50}Grs_{42}Alm_4CaTi_2Prp_2$), respectively. Page et al. (2010) reported average instrumental biases for 92LEW7 and 92LEW10 when corrected using UWG-2 of +6.69‰ and +5.64‰ and these additional errors are taken into consideration in the results section.

Colour Cathodoluminescence Imaging

Cathodoluminescence images were obtained with a Reliotron-based hot cathode CL system at the Geological Survey of Canada (Ottawa). Sample photographs were taken with a vacuum gauge pressure that read between 57 and 82 millitorr, a beam current fluctuation between 40 and 70 microamps, a voltage of 12 kV, a beam focus of 28, and a current limit set at 2 ma. Photographs were taken using the Empix program and an Optronics camera.

Bulk Oxygen Stable Isotope Analysis

Bulk oxygen isotope analysis of garnet was determined at Queen's University, Kingston, Ontario. Oxygen was extracted using a conventional bromine pentafluorine extraction line and the isotopes were measured on a Finnigan Mat 252 isotope ratio mass spectrometer with an analytical uncertainty of ±0.3‰ (K. Klassen, pers. comm., 2011).

RESULTS AND DATA ANALYSIS

Evolution of the Sudbury Igneous Complex Indicated from Silicate Melt Inclusions

Analyses of primary melt inclusions hosted in cumulus apatite from the Transition Zone Gabbro (TZG), norite, and quartz diorite offset dykes of the SIC are used to decipher the thermochemical characteristics of the original melt sheet and trace element partitioning behaviour within the evolving melt sheet. Textural analyses of apatite in the SIC shows that apatite occurs as a cumulus phase in the Main Mass and quartz diorite offset dykes (Fig. 1). Early saturation of apatite in the SIC is supported by microthermometric data that yields melt inclusion minimum trapping temperatures in the TZG and quartz diorite offset dykes between ~1100 to 1200°C.

Apatite-hosted melt inclusions commonly display a negative crystal shape, occur parallel to the c-axis, and commonly occur within a central growth zone, which suggests a primary origin (Fig. 2). Coeval (co-entrapped) melt inclusion compositions show two distinct types: (i) Si-rich liquids that range in composition from tonalitic to granodioritic (60–70 wt% SiO_2, ≤11 wt % FeO) and (ii) Fe-rich liquids that range in composition from syenogabbroic to essexitic to alkali gabbroic (27–49 wt% SiO_2, 16–44 wt% FeO), determined by SEM-EDS and EMP analyses of opened, homogenized melt inclusions (apatite grains heated at 1100 to 1200°C for 3 hours in a box furnace). These contrasting melt pairs may represent the products of immiscibility by either simple cooling of the superheated melt sheet or fractional crystallization.

The position of the bulk liquid composition of the SIC, the equivalent of the chilled margin of the quartz diorite offset dykes and least altered vitric bombs and blocks of the Onaping Formation, falls between immiscible melt pairs and in close proximity to the two-liquid field in the system leucite-fayalite-silica (Fig. 3), which suggests that the onset of immiscibility in the SIC was a consequence of simple cooling of the superheated melt sheet (~1700°C) and not liquidus crystallization that has been indicated to occur in other well studied basaltic layered intrusions.

Trace element data, obtained by LA-ICP-MS analyses of single inclusions and surrounding host apatite, are used to infer Kd values (Fig. 4) between apatite and the two melt types, and between coexisting melt types (Fig. 5; $Kd^{Fe\text{-}rich\ melt/Si\text{-}rich\ melt}$). The Kd values

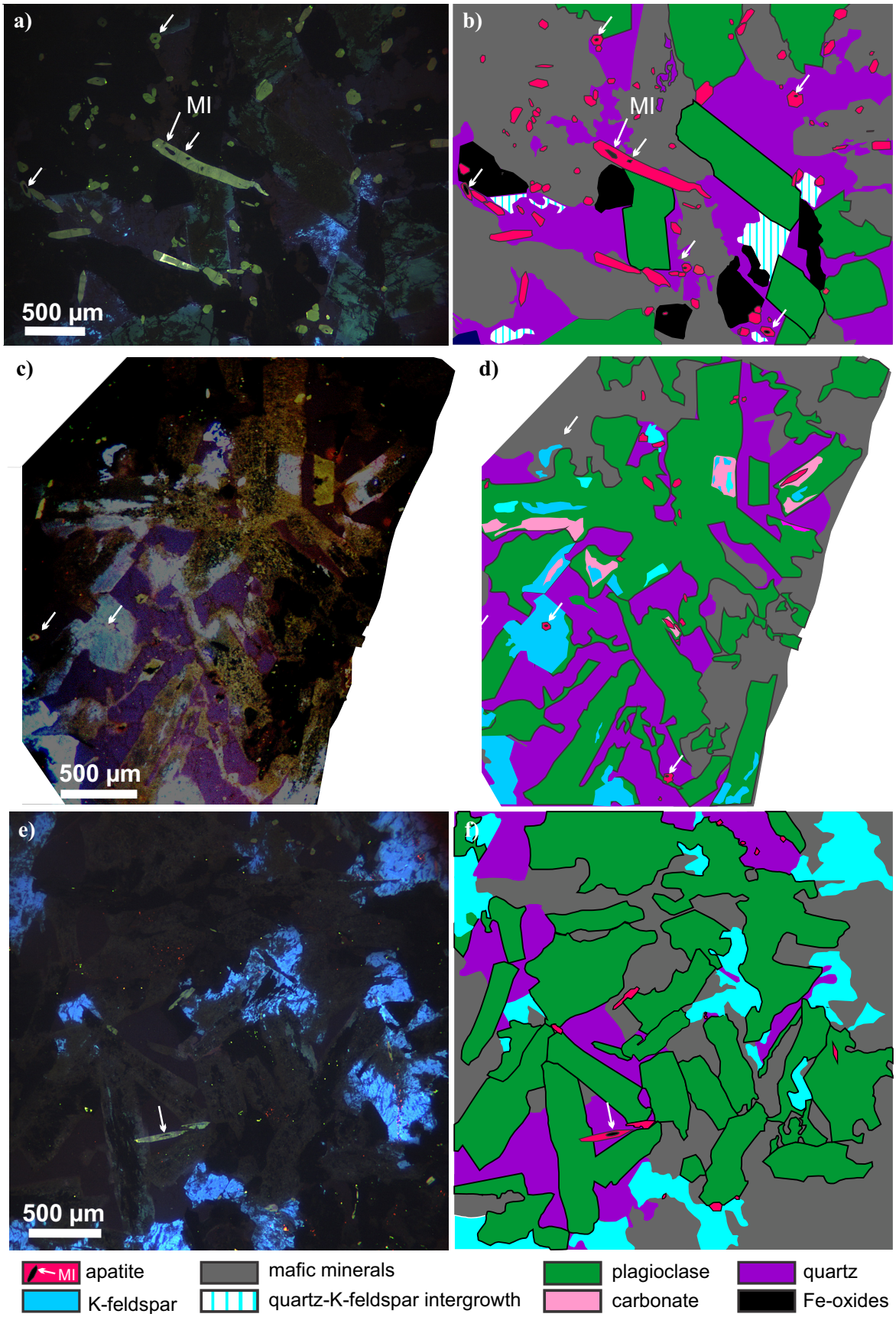

Figure 1. Microphotographs (colour CL) and thin section sketches showing the distribution of apatite and trapped melt inclusions (MI) in the Transition Zone Gabbro and Whistle offset dyke. **a, b)** Apatite from the Transition Zone Gabbro and **(c–f)** apatite from the leucocratic quartz diorite Whistle offset dyke.

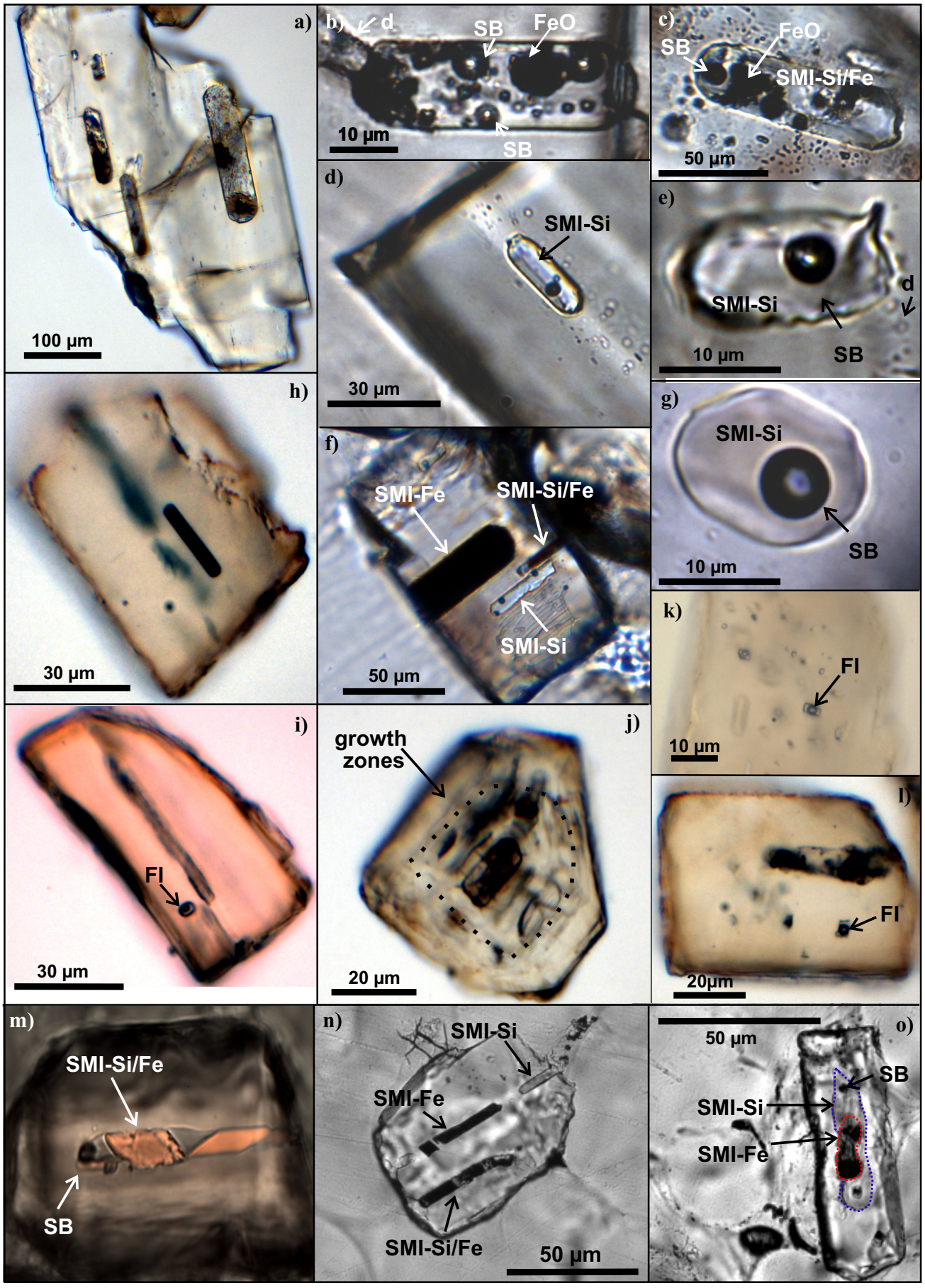
a)
100 µm
b)
d
SB
FeO
10 µm
SB
c)
SB
FeO
SMI-Si/Fe
50 µm
d)
SMI-Si
30 µm
e)
SMI-Si
d
10 µm
SB
h)
30 µm
f)
SMI-Fe
SMI-Si/Fe
SMI-Si
50 µm
g)
SMI-Si
SB
10 µm
k)
Fl
10 µm
i)
Fl
30 µm
j)
growth
zones
20 µm
l)
Fl
20µm
m)
SMI-Si/Fe
SB
n)
SMI-Si
SMI-Fe
SMI-Si/Fe
50 µm
50 µm
o)
SB
SMI-Si
SMI-Fe

between immiscible melt pairs in this study show that the majority of trace elements partition evenly between Si- and Fe-rich liquid, with the incompatible elements (Hf, Zr, Nb, and Ta) showing a slight affinity for the Si-rich liquid and V and Co showing a slight affinity for the Fe-rich liquid in the TZG. Immiscible melt pairs in the norite have Kd values closer to 1, with the exception of Co that prefers the Fe-rich melt. Kd values between immiscible Fe- and Si-rich liquid are also in close agreement to what has been found experimentally for melts with basaltic starting compositions. $Kd^{apatite/melt}$ values for both Si- and Fe-rich melt pairs show that REE, Sr, and Y are compatible in apatite, and As is weakly compatible or incompatible in apatite, whereas the following elements behaved incompatibly (in increasing order of incompatibility: Cr, Ni, Cu, Zr, Co, Cs, Ag, Nb, Hf, Ta, and Rb).

Pathfinder Mineral Chemistry in the Sublayer Environment

The chemistry of biotite in the Totten deposit (south-east corner of Sudbury Igneous Complex) and its surrounding country rocks was investigated. The deposit is a magmatic Ni-Cu-PGE sulphide system hosted within a radial offset dyke of multiphase quartz diorite. Despite evidence of complex interaction with its metasedimentary and metavolcanic country rocks, and overprinting by syn- to post-emplacement igneous, hydrothermal, and metamorphic events, the dyke remains a petrographically distinct unit comprising several phases of quartz dioritic rocks, with an inclusion-rich phase hosting discrete magmatic Ni-Cu-PGE sulphide orebodies (Zurbrigg et al., 1957; Cochrane, 1984; Grant and Bite, 1984; Lightfoot et al., 1997a,b; Lightfoot and Farrow, 2002; Murphy and Spray, 2002; Tuchscherer and Spray, 2002; Stewart, 2011).

LA-ICP-MS and quantitative SEM-EDS analyses of biotite were obtained from representative host rocks to, and igneous rocks of, the SIC in and surrounding the Worthington quartz diorite offset dyke at the Totten Mine (Vale Canada Ltd.). With the exception of Ni, Cr, and Cu, no systematic variations in dissolved trace elements concentrations were observed to be related to proximity to sulphide ore. Enrichment of Cu in biotite (up to two orders of magnitude higher than back-

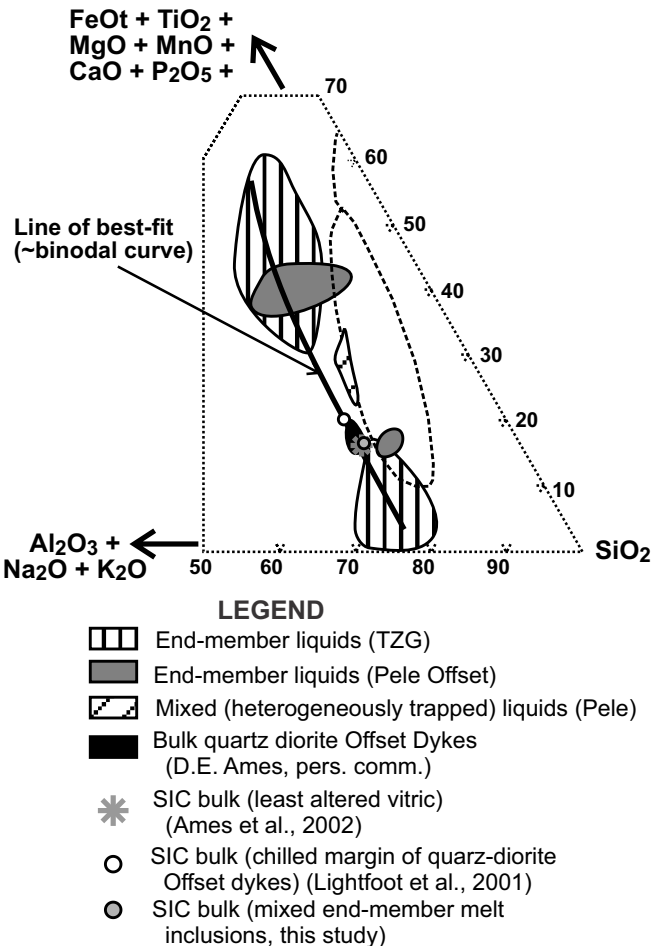

Figure 3. Major element chemistry of apatite-hosted melt inclusions from the Main Mass Transition Zone Gabbro (TZG) and Pele offset dyke are plotted as shaded fields on an enlarged part of the pseudo-ternary Grieg diagram with the bimodal curve separating the one- and two-liquid fields. Major element compositions from the Main Mass TZG and Pele offset dyke are plotted along with the binodal curve that is drawn from a line of best-fit. The Sudbury Igneous Complex (SIC) bulk compositions are represented by the least altered vitric of the Onaping Formation (Ames et al., 2002), the chilled margin of the quartz diorite Offset dykes (Lightfoot et al., 2001),. and the calculated by mixing end-member liquids from this study see discussion for how the calculation was done).The North Range quartz diorite bulk rock compositions are shown plotted (D.E. Ames, pers. comm. 2013) as well as the two-liquid field in the system leucite-fayalite-silica (Roedder, 1979 after Jakobsen et al., 2011).

Figure 2 (opposite page). Melt inclusions hosted in apatite from the North Range Main Mass and offset dykes. Representative melt inclusion types in apatite in (a–g) the Transition Zone Gabbro, (h–l), leucocratic quartz diorite Whistle offset, and (m–o) quartz diorite, Pele offset. **a)** Unhomogenized melt inclusion. **b, c)** Homogenized melt inclusions that show a mixture of Fe- and Si-rich liquid. **d, e)** Homogenized Si-rich melt inclusions, as well as mixed melt inclusions. **f)** A single apatite grain that has trapped both pure end-member Fe-rich homogenized melt inclusions, as well as mixed. **g)** Homogenized Si-rich melt inclusion. **h)** Unhomogenized melt inclusion. **i, j, k)** Large vapour bubble in fluid inclusions from the Whistle offset dyke. **l)** Heterogeneously trapped mixed melt inclusion and fluid inclusion in a single apatite grain from the Whistle offset dyke. **m)** Unhomogenized melt inclusion from the Pele offset dyke (PPL). **n, o)** Homogenized melt inclusions from the Pele offset dyke (plane polarized light). Abbreviations: SB = shrinkage bubble; SMI-Fe = silicate melt inclusion that is Fe-rich; SMI-Si = silicate melt inclusion that is Si-rich; SMI-Si/Fe = silicate melt inclusion that has trapped both end-member types; XPL is cross polarized light.

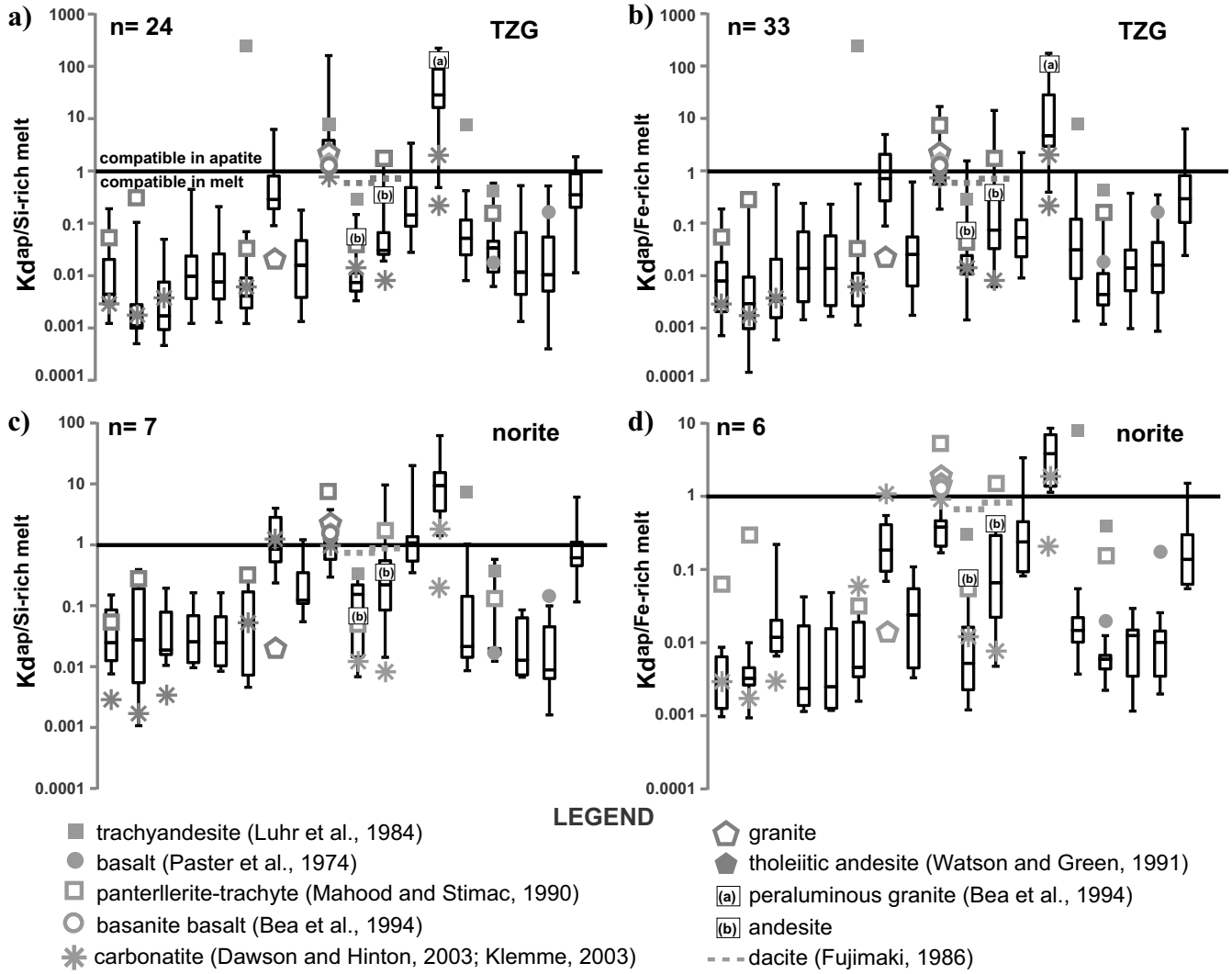

Figure 4. Box-and-whisker plots of the Kd values between apatite and melt inclusions in the Main Mass. **a)** Kd values for the Si-rich melt of the Transition Zone Gabbro (TZG). **b)** Kd values for the Fe-rich melt inclusions of the TZG. **c)** Kd values for the Si-rich melt inclusions of the norite. **d)** Kd values corresponding to the Fe-rich melt of the norite.

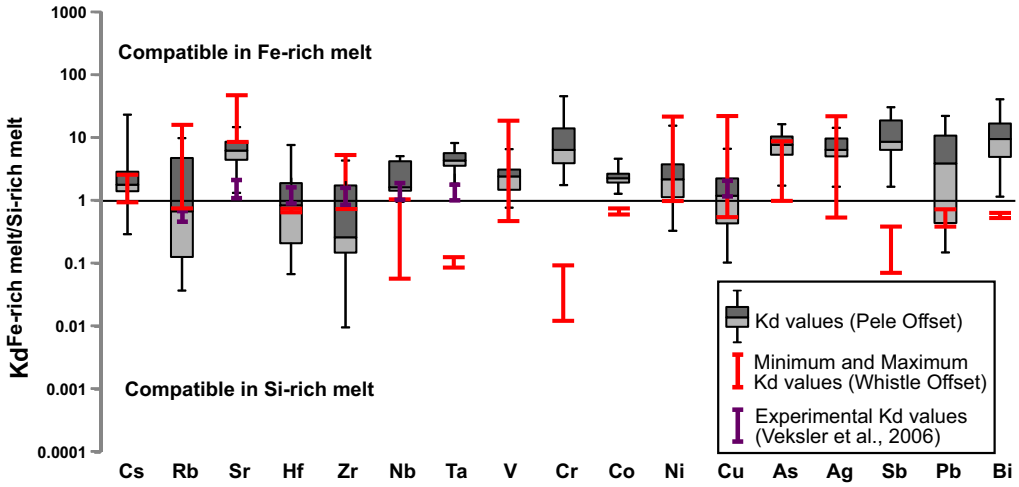

Figure 5. Plot of Kd values between Si-rich and Fe-rich melt in the Pele and Whistle offset dykes. The Kd values for trace elements between Fe- and Si- rich melt inclusions for the Pele offset dykes are shown as box-and-whisker plots, which show that these values are close to 1 and compare favourably to what has been found experimentally (Veksler et al., 2006). The exceptions noted are Sr, the incompatible elements (Nb, Ta), and Sr, Cr, As, Ag, Pb, Sb, and Bi, which show slight affinities for the Fe-rich melt.

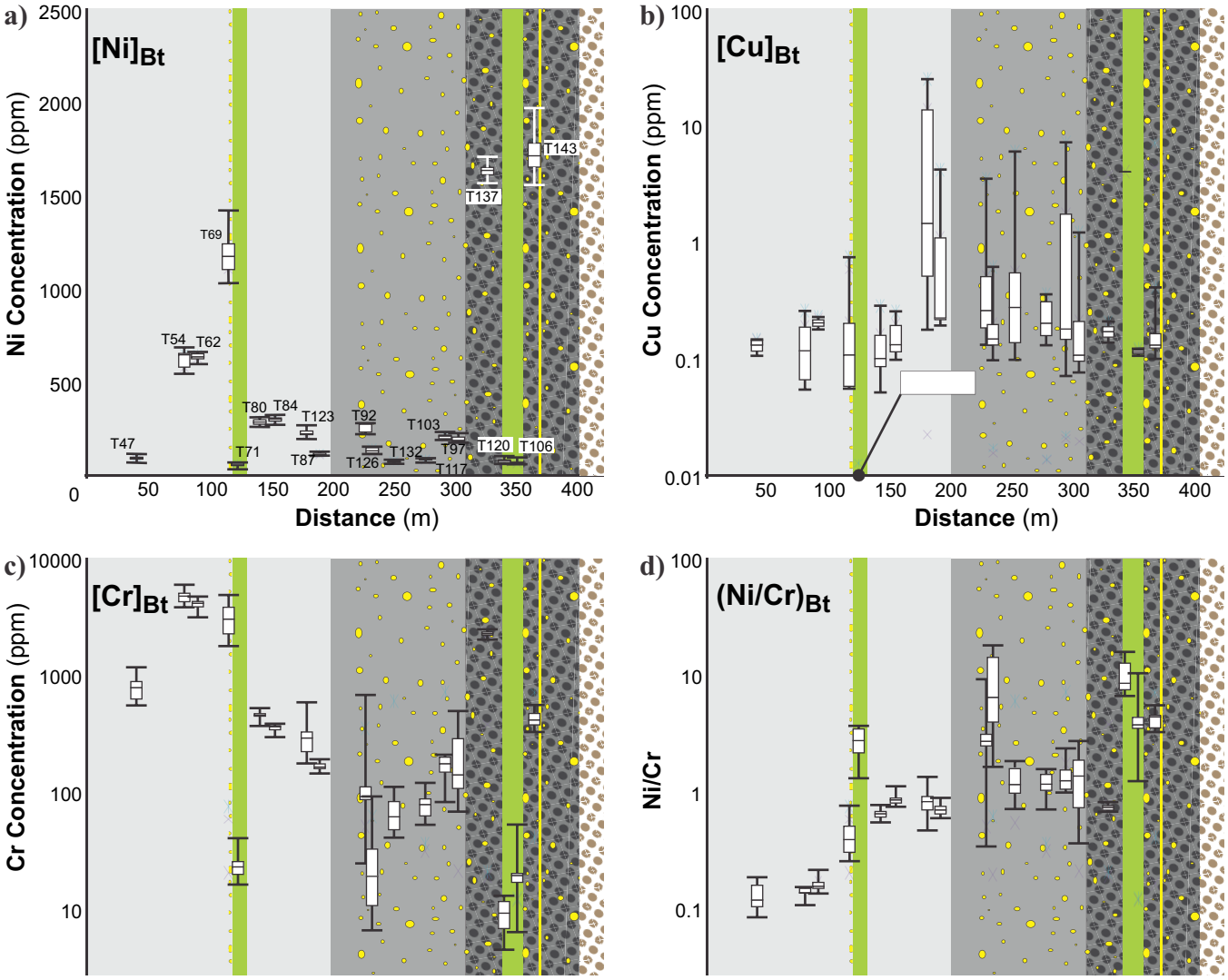

Figure 6. Box-and-whisker plots of the **(a)** $(Ni)_{Bt}$, **(b)** $(Cu)_{Bt}$, **(c)** $(Cr)_{Bt}$, and **(d)** $(Ni/Cr)_{Bt}$ in samples at different distances from the massive sulphide mineralization hosted in IQD (traverse through Totten mine diamond drill hole 1265980 running perpendicular to the dyke trend; based showing lithologies logged from drill core and sample numbers at their positions downhole below collar. All samples contained only type III biotite with the exception of T137 and T143 (type I biotite) and T54, T62 and T69 (type II biotite). For each sample the maximum, minimum, first quartile (upper box), third quartile (lower box), and mean (separation between boxes) values are shown. For Cu, where some values were BDL, the data are shown for only those analyses that were above DL. Although sulphides are shown in both quartz diorite (QD) and inclusion-rich quartz diorite (IQD), the relative proportions of disseminated sulphide mineralization are not distinguished, and the occurrence of massive sulphides are restricted to IQD. Generally, biotite from the sulphide ore-associated IQD has elevated Ni relative to QD and the surrounding country rocks, however anomalously elevated Ni was measured in some country rock biotite. Variable and elevated concentrations of Cu were measured in biotite from QD and country rocks adjacent to IQD, correlating to an increase in the proportion of secondary chalcopyrite in the envelope of rock surrounding IQD. With the exception of Sudbury diabase dykes in which concentrations of Cr in biotite are consistently low relative to other lithologies, Cr concentrations are highly variable and show no systematic variations with distance to mineralization. The Ni/Cr in biotite increases east of a Sudbury diabase dyke hosted within the Huronian country rocks. After Warren et al. (2015).

ground) occurs within barren to weakly mineralized, sublayer quartz diorite and adjacent Huronian metasedimentary rocks within ~200 m of massive sulphide, whereas enrichment in Ni occurs only within the inclusion-rich quartz diorite (Fig. 6). Three distinct populations of Ni- and Cr-enriched biotite were distinguished based on textural and chemical criteria (Fig. 7): (i) type I — isolated, euhedral laths only within inclusion-rich sublayer quartz diorite (IQD; the main mineralized host lithology), and high Ni (>1400 ppm and up to ~2700 ppm) and variable Cr (up to ~2400 ppm) concentrations and variable Ni/Cr ratios (>2); (ii) type II — coarse-grained poikiloblasts (enclosing amphibole, chlorite, and type III biotite) within country rocks, and having moderate to high Ni (~500–1400 ppm) and high Cr (≤6000 ppm) concentrations but low Ni/Cr ratios

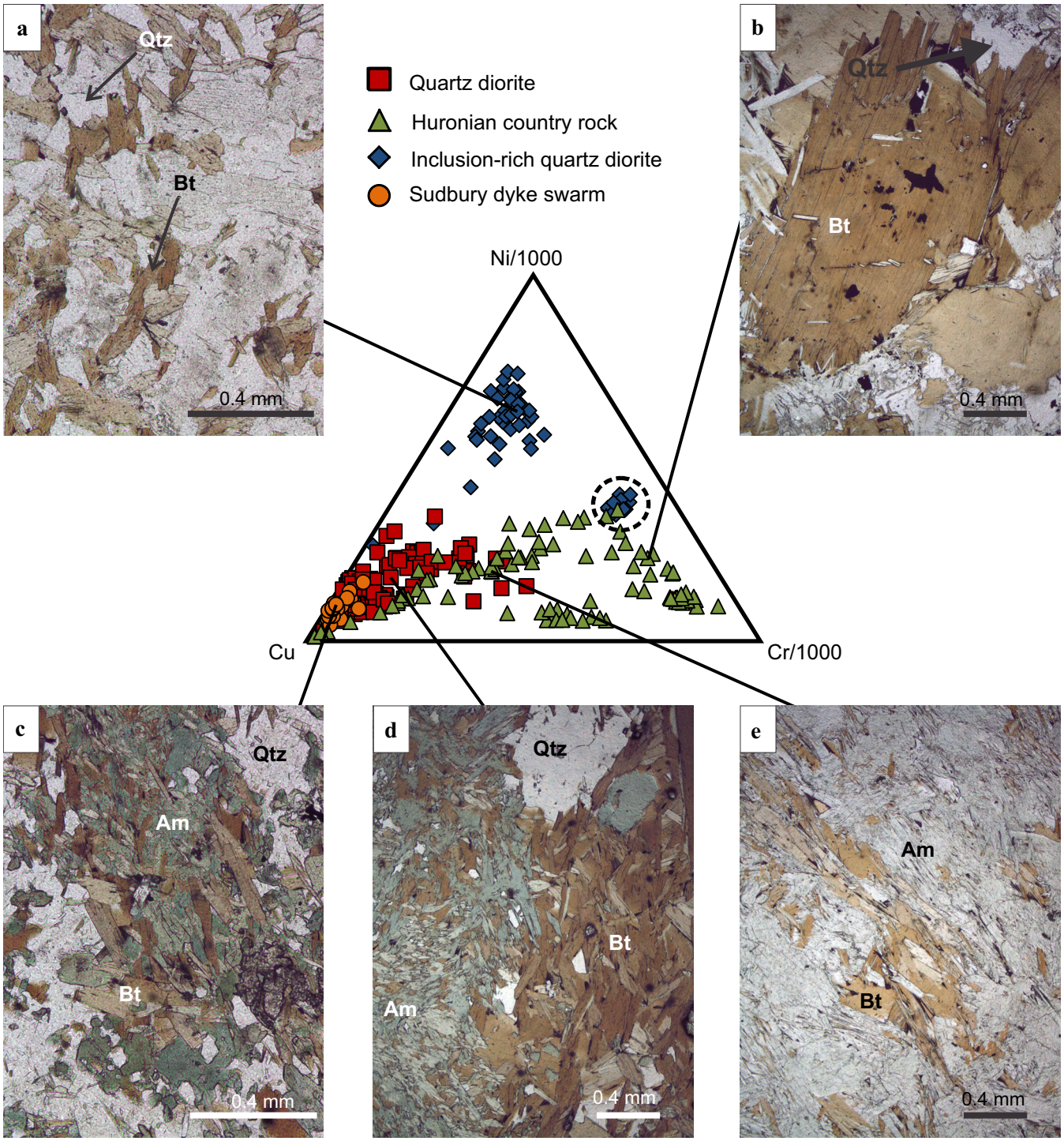

Figure 7. Photomicrographs (transmitted plane polarized light) and compositional fields on a Ni-Cr-Cu ternary diagram (ppm-basis) for biotite populations (by lithology). **a)** High-Ni, type I biotite from mineralized inclusion-rich quartz diorite (IQD). **b)** High-Cr, type II biotite from Huronian country rocks. **c–e)** Variable composition, type III biotite from barren QD, Huronian country rocks, and late Sudbury dykes. Abbreviations: Am = amphibole; Bt = biotite; Qtz = quartz. Analyses of biotite within the dashed circle represent a sample logged and identified (incorrectly) as IQD but with biotite composition characteristic of type II and III biotite, indicating a sample of country rock or barren QD (or inclusion or country rock or barren QD within IQD). After Warren et al. (2015).

(<0.5); and (iii) type III — subhedral to euhedral laths, intergrown with amphibole in dense, foliated aggregates and having low Ni (<300 ppm) and low to moderate Cr (<1200 ppm) concentrations and high Ni/Cr ratios (≤ ~20), found within Huronian country rocks, sublayer quartz diorite (QD), and crosscutting diabase dykes (Sudbury dyke swarm). Two different controls on Ni and Cr cation substitution in biotite were identified: (i) biotite with low Ni+Cr concentrations (<1000 ppm) that show a positive correlation with X_{Mg}, indi-

cating crystallographic controls (e.g. avoidance and permissibility phenomena); (ii) biotite with high Ni+Cr concentrations (>1000 ppm) showing no correlation with XMg, suggesting another control (e.g. host-rock chemistry, proximity to sulphides, or availability of Ni and Cr in magmatic-hydrothermal volatiles) that influences biotite chemistry.

Stable Isotope, Alteration, and Fluid Inclusion Fingerprints of "Low-Sulphide" Mineralization in the Footwall

The North Range footwall of the Sudbury Igneous Complex (SIC) hosts numerous small-volume (relative to other SIC-associated deposits) Cu-Ni-PGE mineral deposits that have seen progressively increasing exploration interest within the last decade due to their high base metal (Cu, Ni) contents and precious metal (Pt, Pd, Ag, and Au) tenors. Farrow et al. (2005) separated footwall deposits at Sudbury into "high-sulphide" (sharp-walled vein) and "low-sulphide" (PGE-rich) systems based on their ore mineralogy, alteration mineralogy, and bulk rock chemistry. Both deposit types have significant representation in the literature and current models for their geneses attribute the formation of high-sulphide mineralization to magmatic/magmatic-hydrothermal mechanisms and/or remobilization by high-temperature volatiles Li et al., 1992; Naldrett et al., 1999; Péntek et al., 2008; Hanley et al., 2011, etc.) and the formation of low-sulphide mineralization to circulating (metal-loaded) hydrothermal fluids (e.g. Péntek et al., 2008; Nelles et al., 2010; Tuba et al., 2010, 2014; White, 2012; etc.). Crosscutting considerations indicate that the formation of low-sulphide mineralization occurred before the deposition of high-sulphide veins. However, at present there is no general characterization in the literature of many of the fluid conditions (fluid sources, transport mechanisms, ambient fO_2 of fluids, fluid compositions, etc.) that resulted in the precipitation of low-sulphide high-PGE systems.

The variable types of low sulphide mineralization are most commonly distinguished on textural (i.e. veinlets, disseminations, blebs, stringers, etc.) and/or mineralogical (alteration phases, precious metal mineral assemblages) bases (Farrow et al. 2005; Gibson et al. 2010; Nelles et al., 2010; Tuba et al. 2010, 2014; White, 2012; Péntek et al., 2013) but general characteristics that encompass all low-sulphide subtypes are (i) <5 volume percent (%) Cu- and Ni-sulphide minerals (bornite, chalcopyrite, millerite), (ii) elevated (can be an order of magnitude higher) bulk rock PGE/S compared to high-sulphide veins, and (iii) hydrous alteration phases intergrown with the ore minerals (sulphide minerals, precious metal minerals). The most common alteration assemblage in low-sulphide environments consists of quartz+epidote+chlorite packages that enclose mineralization; however, more calcic alteration may be observed with the addition of calcite and calcic amphibole to the alteration assemblages.

Alteration assemblages containing hydrothermal garnet are reported for the first time associated with "low-sulphide" high-PGE footwall Cu-Ni-PGE mineralization in a calcite-quartz-garnet-epidote-chlorite-amphibole-sulphide vein from Level 5080 of the Coleman 153 (Vale) orebody (Fig. 8). The garnet exhibits two different growth zones on the basis of their composition (andradite cores, grossular-rich rims) and the sulphides (bornite, chalcopyrite, millerite) are coeval with the grossular-rich rims on garnet as well as the surrounding calcite (~80 vol%) matrix. Calcite-hosted fluid inclusions (Fig. 9) are two phase liquid-vapour (L-V) and are separated into two populations: (1) 23.65 wt% eq. NaCl and (2) 8.26 wt% eq. NaCl. Homogenization temperatures recorded for all reported fluid inclusions have an average of 140.2°C and range from 90.1 to 210.0°C. Secondary ion mass spectrometry (SIMS) analyses were conducted on 10 (sulphide-coeval) calcite grains and the average $\delta^{18}O$ value for these analyses is 5.1 ± 1.2‰, resulting in calculated $\delta^{18}O$ values (O'Neil et al., 1969) of -11.5‰ and -0.02‰ at 100°C and 300°C, respectively, for the hydrothermal fluid at the time of sulphide precipitation.

DISCUSSION AND MODELS

Evolution of the Sudbury Igneous Complex Indicated from Silicate Melt Inclusions

The mass proportion of immiscible Fe-rich to Si-rich liquids (~1:4.5) predicted through melt-inclusion characterization is in close agreement with the volume of granophyric liquid predicted from experiments modelling the fractional crystallization of the SIC melt sheet. However, these experiments have shown that fractional crystallization alone does not account for the observed 1:3 ratio of norite to granophyre along the North Range. Importantly, trapped (immiscible?) Si-rich liquid lower in the SIC must be taken into consideration. If one considers immiscibility as a petrogenetic process for the SIC melt sheet, it may explain the large amount of granophyre in the SIC that has been so poorly understood in the past.

Apatite-hosted melt inclusions from the mineralized Whistle offset dyke are enriched in Ni by up to 4 orders of magnitude compared to melt inclusions trapped in units stratigraphically higher in the SIC, reflecting the loss of these metals to sulphide liquids prior to the crystallization of these units in the SIC. The absence of enrichment in Ni and Cu in melt inclusions from the unmineralized Pele offset dyke suggests that proximity of the trapped melt to the orebodies may influence their

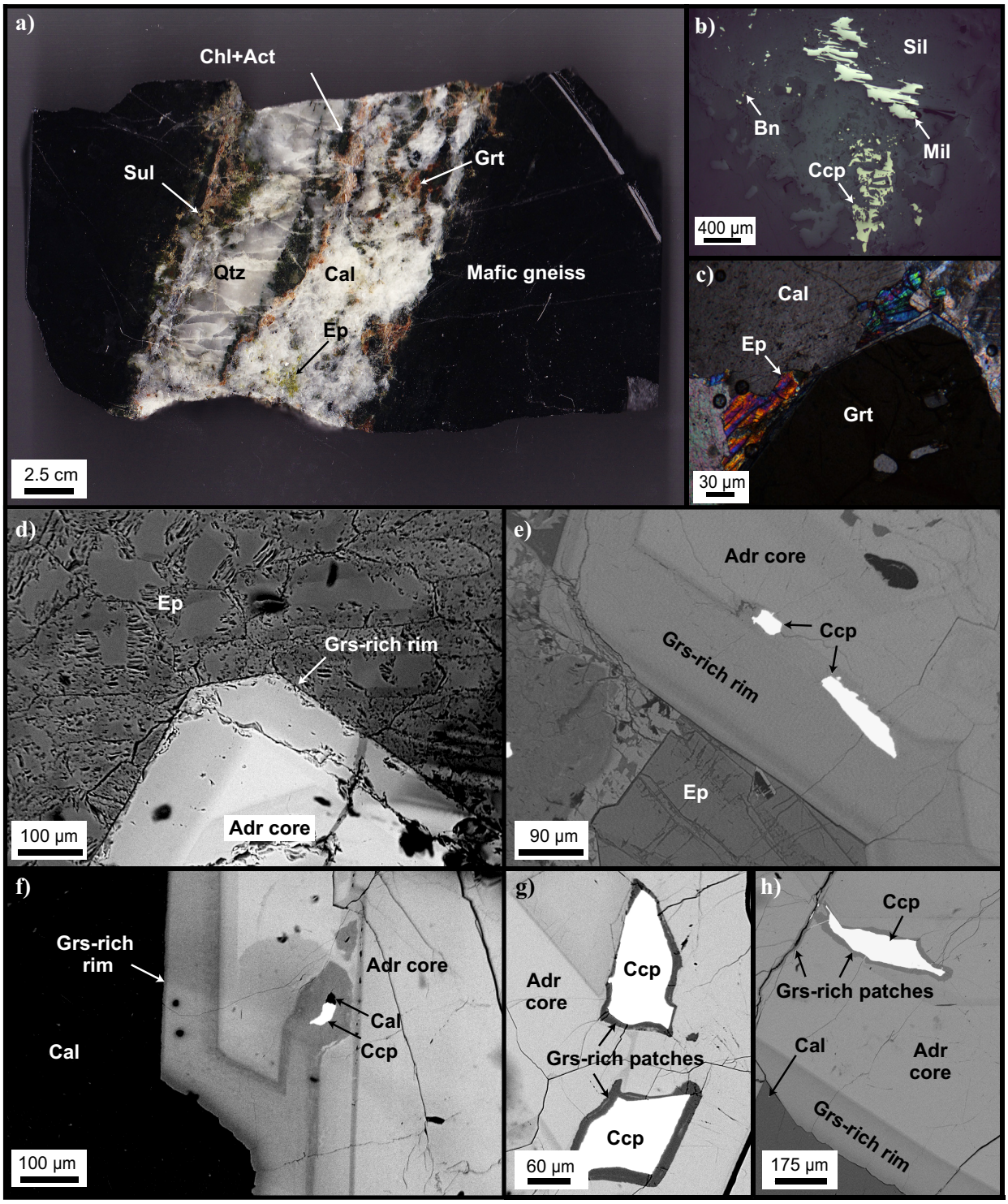

Figure 8. Mineralogical characteristics of the hydrothermal garnet-bearing "low-sulphide" assemblage. **a)** Representative hand sample from a vein displaying a calcite-quartz matrix hosting garnet crystals and patches of epidote, amphibole, chlorite, and sulphides. **b)** Bornite disseminations and networks of chalcopyrite and millerite within a silicate host (plane polarized light). **c)** Garnet hosted in a calcite matrix and in equilibrium with granular epidote (cross-polarized light). **d)** Euhedral crystal of garnet (grossular-rich rim/andradite core) in equilibrium with granular epidote. **e)** Chalcopyrite inclusions hosted in the grossular-rich rim on a garnet crystal. The garnet is in contact with epidote along the outer edge of its rim. **f)** Calcite and chalcopyrite inclusions within the grossular-rich rim of a calcite-hosted garnet crystal. The garnet core is andraditic in composition. **g)** Inclusions of chalcopyrite hosted in grossular-rich patches within the andradite core of a garnet crystal. **h)** Chalcopyrite hosted in a grossular-rich patch within the andradite core of (calcite-hosted) garnet. Grossular-rich patches also occur along the edge of a crack that runs through the andradite core of garnet near the chalcopyrite inclusion (top left). Abbreviations: Act = actinolite; Adr = andradite; Bn = bornite; Cal = calcite; Ccp = chalcopyrite; Chl = chlorite; Ep = epidote; Grs = grossular; Grt = garnet; Mil = millerite; Qtz = quartz; Sil = silicates; Sul = sulphides.

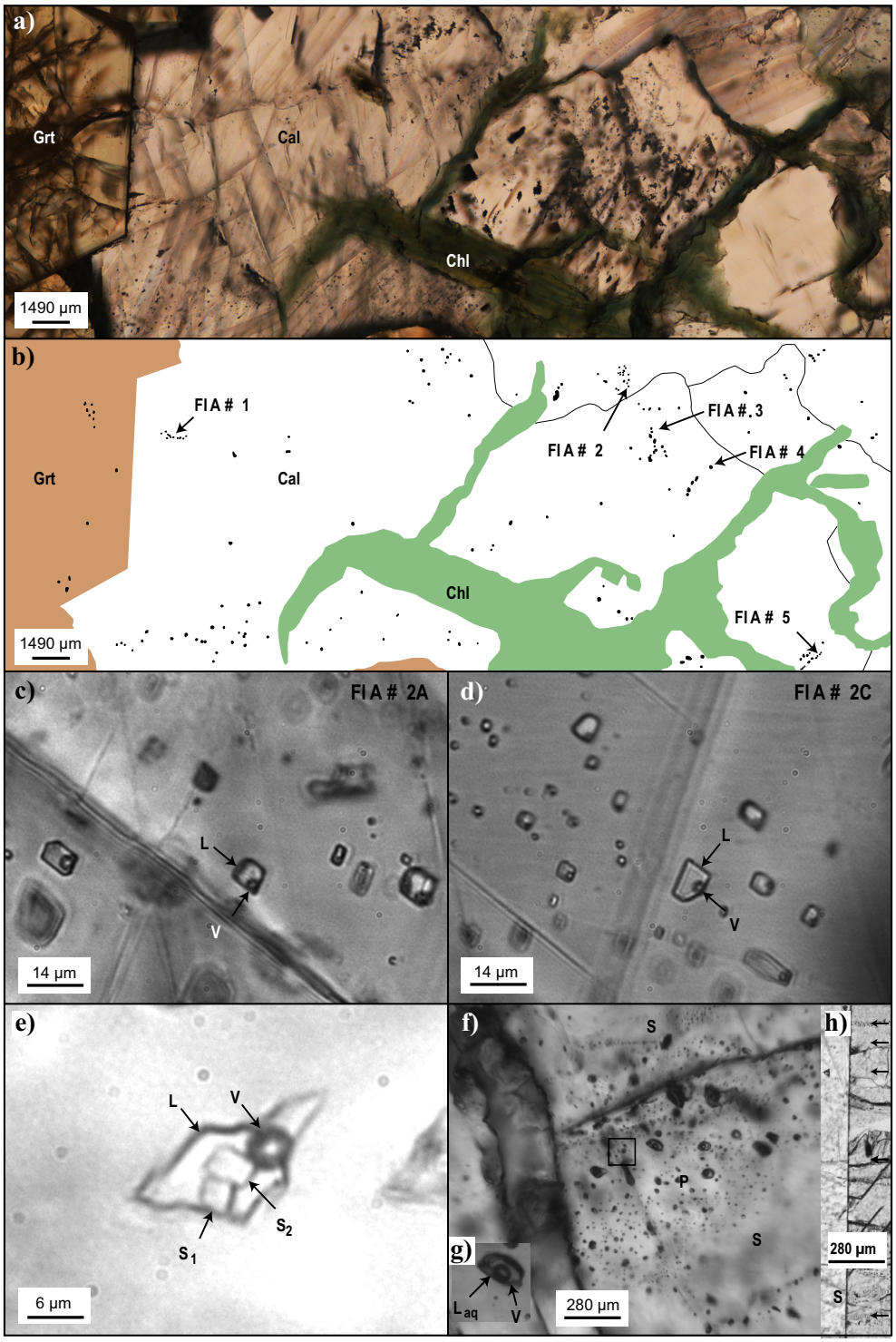

Figure 9. General fluid inclusion characteristics of hydrothermal garnet-bearing "low-sulphide" assemblages. **a)** Photomicrograph displaying the area where fluid inclusion assemblages of interest were analyzed in this study (plane polarized light). **b)** Fluid inclusion map illustrating photomicrograph (a) and the relative locations of the 5 fluid inclusion assemblages (FIA) addressed in this section. **c)** Calcite-hosted trail of primary liquid-vapour (L-V) inclusions at FIA # 2a. **d)** Calcite-hosted trail of primary L-V inclusions at FIA # 2c. **e)** Calcite-hosted liquid-vapour-solid (L-V-S) inclusion of uncertain origin. Measure-ments were not taken on this inclusion and the compositions of the daughter minerals (S_1 and S_2) are not known. This inclusion was not present within the field of view presented in (a, b). **f)** Garnet-core-hosted trails of primary (P) and secondary (S) L-V inclusions. These inclusions were situated outside of the field of view presented in (a, b). **g)** Magnified view of the garnet-core-hosted primary L-V inclusion outlined by the black square in photomicrograph (f). **h)** Segment of a garnet (left) – calcite (right) contact. Secondary fluid inclusion trails in garnet run perpendicular to garnet growth zones and exhibit abrupt terminations at garnet crystal edges (i.e. do not continue into calcite). Five of these trails are highlighted by black arrows. Abbreviations: Cal = calcite; Chl = chlorite; Grt = garnet.

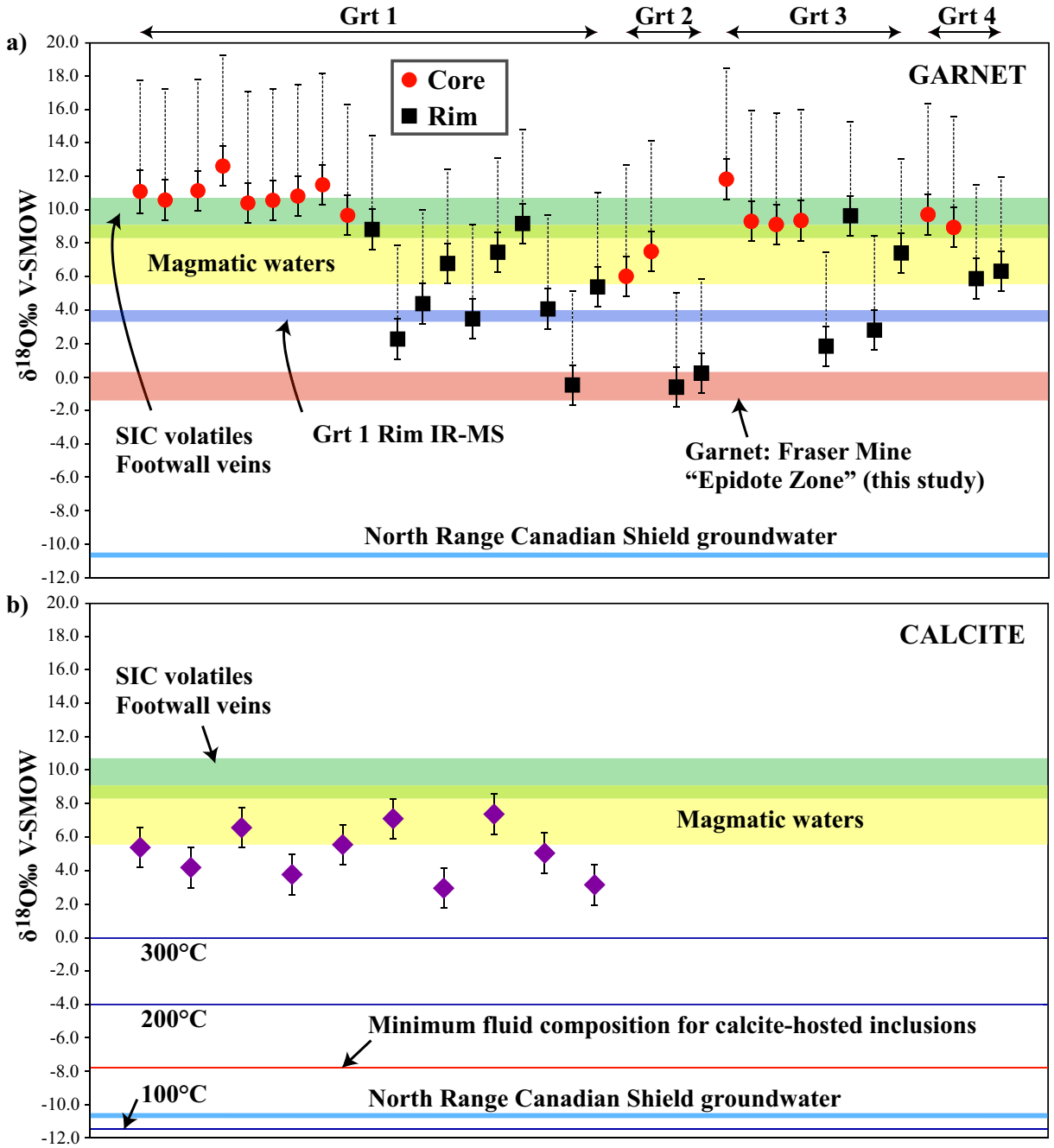

Figure 10. δ18O in garnet and calcite from hydrothermal garnet-bearing "low-sulphide" mineralization. **a)** δ18O‰ V-SMOW results for core and rim spot analyses across 4 garnet grains. Standard deviations are reported at 1σ and all analyses were calibrated using standard UWG-2. Additional positive error bars (dashed lines) account for the inherent instrumental bias in garnet relative to UWG-2, which varies as a function of garnet composition. The average core composition from 15 garnet grains analyzed in this study is $Adr_{99.27}Prp_{0.54}Grs_{0.45}Sps_{0.02}$, which closely matches garnet standard 92LEW7 ($Adr_{89}Grs_{6}Alm_{4}Prp_{1}$). Page et al. (2010) reported an average instrumental bias of +6.69‰ for 92LEW7 when calibrating analyses against UWG-2. The average rim composition from 38 garnet grains analyzed in this study is $Adr_{53.73}Grs_{44.92}Sps_{0.60}Prp_{0.14}Uva_{0.02}$, which closely matches garnet standard 92LEW10 ($Adr_{50}Grs_{42}Alm_{4}CaTi_{2}Prp_{2}$). Page et al. (2010) reported an average instrumental bias of +5.64‰ for 92LEW10 when calibrating analyses against UWG-2. The rim of one garnet (Grt 1) was also analyzed at Queen's University using a Finnigan Mat 252 isotope ratio mass spectrometer (IR-MS) and is represented by the dark blue band. Fields for magmatic waters (Marshall et al., 1999), North Range Canadian Shield groundwater (Kaufmann et al., 1987), SIC volatiles (scapolite; Hanley et al., 2011), footwall veins (sharp-walled vein-associated calcite and quartz; Farrow, 1994), and garnet from alteration assemblages (see text) at the Fraser Mine's "Epidote Zone" (Farrow, 1994) are also illustrated. **b)** δ18O‰ V-SMOW results for 10 spot analyses of calcite grains. Standard deviations are reported at 1σ and all analyses were calibrated using Jop-Cal. Average δ18O V-SMOW for the calcite-forming fluid were calculated at 100°C, 200°C, and 300°C using an equation from O'Neil et al. (1969) and are superimposed on this figure. "Minimum fluid composition for calcite-hosted inclusions" was calculated using the average fluid inclusion T_h measured in calcite and the equation from O'Neil et al. (1969).

metal content. The results of this study have implications for our understanding of the petrogenesis of the SIC melt sheet and the potential effects of sulphide saturation in the presence of immiscible Si- and Fe-rich liquids. Melt inclusion compositions may provide an important proxy for distance to orebodies in the margin of the SIC. The study provides the first in-situ determination of actual ore metal concentrations from early trapped melt of the SIC and trace element partitioning behaviour between immiscible liquids in nature.

Pathfinder Mineral Chemistry in the Sublayer Environment

Type I biotite within IQD is compositionally distinct from those observed in all other lithologies associated with the Sudbury Igneous Complex and its footwall rocks, and can be most readily discriminated in a Ni/Cr versus Ni binary diagram or in a Ni-Cr-Cu ternary diagram by anomalously high Ni content and a Ni/Cr ratio of >2. However, application of such diagrams requires caution. An examination of biotite chemistry in the Sudbury district shows that Ni (and likely Cr) concentrations in biotite vary greatly between different environments (both barren and ore-hosting), indicating the importance of establishing local "background" Ni concentrations in biotite in order to identify what is truly anomalous for that environment. Second, large ranges in Ni-in-biotite data reported previously from microprobe analyses result from analyses not representative of true dissolved concentrations. Introduction of false-anomalous Ni contents in biotite and a high degree of heterogeneity within sample sets may occur where biotite (i) contains discrete sulphide micro-inclusions that contaminate the analytical volume; (ii) occurs in direct contact with coeval sulphide minerals that caused localized changes in biotite composition; and (iii) was altered to chlorite, a process that modified primary metal abundances. Though routine microprobe analysis may be used to discriminate ore-diagnostic biotite using the Ni-Cr-Cu characteristics reported here, LA-ICPMS should be considered to allow identification/selective removal of sulphide inclusions and localized chemical zoning in biotite that is unrelated to lithology-pervasive, primary chemical composition.

Stable Isotope, Alteration, and Fluid Inclusion Fingerprints of "Low-Sulphide" Mineralization in the Footwall

Shifts towards lighter $\delta^{18}O$ values from the paragenetically-early garnet cores (10.0‰) to the synsulphide precipitation rims (4.7‰) track progressive interaction with and dilution by ($CaCl_2$-rich) isotopically-light North Range groundwater (Kaufmann et al., 1987): -10.8 to -10.5‰ (Fig. 10). Recent studies (Hanley et al., 2005; Kerr and Hanley, 2013) have shown that the fluid associated with low-sulphide mineralization was hydrocarbon-rich and numerous observations in this study (sulphide/gangue relationships, garnet trace element zoning, garnet-epidote equilibria chemistry, presence of primary sulpho-bismuthide minerals) indicate that this fluid became more reducing over its evolution. Progressive mixing of meteoric groundwater with hydrocarbon/metal-rich aqueous fluids can achieve both carbonate and sulphide precipitation as well as lower the ambient oxygen fugacity of the mineralizing system. Calcium-rich alteration (calcite, garnet, epidote, calcic amphibole) within the low-sulphide assemblage, which is the focus of this study, represents an apparent end-member to the low-sulphide continuum; where the mineralizing fluid has experienced the most interaction with $CaCl_2$ groundwater. Low Pt+Pd grades and the absence of Pt- and Pd-PGM in this calcium mineral-rich vein suggests that the mineralizing hydrothermal fluid lost the majority of its PGE load at an earlier point in its evolution. Anomalously high Au grades coupled with the presence of primary electrum suggest Au deposition was not temporally linked with the precipitation of the PGM and persisted to the extremities of low-sulphide footwall systems.

IMPLICATIONS FOR EXPLORATION

Melt Inclusion and Apatite Trace Element Chemistry in the Sudbury Igneous Complex Main Mass and Sublayer

Variations in melt composition of different units of the SIC, and in different areas of the SIC, near and distal to sulphide orebodies in the footwall-contact area enables the identification of spatial differences in interstitial melt composition resulting from sulphide separation, indicating melt chemistry (and host apatite chemistry, by association) is an appropriate exploration tool in delineating "metal-depleted" versus "metal-fertile" regions of the SIC sublayer. The immiscible melts found in the SIC Main Mass are devoid of metals compared to melt inclusions from the mineralized quartz diorite in the Whistle offset dyke. The absence of Ni and Cu in melt inclusions from the unmineralized Pele offset and Main Mass of the SIC may reflect loss of these metals to early sulphide liquids, however, if the differentiation of immiscible liquids resulted in a density-stratified melt prior to in situ crystallization processes, the most basal layers in the density-stratified melt sheet would be more mafic and may crystallize the Ni- and Cu-rich sulphide (Lightfoot et al., 2001). The Ni-rich apatite-hosted melt inclusions from the Whistle offset are, therefore, likely a result of trapped immiscible liquid that was in equilibrium with sulphide liquid. Apatite-hosted melt inclusions that were compared between mineralized (Whistle) and unmineralized (Pele) offset dykes revealed that melt inclusions in

close proximity to mineralization contain high (>400 ppm) amounts of Ni. In addition, apatite from the Whistle offset contained the highest amounts of Cu and As. These findings are comparable to what is found in apatite from the mineralized footwall and may be applicable to exploration in the SIC. The conclusions of this study suggest that apatite-hosted melt inclusions from the Whistle offset dyke were in equilibrium with sulphide liquids at the time of their entrapment. Therefore, the metal content of apatite-hosted melt inclusions (and by partitioning association, the apatite host phase itself) in the basal portions of the SIC may serve as a proxy for distance to orebodies within the SIC sublayer, including offset dyke settings.

Biotite Chemistry in the Sublayer

There are two potential applications of the biotite chemistry to exploration. First, in drill core (or surface mapping involving outcrop or till/rubble surveying), differentiation between QD and IQD can be confirmed through analysis of $[Ni]_{Bt}$, provided that the identity of the rock type in question has been confirmed as quartz diorite. The threshold for $Ni_{biotite}$ in inclusion-rich versus inclusion-free phases is proposed tentatively at ~1500 ppm, a concentration level that can be readily identified using LA-ICP-MS, electron microprobe, or even SEM-EDS, provided adequate counting times are utilized during spectrum collection. Textural scrutiny and determination of the absolute concentration of Nibiotite are not essential in this case since inclusion-rich QD contains only a single, high-Ni variety of biotite and inclusion-poor QD biotite is consistently very low in Ni (<300 ppm). Textural analysis can be used to confirm that high-Ni biotite is of the magmatic, "type III" variety described here. Generally, this application may encourage more careful delineation of the two phases of QD in offsets and, although bulk rock assays may be ambiguous, especially at low-sulphide abundances in IQD, biotite compositions consistently show enrichment in Ni and elevated Ni/Cr ratios. The results may be extended to other mafic-ultramafic systems where sulphide-saturated or metal-enriched intrusive phases grew metal-enriched biotite during primary crystallization or through secondary processes of metasomatic enrichment involving remobilization of base metals by magmatic-hydrothermal fluids.

Second, a broader reaching application to surface exploration in uncharacterized and variably covered areas is proposed that involves the analysis of biotite and its weathering products in regolith. In this scenario, the target material is grains of fresh biotite, or secondary hydrobiotite or vermiculite liberated from sulphide-associated mafic lithologies through erosion and weathering. Micaceous grain populations with the characteristically high Ni (> ~1400 ppm) and elevated Ni/Cr ratio (>2) should be suspected as having been liberated from inclusion-rich quartz diorite hidden at depth (if soil formation had been in situ) or distally in cases where micaceous sediment transport by wind or water has occurred. Biotite readily alters at surface conditions and, depending on the "strength" of chemical weathering, it may generate a variety of alteration products (e.g. vermiculite, chlorite, clay minerals, and Fe-oxide minerals; Wilson, 2004, and references therein). The weathering of biotite may begin with vermiculation through the replacement of K by other cations (which may be controlled by the amount of K contained within external solutions; Martin and Sparks, 1985) as well as the loss of octahedral Fe through oxidation (Barshad 1948; Walker, 1949; Rausell-Colom et al., 1964; Newman and Brown, 1966). Despite these structural changes, Gilkes and Suddhiprakarn (1979) have shown in saprolite and pallid zones of lateritic profiles that primary Ni and Cr are largely retained during soil formation, remaining in the most advanced alteration products of biotite (vermiculite, clays) at concentrations equivalent to their primary levels in the protolith. Therefore, the criteria here may be applicable to exploration in a diversity of environments, even those showing advanced stages of chemical weathering. However, the importance must be stressed of establishing bulk compositional or textural criteria to discriminate different types of biotite recovered from regolith, and where possible, establishing "background" levels of Ni and Cu enrichment in representative basement lithologies in a prospective study area.

Stable Isotope, Alteration, and Fluid Inclusion Fingerprints of "Low-Sulphide" Mineralization in the Footwall

Changes in fluid chemistry (reduction, dilution, neutralization, cooling) associated with early mixing events in the footwall are recognizable through systematic mapping of alteration mineralogy and stable isotopes. These changes were responsible for the dissociation of metal complexes leading to the precipitation of base and precious metals. In particular, identification of zones where mixing between calcic, high-salinity brines and oxidized metal-rich fluids (possibly derived from the SIC contact region) took place should be a priority for exploration. Identification of the original fluid pathways (from contact to footwall) within complex structural zones linking the footwall and contact environments is stressed.

FORTHCOMING RELEASES

The study of melt-inclusion chemistry and its applications to understanding SIC evolution and ore formation will be submitted to *Journal of Petrology* in 2015. The study of fluid chemistry, alteration, and stable isotope

systematics of low-sulphide systems will be submitted to *Mineralium Deposita*, in 2015. An article outlining the trace element chemistry of biotite and its application to routine exploration will be published in the *Journal of Geochemical Exploration* in June, 2015 (Warren et al., 2015).

ACKNOWLEDGEMENTS

The authors wish to acknowledge NSERC (Discovery Grant to JH), Vale Canada (Ontario Operations), and the TGI-4 program for research and stipend funding that enabled this multi-faceted project. Joe Petrus at Laurentian University (MERC), Simon Jackson (GSC Ottawa), Ryan Sharpe and Mostafa Fayek (University of Manitoba), and Chris McFarlane (UNB) are acknowledged for their invaluable assistance in obtaining the LA-ICP-MS and SIMS analyses.

REFERENCES

Ames, D.E. and Farrow, C.E.G., 2007. Metallogeny of the Sudbury mining camp, Ontario, *In:* Mineral deposits of Canada: A Synthesis of Major Deposit Types, District Metallogeny, the Evolution of Geological Provinces, and Exploration Methods, (ed.) W.D. Goodfellow; Geological Association of Canada, Mineral Deposits Division, Special Publication 5, p. 329–350.

Ames, D.E., Golightly, J.P., Lightfoot, J.P., and Gibson, H.L., 2002. Vitric compositions in the Onaping formation and their relationship to the Sudbury Igneous Complex, Sudbury Structure; Economic Geology, v. 97, p. 1541–1562.

Ames, D.E. and Kjarsgaard, I.M., 2013. Sulphide and alteration mineral chemistry of low- and high- sulphide Cu-PGE-Ni deposits in the footwall environment, Sudbury, Canada; Geological Survey of Canada, Open File 7331, 1 sheet.

Ariskin, A. A., Deutsch, A., and Ostermann, M., 1999. Sudbury Igneous Complex: Simulating phase equilibria and in situ differentiation for two proposed parental magmas, *In:* Large Meteorite Impacts and Planetary Evolution II, (ed.) B.O. Dresser and V.L. Sharpton; Geological Society of America, Special Paper 339, p. 373–388.

Barshad, I., 1948. Vermiculite and its relation to biotite as revealed by base exchange reactions, X-ray analysis, differential thermal curves and water content; American Mineralogist, v. 33, p. 655–678.

Bea, F., Pereira, M.D., and Stroh, A., 1994. Mineral/leucosome trace element partitioning in a peraluminous migmatite (a laser ablation-ICP-MS study); Chemical Geology, v. 117, p. 291–312.

Chai, G. and Eckstrand, R., 1994. Rare-earth element characteristics and origin of the Sudbury Igneous Complex, Ontario, Canada; Chemical Geology, v. 113, p. 221–244.

Coats, C.J.A. and Snajdr, P., 1984. Ore deposits of the North Range, Onaping-Levack Area, *In:* The Geology and Ore Deposits of the Sudbury Structure, (ed.) E.G. Pye, A.J. Naldrett, and P.E. Giblin; Ontario Geological Survey, Special Publication 1, p. 327–346.

Cochrane, L.B., 1984. Ore deposits of the Copper Cliff, *In:* The Geology and Ore Deposits of the Sudbury Structure, (ed.) E.G. Pye, A.J. Naldrett, and P.E. Giblin; Ontario Geological Survey, Special Publication 1, p. 347–360.

Corfu, F. and Andrews, A.J., 1986. A U-Pb age for mineralized Nipissing diabase, Gowganda, Ontario; Canadian Journal of Earth Sciences, v. 23, p. 107–109.

Dawson, J. and Hinton, R., 2003. Trace element content and partitioning in calcite, dolomite, and apatite in carbonate, Phalaborwa, South Africa; Mineralogical Magazine, v. 67, p. 921–930.

Dicken, A.P., Nguyen, T., and Crocket, J.H., 1999. Isotopic evidence for a single impact melting origin of the Sudbury Igneous Complex, *In:* Large Meteorite Impacts and Planetary Evolution II, (ed.) B.O. Dresser and V.L. Sharpton; Geological Society of America, Special Paper 339, p. 361–371.

Faggart, B.E., Basu, A.R., and Tatsumoto, M., 1985. Origin of the Sudbury Complex by meteoritic impact: neodymium isotopic evidence; Science, v. 230, p. 436–439.

Farrow, C.E.G., 1994. Geology, alteration, and the role of fluids in Cu-Ni-PGE mineralization of the footwall rocks to the Sudbury Igneous Complex, Levack and Morgan Townships, Sudbury District, Ontario; Ph.D. thesis, Carleton University, Ottawa, Ontario, 373 p.

Farrow, C.E.G. and Watkinson, D.H., 1997. Diversity of precious-metal mineralization in footwall Cu-Ni-PGE deposits, Sudbury, Ontario: Implications for hydrothermal models of formation; Canadian Mineralogist, v. 35, p. 817–839.

Farrow, C.E.G., Everest, J.O., King, D.M., and Jolette, C., 2005. Sudbury Cu-(Ni)-PGE systems: Refining the classification using McCreedy West mine and Podolsky project case studies, *In:* Exploration for Deposits of Platinum-Group Elements, (ed.) J.E. Mungall; Mineralogical Association of Canada, Short Course Series, v. 35, p. 163–180.

Fujimaki, H., 1986. Partition-coefficients of Hf, Zr, and REE between zircon, apatite, and liquid; Contributions to Mineralogy and Petrology, v. 94, p. 42–45.

Gibson, A.M., Lightfoot, P.C., and Evans, T.C., 2010. Contrasting styles of mineralization: North Range 148 zone versus South Range 109 FW zone, *In:* Abstracts, 11th International Platinum Symposium, 21–24 June 2010, Sudbury, Ontario, (ed.) G.H. Brown, P.L. Jugo, C.M. Lesher, and J.E. Mungall; Ontario Geological Survey, Miscellaneous Release-Data 269.

Gilkes, R.J. and Suddhiprakarn, A., 1979. Biotite alteration in deeply weathered granite. I. morphological, mineralogical, and chemical properties; Clays and Clay minerals, v. 27, p. 349–360.

Grant, R.W. and Bite, A., 1984. Sudbury quartz diorite offset dikes, *In:* The Geology and Ore Deposits of the Sudbury Structure, (ed.) E.G. Pye, A.J. Naldrett, and P.E. Giblin; Ontario Geological Survey, Special Publication 1, p. 275–300.

Grieve, R.A.F., Stoeffler, D., and Deutsh, A., 1991. The Sudbury structure: controversial or misunderstood?; Journal of Geophysical Research, v. 96, p. 22,753–22,764.

Guillong, M.M., Maier, D.L., Allan, M.M., Heinrich, C.A., and Yardley, B.W.D., 2008. Appendix A6: SILLS: a MATLAB based program for the reduction of laser ablation ICP-MS data of homogeneous materials and inclusions, *In:* Laser Ablation ICP-MS in the Earth Sciences: Current Practices and Outstanding Issues, (ed.) P. Sylvester; Mineralogical Association of Canada, Short Course Series, v. 40, p. 328–333.

Hanley, J.J. and Bray, C.J., 2009. The trace metal content of amphibole as a proximity indicator for Cu-Ni mineralization in the footwall of the Sudbury Igneous Complex, Ontario, Canada; Economic Geology, v. 104, p. 113 –125.

Hanley, J.J. and Mungall, J.E., 2003. Chlorine enrichment and hydrous alteration of the Sudbury Breccia hosting footwall Cu-Ni-PGE mineralization at the Fraser Mine, Sudbury, Ontario, Canada; The Canadian Mineralogist, v. 41, p. 857–881.

Hanley, J.J., Mungall, J.E., Bray, C.J., and Gorton, M.P., 2004. The origin of bulk and water-soluble Cl and Br enrichments in ore-hosting Sudbury Breccia in the Fraser Copper Zone, Strathcona

Embayment, Sudbury, Ontario, Canada; The Canadian Mineralogist, v. 42, p. 1777–1798.

Hanley, J.J., Mungall, J.E., Pettke, T., Spooner, E.T.C., and Bray, C.J., 2005. Ore metal redistribution by hydrocarbon-brine and hydrocarbon-halide melt phases, North Range footwall of the Sudbury Igneous Complex, Ontario, Canada; Mineralium Deposita, v. 40, p. 237–256.

Hanley, J.J., Ames, D.E., Barnes, J., Sharp, Z., and Guillong, M., 2011. Interaction of magmatic fluids and silicate melt residues with saline groundwater in the footwall of the Sudbury Igneous Complex, Ontario, Canada: New evidence from bulk rock geochemistry, fluid inclusions and stable isotopes; Chemical Geology, v. 281, p. 1–25.

Holliger, P. and Cathelineau, M., 1988. In situ U-Pb age determination by secondary ion mass spectrometry; Chemical Geology, v. 70, p. 173.

Jago, B.C., Morrison, G.G., and Little, T.L., 1994. Metal zonation patterns and microtextural and micromineralogical evidence for alkali- and halogen-rich fluids in the genesis of the Victor Deep and McCreedy East footwall copper orebodies, Sudbury Igneous Complex, *In:* Proceedings of the Sudbury – Noril'sk Symposium; Ontario Geological Survey, Special Volume 5, p. 65–75.

Jakobsen, J.K., Veksler, I.V., Tegner, C., and Brooks, C.K., 2011. Crystallization of the Skaergaard intrusion from an emulsion of immiscible iron-and-silica-rich liquids: evidence from melt inclusions in plagioclase; Journal of Petrology, v. 52, p. 345–373.

Kaufmann, R., Frape, S., Fritz, P., and Bentley, H., 1987. Chlorine stable isotope composition of Canadian Shield brines, *In:* Saline Water and Gases in Crystalline Rocks, (ed.) P. Fritz and S.K. Frape; Geological Association of Canada, Special Paper 33, p. 89–93.

Kerr. M.J. and Hanley, J.J., 2013. Preliminary evaluation of trace hydrocarbon speciation and abundance as an exploration tool for footwall-style sulfide ore, Sudbury Igneous Complex, Ontario, Canada, *In:* Abstracts; Goldschmidt conference, Florence, Italy, August 25-30, 2013, p. 1449.

Klemme, S., 2003. Trace element partitioning between apatite and carbonatite melt; American Mineralogist, v. 88, p. 639–646.

Kuo, H.Y. and Crocket, J.H., 1979. Rare earth elements in the Sudbury nickel irruptive: comparison with layered gabbros and implications for nickel petrogenesis; Economic Geology, v. 74, p. 590–605.

Li, C. and Naldrett, A.J., 1993. High chlorine alteration minerals and calcium-rich brines in fluid inclusions from the Strathcona Deep copper zone, Sudbury, Ontario; Economic Geology, v. 88, p. 1780–1796.

Li, C., Naldrett, A.J., Coats, C.J.A., and Johannessen, P., 1992. Platinum, palladium, gold and copper-rich stringers at the Strathcona Mine, Sudbury: Their enrichment by fractionation of a sulfide liquid; Economic Geology, v. 87, p. 1584–1598.

Lightfoot, P.C. and Farrow, C.E.G., 2002. Geology, geochemistry, and mineralogy of the Worthington Offset Dike: a genetic model for offset dike mineralization in the Sudbury Igneous Complex; Economic Geology, v. 97, p. 1419–1446.

Lightfoot, P.C., Keays R.R., Morrison G.G., Bite, A., and Farrell, K.P., 1997a. Geochemical relationships in the Sudbury Igneous Complex: origin of the Main Mass and Offset Dikes; Economic Geology, v. 92, p. 289–307.

Lightfoot, P.C., Keays R.R., Morrison, G.G., Bite, A., and Farrell, K.P, 1997b. Geologic and geochemical relationships between the contact sublayer, inclusions, and the Main Mass of the Sudbury Igneous Complex: a case study of the Whistle Mine embayment; Economic Geology, v. 92, p. 647–673.

Lightfoot, P.C., Reid R.K., and Doherty, W., 2001. Chemical evolution and origin of nickel sulfide mineralization in the Sudbury Igneous Complex, Ontario, Canada; Economic Geology, v. 96, p. 1855–1875.

Luhr, J.F., Carmichael, I.S.E., and Varekamp, J.C., 1984. The 1982 eruptions of El Chichon volcano, Chiapas, Mexico: mineralogy and petrology of the anhydrite-bearing pumices; Journal of Volcanology and Geothermal Research, v. 23, p. 69–108.

Magyarosi, Z., 1998. Metamorphism of the Proterozoic Rocks Associated with the Sudbury Structure; M.Sc. thesis, Carleton University, Ottawa, Ontario, 101 p.

Magyarosi, Z., Watkinson, D.H., and Jones, P.C., 2002. Mineralogy of Ni-Cu-platinum-group element sulfide ore in the 800 and 810 orebodies, Copper Cliff South Mine, and P-T-X conditions during the formation of platinum-group minerals; Economic Geology, v. 97, p. 1471–1486.

Mahood, G.A. and Stimac, J.A., 1990. Trace element partitioning in pantellerites and trachytes; Geochimica et Cosmochimica Acta, v. 54, p. 2257–2276.

Marshall, D., Watkinson, D., Farrow, C., Molnár, F., and Fouillac, A.M. 1999. Multiple fluid generations in the Sudbury Igneous Complex: fluid inclusion, Ar, O, H, Rb and Sr evidence; Chemical Geology, v. 154, p. 1–19.

Martin, H.W. and Sparks, D.L., 1985. On the behaviour of non-exchangeable potassium in soils; Communications in Soil Science and Plant Analysis, v. 16, p. 133–162.

Molnár, F., Watkinson, D.H., and Jones, P.C., 2001. Multiple hydrothermal processes in footwall units of the North Range, Sudbury Igneous Complex, Canada, and implications for the genesis of vein-type Cu-Ni-PGE deposits; Economic Geology, v. 96, p. 1645–1670.

Murphy, A.J. and Spray, J.G., 2002. Geology, mineralization, and emplacement of the Whistle-Parkin Offset Dyke, Sudbury; Economic Geology, v. 97, p. 1399–1418.

Naldrett, A.J., Asif, M., Schandl, E., and Searcy, T., 1999. Platinum-group elements in the Sudbury ores: Significance with respect to the origin of different ore zones and to the exploration for footwall orebodies; Economic Geology, v. 94, p. 185–210.

Nelles, E.W., Lesher C.M., and Lafrance B., 2010. Mineralogy and textures of Cu–PPGE–Au-rich mineralization in the Morrison (Levack footwall) Deposit, Sudbury, Ontario, *In:* Abstracts Volume; Society of Economic Geologists Annual Meeting, Keystone, Colorado, October 2010.

Newman, A.C.D. and Brown, G., 1966. Chemical changes during the alteration of micas; Clay minerals, v. 6, p. 297–309.

Noble, S.R. and Lightfoot, P.C., 1992. U-Pb baddeleyite ages for the Kerns and Triangle Mountain intrusions, Nipissing Diabase, Ontario; Canadian Journal of Earth Sciences, v. 29, p. 1424–1429.

O'Neil, J.R., Clayton, R.N., and Mayeda, T.K., 1969. Oxygen isotope fractionation in divalent metal carbonates; Journal of Chemical Physics, v. 51, p. 5547–5558.

Page, F.Z., Kita, N.T., and Valley, J.W., 2010. Ion microprobe analysis of oxygen isotopes in garnets of complex chemistry; Chemical Geology, v. 270, p. 9–19.

Paster, T.P., Schauwecker, D.S., and Haskin, L.A., 1974. The behavior of some trace elements during solidification of the Skaergaard layered series; Geochimica et Cosmochimica Acta, v. 38, p. 1549–1577.

Péntek, A., Molnár, F., Watkinson, D.H., and Jones, P.C., 2008. Footwall-type Cu-Ni-PGE mineralization in the Broken Hammer area, Wisner township, North Range, Sudbury structure; Economic Geology, v. 103, p. 1005–1028.

Péntek, A., Molnár, F., Tuba, G., Watkinson, D.H., and Jones, P.C., 2013. The significance of partial melting processes in hydrothermal low-sulfide Cu-Ni-PGE mineralization within the footwall of the Sudbury Igneous Complex, Ontario, Canada; Economic Geology, v. 108, p. 59–78.

Peredery, W.V. and Naldrett, A.J., 1975. Petrology of the upper irruptive rocks, Sudbury, Ontario; Economic Geology, v. 70, p. 164–175.

Pope, K.O., Kieffer, S.W., and Ames, D.E., 2004. Empirical and theoretical comparisons of the Chicxulub and Sudbury impact structures; Meteoritics and Planetary Science, v. 39, p. 97–116.

Rausell-Colom, J.A., Sweatman, T.R., Wells, C.B., and Norrish, K., 1964. Studies in the artificial weathering of mica; *In:* Experimental Pedology, (ed.) E.G. Hallsworth and D.V. Crawford; Buttersworths, London, p. 40–72.

Riciputi, L.R., Paterson, B.A., and Ripperdan, R.L., 1998. Measurement of light stable isotope ratios by SIMS: Matrix effects for oxygen, carbon, and sulfur isotopes in minerals; International Journal of Mass Spectrometry, v. 178, p. 81–112.

Roedder, E., 1979. Silicate liquid immiscibility in magmas, Chapter 2, *In:* The evolution of igneous rocks: Fiftieth Anniversary Perspectives, (ed.) H.S. Jr. Yoder; Princeton University Press, Princeton, New Jersey, p. 15–57.

Stewart, M.C., 2002. Petrology and mineralogy of Cu-Ni-PGE ore, Totten area, Worthington offset, Sudbury Igneous Complex; M.Sc. thesis, Carleton University, Ottawa, Ontario, 164 p.

Stewart, R.C., 2011. Halogen geochemistry of footwall breccia and associated units of the Main Mass of the Sudbury Igneous Complex, Ontario; M.Sc. thesis, Saint Mary's University, Halifax, Nova Scotia, 190 p.

Therriault, A.M., Fowler, A.D., and Grieve, R.A.F., 2002. The Sudbury Igneous Complex: A differentiated impact melt sheet; Economic Geology, v. 97, p. 1521–1540.

Thomson, M.L., Barnett, R.L., Fleet, M.E., and Kerrich, R., 1985. Metamorphic assemblages in the South Range norite and Footwall mafic rocks near the Kirkwood mine, Sudbury, Ontario; The Canadian Mineralogist, v. 23, p. 173–186.

Tuba, G., 2012. Multiple hydrothermal systems in the footwall of the Sudbury Igneous Complex: Fluid characteristics, associated alteration, and the role in footwall-type "low-sulphide" Cu-(Ni)-PGE sulphide mineralization (North and East Ranges, Sudbury Structure, Canada); Ph.D. thesis, Eötvös Loránd University, Budapest, 183 p.

Tuba, G., Molnár, F., Watkinson, D.H., Jones, P.C., and Mogessie, A., 2010. Hydrothermal vein and alteration assemblages associated with low-sulfide footwall Cu-Ni-PGE mineralization and regional hydrothermal processes, North and East Ranges, Sudbury structure, Canada, *In:* The Challenge of Finding New Mineral Resources: Global Metallogeny, Innovative Exploration, and New Discoveries Volume I: Gold, Silver, and Copper-Molybdenum, (ed.) R.J. Goldfarb, E.E. Marsh, and T. Monecke; Society of Economic Geologists, Special Publication 15, p. 573–598.

Tuba, G., Molnár, F., Ames, D.E., Péntek, A., Watkinson, D.H., and Jones, P.C., 2014. Multi-stage hydrothermal processes involved in "low-sulfide" Cu(-Ni)-PGE mineralization in the footwall of the Sudbury Igneous Complex (Canada): Amy Lake PGE zone, East Range; Mineralium Deposita, v. 49, p. 7–47.

Tuchscherer, M. G. and Spray, J. G., 2002. Geology, Mineralization, and Emplacement of the Foy Offset Dyke, Sudbury Impact Structure; Economic Geology, v. 97, p. 1377–1397.

Valley, J. W., Kitchen, N., Kohn, M.J., Niendorf, C.R., and Spicuzza, M.J., 1995. UWG-2, a garnet standard for oxygen isotope ratios: Strategies for high precision and accuracy with laser heating; Geochimica et Cosmochimica Acta, v. 59, p. 5223–5231.

Veksler, I.V., Dorfman, A.M., Danyushevsky, L.V., Jakobsen, J.K., and Dingwell, D.B., 2006. Immiscible silicate liquid partition coefficients: implications for crystal-melt element partitioning and basalt petrogenesis; Contributions to Mineralogy and Petrology, v. 152, p. 685–702.

Walker, G.F., 1949. The decomposition of biotite in the soil; Mineralogical Magazine, v. 28, p. 693–703.

Warren, M.R., Hanley, J.J., Ames, D.E., and Simon E. Jackson, S.E., 2015. The Ni–Cr–Cu content of biotite as pathfinder elements for magmatic sulfide exploration associated with mafic units of the Sudbury Igneous Complex, Ontario, Canada; Journal of Geochemical Exploration, v. 153, p. 11–29.

Watson, E.B. and Green, T.H., 1981. Apatite/liquid partition coefficients for the rare earth elements and strontium; Earth and Planetary Science Letters, v. 56, p. 405–421.

White, C.J., 2012. Low-sulfide PGE-Cu-Ni mineralization from five prospects within the footwall of the Sudbury Igneous Complex, Ontario, Canada; Ph.D. thesis, University of Toronto, Toronto, Ontario, 318 p.

Wilson, M.I., 2004. Weathering of the primary rock-forming minerals: processes, products and rates; Clay Minerals, v. 39, p. 233–266.

Zieg, M.J. and Marsh, B.D., 2005. The Sudbury Igneous Complex: viscous emulsion differentiation of a superheated impact melt sheet; Geological Society of America Bulletin, v. 117, p. 1427–1450.

Zurbrigg, H.F., 1957. The Frood-Stobie Mine. *In:* Structural Geology of Canadian Ore Deposits, (ed.) G. Gilbert; Commonwealth Mining and Metallurgical Congress, v. 2, p. 341–350.

GEOLOGICAL SURVEY OF CANADA
OPEN FILE 7856

Targeted Geoscience Initiative 4: Canadian Nickel-Copper-Platinum Group Elements-Chromium Ore Systems — Fertility, Pathfinders, New and Revised Models

Textural character and chemistry of plagioclase and apatite in the Marathon Cu-PGE deposit, Ontario: Implications for mineralizing processes

Maryam Shahabi Far[1], Iain M. Samson[1], Joel E. Gagnon[1], Robert L. Linnen[2], David J. Good[2], and Doreen E. Ames[3]

[1]University of Windsor, Windsor, Ontario
[2]University of Western Ontario, London, Ontario
[3]Geological Survey of Canada, Ottawa, Ontario

2015

© Her Majesty the Queen in Right of Canada, as represented by the Minister of Natural Resources Canada, 2015

This publication is available for free download through GEOSCAN (http://geoscan.nrcan.gc.ca/)

Recommended citation

Shahabi Far, M., Samson, I.M., Gagnon, J.E., Linnen, R.L., Good, D.J., and Ames, D.E., 2015. Textural character and chemistry of plagioclase and apatite in the Marathon Cu-PGE deposit, Ontario: Implications for mineralizing processes, *In:* Targeted Geoscience Initiative 4: Canadian Nickel-Copper-Platinum Group Elements-Chromium Ore Systems — Fertility, Pathfinders, New and Revised Models, (ed.) D.E. Ames and M.G. Houlé; Geological Survey of Canada, Open File 7856, p. 233–243.

Publications in this series have not been edited; they are released as submitted by the author.

Contribution to the Geological Survey of Canada's Targeted Geoscience Initiative 4 (TGI-4) Program (2010–2015)

TABLE OF CONTENTS

Textural character and chemistry of plagioclase and apatite in the Marathon Cu-PGE deposit, Ontario: Implications for mineralizing processes

Maryam Shahabi Far[1]*, Iain M. Samson[1], Joel E. Gagnon[1],
Robert L. Linnen[2], David J. Good[2], and Doreen E. Ames[3]

[1]Department of Earth and Environmental Sciences, University of Windsor, 401 Sunset Avenue, Windsor, Ontario N9B 3P4
[2]Department of Earth Sciences, University of Western Ontario, 1151 Richmond Street N., London, Ontario N6A 5B7
[3]Geological Survey of Canada, 601 Booth Street, Ottawa, Ontario K1A 0E8
*Corresponding author's e-mail: m.shahabifar59@gmail.com

ABSTRACT

The Marathon deposit is hosted within the Two Duck Lake gabbro (TDLG) of the Mesoproterozoic Coldwell alkaline complex, and comprises three zones (Footwall Zone, Main Zone, and W Horizon), which have different textural, mineralogical, and geochemical characteristics. Plagioclase and apatite in the host gabbro units have complex textures and chemistry. Magmatic plagioclase is characterized by a strong positive Eu anomaly, and ΣREE increases from core to rim. Plagioclase with replacement rims occurs adjacent to granophyric patches in the vicinity of the footwall, suggesting alteration by fluids exsolved from the granophyric melts. Apatite both predated and postdated plagioclase. Apatite crystals from the Main and Footwall zones generally have high Cl contents, whereas apatite from the W Horizon has low Cl content. Rocks with higher grades of mineralization in the Main and Footwall zones generally contain apatite with higher Cl contents, whereas, in the W Horizon, higher grades correlate with lower Cl in apatite. In addition, zoning, recrystallization textures, and the presence of primary fluid inclusions are more common in apatite from the Main and Footwall zones. ΣREE in late apatite overlaps that of the core and rim of early apatite, suggesting that late apatite probably crystallized from a new influx of magma rather than from continued crystallization of a resident magma. The spatial variations in apatite Cl/F could be explained if compositionally distinct magma pulses were responsible for each mineralized zone, as most early apatite crystals are euhedral to subhedral, and magmatic. Intracontinental basaltic melts are, however, reported to be poor in Cl, suggesting local addition of Cl. Chalcopyrite in the Main Zone commonly replaces pyrrhotite and is intergrown with hydrous silicate minerals, suggesting Cu (re-)mobilization. Therefore, a zone-refining process in which volatiles, derived from footwall country-rock dehydration, migrated through the crystallizing gabbros and transported Cu to the Main Zone is an attractive model by which Cl could also be added to the system. The low Cl contents of apatite in the W Horizon can be explained if these fluids did not reach the W Horizon, or the W Horizon represents late-stage magma infiltration.

INTRODUCTION

Despite extensive study, aspects of the genesis of contact-style, low sulphide PGE-Cu (-Ni) deposits (e.g. Naldrett, 2004; Mungall, 2005; Zientek, 2012) remains a controversial subject, in particular the relative importance of magmatic and fluid (volatile)-mediated processes in Cu and PGE enrichment remains a point of debate. Many recent studies have discussed this issue, and have suggested that these deposits are magmatic ore deposits modified by syn- or post-magmatic fluid activity (Harris and Chaumba, 2001; Sharman-Harris et al., 2005; Holwell et al., 2007; Gál et al., 2011; Holwell et al., 2014).

The Marathon deposit, Ontario, Canada, is classified as a contact-type PGE-Cu deposit. It is hosted by the Two Duck Lake gabbro (TDLG) of the Mesoproterozoic (1108 ± 1 Ma) Coldwell alkaline complex. The process of platinum-group element (PGE) enrichment in the Marathon deposit is also still controversial: can the concentration mechanisms be dominantly attributed to PGE-rich immiscible sulphide liquids that separated from the host gabbroic magmas (Good and Crocket, 1994; Good, 2010; Ruthart et al., 2010) or were the volatile-rich fluids passing through the crystalline or nearly crystalline rocks also important (Watkinson and Ohnenstetter, 1992; Dahl et al.,

Shahabi Far, M., Samson, I.M., Gagnon, J.E., Linnen, R.L., Good, D.J., and Ames, D.E., 2015. Textural character and chemistry of plagioclase and apatite in the Marathon Cu-PGE deposit, Ontario: Implications for mineralizing processes, *In:* Targeted Geoscience Initiative 4: Canadian Nickel-Copper-Platinum Group Elements-Chromium Ore Systems — Fertility, Pathfinders, New and Revised Models, (ed.) D.E. Ames and M.G. Houlé; Geological Survey of Canada, Open File 7856, p. 233–243.

2001; Barrie et al., 2002). The Marathon deposit comprises three zones of mineralization with different textural, mineralogical, and geochemical characteristics: Footwall Zone, Main Zone, and W Horizon.

In order to improve our understanding of the magmatic and fluid-rock interaction processes that led to the formation of the Marathon deposit, including the thermal history of the rocks, and hence further develop models for contact-type low-sulphide deposits, we have studied the chemical and textural characteristics and evolution of plagioclase and apatite at Marathon, in the context of sulphide distribution in the various mineralized zones.

Major and trace element mineral chemistry, combined with petrography, have been used by a number of authors to elucidate magma-chamber processes, such as magma sources, the nature and degree of fractional crystallization, magma recharge, and fluid-rock interaction (Hall, 1987; Kruger, 1992; Best, 2003; Streck, 2008). Plagioclase chemistry has been long recognized as a good recorder of crystallization history and the chemical evolution of magmas due to the easily recognized compositional zoning (Ginibre et al., 2002; Humphreys et al., 2006; Ginibre et al., 2007; Humphreys, 2009; Gorokhova et al., 2013). Also, the distribution and composition of halogen-bearing minerals can be used to assess the possible role of volatile components during crystallization, and the potential for Cl-bearing fluids to act as metal transport agents (Boudreau and McCallum, 1989; Boudreau et al., 1986; Boudreau and Kruger, 1990; Willmore et al., 2002; Boudreau and Hoatson, 2004). The effects of the migration of Cl-rich fluids in the mobilization of base and precious metal sulphides in the Bushveld and Stillwater complexes have been extensively reported (Boudreau et al., 1986; Boudreau and McCallum, 1989; Boudreau and Kruger, 1990; Willmore et al., 2000). Therefore, the significance of hydrothermal fluids in the mineralizing mechanisms, either directly forming mineralization or causing considerable modification of it, cannot be ignored. In this study, petrographic analyses have been combined with detailed mineral chemical analyses to evaluate the petrogenetic evolution of the Marathon host rocks in the context of magmatic and fluid-rock interaction history as a framework for understanding the relationship of this evolution to the formation of the ore minerals.

RESULTS

Petrography

The TDLG is coarse-grained to pegmatitic, and comprises plagioclase with variable amounts of interstitial ophitic clinopyroxene, olivine, and magnetite. Apatite, biotite, and amphibole are common accessory minerals. Hydrothermal alteration is a common feature, especially in the Main and Footwall zones, and is dominated by replacement of primary igneous minerals by amphibole, chlorite, biotite, and serpentine. Epidote and carbonate are also present as alteration minerals in some samples.

Plagioclase is a ubiquitous silicate phase in the TDLG and occurs as cumulus euhedral to subhedral tabular prisms. The grain size varies typically from a few millimetres to 1 centimetre, but can be considerably coarser. Plagioclase crystals contain a wide variety of internal textures, including resorption surfaces, normal or reverse zoning, oscillatory zoning, and patchy zoning. Plagioclase crystals can be classified into four types based on the nature of internal zonation: (1) homogeneous crystals lacking zonation, (2) crystals showing normal or oscillatory zoning (Fig. 1a, b), (3) plagioclase crystals with resorption surfaces (Fig. 1c, d, e), and (4) crystals with replacement rims (Fig. 1f). Resorption textures are relatively common in plagioclase, and can contain one or two resorption surfaces (i.e. two or three stages of plagioclase growth; Fig. 1c, d).In some cases, in rocks that contain sulphides, the outermost resorption zone is characterized by a porous texture in which the pores are filled with sulphide (Fig. 1e). Finally, plagioclase crystals with replacement rims occur in the vicinity of quartz-feldspar granophyre patches (Fig. 1f).

Apatite is an accessory mineral and mostly occurs as interstitial euhedral to subhedral acicular and tabular prisms, and as anhedral crystals hosted by both altered and unaltered minerals. Although apatite is commonly hosted by plagioclase, it is also hosted by pyroxene, sulphide, magnetite, and hydrous minerals (Fig. 2). In different rocks, apatite either predated (pre-plagioclase apatite; Fig. 2a, b) or postdated plagioclase crystallization (post-plagioclase apatite; Fig. 2g, h). Apatite grains vary in size but are usually not more than a few millimetres. However, unusual oikocryst apatite, up to a few centimetres across, occurs in pegmatitic gabbro. The latter are more common in the W Horizon, and mostly postdate plagioclase crystallization. SEM-CL imaging shows that apatite crystals can exhibit growth (oscillatory) and replacement zoning. Zoning, re-crystallization textures (Fig. 3), and the presence of primary fluid inclusions, are more common in apatite crystals from Main and Footwall zone samples compared to those from the W Horizon.

Sulphide minerals occur as disseminations throughout the gabbro or as massive to semi-massive accumulations of chalcopyrite, pyrrhotite, bornite, minor pentlandite, and accessory pyrite and cubanite. The Footwall Zone contains massive to semi-massive pyrrhotite with minor chalcopyrite, pentlandite, and pyrite. In the Main Zone, interstitial disseminated sulphides comprise chalcopyrite, pyrrhotite ± pentlandite, and cubanite. In some

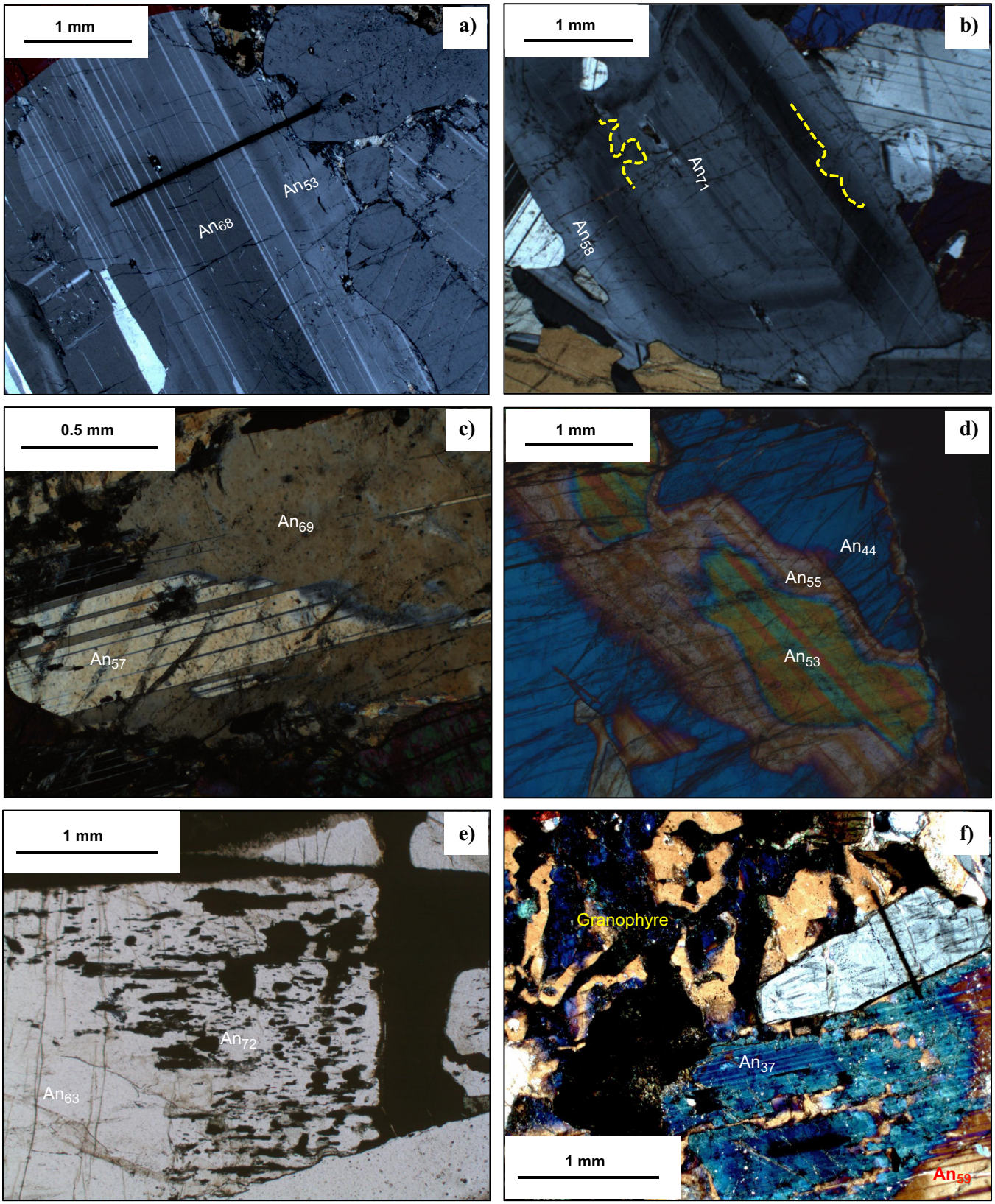

Figure 1. Photomicrographs representing the variation in textural characteristics of plagioclase: **(a)** normal zoning; **(b)** oscillatory zoning (highlighted by a yellow dotted line); **(c)** early crystallized plagioclase resorbed and overgrown by more calcic plagioclase; **(d)** two stages of resorption: early crystallized plagioclase was first resorbed and overgrown by more calcic plagioclase and then a second stage is represented by resorption followed by sodic overgrowth; **(e)** resorption texture with sulphide blebs in the outermost zone (overgrowth); **(f)** replacement rim of more sodic plagioclase replacing a more calcic crystal.

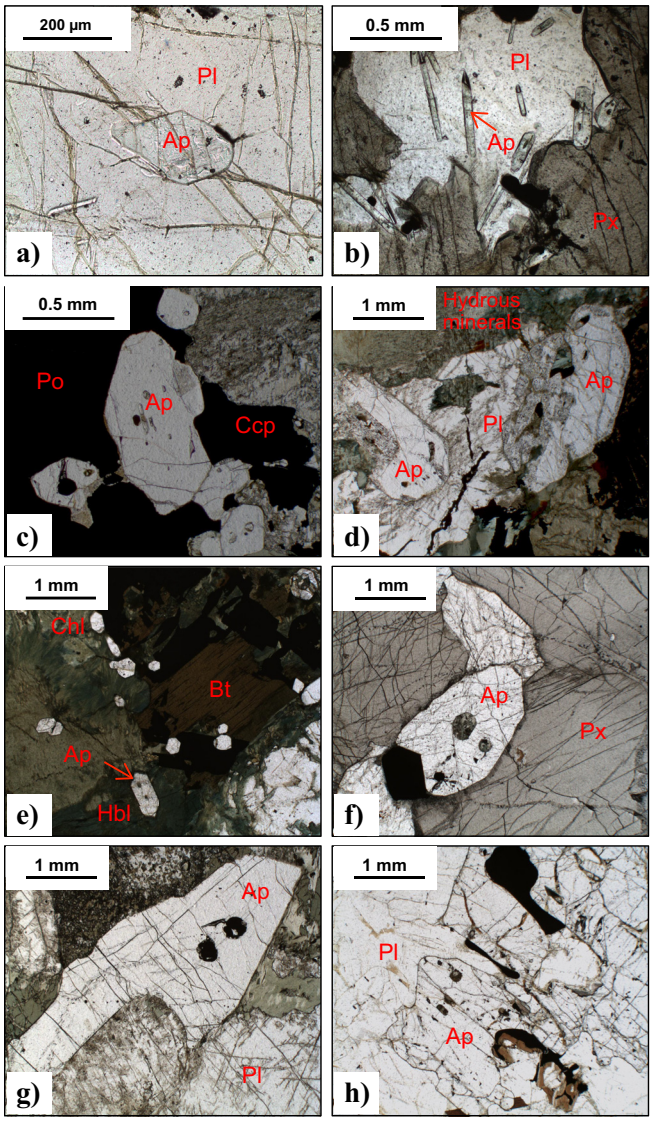

Figure 2. Photomicrographs representing the variation in textural characteristics and host assemblages of apatite from the three mineralized zones: **(a and b)** Main Zone; **(c and d)** Footwall Zone; **(e and f)** W Horizon; and **(g and h)** apatite that postdates plagioclase crystallization. Ap = apatite; Bt = biotite; Ccp = chalcopyrite; Chl = chlorite; Hbl = hornblende; Pl = plagioclase; Po = pyrrhotite; Px = pyroxene.

aggregates, chalcopyrite shares equilibrium boundaries with pyrrhotite. Much of the chalcopyrite in the Main Zone, however, replaced pyrrhotite and is intergrown with hydrous silicate minerals. In both the Footwall and Main zones, sulphides occur as replacing pyroxene lamellae in altered samples. Sulphides in the W Horizon (the highest stratigraphic zone) are characterized by disseminated chalcopyrite, bornite ± pyrrhotite, pentlandite, cubanite, and pyrite. Bornite occurs as irregular patches in chalcopyrite but is mostly represented by flame-like exsolution within chalcopyrite.

Mineral Chemistry

The anorthite content of plagioclase in the TDLG

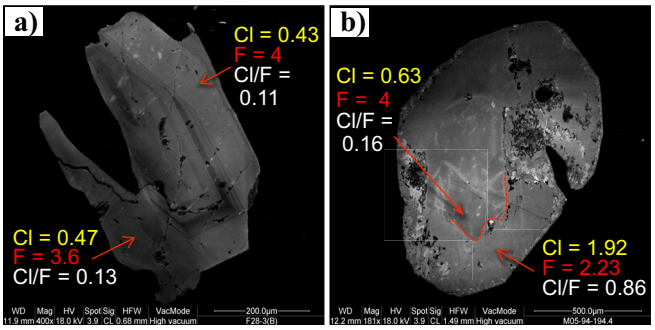

Figure 3. SEM-cathodoluminescence images of apatite crystals with EDS analyses of different zones: **(a)** growth zoning in a crystal from the Main Zone with no variation in Cl/F ratios between zones; **(b)** outer replacement zone with a higher Cl/F ratio than in the relict core (from the Footwall Zone); boundary marked by the dotted line.

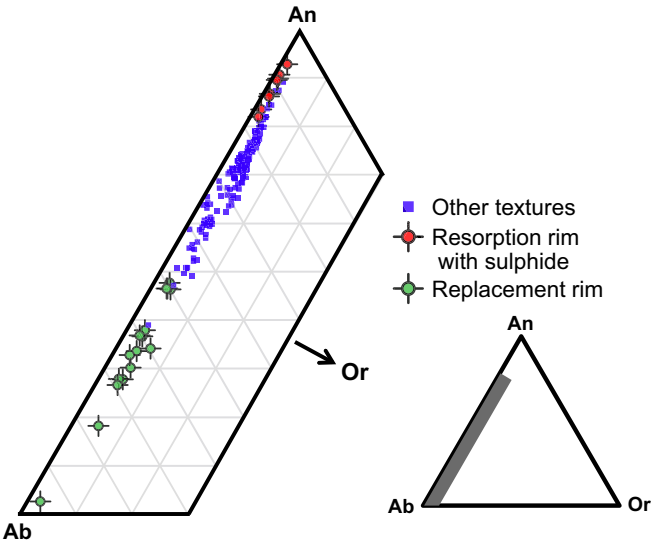

Figure 4. Part of a ternary diagram (grey field in the An-Ab-Or ternary diagram) showing the variations in An content of plagioclase with different textures.

varies widely, from An_{15} to An_{74}. The anorthite content of the plagioclase varies by 4 mol% between different oscillatory zones; however, the general trend is a decrease in An content toward the rim. The later overgrowth phases, after resorption, generally have higher An contents (An_{52-74}) than the earlier stages of crystallization, whereas replacement rims in the vicinity of the granophyric patches have lower An contents (An_{33-50}) compared to the magmatic plagioclase that was replaced (An_{60-75}) (Fig. 4).

Trace element analyses of plagioclase indicate that only the rare earth elements, S, Ni, Cu, Ti, and Pb exhibit significant differences among the three zones, and that other analyzed elements show either no variation or the variation is less than the precision of the analytical method. Magmatic plagioclase with normal or oscillatory zoning is characterized by a distinct positive Eu anomaly, and mostly shows an increase in ΣREE towards the rims of crystals. The change in the

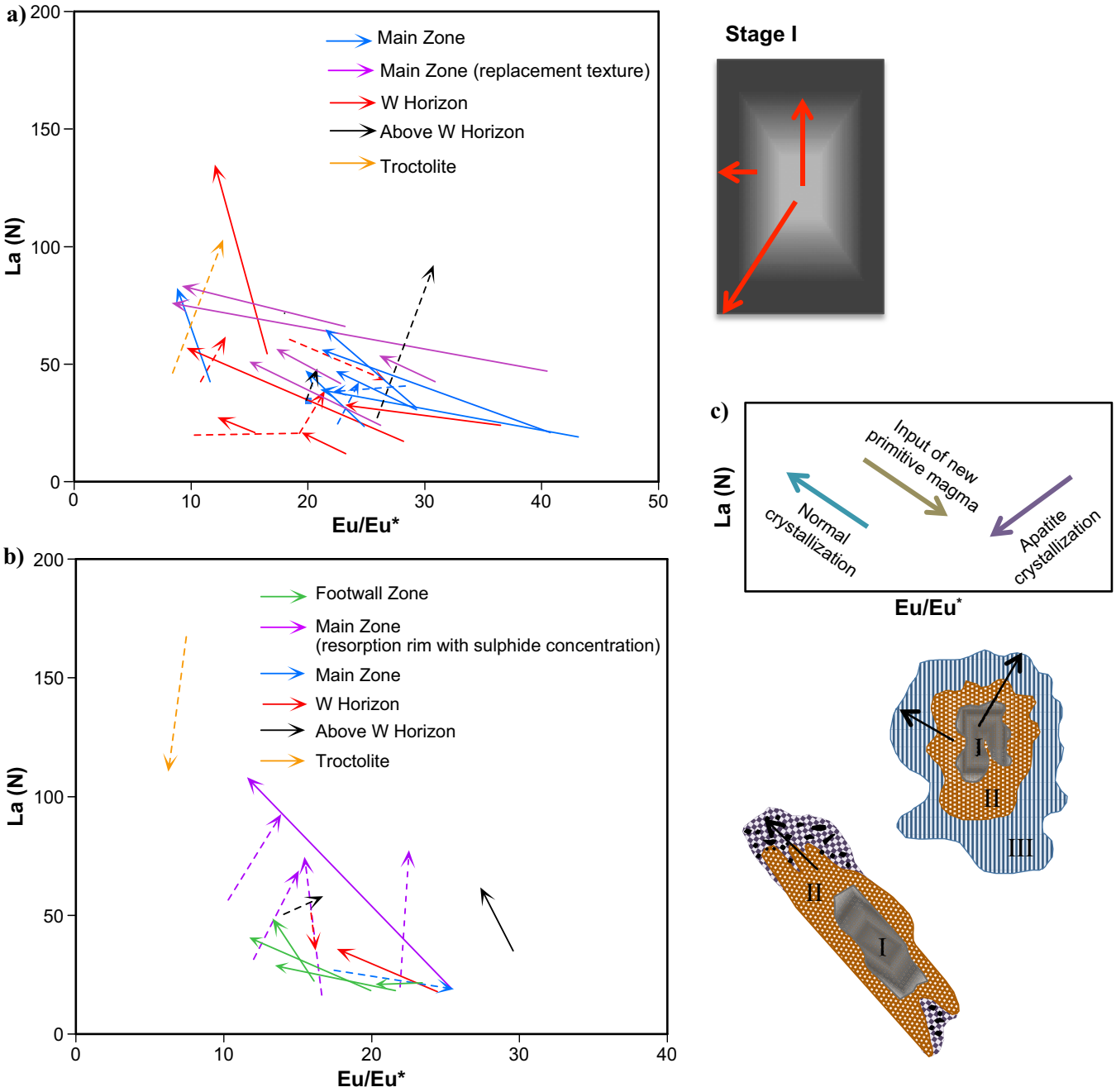

Figure 5. Trace element variation in plagioclase for different textures showing trends from early to late crystallization: **(a)** plagioclase crystallization showing normal or oscillatory zoning without any resorption; **(b)** plagioclase crystals showing overgrowth after resorption; **(c)** sketch showing expected trends of REE for early to late phases of plagioclase based on different scenarios.

magnitude of the Eu anomaly from core to rim of oscillatory zoned plagioclase crystals, however, is different in different crystals. For example, in most plagioclase crystals from the Main and Footwall zones, the magnitude of this anomaly decreases from the earlier to the later crystallized phase, whereas in some crystals from the W Horizon; in gabbro above W Horizon the opposite is observed (Fig. 5a). These different trends in REE character can also be found in plagioclase crystals with overgrowths that postdate resorption, where the Eu anomaly can increase or decrease from an early crystal that has been resorbed to one of the overgrowth phases or from an early overgrowth to a later one (Fig. 5b). The resorption rims characterized by sulphide-filled pores have higher An content than the crystal cores and have higher S, Ni, Cu, and Pb and lower Ti than all other types of plagioclase.

The energy-dispersive X-ray spectrometry (ed.) and wavelength-dispersive X-ray spectrometry (WDS) analyses indicate that the F and Cl contents in apatite

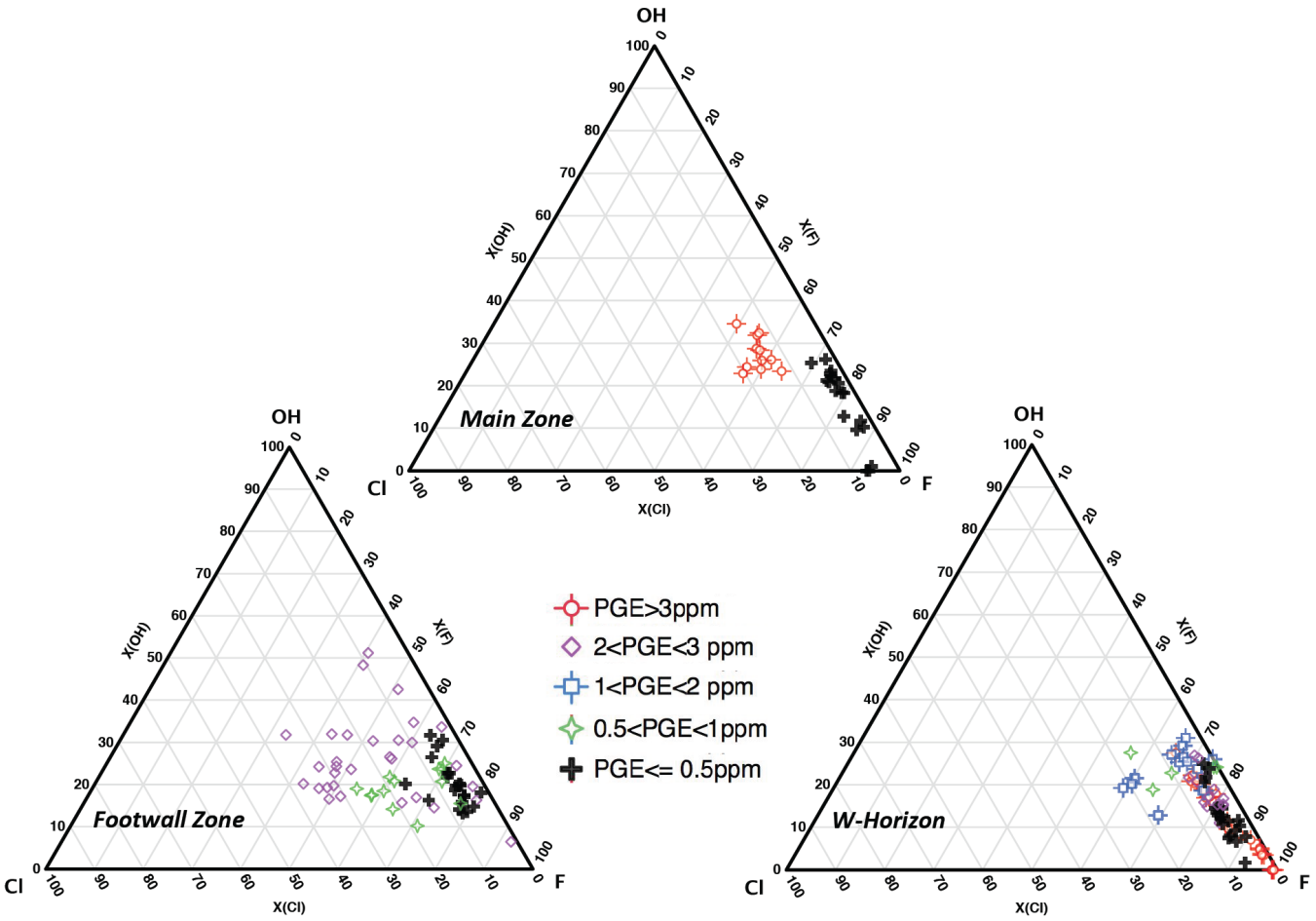

Figure 6. Ternary diagrams showing F-Cl variations in apatite from the different mineralized zones and their relationship to the grade of mineralization.

are variable (Fig. 6). There is a systematic variation of halogen contents in apatite with stratigraphic level and grade of mineralization. Apatite crystals from mineralized Main and Footwall zone samples generally have high Cl contents, whereas apatite from the W Horizon has low Cl contents, and generally have fluorapatite end-member compositions. Apatite crystals from the Footwall Zone have the highest Cl/F values, whereas those from the W Horizon show the lowest Cl/F ratios. Rocks with higher grades of mineralization in the Main and Footwall zones generally contain apatite with higher Cl contents, whereas, in the W Horizon, higher grades correlate with lower Cl in apatite.

Cores of apatite crystals have lower ΣREE contents and a negative Eu anomaly, whereas the rims have higher REE contents and a stronger Eu anomaly. Both cores and rims of apatite crystals exhibit similar positive Ce anomalies. The range of REE compositions for post-plagioclase apatite spans the entire range of compositions for cores and rims of pre-plagioclase apatite. Replacement rims of apatite crystals, however, show lower ∑REE, and higher Cl contents compared to early apatite, and no significant Ce anomaly.

DISCUSSION

Although some crystals of plagioclase in the TDLG show normal zoning, it is common to find evidence of disequilibrium and resorption, indicating repeated input of new magma into the TDLG system, which was out of equilibrium with pre-existing crystals (Fig. 1c, d, e). Magma dynamics, including magma mingling, as recorded by plagioclase crystals, has been discussed in numerous studies (Browne et al., 2006; Ginibre et al., 2007; Gál et al., 2013; Thy et al., 2013). The expected trend from normal crystallization would be an increase in La and a decrease in the magnitude of the Eu anomaly as crystals grow (Fig. 5c). At Marathon, plagioclase crystals that exhibit normal or oscillatory zoning without any evidence of resorption show different chemical trends from core to rim (Fig. 5a). Most of the plagioclase crystals from the Main Zone and Footwall Zone follow this trend, however, some crystals from within and above the W Horizon and from the troctolite represent different trends: the magnitude of the Eu anomaly increases from early to late crystallization. This trend can be explained by changing magma chemistry (through influx of new magma) or crystallization of

other minerals, such as apatite, which could have affected REE concentrations in the magma. However, crystallization of apatite would cause REE depletion in the magma and later-crystallized plagioclase would be expected to show lower La, which is in contrast with what was observed. Therefore, it is more likely that these trends represent changing magma chemistry through the input of new magma. If the new magma was relatively primitive (the same as the original magma), we would expect the later phase to contain lower La because the REE partition coefficients in plagioclase decrease with increasing An content. The new magmas, therefore, probably came from a chamber undergoing fractional crystallization at depth. This model is supported by the observation that many crystals show evidence of resorption and that late-stage, post-resorption overgrowths have a higher An content as well as different REE trends.

The higher An and base metal contents of plagioclase crystals that contain sulphide blebs in post-resorption overgrowths suggests that these resorption rims are related to the mineralization, and crystallized from a sulphide-bearing magma or fluids. This could be attributed to the influx of metal-rich magma, or the interaction of the magma with metal-rich fluid. Both models could explain the higher An content of these resorptions rims than in the earlier stages of crystallization. One possible source of metal-rich fluids is the late-stage granophyric melts that were present in the system. Plagioclase replacement rims that occur in the vicinity of quartz-feldspar granophyric patches (Fig. 1f), however, have low An contents (An_{33-50}; Fig. 4c), consistent with alteration by fluids exsolved from the granophyric melts, which are therefore unlikely to have formed the sulphide-associated Ca-rich overgrowths (Fig. 4c).

The observed spatial variations in Cl/F in apatite can be explained by compositionally distinct magma pulses being responsible for the formation of the different mineralized zones, as most apatite crystals are euhedral to subhedral, formed early in the paragenetic sequence, and are magmatic. Boudreau et al. (1997) showed that magmas formed by simple extensional decompression melting are relatively volatile-poor and apatite that crystallizes from such magmas would be fluorine-rich. Given that the Marathon deposit is related to magmas formed in an intracontinental rift, we can therefore expect that the TDL magmas were relatively dry, and that apatite crystallizing from such a melt would be fluorapatite. This is supported by the lower Cl/F ratio of apatite from the TDLG compared to those from the Stillwater and Bushveld complexes (Boudreau et al., 1997).

Much of the chalcopyrite in the Main Zone has replaced pyrrhotite and is intergrown with hydrous silicate minerals, which suggests that Cu was introduced into the system by fluids. This observation can be explained by a process in which fluids flux through the Footwall Zone, transporting Cu to the Main Zone during its upward migration. Therefore, a zone-refining process, in which volatiles that were derived from footwall country-rock dehydration migrated up through the crystallizing gabbro, is an attractive alternative by which Cl could be added to the system. Zoning and recrystallization textures of Cl-rich apatite also indicate that Cl was not incorporated at the time of apatite crystallization, but rather Cl addition occurred at some point after the crystallization of apatite started. The low Cl contents of apatite in the W horizon can be explained if these fluids did not migrate up as far as the W Horizon. Alternatively, the W Horizon represents a late stage of magma intrusion, after the Cl-rich fluids had fluxed through the lower portions of the TDLG. Thus, the alteration of the primary igneous minerals, the re-crystallization textures, the high Cl/F exhibited by apatite within the Footwall and Main zones, and higher Cl and transition metal contents of the apatite replacement rims can be attributed to the interaction of a fluid phase at suprasolidus and/or subsolidus conditions.

IMPLICATIONS FOR EXPLORATION

A multistage-dissolution upgrading model has been widely accepted for the genesis of magmatic PGE-Cu deposits, and has been proposed for the formation of the Marathon deposit (Good, 2010). In this model, new, S-under-saturated magma pulses through magma conduits, resulting in dissolution of pre-existing sulphide but not PGE (Kerr and Leitch, 2005), and produces very high PGE/Cu and PGE/S ratios. The textures and chemistry of plagioclase and apatite indicate multiple influxes of magma into the Marathon gabbros, which would support this model. Therefore, the textural and chemical features described in this study can be used to indicate that these processes have occurred and thus could be used as an indicator of fertility of gabbro in exploration.

ACKNOWLEDGEMENTS

The authors wish to thank Melissa Price for her support during analyses, and Matthew Brzozowski, Rachel Epstein, Ryan Ruthart, and Katrina McLean for assistance during field sampling. Financial support has been provided by Stillwater Canada Ltd., NSERC, and the TGI-4 Ni-Cu-PGE-Cr project of the Geological Survey of Canada.

REFERENCES

Barrie, C.T., MacTavish, A.D., Walford, P.C., Chataway, R., and Middaugh, R., 2002. Contact-type and magnetitite reef-type Pd-Cu mineralization in ferroan olivine gabbros of the

Coldwell Complex, Ontario, *In:* The Geology, Geochemistry, Mineralogy and Mineral Beneficiation of Platinum-Group Elements, (ed.) L.J. Cabri); Canadian Institute of Mining, Metallurgy and Petroleum, Special Volume 54, p. 321–337.

Best, M.G., 2003. Igneous and Metamorphic Petrology, Second Edition; Blackwell Publishing 729 p.

Boudreau, A. and Hoatson, D., 2004. Halogen variation in the Paleoproterozoic layered mafic-ultramafic intrusions of east Kimberley, Western Australia: implication for platinum group element mineralization; Economic Geology, v. 99, p. 1015–1026.

Boudreau, A. and Kruger, F., 1990. Variation in the composition of apatite through the Merensky cyclic unit in the western Bushveld Complex; Economic Geology, v. 85, p. 737–745.

Boudreau, A., Mathez, E., and McCallum, I., 1986. Halogen geochemistry of the Stillwater and Bushveld complexes: evidence for transport of the platinum-group elements by Cl-rich fluids; Journal of Petrology, v. 27, p. 967–986. doi:10.1093/petrology/27.4.967

Boudreau, A. and McCallum, I., 1989. Investigations of the Stillwater Complex: Part V. Apatites as indicators of evolving fluid composition; Contributions to Mineralogy and Petrology, v. 102, p. 138–153.

Boudreau, A.E., Stewart, M.A., and Spivack, A.J., 1997. Stable chlorine isotopes and the origin of high-Cl magmas of the Stillwater Complex, Montana; Geology, v. 25, p. 791–794.

Browne, B.L., Eichelberger, J.C., Patino, L.C., Vogel, T.A., Uto, K., and Hoshizumi, H., 2006. Magma mingling as indicated by texture and Sr/Ba ratios of plagioclase phenocrysts from Unzen volcano, SW Japan; Journal of Volcanology and Geothermal Research, v. 154, p. 103–116. doi:10.1016/j.jvolgeores.2005.09.022

Dahl, R., Watkinson, D.H., and Taylor, R.P., 2001, Geology of the Two Duck Lake intrusion and the Marathon Cu-PGE deposit, Coldwell complex, northern Ontario; Exploration and Mining Geology, v. 10, p. 51–65.

Gál, B., Molnár, F., Guzmics, T., Mogessie, A., Szabó, C., and Peterson, D.M., 2013, Segregation of magmatic fluids and their potential in the mobilization of platinum-group elements in the South Kawishiwi Intrusion, Duluth Complex, Minnesota — Evidence from petrography, apatite geochemistry and coexisting fluid and melt inclusions; Ore Geology Reviews, v. 54, p. 59–80. doi:10.1016/j.oregeorev.2013.03.001

Gál, B., Molnar, F., and Peterson, D.M., 2011. Cu-Ni-PGE mineralization in the South Filson Creek Area, South Kawishiwi Intrusion, Duluth Complex: Mineralization styles and magmatic and hydrothermal processes; Economic Geology, v. 106, p. 481–509. doi:10.2113/econgeo.106.3.481

Ginibre, C., Kronz, A., and Wörner, G., 2002. High-resolution quantitative imaging of plagioclase composition using accumulated backscattered electron images: new constraints on oscillatory zoning; Contributions to Mineralogy and Petrology, v. 142, p. 436–448. doi:10.1007/s004100100298

Ginibre, C., Wörner, G., and Kronz, A., 2007. Crystal zoning as an archive for magma evolution; Element, v. 3, p. 261–266.

Good, D., 2010, Applying multistage dissolution upgrading and 3d-GIS to exploration at the Marathon Cu-PGE deposit, Canada, In: Abstracts; 11th International Platinum Symposium, p. 1–4.

Good, D. and Crocket, J.H., 1994. Genesis of the Marathon Cu-platinum-group element deposit, Port Coldwell alkalic complex, Ontario: A midcontinent rift-related magmatic sulfide deposit; Economic Geology, v. 89, p. 131–149.

Gorokhova, N.V., Melnik, O.E., Plechov, P.Y., and Shcherbakov, V.D., 2013. Numerical simulation of plagioclase rim growth during magma ascent at Bezymianny Volcano, Kamchatka; Journal of Volcanology and Geothermal Research, v. 263, p. 172–181. doi:10.1016/j.jvolgeores.2013.03.020

Hall, A., 1987. Igneous Petrology; Longman Scientific & Technical, 586 p.

Harris, C. and Chaumba, J., 2001. Crustal contamination and fluid–rock interaction during the formation of the Platreef, northern limb of the Bushveld Complex, South Africa; Journal of Petrology, v. 42, p. 1321–1347.

Holwell, D., Boyce, A., and McDonald, I., 2007. Sulfur isotope variations within the Platreef Ni-Cu-PGE deposit: Genetic implications for the origin of sulfide mineralization; Economic Geology, v. 102, p. 1091–1110.

Holwell, D., Keays, R., Firth, E., and Findlay, J., 2014. Geochemistry and mineralogy of platinum group element mineralization in the River Valley Intrusion, Ontario, Canada: A model for early-stage sulfur saturation and multistage emplacement and the implication for "contact-type" Ni-Cu-PGE sulfide mineralization; Economic Geology, v. 109, p. 689–712.

Humphreys, M.C.S., 2009. Chemical evolution of intercumulus liquid, as recorded in plagioclase overgrowth rims from the Skaergaard Intrusion; Journal of Petrology, v. 50, p. 127–145. doi:10.1093/petrology/egn076

Humphreys, M.C.S., Blundy, J.D., and Sparks, R.S.J., 2006. Magma evolution and open-system processes at Shiveluch Volcano: Insights from phenocryst zoning; Journal of Petrology, v. 47, p. 2303–2334. doi:10.1093/petrology/egl045

Kerr, A. and Leitch, A., 2005. Self-destructive sulfide segregation systems and the formation of high-grade magmatic ore deposits; Economic Geology, v. 100, p. 311–332.

Kruger, F.J., 1992. The origin of the Merensky cyclic unit: Sr-isotopic and mineralogical evidence for an alternative orthomagmatic model; Australian Journal of Earth Sciences, v. 39, p. 255–261. doi:10.1080/08120099208728021

Mungall, J.E., 2005. Magmatic geochemistry of the platinum-group elements, Chapter 1 *In:* Exploration for Platinum-Group Element Deposits; Mineralogical Association of Canada, Short Course Series Volume 35, p. 1–34.

Naldrett, A.J., 2004. Magmatic Sulfide Deposits: Geology, Geochemistry, and Exploration; Springer-Verlag, 728 p.

Ruthart, R., Linnen, R., Samson, I., and Good, D., 2010. Characterization of high-PGE low-sulphur mineralization at the Marathon PGE-Cu deposit, Ontario, *In:* Abstracts; 11th International Platinum Symposium, 21-24 June 2010, Sudbury, Ontario, p. 1–4.

Sharman-Harris, E.R., Kinnaird, J.A., Harris, C., and Horstmann, U.E., 2005. A new look at sulphide mineralisation of the northern limb, Bushveld Complex: a stable isotope study; Applied Earth Science, v. 114, p. 252–263. doi:10.1179/037174505X82134

Streck, M.J., 2008. Mineral textures and zoning as evidence for open system processes; Reviews in Mineralogy and Geochemistry, v. 69, p. 595–622. doi:10.2138/rmg.2008.69.15

Thy, P., Lesher, C.E., and Tegner, C., 2013. Further work on experimental plagioclase equilibria and the Skaergaard liquidus temperature; American Mineralogist, v. 98, p. 1360–1367. doi:10.2138/am.2013.4044

Watkinson, D.H. and Ohnenstetter, D., 1992. Hydrothermal origin of platinum-group mineralization in the Two Duck Lake intrusion, Coldwell complex, northwestern Ontario. Canadian Mineralogist, v. 30, p. 121–136.

Willmore, C., Boudreau, A., and Kruger, F., 2000. The halogen geochemistry of the Bushveld Complex, Republic of South Africa: implications for chalcophile element distribution in the lower and critical zones; Journal of Petrology, v. 41, p. 1517–1539.

Willmore, C.C., Boudreau, A.E., Spivack, A., and Kruger, F.J., 2002. Halogens of Bushveld Complex, South Africa: $\delta^{37}Cl$ and Cl/F evidence for hydration melting of the source region in a back-arc setting; Chemical Geology, v. 182, p. 503–511.

Zientek, M.L., 2012. Magmatic ore deposits in layered intrusions — descriptive model for reef-type PGE and contact-type Cu-Ni-PGE deposits; U.S. Geological Survey, Open-File Report 2012-1010, 48 p.

GEOLOGICAL SURVEY OF CANADA
OPEN FILE 7856

Targeted Geoscience Initiative 4: Canadian Nickel-Copper-Platinum Group Elements-Chromium Ore Systems — Fertility, Pathfinders, New and Revised Models

Variation in vein mineralogy and mineral chemistry around the Marathon Cu-Pd deposit, Ontario: Insights into the development of an exploration tool

Matthew J. Brzozowski[1], Iain M. Samson[1], Joel E. Gagnon[1], Robert L. Linnen[2], David J. Good[2], Doreen E. Ames[3], and Roberta L. Flemming[2]

[1]University of Windsor, Windsor, Ontario
[2]University of Western Ontario, London, Ontario
[3]Geological Survey of Canada, Ottawa, Ontario

2015

© Her Majesty the Queen in Right of Canada, as represented by the Minister of Natural Resources Canada, 2015

This publication is available for free download through GEOSCAN (http://geoscan.nrcan.gc.ca/)

Recommended citation

Brzozowski, M.J., Samson, I.M., Gagnon, J.E., Linnen, R.L., Good, D.J., Ames, D.E., and Flemming, R.L., 2015. Variation in vein mineralogy and mineral chemistry around the Marathon Cu-Pd deposit, Ontario: Insights into the development of an exploration tool, *In:* Targeted Geoscience Initiative 4: Canadian Nickel-Copper-Platinum Group Elements-Chromium Ore Systems — Fertility, Pathfinders, New and Revised Models, (ed.) D.E. Ames and M.G. Houlé; Geological Survey of Canada, Open File 7856, p. 245–255.

Publications in this series have not been edited; they are released as submitted by the author.

Contribution to the Geological Survey of Canada's Targeted Geoscience Initiative 4 (TGI-4) Program (2010–2015)

TABLE OF CONTENTS

Variation in vein mineralogy and mineral chemistry around the Marathon Cu-Pd deposit, Ontario: Insights into the development of an exploration tool

Matthew J. Brzozowski[1]*, Iain M. Samson[1], Joel E. Gagnon[1], Robert L. Linnen[2], David J. Good[2], Doreen E. Ames[3], and Roberta L. Flemming[2]

[1]Department of Earth and Environmental Sciences, University of Windsor, 401 Sunset Avenue, Windsor, Ontario N9B 3P4
[2]Department of Earth Sciences, University of Western Ontario, 1151 Richmond Street N., London, Ontario N6A 3K7
[3]Geological Survey of Canada, 601 Booth Street, Ottawa, Ontario K1A 0E8
*Corresponding author's e-mail: brzozowm@uwindsor.ca

ABSTRACT

The Marathon Cu-Pd deposit (125 Mt at 0.26% Cu, 0.72 ppm Pd, 0.25 ppm Pt, and 0.08 ppm Au) is hosted within the Two Duck Lake Intrusion (TDLI), a late-stage phase of the Eastern Gabbro in the Coldwell Complex. Late-stage chlorite±calcite veins are present in and around the Marathon deposit, indicating subsolidus movement of fluids throughout mineralized and barren rocks. The hypothesis to be tested is did fluids migrating upwards through mineralized rock mobilize metals into overlying barren rock and was this movement recorded in the chemistry of vein minerals? Chlorite- and calcite-bearing veins were collected from drillholes throughout the deposit. The drill-core samples contain veins hosted in variably mineralized and barren host rocks. Chlorite, the dominant phase, occurs as very fine-grained, bladed crystals in massive, radiating, or aligned aggregates. The veins also contain minor saponite, talc, serpentine, and/or amphibole. Mineral chemistry data from energy- and wavelength-dispersive spectroscopy indicate that the Fe/Mg ratio in chlorite (chamosite to clinochlore) is highly variable, and varies as a function of host-rock type.

Laser ablation ICP-MS analyses were carried out on 52 chlorite samples collected throughout the deposit and barren host rocks. Transition metals were detected in all chlorite veins, whereas metalloids were only detected in a subset of samples. Titanium, Cr, Mn, Zn, and metalloid concentrations do not correlate with host-rock type. Transition metal concentrations in vein chlorite that crosscuts plagioclase, pyroxene, and pyrrhotite are comparable; however, chlorite in veins that occur in magnetite, altered olivine, and chalcopyrite have distinctive transition metal signatures (e.g. significantly higher Ti and V concentrations in veins hosted by magnetite), indicating that chlorite chemistry was controlled on a very local scale. Cobalt, Ni, and Cu concentrations are greater above mineralization than within mineralization. The Mn concentrations in chlorite increase linearly towards mineralization, whereas Co, Ni, and Zn decrease. When employing chlorite chemistry as a vector to mineralization, grain-scale variations in chlorite must be considered. Our results show that when these small-scale controls on chlorite composition are recognized, the chemistry of chlorite can be a successful exploration tool.

INTRODUCTION

Mineral deposits generally occupy small areas and/or may be located below the surface, making them difficult to locate using normal surface mapping techniques. To increase the target area, geochemical-mineralogical haloes can be used to vector towards deposits (Kelley et al., 2006). However, very few studies have focused on using the chemistry of vein minerals for Cu-PGE exploration.

The contact-type Marathon Cu-platinum-group element (PGE) deposit, located near Marathon, Ontario, is hosted within the Two Duck Lake (TDL) gabbro, a late-stage intrusion within the Eastern Gabbro of the Coldwell Complex (Watkinson and Ohnenstetter, 1992; Good and Crocket, 1994; Dahl et al., 2001; Good et al., in press). The Eastern Gabbro is an arcuate, composite intrusion located at the base of the Coldwell Complex, and is the oldest intrusive phase within the complex (Shaw, 1997; Barrie, 2002; Good et al., in press). Recent studies by Good et al. (in press) have led to new subdivisions of the Eastern Gabbro into three gabbroic series: the Fine-Grained Series, the Layered Series, and the Marathon Series, the latter of which is host to the majority of the mineralization.

The Fine-Grained Series is tholeiitic in composition, occurs at the base of the Eastern Gabbro, and is compositionally homogenous (Good et al., in press). The Layered Series makes up the majority of the Eastern

Brzozowski, M.J., Samson, I.M., Gagnon, J.E., Linnen, R.L., Good, D.J., Ames, D.E., and Flemming, R.L., 2015. Variation in vein mineralogy and mineral chemistry around the Marathon Cu-Pd deposit, Ontario: Insights into the development of an exploration tool, *In:* Targeted Geoscience Initiative 4: Canadian Nickel-Copper-Platinum Group Elements-Chromium Ore Systems — Fertility, Pathfinders, New and Revised Models, (ed.) D.E. Ames and M.G. Houlé; Geological Survey of Canada, Open File 7856, p. 245–255.

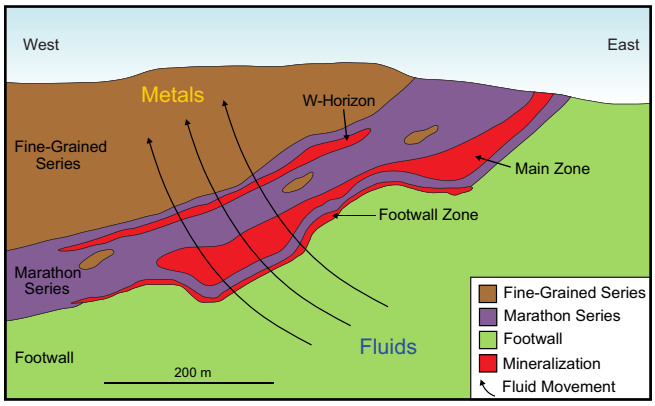

Figure 1. East-west cross-section of the Marathon deposit showing relative locations of the main rock series and mineralized zones (modified after Ruthart, 2013). Curved arrows illustrate the hypothetical movement of fluid upward through mineralized and barren rock.

Gabbro and occurs stratigraphically above the Fine-Grained Series. It is geochemically and texturally similar throughout the Coldwell Complex and is characterized by massive to modally layered olivine gabbro (Good et al., in press). The Marathon Series is defined as including all mafic and ultramafic intrusive rocks that host Cu and PGE mineralization (Good et al., in press). It comprises mainly the TDL gabbro, an unmetamorphosed and undeformed body formed from multiple intrusions of crystal-laden magma into the Fine-Grained Series (Good and Crocket, 1994; Good et al., in press). It is coarse grained to pegmatitic and displays ophitic to subophitic textures (Good and Crocket, 1994; Good et al., in press).

Mineralization within the Marathon Series occurs in three zones: the Footwall Zone, the Main Zone, and the W-Horizon (Ruthart, 2013; Good et al., in press). The Footwall Zone is located between the contact of the footwall and TDL gabbro (Ruthart, 2013; Good et al., in press). Sulphides are interstitial to the silicates and consist of, in decreasing abundance, pyrrhotite, chalcopyrite, pyrite, and pentlandite. The sulphides are typically disseminated, but can occur as net-textured assemblages and as semi-massive blebs (Ruthart, 2013; Good et al., in press). The Main Zone is located in the lower part of the TDL gabbro (Ruthart, 2013; Good et al., in press). Sulphides here are dominated by chalcopyrite and pyrrhotite with minor bornite, pentlandite, and pyrite, and occur as lenses of disseminated mineralization where chalcopyrite commonly replaces pyrrhotite (Good and Crocket, 1994; Dahl et al., 2001). Platinum-group minerals are, in part, associated with chalcopyrite and an alteration assemblage dominated by chlorite and/or actinolite, with or without epidote, sericite, and calcite (Watkinson and Ohnenstetter, 1992; Dahl et al, 2001). The W-Horizon is hosted by the TDL gabbro and sits above the Main Zone, but offset from it. Due to the low sulphide content of the W-Horizon, it can only be distinguished from the Main Zone by its distinctly low S contents, low Cu/Pd (average <3500, high grade <215) and S/Se ratios, and a mineralogy that comprises chalcopyrite and bornite, rather than chalcopyrite and pyrrhotite (Ruthart, 2013; Good et al., in press).

The presence and effects of fluids within the Marathon deposit were described by Watkinson and Ohnenstetter (1992) and Barrie et al. (2002). The working hypothesis of this study is that fluids passing through the Cu-PGE deposit mobilized metals (e.g. Cu, Ni) out of the mineralized Marathon Series and into the barren Marathon and Fine-Grained Series, and influenced the chemistry of the vein minerals (Fig. 1). The objective of this study is to systematically characterize variations in late vein-mineral chemistry and determine which, if any, elements and minerals may be used as a vectoring tool for Cu-PGE exploration in the Coldwell Complex and elsewhere. Understanding how and why mineral chemistry varies is critical in the development of an exploration vector because controls on mineral chemistry at, for example, the grain-scale, may complicate or invalidate its use as an exploration tool.

RESULTS AND DATA ANALYSIS

Drillhole Sampling and Vein Density

Samples of veins were collected from ten drillholes, which are distributed along a 5.2 km line from the northern end of the 4 km long Marathon deposit to its southern end. Samples were taken from within and above the mineralized zones, at varying distances from the mineralization. Thin (<1 mm) veins are ubiquitous in the Marathon deposit and the surrounding barren gabbros. Vein density, quantified by counting the number of veins occurring over a 3 m interval, varies considerably (Fig. 2). An obvious correlation exists between vein density and mineralization, with mineralized rocks having distinctly lower vein densities; this relationship was observed in all of the drillholes examined, and is particularly obvious in drillhole M-06-221.

Petrography

Chlorite and calcite are the only abundant vein minerals that were observed. Chlorite is extremely fine grained, and occurs as randomly oriented, radiating, or aligned aggregates of bladed crystals (Fig. 3). In thin section, chlorite is commonly light to dark brown, but can also be colourless, pale to light green, yellow, or orange. It exhibits weak pleochroism and a range of first-order interference colours. Multiple optically distinguishable varieties of chlorite are generally present within a given vein, either intergrown or in separate

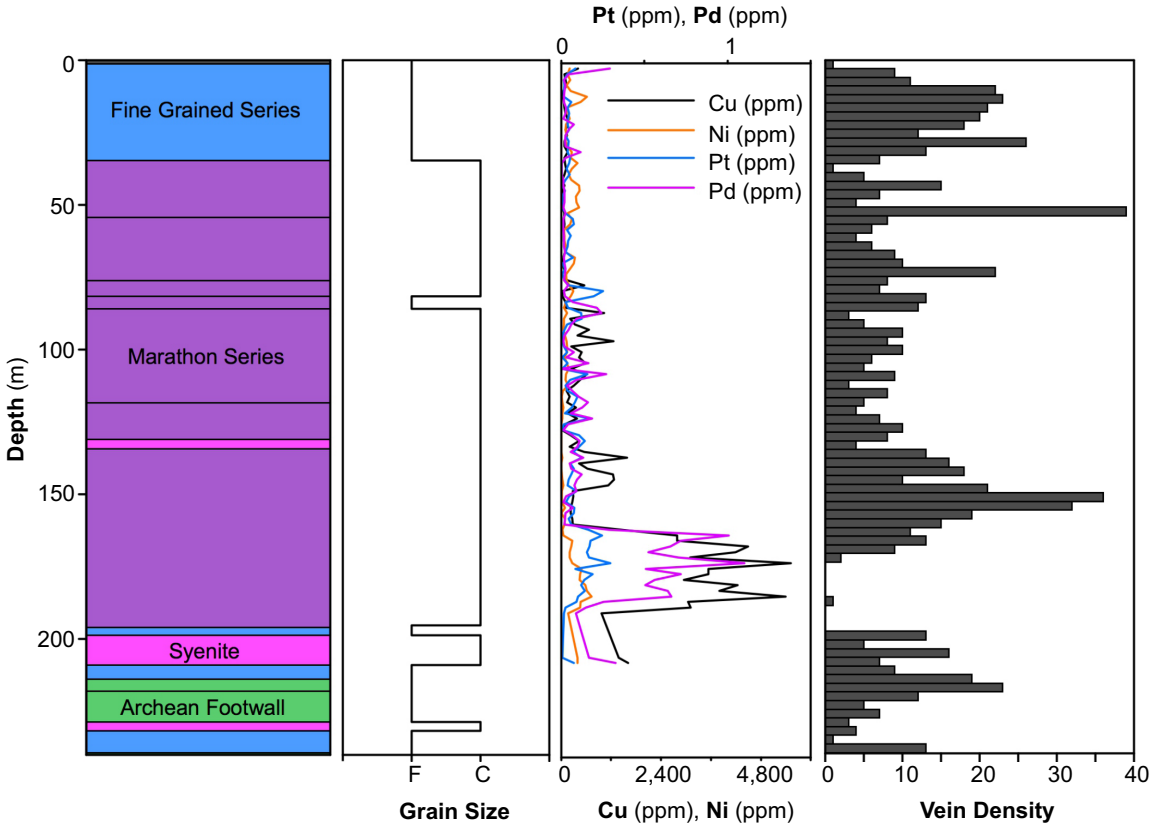

Figure 2. Downhole profile of drillhole M-06-221 illustrating the lithology, grain size, Cu, Ni, Pt, and Pd assay (ppm), and vein density.

zones with gradational or sharp contacts (Fig. 3). Light green to colourless Mg-rich chlorite is restricted to the outer zones of veins, where they crosscut plagioclase, and is absent from veins that crosscut pyroxene or olivine (Fig. 3c,d).

Calcite is commonly a vein component (Fig. 3g,h), but is much less abundant than chlorite, typically occupying <10 to 20% of the vein. Fine-grained anhedral calcite grains occur in aggregates in the vein cores, as isolated crystals, and occasionally as very fine-grained disseminated crystals. Calcite is rarely the dominant vein mineral, but can comprise up to ~80 to 90% (Fig. 3g,h). Results from energy-dispersive spectroscopy (EDS), wavelength-dispersive spectroscopy (WDS), and Raman spectroscopy (described below) indicate that minor amounts of amphibole, serpentine, talc, and/or saponite are present in the veins. They are very fine-grained and exist as mixtures with chlorite or as the main phase within the vein; however, they are not distinguishable optically as their optical properties are similar to those of chlorite. Sulphides do not occur in the veins.

Major Element Chemistry

Chlorite from 61 vein samples was analyzed by EDS, and a subset of these by WDS. Analyses of single crystals proved difficult due to the extremely small size of most of the chlorite crystals (<1–10 μm) and, as a result, analyses represent the composition of crystal aggregates. Typically 3 to 5 analyses within individual zones in the veins were used to confirm homogeneity of chlorite composition. Aluminum contents of chlorite do not vary significantly, however, the Si/Al ratio and the concentration of Fe and Mg vary among rock series. The Si/Al ratio is only slightly higher (mean = 4.5) in veins hosted within Archean footwall and slightly lower (mean = 2.75) in veins hosted in Layered Series gabbro, compared to the other rock series. Average total Fe concentrations range from ~6 to ~13 at.%; the lowest average values are in veins hosted by Archean footwall, and the highest in veins hosted in augite syenite, with gabbro-hosted chlorite ranging from ~7 to ~10 at.%. Magnesium concentrations show the opposite trend. Calcium was detected (<1 at.%) in many analyses, with concentrations slightly higher in veins hosted in Archean footwall and Layered Series rocks, compared to the other rock types.

Figure 4 illustrates the relative proportions of Al, Fe, and Mg in vein chlorite, which ranges in composition from clinochlore to chamosite; average atomic Mg/(Mg+Fe) ratios are between ~0.15 and ~0.6. Both chamosite and clinochlore veins are present in all of the rock series in the Eastern Gabbro. Some veins have compositions that are consistent with the presence of

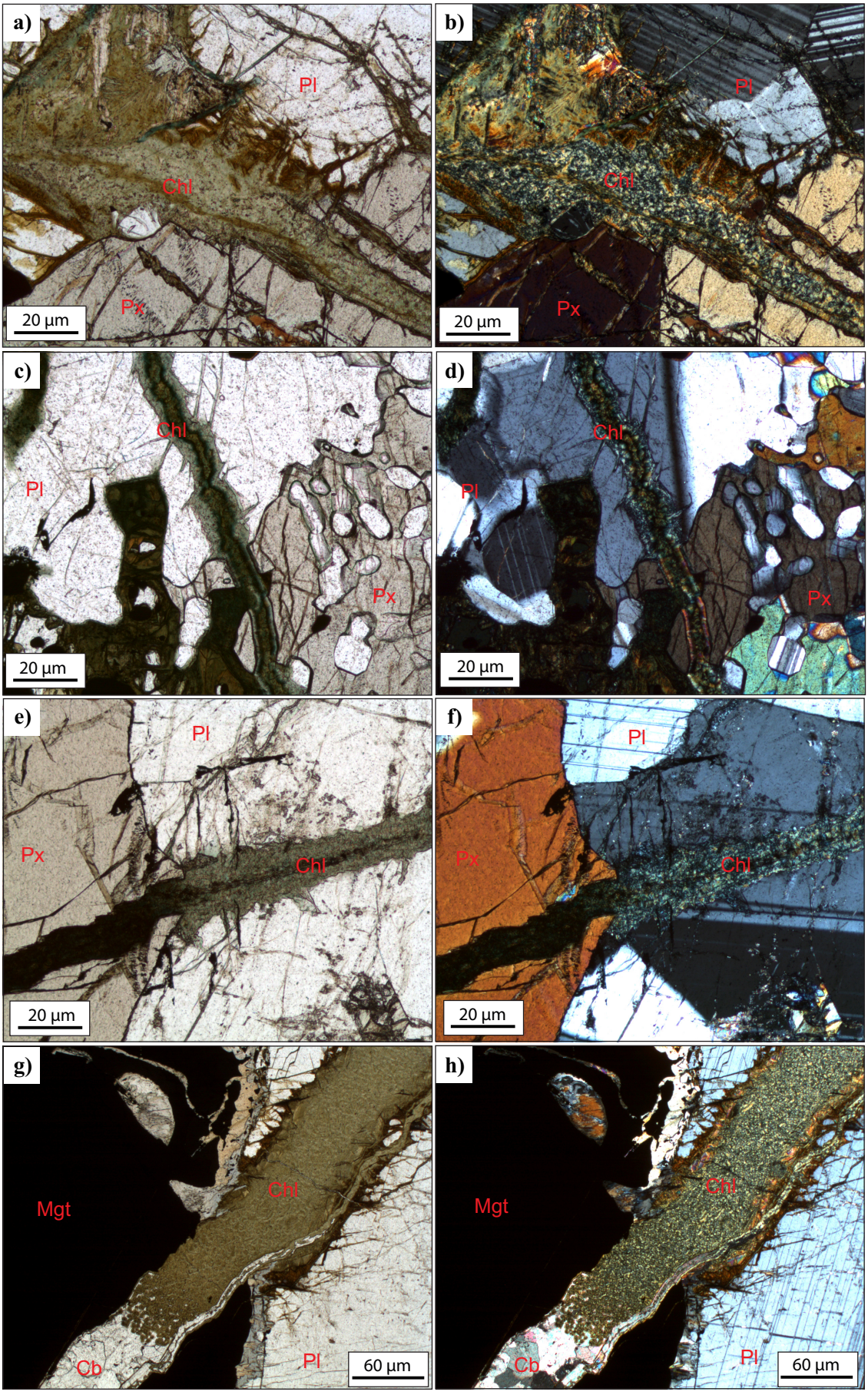
a)
Pl
Chl
Px
20 µm
b)
Pl
Chl
Px
20 µm
c)
Chl
Pl
Px
20 µm
d)
Chl
Pl
Px
20 µm
e)
Pl
Px
Chl
20 µm
f)
Pl
Px
Chl
20 µm
g)
Mgt
Chl
Cb
Pl
60 µm
h)
Mgt
Chl
Cb
Pl
60 µm

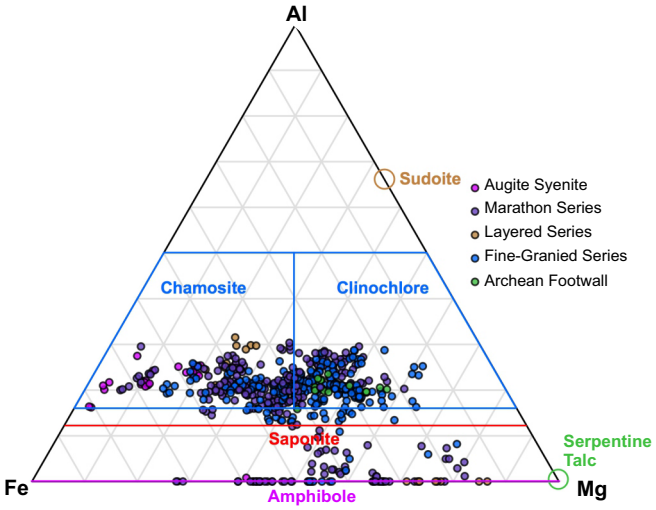

Figure 4. Ternary diagram showing the relative atomic proportions of Al, Fe, and Mg in vein minerals. Compositional fields for chlorite, saponite, amphibole, serpentine, talc, and sudoite are also shown (Bailey, 1988; Deer et al., 1996). Symbol colours represent the host-rock type.

saponite, amphibole, serpentine, and talc, or some combination of these minerals. Pale green and colourless chlorite varieties are consistently devoid of Ca and have the most consistent Si concentrations.

Raman Spectroscopy and Micro X-Ray Diffraction

Raman spectroscopy (McMillan, 1989) and micro X-ray diffraction (Flemming, 2007) were useful tools for identifying vein minerals, as these instruments are capable of identifying minerals occurring as mixtures with high degrees of spatial resolution. Both techniques were used to identify different hydrous silicates occurring as mixtures within the veins (e.g. chlorite versus serpentine, amphibole), however, the spectra did not allow us to distinguish different varieties of chlorite (i.e. chamosite versus clinochlore).

Trace Element Chemistry

Chlorite veins from 52 thick sections, collected at various depths in nine drillholes spanning the entire Marathon deposit, were analyzed by LA-ICP-MS for major elements, transition metals (Ti, V, Cr, Mn, Co, Ni, Cu, Zn, Cd), and metalloids (As, Sn, Sb, Pb, Bi). Transition metals are present in all the chlorite veins analyzed, whereas metalloids in only a subset. With the exception of Cd, all transition metals are present in higher concentration than metalloids. Median concentrations for transition metals range from 0.15 ppm for Cd up to 1500 ppm for Mn, whereas those for metalloids range from as low as 0.03 ppm for Bi to 0.64 ppm for As. Representative metal concentrations of vein chlorite are provided in Table 1.

Local Controls on Chlorite Trace-Element Chemistry

It is important to understand the effects that other variables (e.g. host-rock type, host mineral) have on vein chlorite chemistry so that such effects can be taken into account when interpreting the relationship between chlorite chemistry and mineralization. Chlorite veins hosted in Marathon Series (±Cu-PGE), Fine-Grained Series (barren), Layered Series (barren), and Archean Footwall rocks were analyzed. Vanadium is present in greater concentrations, and Cd in lower concentrations, in chlorite veins hosted within Archean Footwall compared to those hosted in other rock types. Cobalt and Ni, and to some extent, Cr and Zn, are present in higher concentrations in chlorite veins hosted in Archean Footwall and Fine-Grained Series rocks compared to those hosted in the other mineralized and barren rock types. To assess the spatial variations in chlorite chemistry independent of any host-rock influence, metal concentrations were normalized to a representative host-rock metal content for the Fine-Grained Series and Marathon Series (Table 2). Normalized Co, Ni, and Cu concentrations are greater in chlorite veins hosted in Fine-Grained Series than in Marathon Series rocks. The unnormalized concentration of Cr, Co, and Ni is greater in some chlorite veins hosted by rocks with high magnetite content compared to those with low magnetite content, whereas Mn concentrations are lower.

The concentrations of transition metals and metalloids in chlorite hosted by plagioclase, pyroxene, and pyrrhotite show similar ranges throughout the sample suite. The exception is Cd, which has significantly higher concentrations in pyrrhotite-hosted veins compared to those hosted in the other minerals. Magnetite-hosted veins consistently have higher concentrations of Ti and V compared to those in other mineral hosts. Although few chalcopyrite-hosted and altered olivine-hosted veins were present and analyzed, some notable correlations were observed. Chlorite hosted by chalcopyrite has anomalously high Cu concentrations; however, the concentrations of Ti and Co are only marginally lower than those in the previously mentioned minerals. Altered olivine-hosted veins have significantly lower Ti and V, but significantly higher Co, Ni,

Figure 3 (opposite page). Photomicrographs in plane-polarized and cross-polarized light illustrating (**a-b)** mixtures of chlorite with other minerals in a vein, **(c-f)** variations in chlorite morphology and optical properties as a function of host mineral, and **(g-h)** a chlorite-calcite vein in which calcite is the predominant mineral in portions of the vein. Abbreviations: Cb = carbonate, chl = chlorite, mgt = magnetite, pl = plagioclase; and px = pyroxene.

Table 1. Representative trace metal concentrations (ppm) in vein chlorite from mineralized and barren sections of each drillhole sampled. Concentrations for each sample represent an individual laser ablation analysis.

Sample	Location to Mineralization	Host-Rock Series	Ti ppm	V ppm	Cr ppm	Mn ppm	Co ppm	Ni ppm	Cu ppm	Zn ppm	As ppm	Cd ppm	Sn ppm	Sb ppm	Pb ppm	Bi ppm
MB-151-04	Above	Fine-Grained	93	0.9		1574	24	7	37	13			11		3	
MB-151-20	Within	Marathon	65	3	0.7	1678	10	2	17	9			1	0.03	16	
MB-221-026	Above	Marathon	84	9	6	1168	4	15	5	8		0.06	0.2	0.09	0.4	
MB-221-035	Within	Marathon	46	8	3	1357	3	30	5	6			0.3		0.2	
MB-366-23	Above	Fine-Grained	332	19	21	446	50	164	3	16	2	0.1	5		2	0.01
MB-366-40	Within	Fine-Grained	59	77	0.9	1213	4	4	11	4			10		0.4	
MB-391-25	Above	Marathon	127	35		1296	80	453	1	52		0.2	0.5		0.1	0.08
MB-391-31	Within	Marathon	31	79	2	1707	14	36	13	27		0.2	8		0.6	
MB-424-017	Above	Fine-Grained	8			1995	90	297	0.8	48			0.2		0.07	
MB-424-036	Within	Marathon	38	4	2	1761	58	98	7	59			0.3		1	
MB-513-003	Above	Augite Syenite	22			8606	3	2	0.4	1		0.07	0.3		0.1	
MB-513-011	Within	Marathon	75	1		4705	28	149	3	95	0.4		0.2	0.08	2	
MB-99-10	Above	Fine-Grained	178	52	47	867	1	7	1	7		0.1	0.7		0.9	
MB-99-16	Within	Marathon	52	3	0.5	1541	1	16	2	6		0.07	0.2		0.07	
MB-MW05-02	Above	Marathon	70	8		1997	16	2	1	5			0.2		0.09	
MB-MW05-05	Within	Marathon	25	0.8	0.5	2480	8	11	37	13			1		8	
MB-MW06-01	Above	Layered	255	9		6108	13	0.9	1	7		0.1	1		0.1	

Note: Blank cells represent elements that are below detection.

Table 2. Metal concentrations (ppm) of host rocks from Good et al. (in press) used to normalize metal concentrations in vein chlorite. Representative host rock normalized trace metal concentrations (ppm) of vein chlorite from mineralized and barren sections of each drillhole sampled. Concentrations for each sample represent an individual laser ablation analysis.

Rock Type	Co ppm	Cr ppm	Cu ppm	Ni ppm	V ppm	Zn ppm	TiO_2 wt%	MnO wt%
Augite Troctolite	76.7	67.7	71.0	172	238	97	0.7	0.2
Olivine Gabbro	60	10	300	7	259	210	3.12	0.34
Two Duck Lake Gabbro	74.3	146	1766	242	393	86	0.86	0.17
Gabbro	57.1	348	51	146	351	97	1.26	0.18
Picritic Gabbro	101	1523	88	853	263	112	1.25	0.21
Lower Oxide Melatroctolite	126	233	1634	148	1623	331	6.28	0.38

Sample	Co	Cr	Cu	Ni	V	Zn	Ti	Mn
MB-151-04	0.4		0.7	0.05		0.1	0.01	1
MB-151-20	0.1		0.01	0.01	0.01	0.1	0.01	1
MB-221-026	0.05	0.04		0.06	0.02	0.09	0.02	0.9
MB-221-035	0.05	0.02		0.1	0.02	0.07	0.01	1
MB-366-23	0.9	0.06	0.05	1	0.06	0.2	0.04	0.3
MB-366-40	0.07		0.2	0.03	0.2	0.04	0.01	0.9
MB-391-25	1			2	0.09	0.6	0.02	1
MB-391-31	0.2	0.02	0.01	0.2	0.2	0.3	0.01	1
MB-424-017	2		0.02	2		0.5		1
MB-424-036	0.8	0.02		0.4	0.01	0.7	0.01	1
MB-513-011	0.2			1		0.3		2
MB-99-10	0.01	0.03	0.01	0.01	0.2	0.06	0.02	0.5
MB-99-16	0.01			0.07	0.01	0.07	0.01	1
MB-MW05-02	0.2			0.01	0.02	0.06	0.01	2
MB-MW05-05	0.1		0.02	0.04		0.2		2
MB-MW06-01	0.2			0.1	0.03	0.03	0.01	2

Note: Blank cells represent elements that are below detection; host-rock metal concentrations from Good et al. (in press)

and Zn concentrations than veins hosted by other minerals.

Relationship between Trace-Element Chemistry and Mineralization

Figure 5 illustrates the spatial relationship between chlorite trace-element chemistry and Cu-PGE mineralization in aggregated downhole plots that incorporate data from all of the drillholes sampled. The boundary of the mineralization is defined as the initial spike in Cu and Ni in the downhole assay data. As mineralization is approached, vein-chlorite concentrations of Mn, Co, Ni, and Zn vary systematically. Manganese concentrations increase linearly by roughly an order of magnitude, whereas Co, Ni, and Zn concentrations decrease by almost two orders of magnitude as mineralization is approached. Concentrations of Co, Ni, and Zn all decrease nonlinearly, however, the trend for Ni is different from that of Co and Zn.

Patchy Chlorite Alteration

In addition to occurring in late-stage veins, chlorite also occurs in patchy alteration as aggregates of fine- to coarse-grained crystals that have replaced pyroxene and plagioclase in the TDL gabbro. This patchy chlorite is commonly associated with sulphides, but can occur where no sulfides are present. The major element chemistry of this chlorite is distinctly different from that of vein chlorite. Silicon is greater in vein chlorite compared to patchy chlorite (mean = 15 versus 11 at.%), whereas Al has the opposite relationship (mean = 4.5 versus 8 at.%), resulting in a Si/Al ratio that is consistently greater in vein chlorite (mean = 3.5 versus 1.5). There is generally no Ca detected in patchy chlorite, whereas up to 1 at.% is present in vein chlorite. The major element chemistry of patchy chlorite displays no difference whether or not it is associated with sulphides. However, the trace element chemistry of patchy chlorite is different from that of vein chlorite. Concentrations of Cr, As, Sn, and Sb are greater in vein chlorite than patchy chlorite, whereas Mn, Co, Ni, and Zn concentrations are greater in patchy chlorite. These concentration differences are less than an order of magnitude. Concentrations of trace metals are comparable in patchy chlorite associated with sulphides with those isolated from sulphides.

DISCUSSION

Few studies (e.g. Hanley and Bray, 2009; Tuba et al., 2014) have been published that have characterized silicate vein mineral chemistry and its relationship to Ni-Cu-PGE mineralization. A recent study by Hanley and Bray (2009) tested Ni concentrations in vein amphibole as an exploration vectoring tool for Cu-(Ni)-PGE mineralization in the Sudbury footwall of the Sudbury Igneous Complex. Their study showed that the concentration of Ni in vein-hosted amphibole ([Ni]amp) increased with increasing proximity to mineralization based on the model $[Ni]amp = 5100\ (D)^{-0.45}$, where D is the distance in metres from the initial signs of mineralization. Amphibole poikiloblasts contained only background Ni values.

Chlorite and/or chlorite-calcite veins are ubiquitous throughout the Marathon Cu-PGE deposit and Eastern Gabbro and their density varies with respect to mineralization (Fig. 2). Therefore, vein density itself may have the potential to be used as an exploration tool by vectoring towards areas with low vein density. Chlorite mineral chemistry is variable, ranging from Fe-rich varieties (chamosite) to Mg-rich varieties (clinochlore). The aluminum content, however, does not vary significantly, suggesting that all vein chlorite formed at similar temperatures (cf. Cathelineau, 1988). Patchy chlorite has consistently higher Al concentrations, suggesting that it formed at higher temperatures than the vein chlorite. Calcium is typically not incorporated into chlorite (Bailey, 1988), but is present in some vein chlorite from Marathon, yet generally absent from patchy chlorite. This, along with mineral compositions that fall outside of the chlorite compositional field (Fig. 3), indicates that, in some cases, the veins comprise mixtures of chlorite and other hydrous silicates containing Ca or fine-grained crystals of calcite, whereas patchy chlorite does not. Trace element contents of vein and patchy chlorite are also different (e.g. Cr, Co, Ni, and Zn). These observations demonstrate that patchy and vein chlorite formed during different events and at different temperatures, with the former associated with an earlier event that was more closely tied to the mineralization.

Revised Model

The trace element chemistry of vein-hosted chlorite is consistent with a model whereby fluids moved upwards through mineralized gabbros (TDL) at some time after the rocks had been mineralized, and carried metals into the overlying, barren gabbros. Cobalt, Ni, and Cu are elements indicative of fertility, whereby their normalized concentrations in chlorite are greater in veins hosted by the barren Fine Grained Series that lies above mineralization compared to veins hosted in mineralized Marathon Series. Of the transition metals analysed, only Mn, Co, Ni, and Zn show a variation with proximity to mineralization; Mn concentrations increase linearly with proximity to mineralization, and Co, Ni, and Zn concentrations decrease nonlinearly, providing new pathfinder elements for the Cu-PGE mineralization in the Coldwell Complex. It is expected that metal concentrations in vein chlorite would be greatest proximal to mineralization as that is where an

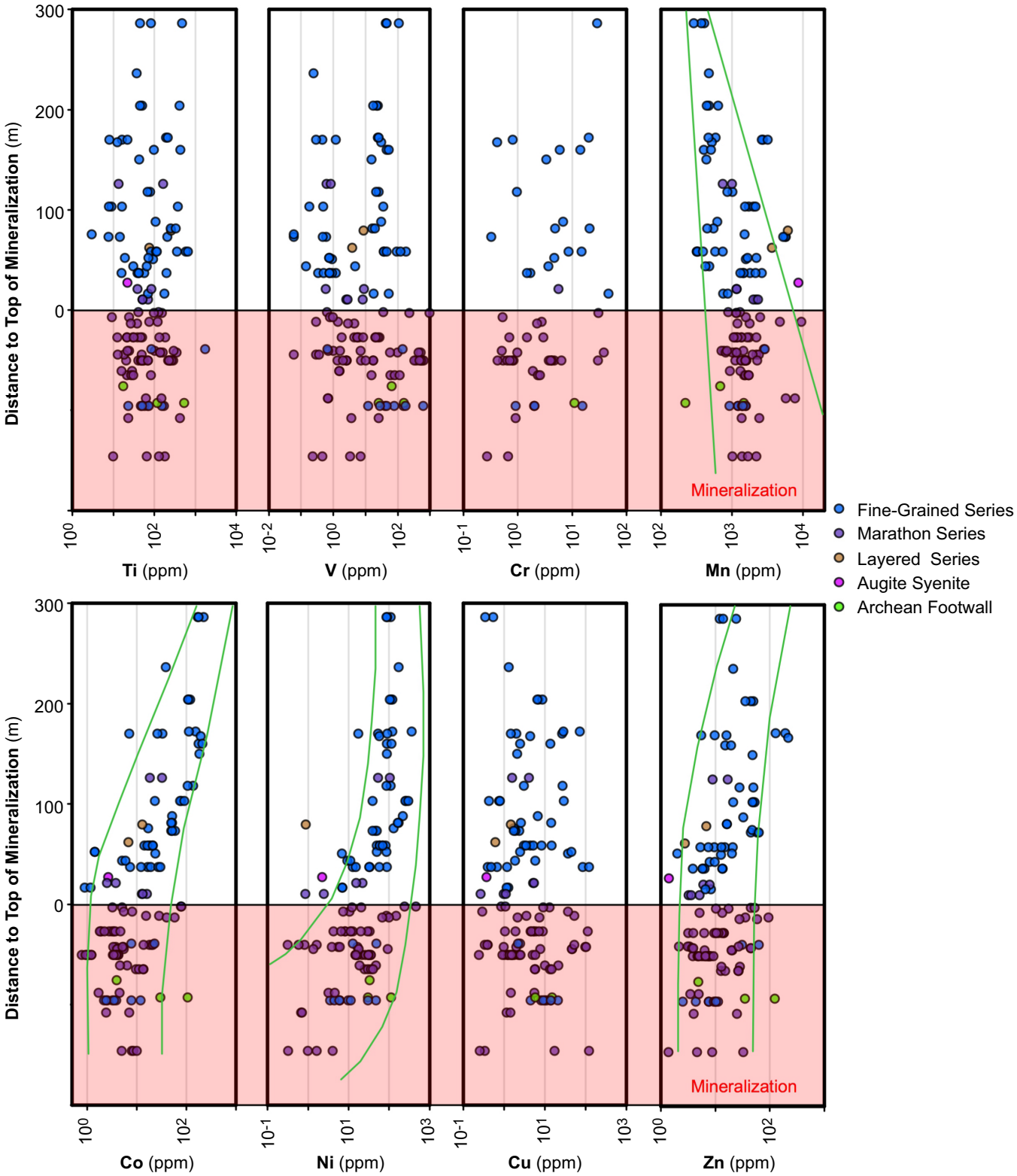

Figure 5. Composite downhole trace-element profiles demonstrating variations in vein-chlorite metal concentration as a function of proximity to mineralization. The top of mineralization was taken as the initial spike in Cu, Ni, Pt, and Pd in assay data. Symbol colours represent veins hosted in different rock series.

upwardly migrating fluid, having passed through a mineralized section and subsequently precipitated chlorite, would have the greatest concentration of metals. Manganese concentrations follow this trend; however, Co, Ni, and Zn display the opposite trend and decrease with proximity to mineralization. The reason for this is not yet understood, however, two things to consider are (1) a model in which fluids migrated

solely in an upward direction may be an oversimplification, and (2) the behaviour and sources of Mn, versus Co, Ni, and Zn are fundamentally different.

Care must be taken when analyzing vein-hosted chlorite and interpreting the relationships between mineral chemistry and mineralization, as host-rock mineralogy (i.e. the mineral in which the vein occurs) has an effect on vein chlorite chemistry. Interpretations should be based on those veins hosted by plagioclase, pyroxene, and pyrrhotite, as these minerals do not appear to exert a strong influence on the trace element chemistry of chlorite at a local scale.

IMPLICATIONS FOR EXPLORATION

Although the use of mineral chemistry as vectoring tool towards mineralization is not a new concept for many ore deposit types (i.e. indicator minerals), the relationship between post-mineralization vein-hosted mineral chemistry (e.g. chlorite) and Cu-PGE magmatic(-hydrothermal) mineralization has rarely been tested. In this study, we have illustrated how the chemistry of vein-hosted chlorite can be used to vector towards Cu-PGE mineralization in the Marathon deposit, and identified a few caveats to consider when interpreting an exploration survey database. Given the ubiquity of veins throughout mineralized and barren rocks, this exploration method has the potential to be applicable to a wide array of Cu-PGE ore systems.

ACKNOWLEDGEMENTS

Funding for this project was provided by NSERC, Stillwater Canada Inc., and the Geological Survey of Canada's TGI4 Ni-Cu-PGE-Cr project. The authors would like to thank Katrina McLean and Ryan Ruthart (Stillwater Canada Inc.) for providing access to their geological information and drill core. We are very grateful to Rachel Epstein for her insights into the Marathon geology and would like to thank Melissa Price, Sharon Lackie, and J.C. Barrette (University of Windsor) for their assistance in operating various analytical instruments.

REFERENCES

Bailey, S.W., 1988. Chlorites: structures and crystal chemistry, *In:* Hydrous Phyllosilicates (exclusive of micas), (ed.) S.W. Bailey; Mineralogical Society of America, v. 19, p. 347–398.

Barrie, C.T., MacTavish, A.D., Walford, P.C., Chataway, R., and Middaugh, R., 2002. Contact-type and magnetite reef-type Pd-Cu mineralization in the ferroan olivine gabbros of the Coldwell Complex, Ontario, *In:* Cabri, L.J., ed., The Geology, Geochemistry, Mineralogy and Mineral Beneficiation of Platinum-Group Elements; Canadian Institute of Mining, Metallurgy and Petroleum, Special Volume 54, p. 321–338.

Cathelineau, M., 1988. Cation site occupancy in chlorites and illness as a function of temperature; Clay Minerals, v. 23, p. 471–485.

Dahl, R., Watkinson, D.H., and Taylor, R.P., 2001. Geology of the Two Duck Lake Intrusion and the Marathon Cu-PGE Deposit, Coldwell Complex, Northern Ontario; Exploration and Mining Geology, v. 10, p. 51–65.

Deer, W.A., Howie, R.A., and Zussman, J., 1996. An Introduction to the Rock-Forming Minerals; Prentice Hall, 712 p.

Flemming, R.L., 2007. Micro X-ray Diffraction (μXRD): A versatile technique for characterization of Earth and planetary materials; Canadian Journal of Earth Sciences, v. 44, p. 1333–1346.

Good, D.J. and Crocket, J.H., 1994. Genesis of the Marathon Cu-platinum-group element deposit, Port Coldwell Alkalic Complex, Ontario: A midcontinent rift-related magmatic sulfide deposit; Economic Geology, v. 89, p. 131–149.

Good, D.J., Epstein, R., McLean, K., Linnen, R.L., and Samson, I.M., 2015. Evolution of the Main Zone at the Marathon Cu-PGE sulfide deposit, Midcontinent Rift, Canada: Spatial relationships in a magma conduit setting; Economic Geology, v. 110, p. 983–1008.

Hanley, J.J. and Bray, C.J., 2009. The trace metal content of amphibole as a proximity indicator for Cu-Ni-PGE mineralization in the footwall of the Sudbury Igneous Complex, Ontario, Canada; Economic Geology, v. 104, p. 113–125.

Kelley, D.L., Kelley, K.D., Coker, W.B., Caughlin, B., and Doherty, M.E., 2006. Beyond the obvious limits of ore deposits: The use of mineralogical, geochemical, and biological features for the remote detection of mineralization; Economic Geology, v. 101, p. 729–752.

McMillan, P.F., 1989. Raman spectroscopy in mineralogy and geochemistry; Annual Reviews in Earth and Planetary Sciences, v. 17, p. 255–283.

Ruthart, R., 2013. Characterization of High-PGE, Low-Sulphur Mineralization at the Marathon PGE-Cu Deposit, Ontario; M.Sc. thesis, University of Waterloo, Waterloo, Ontario, 145 p.

Shaw, C.S.J., 1997. The petrology of the layered gabbro intrusion, eastern gabbro, Coldwell alkaline complex, Northwestern Ontario, Canada: evidence for multiple phases of intrusion in a ring dyke; Lithos, v. 40, p. 243–259.

Tuba, G., Molnár, F., Ames, D. E., Péntek, A., Watkinson, D.H., and Jones, P., 2014. Multi-stage hydrothermal processes involved in "low-sulfide" Cu(-Ni)-PGE mineralization in the footwall of the Sudbury Igneous Complex (Canada): Amy Lake PGE zone, East Range; Mineralium Deposita, v. 49, p. 7–47.

Watkinson, D.H. and Ohnenstetter, D., 1992. Hydrothermal origin of platinum-group mineralization in the Two Duck Lake intrusion, Coldwell Complex, Northwestern Ontario; Canadian Mineralogist, v. 30, p. 121–136.

GEOLOGICAL SURVEY OF CANADA
OPEN FILE 7856

Targeted Geoscience Initiative 4: Canadian Nickel-Copper-Platinum Group Elements-Chromium Ore Systems — Fertility, Pathfinders, New and Revised Models

Trace element distribution in sulphide assemblages of the Levack-Morrison ore system, Sudbury, Ontario: Looking for chemical fingerprints of mineralization processes

Moji Adibpour[1], Pedro J. Jugo[1], and Doreen E. Ames[2]

[1]Laurentian University, Sudbury, Ontario
[2]Geological Survey of Canada, Ottawa, Ontario

2015

© Her Majesty the Queen in Right of Canada, as represented by the Minister of Natural Resources Canada, 2015

This publication is available for free download through GEOSCAN (http://geoscan.nrcan.gc.ca/)

Recommended citation

Adibpour, M., Jugo, P.J., and Ames, D.E., 2015. Trace element distribution in sulphide assemblages of the Levack-Morrison ore system, Sudbury, Ontario: Looking for chemical fingerprints of mineralization processes, *In:* Targeted Geoscience Initiative 4: Canadian Nickel-Copper-Platinum Group Elements-Chromium Ore Systems — Fertility, Pathfinders, New and Revised Models, (ed.) D.E. Ames and M.G. Houlé; Geological Survey of Canada, Open File 7856, p. 257–268.

Publications in this series have not been edited; they are released as submitted by the author.

Contribution to the Geological Survey of Canada's Targeted Geoscience Initiative 4 (TGI-4) Program (2010–2015)

TABLE OF CONTENTS

Trace element distribution in sulphide assemblages of the Levack-Morrison ore system, Sudbury, Ontario: Looking for chemical fingerprints of mineralization processes

Moji Adibpour[1]*, Pedro J. Jugo[1], and Doreen E. Ames[2]

[1]Department of Earth Sciences, Laurentian University, 935 Ramsey Lake Road, Sudbury, Ontario P3E 2C6
[2]Geological Survey of Canada, 601 Booth Street, Ottawa, Ontario K1A 0E8
*Corresponding author's e-mail: mx_adibpour@laurentian.com

ABSTRACT

One challenge in the exploration for Cu-Ni-PGE mineralization in the footwall of the Sudbury Igneous Complex (SIC) is the uncertainty of its origin. The relative proximity of mineralization to the SIC is consistent with models of magmatic fractionation, but the common association of ore in the SIC footwall with amphibole and epidote alteration is consistent with a hydrothermal origin. Although these processes are not mutually exclusive (e.g. ores of magmatic origin could have been later remobilized by hydrothermal fluids), better constraints on which processes operated would greatly assist exploration. This project is a pilot study to assess whether chemical fingerprints can be established for four distinct mineralization types in the Levack-Morrison ore system: (a) contact; (b) a transition zone between contact and footwall ore; (c) sharp-walled veins; and (d) disseminated, S-poor, PGE-rich ores.

Sulphide assemblages consisting primarily of pyrrhotite, chalcopyrite, and pentlandite were characterized in detail (petrography, SEM, EPMA, LA-ICP-MS). The results indicate that (a) Se content increases with depth; and (b) some trace elements (e.g. Cd vs. Se in chalcopyrite, Co vs. Se in pentlandite and pyrrhotite) can discriminate among different ore types. Calculated partition coefficients ($\pm 2\sigma$) for Se in chalcopyrite and pentlandite (1.2 ± 0.1 for contact and transition ores, 0.5 ± 0.2 for sharp-walled veins) are significantly different, which is consistent with different mineralization processes for those ore types. In addition to trace element content calculation in major sulphides, element distribution maps were created from LA-ICP-MS spectra of sulphide assemblages. Some contact-style samples contained abundant euhedral pyrite but pyrite was also present in samples of other ore types. The maps showed complex trace element zonation (e.g. Se, Co, and As) in pyrite in contact ore, as well as some PGE minerals (notably Ir and Os). In contrast, no PGEs were detected in any of the other sulphides or any compositional zoning. Because Ir has very low solubility under most hydrothermal conditions, Co-rich, Ir-bearing pyrite was interpreted to have formed from the cooling of a sulphur-rich sulphide liquid. Such pyrite (when present) could be used as an indicator of a magmatic signature.

To further refine these results, future work would need to focus on three areas: (1) analyses of additional samples from the Morrison-Levack ore system to validate the discrimination diagrams for different ore types; (2) similar work would need to be undertaken elsewhere in the Sudbury mining district, to establish if the proposed discrimination plots are applicable basin-wide; (3) better constraints would need to be established for the origin of the Co-rich, PGE-bearing pyrite to enable it to be used as a marker of ore type.

INTRODUCTION

The 1.85 Ga Sudbury impact structure, located at the boundary between the Archean Superior Province and the Proterozoic Huronian Supergroup of the Southern Province (Fig. 1a), hosts some of the largest Ni-Cu-platinum group element (PGE) resources in the world (Ames and Farrow, 2007). The Ni-Cu-PGE ore deposits in the Sudbury District have been divided into three main types: (1) contact-type deposits, with sulphides concentrated in embayments near the base of the Sudbury Impact Complex (SIC); (2) offset-type deposits, hosted by radial and concentric offset dykes; and (3) footwall-type deposits, hosted by shock-derived impact breccia in the SIC footwall (Morrison et al., 1994). Figure 1b shows the schematic relationship between contact-type mineralization and footwall ores. The magmatic origin of high-Ni, low-PGE contact-type deposits has been reasonably well established.

Adibpour, M., Jugo, P.J., and Ames, D.E., 2015. Trace element distribution in sulphide assemblages of the Levack-Morrison ore system, Sudbury, Ontario: Looking for chemical fingerprints of mineralization processes, *In:* Targeted Geoscience Initiative 4: Canadian Nickel-Copper-Platinum Group Elements-Chromium Ore Systems — Fertility, Pathfinders, New and Revised Models, (ed.) D.E. Ames and M.G. Houlé; Geological Survey of Canada, Open File 7856, p. 257–268.

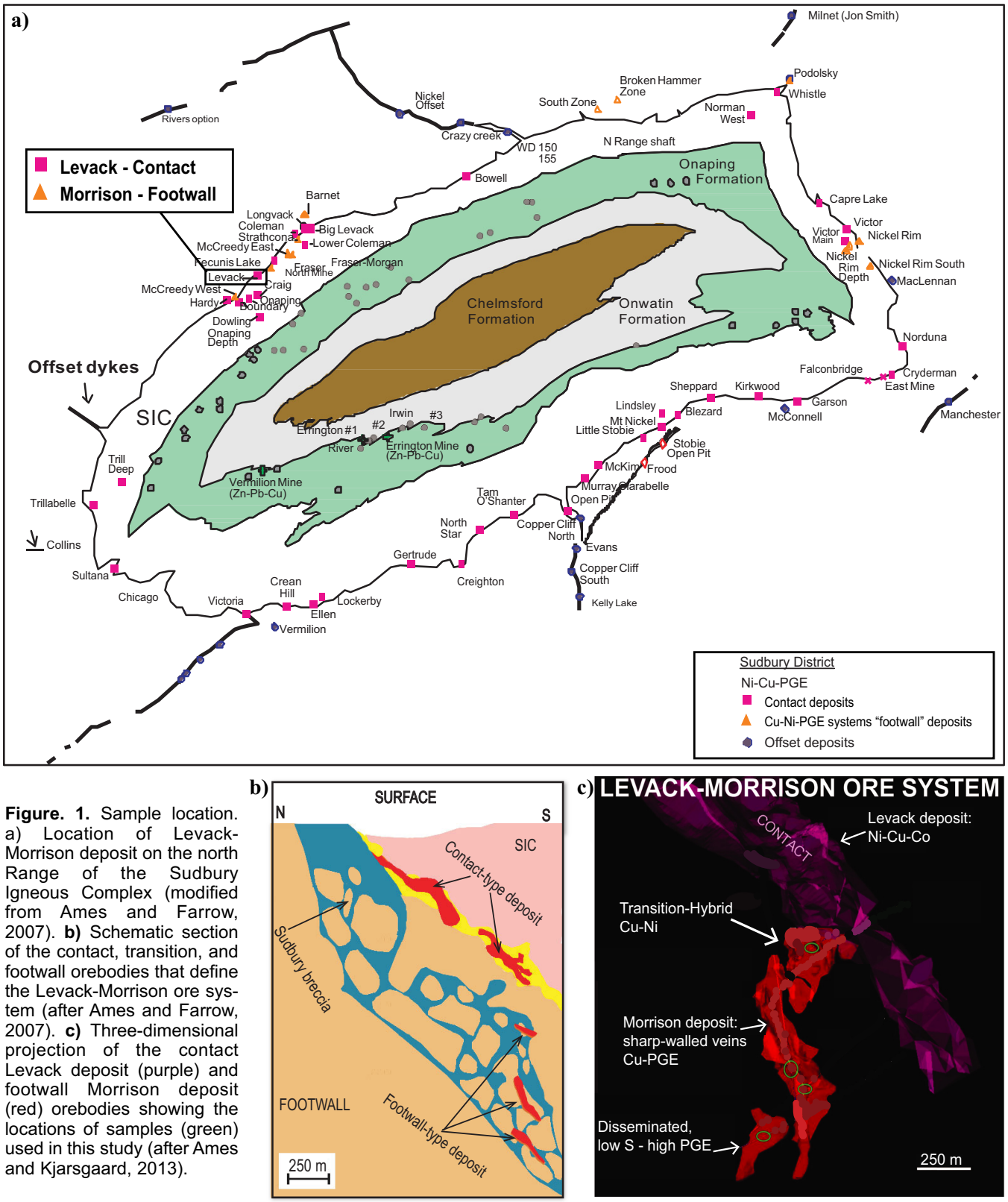

Figure. 1. Sample location. a) Location of Levack-Morrison deposit on the north Range of the Sudbury Igneous Complex (modified from Ames and Farrow, 2007). **b)** Schematic section of the contact, transition, and footwall orebodies that define the Levack-Morrison ore system (after Ames and Farrow, 2007). **c)** Three-dimensional projection of the contact Levack deposit (purple) and footwall Morrison deposit (red) orebodies showing the locations of samples (green) used in this study (after Ames and Kjarsgaard, 2013).

These deposits are widely recognized as segregations of immiscible sulphide melts that accumulated along the floor and embayments of the SIC during cooling of the impact melt sheet after meteoritic impact (Ames and Farrow, 2007). In contrast, the origin of mineralization within the footwall is not well understood, in part because of the different styles of mineralization that are present. Kjarsgaard and Ames (2010) showed that mineral assemblages in the footwall ores have been affected by multiple processes (magmatic, meta-

morphic, and hydrothermal). It has been hypothesized that the footwall ore deposition was related to magmatic processes (e.g. Stewart and Lightfoot, 2010); in contrast, the quartz, epidote, and amphibole alteration assemblages may indicate mineralization by hydrothermal or metamorphic processes (e.g. Farrow and Watkinson, 1997; Gibson, 2010). In order to develop a good exploration model for mineralization related to the footwall of the SIC, it must be established to what extent the mineralization was directly related to sulphide melts (i.e. directly related to the impact event) and or related to deposition from subsequent hydrothermal fluids.

The Levack-Morrison ore system (Fig. 1c), on the north range of the SIC, is one of a few places in which a contact-type orebody (Levack) is in spatial continuity with the footwall ores (Morrison deposit). Mineralization within the Morrison footwall Cu-PGE-Ni ores can be divided in three mineralization types: (a) transition ore (with Ni ≈ Cu), which is a hybrid between contact and footwall-style mineralization; (b) sharp-walled veins (with Cu > Ni, PGE); and (c) low-S, high-PGE disseminated ore (Ames and Kjarsgaard, 2013). In general, transition, sharp-walled veins, and disseminated ores occur progressively deeper and away from contact-style ores. The primary goal of this project was to assess whether the trace element content in major sulphides (pyrrhotite, pentlandite, chalcopyrite) can be used to 'fingerprint' mineralization styles, and if so, which chemical fingerprints can be used as indicators for the different ore formation processes. In addition, element distribution maps were created to characterize and understand occurrences of Co-rich and PGE-bearing pyrite in contact-style deposits, and to test whether this type of pyrite is useful as an indicator of a specific mineralization process.

RESULTS AND DATA ANALYSIS

Samples and Methods

Fourteen samples from different sections of the Levack-Morrison ore system were analysed: three contact- type ore (Levack deposit); two from transition-type ore; two sharp-walled veins; three disseminated, low-sulphur, high-PGE ore. Sulphide assemblages were characterized under reflected light microscopy and SEM. Major element composition was obtained by electron probe microanalysis. Selected areas were analysed by LA-ICP-MS in two ways: (a) trace element content were obtained using spot analyses with a 90 μm laser beam diameter; (b) trace element distribution maps were created using a smaller laser beam diameter (~20 μm) for better spatial resolution. Trace element contents were obtained using Po725 a synthetic pyrrhotite standard and NIST-610 glass as calibration standards. The Fe content of each mineral was used for internal standardization.

Sulphide Mineralogy and Textures

Representative images of the samples analysed are shown in Figure 2. Samples from Levack (Fig. 2a) contain pyrrhotite, chalcopyrite, pentlandite, pyrite, and magnetite. Two types of pentlandite (blocky and flame) are present (Fig. 2b) as well as minor amounts of sphalerite and galena. Transition-type ore (Fig. 2c) contains massive pyrrhotite, chalcopyrite, blocky and flame pentlandite, and magnetite. Samples from sharp-walled veins (Fig. 2d) contain massive chalcopyrite-cubanite intergrowths, blocky and flame pentlandite, magnetite, and small amounts of sphalerite disseminated in chalcopyrite. Samples from low-sulphide, high-PGE disseminated ores (Fig. 2e) contain little sulphide, mostly as chalcopyrite, minor amounts of pentlandite, magnetite grains with ilmenite exsolution, very small (<50 μm) euhedral pyrite, and tiny (<50 μm) galena inclusions disseminated in chalcopyrite.

Sulphide Composition

The composition of the sulphides is summarized in Table 1 (S, Fe, Cu, Ni, Co, Zn) and Table 2 (trace elements). Three different groups of elements were analysed: (a) highly siderophile elements (HSE = PGE plus Re and Au); (b) metalloids (As, Se, Sb, Te, Bi); (c) other chalcophile or siderophile elements (Co, Zn, Mo, Ag, Cd, Sn, Pb). Elements that were below detection limits (e.g. HSE) are not included in the Tables. Element distribution maps of sulphide assemblages are discussed below.

DISCUSSION

Chemical Fingerprinting and Geochemical Discrimination of Ore Types

One goal of this study was to identify elements that can be measured routinely, thus the focus was on elements that were consistently above detection limits. Elements that were too close to detection limits were deemed not reliable or useful because analytical uncertainties are deemed too high. Initially, Zn was targeted because Nelles (2012) noted a correlation between PGE and Zn content based on whole rock analyses, and Zn and Cd are markedly enriched in footwall Cu-PGE ores (Ames and Farrow, 2007). The working hypothesis was that because Zn partitions preferentially into Cu-rich melt, therefore the Zn content in chalcopyrite should track the fractionation of such melts. However, the Zn content in chalcopyrite was approximately the same for all the samples analysed. Revised petrography and SEM analyses revealed that all the samples contained sphalerite (often only as very small grains <50 μm), indicating that the Zn content in chalcopyrite is at spha-

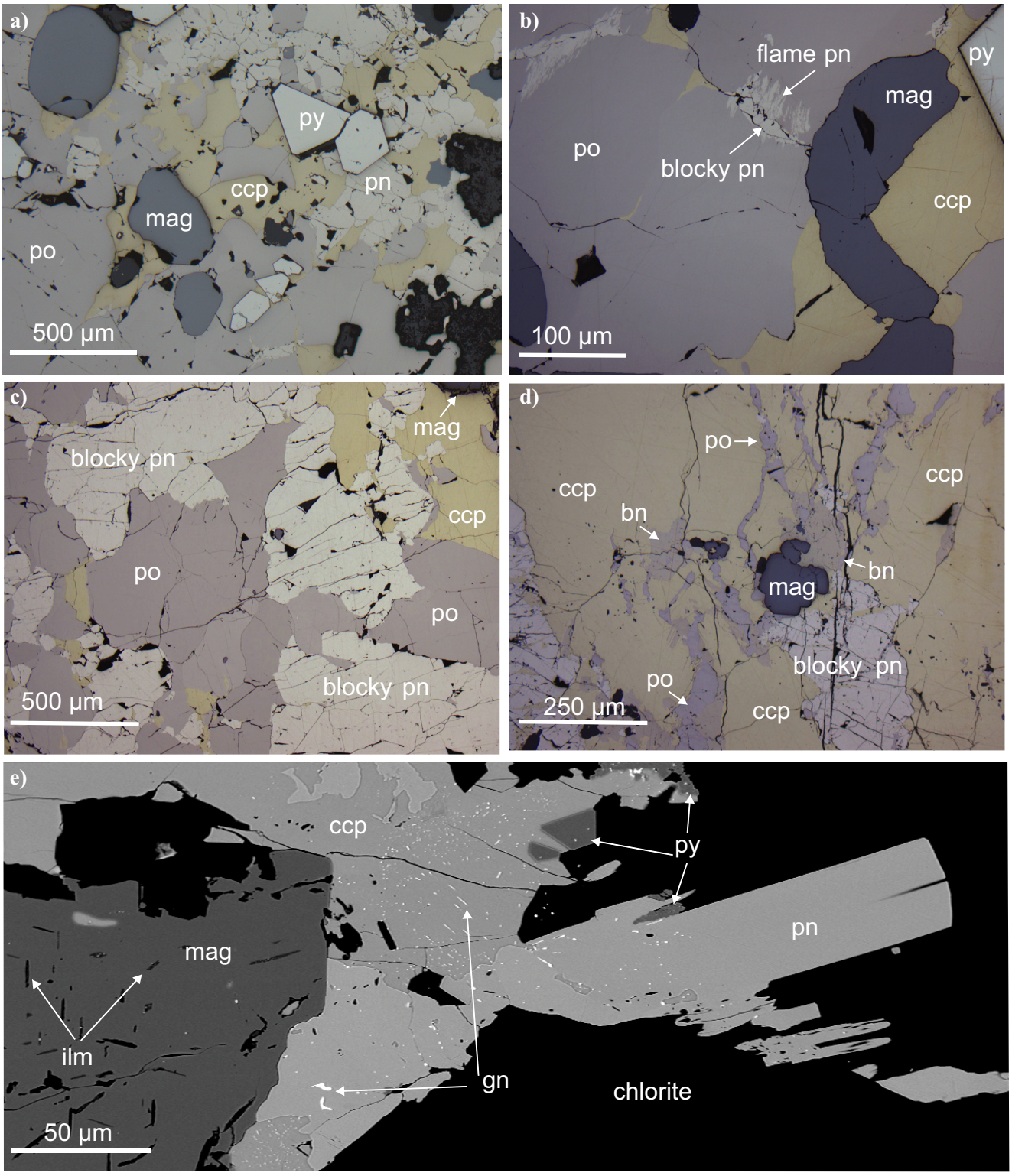

Figure 2. Ore textures and mineral associations in various ore types from the Levack-Morrison ore system. Typical assemblages contain variable amounts of chalcopyrite (ccp), magnetite (mag), pyrrhotite (po), and pentlandite (pn). **a)** Contact ore with euhedral pyrite (py) grains (sample 99AV-122). **b)** Detailed view of the two types of pn found in contact ore samples (sample 99AV-122). **c)** Footwall-contact transitional assemblage (sample 08AV-08) containing massive po, ccp, blocky and flame pn (similar to contact ore), and mag. **d)** Footwall sharp-walled veins (sample 05AV-11A) containing massive ccp in association with blocky and flame pn and strongly fractured anhedral to subhedral grains of mag. Pyrrhotite and bornite (bn) are minor phases in this sample. **e)** Backscattered electron image (BEI) of footwall-disseminated ore (sample 08AV-02A) showing ccp and minor amounts of pn and mag with ilmenite (ilm) exsolution, small galena (gn) inclusions disseminated in ccp, as well as small subhedral to euhedral py grains.

Table 1. Major element content (wt.%) of chalcopyrite, pentlandite, and pyrrhotite (by electron microprobe analysis) for the four types of mineralization present in the Levack-Morrison ore system in Sudbury Igneous Complex.

Sample	n		S	Fe	Cu	Ni	Co	Total
Chalcopyrite								
99AV-122 (Levack)	7	Ave.	35.0	30.6	34.5	<0.25		100.1
Contact		Std.	0.1	0.1	0.2			
08AV-08 (Morrison)	8	Ave.	35.0	30.3	34.4	<0.25		99.6
Transition		Std.	0.1	0.1	0.1			
05AV-11A (Morrison)	8	Ave.	35.0	30.8	34.2	<0.25		100.0
Sharp-walled veins		Std.	0.1	0.1	0.1			
08AV-02A (Morrison)	1		34.7	30.0	34.0	<0.25		98.6
Disseminated								
Pentlandite								
99AV-122 (Levack)	15	Ave.	33.5	30.4	<0.25	34.9	1.00	99.8
Contact		Std.	0.2	0.6		0.6	0.12	
08AV-08 (Morrison)	11	Ave.	33.4	30.5	<0.25	35.4	0.27	99.5
Transition		Std.	0.1	0.2		0.2	0.03	
05AV-11A (Morrison)	8	Ave.	33.5	34.9	<0.25	31.4	0.21	100.0
Sharp-walled veins		Std.	0.2	0.1		0.1	0.01	
Pyrrhotite								
99AV-122 (Levack)	10	Ave.	39.8	60.1	<0.25	0.489	0.025	100.4
Contact		Std.	0.1	0.1		0.053	0.003	
08AV-08 (Morrison)	8	Ave.	39.8	59.9	<0.25	0.444	0.026	100.1
Transition		Std.	0.1	0.2		0.114		
05AV-11A (Morrison)	8	Ave.	39.1	61.5	<0.25	0.072		100.2
Sharp-walled veins		Std.	0.1	0.1		0.005		

Note: n = sample size

lerite saturation, which renders Zn not useful for chemical fingerprinting in this system. Of the other elements that might be used to discriminate among the different ore types Se was the most notable. Selenium was chosen as the main variable for discrimination because it is present in all major sulphides and was shown to increase systematically with depth. For example, when Cd content in chalcopyrite is plotted versus Se content in chalcopyrite (Fig. 3a) there is a notable increase in Se content with distance from the contact ores; the Cd content helps separate the fields further although Cd content does not seem to systematically correlate with Se. Data from unaltered and slightly altered contact-style orebodies in McCreedy East (Dare et al., 2011) are shown for comparison (Fig 3a). The altered sample has higher Se and lower Cd, indicating that hydrothermal processes maybe responsible for the Se increase (and Cd decrease) relative to contact ores. However, the high Cd content in chalcopyrite from sharp-walled veins is not consistent with a hydrothermal origin. The As versus Se content in pentlandite (Fig. 3b) illustrates a similar behaviour to that Cd versus Se in chalcopyrite (Fig 3a), however, the Se content in pentlandite from sharp-walled veins (green triangles: Fig. 3b) is variable and has a positive correlation with As, indicating that both Se and As are compositionally zoned in pentlandite. Cobalt content in pentlandite (Fig. 3c) and in pyrrhotite (Fig. 3d) is significantly higher in contact ore than in other ore types, which also is an indicator that different ore processes involved in the formation of the contact ores relative to the footwall ores.

Table 2. Trace element content (in ppm) of chalcopyrite, pentlandite, and pyrrhotite (by electron microprobe analysis) for the four types of mineralization present in the Levack-Morrison ore system in Sudbury Igneous Complex.

Sample	n		Ag^{109}	As^{75}	Bi^{209}	Cd^{111}	Co^{59}	Mo^{95}	Pb^{208}	Sb^{121}	Se^{77}	Sn^{118}	Te^{125}	Zn^{66}	Zn^{68}
Chalcopyrite															
Contact	10	Ave	19	3.28	2.19	9.6	2.0	0.116	12.3	0.064	43.3	24.4	1.0	640	560
(Levack; 99AV-122)		Std	17	0.36	0.95	2.0	1.8	0.065	4.7	0.028	1.7	3.6	1.6	150	120
Transition	9	Ave	2.9	3.3	0.046	3.00	1.3	1.9	14.7	0.059	88.3	2.53	0.090	488	440
(Morrison; 08AV-08)		Std	1.0	1.4	0.026	0.53	1.6	1.6	6.4	0.016	6.7	0.72	0.061	55	55
Sharp-walled veins	8	Ave	11.0	2.12	0.058	23.5	0.095	0.059	46	0.050	155	81.5	5.9	560	467
(Morrison; 05AV-11A)		Std	1.1	0.19	0.030	2.9	0.048	0.084	27	0.016	13	6.6	1.3	180	78
Disseminated	13	Ave	174	2.04	1.23	6.4	0.93	0.056	44	0.082	264	41	0.77	510	460
(Morrison; 08AV-02A)		Std	34	0.16	0.66	1.8	0.91	0.021	32	0.016	11	13	0.18	170	150
Pentlandite															
Contact	7	Ave	2.29	4.8	4.3	0.50	13600	0.27	28	0.143	37.4	5.3	0.92	118	111
(Levack; 99AV-122)		Std	0.76	1.1	2.2	0.29	1100	0.11	14	0.023	2.6	2.3	0.35	99	88
Transition	7	Ave	4.6	2.08	0.088	0.040	2750	0.79	5.4	0.046	70.0	0.065	bdl	2.4	bdl
(Morrison; 08AV-08)		Std	1.0	0.30	0.041	0.026	110	0.80	2.4	0.016	2.1	0.043		1.5	
Sharp-walled veins	9	Ave	39	13.3	0.58	0.51	2455	0.036	60	0.113	296	4.6	205	15	bdl
(Morrison; 05AV-11A)		Std	24	7.9	0.56	0.54	57	0.022	87	0.025	85	2.5	94	10	
Pyrrhotite															
Contact	8	Ave	0.38	4.34	1.57	bdl	154	0.093	1.87	0.085	37.9	bdl	bdl	2.15	bdl
(Levack; 99AV-122)		Std	0.14	0.40	0.26		45	0.056	0.59	0.016	2.2			0.93	
Transition	7	Ave	0.333	2.86	0.241	bdl	22.5	0.45	2.09	0.055	81.8	0.10	bdl	1.80	bdl
(Morrison; 08AV-08)		Std	0.063	0.17	0.079		2.5	0.67	0.71	0.013	3.9	0.13		0.78	

Note: bdl = below detection limit; n = sample size

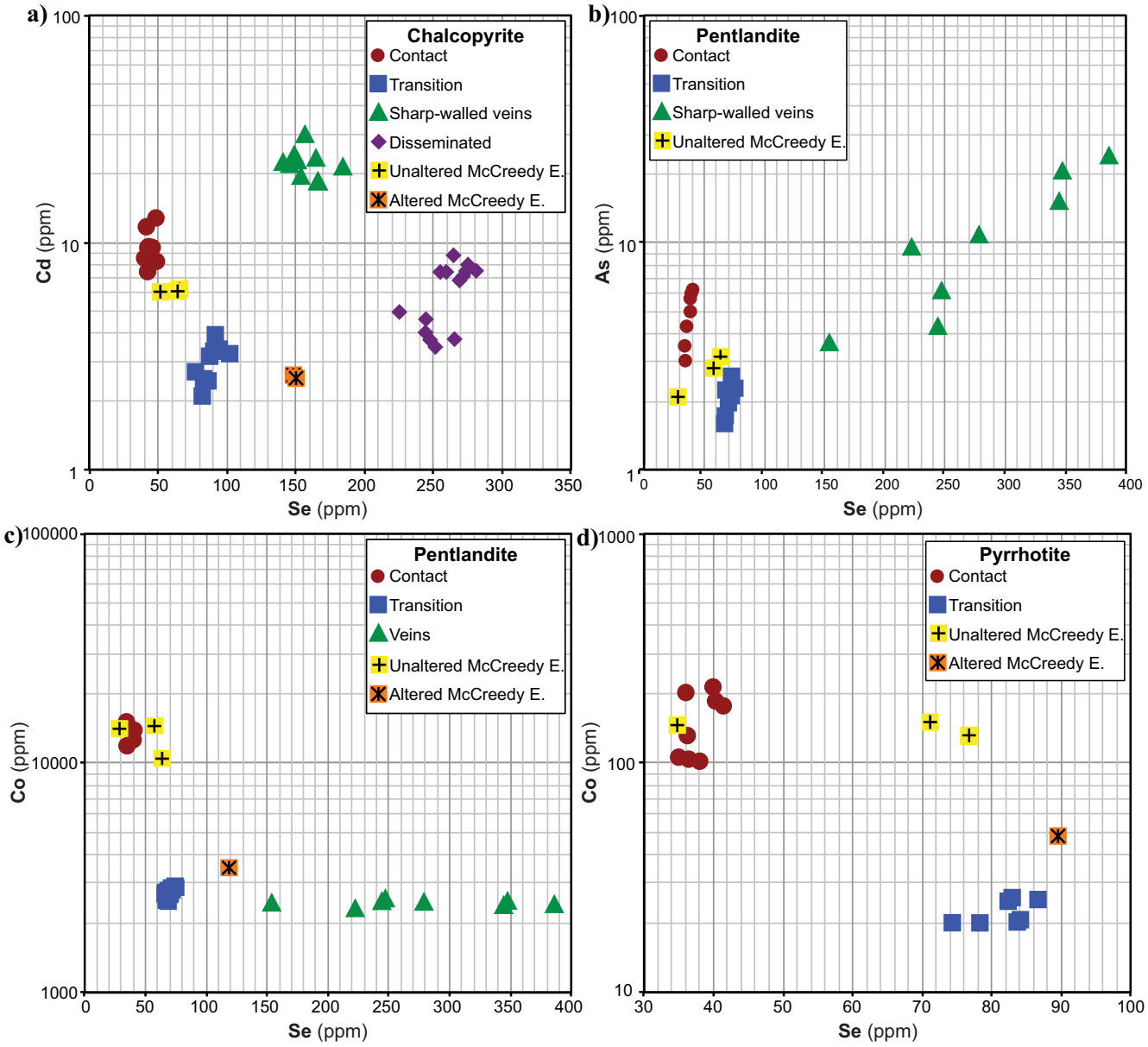

Figure 3. Examples of trace elements in major sulphides that can be used to discriminate between different ore types. **a)** Cd vs. Se content in chalcopyrite. **b)** As vs. Se content in pentlandite. **c)** Co vs. Se content in pentlandite. **d)** Co vs. Se content in pyrrhotite. Data for McCreedy East samples are from Dare et al. (2011).

Partition coefficients of trace elements in chalcopyrite, pentlandite, and pyrrhotite were calculated for contact, transitional, and sharp-walled veins. Partition coefficients are affected by intensive variables, such as temperature, pressure, oxygen fugacity, sulphur fugacity, etc. (e.g. Mungall et al, 2005). All these variables are indicators of the mineralization environment; hence, differences in partition coefficients are reliable indicators of different processes of formation. The propagated uncertainties for most of the elements that were analysed are too large for meaningful comparisons; however, the partition coefficient ($\pm 2\sigma$) of Se between chalcopyrite and pentlandite is 1.2 ± 0.1 for contact and transition ores but only 0.5 ± 0.2 for vein-type ores, indicating that veins formed by different process than contact and transition ores (e.g. Hanley et al., 2005; Pentek et al., 2013).

Element Distribution Maps of Sulphide Assemblages

Zonation of trace elements, including some HSE, in pyrite from contact ore (Levack) was documented; no HSE was detected in the major sulphides (pyrrhotite, chalcopyrite, pentlandite). Figure 4 illustrates some of the most significant features that were observed. The area mapped contains a trapezoidal section of one euhedral pyrite grain surrounded by pyrrhotite, chalcopyrite, and minor pentlandite (Fig. 4a). Some small

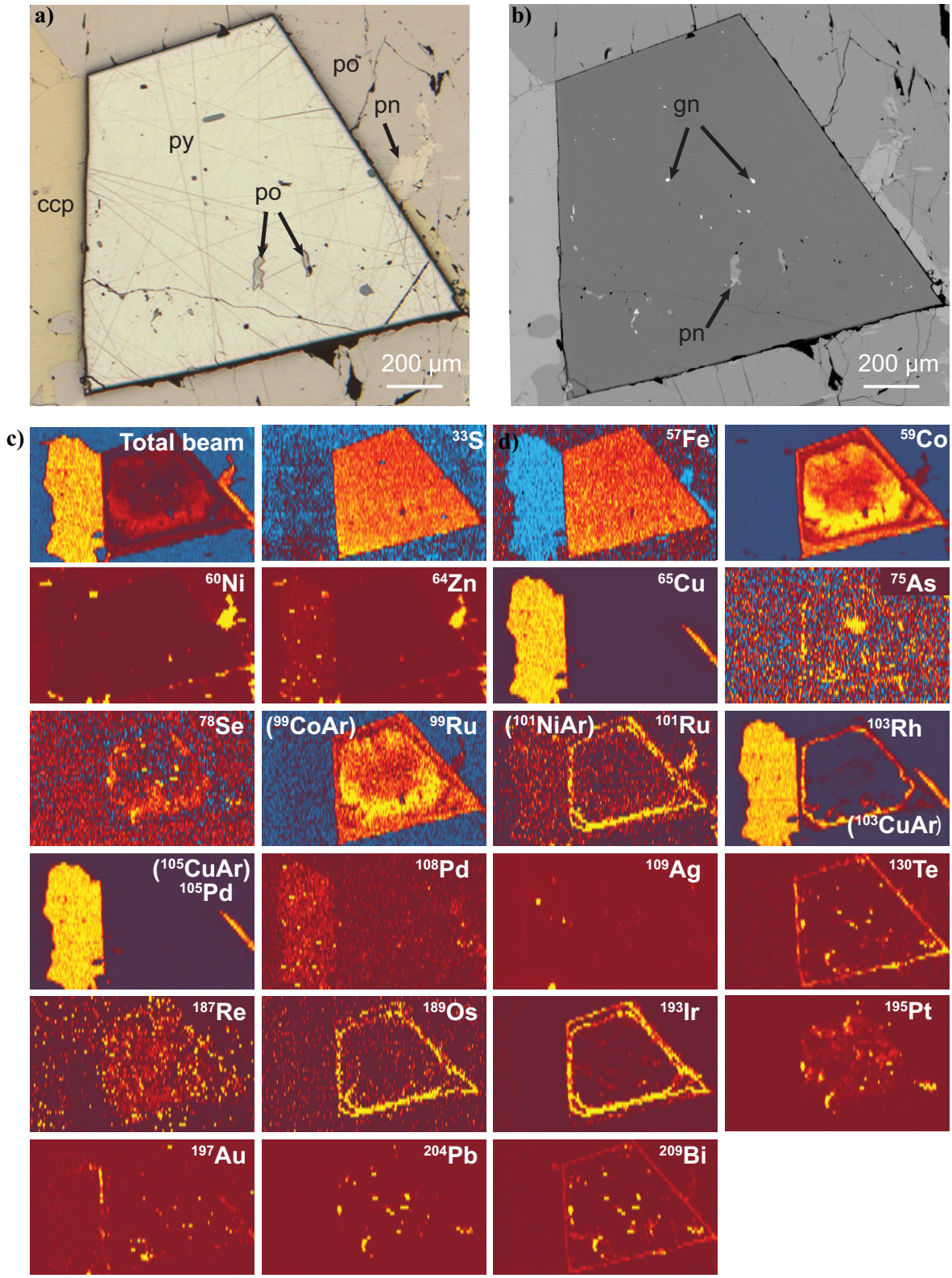

Figure 4. LA-ICP-MS trace element mapping of euhedral pyrite (py) and surrounding pyrrhotite-pentlandite-chalcopyrite (po-pn-ccp) assemblage from contact ore, Levack deposit. **a)** Reflected light photomicrograph for reference. **b)** Backscattered electron image of the same slide as (a) showing inclusions of galena (gn) and other sulphides (e.g. pentlandite) in pyrite. **c)** Element distribution maps (in relative signal intensities) of the same slide. No significant trace element concentrations were detected in the major sulphides. However, pyrite displays (i) a complex zoning of Co, Se, and As; (ii) thin rims containing Ru, Rh, Os, Ir, Te, and Bi, as well as discrete inclusions containing Pt, Au, Pb, Bi, and Te. Maps use a 'warm-cold' scale with yellow being of highest relative intensity, and blue lowest). The signal shown is not corrected for argide-metal interferences of lighter isotopes on higher masses (e.g. ^{59}Co, ^{63}Cu, ^{65}Cu on ^{99}Ru, ^{103}Rh, ^{105}Pd, respectively) or isobaric interferences (e.g. ^{108}Cd on ^{108}Pd).

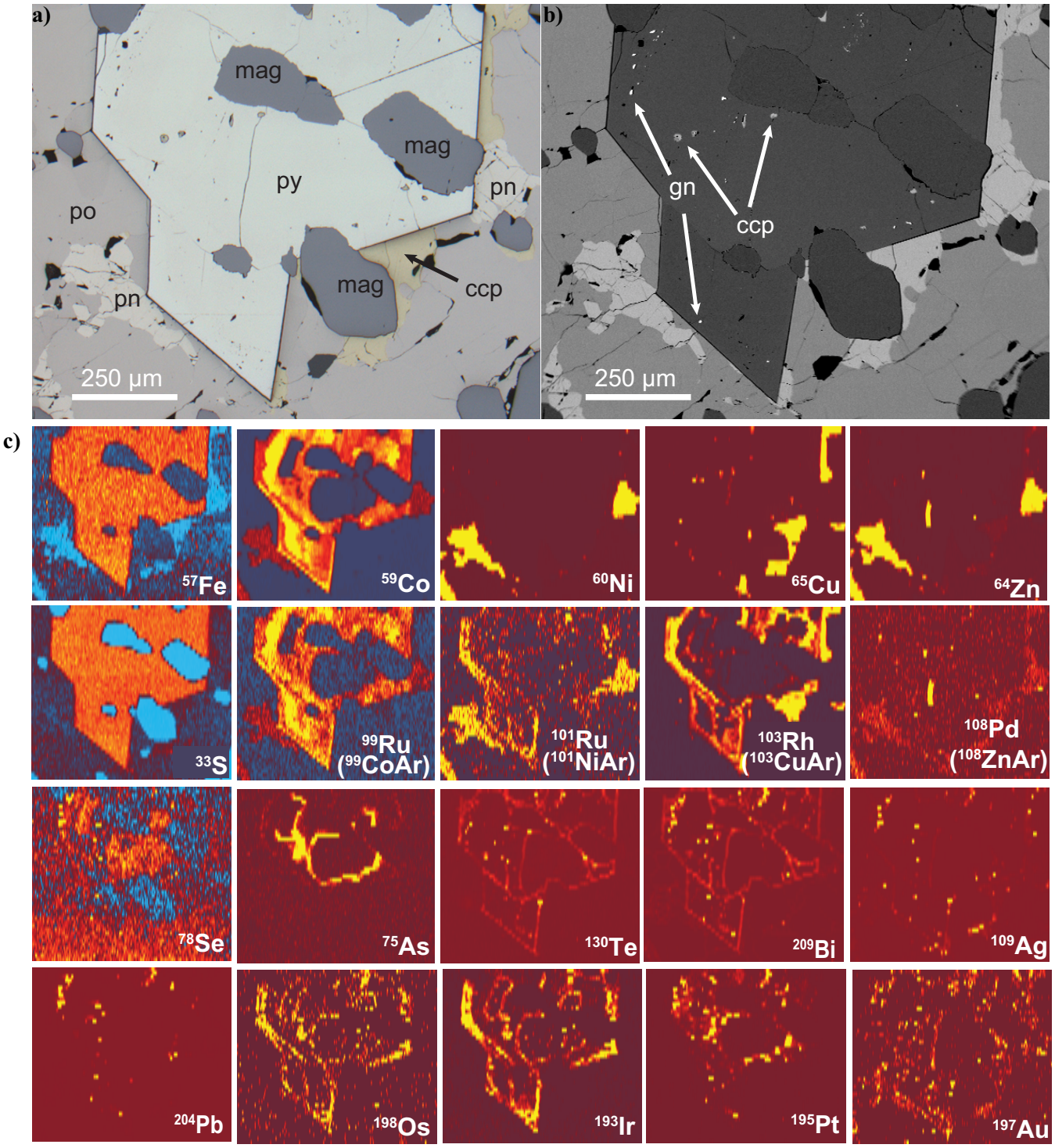

Figure 5. LA-ICP-MS trace element mapping of a composite pyrite (py) grain from contact ore, Levack deposit. **a)** Reflected light photomicrograph showing a large euhedral composite grain of pyrite, enclosing anhedral magnetite (mag) and surrounded by chalcopyrite (ccp), pentlandite (pn), and pyrrhotite (po). **b)** BEI highlighting small galena (gn) and chalcopyrite inclusions in the pyrite grain. **c)** Element distribution maps showing complex zoning of Se, As, and Co (e.g. areas with relatively high Se have no detectable Co; high As areas 'outline' Se-rich areas and are then surrounded by complex Co zonation). The distribution of Ru, Rh, Os, and Ir matches regions within the Co-rich zoned pyrite that are close to the edges of the grain. The Te and Bi distribution outline pyrite grain boundaries and subdomains. The distribution of Pt in pyrite matches that of As and also some discrete Bi as well as some of the galena inclusions.

galena inclusions were observed within pyrite but no HSE-bearing minerals were detected (Fig. 4b). Figure 4c is a set of element distribution maps on a yellow-blue (warm-cold) colour scale. Each map is normalized to the highest signal intensity for the element represented; thus the maps are not meant to provide information (or comparisons) about element concentrations but to illustrate element zonation and rims (e.g. Co, Ru, Rh, Os, Ir, Te, and Bi in pyrite) as well as the presence and distribution of micrometre- and nanometre-scale nuggets (e.g. Te, Pt, Au, Pb, and Bi in pyrite). Figure 5 shows a more complex element zonation of pyrite and again illustrates that most trace elements of interest are dominantly in pyrite rather than chalcopyrite, pentlandite, or pyrrhotite. The maps (Fig. 5c) illustrate several stages of growth in pyrite: (i) a Co-poor but relatively Se-rich stage (centre of the composite grain), followed by (ii) an As-rich stage, followed by (iii) growth of Co-rich areas. Four HSE elements (Ru, Rh, Os, and Ir) are present mostly near the euhedral grain edges of the composite pyrite grain. Tellurium and Bi seem to delineate fractures and the boundaries of the subgrains within the pyrite grains. What is most significant about Co-rich, HSE-bearing pyrite is that it records the geochemical processes that affected the distribution of HSE and key elements (As, Bi, Te). These elements were involved in the formation of the most common platinum group metals in the footwall ores (e.g. merenskyite, moncheite, sperrylite; Cabri and LaFlamme, 1976). Thus, understanding the origin of such pyrite should provide valuable information about the ore-forming processes.

IMPLICATIONS FOR EXPLORATION

These results provide several insights that are relevant for exploration in the challenging footwall environment. Fingerprinting of distinctive trace element signatures can help identify each of the mineralization types present (i.e. contact, transition, sharp-walled veins, disseminated) which further can aid in identify the processes of their formation. The Se content in major sulphides was shown to increase with depth and when compared with Se content in slightly altered contact-style samples from McCreedy East (Fig. 3), indicates that this increase is likely due to hydrothermal activity. Partition coefficients for Se in chalcopyrite and in pentlandite are similar for contact and transition ores but are different for Se in chalcopyrite and in pentlandite from sharp-walled veins, indicating that contact and transition ores may share the same origin but that sharp-walled veins were produced under different conditions. This supports the concept that the contact and transition ores were formed through magmatic processes but that different processes, likely a magmatic-hydrothermal origin have affected the sharp-walled veins. No PGEs were detected in any of the major sulphide minerals (pyrrhotite, pentlandite, chalcopyrite) but pyrite from contact ore displayed complex zoning of many trace elements, including Co, Se, As, and several PGE elements, notably Ir and Os. Although the origin of this pyrite is not clear, it is of significance as it may provide important information about the mineralization processes. For example, if it can be shown that the Co-rich, PGE-bearing pyrite was of magmatic origin (i.e. by cooling of an immiscible sulphide melt) then the presence of pyrite with similar characteristics (even in small amounts) in footwall ores would be a marker of sulphide melt infiltration (for example, transition ore samples contain anhedral pyrite grains with relatively high As and Pt cores). Alternatively, if it can be shown that the Co-rich, PGE-bearing pyrite was of hydrothermal origin, then the presence of such pyrite in contact ores would indicate that contact ores were affected by hydrothermal processes. However, at present there is not enough data to properly constrain the origin of Co-rich, PGE-bearing pyrite.

FORTHCOMING PRODUCTS

Two papers are in preparation for submission (spring 2015) to peer-reviewed journals. The first paper discusses the trace element content of the major sulphides in the contact and footwall of the Levack-Morrison ore system, with focus on trace elements (e.g. Se, Co, Cd) that have potential for discriminating among different ore types. The second paper documents the trace element distribution maps, the complex zoning in pyrite, and the potential implications of the presence of Co-rich, PGE-bearing pyrite for exploration.

ACKNOWLEDGEMENTS

We would like to thank Pat Hunt (GSC) for assistance with the SEM, Joe Petrus (Laurentian University) for assistance with LA-ICP-MS element mapping and spot analysis, and M.Sc. thesis committee (first author) members, M. Lesher and A. McDonald for discussion.

REFERENCES

Ames, D.E. and Farrow, C.E.G., 2007. Metallogeny of the Sudbury mining camp, Ontario, *In:* Mineral Deposits of Canada: A Synthesis of Major Deposit Types, District Metallogeny, the Evolution of Geological Provinces, and Exploration Methods, (ed.) W.D. Goodfellow; Geological Association of Canada, Mineral Deposits Division, Special Publication No. 5, p. 329–350.

Ames, D.E. and Kjarsgaard, I.M., 2013. Sulphide and alteration mineral chemistry of low- and high-sulphide Cu-PGE-Ni deposits in the footwall environment, Sudbury, Canada; Geological Survey of Canada, Open File 7331.

Cabri, L.J. and Laflamme, J.H.G., 1976. The Mineralogy of the platinum-group elements from some copper-nickel deposits of the Sudbury area, Ontario; Economic Geology, v. 71, p. 1159–1195.

Dare, S.A.S., Barnes, S-J., Prichard, H.M., and Fisher, P.C., 2011. Chalcophile and platinum-group element (PGE) concentrations in the sulphide minerals from the McCreedy East deposit, Sudbury, Canada, and the origin of PGE in pyrite; Mineralium Deposita, v. 46, p. 381–407.

Farrow C.E.G. and Watkinson, D.H., 1997. Diversity of precious metal mineralization in footwall Cu-Ni-PGE deposits, Sudbury, Ontario: implications for hydrothermal models of formation; The Canadian Mineralogist, v. 35, p. 817–839.

Gibson, A., 2010. Contrasting styles of mineralization: North Range 148 zone versus South Range 109 FW zone, *In:* Abstracts, 11th International Platinum Symposium, 21–24 June 2010, Sudbury, Ontario, (ed.) G.H. Brown, P.L. Jugo, C.M. Lesher, and J.E. Mungall; Ontario Geological Survey, Miscellaneous Release-Data 269.

Hanley, J.J., Mungall, J.E., Pettke, T., Spooner, E.T.C., and Bray, C.J., 2005. Ore metal redistribution by hydrocarbon brine and hydrocarbon-halide melt phases, North Range footwall of the Sudbury Igneous Complex, Ontario, Canada; Mineralium Deposita, v. 40, p. 237–256.

Kjarsgaard, I.M. and Ames, D.E., 2010. Ore mineralogy of Cu-Ni-PGE deposits in the North Range footwall environment, Sudbury, Canada, *In:* Abstracts, 11th International Platinum Symposium, 21–24 June 2010, Sudbury, Ontario, (ed.) G.H. Brown, P.L. Jugo, C.M. Lesher, and J.E. Mungall; Ontario Geological Survey, Miscellaneous Release Data 269.

Morrison G.G., Jago B.C., and White T.L., 1994. Footwall mineralization of the Sudbury Igneous Complex. *In:* Proceedings of the Sudbury–Noril'sk symposium, (ed.) P.C. Lightfoot and A.J. Naldrett; Ontario Geological Survey, Special Volume 5, p. 57–64.

Mungall J.E., Andrews, D.R.A., Cabri, L.J., Sylvester, P.J., and Tubrett, M., 2005. Partitioning of Cu, Ni, Au, and platinum-group elements between monosulfide solid solution and sulfide melt under controlled oxygen and sulfur fugacities; Geochimica et Cosmochimica Acta, v. 69, p. 4349–4360.

Nelles, E.W., 2012. Genesis of Cu-PGE-rich footwall-type mineralization in the Morrison deposit, Sudbury; M.Sc. thesis, Laurentian University, Sudbury, Ontario, 96 p.

Pentek, A., Molnar, F., Tuba, G., Watkinson, D.H., and Jones, P.C., 2013. The significance of partial melting processes in hydrothermal low-sulfide Cu-Ni-PGE mineralization within the footwall of the Sudbury Igneous Complex, Ontario, Canada; Economic Geology, v. 108, p. 59–78.

Stewart, M.C. and Lightfoot, P.C., 2010. Diversity in platinum group element (PGE) mineralization at Sudbury: New discoveries and process controls, *In:* Abstracts, 11th International Platinum Symposium, 21–24 June 2010, Sudbury, Ontario, (ed.) G.H. Brown, P.L. Jugo, C.M. Lesher, and J.E. Mungall; Ontario Geological Survey, Miscellaneous Release Data 269.

GEOLOGICAL SURVEY OF CANADA
OPEN FILE 7856

Targeted Geoscience Initiative 4: Canadian Nickel-Copper-Platinum Group Elements-Chromium Ore Systems — Fertility, Pathfinders, New and Revised Models

Epidote-amphibole and accessory phase mineral chemistry as a vector to low-sulphide platinum group element mineralization, Sudbury: laser ablation ICP-MS trace element study of hydrothermal alteration

Doreen E. Ames[1] and Györgyi Tuba[2]

[1]Geological Survey of Canada, Ottawa, Ontario
[2]Wallbridge Mining Company Ltd., Lively, Ontario

2015

© Her Majesty the Queen in Right of Canada, as represented by the Minister of Natural Resources Canada, 2015

This publication is available for free download through GEOSCAN (http://geoscan.nrcan.gc.ca/)

Recommended citation

Ames, D.E. and Tuba, G., 2015. Epidote-amphibole and accessory phase mineral chemistry as a vector to low-sulphide platinum group element mineralization, Sudbury: laser ablation ICP-MS trace element study of hydrothermal alteration, *In:* Targeted Geoscience Initiative 4: Canadian Nickel-Copper-Platinum Group Elements-Chromium Ore Systems — Fertility, Pathfinders, New and Revised Models, (ed.) D.E. Ames and M.G. Houlé; Geological Survey of Canada, Open File 7856, p. 269–286.

Publications in this series have not been edited; they are released as submitted by the author.

Contribution to the Geological Survey of Canada's Targeted Geoscience Initiative 4 (TGI-4) Program (2010–2015)

TABLE OF CONTENTS

Epidote-amphibole and accessory phase mineral chemistry as a vector to low-sulphide platinum group element mineralization, Sudbury: laser ablation ICP-MS trace element study of hydrothermal alteration

Doreen E. Ames[1]* and Györgyi Tuba[2]

[1]Geological Survey of Canada, 601 Booth Street, Ottawa, Ontario K1A 0E8
[2]Wallbridge Mining Company Limited, 129 Fielding Road, Lively, Ontario P3Y 1L7
*Corresponding author's e-mail: dames@nrcan.gc.ca

ABSTRACT

In Sudbury, one of the world's largest Ni-Cu-Co mineral districts, geophysical methods have been successfully employed for detecting traditional contact and offset types of Ni-Cu-PGE ore for over a century. Recent discoveries of low- to no-sulphide, high-PGE tenor orebodies, defined in 2005 in the footwall environment to the Sudbury Igneous Complex (SIC), caused a shift in exploration focus to the detection of these precious metal-rich resources. These high-grade orebodies are hosted in randomly distributed impact-derived breccia (Sudbury breccia) entirely within Archean and Proterozoic country rocks and comprise two footwall styles: a) high-sulphide vein-style Cu-PGE ores (i.e. Strathcona, McCreedy East 153 chalcopyrite veins) with a widely recognized magmatic-hydrothermal origin and b) low-sulphide disseminations, blebs and stringers with high PGE tenor and dominated by silicate assemblages of hydrothermal origin. This second, low- to no-sulphide, high-PGE footwall ore-style is a challenge to detect in the field with traditional geophysical methods used for magmatic deposits due to the absence of chalcopyrite or sulphide minerals, resulting in a need for development of non-conventional exploration techniques.

Proper classification is important for guiding future exploration for the low-sulphide metal-rich deposits in the footwall to the Sudbury Igneous Complex. Key hydrothermal alteration assemblages with distinct trace element signatures may aid the development of discriminant mineral chemistry diagrams to yield criteria that help find these high-grade PGE hydrothermal footwall ores. The aim of this study was to establish typical element-associations and behaviours for the paragenetically different hydrothermal assemblages produced during the diverse post-impact magmatic-hydrothermal history of the footwall and hanging-wall units of the Sudbury structure to detect a unique signature for alteration related to the high-tenor PGE mineralization. Factors affecting the trace element distribution patterns in epidote, amphibole, titanite, and allanite are examined, including the element partitioning between coeval minerals, the crystal structural control, and the effect of country rocks on the fluid-rock interaction, and detection of pathfinder elements. As and Zn in epidote and amphibole are host-rock dependant. The pathfinder elements Ni, Pb, Sn, and Co in epidote and amphibole are the most reliable elements to distinctly fingerprint the PGE mineralizing alteration in the footwall. However, mineral-pair partitioning of elements between epidote-amphibole-titanite and allanite indicate that single mineral phases or elements should not be used.

INTRODUCTION

World-class Ni deposits, mined for over 125 years in the camp, are hosted within igneous rocks along and near the basal contact of the Sudbury Igneous Complex (SIC) and its offset dyke structures. The last fifteen years witnessed the evolution of exploration, which was initially focussed on locating Ni-Cu ores in igneous-hosted, contact and offset magmatic-dominant environments, shift towards searching for PGE-rich deposits within impact, shock-derived breccia, the so-called Sudbury breccia, in magmatic-hydrothermal and hydrothermal footwall environments. The two "footwall-styles" of mineralization (1) sharp-walled, high-sulphide vein and (2) disseminated, blebby and stringer, low-sulphide ore (Farrow et al., 2005) have different metal associations, alteration assemblages, and most significantly timing and processes of formation.

The aim of this study was to establish typical element-associations and behaviours for the paragenetically different hydrothermal assemblages produced during the diverse post-impact magmatic-hydrothermal

Ames, D.E. and Tuba, G., 2015. Epidote-amphibole and accessory phase mineral chemistry as a vector to low-sulphide platinum group element mineralization, Sudbury: laser ablation ICP-MS trace element study of hydrothermal alteration, *In:* Targeted Geoscience Initiative 4: Canadian Nickel-Copper-Platinum Group Elements-Chromium Ore Systems — Fertility, Pathfinders, New and Revised Models, (ed.) D.E. Ames and M.G. Houlé; Geological Survey of Canada, Open File 7856, p. 269–286.

history of the footwall and hanging-wall units along the North and East Ranges of the Sudbury structure to potentially detect a unique signature for alteration related to the high-tenor PGE mineralization. Recognizing and classifying the footprint of low- (to no-) sulphide PGE mineralization involved discriminating the mineral chemistry of the pre-, syn- and post-impact (1850 Ma) hydrothermal alteration assemblages. The goals of this study were to (1) characterize the mineral chemical signatures of epidote-allanite, amphibole, and titanite formed by multiple hydrothermal events in different settings, processes, and fluid sources, in order to discriminate PGE-mineralized from barren zones; (2) determine the robustness of the epidote trace-element signature with an enlarged dataset from orebodies and showings across the North Range; and (3) illustrate the factors affecting epidote-amphibole, epidote-titanite, and amphibole-titanite mineral pair compositions to provide effective diagrams for use in detecting PGE-endowed orebodies.

GEOLOGICAL SETTING OF THE SUDBURY HYDROTHERMAL SYSTEM

The Sudbury structure is the product of a comet (Pope et al., 2004; Petrus et al., 2014) that impacted the Archean and Proterozoic crust 1850 Ma ago (Krogh et al., 1984) and whose most prominent feature, the SIC controls the distribution of Ni-Cu-PGE ores in the Sudbury mining camp (Fig. 1). The originally flat-lying, ~150–200 km diameter x 3 km thick igneous body (SIC) was tectonically deformed, folded into a doubly plunging syncline, and eroded into its present much smaller shape. Following the impact, a large hydrothermal system was generated (Ames et al., 1998) that was heated by the cooling SIC and impacted crust and resulted in fluid/volatile circulation through the breccia and structures, both above and below the SIC (Farrow and Watkinson, 1992; Li and Naldrett, 1994; Hanley and Mungall, 2003; Hanley et al., 2004; Ames et al., 2006) (Fig. 1b).

Impact-generated hydrothermal systems may circulate many types of fluids and gases in the impact craters above, below, and within the melt sheet (e.g. Sudbury), at the central uplift (e.g. Manson, Chicxulub) and along impact-derived and pre-existing crustal structures (e.g. Chicxulub, Haughton) (McCarville and Crossey, 1996; Osinski et al., 2001; Naumov, 2002; Abramov and Kring, 2004; Ames et al., 2004). Groundwater, deep crustal fluids, seawater, if present in the target area, and basement fluids commonly recharge an impact site after the initial impact stage, when both target materials and the bolide are volatilized, the crust is melted, and then faulted and the impact site is cooled to the geothermal gradient over a protracted time period. The circulation of mixed fluids and volatiles is strongly dependent on host-rock permeability and the duration of the impact-generated hydrothermal system, which in turn is controlled by crater size, i.e., with little to no alteration in small craters (Melosh, 1989; Abramov and Kring, 2004). Fluids may utilize permeable pathways, such as shallow and deep-seated fault structures in large-scale (~200 km) modified craters, as well as impact-derived breccias developed around the transient crater in the target rocks (pseudotachylite/cataclasite; e.g. Sudbury breccia). Evidence for the Sudbury impact-induced hydrothermal system is based on field observation, mineralogical mapping, fluid inclusion, stable and radiogenic isotopic evidence for fluid and volatile flow, below, within and above the SIC (Farrow and Watkinson, 1992; Ames et al., 1998; Farrow and Watkinson, 1999; Hanley et al., 2005, 2011; Ames and Farrow, 2007; Campos-Alvarez et al., 2010; Tuba et al., 2014; Kerr et al., 2015). Fluids and volatile sources identified in the Sudbury crater include (1) groundwater and deep brines; (2) orthomagmatic volatiles released from impact generated melts; (3) Proterozoic seawater; and (4) an exotic footwall hydrocarbon-bearing fluid (Farrow and Watkinson, 1992, 1999; Ames et al., 1998; Molnar et al., 2001; Hanley et. al., 2005, 2011; Ames et al., 2006; Kerr et al., 2014) (Fig. 1b).

Hydrothermal assemblages with albite-K-feldspar, epidote, amphibole, chlorite, quartz, titanite, or scapolite are present above, below, and within the SIC. Non-aqueous fluid constituents, such as CO_2 and more recently, hydrocarbons are known components of the Sudbury hydrothermal system, as evidenced above the SIC by large (60 x 1 km) semi-conformable calcite alteration zones in the upper part of the Onaping Formation (Ames et al., 1998, 2006), calcite-quartz and actinolite-epidote below the SIC in the footwall PGE / Cu-PGE mineralized zones (Farrow and Watkinson, 1992; MacMillan, 2014), and the recognition of hydrocarbons in fluid inclusions in the ores and pre-impact target rocks (Bunch et al., 1999; Hanley et al., 2005; Mungall et al., 2007; Wright et al., 2010; Kerr et al., 2015).

SAMPLING AND METHODOLOGY

Alteration Assemblage Samples

Eight alteration types from the footwall and hanging wall of the SIC were identified across the North and East ranges of the Sudbury structure and are described in general paragenetic order relative to the main Cu-sulphide mineralizing stage for the footwall types (Ames et al., 1998, 2006; Tuba et al., 2010, 2014), (Figs. 2, 3, Table 1). Alteration assemblages with epidote (Fig. 2) and/or amphibole (Fig. 3) that are pre-sulphide mineralization (i.e. chalcopyrite-PGM veins) and generally barren are found as miarolitic cavities in "footwall granophyre" (Fig. 2a), pervasive epidote-

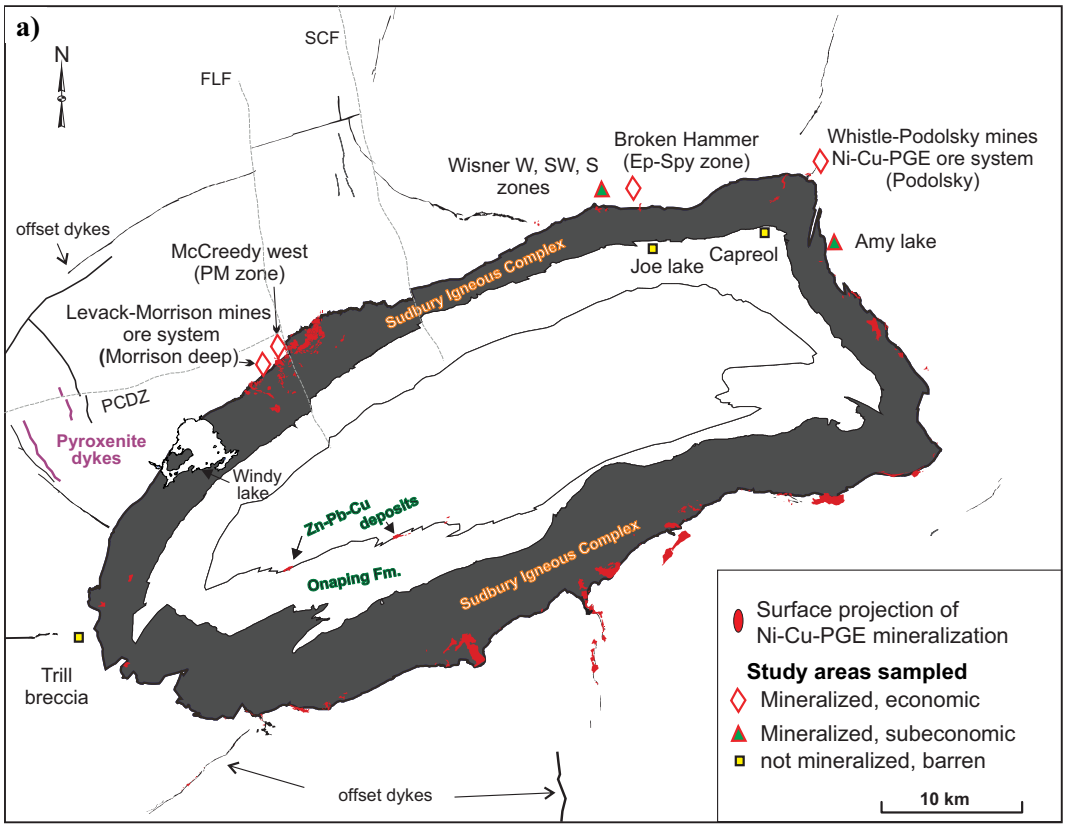

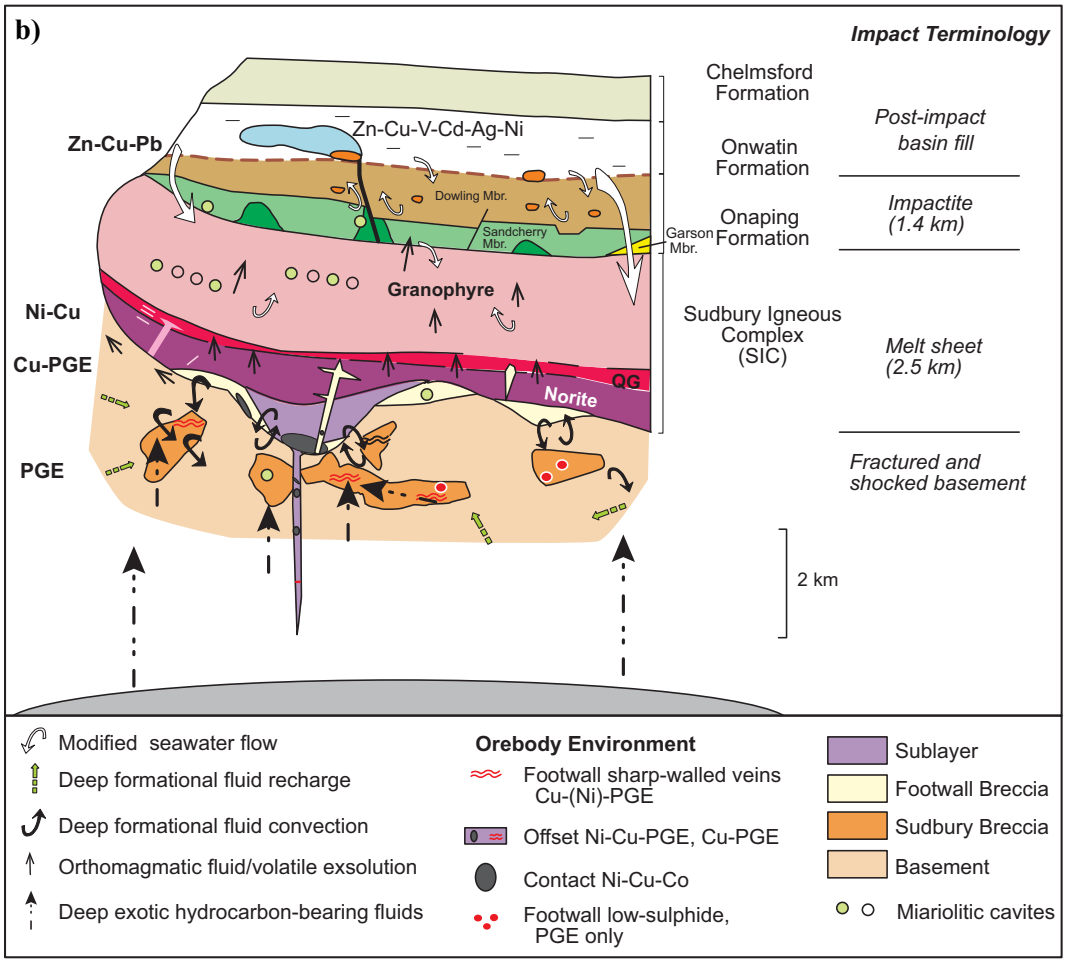

Figure 1. a) Location map of the barren and mineralized hydrothermal alteration studied in the Sudbury structure. **b)** Schematic section of the Sudbury hydrothermal system showing the relative stratigraphic location of ore types, fluid sources, and fluid/volatile flow (after Ames and Farrow, 2007).
Abbreviations:
Ep = epiidote;
FLF = Flack Lake fault;
Fm = Formation;
PCDZ = Pumphouse Creek deformation zone;
SCF = Sandcherry Creek fault;
Spy = sperrylite.

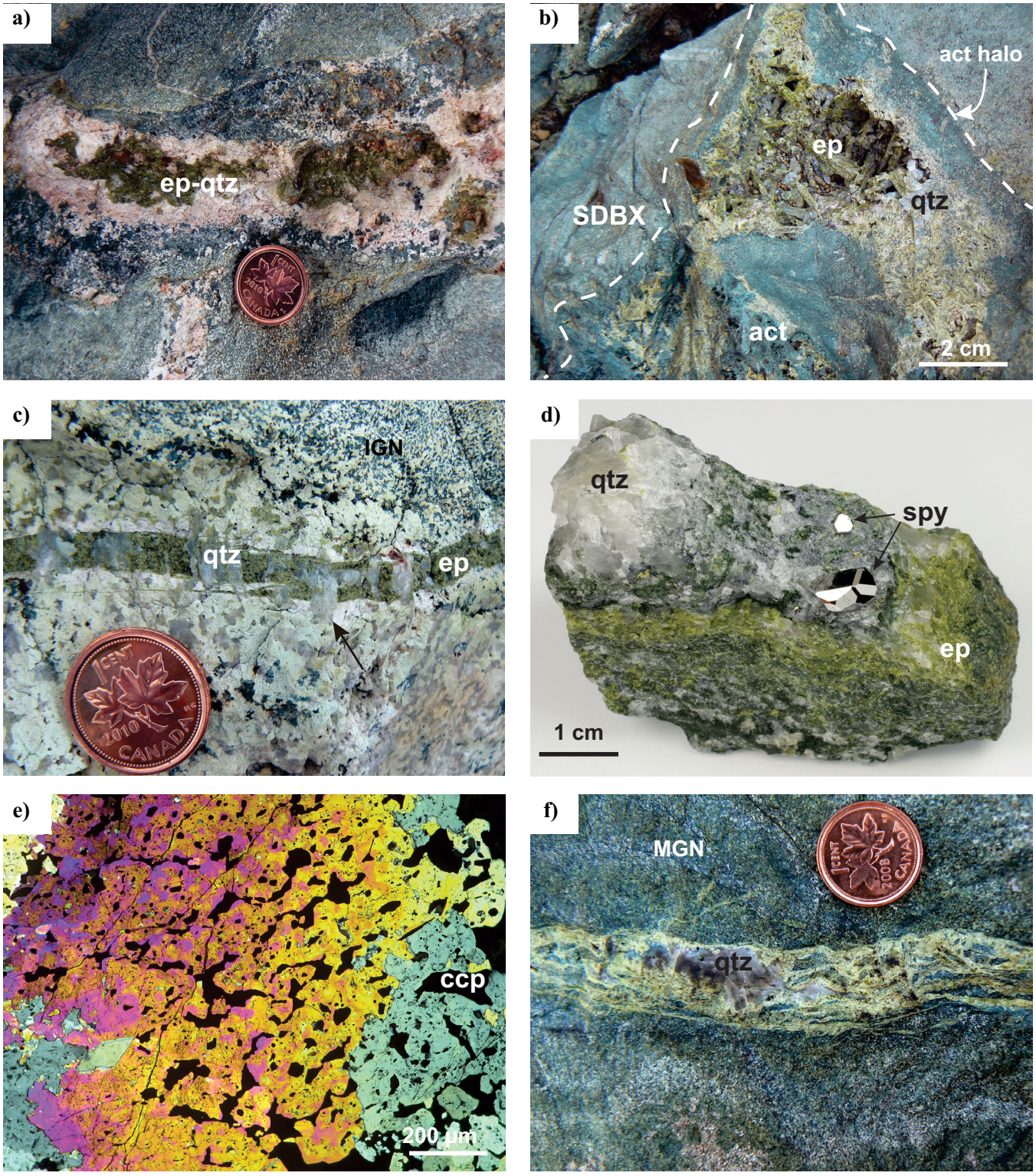

Figure 2. Examples of pre-, syn-, and post-mineralization epidote in the Sudbury structure. **a)** Miarolitic cavity in footwall granophyre, filled by epidote and quartz. Coin is 2 cm. **b)** Pre-sulphide, high-PGE, coarse prismatic epidote-quartz-actinolite open-space filling assemblage in Sudbury Breccia. Note the fine-grained amphibole halo. **c)** Extensional epidote-quartz vein cross-cuts intermediate gneiss with an overgrowth of rock-forming quartz into the vein cavity (arrow). This is a typical feature of barren extensional epidote-quartz veins. **d)** Hand sample of quartz-epidote-euhedral sperrylite ($PtAs_2$) assemblage from the margin of the Broken Hammer bulk sample pit. Note the bonanza platinum mineralization and absence of sulphide minerals. **e)** Poikilitic intergrowth of epidote and chalcopyrite, the characteristic textural feature of footwall high- and low-S mineralization. **f)** Example of a late, post-Sudbury shear-type epidote-quartz vein within mafic gneiss. Abbreviations: act = actinolite; ccp = chalcopyrite; ep = epidote; IGN = indiate gneiss; MGN = mafic gneiss; qtz = quartz; SDBX = Sudbury Breccia; spy = sperylitte.

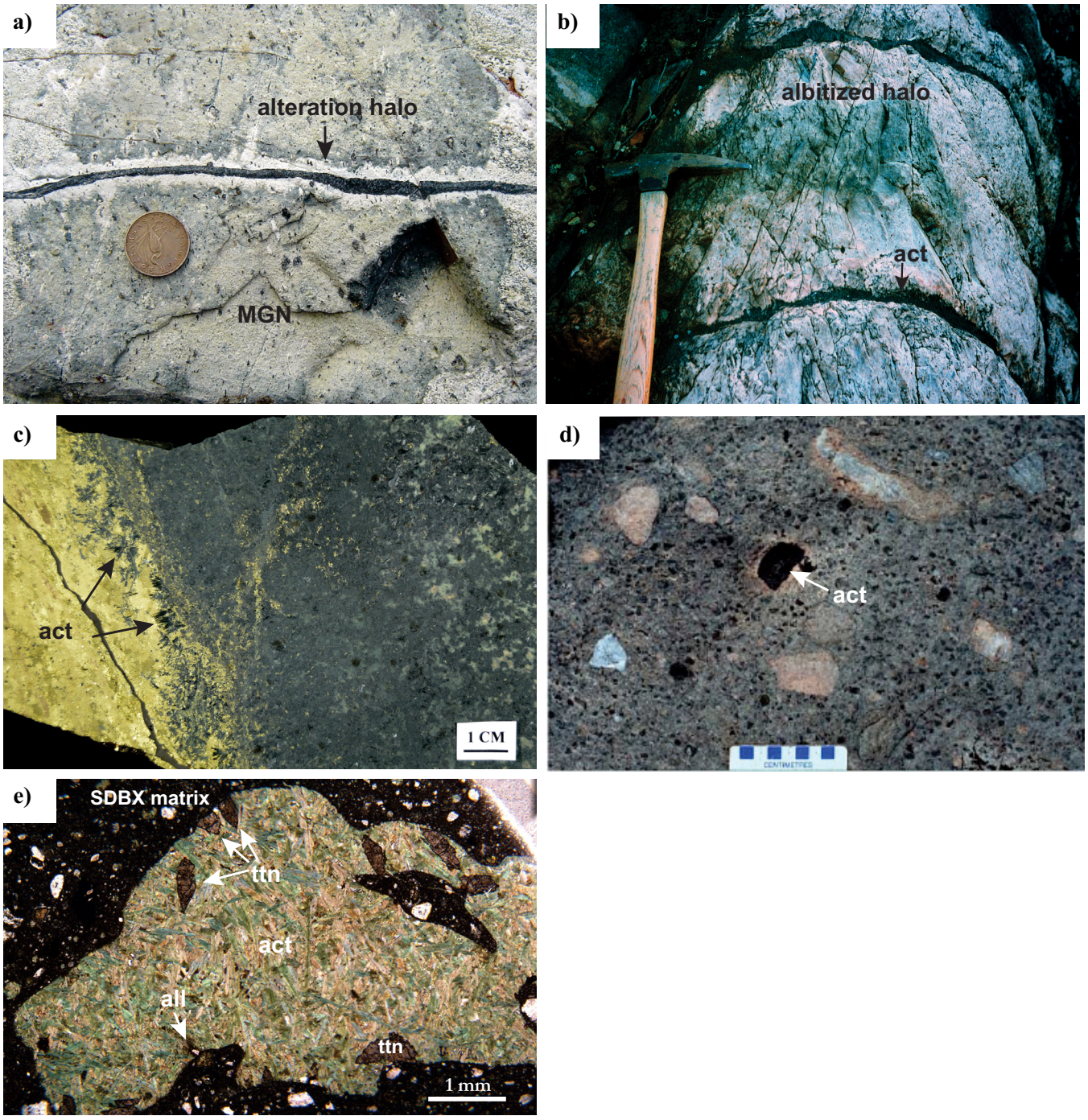

Figure 3. Diverse barren and mineralized alteration zones with amphibole in veins, amygdules, and replacement zones in the footwall and hanging wall of the Sudbury Igneous Complex. **a)** Amphibole vein in mafic gneiss, Amy Lake area. Note the white alteration halo of recrystallized feldspar, similar to that of the pre-sulphide pervasive and vein assemblages. **b)** Amphibole veins above the SIC in the Onaping Formation. Close-up of 1–2 cm actinolite veins and 12–18 cm alteration haloes within in a 3 m diameter zone with pervasive albite-quartz alteration haloes in close proximity to a fluidal breccia sill-dyke complex, Rockcut Lake, Capreol. **c)** Coarse amphibole (arrows) at the margin of a sharp-walled chalcopyrite-PGE vein and gabbro, Podolsky mine. **d)** Intense albitization in hanging-wall andesite breccia, Sandcherry member, Onaping Formation, with actinolite-filled amygdule (arrow). The altered equant-shard unit contains partially albitized (pink hue) quartzite fragments, matrix, and shards. Shards are actinolite-rich. Actinolite occurs in patches rimmed by albite and vice versa, Joe Lake area. **e)** Photomicrograph of amygdules filled with coarse amphibole (actinolite), titanite, and trace allanite hosted in Sudbury breccia, Trill area. Abbreviations: act = actinolite; all = allanite; MGN = mafic gneiss; SDBX = Sudbury Breccia; ttn = titanite.

Table 1. Summary of alteration styles and minerals analyzed in barren and mineralized environments.

Alteration type	Epidote	Allanite	Amphibole	Titanite	Mineralization style
Miarolitic cavities	coarse prismatic	in epidote core	coarse euhedral	euhedral	barren
Pervasive epidote-amphibole alteration, pre-sulphide mineralization	coarse prismatic	in epidote core	coarse euhedral, fibrous in halo		barren; occasionally high PGE
Epidote vein, pre-sulphide mineralization	coarse prismatic		fibrous in halo	euhedral	barren
Amphibole amygdules		euhedral -Trill	acicular -Trill coarse euhedral -Onaping	coarse euhedral (Trill only)	barren
1. Broken Hammer epidote-quartz-sperrylite assemblage	coarse prismatic				high PGE
2. Footwall mineralization, extensional silicate vein	coarse prismatic (in epidote-quartz veins)		acicular euhedral (in amphibole veins)	euhedral (in amphibole veins)	occasionally high PGE; barren
3. Footwall mineralization, sulphide-silicate assemblage	poikilitic		euhedral		high- and low-sulphide, high-PGE
Post-Sudbury shear-type veins	fine- to medium-grained euhedral				barren

amphibole (Fig. 2c), epidote-quartz veins (Fig. 2b), and amygdules in Sudbury breccia (Fig. 3a). The epidote-quartz-sperrylite ($PtAs_2$) bonanza ore at Broken Hammer (Ames et al., 2014), (Fig. 2d) is pre-sulphide mineralization and early in the mineralizing sequence, followed by extensional silicate veins (Fig. 2b) that are cut by high-sulphide chalcopyrite-rich sharp-walled veins that may contain marginal amphibole (Fig. 2c) or poikilitic epidote (Fig. 3e). Late "post-Sudbury", shear-type epidote-quartz veins are the youngest alteration assemblage studied in the footwall environment. Amphibole veins with albitized margins are present in the footwall and hanging wall, as are amphibole-filled amygdules whose paragenetic sequence is unknown (Fig. 3a,b,d,e).

To properly classify and fingerprint alteration assemblages indicative of Sudbury footwall (Cu)-PGE mineralization, an extensive suite of 62 samples and four alteration minerals representing a diversity of post-impact alteration assemblages were analysed in situ by LA-ICP-MS and electron microprobe. Trace element data of 54 elements were collected from epidote, allanite, amphibole, and titanite to establish typical element-associations and classification criteria, with special emphasis on alteration assemblages associated with PGE mineralization, to test the robustness of the PGE-ore geochemical fingerprint identified earlier from a smaller dataset (Tuba et al., 2014).

Background host-rock compositions were determined from representative least-altered host rocks that were collected distal to the altered sample in the same locality and were used to normalize the epidote mineral chemistry (Table A1 in Tuba and Ames, in press). Normalization of the mineral chemical data to bulk host-rock composition eliminates the chemical effects of fluid-rock alteration that were significant in a few of the alteration assemblages. The complete mineralogical and geochemical dataset, including detailed descriptions, the full mineral chemical databases, and methodologies used (electron microprobe and laser ablation ICP-MS of epidote, allanite, amphibole, and titanate) can be found in Tuba and Ames (2015).

Samples collected from North Range footwall environments include the Deep zone of the Morrison deposit, the PM zone of the McCreedy West deposit, the North zone of the Podolsky deposit, the epidote-quartz-sperrylite zone of the Broken Hammer deposit, all with economic low-sulphide PGE mineralization. Exploration trenches exposing sub-economic low-sulphide mineralization at Wisner West, Southwest and South zones in the North Range as well as Amy Lake-PGE zone in the East Range were also sampled (Fig. 1). Hydrothermal alteration is present in the SIC's footwall and hanging wall, with similar mineral assemblages but lacking PGE mineralization. These barren hydrothermally altered rocks were collected in the Trill and Windy Lake footwall environment and in the Joe and Rockcut Lake areas in the hanging-wall environment, along the North and East ranges (Ames and Gibson, 2004 a,b) (Fig. 1).

RESULTS AND DATA ANALYSIS

Epidote is a ubiquitous mineral in many barren and mineralized alteration assemblages along the Sudbury

North Range (Table 1, Fig. 1b). Epidote associated with Sudbury Cu-PGE and PGE deposits has similar major-element compositional ranges with $Fe^{3+}/(Fe^{3+}+Al)$ compositions, (X_{Fe}= 0.18–0.37) and average ratios (X_{Fe}=26, n=72 high-S, and n=41 low-S; Ames et al., 2015) that generally imply oxidizing conditions for low-sulphide PGE-rich mineralization. However, the major-element substitution is complicated as it can be also affected by temperature, fluid, and bulk-rock compositions, CO_2 fugacity, and pressure (Arnason et al., 1993). In addition, the rare-earth and trace-element compositions of the common minerals epidote and amphibole and accessory minerals allanite and titanite were characterized. The elements analysed in minerals were plotted on three diagrams and include (1) pathfinder elements — Co, Ni, Cu, Zn, As, Pd, Ag, Sn, Sb, Pt, Au, Pb, and Bi; (2) other elements — Mg, Sc, V, Cr, Mn, Rb, Sr, Y, Zr, Nb, Mo, Rh, Cd, Cs, Ba, Th, and U; and then (3) rare-earth elements (Figs. 4, 5). Elements close to the detection limit of the ICP-MS in both epidote and amphibole, included Ag, Sb, Pt, Au, Bi, Mo, Rh, Cd, and Cs, and others usually detected in very low concentrations regardless of the alteration type include Pd and Bi in epidote.

Rare-Earth Element Characteristics of Epidote-Allanite, Amphibole, and Titanite

The mineral trace-element data were normalized to the bulk rock geochemistry of the host rock for all data to minimize the influence of host rock (Tuba and Ames, 2015: Table A1). Trace element data show that certain rare-earth element (REE) patterns are more frequent in some alteration groups, although REE concentrations vary significantly within these groups and, in some cases, even within a sample (Fig. 4). The most useful feature of the host rock-normalized REE plots in the characterization of the alteration groups is the diagram topology, whereas other features (e.g. size of Eu anomaly, level of REE-enrichment of a single mineral) do not show systematic variations. Classification of the alteration groups based on mathematically expressed La:Lu (or other light REE:heavy REE) ratios was not possible as individual analyses in heterogeneous samples may scatter in a wide range; therefore the topology of REE plots defined by all analyses in a given sample (typically around 10 ablation spots) was studied. A REE pattern was considered characteristic if it appeared in about 90% of the samples within an alteration group. The presence or absence of the three REE-bearing minerals epidote, titanite, and allanite strongly affects the patterns of individual minerals in the various alteration assemblages (Fig. 5) (Tuba and Ames, 2015).

The overall REE content of the alteration assemblages is strongly dependent on the presence of allanite and titanite. Miarolitic cavities and pervasive epidote-amphibole alteration contained minerals bearing the highest concentrations of REE (titanite average REE_{tot} = 9,256 ppm, and allanite average REE_{tot} =144,260 ppm, respectively), (Fig. 5). Titanite in amphibole amygdules in the Trill Sudbury breccia has similar REE levels as the titanite in pre-sulphide epidote veins (Fig. 5a,e). The REE content of titanite decreases more in the pre-sulphide epidote veins than in the mineralization-related extensional actinolite veins (Fig. 5f). Epidote is the main REE-carrier in extensional epidote veins, mineralized sulphide-silicate assemblages, and late shear-type veins; these assemblages are generally low in REE (REE_{tot} = 76–286 ppm) with the exception of extensional epidote and actinolite veins from the vicinity of the Broken Hammer sperrylite zone, which are unusually enriched (average REE_{tot} = 1,382 ppm).

Epidote and amphibole in the different alteration assemblages exhibit host–rock-normalized REE patterns with characteristic topologies that are best described with nLREE to nHREE relations (Fig. 4). High-REE (with additional Y, Th, and U) assemblages are found in miarolitic cavities and pervasive epidote-amphibole alteration that predate the Sudbury footwall mineralization as these contain the REE-rich minerals allanite and titanite, whereas, in other alteration styles these minerals are absent. Vein-type pre-sulphide assemblages are comparably lower in REE, whereas sulphide-silicate assemblages of footwall mineralization and associated extensional silicate veins, as well as post-Sudbury shear-type veins are REE-poor.

Pathfinder Mineral Chemistry of Epidote-Allanite and Amphibole

Epidote-Group Minerals

Of all of the >25 trace elements analysed in epidote, Pb and Ni proved to be most useful for classifying the alteration groups. Epidote-bearing assemblages predating the sulphide Cu-PGE mineralization are dominantly lower in Pb (<5 ppm) than those associated with the sulphide-bearing system, although the two groups overlap slightly (Fig. 6a,b). Among the pre-sulphide assemblages, Ni is lowest (<1 ppm) in the miarolitic epidote, and highest (typically a few 100 ppm) in the high-PGE pervasively epidotized alteration. Vein-type epidote and most of the low-PGE pervasive epidote plot in between. Nickel in poikilitic epidote of the sulphide-silicate assemblage and in extensional veins ranges widely from ~0.1 to 300 ppm). Although the pre-sulphide and sulphide-bearing systems may be distinguished based on the Pb content of epidote, the Pb and Ni values of epidote in post-Sudbury shear-type veins overlap with both groups. The observations regarding Pb and Ni patterns as discussed above are

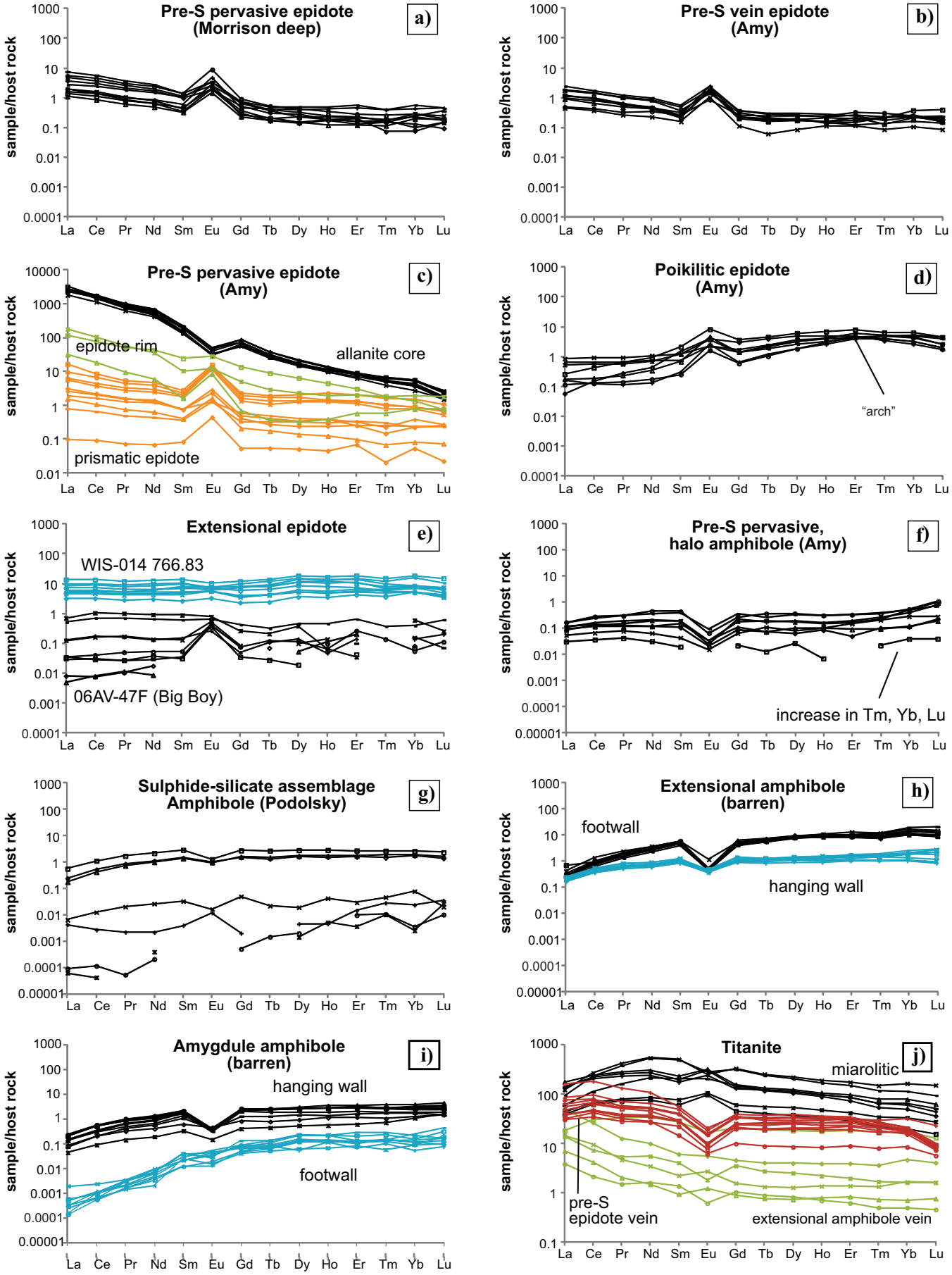
Pre-S pervasive epidote
(Morrison deep)
a)
Pre-S vein epidote
(Amy)
b)
Pre-S pervasive epidote
(Amy)
c)
epidote rim
allanite core
prismatic epidote
Poikilitic epidote
(Amy)
d)
"arch"
Extensional epidote
e)
WIS-014 766.83
06AV-47F (Big Boy)
Pre-S pervasive,
halo amphibole (Amy)
f)
increase in Tm, Yb, Lu
Sulphide-silicate assemblage
Amphibole (Podolsky)
g)
Extensional amphibole
(barren)
h)
footwall
hanging wall
Amygdule amphibole
(barren)
i)
hanging wall
footwall
Titanite
j)
miarolitic
pre-S
epidote vein
extensional amphibole vein
sample/host rock
La Ce Pr Nd Sm Eu Gd Tb Dy Ho Er Tm Yb Lu

generally in agreement with the findings of Tuba et al. (2014).

The positive correlation previously found between Co and Ni in epidote (Tuba et al., 2014) is less pronounced in this extended database (Fig. 6c,d). A strong positive correlation between these elements does occur in poikilitic epidote (and a weaker correlation in the shear-type epidote group); however, there is no clear linear relationship between Co and Ni in other alteration groups. There is a link between these elements in the fluids associated with footwall PGE mineralization. Furthermore, comparison of the absolute and host-rock normalized Co versus Ni plots (Fig. 6c,d) shows that the host-rock composition influenced the concentration of Co in epidote in most alteration assemblages. Significantly, the late shear-type and PGE-mineralized poikilitic epidote samples do not show a major change in the topology of Co versus Ni plots and thus, are not affected by wall rock.

Amphibole and Chlorite

The Ni content is highest in chlorite (<3.4 wt%), followed by amphibole (<1.3 wt%) and biotite (<1 wt%) and also occurs in epidote and stilpnomelane in the mineralized footwall environment (Ames et al., 2013). The magnesian- and nickel-rich compositions of chlorite associated with both low-sulphide-PGE and sharp-walled-vein Cu-PGE mineralization has been recognized (Péntek et al., 2008; Tuba et. al., 2010; Ames and Kjarsgaard, 2013) and is also manifested by Ni-rich amphibole in alteration assemblages produced in higher contact metamorphic grades in the thermal aureole of the SIC (Hanley and Bray, 2009). Ni-enriched ferromagnesian phases identified proximal to Ni-Cu-PGE mineralization include amphibole, chlorite, and biotite (Farrow and Watkinson, 1992; Hanley et al., 2011; White, 2010; Warren et al., 2015). Systematic sampling towards high-sulphide Cu-PGE veins in the footwall identified a vectoring tool using Ni in amphibole (Hanley and Bray, 2009). However, the usefulness of these observations are significant to PGE fertility only when comparing these compositions with other amphibole in the Sudbury environment to detect a unique signature for alteration related to the high-tenor PGE mineralization.

Amphibole-bearing assemblages may be fingerprinted based on their Ni and Sn content (Fig. 7). Pre-sulphide, pervasively altered assemblages associated with high-PGE contain the highest amounts of Ni (0.2 wt% Ni average) in amphibole that occurs with both prismatic epidote and forms the finer grained actinolite halo around the alteration (Fig. 3b). The actinolite halo around pre-sulphide epidote veins, as well as amphibole-filled amygdules in Sudbury breccia are both Ni-poor (<300 ppm). Euhedral amphibole in sulphide-silicate assemblages in the low-sulphide footwall mineralization is enriched in Ni, with values above 0.1 wt% and as high as 1 wt% Ni. Such high concentration of Ni in this type of amphibole was already known from the Sudbury footwall (Farrow, 1994; Magyarosi et al., 2002; Kjarsgaard and Ames, 2010; Tuba et al., 2010, 2014). Unmineralized extensional amphibole veins fall into the low-Ni area of the diagrams, typically with 100–200 ppm Ni; among them, however, two samples with trace microscopic chalcopyrite had anomalous bulk PGE contents (0.01 ppm) and plot closer to the high-PGE field. The Ni content of amphibole in high-PGE extensional veins (samples 12AV-15B and BLT-06) is typically 0.04 to 0.1 wt%.

Nickel content in extensional amphibole as a function of bulk total precious metal content and/or proximity to footwall mineralization was documented by Hanley and Bray (2009) and Tuba et al. (2010). Tin in amphibole is also enriched (>1 ppm) in sulphide-silicate assemblages and extensional amphibole veins in footwall ore systems, whereas the concentrations of Sn in the extensional amphibole veins from the hanging wall (Onaping Formation) are below 1 ppm.

Figure 4 (opposite page). Representative examples of the rare earth element (REE) distribution patterns in pre-sulphide epidote, amphibole, titanite, and sulphide-silicate assemblages. Typical REE pattern of pre-sulphide epidote in **(a)** pervasive replacement (sample 08AV-05A) and **(b)** vein epidote (sample 12AV-63) assemblages with moderate negative slope and pronounced Eu anomaly. The slightly negative slope is characteristic and discriminatory of pre-sulphide epidote. **c)** REE patterns of pre-sulphide pervasive alteration with coexisting allanite and epidote (sample 12AV-60). **d)** "Arch-like" heavy REE pattern of poikilitic epidote associated with platinum-group element (PGE) mineralization (sample FAL-12). **e)** REE pattern in extensional epidote is commonly flat with a slight Eu anomaly. The anomaly increases with decreasing concentrations of REE. **f)** A slight increase in Tm, Yb, and Lu is visible in the REE plots of pre-sulphide amphibole (sample 12AV-60). **g)** Euhedral amphibole from the mineralized sulphide-silicate assemblage is usually low in REE and may show large intra-sample variations (sample 11AV-62F). **h)** Typical REE pattern of extensional amphibole from both the footwall (sample BLT-05) and hanging wall (sample AV-488B) of the Sudbury Igneous Complex(SIC), which show a similar topology to the **(i)** hanging-wall actinolite amygdules (Joe Lake Onaping Formation, sample AV-524A) as they are all mono-mineralic assemblages. This is in contrast to the amphibole assemblage with allanite and titanite in the footwall amygdules (Trill Sudbury Breccia) below the SIC. **j)** REE in titanite decreases from the miarolitic cavities (sample 12AV-57) to pre-sulphide (pre-S) epidote veins (sample 12AV-63) and extensional amphibole veins (sample 12AV-78).

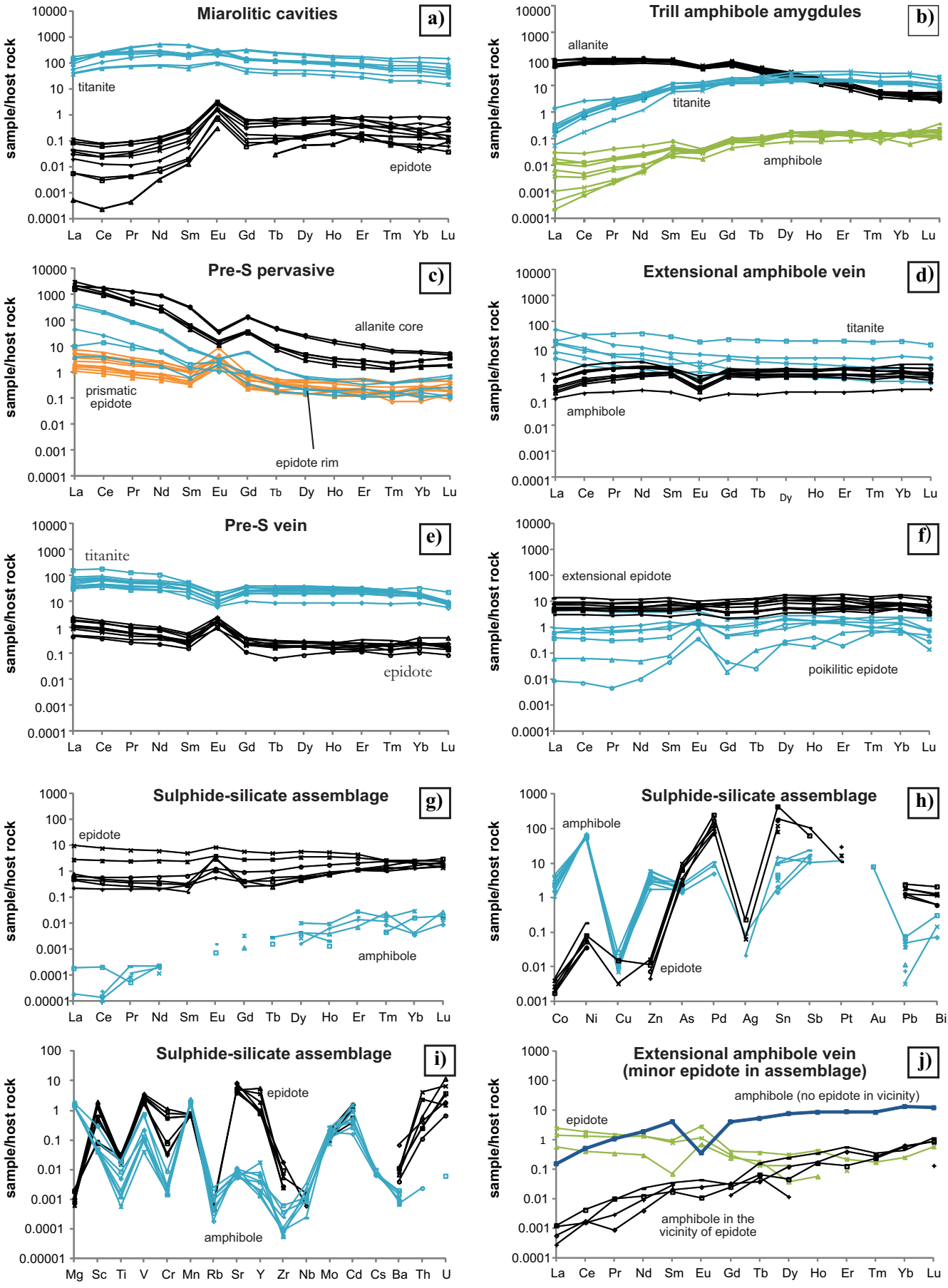
Miarolitic cavities
a)
titanite
epidote
Trill amphibole amygdules
b)
allanite
titanite
amphibole
Pre-S pervasive
c)
allanite core
prismatic epidote
epidote rim
Extensional amphibole vein
d)
titanite
amphibole
Pre-S vein
e)
titanite
epidote
extensional epidote
f)
poikilitic epidote
Sulphide-silicate assemblage
g)
epidote
amphibole
Sulphide-silicate assemblage
h)
amphibole
epidote
Sulphide-silicate assemblage
i)
epidote
amphibole
Extensional amphibole vein (minor epidote in assemblage)
j)
amphibole (no epidote in vicinity)
epidote
amphibole in the vicinity of epidote
sample/host rock
La Ce Pr Nd Sm Eu Gd Tb Dy Ho Er Tm Yb Lu
Co Ni Cu Zn As Pd Ag Sn Sb Pt Au Pb Bi
Mg Sc Ti V Cr Mn Rb Sr Y Zr Nb Mo Cd Cs Ba Th U

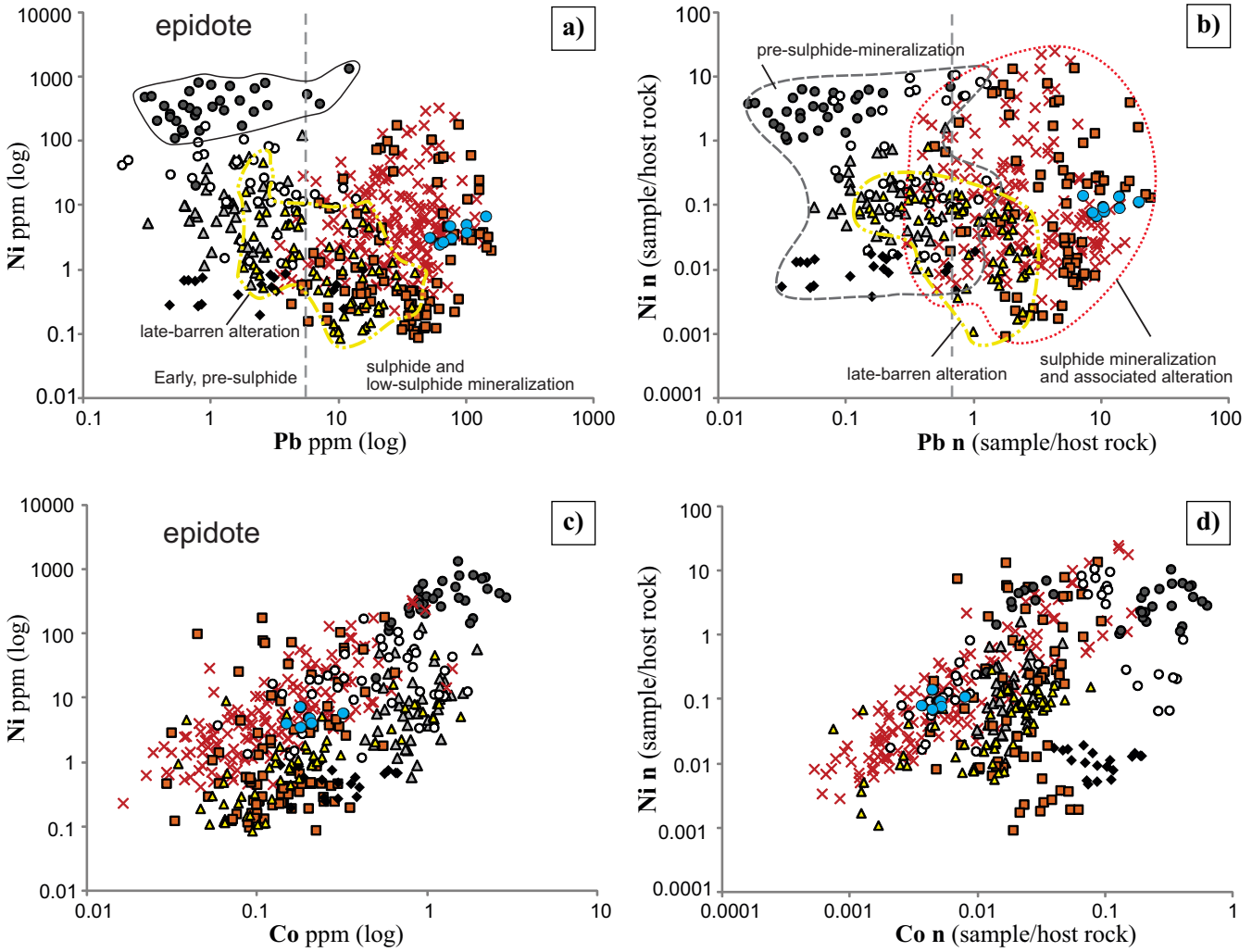

Epidote legend

Pre-sulphide-mineralization
- miarolitic cavities
- pervasive epidote-amphibole (high-PGE)
- pervasive epidote-amphibole (low-PGE)
- epidote vein

Footwall mineralization
- sulphide-silicate assemblage
- extensional epidote-quartz veins
- epidote-quartz-sperrylite assemblage (Broken Hammer)

Post-Sudbury alteration
- shear-type veins

Figure 6. Results for epidote from multiple hydrothermal assemblages showing the relationship of important pathfinder elements, Ni, Pb, and Co, on absolute, and host-rock normalized concentration plots. **a)** Absolute concentration plot of Pb versus Ni, and **(b)** host-rock normalized Pb versus Ni diagram. Vertical dashed line at 5 ppm Pb. Barren and PGE-enriched, pre-sulphide assemblages may be distinguished from those associated with low-sulphide footwall mineralization based on the lower Pb content (vertical dashed line is at 5 ppm Pb). Post-Sudbury shear-type veins (yellow outline) overlap with both groups. Among pre-sulphide assemblages, high-PGE pervasive epidote samples show the highest Ni values. **c)** Absolute and **d)** host-rock normalized concentration of Co and Ni in epidote. Note the pronounced difference in the topologies of alteration groups in the two plots, indicating the effect of host-rock composition on the Co concentration in all assemblages, except for poikilitic and shear-type epidote. Co and Ni correlates well in the sulphide-silicate assemblage (poikilitic epidote).

Figure 5 (opposite page). Representative rare earth element (REE) plots of epidote-, amphibole-, titanite-, and allanite-bearing alteration assemblages showing the mineral reservoirs for REE in paragenetic order from early pre-sulphide to syn-sulphide assemblages **(a-f)**. A gradual decrease in bulk REE can be observed with higher REE concentrations associated with pre-sulphide assemblages (pervasive: sample 08AV-05A, vein: sample 12AV-63) and low REE being typical for footwall mineralization systems (poikilitic epidote: sample 06AV-37A, extensional amphibole vein: sample 12AV-78, extensional epidote vein: sample WIS-014 766.83). Allanite and titanite in the Trill amphibole amygdule assemblage (sample TR-1005) shows REE values as high as silicates in the miarolitic cavities (sample 12AV-57) and pre-sulphide epidote veins. **g-j)** Element partitioning between epidote (black) and amphibole (blue) in a mineralized sulphide-silicate assemblage at the Podolsky deposit (sample 02AV-642, bornite-bearing) showing **(g)** REE profiles, **(h)** pathfinder element suite and **(i)** other trace elements. Similar element partitioning between epidote and amphibole was found in additional 11 samples. **(j)** Characteristic epidote-amphibole and amphibole-only REE patterns where the epidote-free pattern has a positive slope and pronounced negative europium anomaly.

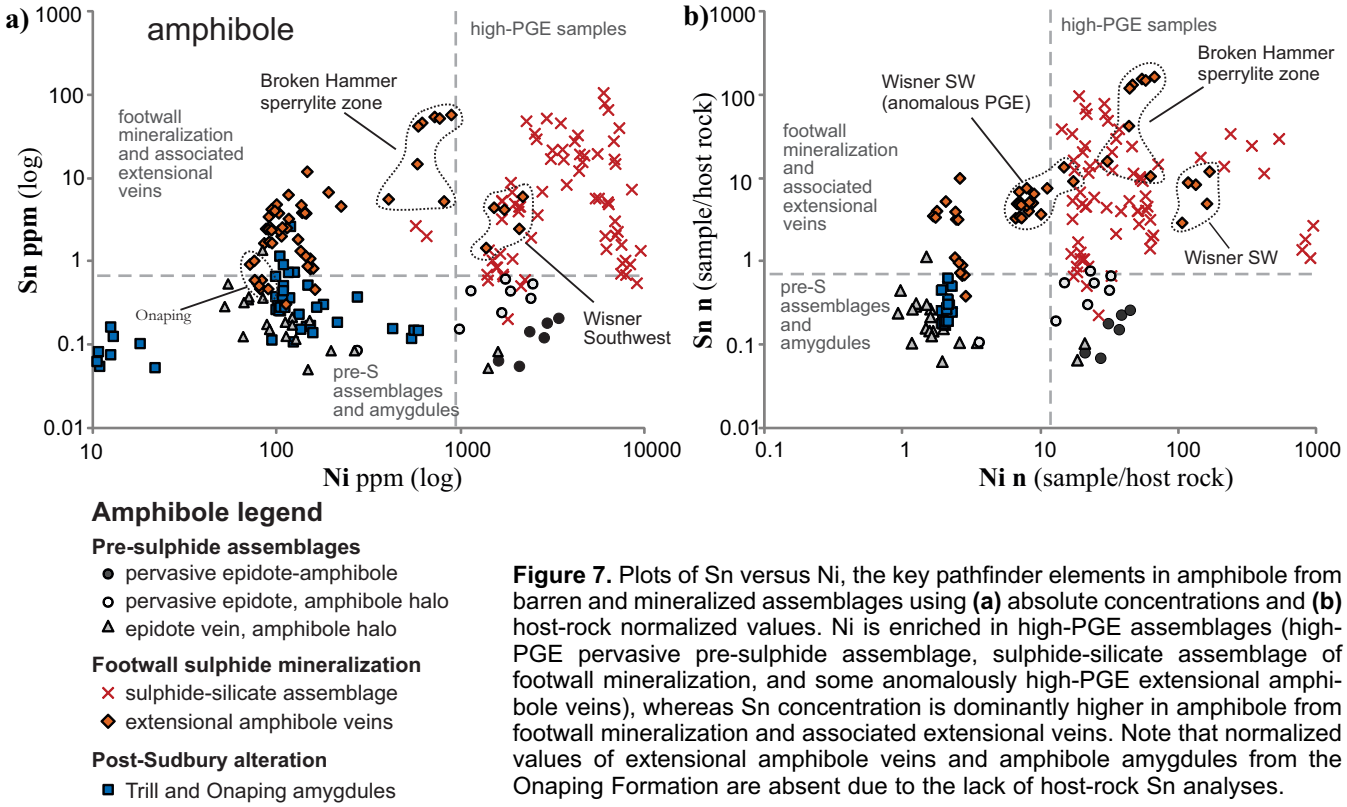

Figure 7. Plots of Sn versus Ni, the key pathfinder elements in amphibole from barren and mineralized assemblages using **(a)** absolute concentrations and **(b)** host-rock normalized values. Ni is enriched in high-PGE assemblages (high-PGE pervasive pre-sulphide assemblage, sulphide-silicate assemblage of footwall mineralization, and some anomalously high-PGE extensional amphibole veins), whereas Sn concentration is dominantly higher in amphibole from footwall mineralization and associated extensional veins. Note that normalized values of extensional amphibole veins and amphibole amygdules from the Onaping Formation are absent due to the lack of host-rock Sn analyses.

DISCUSSION

The alteration minerals quartz, carbonate, chlorite, epidote, and amphibole and accessory titanite and allanite are found in diverse ore-system settings with volcanogenic massive sulphide (VMS), porphyry, gold, and Ni-Cu-PGE deposits. The major elements Fe^{3+} and Al^{3+} of epidote in various mineralizing and barren settings have been used to determine the redox and/or temperature conditions of epidote alteration zones in modern and ancient volcanogenic massive sulphide and recently in porphyry systems (Hannington et al., 2003 and references therein; Frikken et al., 2005; Cooke et al., 2014). Many authors working on different low-sulphide footwall PGE mineralization zones in the Sudbury Ni-Cu-PGE mining district (e.g. White (2010): Vale properties; Tuba (2010): Wallbridge properties; Ames (2005–2010): FNX, Wallbridge and Vale properties) simultaneously recognized poikilitic epidote spatially associated with low-sulphide PGE and some high-sulphide Cu-PGE mineralization.

The trace element contents in minerals are influenced by (1) fluid/melt composition, (2) host-rock composition, and/or (3) co-precipitating minerals. In order to rule out the latter as a major influence on trace element distribution in paragenetically different alteration assemblages, coeval mineral pairs were tested for element partitioning.

Significance of Host-Rock Normalized Mineral Chemistry

Normalization of the data to the composition of the host rock does not usually result in major differences between the topology of the two diagrams — one showing the absolute and the other the normalized values — just "tightening up" the samples within the groups by removing outliers (Figs. 6, 7). As such, the relative position of the groups generally does not change but where it does, it likely indicates that fluid-rock interaction had an impact on certain alteration assemblages. For example, normalizing As in epidote results in a significant shift of poikilitic samples though others preserve their relative position, suggesting that As in the sulphide-silicate assemblage is at least partly dependent on the host rock. Similarly Zn is also host-rock dependent in mineralized and extensional silicate assemblages.

Pathfinder elements Ni, Pb, Sn, and Co are most distinctive in fingerprinting the ore-bearing alteration assemblages. The highest concentrations are associated with silicates from footwall mineralization and the accompanying extensional veins, emphasizing the genetic link between the two assemblages. High-PGE pre-sulphide assemblages are characterized by high Ni and Co but low Pb and Sn values. Other assemblages are notably depleted in these elements. The topologies of the Pb versus Ni diagrams are very similar, regardless of the values plotted (absolute concentrations in

ppm or host-rock normalized values; Fig. 6a and b, respectively), suggesting that the concentrations of these elements are not a function of host-rock composition but rather of fluid composition. The elements Ni, Co, Pb, and Sn are the discriminant elements in epidote and/or amphibole, as the highest amounts of Ni, Co, Pb, and Sn was found in epidote and amphibole in footwall ore as well as in high-PGE pre-sulphide samples that contain Ni-sulphides and significant amounts of Pb- and Sn-bearing trace minerals. High Ni-values in the minerals are also associated with high-PGE pre-sulphide samples, where minor to trace millerite may be present. Sn is more erratic, with only the poikilitic epidote in the selvage of the cassiterite-millerite-bearing sharp-walled vein at Broken Hammer having a high Sn-Ni correlation (Ames et al., 2007). Pre-existing structures provide permeable pathways for the mineralizing fluids; hence, some extensional amphibole and/or epidote-quartz veins are PGE enriched and others are not (Table 1). The amounts of REE, Y, Th, and U are interpreted to reflect the composition of the parental fluids; low-S mineralization is not distinctive based on these elements.

Possible Controls on the Trace Element Distribution in Epidote

Element Partitioning among Minerals

Trace element partitioning between epidote and amphibole, the two most common alteration minerals in the Sudbury footwall, was tested on 12 samples. Element partitioning between titanite and amphibole and between titanite and epidote were tested with a smaller dataset (n= 4 samples; Table 2). The trace element concentration of epidote/amphibole may be influenced by (1) the parental fluid composition (e.g. REE, U, Th, Ni, Pb, Sn), (2) host rock, particularly mafic rocks (e.g. As, Zn), and/or (3) the crystal structural properties of the minerals (e.g. Mg and Sr in epidote).

In samples with coexisting epidote and amphibole, epidote appears to have preferentially incorporated REE, Pb, Bi, and Sn, amphibole is significantly enriched in Co, Ni, and Zn, and As is distributed equally between the two minerals (Table 2; see Fig. 13a to c in Tuba and Ames, in press). The systematic distribution of REE was observed in all of these samples (Fig. 4), and over 90% of the samples showed the same partitioning of the pathfinder elements (Pb, Bi, Sn, Co, Ni, Zn, As, Cu). Copper prefers amphibole or is distributed equally between the two minerals, whereas Pd and Ag are never enriched in amphibole. The behaviour of Sb was found to be erratic.

This partitioning behaviour has a significant effect on the topology of REE plots, and, in fact, may be an explanation for some REE patterns that differ profoundly from the average, most frequent REE patterns

Table 2. Summary of systematic element partitioning among coexisting minerals in footwall alteration zones.

Mineral	REE and pathfinder elements	Other trace elements
Epidote-amphibole		
ep>amph	REE, Pb, Bi, Sn	Sr, U
amph>ep	Co, Ni, Zn	Mn, Rb
ep~amph	As	
Based on 12 samples representing 4 alteration groups. Observed frequency of given element distribution among mineral pairs: min. 90%.		
Titanite-amphibole		
ttn>amph	REE, Sn, Bi	V, Y, Zr, Nb, Mo, Th, U
amph>ttn	Co, Ni, Zn	Sc, Mn, Ba
ttn~amph	Cu	Rb
Based on 4 samples representing 2 alteration groups. Observed frequency of given element distribution among mineral pairs: 100%.		
Titanite-epidote		
ttn>ep	REE, As, Sn, Pb	Sc, V, Cr, Y, Zr, Nb, Mo, Th, U
ep>ttn	Co	Mn, Sr
ttn~ep	Zn, Sb	Mg, Ba
Based on 2 samples representing 2 alteration groups. Observed frequency of given element distribution among mineral pairs: 100%. For informational purposes only.		

Abbreviations: amph = amphibole; ep = epidote; ttn = titanite.

in the same alteration group. The typically low-REE content of euhedral actinolite in the mineralized sulphide-silicate assemblage is likely due to the REE-scavenging behaviour of the poikilitic epidote with which the amphibole is associated (Fig. 4a). Whereas, in amphibole-dominated, essentially monomineralic assemblages (e.g. extensional actinolite veins and Onaping amygdules) where the amphibole is the main REE-bearing phase, it is significantly more enriched in REE than the amphibole occurring with epidote, titanite, or allanite in other assemblages (Fig. 4 h,i).

Element partitioning between titanite and amphibole as well as titanite and epidote from four samples representing three alteration groups (miarolitic cavities, extensional amphibole veins, and Sudbury breccia-hosted amygdules) showed that REE, Sn, Zr, Nb, Yb, Th, and U partition preferentially into titanite and Co, Ni and Zn into amphibole (Tuba and Ames, in press).

IMPLICATIONS FOR EXPLORATION

The examination of hydrothermal minerals (epidote, amphibole, titanite, and allanite) formed during multiple pre-, syn-, and post-magmatic hydrothermal events in barren and PGE-fertile assemblages provides diagnostic geochemical signatures of the major minerals epidote and amphibole to aid in the detection of precious-metal mineralization in the Sudbury footwall environment. Pathfinder elements Ni, Pb, Sn, and Co in

epidote and amphibole are the most reliable and robust elements to distinctly fingerprint the PGE-mineralizing alteration in Sudbury's footwall environment.

Trace element partitioning occurs between texturally coeval minerals, such as epidote and amphibole (REE, Pb, Bi, and Sn partition into epidote; Co, Ni, and Zn show affinity to amphibole). In titanite-amphibole assemblages, the elements REE, Sn, Zr, Nb, Yb, Th, and U partition into titanite and Co, Ni, and Zn have an affinity to amphibole. This scavenging phenomenon greatly affects the element distribution of the mineral pairs; therefore, conclusions drawn on the trace element concentrations of a single mineral should be avoided.

An unconventional exploration technique was developed for detection of the "no-see-um" precious-metal (PGE) mineralization in the world-class Sudbury mining district, using alteration-mineral chemical-pathfinder elements. We highlighted the effects of host-rock compositions and mineral-pair partitioning of elements in the indicator minerals, and show that single mineral phases and single elements should not be used.

Although this study only briefly touches on the role of structure, on fluid and metal mobility through the reactivation of older, impact-generated and extensional structures that host the highest grade PGE-only orebodies, a major knowledge gap remaining that has been overlooked is the physical hydrology of the magmatic-hydrothermal system. Determining the physical controls on the magma, multiple fluids (including copper "fluids"), and volatile expulsion is key to understanding the metallogenesis of the world-class camp and thus, help explorers target more efficiently, contributing to the economic potential of the district.

ACKNOWLEDGEMENTS

This study was carried out under Natural Resources Canada's Targeted Geoscience Initiative 4 (TGI-4) with the support of Zhaoping Yang and Simon Jackson in the GSC LA-ICP-MS facility along with Ingrid Kjarsgaard and Katherine Venance for electron microprobe analyses. We are particularly thankful to exploration companies and geologists for access to properties, particularly Joshua Bailey and Attilla Péntek (Wallbridge Mining), John Everest, Catharine Farrow and Gord Morrison (KGHM née FNX), and Matthew Stewart (Vale).

REFERENCES

Abramov, O. and Kring, D.A., 2004. Numerical modelling of an impact-induced hydrothermal system at the Sudbury crater; Journal of Geophysical Research, v. 109, E1007.

Ames, D.E. and Gibson, H.L., 2004a. Geology, alteration and mineralization of the Onaping Formation, Rockcut Lake area, Norman Township, Sudbury, Ontario; Geological Survey of Canada, Open File 4565,1 sheet with 2 colour maps, 4 figures and 1 table, scale 1:2000.

Ames, D.E. and Gibson, H.L., 2004b. Geology, alteration and mineralization of the Onaping Formation, Joe Lake area, Wisner Township, Sudbury, Ontario; Geological Survey of Canada, Open File 4566, 1 sheet, 2 colour maps, 5 figures and 1 table, scale 1:2000.

Ames, D.E. and Farrow, C.E.G., 2007. Metallogeny of the Sudbury mining camp, Ontario, *In:* Mineral deposits of Canada: A Synthesis of Major Deposit Types, District Metallogeny, the Evolution of Geological Provinces, and Exploration Methods, (ed.) W.D. Goodfellow; Geological Association of Canada, Mineral Deposits Division, Special Publication 5, p. 329–350.

Ames, D.E. and Kjarsgaard, I.M., 2013. Sulphide and alteration mineral chemistry of low- and high-sulphide Cu-PGE-Ni deposits in the Footwall environment, Sudbury, Canada; Geological Survey of Canada, Open File 7331. doi:10.4095/292707

Ames, D.E., Watkinson, D.H., and Parrish, R.R., 1998. Dating of a regional hydrothermal system induced by the 1850 Ma Sudbury impact event; Geology, v. 26, p.447–450.

Ames, D.E., Pope, K.O., Dressler, B., and Pilkington, M., 2004. Secondary alteration of the impactite and mineralization in the basal Tertiary sequence, Yaxcopoil-1, Chicxulub impact crater, Mexico. Meteoritics and Planetary Science, v. 39, no. 6/7, p. 1145–1168.

Ames, D.E., Jonasson, I.R., Gibson, H.L., and Pope, K.O., 2006. Impact-generated hydrothermal system- Constraints from the large Paleoproterozoic Sudbury crater, Canada, *In:* Biological Processes associated with impact events, Impact Studies, (ed.) C. Cockell, I. Gilmour, and C. Koeberl; Berlin-Heidelberg, Springer-Verlag. p. 55–100.

Ames, D.E., McClenaghan, M.B., and Averill, S.A., 2007. Footwall-hosted Cu-PGE (Au-Ag), Sudbury Canada: Towards a new exploration vector, *In:* Proceedings of Exploration: Fifth Decennial International Conference on Mineral Exploration, (ed.) B. Milkereit; Exploration 07, 5th Decennial International Conference on Mineral Exploration, Toronto, Canada, September 9 to 12, p. 1013–1017.

Ames, D.E., Kjarsgaard, I.M., and McClenaghan, M.B., 2013. Target characterization of footwall Cu-(Ni)-PGE deposits, Sudbury; Geological Survey of Canada, Open File 7329. doi:10.4095/292379

Ames, D.E., Hanley, J.J., and Jackson, S.E., 2014. Low sulfide high-grade sperrylite-epidote-quartz zone, (Sudbury, Canada): implications for hydrothermal-magmatic processes, *In:* Abstracts; International Mineralogical Association 2014, Johannesburg, South Africa.

Ames, D.E., Kjarsgaard, I.M., and Tuba, G., 2015. Mineral chemistry database of 39 Ni-Cu-Platinum group element sulphide and low sulphide deposits and occurrences, Sudbury mining district, Canada; Geological Survey of Canada, Open File 7596.

Arnason, J.G., Bird, D.K., and Lion, J.G., 1993. Variables controlling epidote composition in hydrothermal and low-pressure regional metamorphic rocks, *In:* 125 years Knappenwand Proceedings of a symposium held in Salzburg, Austria, (ed.) V. Hock, and F. Koller;Abhablungen der Geologische Bundesonstat, p. 17–25.

Bunch , T.E., Becker, L., Des Marais, D., Tharpe, A., Shultz, P.H., Wolbach, W., Gavin, D.P., Brinton, K.L., and Bada, J.L., 1999. Carbonaceous matter in the rocks of the Sudbury Impact Basin, Ontario, Canada, *In:* Large Meteorite Impacts and Planetary Evolution II, (ed.) B.O. Dressler and V.L. Sharpton; Geological Society of America, Special Paper 339, p. 331–341.

Campos-Alvarez, N., Samson, I.M., Fryer, B.J., and Ames, D.E., 2010. Sr isotopic composition of hydrothermal epidote and car-

bonate in the Sudbury Structure from LA-ICPMS analysis: Implications for fluid sources and architecture; Chemical Geology, v. 278, p. 131–150.

Cooke, D.R., Baker, M., Hollings, P., Sweet, G., Chang, Z., Danyuchevsky, L., Giolbert, S., Zhou, T., White, N.C., Gemmell, J.B., and Inglis, S., 2014. New advances in detecting the distal geochemical footprints of porphyry systems- Epidote mineral chemistry as a tool for vectoring and fertility assessments, *In:* The Challenge of Finding New Mineral Resources: Global Metallogeny, Innovative Exploration, and New Discoveries Volume I: Gold, Silver, and Copper-Molybdenum, (ed.) R.J. Goldfarb, E.E. Marsh, and T. Monecke; Society of Economic Geologists, Special Publication 15, p. 127–152.

Farrow, C.E.G., 1994, Geology, alteration, and the role of fluids in Ni-Cu-PGE mineralization of the footwall rocks to the Sudbury Igneous Complex, Levack and Morgan townships, Sudbury District, Ontario; Ph.D. thesis, Carleton University, Ottawa, Ontario, 373 p.

Farrow, C.E.G. and Watkinson, D.H., 1992. Alteration and the role of fluids I Ni, Cu and platinum-group element deposition, Sudbury igneous complex contact, Onaping-Levack Area, Ontario; Mineralogy and Petrology, v. 46, p. 67–83.

Farrow, C.E.G. and Watkinson, D.H., 1999. An evaluation of the role of fluids in Ni-Cu-PGE-bearing, mafic-ultramafic systems, In: Dynamic processes in magmatic ore deposits and their application in mineral exploration; Geological Association of Canada, Short Course Notes, v. 13, p. 31–67.

Farrow, C.E.G., Everest, J.O., King, D.M., and Jolette, C., 2005. Sudbury Cu-(Ni)-PGE systems: Refining the classification using McCreedy West mine and Podolsky project case studies, *In:* Exploration for Deposits of Platinum-Group Elements, (ed.) J.E. Mungall; Mineralogical Association of Canada, Short Course Series v. 35, p. 163–180.

Frikken, P.H., Cooke, D.R., Walsh, J.L., Archibald, D., Skarmeta, J., Serranol L., and Vargas, R., 2005. Mineralogical and isotopic zonation in the Sur-Sur tourmaline breccia, Rio Blanco-Lops Brpces Cu-Mo deposit Chile Implications for ore genesis; Economic Geology, v. 100, p. 935–961.

Hannington, M.D., Santaguida, F., Kjarsgaard, I.M., and Cathles, L.M., 2003. Regional-scale hydrothermal alteration in the Central Blake River Group, western Abitibi subprovince, Canada: implications for VMS prospectivity; Mineralium Deposita, v. 38, p. 393 –422

Hanley, J.J. and Mungall, J.E., 2003. Chlorine enrichment and hydrous alteration of the Sudbury Breccia hosting footwall Cu-Ni-PGE mineralization at the Fraser mine, Sudbury, Ontario, Canada; The Canadian Mineralogist, v. 41, p. 857–881.

Hanley, J.J. and Bray, C.J., 2009. The trace metal content of amphibole as a proximity indicator for Cu-Ni-PGE mineralization in the footwall of the Sudbury Igneous Complex, Ontario, Canada; Economic Geology, v. 104, p. 113–125.

Hanley, J.J., Mungall, J.E., Bray, C.J., and Gorton, M.P., 2004. The origin of bulk and water-soluble Cl and Br enrichments in ore-hosting Sudbury Breccia in the Fraser Copper Zone, Strathcona Embayment, Sudbury, Ontario, Canada; The Canadian Mineralogist, v. 42, p. 1777–1798.

Hanley, J.J., Mungall, J.E., Pettke, T., Spooner, E.T.C., and Bray, C.J., 2005. Ore metal redistribution by hydrocarbon-brine and hydrocarbon-halide melt phases, North Range footwall of the Sudbury Igneous Complex, Ontario, Canada; Mineralium Deposita, v. 40, p. 237–256.

Hanley, J., Ames, D., Barnes, J., Sharp, Z., and Guillong, M., 2011. Interaction of magmatic fluids and silicate melt residues with saline groundwater in the footwall of the Sudbury Igneous Complex, Ontario, Canada: New evidence from bulk rock geochemistry, fluid inclusions and stable isotopes; Chemical Geology, v. 281, p. 1–25.

Kerr, M., Hanley, J., Morrison, G., Everest, J., and Bray, C., 2015. Preliminary evaluation of trace hydrocarbon speciation and abundance as exploration tool for footwall-style sulfide ores associated with the Sudbury Igneous Complex, Ontario, Canada; Economic Geology, v. 110, p. 50–76.

Kjarsgaard, I.M and Ames, D.E., 2010. Ore mineralogy of Cu- Ni-PGE deposits in the North Range footwall environment, Sudbury, Canada, *In:* Extended Abstracts; 11th International Platinum Symposium, Ontario Geological Survey, Miscellaneous Release_Data 269, p. 1–4.

Krogh, T.E., Davis, D.W., and Corfu, F., 1984. Precise U-Pb Zircon and Baddeleyite Ages for the Sudbury Area, Chapter 20 *In:* The Geology and Ore Deposits of the Sudbury Structure, (ed.) E.G. Pye, A.J. Naldrett, and P.E. Giblin; Ontario Geological Survey, Special Volume 1, p. 431–447.

Li, C. and Naldrett, A.J., 1994. A numerical model for the compositional variations of Sudbury sulfide ores and its application of exploration; Economic Geology, v. 89, p. 1599–1607.

MacMillan, M. A., 2014. Mineralogical, fluid inclusion, and stable isotope constraints on the origin of footwall-style "high-sulfide" and "low-sulfide" Cu-Ni-PGE mineralization at the Coleman Mine, Sudbury Igneous Complex (SIC), Sudbury, Canada; M.Sc. thesis, Saint Mary's University, Halifax, Nova Scotia, 152 p.

Magyarosi, Z., Watkinson, D.H., and Jones, P.C., 2002. Mineralogy of Ni-Cu-platinum-group element sulfide ore in the 800 and 810 orebodies, Copper Cliff South mine, and P-T-X conditions during the formation of platinum-group minerals; Economic Geology, v. 97, p. 1471–1486.

McCarville, P. and Crossey, L.J., 1996. Post-impact hydrothermal alteration of the Manson impact crater, Manson, Iowa, *In:* The Manson Impact Structure Iowa: Anatomy of an Impact Crater, (ed.) C. Koeberl and R.R. Anderson; Geological Society of America, Special Paper 302, p. 347–376.

Melosh, H.J., 1989. Impact cratering: A geological process; Oxford University Press, New York, 25 p.

Molnár, F., Watkinson, D.H., and Jones, P.C., 2001. Multiple hydrothermal processes in footwall units of the North Range, Sudbury Igneous Complex, Canada, and implications for the genesis of vein-type Cu-Ni-PGE deposits; Economic Geology, v. 96, p. 1645–1670.

Mungall, J.E., Ames, D. E., and Hanley, J.J., 2004. Geochemical evidence from the Sudbury structure for crustal redistribution by large bolide impacts; Nature, v. 429, 546–548.

Naumov, M.V., 2002. Impact-generated hydrothermal systems: Data from Popigai, Kara, and Puchez-Katunki impact craters, *In:* Impacts in Precambrian Shields, (ed.) J. Plado and L.J. Pesonen; Springer-Verlag, New York, p. 117–171.

Osinski, G.R., Spray, J.G., and Lee, P., 2001. Impact-induced hydrothermal activity in the Haughton impact structure, Canada: Generation of a transient, warm, wet oasis; Meteoritics and Planetary Science, v. 36, p. 731–745.

Péntek, A., Molnár, F., Watkinson, D.H., and Jones, P.C., 2008. Footwall-type Cu-Ni-PGE mineralization in the Broken Hammer area, Wisner township, North Range, Sudbury structure; Economic Geology, v. 103, p. 1005–1028.

Petrus, J.A., Ames, D.E., and Kambor, B.S., 2014. On the track of the elusive Sudbury impact: geochemical evidence for a chondrite or comet bolide; Terra Nova, v. 26, issue 7, p. 1–12. doi: 10.1111/ter.12125

Pope, K.O., Kieffer, S.W., and Ames, D.E., 2004. Empirical and theoretical comparisons of the Chicxulub and Sudbury Impact Craters; Meteoritics and Planetary Science, v. 39, no. 1, p. 97–116.

Tuba, G. and Ames, D.E., in press. Trace element signature of hydrothermal alteration assemblages (epidote, allanite, actinolite, titanite) in the footwall of the Sudbury Igneous Complex: A laser ablation ICP-MS trace element vectoring and fertility study; Geological Survey of Canada, Open File 7757.

Tuba, G., Molnár, F., Watkinson, D.H., Jones, P.C., and Mogessie, A., 2010. Hydrothermal vein and alteration assemblages associated with low-sulfide footwall Cu-Ni-PGE mineralization and regional hydrothermal processes, North and East Ranges, Sudbury structure, Canada, *In:* The Challenge of Finding New Mineral Resources: Global Metallogeny, Innovative Exploration, and New Discoveries Volume I: Gold, Silver, and Copper-Molybdenum, (ed.) R.J. Goldfarb, E.E. Marsh, and T. Monecke; Society of Economic Geologists, Special Publication 15, p. 573–598.

Tuba, G., Molnár, F., Ames, D.E., Péntek, A., Watkinson, D.H., and Jones, P.C., 2014. Multi-stage hydrothermal processes involved in "low-sulfide" Cu(-Ni)-PGE mineralization in the footwall of the Sudbury Igneous Complex (Canada): Amy Lake PGE zone, East Range; Mineralium Deposita, v. 49, p. 7–47.

Warren, M.R., Hanley, J.J., Ames, D.E. and Jackson, S.E., 2015. The Ni-Cu-PGE content of biotite as pathfinder elements for magmatic sulfide exploration associated with mafic units of the Sudbury Igneous Complex, Ontario, Canada; Journal of Geochemical Exploration, v. 153, p. 11–29.

White, C.J., 2010. Low-sulfide PGE-Cu-Ni mineralization from five prospects within the footwall of the Sudbury Igneous Complex, Ontario, Canada; Ph.D. thesis, University of Toronto, Toronto, Ontario, 337 p.

Wright, A.J., Parnell, J., and Ames, D.E., 2010. Carbon spherules in Ni-Cu-PGE sulphide deposits in the Sudbury impact structure, Canada; Precambrian Research, v. 177, p. 23–38.

GEOLOGICAL SURVEY OF CANADA
OPEN FILE 7856

Targeted Geoscience Initiative 4: Canadian Nickel-Copper-Platinum Group Elements-Chromium Ore Systems — Fertility, Pathfinders, New and Revised Models

A geological, petrological, and geochronological study of the Grey Gabbro unit of the Podolsky Cu-(Ni)-PGE deposit, Sudbury, Ontario, with a focus on the alteration related to the formation of sharp-walled chalcopyrite veins

Daniel J. Kontak[1], Linette M. MacInnis[1], Doreen E. Ames[2], Nicole M. Rayner[2], and Nancy Joyce[2]

[1]Laurentian University, Sudbury, Ontario
[2]Geological Survey of Canada, Ottawa, Ontario

2015

© Her Majesty the Queen in Right of Canada, as represented by the Minister of Natural Resources Canada, 2015

This publication is available for free download through GEOSCAN (http://geoscan.nrcan.gc.ca/)

Recommended citation

Kontak, D.J., MacInnis, L.M., Ames, D.E., Rayner, N.M., and Joyce, N., 2015. A geological, petrological, and geochronological study of the Grey Gabbro unit of the Podolsky Cu-(Ni)-PGE deposit, Sudbury, Ontario, with a focus on the alteration related to the formation of sharp-walled chalcopyrite veins, *In:* Targeted Geoscience Initiative 4: Canadian Nickel-Copper-Platinum Group Elements-Chromium Ore Systems — Fertility, Pathfinders, New and Revised Models, (ed.) D.E. Ames and M.G. Houlé; Geological Survey of Canada, Open File 7856, p. 287–301.

Publications in this series have not been edited; they are released as submitted by the author.

Contribution to the Geological Survey of Canada's Targeted Geoscience Initiative 4 (TGI-4) Program (2010–2015)

TABLE OF CONTENTS

A geological, petrological, and geochronological study of the Grey Gabbro unit of the Podolsky Cu-(Ni)-PGE deposit, Sudbury, Ontario, with a focus on the alteration related to the formation of sharp-walled chalcopyrite veins

Daniel J. Kontak[1]*, Linette M. MacInnis[1], Doreen E. Ames[2], Nicole M. Rayner[2], and Nancy Joyce[2]

[1]Mineral Exploration Research Centre, Department of Earth Sciences, Laurentian University, 935 Ramsey Lake Road, Sudbury, Ontario P3E 2C6
[2]Geological Survey of Canada, 601 Booth Street, Ottawa, Ontario K1A 0E8
*Corresponding author's e-mail: dkontak@laurentian.ca

ABSTRACT

An integrated geological, petrological, and geochronological study of the Grey Gabbro (GG) unit of the Podolsky Cu-(Ni)-PGE deposit, which is located in a radial dyke of the 1850 Ma Sudbury Igneous Complex (SIC), indicates it is a dislodged fragment of alkalic gabbroic basement rock with a minimum age of ca. 2714 Ma (U-Pb zircon). Petrographic textures in the GG record both the impact event (e.g. planar deformation features in zircon) and subsequent thermal overprinting from the cooling SIC melt sheet; U-Pb dating of epitaxial zircon overgrowths yielded concordant dates at ca. 1850 Ma. Petrological study of the GG adjacent to sharp-wall chalcopyrite veins provides a number of insights into the origin of mineralization in the high-sulphide Cu-PGE Podolsky deposit. 1) Actinolite fibres (<1–2 cm) occur both at vein margins and within the sulphide veins, indicating that they are synchronous with or pre-date vein injection. 2) Intense alteration with the formation of actinolite-epidote-quartz-chalcopyrite-magnetite assemblages is restricted in the GG to within <1–2 cm of vein margins. The same alteration assemblage does occur <20–30 cm into the GG but as micro-clots (<1 mm) and post-dates the thermal effects of the cooling SIC; hence, this provides a time frame for massive chalcopyrite vein formation. (3) At distances of >1 m from the sulphide veins, geochemical modification from fluid:rock interaction is minimal in the GG, with Cu the only distal indicator of mineralization (i.e. 100s ppm Cu). 4) Isotopic data (Sr, O, S) indicate that S in the Podolsky deposit is similar to that of the Whistle contact Ni-Cu deposit and is sourced from the melt sheet ($\delta^{34}S_{cpy}$ = 4.3‰). These observations indicate that alteration within the GG is the result of the equilibration of high-temperature magmatic-derived fluids with the GG and that the GG is part of the pre-impact history of the area. Intense hydrothermal alteration in the GG occurs only adjacent (<10s cm) to the sharp-walled sulphide veins and thus does not provide a significant vector for exploration.

INTRODUCTION

The Podolsky Cu-(Ni)-PGE deposit, located in Norman township ~35 km north-northeast of Sudbury, is hosted by the Whistle-Parkin radial offset dyke that radiates outwards from an embayment structure in the Paleoproterozoic 1850 Ma (Krogh et al., 1984) Sudbury Igneous Complex (SIC; Fig. 1a,b). The Podolsky 2000 deposit (Fig. 1b) was an underground mine that produced ~1.5 M tonnes of 4.29% Cu, 0.38% Ni, 0.051 oz/t Pt, 0.054 oz/t Pd, and 0.024 oz/t Au, between 2007 and 2011 (Courtesy of KGHM International Ltd.). This deposit is a hybrid style deposit that displays aspects of both "sharp-walled" and "low-sulphide" style mineralization in the Sudbury Structure (Farrow et al., 2005). The 2000 deposit is situated ~650 m below the formerly producing Ni-Cu-Co Whistle deposit, which is located at the basal contact of the SIC and the radial Whistle-Parkin offset structure (Fig. 1b,c). This offset, which is host to the Podolsky 2000 deposit, is a northeast-trending structure and is atypical compared to most radial offset structures, which are generally composed of quartz diorite material. Instead, this offset dyke is dominated by metabreccia rock (i.e. metamorphosed breccia rock) that contains small bodies of quartz diorite rock, inclusion-bearing quartz diorite, and pods of other intrusive phases that vary in size (i.e. <1 cm to 10s of m; Carter et al., 2009). One such pod in this offset dyke is a large fragment of gabbroic rock, which has been referred to informally as the grey gabbro (GG), that hosts part of

Kontak, D.J., MacInnis, L.M., Ames, D.E., Rayner, N.M., and Joyce, N., 2015. A geological, petrological, and geochronological study of the Grey Gabbro unit of the Podolsky Cu-(Ni)-PGE deposit, Sudbury, Ontario, with a focus on alteration related to formation of sharp-walled chalcopyrite veins, *In:* Targeted Geoscience Initiative 4: Canadian Nickel-Copper-Platinum Group Elements-Chromium Ore Systems — Fertility, Pathfinders, New and Revised Models, (ed.) D.E. Ames and M.G. Houlé; Geological Survey of Canada, Open File 7856, p. 287–301.

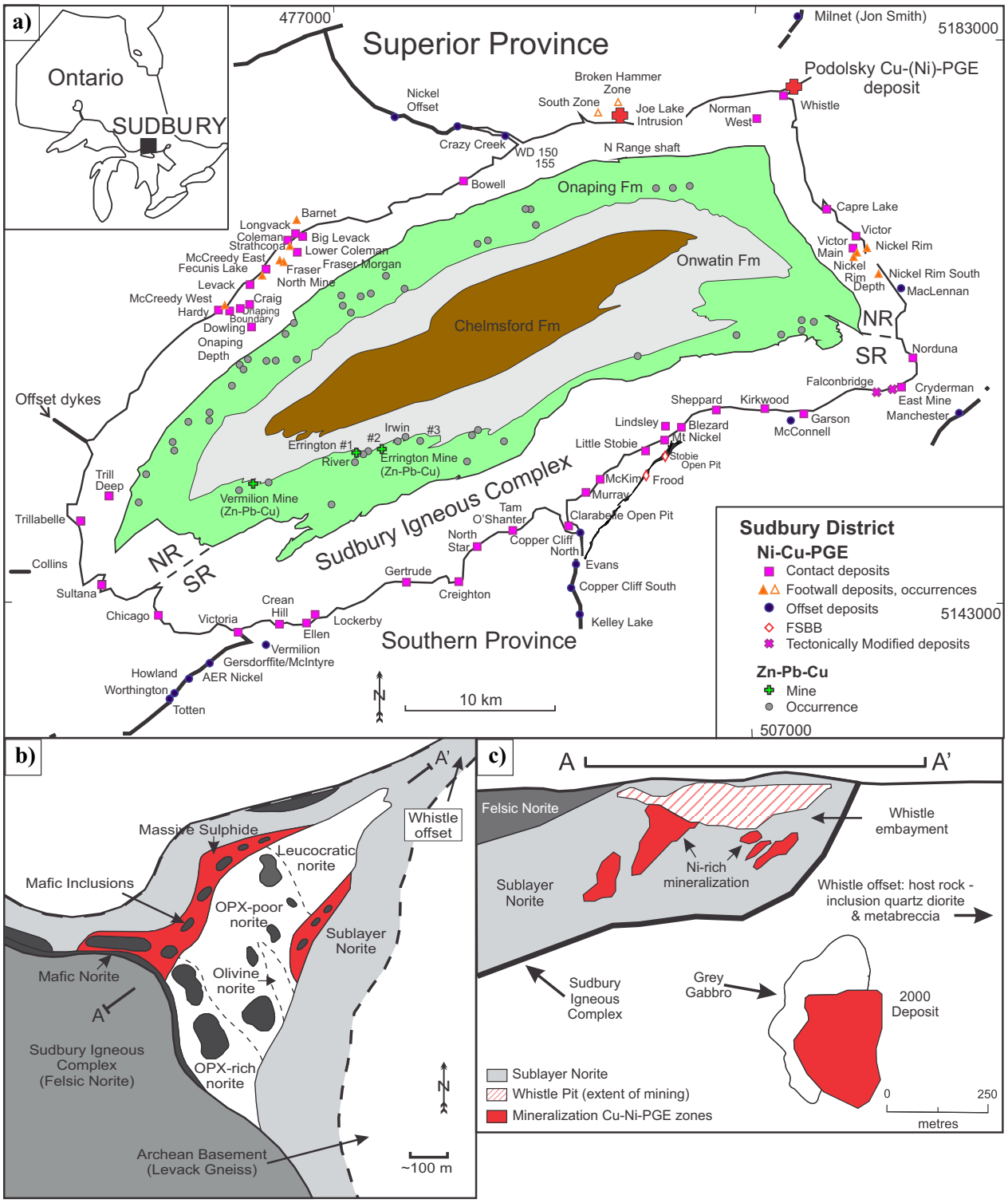

Figure. 1. a) Simplified geological map of the Sudbury Structure showing the footwall rocks, the Sudbury Igneous Complex (SIC) and related offset and concentric dyke rocks, and basin-fill material, as well as the location of the different types of sulphide deposits (i.e. contact, offset, footwall). Note the location of the Podolsky deposit and Joe Lake gabbro, both in the north part of the map area (red filled circles), which are referred to in the text. The figure is modified from Ames and Farrow (2007). **b)** A schematic plan view of the Whistle embayment structure of the SIC in relation to the Whistle-Parkin offset (modified from Lightfoot et al., 1997). The map shows the relationship between the main rock types of the SIC along with the beginning of the NE-trending Whistle-Parkin offset. Note the presence of SIC units, which include the inclusion-rich sublayer norite that hosted the Ni-rich contact-style mineralization mined from the Whistle Pit by INCO. **c)** A northeast long section (line A and A' in Fig. 1b) of the Whistle embayment that shows, from top down, felsic norite, sublayer norite, Ni-rich mineralization, Whistle-Parkin offset, the Grey Gabbro (GG) unit and the 2000 deposit. The study area was located in the GG fragment which hosts a series of sharp-walled chalcopyrite veins from the 2000 deposit. Figure has been modified from Farrow et al. (2005).

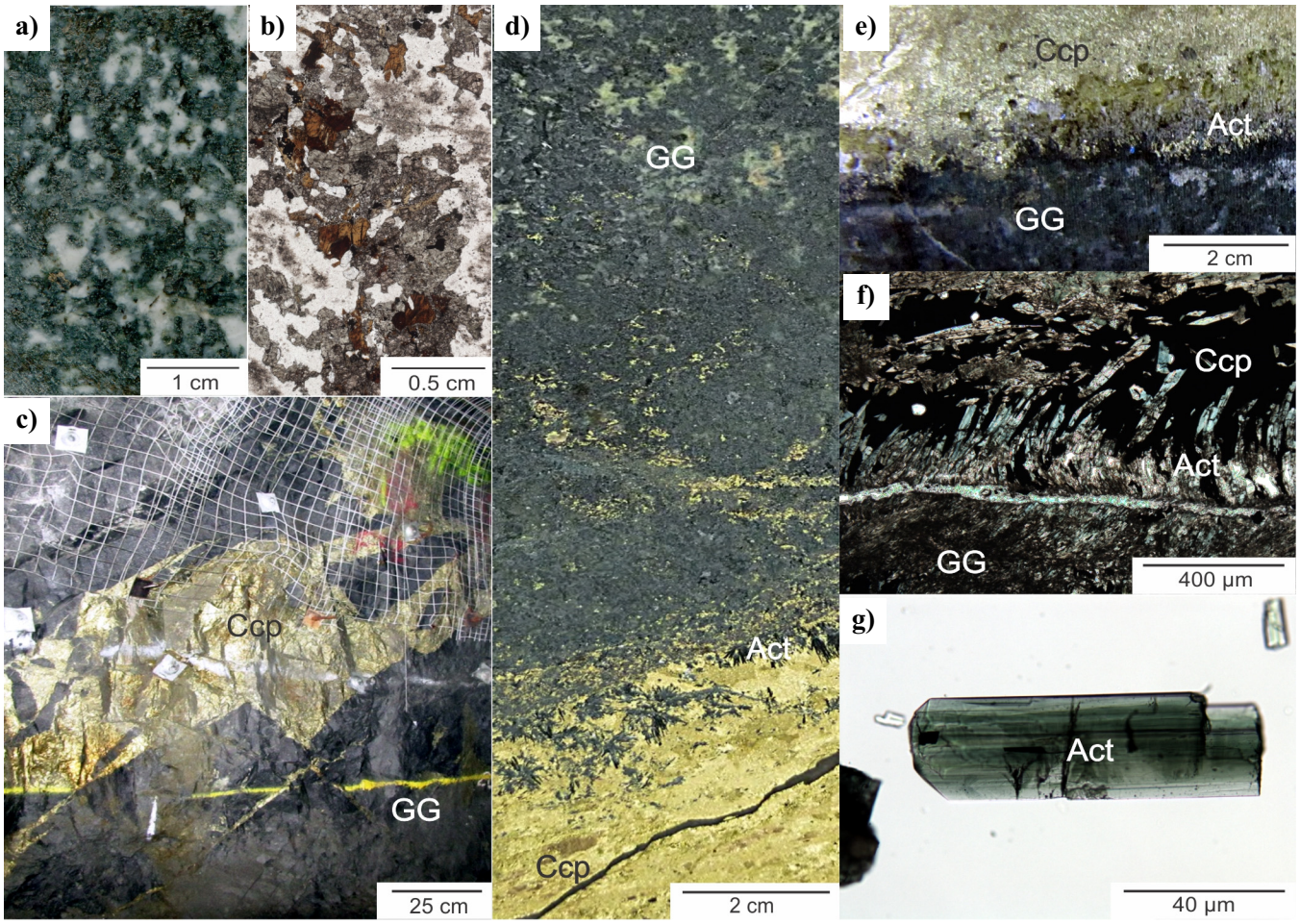

Figure. 2. Images of the Grey Gabbro (GG) unit and sharp-walled sulphide veins. **a)** Scanned rock slab of sample LM-P-007 showing the texture typical of the GG unit with mafic (i.e. pyroxene, amphibole, biotite) and felsic (i.e. plagioclase) domains. **b)** Thin section scan of sample LM-P-007 (in plane polarized light) showing the typical gabbroic-like texture, but note the unusual scalloped outlines of the plagioclase against the mafic domains and the dusty cores of the plagioclase due to alteration. The brown phase is biotite. **c)** Underground photo (1925 level) of a sharp-walled chalcopyrite vein cutting GG. **d)** Cut slab of sample LM-P-060 collected from the 1700 level. The sample shows, from top to bottom, the GG, intensely altered GG (actinolite-epidote), actinolite grains or fibres (Act) and massive chalcopyrite (Ccp) that entrains the actinolite grains. **e)** The GG in contact with a chalcopyrite sharp-walled vein with actinolite along the contact, as seen in drillhole FNX40272. **f)** Thin section photomicrograph (in plane polarized light) of sample LM-P-060 showing rotated actinolite fibres along the contact of a chalcopyrite vein. **g)** A grain of actinolite from a prepared mineral separate from sample LM-P-060 (see Fig. 2d) that was used for $^{40}Ar/^{39}Ar$ dating and isotope analyses (O, Sr).

the "sharp-walled" vein systems of the Podolsky 2000 deposit.

This paper summarizes the results of a graduate thesis project by the second author (L. MacInnis, M.Sc. thesis, in prep.) that documents the nature and extent of alteration in the GG unit (Figs. 2a,b, 3a,b), both proximal and distal to its contained footwall-style mineralization (Fig. 2c). The GG unit is, as noted above, a large (230 m by 270 m) fragment that occurs in the Whistle offset dyke, which hosts thick (<1 m) sharp-walled veins of massive chalcopyrite, many of which contain narrow (i.e. cm-scale) epidote-actinolite-magnetite-bearing alteration halos (Fig. 2d-f). More specifically, the focus of the study was to characterize the mineralogy and geochemistry of the alteration specific to the sharp-walled vein mineralization to further our understanding of footwall-styled ore systems and to see if such data may provide criteria for vectoring towards mineralization in other footwall environments of the SIC. The massive and homogenous nature of the GG unit, combined with underground access to it and the sharp-walled veins in addition to the availability of historic drill core, made this site ideal for such a project. The study was broken into two parts in order to achieve its objectives:

- Characterize the mineralogy and geochemistry of the least altered host rock (i.e. GG) to the mineralization, as this formed the basis for the subsequent alteration study;
- Assess the nature and origin of the alteration asso-

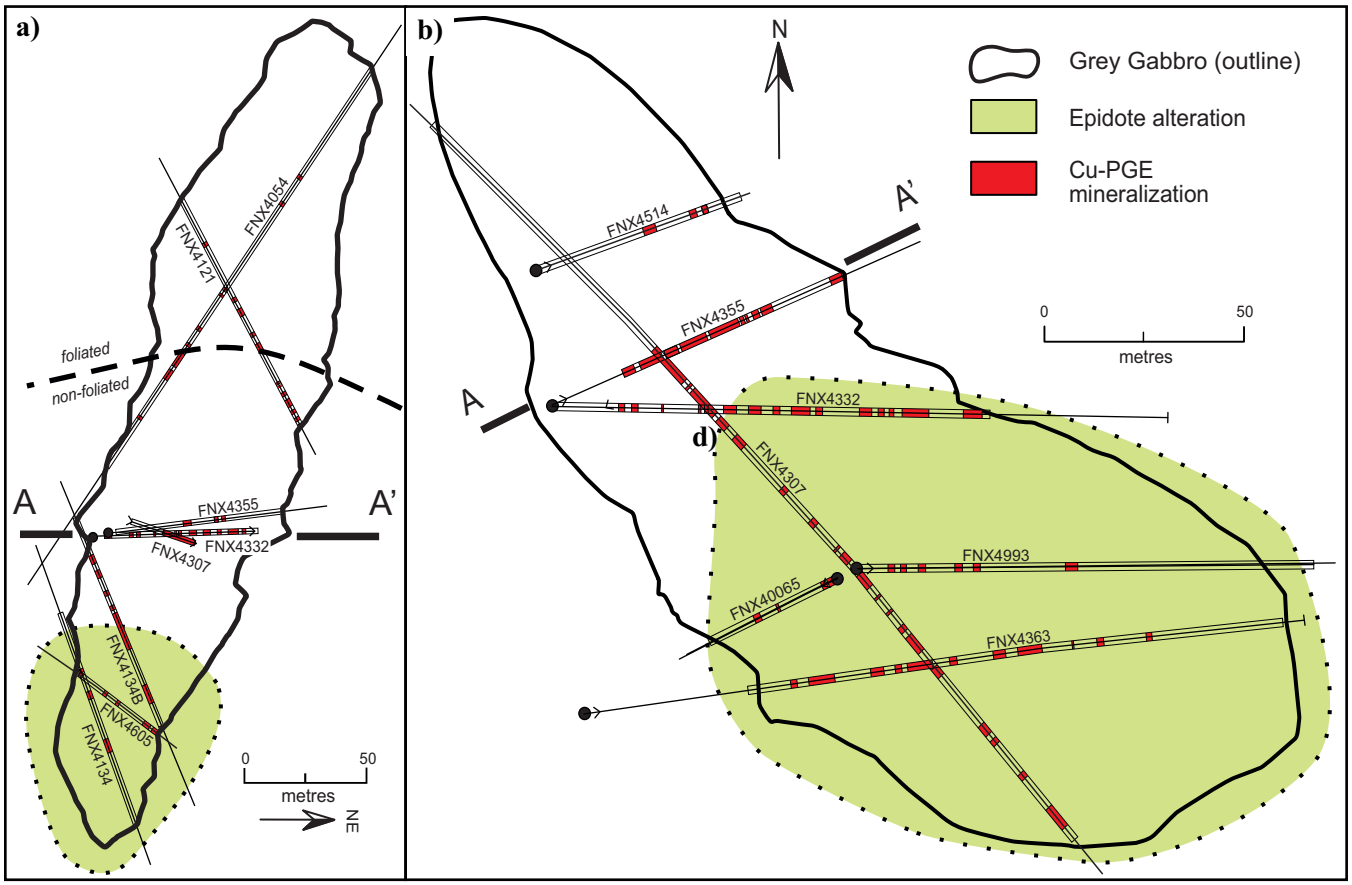

Figure 3. Remapped vertical (facing northwest) and plan view of the Podolsky Grey Gabbro fragment depicting the relationship of epidote alteration and foliation in relation to the sharp-walled Cu-(Ni)-PGE mineralization trend. Note where A and A' are in relation to the vertical and plan view maps.

ciated with the sharp-walled veins and compare it to the other known alteration present in the footwall environment of the SIC (e.g. Tuba et al., 2014 and references therein). The characterization and chemical fingerprinting of alteration-specific mineralization could provide criteria for targeting mineralization in other footwall environments.

METHODOLOGY

Mapping of the Grey Gabbro

The nature and origin of the GG unit had not previously been addressed, thus its genetic relationship to mineralization was not considered. For example, whether the GG unit was a passive host or active participant to mineralization has not been considered before this study. In order to answer this outstanding problem, the GG was studied to address two possible hypotheses: 1) The GG represented an 1850 Ma impact-generated melt compositionally related to the SIC or another source (i.e. mantle input); or 2) the GG represents a fragment of the pre-existing target area. At the time of this study, the provenance of GG was not known. To further our understanding of the unit, a comprehensive suite of 12 drillholes, which penetrated the GG unit horizontally and vertically, were re-logged using archived photos provided by KGHM International Ltd. and a geological map was produced (Fig. 3a,b). In order to assess the homogeneity of the GG unit, it was logged in 1.5 m intervals based on lithology, grain size, and texture in addition to the presence of alteration, foliation, and mineralization. The intensity of mineralization and alteration were also assessed based on the relative abundances of present phases present (see MacInnis et al., 2014). Information from several drill cores that penetrated the GG unit combined with underground visits were used to verify the maps that been produced from the photo library.

Sampling of Whole-Rock Materials and Geochemical Analysis

Seventy samples of the GG unit and its contained mineralization were collected from both underground workings and archived drill core; these samples provided the basis for petrological studies, including complete major and trace element chemistry, with a subset used for stable (O, S) and radiogenic (Sr) isotopic analysis (see below). The sample suite consisted of 19 least altered GG samples, 30 altered samples of GG, and 21 mineral-

ized samples. The underground samples were collected between the 1700 and 2450 working levels of the deposit and included multiple transects leading up to sharp-walled chalcopyrite veins that were collected by using a diamond air saw. Full details of the sample locations and analytical techniques along with the geochemical data are presented in MacInnis et al. (2014).

Isotopic Analysis (O, Sr, S) and Geochronology (U-Pb and Ar-Ar dating)

A total of 20 samples, including nineteen whole-rock samples of the GG and one actinolite separate (see Fig. 2g), were analyzed for $\delta^{18}O$ at the Queen's University Facility for Isotopic Analysis, Kingston, Ontario. The same actinolite separate, 2 samples of least altered GG, a sample of the Joe Lake gabbro, which is an inferred-age equivalent to the GG (see below)), and, for comparison with SIC compositions, 9 North Range offset dyke samples and 1 South Range grey gabbro (Segway), were analysed for $^{87}Sr/^{86}Sr$ isotopes at the Carleton University Isotope, Geochemistry and Geochronology Research Centre, Ottawa, Ontario. A comprehensive suite of 15 chalcopyrite samples collected from massive chalcopyrite sharp-walled veins in the GG, which included 3 detailed transects from 4 levels of the mine, were analysed for sulphur isotopes ($\delta^{34}S$) at the G.G. Hatch Isotope Laboratories, Ottawa, Ontario. Methods and results for O, Sr, and S isotopic analyses are provided in MacInnis et al. (2014) and MacInnis (M.Sc. thesis, in prep.).

A sample of least altered, medium-grained GG with "salt-and-pepper" texture from the 1700 level of the Podolsky mine was selected for U-Pb zircon geochronology and was processed using conventional methods at the Geological Survey of Canada (sample 11AV-74; lab number z10633). The zircon separates, along with the host rock, were first characterized petrographically, which was followed by scanning electron microscopy (SEM) with backscattered electron (BSE) and catholuminescence (CL) imaging to fully characterize the unusual habit of the zircon (see the more detailed discussion below). The zircon grains were then dated using both isotope dilution-thermal ionization mass spectrometry (ID-TIMS; Mattinson, 2005) and the sensitive high-resolution ion microprobe (SHRIMP; Stern, 1997; Stern and Amelin, 2003). The same sample of actinolite used for O and Sr isotopic analyses, which was collected along the contact of the GG and a massive sulphide vein (see Fig. 2c,f), was selected for Ar-Ar dating. This vein sample was processed using standard methods (i.e. crushing, sieving, heavy liquids, hand picking) to generate a high-purity separate (Fig. 2g), which was subsequently irradiated and analysed at the Geological Survey of Canada; full details and results can be found in MacInnis et al. (2014).

RESULTS AND SUMMARY

Map of the Grey Gabbro Unit

Figure 3 shows a plan (1925 level) and sectional map for the GG unit and highlights the distribution of epidote alteration and mineralization, the latter represented by sharp-walled sulphide veins. The epidote alteration is confined to a portion of the GG and, based on mapping, does not appear to have any significant spatial association with the density of the sulphide mineralization, as might have been expected given the association of epidote with some mineralization in Sudbury area (e.g. Fraser deposit; Farrow and Watkinson, 1996). In addition, a weak foliation in the GG unit was observed at its northern end. This feature is also seen microscopically as an alignment of light and dark domains (a mixture of pyroxene, amphibole, and biotite). Another feature of interest was small leucocratic pegmatite bodies ($\leq$1–2 m^2) that occur rarely in the GG; however, these were too small and rare to portray on this map and, in addition, did not appear to have any obvious spatial distribution within the GG.

Petrology of the Grey Gabbro

The least altered GG is in general a medium- to fine-grained, homogeneous unit, with a "salt-and-pepper" texture that is somewhat analogous to ophitic textured gabbro with felsic and mafic domains (Fig. 2a,b). Rare occurrences of possible chilled margins were noted in logging the GG, which was subsequently confirmed by company geologists based on their underground observations. Detailed petrographic studies integrated with imaging and chemical analyses using an SEM coupled to an energy dispersive system (EDS) indicate that the GG records a complex, multi-stage history involving initial crystallization and deuteric alteration, a shock metamorphic event, a thermal overprint, and finally a hydrothermal alteration event, as shown in representative petrographic images in Figure 4 and summarized as follows: 1) Domains of what is inferred to have been originally single grains of magmatic plagioclase now consist of sub-domains of granoblastic-textured plagioclase of 10–50 μm and An_{50} composition (Fig. 4a,c,d). This feature is considered to reflect dynamic recrystallization due to thermal heat from the melt sheet. 2) Plagioclase is altered along internal grain boundaries and interiors to a quartz-An_{20} plagioclase-epidote assemblage (Fig. 4d) and also to sericite, due to later fluid-mediated alteration related to the sulphide veins. In rare cases, the plagioclase occurs as patches of a ternary feldspar-like orthoclase phase. Interstitial to the grains are mafic clots consisting of mixed silicates (i.e. pyroxene, amphibole, biotite, Fe-Ti oxides, actinolite; Fig. 4e,f), which have a bulk composition equating to stoichiometric augitic pyroxene. These

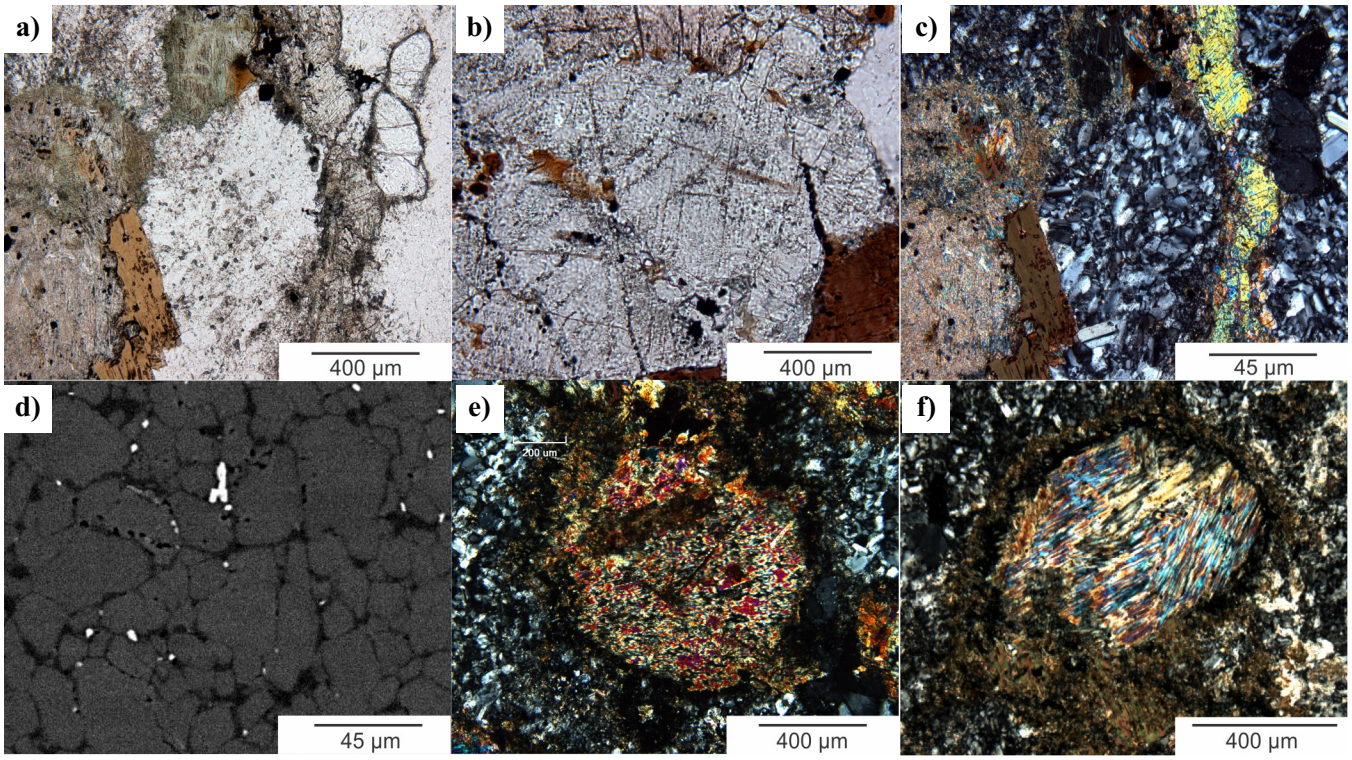

Figure 4. Photomicrographs of Grey Gabbro that highlight the two main domains of primary clinopyroxene and plagioclase and also examples of alteration. **a)** Plagioclase grain (in plane polarized light) with a subhedral outline that appears to be largely (?) unaltered. Note the euhedral apatite grains to the right, and biotite and altered pyroxene grains to the left. **b)** Clinopyroxene grain (in plane polarized light) that has a subhedral outline and a fresh interior; **c)** Same plagioclase grains seen in image (a) that in cross-polarized light displays a granoblastic texture due to thermally induced recrystallization. **d)** Backscatter electron image of the granoblastic-textured plagioclase of An_{50} composition. The bright phases are epidote and the dark phases that are intergranular to plagioclase are quartz and An_{20} plagioclase. **e, f)** Examples (in cross polarized light) of clinopyroxene partially to completely pseudomorphed by actinolite.

clots likely represent the combined effects of shock-related modification to the primary magmatic augitic pyroxene and later alteration due to fluids. 3) Zircon with planar deformation features (PDFs) and overgrowths of neomorphic zircon (se discussion below). The latter features in the zircons are considered to be related to the impact event. 4) Variable development of sericite, carbonate, and epidote with some sulphides disseminated in the GG as a result of fluid infiltration during sulphide vein formation. Proximal to sharp-walled veins, the GG is enriched in hydrothermal minerals (e.g. sericite, chlorite, quartz, actinolite, calcite, epidote, magnetite) along fractures and within dissolution features; the most intense development occurs <10 cm from the sulphide veins (Fig. 2d).

The volumetrically small pegmatite bodies, which consist of albite and quartz ± potassium feldspar, are very fresh and notably do not record petrographic evidence of the complex textures seen in the GG unit, hence a different petrogenesis is probable. Further work is required, but we tentatively suggest that they may represent partial melting of the GG due to thermal metamorphism, which would be analogous to the generation of plagiogranite found in ophiolite complexes (e.g. Grimes et al., 2013).

The major element chemistry of the GG is very uniform, which is consistent with our drill-core logging and petrographic study, and equates to a gabbro of 50 wt% SiO_2 with some chemical evidence of a cumulate component (i.e. clinopyroxene accumulation). In addition, a subalkaline character for the GG is indicated from its Zr/TiO_2 ratio. The elemental abundances and mantle-normalized profile for the trace element data show enrichment of the large ion lithophile elements (LILE), depletion of high field strength elements (HFSE: in particular strongly negative Ta-Nb anomalies), a strong fractionation of the rare earth elements (REE) with (La/Lu)N ~40, and only a slightly negative Eu anomaly; these geochemical features are consistent with derivation of the GG from a previously metasomatized subcontinental lithospheric mantle reservoir. When compared to other intrusive rocks in the Sudbury area (e.g. dyke rocks, SIC units), the GG is geochemically most similar to the 2657± 9 Ma (Bleeker et al., 2013) Joe Lake intrusion that is located just west of Podolsky (Fig. 1). In broader terms, the trace-element chemistry and extended spider plots compare most

favourably to those of ocean island basalts (OIB; Sun and McDonough, 1989).

Petrology of Altered Grey Gabbro

Adjacent to sharp-walled sulphide veins, the GG unit records two features that reflect reaction with a fluid. The first feature, seen immediately against the sulphide veins, is the presence of a thin layer of mono-mineralic actinolite fibres that are <1 to 2 cm in width and are oriented perpendicular to the wall rock GG (Fig. 2d-f). The second feature is intense alteration haloes of actinolite-epidote-quartz-sulphide-magnetite-chalcopyrite. These alteration haloes are <1to 2 cm wide and are bordered by a zone of variably altered GG that gives way to least altered GG over 10 to 30 cm. The most notable petrographic feature of this alteration as observed in thin section is the presence of a network of connected pores that are commonly lined with epidote-actinolite-magnetite±chalcopyrite; these features are spatially coincident with the sericitic alteration of plagioclase near rare carbonate veins. We also note that quartz nearest the sulphide veins is intergrown with epidote and contains abundant hypersaline fluid inclusions with multi-solid phases that are petrographically similar to those observed in PGE-rich, low-sulphide footwall systems of the Sudbury Structure (e.g. Farrow et al., 1994; Molnár et al., 2001; Péntek et al., 2011; Tuba et al., 2014).

Geochemical analyses of samples collected across these alteration zones did not reveal appreciable chemical or mass change except close to the sharp-walled sulphide veins where the most altered samples show a mass gain relative to least altered samples and minor development of Eu anomalies due to alteration of plagioclase. Absolute changes in metal abundances occurred over only short distances from the veins (<20–30 cm), in particular gains of Cu, Ni, Au, Sn, Pd, Pt, Ag, and Zn. Interestingly, Cu is singularly enriched furthest from the veins without accompanying metal enrichment. In addition, sulphur, ferric iron, and loss on ignition reflected some mass gains relative to all other elements.

Stable and Radiogenic Isotopes

Oxygen isotopes were measured on four samples of least altered samples of GG and for traverses away from the veins into the GG; there was no apparent spatial correlation between $\delta^{18}O$ values of the GG unit and the sharp-walled chalcopyrite veins. The $\delta^{18}O$ values for the least altered GG of 6.7 to 8.1‰ (average = 7.3‰) compare to values of 6.5 ± 0.5‰ for samples from traverses adjacent the sharp-walled veins (see MacInnis et al. (2014) for data and details of samples). The $\delta^{18}O$ data indicate that there was no modification of the $\delta^{18}O$ signature of the GG due to vein-related fluid infiltration and is consistent, which is in agreement with the geochemical data discussed previously. An actinolite separate collected from immediately against the sulphide vein had a $\delta^{18}O$ value of 5‰, which equates to a $\delta^{18}O_{H_2O}$ value between 6.1 and 6.9‰ at 400 to 600°C (Zheng, 1993) and is consistent with a fluid of unknown origin equilibrating with the GG unit and generating the actinolite under a low fluid:rock ratio and, hence, inheriting the $\delta^{18}O$ value of the GG unit.

Table 1. Sr isotope whole-rock data for mafic rocks in the Sudbury mineral district.

Sample	$\frac{^{87}Sr}{^{86}Sr}_i$	$\frac{^{87}Rb}{^{86}Sr}$	$\frac{^{87}Sr}{^{86}Sr}$[1]	±SE[2]	Description of Lithology
[a]Podolsky Cu-PGE deposit					
LM-P-007	0.70183	0.1279	0.70683	0.000024	Least altered Grey Gabbro
LM-P-043G	0.70079	0.1812	0.70787	0.000008	Representative Grey Gabbro
LM-P-060	0.70209	0.0776	0.70512	0.000005	Intensely altered Grey Gabbro (actinolite separate)
[a]Levack gneiss gabbro					
12-AV-44	0.70167	0.0877	0.70509	0.000019	Joe Lake mafic intrusion
[b]Offset dykes, SIC					
13-AV-06	0.70577	0.4148	0.71681	0.000020	Hess quartz diorite, margin
13-AV-08	0.70969	0.7164	0.72876	0.000014	Ermatinger quartz diorite, core
13-AV-10	0.69999	0.7157	0.71905	0.000015	Ermatinger quartz diorite, core
13-AV-12	0.71785	0.6991	0.73645	0.000006	Ministic quartz diorite, core
13-AV-13	0.70608	0.1622	0.71040	0.000006	Parkin quartz diorite, margin
13-AV-15	0.70708	0.4763	0.71976	0.000006	Parkin quartz diorite, margin
13-AV-17	0.71042	1.0357	0.73799	0.000012	Pele quartz diorite, margin
05-AV-15	0.71038	0.3218	0.71895	0.000005	Segway grey gabbro
13-AV-04	0.70722	0.4904	0.72027	0.000052	Trill quartz diorite, core
05-AV-33	0.67327	1.1956	0.70509	0.000019	Trill quenched quartz diorite

[1]analyzed with Thermofinnigan Triton T1 thermal ionization mass spectrometer, IGGRC Carleton University
[2]Uncertainties are presented as ±2 standard errors (SE)
[a]initial Sr (i) calculated at 2700Ma, [b]initial Sr (i) calculated at 1850 Ma

Sulphur isotopic data across the sharp-walled veins (<1 m thick) are consistent with an average $\delta^{34}S$ value of 4.3 ± 0.3‰ (McInnis et al., 2014). These values are similar to those reported by other workers for the sulphide mineralization related to the SIC (e.g. Ames et al., 2010; Tuba et al., 2014), and therefore indicate a uniform isotopic reservoir for the S. This also suggests that the sulphides were deposited in the Whistle-Podolsky ore system under similar physio-chemical conditions since no variation, which would result from fractionation, is recorded. Furthermore, the data are consistent, as expected, with a dominantly crustal reservoir for the S versus a mantle source (i.e. departure from 0‰; Ohmoto and Rye, 1979).

Strontium isotopic data (i.e. $^{87}Sr/^{86}Sr$, Table 1) obtained for two samples of least altered GG indicate measured $^{87}Sr/^{86}Sr$ values of 0.70512, 0.70683, and 0.70787, which give age-corrected initial Sr isotope (Sr_i) values of 0.70079 to 0.70209 at 2700 Ma, the minimum estimated time for crystallization of the GG (see below), and Sr_i values of 0.70305 and 0.703042 at 1850 Ma, the age of the impact event and the sulphide mineralization. The Sr_i values for the GG at 2700 Ma overlaps with a single Sr_i value of 0.70167 for the geo-

chemically similar Joe Lake gabbro (also at 2700 Ma, Table 1) and are much lower than the Sr_i values for the offset dyke component of the radiogenic SIC (6 North Range offset dykes; Table 1). The single actinolite sample analysed yielded an initial $^{87}Sr/^{86}Sr$ value of 0.70305, its low Rb content not requiring age-correcting. That the initial $^{87}Sr/^{86}Sr$ value for the actinolite is similar to the GG value at 1850 Ma suggests that the actinolite formed due to reaction of a fluid with the GG at this time and is consistent with the $^{40}Ar/^{39}Ar$ dating of the actinolite (see below).

Geochronology

$^{40}Ar/^{39}Ar$ Age Dating

The results of 10 out of 14 total fusion analyses of actinolite grains from adjacent a sharped-wall sulphide vein indicate a weighted mean age of 1850 ± 30 Ma (see MacInnis et al. (2014) for full results). This age is interpreted to record cooling of the actinolite below the argon blocking temperature, which is taken to be around 350 to 400°C in this phase (McDougall and Harrison, 1999). Importantly, the age overlaps (within error) the time of the Sudbury impact event (1849.53 ± 0.21 Ma; Davis, 2008) and indicates, therefore, that in the study area a subsequent reheating to above 350 or 400°C did not occur after 1820 Ma, although we cannot say it did not occur prior to this time and after 1850 Ma. This latter interpretation is further verified based on the results of step-wise heating of actinolite grains from the same sample, which yielded flat age spectra profiles (MacInnis et al., 2014).

Zircon Morphology and U-Pb Thermal Ionization Mass Spectrometry and Sensitive High-Resolution Ion Microprobe Dating

Zircon Morphology

Examination of the zircon hosted by the GG unit indicated two distinct morphological types which, based on their proportions in the mineral separate prepared for dating, appear to be in roughly equal proportion. One of these zircon sub-populations consists of clear, colourless, euhedral, prismatic (elongate to stubby), well faceted, and terminated crystals with few fractures and rare clear inclusions (Fig. 5a). When examined in CL (Fig. 5b), the euhedral zircon grains are strongly luminescent and exhibit sharp oscillatory and sector zoning, which are features most commonly ascribed to growth from a silicate melt (Corfu et al., 2003). This morphological type of clear zircon was analysed for U-Pb dating by isotope dilution - thermal ionization mass spectrometry (ID-TIMS).

The second zircon sub-population consists of highly fractured, anhedral, pale brown to reddish brown, cloudy fragments (Fig. 5c) that occur as cores to the overgrowths of the clear, colourless zircon, which is tentatively linked to the euhedral morphology described above. The fractured zircon has relatively poor CL response, appearing as medium to dark grey (Fig. 5d), whereas the clear overgrowths luminesce strongly (Fig. 5d). Corresponding back scatter electron (BSE) images faintly mimic the zoning in the CL images, but more clearly illustrate the presence of fractures and inclusions (Fig. 5d). The BSE images clearly show that anhedral zircon is characterized by the presence of crystallographically oriented features, including short fractures or small pits. These features have been noted in zircons elsewhere and were attributed to planar deformation features resulting from shock impact (Krogh et al,. 1984; Bohor et al, 1993; Krogh et al., 1993a, b; Pidgeon et al., 2011). Anhedral zircon, both with and without the euhedral overgrowths, was analysed for U-Pb dating by sensitive high-resolution ion microprobe (SHRIMP).

U-Pb Age Dating

Six single-grain fractions of euhedral zircon were analysed using ID-TIMS with five of the most concordant analyses (0.1–0.3%) yielding a mean $^{207}Pb/^{206}Pb$ age of 1849.9 ± 1.0 Ma; the sixth zircon analysed was more discordant (0.7%) and gave an age of 1854 Ma (Fig. 6, Table 2). The 1849.9 ± 1.0 Ma age is considered to represent the time at which these euhedral zircon grains grew, which is equate to the Sudbury impact event. Twenty-one U-Pb SHRIMP analyses were carried out on fifteen anhedral zircon grains, with a few analyses also hitting the euhedral overgrowths on these grains. These zircon analyses yielded a range of $^{207}Pb/^{206}Pb$ ages between 2606 Ma and 1706 Ma and were typically 3-10% discordant. Examination of the data in a concordia diagram (Fig. 6b) indicate that a linear array is defined with an upper intercept of ca. 2714 ± 52 Ma, which is derived by anchoring the lower intercept at 1850 Ma, the inferred time of impact and resetting of the zircons (Fig. 6b, Table 3). The upper intercept is considered the best approximation of a minimum age for the GG, whereas the lower intercept is considered to reflect a resetting event and when the PDF in the zircon formed, which equates to the time of the Sudbury impact event.

SUMMARY OF THE FINDINGS AND IMPLICATIONS FOR EXPLORATION

1. The GG unit represents a large dislodged fragment of a previously crystallized alkali gabbro rock that formed at or before ca. 2714 Ma. This unit is correlated with its petrologically equivalent unit in the North Range footwall environment, the Joe Lake Gabbro, which has a minimum age of ca. 2657 ± 9 Ma based on U-Pb dating of inferred metamorphic

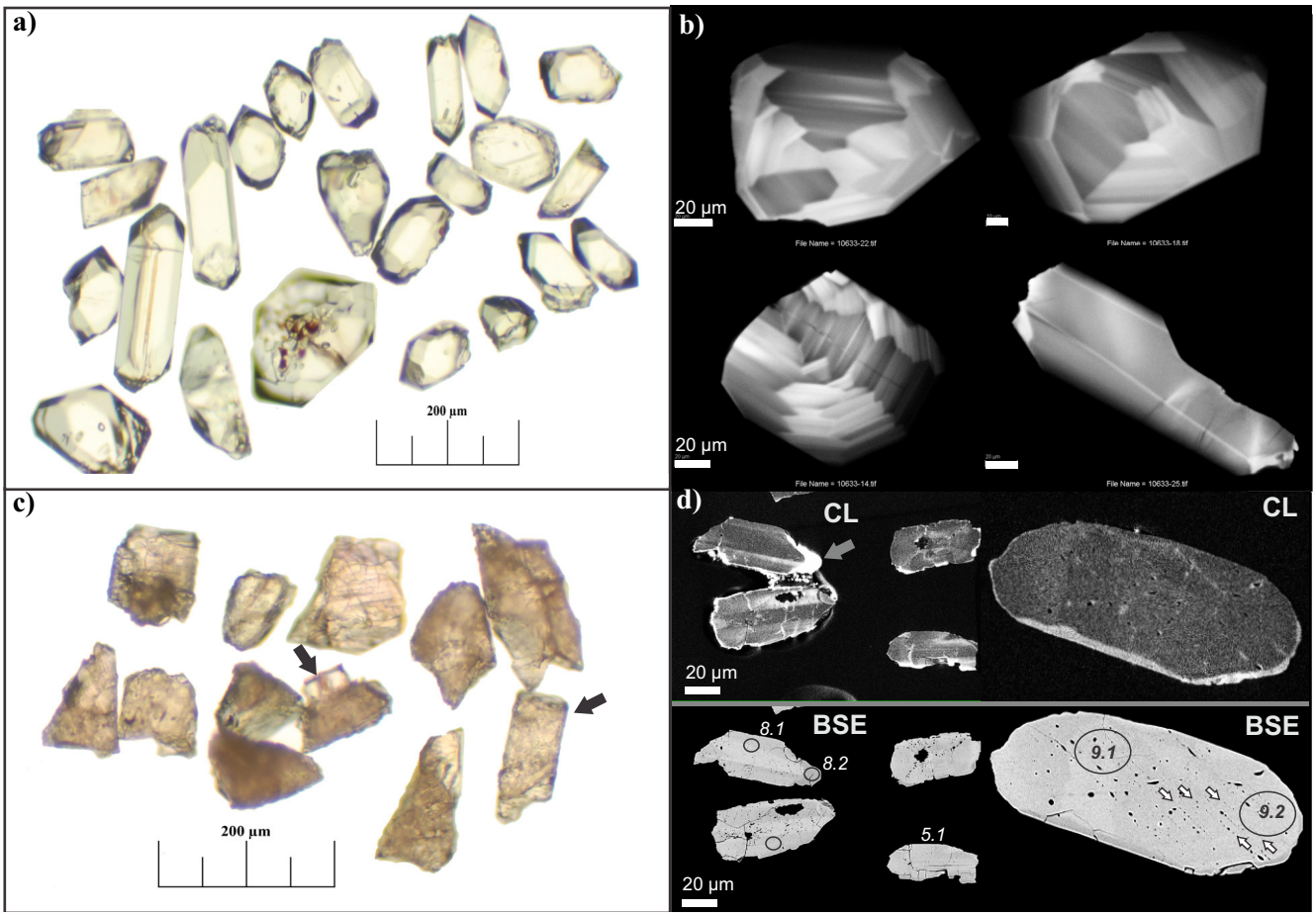

Figure 5. Photographs summarizing the various textures of zircon extracted from a sample of Grey Gabbro. **a)** Transmitted light photomicrograph of euhedral, prismatic zircon grains, after annealing for 48 h at 1000°C; photograph includes zircon grains analysed by TIMS. **b)** Cathodolumi-nescence (CL) images of euhedral, prismatic zircon. **c)** Transmitted light photomicrograph of anhedral zircon inferred to record shock metamorphic textures; some of these grains were selected for SHRIMP analysis. The arrows indicate the presence of overgrowths of euhedral zircon on the earlier, shocked zircon. **d)** Complementary CL (top) and BSE (bottom) images of shocked zircon with the grey arrow indicating an area of zircon overgrowth. Note the enhanced brightness of the euhedral zircon overgrowth relative to the anhedral shocked zircon. The crystallographically oriented features seen in the BSE (indicated by pairs of small, white arrows) are interpreted as impact-related planar deformation features. SHRIMP analysis sites are shown by black ellipses labelled with corresponding spot name shown in Table 3.

zircons (Bleeker et al., 2013). The geochemistry of the GG, and also the age and geochemically equivalent Joe Lake gabbro, indicates it was sourced from a previously metasomatised subcontinental lithospheric mantle and is unrelated to the SIC.

2. The GG is a macroscopically homogeneous unit, but detailed petrographic and SEM-EDS imaging studies indicate a complex textural history that involved extensive mineral re-equilibration. The latter feature is interpreted to reflect shock-induced metamorphism at ca. 1850 Ma due to the Sudbury impact event (e.g., zircon PDF features and overgrowths), then shortly thereafter thermal annealing related to the cooling melt sheet that overlay the site (e.g. plagioclase textures), and then superimposed hydrothermal alteration related to the emplacement of sharp-walled sulphide veins.
3. $^{40}Ar/^{39}Ar$ age-dating of actinolite found along the contact of GG and sharp-walled sulphide veins records cooling of the area below ~350–400°C at ca. 1850 Ma and, furthermore, its flat age spectra indicates the area did not subsequently experience heating above this temperature.
4. Hydrothermal alteration of the GG adjacent to the sharp-walled sulphide veins is most intense nearest the veins (i.e. ≤10–20 cm) with formation of a quartz-epidote-actinolite-magnetite-chalcopyrite zone that quickly becomes cryptic into the wall rock. Geochemically, the most distal indicator of the mineralization is elevated Cu (to 100s ppm up to 1 m away) without enrichment of other metals.
5. Isotopic analyses (Sr, O, S) indicate that the GG retains its primary isotopic signal for Sr and O despite alteration, whereas the O data for actinolite records $\delta^{18}O_{H_2O}$ values of 6.1 to 6.9‰ at 400 to

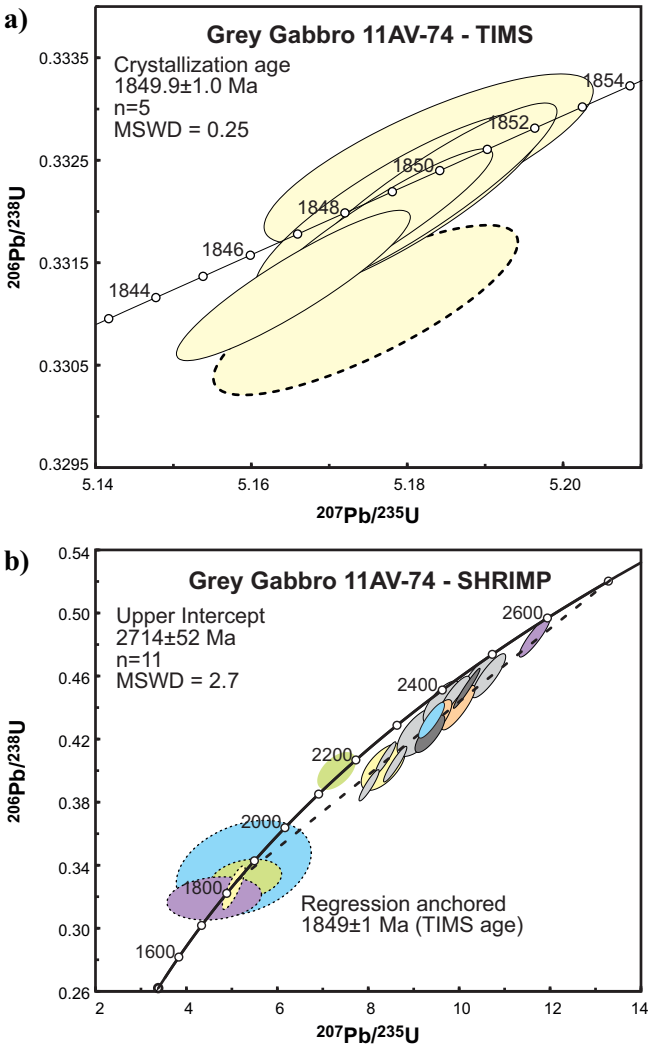

Figure 6. U-Pb concordia diagrams for zircon from the Grey Gabbro unit. a) Results for six zircon grains analysed by ID-TIMS with error ellipses plotted at 2σ. The calculated age of 1849.9 Ma excluded the most discordant sample, which is shown by the dashed ellipse. b) Results of SHRIMP analyses with error ellipses plotted at 2σ. Note the following: (1) pairs of analyses on a single grain are shown by colours other than light grey, (2) analyses of shocked zircon grains are shown by solid outlines and cluster towards 2400 Ma, (3) euhedral overgrowths are shown by dashed outlines and cluster at 1800 to 2000 Ma, and (4) the analysis excluded from regression (ellipse at 2200 Ma) is shown with no outline. Note that the regression line shown (dashed line) is anchored at 1850 Ma, the time of the impact event at Sudbury.

Table 2. U-Pb TIMS analytical data of six grain fractions of a euhedral zircon found in sample 11AV-74 (Z10633).

Fract.[1]	Description[2]	Wt. ug	U ppm	Pb[3] ppm	$\frac{206Pb}{204Pb}$	Pb[5] pg	$\frac{208Pb}{206Pb}$	$\frac{207Pb}{235U}$	±1SE Abs	$\frac{206Pb}{238U}$	±1SE Abs	Corr.[7] Coeff.	$\frac{207Pb}{206Pb}$	±1SE Abs	$\frac{206Pb}{238U}$	±2SE	$\frac{207Pb}{235U}$	±2SE	$\frac{207Pb}{206Pb}$	±2SE	% Disc
Sample 11AV-74 (Z10633)																					
A16-1	Clr, Co, El, Pr, NM0	4	51	29	1781	2	0.87	5.1789	0.0075	0.33207	0.00037	0.857111505	0.11311	0.00009	1848.4	3.6	1849.1	2.5	1850.0	2.7	0.1
A16-2	Clr, Co, El, Pr, NM0	5	78	45	3977	2	0.90	5.1652	0.0061	0.33128	0.00030	0.908397397	0.11308	0.00006	1844.6	2.9	1846.9	2.0	1849.5	1.9	0.3
A16-3	Clr, Co, St, Pr, nln, NM0	12	21	12	1190	4	0.84	5.1745	0.0080	0.33104	0.00034	0.800901953	0.11337	0.00011	1843.4	3.3	1848.4	2.6	1854.1	3.4	0.7
C16-1	Clr, Co, El, Pr, M1	6	59	35	7873	1	0.98	5.1758	0.0061	0.33186	0.00031	0.926939444	0.11311	0.00005	1847.4	3.0	1848.6	2.0	1850.0	1.7	0.2
C16-2	Clr, Co, El, Pr, M1	6	33	19	3776	0	0.92	5.1821	0.0069	0.33216	0.00037	0.908311575	0.11315	0.00006	1848.8	3.5	1849.7	2.3	1850.6	2.1	0.1
C16-3	Clr, Co, El, Pr, M1	4	42	24	975	4	0.93	5.1826	0.0086	0.33252	0.00034	0.800641518	0.11304	0.00012	1850.6	3.3	1849.8	2.8	1848.8	3.7	-0.1

[1]All zircon fractions are composed of single grains and were chemically abraded using a modified procedure from Mattinson (2005); all fractions composed of single grains
[2]Zircon descriptions: Co=colourless, Clr=clear, El=elongate, Eu=euhedral, nIn=numerous inclusions, Pr=prismatic, St=stubby prism, NM0=non-magnetic @1.8A 0oSS, M1=magnetic @ 1.8A 1oSS.
[3]Radiogenic Pb
[4]Measured ratio, corrected for spike and fractionation
[5]Total common Pb in analysis corrected for fractionation and spike
[6]Corrected for blank Pb and U and common Pb, errors quoted are 1 sigma absolute; procedural blank values for this study are 0.1 pg U and 1 pg Pb
Pb blank isotopic composition is based on the analysis of procedural blanks; corrections for common Pb were made using Stacey and Kramers (1975) compositions
[7]Correlation Coefficient
[8]Corrected for blank and common Pb, errors quoted are 2σ in Ma
The error on the calibration of the GSC ^{205}Pb-^{233}U-^{235}U spike utilized in this study is 0.22% (2s)

Table 3. U-Pb SHRIMP analytical data for zircon from sample 11AV-74 (Z10633).

Spot name	U (ppm)	Th (ppm)	Th/U	Yb (ppm)	Hf (ppm)	$^{204}Pb/^{206}Pb$	% ±	$^{206}Pb^*$ (ppm)	$f(206)^{204}$ %	$^{208*}Pb/^{206*}Pb$	% ±	$^{207*}Pb/^{235}U$	% ±	$^{206*}Pb/^{238}U$	% ±	Corr Coeff	$^{207*}Pb/^{206*}Pb$	% ±	$^{206*}Pb/^{238}U$	±	$^{207*}Pb/^{206*}Pb$	±	Disc. %
10633-8.2	11	20	1.94	61	7870	3.2E-3	20	3	5.587	0.547	4.2	4.60	9.3	0.319	1.75	0.188	0.1046	9.2	1784	27	1707	169	-5.2
10633-36.2	29	51	1.85	79	9640	7.9E-5	46	8	0.137	0.575	2.9	5.03	2.1	0.325	1.74	0.845	0.1121	1.1	1816	28	1834	20	1.1
10633-1.2	12	20	1.74	64	7091	3.4E-3	20	3	5.821	0.476	3.8	5.25	11.6	0.338	3.67	0.315	0.1128	11.0	1876	60	1845	200	-1.9
10633-2.2	19	34	1.86	73	7716	2.4E-3	20	5	4.154	0.552	3.0	5.29	6.1	0.331	1.56	0.254	0.1160	5.9	1843	25	1896	107	3.2
10633-2.1	89	122	1.42	121	9867	8.9E-4	20	30	1.536	0.418	2.4	7.31	2.4	0.399	1.23	0.518	0.1326	2.0	2167	23	2133	36	-1.8
10633-7.1	126	242	1.98	182	9100	3.0E-5	85	44	0.052	0.574	1.1	8.39	1.1	0.408	1.03	0.927	0.1491	0.4	2206	19	2335	7	6.6
10633-15.1	81	87	1.10	67	9579	-2.7E-5	37	27	-0.047	0.330	1.8	8.03	1.1	0.390	1.04	0.915	0.1491	0.5	2125	19	2336	8	10.6
10633-36.1	38	55	1.52	81	7516	3.1E-4	64	13	0.531	0.429	2.3	8.34	2.4	0.402	1.50	0.632	0.1504	1.8	2179	28	2351	32	8.6
10633-19.1	111	226	2.10	204	6823	3.6E-5	41	38	0.063	0.623	1.1	8.61	1.2	0.404	1.14	0.930	0.1545	0.4	2187	21	2396	8	10.3
10633-6.1	108	197	1.90	181	10083	2.8E-4	62	39	0.490	0.546	2.2	9.15	2.3	0.425	1.51	0.668	0.1562	1.7	2281	29	2415	28	6.6
10633-10.1	161	404	2.58	306	7629	5.4E-5	234	61	0.094	0.746	1.4	9.63	1.7	0.443	1.24	0.718	0.1576	1.2	2364	25	2430	20	3.2
10633-1.1	69	146	2.19	153	6941	1.7E-4	33	26	0.298	0.643	1.3	9.40	1.2	0.432	1.07	0.857	0.1579	0.6	2313	21	2434	11	5.9
10633-23.2	90	189	2.16	191	7685	1.8E-4	34	34	0.310	0.601	1.9	9.49	1.6	0.432	1.27	0.803	0.1594	0.9	2313	25	2449	16	6.6
10633-9.1	173	202	1.21	185	10034	2.6E-4	28	63	0.448	0.336	2.1	9.37	1.4	0.423	1.14	0.789	0.1605	0.9	2275	22	2461	15	8.9
10633-21.1	139	257	1.91	211	8744	6.8E-5	65	51	0.117	0.548	1.0	9.49	1.1	0.428	1.03	0.897	0.1608	0.5	2298	20	2464	9	8.0
10633-11.1	105	207	2.04	205	8034	8.7E-5	21	40	0.150	0.572	1.9	9.92	1.4	0.447	1.17	0.842	0.1610	0.7	2381	23	2466	13	4.1
10633-9.2	232	212	0.95	149	11253	2.2E-5	41	90	0.038	0.275	1.1	10.19	1.2	0.452	1.14	0.971	0.1635	0.3	2405	23	2492	5	4.2
10633-23.1	132	249	1.95	221	8729	5.3E-5	50	50	0.092	0.521	1.9	10.00	1.5	0.440	1.31	0.865	0.1650	0.8	2350	26	2507	13	7.5
10633-4.1	64	106	1.71	108	8233	4.8E-5	71	25	0.083	0.474	2.6	10.44	1.6	0.458	1.28	0.793	0.1653	1.0	2432	26	2511	17	3.8
10633-5.1	85	167	2.02	184	8385	-1.1E-5	38	34	-0.019	0.577	1.9	10.67	1.4	0.460	1.24	0.861	0.1683	0.7	2439	25	2541	12	4.8
10633-8.1	221	571	2.67	376	7531	7.7E-5	39	92	0.133	0.757	1.1	11.70	1.2	0.485	1.08	0.903	0.1750	0.5	2548	23	2606	9	2.7

Spot name follows the convention x-y.z; where x = sample number, y = grain number and z = spot number

$f(206)^{204}$ refers to mole percent of total ^{206}Pb that is due to common Pb, calculated using the ^{204}Pb-method; common Pb composition used is the surface blank (4/6: 0.05770; 7/6: 0.89500; 8/6: 2.13840)

* refers to radiogenic Pb (corrected for common Pb)

Errors are reported at 1σ uncertainty level unless otherwise noted

Analytical details:

IP665: 25 µm spot; 5 or 6 scans; ~9nA O- primary beam intensity, U-Pb calibration error 1.0% (included)

No mass fractionation correction applied

600°C, which suggests isotopic equilibration with the GFG unit at low fluid:rock interaction. The S isotopic data for the sharped-wall vein sulphides, with average $\delta^{34}S$ value of 4.3‰, is consistent with a single homogeneous crustal reservoir, which was likely sourced from the melt sheet.

In summary, this study has shown that the GG is part of the pre-impact history at 1850 Ma and although there is an intense hydrothermal alteration adjacent to the sharp-walled sulphide veins, its extent is limited to 10s cm and thus does not provide a significant vector for exploration.

FORTHCOMING PRODUCTS

A petrological and geochronological study of the grey gabbro unit of the Podolsky Cu-Ni-PGE deposit, Sudbury, Ontario: A 2.6 Ga Gabbro Hosting 1.85 Ga impact-related mineralization. Authors: Linette M. MacInnis, Daniel J. Kontak, Doreen E. Ames, and Nicole Rayner, January, 2015, CJES.

The chemical fingerprint of alteration marginal to a sharp-walled Cu(-Ni)-PGE vein setting: Podolsky deposit, Sudbury, Ontario. Authors: Linette M. MacInnis, Daniel J. Kontak, Doreen E. Ames, and Nancy Joyce, January 2015, SEG.

ACKNOWLEDGEMENTS

The authors would like to thank KGHM International Ltd.'s Podolsky 2012-2013 team for their guidance, access, feedback, coordination, and insight with their computer programs, facilities, and logistics. This work was initiated and funded by the Targeted Geoscience Initiative 4 (TGI-4) program of the Geological Survey of Canada (GSC) within the Ni-Cu-PGE–Cr project including support to the second author (L.M. MacInnis) under the Research Affiliate Program 2012-2014 of Natural Resources of Canada.

REFERENCES

Ames, D.E. and Farrow, C.E.G., 2007. Metallogeny of the Sudbury mining camp, Ontario; Geological Association of Canada, Mineral Deposits Division, Special Publication 5, p. 329–350.

Ames, D.E., Golightly, J.P. and Zierenberg, R.A., 2010. Trace element and sulfur isotope composition of Sudbury Ni-Cu-PGE ores in diverse settings, *In:* Extended Abstracts;. Society of Economic Geologists (SEG), 2010 Keystone conference, Keystone, Colorado, October 2–5, 2010, 4 p. (DVD).

Bleeker, W., Kamo, S., and Ames, D., 2013. New field observations and U-Pb age data for footwall (Target) rocks at Sudbury: Towards a detailed cross-section through the Sudbury Structure, *In:* Lunar and Planetary Institute Abstract Collection; Lunar and Planetary Institute Conference, Large Meteorite Impacts and Planetary Evolution V, Sudbury, Ontario, August 5 to 8, 3112.pdf.

Bohor, B.F., Betterton, W.J., and Krogh, T.E., 1993. Impact-shocked zircons: discovery of shock-induced textures reflecting increasing degrees of shock metamorphism; Earth and Planetary Science Letters, v. 119, p. 419–424.

Carter, W.M., Watkinson, D.H., Ames, D.E., and Jones, P.C., 2009. Quartz diorite magmas and Cu-(Ni)-PGE mineralization, Podolsky deposit, Whistle offset structures, Sudbury, Ontario; Geological Survey of Canada, Open File 6134, 58 p., 1 CD-ROM. doi:10.4095/247514

Corfu, F., Hanchar, J.M., Hoskin, P.W.O., and Kinny, P., 2003. Atlas of zircon textures; Reviews in Mineralogy and Geochemistry, v. 53, p. 469–500.

Davis, D., 2008. Sub-million-year age resolution of Precambrian igneous events by thermal extraction-thermal ionization mass spectrometer Pb dating of zircon: Application to crystallization of the Sudbury impact melt sheet; Geology, v. 36, p. 383–386.

Farrow, C.E.G., Watkinson, D.J., and Jones, P.C., 1994. Fluid inclusion in sulfides from North and South Range Cu-Ni-PGE deposit, Sudbury Structure, Ontario; Economic Geology, v. 89, p. 647–655.

Farrow, C.E.G. and Watkinson, D.H., 1996. Geochemical evolution of the epidote zone, Fraser Mine, Sudbury, Ontario: NI-Cu-PGE remobilization by saline fluids; Exploration and Mining Geology, v. 5, p. 17–31.

Farrow, C.E.G., Everest, J.O., King, D.M., and Jolette, C., 2005. Sudbury Cu-(Ni)-PGE systems: Refining their classification using McCreedy West Mine and Podolsky Project Case Studies, *In:* Exploration for Deposits of Platinum-Group Elements, (ed.) J.E. Mungall; Mineralogical Association of Canada, Short Course Series, v. 35, p. 163–180.

Grimes, C.B., Ushikubo, T., Kozdon, R., and Valley, J., 2013. Perspectives on the origin of plagiogranite in ophiolites from oxygen isotopes in zircon; Lithos, v. 179, p. 48–66.

Krogh, T.E., Davis, D.W., and Corfu, F., 1984. Precise U-Pb zircon and baddeleyite ages for the Sudbury area, *In:* Geology and Ore Deposits of the Sudbury Structure, (ed.) E.G. Pye, A.J. Naldrett, and P.E. Giblin; Ontario Geological Survey, Special Volume 1, p. 431–446.

Krogh, T.E., Kamo, S.L., and Bohor, B.F., 1993a. Fingerprinting the K/T impact site and determining the time of impact by U-Pb dating of single shocked zircons from distal ejecta; Earth and Planetary Science Letters, v. 119, p. 425–429.

Krogh, T.E., Kamo, S.L., Sharpton, V.L., Marin, L.E., and Hildebrand, A.R., 1993b. U-Pb ages of single shocked zircons linking distal ejecta to the Chicxulub crater; Nature, v. 366, p. 731–734.

Lightfoot, P.C., Keays, R.R., Morrison, G.C., Bite, A., and Farrell, K.P., 1997. Geochemical relationships in the Sudbury Igneous Complex: Origin of the Main Mass and Offset Dikes; Economic Geology, v. 92, p. 289–307.

MacInnis, L.M., Kontak, D.J., Ames, D.E., and Joyce, N.L., 2014. Alteration proximal to the sharp-walled Cu-(Ni)-PGE vein footwall mineralization of the Podolsky deposit; Geological Survey of Canada, Open File 7666, 19 p. doi:10.4095/295482

Mattinson, J.M., 2005. Zircon U-Pb chemical abrasion ("CA-TIMS") method: combined annealing and multi-step partial dissolution analysis for improved precision and accuracy of zircon ages; Chemical Geology, v. 22, p. 47–66.

McDougall, I. and Harrison, T.M., 1999. Geochronology and Thermochronology by the $^{40}Ar/^{39}Ar$ Method; Oxford University Press, New York, 269 p.

Molnár, F., Watkinson, D.H., and Jones, P.C., 2001. Multiple hydrothermal processes in footwall units of the North Range, Sudbury Igneous Complex, Canada, and Implications for the genesis of vein-type Cu-Ni-PGE deposits; Economic Geology, v. 96, p. 1645–1670.

Ohmoto, H. and Rye, R.O., 1979. Isotopes of sulphur and carbon, *In:* Geochemistry of Hydrothermal Ore Deposits, (ed.) H.L. Barnes; J. Wiley & Sons, New York, p. 509–567.

Péntek, A., Molnár, F., Watkinson, D.H., Jones, P.C., and Mogessie, A., 2011. Partial melting and melt segregation in footwall units within the contact aureole of the Sudbury Igneous Complex (North and East Ranges, Sudbury Structure), with implications for their relationship to footwall Cu-Ni-PGE mineralization; International Geology Review, v. 53, p. 291–325.

Pidgeon, R.T., Nemchin, A.A., and Kamo, S.L., 2011. Comparison of structures in zircons from lunar and terrestrial impactites; Canadian Journal of Earth Sciences, v. 48, p. 107–116.

Stacey, J.S. and Kramers, J.D., 1975. Approximation of terrestrial lead isotope evolution by a 2-stage model; Earth and Planetary Science Letters, v. 26, p. 207–221.

Stern, R.A., 1997. The GSC sensitive high-resolution ion microprobe (SHRIMP): analytical techniques of zircon U-Th-Pb age determinations and performance evaluation, in Radiogenic Age and Isotopic Studies, Report 10; Geological Survey of Canada, Current Research 1997-F, p. 1–31.

Stern, R.A. and Amelin, Y., 2003. Assessment of errors in SIMS zircon U-Pb geochronology using a natural zircon standard and NIST SRM 610 glass; Chemical Geology, v. 197, p. 111–146.

Sun, S.-S. and McDonough, F., 1989. Chemical and isotopic systematic of oceanic basalts; implications for mantle composition and processes, *In:* Magmatism in the ocean basins; Geological Society, Special Publication, v. 42, p. 312–345.

Tuba, G., Molnár, F., Ames, D.E., Péntek, A., Watkinson, D.H., and Jones, P.C., 2014. Multi-stage hydrothermal processes involved in "low-sulfide" Cu(-Ni)-PGE mineralization in the footwall of the Sudbury Igneous Complex (Canada): Amy Lake PGE zone, East Range; Mineralium Deposita, v. 49, p. 7–47.

Zheng, Y.-F., 1993. Calculation of oxygen isotope fractionation in hydroxyl-bearing silicates; Earth and Planetary Science Letters, v. 120, p. 247–263.